QA: QA

MDL-WIS-PA-000005 REV00

January 2008

Total System Performance Assessment Model/Analysis for the License Application

Volume II

Prepared for:
U.S. Department of Energy
Office of Civilian Radioactive Waste Management
Office of Repository Development
1551 Hillshire Drive
Las Vegas, Nevada 89134-6321

Prepared by:
Sandia National Laboratories
OCRWM Lead Laboratory for Repository Systems
1180 Town Center Drive
Las Vegas, Nevada 89144

Under Contract Number
DE-AC04-94AL85000

DISCLAIMER

This report was prepared as an account of work sponsored by an agency of the United States Government. Neither the United States Government nor any agency thereof, nor any of their employees, nor any of their contractors, subcontractors or their employees, makes any warranty, express or implied, or assumes any legal liability or responsibility for the accuracy, completeness, or any third party's use or the results of such use of any information, apparatus, product, or process disclosed, or represents that its use would not infringe privately owned rights. Reference herein to any specific commercial product, process, or service by trade name, trademark, manufacturer, or otherwise, does not necessarily constitute or imply its endorsement, recommendation, or favoring by the United States Government or any agency thereof or its contractors or subcontractors. The views and opinions of authors expressed herein do not necessarily state or reflect those of the United States Government or any agency thereof.

Total System Performance Assessment Model/Analysis for the License Application

Volume II

MDL-WIS-PA-000005 REV00

January 2008

CONTENTS

Page

CONTENTS (Continued)

Page

FIGURES

Page

FIGURES (Continued)

Page

FIGURES (Continued)

Page

FIGURES (Continued)

Page

FIGURES (Continued)

Page

FIGURES (Continued)

Page

FIGURES (Continued)

Page

FIGURES (Continued)

Page

FIGURES (Continued)

Page

FIGURES (Continued)

Page

FIGURES (Continued)

Page

FIGURES (Continued)

Page

FIGURES (Continued)

Page

FIGURES (Continued)

Page

FIGURES (Continued)

Page

FIGURES (Continued)

Page

TABLES

Page

TABLES (Continued)

Page

7. VALIDATION AND CONFIDENCE BUILDING

The intended purpose of the Total System Performance for the License Application (TSPA-LA) Model, as defined in Section 1.1 of *Technical Work Plan for: Total System Performance Assessment FY 07-08 Activities* (SNL 2008 [DIRS 184920], Section 2.3.5), is to provide the TSPA-LA Model for use in evaluations of compliance with the quantitative postclosure requirements of U.S. Nuclear Regulatory Commission (NRC) Proposed Rule 10 CFR Part 63 (DIRS 178394] and [DIRS 180319]).

The TSPA-LA Model analyzes the complex system of features, events, and processes (FEPs), natural disruptive events, such as igneous intrusion, volcanic eruption, seismic ground motion and fault displacement, and a human-intrusion scenario that could occur at the Yucca Mountain Repository after closure of the repository during the first 10,000 years but within the period of geologic stability (i.e., to and at 1,000,000 years after disposal) (NRC Proposed Rule 10 CFR 63.302 [DIRS 178394]). The FEPs' screening and scenario development for the TSPA-LA Model are discussed in Section 6.1.1. The modeling cases to address the scenario classes are discussed in Section 6.1.2. The modeling cases include:

- Nominal Modeling Case
- Drip Shield Early Failure (EF) Modeling Case
- Waste Package Early Failure (EF) Modeling Case
- Igneous Intrusion Modeling Case
- Volcanic Eruption Modeling Case
- Seismic Ground Motion (GM) Modeling Case
- Seismic Fault Displacement (FD) Modeling Case
- Human Intrusion Scenario.

Validation of the TSPA-LA Model consists of a sequence of activities as described in the *Technical Work Plan for: Total System Performance Assessment FY 07-08 Activities* (SNL 2008 [DIRS 184920], Section 2.3.5). These activities are consistent with the requirements contained in *Quality Assurance Requirements and Description* (QARD) (DOE 2007[DIRS 182051], Supplement SIII.2.6), and Section 6.3 in SCI-PRO-006, *Models*, and are designed to build confidence in the results of the TSPA-LA Model. The activities include verification that consists of checking that the inputs are correct and the software is passing information correctly among its submodels and model components. Several computer software and associated electronic input files were used in developing the TSPA-LA Model. These software and input files are controlled by IM-PRO-003, *Software Management.* The procedural control of the model validation activities, and the software and input files used in developing the TSPA-LA Model, are necessary to ensure overall fidelity and confidence in the results of the TSPA-LA Model.

The verification activities were carried out during development of the TSPA-LA Model, where development follows the generalized approach shown on Figure 7.1-1. These verification activities and the activities conducted for validation of the TSPA-LA Model after its development are shown on Figure 7.1-2.

The during-development activities of model validation include the following:

- Verification of inputs and software (Section 7.2)
- Stability testing (Section 7.3)
- Uncertainty characterization reviews of the values of direct-input parameters and uncertainty and sensitivity analyses (Section 7.4) of the parameters
- Surrogate waste form analyses (Section 7.5) for U.S. Department of Energy (DOE)-owned spent nuclear fuel (DSNF) and naval spent nuclear fuel (NSNF).

Post-development model validation activities were conducted to provide confidence in the results of the TSPA-LA Model and include the following:

- Corroboration of abstraction results with the underlying validated process models (Section 7.6)
- Corroboration of the TSPA-LA Model results with auxiliary analyses (Section 7.7)
- Corroboration of the TSPA-LA Model results with relevant man-made and natural analogues (Section 7.8)
- Incorporation of the comments and recommendations from independent technical reviews (Section 7.9).

A summary of the analyses conducted for validation of the TSPA-LA Model is presented in Table 7.1-1.

The strategy for the model validation is discussed in Section 7.1, followed by discussions of the specific activities conducted to validate the TSPA-LA Model (Figure 7.1-2). Section 7.2 presents testing and input verification activities. Section 7.3 contains a discussion of the statistical, temporal, and spatial discretization tests which are necessary to evaluate model convergence to a stable mean value of the distribution of results. Section 7.3 also evaluates the accuracy of the computed results. Section 7.4 provides a review of the treatment of uncertainties associated with the TSPA-LA Model and parameter input values. Section 7.4 includes a description of the criteria used in the uncertainty review, the review findings, and the corrective actions taken for the situations where the review identified issues in uncertainty treatment of the values of the TSPA-LA direct-input parameters. This section also summarizes the parameter uncertainty and sensitivity analyses performed on the TSPA-LA Model parameters with the details of the analyses presented in Appendix K. Section 7.5 describes application of the TSPA modeling approach to the development of the surrogate waste forms used to represent DSNF and NSNF.

Sections 7.6 to 7.9 describe validation activities conducted for the TSPA-LA Model. Section 7.6 provides a corroborative evaluation of the results of the abstractions that serve as the basis for the TSPA-LA Model. Section 7.6 also evaluates the consistency of the results of model abstractions relative to those obtained with the underlying process models. Section 7.7 describes the results

of a number of auxiliary analyses that were performed in order to corroborate the results of the TSPA-LA Model; in particular, to add confidence by a set of performance margin analyses that the TSPA-LA Model results are indeed conservative without producing any significant risk-dilution, to demonstrate that the TSPA-LA Model is performing as expected and that the TSPA-LA Model results are not sensitive to changes in submodel representations. The various auxiliary analyses performed are of four distinct mutually complementing categories, which were identified to evaluate the reasonableness of the TSPA-LA Model results by applying techniques that are different from those used in the development of the TSPA-LA Model. These auxiliary analyses categories are (1) single realization analyses, (2) comparison of the results of the TSPA-LA Model with a Simplified TSPA Analysis that was developed using a separate numerical code, (3) comparison of the results of the TSPA-LA Model with the performance assessment model developed by the Electric Power Research Institute (EPRI), and (4) a performance margin analyses. Section 7.8 discusses the use of several man-made and natural analogues, which provide confidence in the results of the TSPA-LA Model. Section 7.8 contains quantitative modeling comparisons with the Cerro Negro volcanic eruption of 1995, an analogue for a future potential volcanic eruption at the Yucca Mountain site. In addition, Section 7.8 includes a qualitative comparison of the relevant components of the TSPA-LA Model with those of the Nopal I uranium deposit in the sierra Peña Blanca, Chihuahua, Mexico. Section 7.9 presents summaries of reviews of previous TSPA analyses of the Yucca Mountain Repository including a 1998 peer review of the Total System Performance Assessment for the Viability Assessment (TSPA-VA), a 2001 International Review Team (IRT) evaluation of the performance assessment model used for the Yucca Mountain site recommendation, and a 2006 Independent Validation Review Team (IVRT) evaluation of drafts of the TSPA-LA Model and its supporting process models and submodels. Section 7.9 includes a discussion of the findings and recommendations provided by the IVRT, and summarizes responses to the IVRT's findings and the implementation of the IVRT's recommendations. Section 7.10 provides a summary of the material presented in Sections 7.1 through 7.9.

In addition to the validation activities mentioned above, potential impact on the TSPA-LA Model results due to issues identified after the model runs were completed was evaluated as stated in *Technical Work Plan for: Total System Performance Assessment FY 07-08 Activities* (SNL 2008 [DIRS 184920], Section 2.3.5.3). Appendix P contains the results of this evaluation. No significant impact on the TSPA-LA results was noted.

INTENTIONALLY LEFT BLANK

7.1 MODEL VALIDATION STRATEGY

7.1.1 Introduction

Validation of a computer model for a physical system involves a series of activities designed to generate and enhance confidence in the model's conceptualization and results during and after model development. The modeling process starts with the modeler's understanding of the physical system. A conceptual model is then formulated based on available information, using assumptions, simplifications, and idealizations. The conceptual model is translated into a mathematical model and then implemented into a numerical model. An appropriate computer code/software suite is selected or developed to implement the numerical model. The input to the computer code is prepared, and the code is executed to obtain the model output. This process is illustrated on Figure 7.1-1.

Converting the numerical model to a set of computer code algorithms is a process that must be transparent and traceable. Model inputs are checked, controlled, and documented (Section 4). The process of checking both the development of the computer code and the associated inputs and documentation of decisions generates confidence in the validity of the model during model development (SCI-PRO-002, *Planning for Science Activities*, Attachment 3, Level I Validation). IM-PRO-005, *Software Independent Verification and Validation*, controls computer code verification and validation to ensure that the code implements the numerical model correctly. In conventional modeling practice, model validation is achieved by comparing model results with experimental measurements. However, such measurements are impossible to obtain at the temporal and spatial scales of interest for postclosure performance of the Yucca Mountain repository. From a strictly computational perspective, a well-designed, correctly implemented numerical model should produce results that are explainable and appropriate for its intended purpose. Validation of the TSPA-LA Model is a process to establish confidence that the model adequately represents with sufficient accuracy the postclosure performance of the repository and satisfies its intended purpose.

Preparation of a validated model for a complex system such as the Yucca Mountain repository is an iterative evolutionary process (Eisenberg et al. 1999 [DIRS 155354]). Model development proceeds as the FEPs that could affect the repository system are progressively better understood through testing, analyses, and refinement of the conceptual models, and improvements are made in the computer software needed to implement the numerical model. The TSPA-LA Model is a result of such an evolutionary process of progressive improvements in the database development, refining the process models used as inputs to the next iteration of the TSPA models and their internal as well as external peer reviews. The earlier versions of the performance assessment model, such as the TSPA-VA Model and the Total System Performance Assessment for the Site Recommendation (TSPA-SR) Model, as well as key process models that directly supported the performance assessment models, were subjected to independent reviews. The TSPA-SR Model is the direct precursor to the TSPA Final Environmental Impact Statement (FEIS) Model (Williams 2001 [DIRS 157307]) from which the TSPA-LA Model was developed. The DOE subjected the TSPA-SR Model to a peer review by the Organization for Economic Cooperation and Development (OECD), Nuclear Energy Agency (NEA), and International Atomic Energy Agency (IAEA) IRT (OECD and IAEA 2002 [DIRS 158098]). To quote from their findings:

> "…the TSPA-SR methodology is soundly based and has been implemented in a competent manner… Overall the IRT considers that the implemented performance assessment approach provides an adequate basis for supporting a statement on likely compliance within the regulatory period of 10,000 years."

The IRT also recommended a number of improvements and changes to result in more confidence in and robustness of the TSPA Model. Appendix E, Table E-1, provides a summary of the IRT's comments and identifies the work conducted to improve the TSPA Model as development progressed to the TSPA-FEIS Model and then to the TSPA-LA Model. Given that the TSPA-LA Model evolved directly from the TSPA-SR and TSPA-FEIS Model (Williams 2001 [DIRS 157307]) using the same methods and approach, IRT review and DOE's subsequent favorable response to recommendations provide confidence in the validity of the developmental approach for the TSPA-LA Model.

As a part of the continued effort for confidence building, in addition to the IRT review of the TSPA-SR Model, the TSPA-LA Model was the subject of an independent model validation review conducted on earlier iterations of the model by a team of experts who were independent of the TSPA-LA Model development. Section 7.9 presents additional information on the review by the IVRT. The IVRT review observed that the draft TSPA-LA Model was developed through a recognized iterative and evolutionary process. The recommendations and comments of the IVRT (Section 7.9.3) have been addressed in development of the supporting models and the TSPA-LA product. This provides an enhanced technical basis for the work, and increases confidence in the technical quality and defensibility of the TSPA-LA Model.

Confidence in the results of the TSPA-LA Model is partly based on the results of conducting the checking and documentation activities as required by SCI-PRO-006, *Models*. There are two main categories of procedural activities required for developing a model that is valid for its intended use: (1) those conducted during development of the model (described in SCI-PRO-002, Attachment 3, Validation Level I), and (2) those conducted after development of the model (described in Section 6.3.2. of SCI-PRO-006). Figure 7.1-2 is a flow diagram indicating how the activities identified in the two procedures were applied to the TSPA-LA Model. The basis for the activities conducted for verification and validation of the TSPA-LA Model is documented in *Technical Work Plan for: Total System Performance Assessment FY 07-08 Activities* (SNL 2008 [DIRS 184920], Section 2.3.5). The goal of these activities is to support the demonstration that the results of the procedurally validated TSPA-LA Model satisfy the applicable NRC's individual dose and groundwater protections requirements. The activities are also to address the applicable TSPA-LA Model acceptance criteria identified by the NRC in its Yucca Mountain Review Plan. Table H-1 in Appendix H provides a roadmap of the NRC requirements and the Yucca Mountain Review Plan acceptance criteria applicable to the TSPA-LA Model.

The analyses planned for the verification and validation in the technical work plan (SNL 2008 [DIRS 184920], Section 2.3.5) are described in Table 7.1-1, which generally corresponds to the organization of Section 7.

The technical work plan (SNL 2008 [DIRS 184920], Section 2.3.5.1) describes the activities conducted during development to verify the TSPA-LA Model, as required by SCI-PRO-002, Attachment 3, Validation Level I. Section 2.3.5.2 of the technical work plan (SNL 2008

[DIRS 184920]) describes the post-development activities conducted to validate the TSPA-LA Model to the required validation Level II (as required by SCI-PRO-006, Section 6.3.2). Section 7.1.2 summarizes the activities conducted during development, and Section7.1.3 summarizes the post-development activities. Figure 7.1-2 provides a conceptual flow of model-validation activities performed during and after the development of the TSPA-LA Model and maps these validation activities to the corresponding sections of SCI-PRO-006.

Table 7.1-1 shows the TSPA-LA Model analyses that support the various validation activities. Table 7.1-1 shows the category/subcategory of each model activity (analysis or set of analyses), the purpose of the activity, a brief description of the activity, and the section where the detailed discussions of the results are found. Section 7 and the output data tracking number (DTN) describe the results of each of the analyses in Table 7.1-1. The output DTN contains the run log for the analysis, raw results, and any transformations to produce the figures and tables used in the discussion of the analysis. A complete set of output DTNs is provided in Appendix B.

7.1.2 During-Development Model Validation Activities

The following during-development activities, listed in Section 2.3.5.1 of the technical work plan (SNL 2008 [DIRS 184920]), were performed to demonstrate the validation of the TSPA-LA Model in relationship to its intended use and required level of confidence, are as follows:

1. Selection of input parameters and/or input data and a discussion of how the selection process builds confidence in the model (SCI-PRO-002, Attachment 3, Level I, Validation 1).

2. Description of calibration activities, and/or initial boundary condition simulations, and/or simulation convergences, and a discussion of how the activity or activities build confidence in the model. Includes a discussion of impacts of any run non-convergences (SCI-PRO-002, Attachment 3, Level I, Validation 5).

3. Discussion of the impacts of uncertainties on the results (SCI-PRO-002, Attachment 3, Level I, Validation 4 and 6).

In addition, the TSPA-LA Model input parameter values and abstraction models, including their ranges of applicability, were reviewed and verified for accuracy (Section 7.2). Stability tests were conducted to identify the appropriate number of realizations, timestep size, and spatial discretization to ensure that the model was stable for each modeling case (Section 7.3).

In addition to the discussion on the uniform treatment of uncertainty throughout the model in Section 6.1.3, Section 7.4 presents uncertainty characterization reviews that were conducted to evaluate characterization of the uncertainty associated with the direct-input parameters of the key submodels that support the TSPA-LA Model. Section 7.4 includes a summary of the parameter uncertainty and sensitivity analyses performed on the TSPA-LA Model parameters, with the details of the analyses presented in Appendix K.

The technical work plan (SNL 2008 [DIRS 184920]) includes two additional considerations related to model development and validation:

1. Formulation of defensible assumptions and simplifications (SCI-PRO-002, Attachment 3, Level I, Validation 2).

2. Consistency with physical principles, such as conservation of mass, energy, and momentum (SCI-PRO-002, Attachment 3, Level I, Validation 3).

Formulation of defensible assumptions and simplifications: The TSPA-LA Model was developed by integrating assumptions, process models, abstractions, and the results of analysis or model reports. Section 5 presents the assumptions that support the TSPA-LA Model. These TSPA-LA Model assumptions reflect the relevant assumptions from the supporting analysis or model reports. Section 5 provides the assumptions, their bases for the individual scenario classes, and references to the source submodels where the assumptions were justified.

In addition to the assumptions described in Section 5, the subsections of Section 6.3 describe modeling decisions that describe the technical bases for the TSPA-LA Model and its submodels.

Section 6.1.3 describes how the uncertainties in the direct inputs to the TSPA-LA Model (Table 4-1) were addressed. The uncertainty treatments used in the individual abstraction models are presented in the source reports referenced in Table 4-1. Section 7.4 contains a review of the uncertainty characterizations of the inputs to the TSPA-LA Model, along with the implemented remedies for the uncertainty issues identified during the review.

Section 6.1.4 describes the mechanisms and reasoning used in integrating the process models and submodels from the supporting analysis or model reports into the TSPA-LA Model. The post-development model validation activities, especially the suite of auxiliary analyses, were designed to increase confidence that the TSPA-LA Model results are reasonable, given the complexity of the repository system.

Consistency with physical principles, such as conservation of mass, energy, and momentum: Section 6 describes the development of the TSPA-LA Model. Implicit in the model description is ensuring that the physical principles such as conservation of mass, energy, and momentum are strictly followed in development of mathematical relationships; for example, the particular flow and transport components used in modeling the performance of the engineered and natural barrier systems. The mathematical relationships describing the physical components of models or calculations were developed and presented in the direct-input parameters (Table 4-1) and in their underlying process models and calculations. The Parameter Uncertainty Team, which consisted of a team of subject matter experts (SMEs), evaluated the appropriateness of the input parameters and addressed the uncertainty issues associated with key parameter.

The input verification tests described in Section 7.2 ensure that the inputs, for example, equations describing the abstracted model, are functioning as expected. The calibration and stability testing described in Section 7.3 ensures that the TSPA-LA Model runs are statistically, temporally, and spatially stable and the model produces reliable results, identifies any residual issues, and implements remedial actions. All of these activities ensure that the physical principles on which the process models and calculations were developed were incorporated during the development of the TSPA-LA Model.

In addition to the validation activities mentioned above, potential impact on the TSPA-LA Model results due to issues identified after the model runs were completed was evaluated as stated in *Technical Work Plan for: Total System Performance Assessment FY 07-08 Activities* (SNL 2008 [DIRS 184920], Section 2.3.5.3). Appendix P contains the results of this evaluation. No significant impact on relevant TSPA-LA performance measures (i.e., mean dose) was noted. As a part of the continuing improvement effort by the Project, the impact on the results of this version of the TSPA-LA Model will be included in an addendum to this TSPA-LA Model report.

7.1.2.1 Input Selection and Verification

The TSPA-LA Model is composed of linked submodels. To permit checking of submodel implementation, Section 6.1.5 documents the links from the TSPA-LA Model documentation to submodels in the GoldSim model file (V. 9.60. STN: 10344-9.60-00 [DIRS 181903]). The supporting analysis or model reports for these submodels document the validation of the underlying process models or abstracted models. Each submodel was validated before being integrated into the TSPA-LA Model. Therefore, although the submodels of the TSPA-LA Model were individually validated, validation of the TSPA-LA Model is still necessary. The input verification described in the technical work plan (SNL 2008 [DIRS 184920], Section 2.3.5.1) (Figure 7.1-2), includes the comparison of TSPA-LA Model inputs with the source analyses and model reports from which they were derived. More specifically, this activity consists of checking the input information and models in the TSPA-LA Model against the source analysis or model report results, making certain that individual submodel results do not exceed the validity range of successive submodels, and confirming that the coupling from one submodel to the next is correct. Where submodels yield values that exceed the validity range of a successive submodel, an appropriate value within the valid range is selected. The documentation of the process of selecting submodel input parameters and/or data, including their uncertainties, is included in the relevant supporting document and not in this document. However, it is conceivable that the coupling of submodels in the TSPA-LA Model might generate conditions that cause one or more submodels to produce output that is beyond the validated range of input for the next successive submodel. Occurrence of out-of-valid-range samples for which a valid value is selected is documented in the source analysis or model abstraction report that provides the input in question to the TSPA-LA Model. Section 7.2 presents the results of the computer code and input verification.

Additional measures were added to the computer code verification and input selection activities required by SCI-PRO-002, Attachment 3, because of the critical role of the TSPA-LA Model in estimating repository performance, and because the TSPA-LA Model couples and integrates numerous computer codes and submodels. These measures are intended to verify that the suite of software codes and their associated input files are properly implemented in the integrated TSPA-LA Model. Computer code and input verification and selection consist of the following activities:

- **Selection and Verification of the Integrated System Software: GoldSim**—The integrated system code, GoldSim (V. 9.60. STN: 10344-9.60-00 [DIRS 181903]), is fully verified by the code vendor, GoldSim Technology, and has been qualified for use for TSPA in accordance with IM-PRO-004, *Qualification of Software*.

- **Verification of the Dynamically Linked Libraries as Single Modules and in an Integrated System**—Some of the submodels used within the TSPA-LA Model are implemented as dynamically linked libraries (DLLs) that are separately compiled as linked modules or subroutines that can be called by GoldSim. Examples of single module DLLs are the Waste Package Degradation DLL (WAPDEG V. 4.07, STN: 10000-4.07-00 [DIRS 161240]) and the unsaturated zone (UZ) transport module finite element, heat and mass transfer code (FEHM) (FEHM V. 2.24. STN: 10086-2.24-01-00 [DIRS 179419]). The DLLs for single modules have been validated as adequate representations of their underlying conceptual and mathematical models, and verified in terms of their mechanical operation as DLLs. Because the ability to properly call DLLs is a feature for which GoldSim has been validated, the DLLs are, by default, qualified when called from within the TSPA-LA Model. However, the input to and output from each DLL must be confirmed (Section 7.2.2).

  There are two aspects to confirmation of the DLLs within the integrated TSPA-LA Model. The first is the potential for two or more DLLs to conflict with each other in terms of memory requirements, duplicate input, or output file unit numbers. The second is the potential interaction between DLLs, such as when an output file generated by one DLL is used as an input file to another DLL. Appropriate test cases documented during model development ensure that these types of confirmation issues have been properly resolved (Section 7.2.2).

- **Verification of Inputs in the TSPA Database**—Input to the TSPA-LA Model is controlled by the TSPA Input Database described in Section 4. Input parameters are manually extracted from DTNs stored in the Technical Data Management System, analysis or model reports, and other sources. Table 4-1 summarizes the inputs to the TSPA-LA Model. Parameter Entry Forms, discussed in Section 4.1, provide traceability of the input to its source in the cited document or a DTN. Parameters entered into the TSPA Input Database were checked and confirmed against their sources (Section 7.2.3).

- **Validation and Verification of Single Model Components**—The submodels in the integrated TSPA-LA Model were validated before incorporation into the TSPA-LA Model as described in the analysis or model reports. Section 7.2.4 describes the verification of the proper implementation of submodels within the TSPA-LA Model.

- **Verification of Coupling among Submodels and Model Components**—Section 7.2.5 describes the verification of proper information transfer between connected submodels and software within the integrated TSPA-LA.

The parameter uncertainty and variability, along with model and scenario uncertainty, comprise the overall uncertainty in the TSPA-LA Model results. The parameter uncertainty and variability in the TSPA-LA Model causes a spread of results of the mean dose between the 5th and 95th percentile of about two to three orders of magnitude depending on the modeling case (Section 7.4). The criterion for verification of input parameters to the TSPA-LA Model DLLs and submodels is that the parameter values should be the exact same value as the inputs used in the DLL and/or submodel validation process presented in the respective analysis or model reports. The verification criterion for the results calculated within the TSPA-LA Model and

passed from one submodel to another and/or calculated by DLLs that use abstracted models is that they should agree, within five percent, with the validation results presented in the respective analysis or model reports. The five percent criterion was chosen arbitrarily. Differences between the results from the two calculations are derived from different solution techniques and/or differences in the numbers and durations of the model timesteps between the calculations. The calculation results from individual submodels presented in the respective analysis or model reports and those calculated with the TSPA-LA Model should agree within five percent. The choice of the acceptance criterion of a five percent difference in the results was arbitrary but is justified in view of the overall uncertainty in the TSPA-LA Model.

The tests outlined above are described in detail in Section 7.2. Completion of computer code and input verification is a necessary condition for model validation but, by itself, is insufficient to ensure confidence in the TSPA-LA Model without completion of additional activities, such as those described in the following sections.

7.1.2.2 Model Stability Testing

Model stability testing activities include three types of stability tests: statistical stability, temporal stability, and spatial stability or discretization. Collectively, these three tests are referred to as model stability testing.

Statistical stability (Section 7.3.1) testing involves a number of activities related to demonstrating that a sufficient number of stochastic realizations have been run to achieve a numerically stable mean dose, including: (1) determining confidence intervals (with 3 replicates and using t-test) around the total mean annual dose and mean annual dose for each modeling case (Section 7.3.1); (2) demonstrating numerical accuracy of mean annual dose for the Nominal Modeling Case by comparing the results of the base case 300 realizations with those using 1,000 realizations (Section 7.3.2); (3) demonstrating the numerical accuracy of the expected dose calculations for the Igneous and Seismic Scenario Classes and for the Human Intrusion Scenario (Section 7.3.2); (4) demonstrating for the Seismic GM Modeling Case for 10,000 years that the simplification from *Seismic Consequence Abstraction* (SNL 2007 [DIRS 176828]) used in the calculation of the expected dose is reasonable for: (a) omitting rupture and puncture mechanisms for breaching waste packages (WPs) and omission of rockfall effects on temperature and seepage entering the repository drifts (Section 7.3.2), and (b) assuming that drip shields (DSs) remain intact for 10,000 years (Section 7.3.2); and, (5) checking UZ transport modeling to: (a) ensure that the particle tracking conserves mass, and (b) obtain a sufficient number of particles for the Igneous Intrusion and Seismic GM Modeling Cases (7.3.5).

Temporal stability refers to the use of an appropriate timestep size necessary to achieve a stable solution. Section 7.3.3 describes timestep size evaluation for the Waste Package EF, Igneous Intrusion, Seismic GM and Human Intrusion Modeling Cases, which collectively encompass the range of events and processes that lead to radionuclide mobilization and transport. The degree of stability shown in the graphical comparisons of the results of the stability analysis, using timesteps as short as one year, indicated that a statistical comparison of timestep changes was not necessary.

Spatial stability/discretization in the TSPA-LA Model involves studying the scale at which the repository must be modeled. In particular, because of computational constraints, the TSPA-LA Model does not simulate the individual performance of each of the 11,629 WPs to be emplaced in the repository but groups the WPs into representative WP groups. Section 7.3.4 evaluates the effect of the WP groupings on TSPA-LA Model results.

7.1.2.3 Uncertainty Characterization Reviews and Uncertainty and Sensitivity Analyses

Uncertainty characterization reviews on the direct-input TSPA-LA parameters were undertaken to ensure that appropriate treatment of parameter uncertainty and variability was implemented in preparation of the TSPA-LA Model as required by the technical work plan (SNL 2008 [DIRS 184920], Section 2.3.5.1, Criterion 3). Uncertainty and sensitivity analyses were performed to ensure that the parameter uncertainty is appropriately propagated during the TSPA-LA Model development and the sensitivity of the dose calculations to the parameter uncertainty during and after the model development were identified and addressed.

Section 7.4 documents the results of the activities performed for the uncertainty characterization reviews, and the uncertainty and sensitivity analyses. The discussion presented in Section 7.4 include: (1) approach used for the reviews (Section 7.4.1); (2) risk-informed ranking of the TSPA-LA scenario classes and modeling cases so as to focus the reviews on those modeling cases that have a significant impact on dose (Section 7.4.2), which resulted in identification of three key modeling cases: Seismic GM Modeling Case; Igneous Intrusion Modeling Case; and Volcanic Eruption Modeling Case (Section 7.4.2); (3) performing risk-informed identification and prioritization of the key uncertain parameters that are important to dose in the Seismic, Igneous, and Nominal Scenario Classes (Section 7.4.3); (4) scope of the uncertainty reviews, including identifying the appropriate review team to cover the breadth and depth of the scope of the review, conducting the reviews, and documenting the results in appropriate analysis or model reports (Section 7.4.4); (5) corrective actions for the key uncertainty-related issues identified during the reviews; and, (6) summary of the results of the uncertainty and sensitivity analyses, the details of which are presented in Appendix K as mentioned in the paragraph below.

Appendix J describes the strategy for separating aleatory and epistemic uncertainty including the overall computational strategy, the derivation of the expected annual dose to the reasonably maximally exposed individual (RMEI) for each of the modeling case considered, and presents the results of expected dose calculations. Appendix K discusses uncertainty results for physical processes associated with the release, flow, and transport of radionuclides, and presents sensitivity analysis results for both physical processes and expected dose.

7.1.2.4 Surrogate Waste Form Analyses

Section 7.5 describes the application of the TSPA-LA modeling approach to develop the surrogate waste forms to represent DSNF and NSNF. Section 7.5 includes: (1) discussions on methodology as to how the surrogate waste form represents the DOE and naval waste forms and how the modeling was conducted; (2) a description of the spent fuel categories and how they are represented in the TSPA-LA Model; (3) a discussion of the naval spent fuel Category 1; (4) a representation of the DSNF Category 2 through Category 11; and (5) the results of the analyses that applying the surrogate waste forms.

7.1.3 Post-Development Model Validation Activities

This section discusses the post-development validation activities performed. Post-development model validation activities (SNL 2008 [DIRS 184920], Sections 2.3.5.2 and 2.3.5.3) include possible analyses and evaluations to build the level of confidence that is necessary to demonstrate that the TSPA-LA Model is valid for its intended use. The required validation level for the TSPA-LA Model falls into the Level II Validation category (SCI-PRO-002, *Planning for Science Activities,* Attachment 3) that requires use of at least two of the activities from Section 6.3.2 of SCI-PRO-006. Exceeding the procedural requirements, the technical work plan (SNL 2008 [DIRS 184920], Sections 2.3.5.2 and 2.3.5.3) identified several post-development model validation activities and a number of possible analyses and evaluations for the individual activities to ensure the model is validated.

These activities include the following:

- Corroborating the direct-input abstraction results to the results of the validated mathematical model or process model from which the abstraction was derived (Section 7.6; Figure 7.1-2).

- Performing auxiliary analyses to corroborate the results provided by the TSPA-LA Model or model abstractions and/or submodels used in the TSPA-LA Model (Section 7.7; Figure 7.1-2). The auxiliary analyses include comparison of the TSPA-LA Model results with: (1) those of analyses of single realizations that are significant contributors to dose (Section 7.7.1); (2) the results of a Simplified TSPA Analysis (Section 7.7.2); (3) results calculated by EPRI for the repository using its own performance assessment code (Section 7.7.3); and (4) results of performance margin analyses to provide objective evidence for assessing performance margin and degree of conservatism or non-conservatism in the TSPA-LA Model (Section 7.7.4; Figure 7.1-2).

- Comparing the relevant portions of the TSPA-LA Model with appropriate analogue information. The comparison included quantitative comparisons of the TSPA-LA Model components with: (1) an analogous volcanic eruption (Cerro Negro); and (2) a qualitative description of the groundwater flow and transport of radionuclides in a natural system (Peña Blanca) analogous to Yucca Mountain (Section 7.8; Figure 7.1-2).

- As an additional confidence building activity, the comments and recommendations by past technical reviews, including those by the IVRT review of earlier drafts of the TSPA-LA were addressed and implemented as appropriate (Section 7.9; Figure 7.1-2).

The technical work plan (SNL 2008 [DIRS 184920], Section 2.3.5.3) contains additional contingent activities planned to further build confidence in the TSPA-LA results and complementing the post-development confidence building activities described above. These activities include sensitivity analyses to ensure that the TSPA-LA results remain unchanged due to any essential future revision made in the parameter inputs or submodels. These analyses, if needed, will be conducted utilizing the updated information to evaluate the effect of the changes on the results or conclusions obtained using the TSPA-LA Model. Results of any such

supplemental sensitivity analyses will be documented and reviewed to ensure that the model validation was not adversely impacted through incorporation of the revised information.

Successful completion of the during- and post-development model verification and validation activities described above satisfies the Level II requirements in SCI-PRO-006, Section 6.3.2, for validation of the TSPA-LA Model for its intended purpose.

7.1.3.1 Corroboration of Abstraction Model Results with Validated Process Models

The TSPA-LA Model's abstraction models and their underlying process models were validated during their individual development and post-development validation phases following SCI-PRO-006 and performing the needed activities planned in the appropriate technical work plans. The details of the validation activities and the results of such activities for the process models that served as direct inputs (Table 4-1) to the TSPA-LA Model are documented in the respective analysis or model reports. Validation that the abstraction model results agree with the underlying process model results and quantitatively represent their respective process models before and after their implementation in the TSPA-LA Model is essential to the validation of the TSPA-LA Model. These submodels must function coherently when linked together as integral components of the TSPA-LA Model to provide results that are stable and properly represent the contributing abstraction models. This linkage of individually validated submodels is evaluated by performing input-verification and stability testing activities during the TSPA-LA Model development.

The integrity of the abstraction models during their implementation in the TSPA-LA Model is ensured by performing: (1) independent checks to confirm that the direct inputs are accurately applied in the TSPA-LA Model simulations; and (2) independent verification, for example, by model re-runs to confirm that the inputs produce the result that is expected. The checking and verification activities are documented controlled processes. The verification activities are summarized in Section 7.1.2.1, and a discussion of the verification analyses is provided in Section 7.2. The checking and verification activities ensure that the TSPA-LA Model is built on verified inputs and that the abstraction models accurately reflect the underlying process models. Section 7.1.2.2 summarizes model stability analyses. Section 7.3 provides a discussion of these analyses and the results obtained.

Once the integrity of the underlying process models are ensured through the abstraction and implementation processes used in the TSPA-LA Model, and it is clear that the individual abstraction models are functioning well when they are applied together as components during the computation of the TSPA-LA Model itself, certain post-development model validation and confidence building activities that are unrelated to the TSPA-LA Model development activities need to be performed in order to assess that the TSPA-LA Model, which is built on the abstraction models, is valid for its intended use.

Ensuring the integrity of the direct-input process models during abstraction and their successful application in the TSPA-LA Model is the first step toward defining and executing these follow-up post-development validation and confidence building activities and addressing the intent of the technical work plan goal for Corroboration of Abstraction Model Results with Validated Process Models [Section 7.6]. The technical work plan (SNL 2008 [DIRS 184920],

Section 2.3.5.2) identified corroboration of abstraction model results with those of the respective underlying validated process models as a TSPA-LA Model validation criterion to demonstrate that the actual results of the abstracted models do, in fact, corroborate with those of the respective underlying process models that were abstracted. To accomplish this confirmation, the abstraction models' results were compared with those of the respective process models. Details of the comparisons are presented in Section 7.6.

7.1.3.2 Corroboration of Results with Auxiliary Analyses

Auxiliary analyses are confidence building activities often based on the use of stylized inputs or test cases that help to demonstrate that the TSPA-LA Model and its submodels are functioning correctly. If the outputs from these stylized cases do not agree with scientific judgment and intuition, then an explanation of these counterintuitive results would have to be sought through additional analyses of the underlying processes. Conversely, if the stylized cases produce results that are logical, confidence in the model is enhanced. The auxiliary or stylized analyses for the TSPA-LA Model (Section 7.7) include analyses of selected realizations (e.g., upper-bound realizations at peak mean-dose times) from the full suite of probabilistic realizations (Section 7.7.1); comparison of the results of the TSPA-LA Model with a Simplified TSPA Analysis (Section 7.7.2); a comparison of the TSPA-LA Model results with those from an independent organization (Section 7.7.3); and analyses of performance margins (Section 7.7.4). The impact analyses examine alternative submodels as they relate to issues of conservatism and consistency that were identified by the IVRT. Performance margin analyses provide objective evidence for assessing performance margin and the degree of conservatism or non-conservatism present in the TSPA-LA Model. Specifically, the performance margin analyses will utilize revisions to selected component models in the TSPA-LA compliance model, including alternative conceptual models and/or alternative probability density functions for specific parameters, to assess the performance margin in the TSPA-LA Model (i.e., the degree to which repository system performance is underestimated by the TSPA-LA Model). The Performance Margin Analysis is specifically designed to address IVRT comments. The analyses were conducted both with individual model-component revisions as well as with a combined analysis that incorporates all of the selected component revisions.

7.1.3.3 Corroboration of Results with Analogues

In accordance with SCI-PRO-006*,* Section 6.3.2, comparisons with several analogues that are relevant to barrier performance of the Yucca Mountain repository were conducted for the TSPA-LA Model. Section 7.8 provides a summary of these comparisons. Specifically, a detailed quantitative comparison was conducted for the atmospheric dispersal and deposition of tephra from a potential volcanic eruption (SNL 2007 DIRS 177431] to ash fall at Cerro Negro, Nicaragua, using the code ASHPLUME [181035], an analogue for the Volcanic Eruption Modeling Case (Section 7.8.1). In addition, Section 7.8.2 provides a qualitative comparison of the Nopal I uranium mine, located in the Sierra Peña Blanca, Chihuahua, Mexico, to the performance of the Yucca Mountain repository. The Nopal I uranium deposit is a natural analogue for groundwater transport of radionuclides in the TSPA-LA modeling cases. These two natural analogues were selected because they incorporate significant components of the TSPA-LA Model. Cerro Negro enhances confidence in the ash distribution model, and Peña

Blanca enhances confidence in the groundwater transport models for the UZ and saturated zone (SZ) of the natural system of the Yucca Mountain repository.

7.1.3.4 Independent Technical Reviews

The TSPA methodology is iterative. The TSPA process adopted by the DOE is based generally on the methodology developed by Cranwell et al. (1990 [DIRS 101234], Sections 2 and 3). Over time, the methodology has been enhanced and applied to numerous projects by various international organizations involved in radioactive waste management. The TSPA-LA Model was developed initially to analyze the ability of the natural and engineered systems of the Yucca Mountain repository to isolate nuclear waste following repository closure. Performance Assessments and related supplemental analyses of the Yucca Mountain repository have been conducted following the publication of the Nuclear Waste Policy Act as Amended in 1987, Public Law No. 100-203 [DIRS 100016]. TSPAs of the Yucca Mountain repository have been iterative and periodically updated, each building on the previous TSPAs. The iterative assessments incorporate both an improved understanding of the processes affecting repository performance and, through additional field observations and laboratory analyses, better identification and quantification of the values of the parameters used in the TSPAs.

Early iterations of probabilistic TSPAs for the Yucca Mountain repository include TSPA-91 (Barnard et al. 1992 [DIRS 100309]), TSPA-93 (Wilson et al. 1994 [DIRS 100191]), TSPA-95 (CRWMS M&O 1995 [DIRS 100198]), and *Total System Performance Assessment – Viability Assessment of a Repository at Yucca Mountain (TSPA-VA)* (DOE 1998 [DIRS 100550], Volume 3). The more recent TSPA iterations include *Total System Performance Assessment for the Site Recommendation* (TSPA-SR) (CRWMS M&O 2000 [DIRS 153246]) and the application of the Total System Performance Assessment-Site Recommendation Model to the Final Environmental Impact Statement for the Yucca Mountain repository (Williams 2001 [DIRS 157307]).

Previous performance assessments of the Yucca Mountain repository have been evaluated and independently reviewed by technical staff and various external organizations, and reviewers generally make recommendations for improvements for consideration in future TSPA iterations. Examples of empanelled reviews include the TSPA Peer Review conducted by Budnitz et al. (1999 [DIRS 102726]) and an evaluation by an IRT that is summarized in *An International Peer Review of the Yucca Mountain Project TSPA-SR, Total System Performance Assessment for the Site Recommendation (TSPA-SR)* (OECD and IAEA 2002 [DIRS 158098]). These independent technical reviews for the TSPA-LA development process are summarized in Section 7.9.1. As mentioned earlier, the IVRT reviewed the earlier iterations of the TSPA-LA Model. A detailed discussion on the IVRT review is presented in Section 7.9.2.

Table 7.1-1. TSPA-LA Model Validation Analyses

Activity Category/Subcategory	Purpose	Activity Description	Document Section
During–Development Validation Activities (Technical Work Plan Validation (SNL 2008 [DIRS 184920], Section 2.3.5.1))			
Computer Code and Input Verification			
Model Testing and Verification	Testing of software that is the basis for the TSPA-LA Model.	Verify GoldSim software.	7.2.1
	Checking to determine whether the correct input parameters are used.	Verify input parameters.	7.2.3
	Test cases to determine whether the model is working correctly, saving appropriate results, interfacing with DLLs, feeding the correct information among model components, and not exceeding the applicable range of model components.	Includes verification of DLLs, submodels, model components, and coupling among submodels and model components; and comparison with other models (e.g., stand-alone models from analysis model reports). In addition, the verification of coupling among submodels and model components includes subsystem analyses of annual release across model interfaces, drift-wall condensation, and localized corrosion initiation.	7.2.2, 7.2.4, 7.2.5; Tables 7.2-1 and 7.2-2
Model Stability Testing			
Statistical Stability of Mean Annual Dose	Determine confidence interval around total mean annual dose and mean annual dose for each modeling case using three replicates.	Generate total mean annual dose and mean annual dose for each modeling case using three replicates with different random seeds. Determine a confidence interval around the estimate of the overall mean with a *t*-test.	7.3.1
Numerical Accuracy of Expected Annual Dose Calculation – Igneous Scenario Class	Demonstrate accuracy of calculation of expected annual dose for the modeling cases of the Igneous Scenario Class.	For the Igneous Intrusion Modeling Case, demonstrate accuracy of the quadrature integration technique by increasing the discretization used in the integral. Increase the number of specified event times from 10 to 50. Calculate expected annual dose for five epistemic realizations for both 10,000 and 1,000,000 years. For the Volcanic Eruption Modeling Case for 10,000 years, demonstrate accuracy of the combined Monte Carlo and quadrature integration techniques by increasing the sample size used in the Monte Carlo integration and the discretization used in the quadrature integration. Calculate expected annual dose for 10,000 years for five epistemic realizations, increasing the aleatory LHS sample size from 40 to 120, and the number of specified event times from 10 to 20. Conclusions for 10,000 years apply to the 1,000,000 year calculations.	7.3.2

Table 7.1-1. TSPA-LA Model Validation Analyses (Continued)

Activity Category/Subcategory	Purpose	Activity Description	Document Section
Model Stability Testing (Continued)			
Numerical Accuracy of Expected Annual Dose Calculation – Seismic Scenario Class	Demonstrate accuracy of calculation of expected annual dose for the modeling cases of the Seismic Scenario Class.	For the Seismic GM Modeling Case for 1,000,000 years, demonstrate the accuracy of the Monte Carlo integration technique by means of increased sample size. Repeat Replicate 1 (300 epistemic realizations) with a different aleatory seed to generate a second set of 9,000 dose histories (30 independent aleatory samples for each epistemic realization). Pool the two sets of 9,000 dose histories and generate expected annual dose based on the pooled set of 60 independent aleatory samples per epistemic realization, and compare to expected annual dose for the base case of 30 independent aleatory samples per epistemic realization. For the Seismic GM Modeling Case for 10,000 years, demonstrate accuracy of the quadrature integration technique by increasing the discretization used in each integral. Increase the number of specified event times from 6 to 12 and the number of specified damage levels from 4 to 8. Calculate expected annual dose for 5 epistemic realizations. For the Seismic FD Modeling Case, demonstrate accuracy of the quadrature integration technique by increasing the discretization used in each integral. Increase the number of specified event times from 6 to 12 and the number of specified damaged areas from 3 to 6. Calculate expected annual dose for 5 epistemic realizations for both 10,000 and 1,000,000 years.	7.3.2

Table 7.1-1. TSPA-LA Model Validation Analyses (Continued)

Activity Category/Subcategory	Purpose	Activity Description	Document Section
Model Stability Testing (Continued)			
Justification of Simplifications for the Seismic GM Modeling Case for 10,000 Years	For the Seismic GM Modeling Case for 10,000 years, demonstrate that simplifications of the Seismic Consequences Abstraction used in the calculation of expected annual dose are reasonable.	Justify omission of TAD waste packages for SCC damage by computing the probability of SCC damage to the TAD over 10,000 years. Justify omission of the rupture mechanism for breaching WPs by computing the probability of rupture for the CDSP and TAD WPs over 10,000 years. Justify omission of the puncture mechanism for breaching WPs by computing the probability of puncture for the CDSP and TAD WPs over 10,000 years. Justify assumption that the DS remains intact for 10,000 years by computing the probability of DS framework and plate failure over 10,000 years and estimating the consequent dose assuming plate failure before 10,000 years. Justify omission of rockfall effects on temperature and seepage entering the drift by computing the expected and 95th percentile volumes of rockfall over 10,000 years.	7.3.2
Temporal Stability	Demonstrate stability of expected annual dose for temporal discretization in GoldSim.	Comparison of expected annual dose histories for five epistemic vectors for the following modeling cases: Nominal; Seismic GM (10,000 years); Igneous Intrusion (10,000 and 1,000,000 years); and Drip Shield EF (10,000 years). Compare expected annual dose histories for three different temporal discretizations.	7.3.3
Spatial Discretization	Evaluate the impact due to the spatial discretizations inherited by the TSPA-LA Model from the supporting natural and engineered-barrier process models.	Evaluate the appropriateness of use of the inherited spatial discretization schemes of the process model abstractions that feed the TSPA-LA. These abstractions include the process models: Mountain-Scale UZ Flow, EBS TH Environment, UZ Transport, and SZ Flow and Transport abstractions.	7.3.4.1
	Evaluate the impact due to the spatial discretizations created within the TSPA-LA Model.	Describe the spatial discretization of the repository on the basis of percolation subregions and the binning of the percolation subregions by quantiles (0.0 to 0.05, 0.05 to 0.3, 0.3 to 0.7, 0.7 to 0.95, and 0.95 to 1.0).	7.3.4.2
		Demonstrate the appropriateness and validity of using the representative TH histories as inputs to the EBS Thermal-Hydrologic Environments Submodel of the TSPA-LA, as opposed to using the comprehensive data set available from the MSTHM.	7.3.4.3

Table 7.1-1. TSPA-LA Model Validation Analyses (Continued)

Activity Category/Subcategory	Purpose	Activity Description	Document Section
Model Stability Testing (Continued)			
Stability of UZ Transport Modeling for the Igneous Intrusion Modeling Case	Evaluate the stability of results in reference to the maximum number of particles allowed per species for the Igneous Intrusion Modeling Case for 1,000,000 years.	Analyze the differences in UZ releases of ^{99}Tc, ^{233}U, ^{234}U, ^{237}Np, and ^{239}Pu, and in cumulative dose for three cases (500,000; 750,000; and 900,000 particles).	7.3.5
Stability of UZ Transport Modeling for the Seismic GM Modeling Case	Evaluate the stability of results in reference to the maximum number of particles allowed per species for the Seismic GM Modeling Case for 10,000 years.	Analyze the differences in UZ releases of ^{99}Tc, ^{233}U, ^{234}U, ^{237}Np, and ^{239}Pu and in cumulative dose for three cases (500,000; 750,000; and 900,000 particles.).	7.3.5
Stability of UZ Transport Modeling for the Drip Shield EF Modeling Case	Evaluate the stability of results in reference to the maximum number of particles allowed per species for the Drip Shield EF Modeling Case for 1,000,000 years.	Analyze the differences in UZ releases of ^{99}Tc, ^{233}U, ^{234}U, ^{237}Np, and ^{239}Pu, and in cumulative dose for three cases (500,000; 750,000; and 900,000 particles).	7.3.5
Uncertainty Characterization Reviews			
Ranking of Scenario Classes	Prioritize scenario classes of higher significance to dose.	Develop a risk-based ranking of TSPA-LA scenario classes and modeling cases in order to focus the uncertainty characterization reviews of the most important component model abstractions.	7.4.2
Key Uncertain Parameters	Identify the key uncertain parameters that are important to dose.	Select the key uncertain parameters that are important to dose in the Seismic, Igneous, and Nominal Modeling Cases for characterization review based on both importance rankings from past TSPA scoping studies and recommendations provided by model abstraction developers and experienced TSPA analysts.	7.4.3
Uncertainty-Characterization Review Findings and their Implementation	Review uncertainty characterization and address findings.	Perform uncertainty characterization of the selected key parameters impacting dose for the Seismic, Igneous, and Nominal Modeling Cases and implement corrective actions for observed deficiencies.	7.4.4

Table 7.1-1. TSPA-LA Model Validation Analyses (Continued)

Activity Category/Subcategory	Purpose	Activity Description	Document Section
Surrogate Waste Form Validation			
Spent Fuel Categories	Comparison of naval surrogate fuel to naval fuel (Category 1).	Perform probabilistic runs to compare the naval surrogate (Zircaloy-clad commercial fuel) with naval fuel for Nominal, Igneous Intrusion, and Volcanic Eruption Modeling Cases.	7.5.3
	Comparison of the DOE surrogate fuel to each DOE spent fuel category (Category 2 through Category 11).	Perform probabilistic run using Drip Shield EF Modeling Case to compare the DOE surrogate with plutonium/uranium alloy spent fuel (Category 2), plutonium/uranium-carbide spent fuel (Category 3), mixed-oxide spent fuel (Category 4), uranium/thorium-carbide spent fuel (Category 5), uranium/thorium-oxide spent fuel (Category 6), uranium-metal spent fuel (Category 7), uranium-oxide spent fuel (Category 8), aluminum-based spent fuel (Category 9), miscellaneous spent fuel (Category 10) for two inventories, and uranium-zirconium hydride spent fuel (Category 11).	7.5.4
Selected Sensitivity Analyses	Justification of the DOE surrogate dissolution model.	Perform probabilistic comparison of fuel degradation models for Category 2 through Category 11 and air alteration rates for Category 5 and Category 7.	7.5.5
	Justification of the DOE surrogate dissolution model.	Perform comparison of uranium-metal dissolution model, uranium-metal dissolution model with air alteration, and instantaneous dissolution (Category 7). Perform similar comparison for the uranium/thorium-carbide dissolution model (Category 5).	7.5.5
	Effects of fuel surface area and free inventory and uncertainty of radionuclide inventory.	Perform probabilistic comparison of uranium-metal nominal surface area with bounding surface area and free inventory and comparison of nominal inventory with the bounding inventory (Category 7).	7.5.5
	Uncertainty in number of WPs.	Perform probabilistic comparison of aluminum-based spent fuel for nominal and bounding number of WPs (Category 9).	7.5.5
	Comparison of radionuclides that contribute to annual dose from surrogate DOE spent fuel, HLW, uranium-metal spent fuel (Category 7), uranium/thorium-carbide spent fuel (Category 5), and uranium/thorium-oxide spent fuel (Category 6).	Analyze plots of key radionuclides that contribute to total annual dose for the DOE surrogate spent fuel only, HLW only, Category 7 only, Category 5 only, and Category 6 only.	7.5.5
	Justification of the DOE surrogate fuel.	Compare of the weighted sum of Category 2 through Category 11 spent fuel with a single WP of the DOE surrogate spent fuel.	7.5.5

Table 7.1-1. TSPA-LA Model Validation Analyses (Continued)

Activity Category/Subcategory	Purpose	Activity Description	Document Section
Post–Development Validation Activities (Technical Work Plan Validation (SNL 2008 [DIRS 184920], Section 2.3.5.2))			
Corroboration of Direct Input Abstraction Results with Validated Process Models			
Corroboration of Abstraction Results with Underlying Process Models	Evaluate consistency of the abstraction results with the underlying validated key natural system environment models.	Perform quantitative and qualitative evaluation of how well the direct input abstraction results corroborate with the underlying validated key natural system environment models. Provide the evidence that builds confidence in the direct inputs.	7.6. 4.1
	Evaluate consistency of the abstraction results with the underlying validated key engineered barrier system models.	Perform quantitative and qualitative evaluation of how well direct input abstraction results corroborate the underlying validated key EBS models. Provide the evidence that builds confidence in the direct inputs.	7.6.4.2
	Evaluate consistency of the abstraction results with the underlying validated key DS, WP, and waste form degradation and mobilization models.	Perform quantitative and qualitative evaluation of how well the direct input abstraction results corroborate the underlying validated key DS, WP, and waste form degradation and mobilization models. Provide the evidence that builds confidence in the direct inputs.	7.6.4.3
	Evaluate consistency of the abstraction results with the underlying validated key disruptive events models.	Perform quantitative and qualitative evaluation of how well the direct input abstraction results corroborate the underlying validated key seismic and igneous disruptive events models. Provide the evidence that builds confidence in the direct inputs.	7.6.4.4
	Evaluate consistency of the abstraction results with the underlying validated biosphere model.	Provide the evidences that build confidence in the direct inputs from the biosphere model to the TSPA-LA Model.	7.6.4.5
Corroboration of Results with Auxiliary Analyses			
Analysis of Single Realizations	Evaluate the realization that contributes significantly to mean annual dose for the Early Failure Modeling Cases.	Select a realization each from the Waste Package EF Modeling Case and Drip Shield EF Modeling Case and analyze it to examine how the transport of key radionuclides is affected by coupling various components of the EBS, UZ, and SZ domains following the WP failure under varying physical-chemical-thermal-mechanical conditions.	7.7.1
	Evaluate the realization that contributes significantly to mean annual dose for the Igneous Intrusion Modeling Case.	Select a realization from the Igneous Intrusion Modeling Case and analyze it to examine how the transport of key radionuclides is affected by coupling various components of the EBS, UZ, and SZ domains following the waste package failure under varying physical-chemical-thermal-mechanical conditions	7.7.1
	Evaluate the realization that contributes significantly to mean annual dose for the Seismic GM Modeling Case.	Select a realization from the Seismic GM Modeling Case and analyze it to examine how the transport of key radionuclides is affected by coupling various components of the EBS, UZ, and SZ domains following the WP failure under varying physical-chemical-thermal-mechanical conditions.	7.7.1

Table 7.1-1. TSPA-LA Model Validation Analyses (Continued)

Activity Category/Subcategory	Purpose	Activity Description	Document Section
Corroboration of Results with Auxiliary Analyses (Continued)			
Comparison with Other Simple Models	Compare the TSPA-LA Model component results with a simplified analysis.	Perform an Simplified TSPA Analysis and compare the results with those of the TSPA-LA Model.	7.7.2
	Compare with the Energy and Power Research Institute (EPRI) TSPA Analysis.	Develop a comparison of the approach and results of the TSPA independently conducted by EPRI using its code IMARC for the postclosure performance of the Yucca Mountain repository.	7.7.3
Performance Margin Analyses	Provide objective evidence for assessing performance margin and degree of conservatism or non conservatism in the TSPA-LA Model.	Conduct several auxiliary analyses (see Section 7.7.4 for the list) utilizing revisions to selected component models in the TSPA-LA compliance model, including conceptual or uncertainty alternatives, to assess the performance margin in the compliance model and to evaluate whether the compliance model dose is underestimated. The analyses include both individual component revisions as well as a combined analysis that incorporates all of the selected component revisions.	7.7.4
Corroboration of Results with Natural Analogues			
Cerro Negro	Validation of ASHPLUME for the Volcanic Eruption Modeling Case.	Compare of Cerro Negro ash-fall measurements to the results from ASHPLUME.	7.8.1
Peña Blanca	Validation of the UZ and SZ Transport Model.	Compare of field data from Peña Blanca with the TSPA-LA Model results using a modified TSPA model.	7.8.2
Independent Technical Reviews Performed in Preparation of TSPA-LA Model			
TSPA-VA Peer Review	Evaluate the TSPA-VA methodology and prediction of the future behavior of the total system.	Performed peer review of the TSPA-VA and the supporting process models. The review was to be conducted by an independent group of external experts. 1997 -1999	7.9.1
TSPA-SR Peer Review	Evaluation of the TSPA-SR for methodology and ability to meet the needs for SR and future LA compliance.	Performed peer review of the TSPA-SR and selected supporting documents to evaluate the approach used in the performance assessment, and how well the TSPA-SR and the future TSPA-LA needs were addressed. The review was to be conducted by an international panel of experts managed by the OECD/NEA in 2002.	7.9.2
Draft TSPA-LA Technical Review	Evaluate the earlier draft iterations of the TSPA-LA Model as they were being drafted as to the degree of validation of the model for its intended purpose.	Perform technical review on the evaluation of the degree to which the draft TSPA-LA Model was valid for its intended purpose for the 10,000 years compliance period for which the model was prepared. The review was to be conducted by a team of experts during 2004, 2005, and early part of 2006.	7.9.3

INTENTIONALLY LEFT BLANK

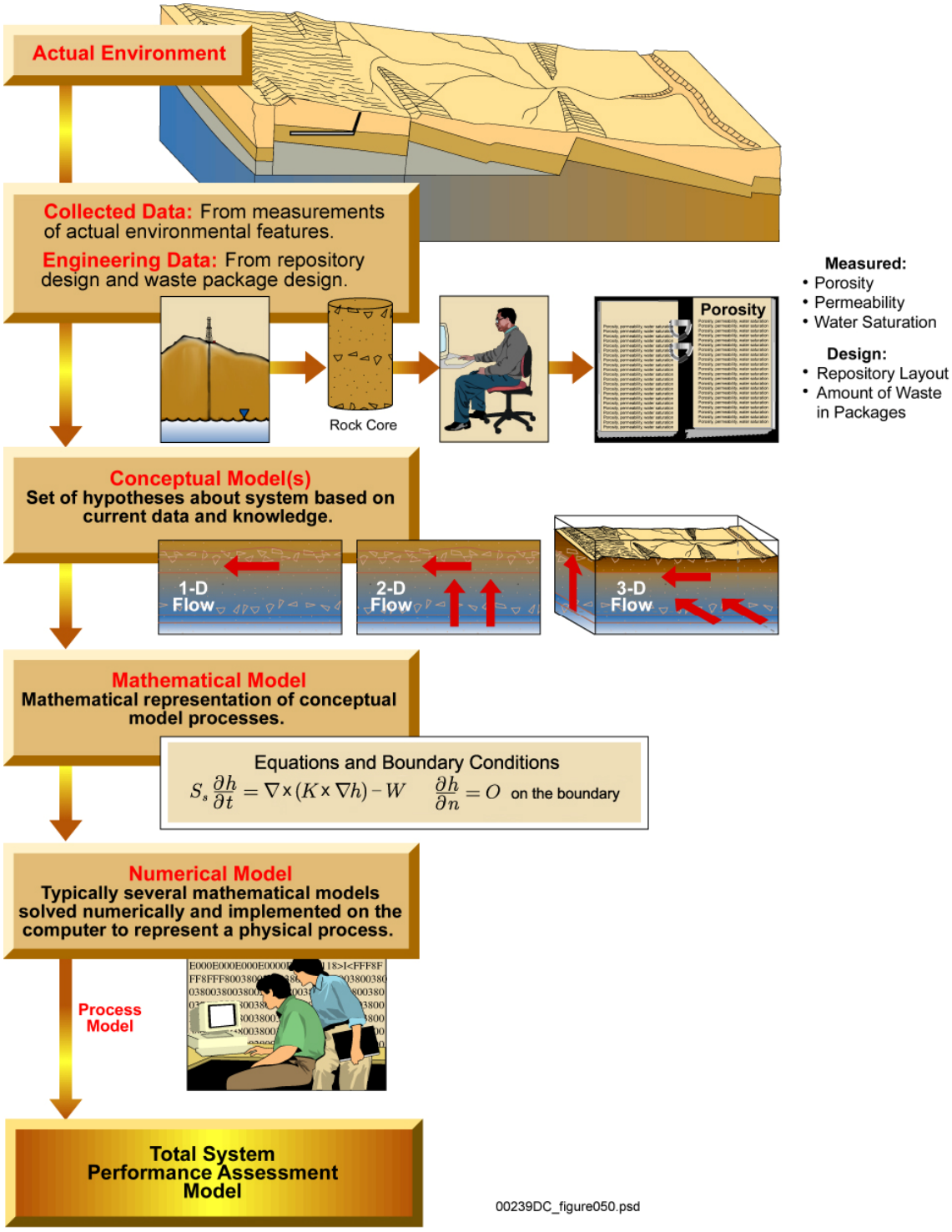

Figure 7.1-1. Generalized Performance Assessment Approach

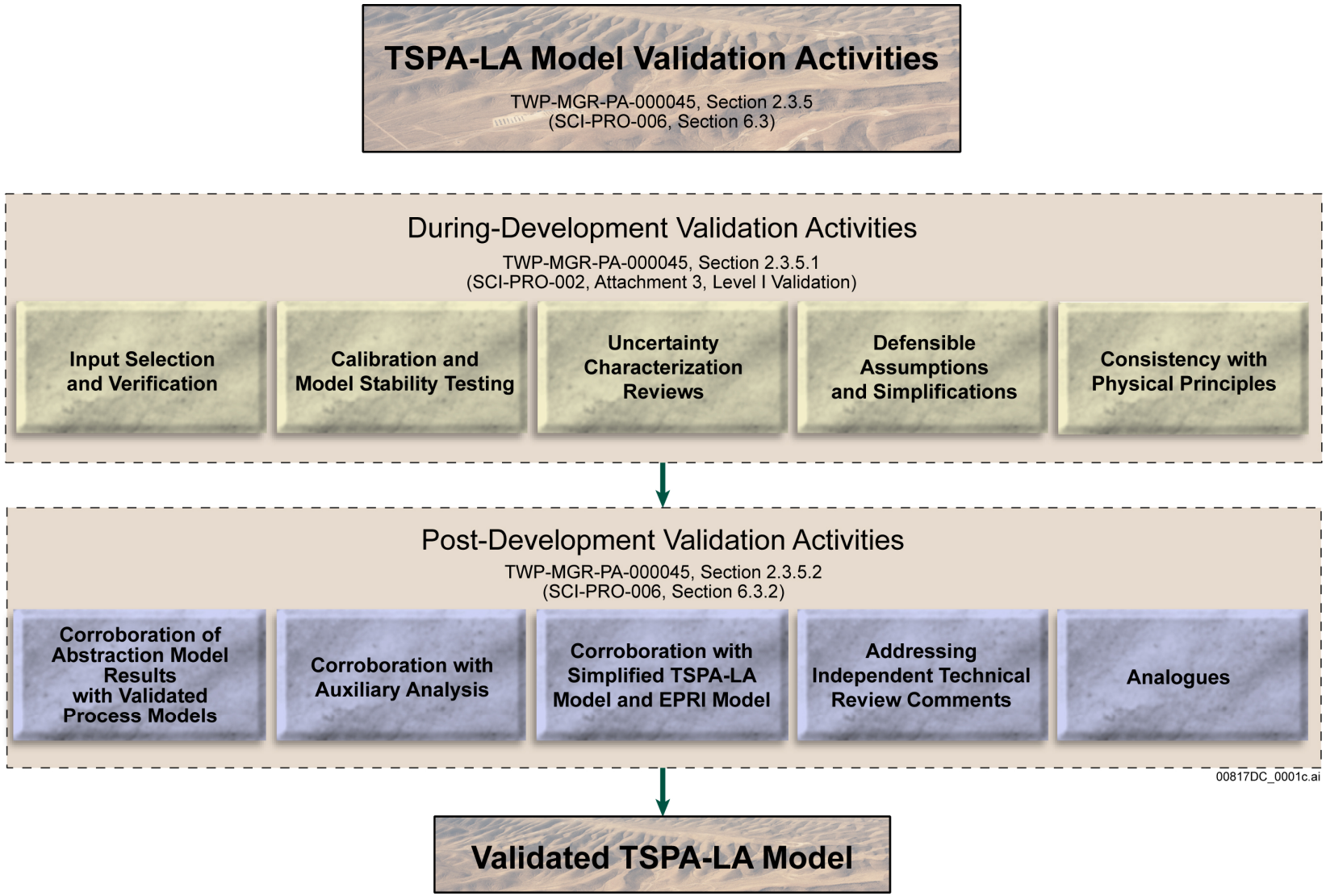

NOTE: The model validation activities, discussed in the TSPA TWP, are shown in the boxes. The corresponding procedural activities are in parenthesis.

Figure 7.1-2. Model Validation Approach

7.2 COMPUTER CODE AND INPUT VERIFICATION

The activities discussed in this section were conducted to comply with the requirements of SCI-PRO-006, *Models,* and Section 2.3.5.1 of *Technical Work Plan for: Total System Performance Assessment FY 07-08 Activities* (SNL 2008 [DIRS 184920]). They include verification of the integrated TSPA-LA Model software (GoldSim), verification of DLL implementations within the TSPA-LA Model, verification of model inputs entered into the TSPA Input Database, and verification of the implementation of the submodel abstractions within the TSPA-LA Model. Verification of the DLL/abstraction implementations was conducted by executing the TSPA-LA Model with a known set of input parameters and comparing the calculated results to those presented in the DLL/abstraction supporting documentation (Sections 7.2.2 and 7.2.4). Coupling between submodels within the TSPA-LA Model is examined by verifying that the information generated by one submodel is fed correctly to successive submodels, and the information does not exceed the applicable range of the successive submodel (Section 7.2.5). Additional information related to the use of the TSPA-LA software codes mentioned in the verification process is provided in Section 3.0.

7.2.1 Selection and Verification of the Integrated System Software: GoldSim

The GoldSim software (V9.60.100, STN: 10344-9.60-01 [DIRS 181903]) was selected as the TSPA Model's integration software based on its capabilities and use in similar applications. The TSPA-LA Model was developed within the GoldSim software framework. GoldSim provides the capability for the user to:

- address the inherent variability and uncertainty that is present in real-world systems by using Monte Carlo simulation
- superimpose the occurrence and consequences of discrete events onto continuously varying systems
- build top-down models using hierarchical containers that facilitate the simulation of large, complex systems while keeping them easy to understand and navigate
- dynamically link external programs or spreadsheets directly to the GoldSim software
- directly exchange information between any open connectivity-compliant database and
- simulate the release, transport, and ultimate fate of mass within the system with an included contaminant transport module.

The GoldSim software application was originally developed specifically for use in the evaluation of radioactive waste disposal facilities. In the past decade, the following are some examples of applications of GoldSim (GoldSim Technology Group 2007 [DIRS 184807]):

- Evaluation of the safety of the proposed high-level radioactive waste (HLW) repository at Yucca Mountain, including the SR

- Evaluation of potential host rocks as part of a program to select a disposal site for the Spanish Radioactive Waste Disposal Research efforts

- Evaluation of waste disposal sites in Los Alamos, New Mexico, to aid in risk characterization and to help identify monitoring requirements for low-level radioactive waste disposal areas

- Evaluation of alternative remediation and closure options for abandoned uranium mill tailings facilities and mine workings in Germany and Canada

- Sensitivity calculations for various applications to supplement the Performance Assessments of the Waste Isolation Pilot Plant in Carlsbad, New Mexico

- Evaluation of different conceptual models of the groundwater flow system on estimates of radionuclide migration at the Nevada Test Site.

Prior to release of each version of the software, the vendor, GoldSim Technology Group, executed tests in an internal verification plan that are included in *Design Document for: GoldSim v9.60* (DOE 2007 [DIRS 181107]). This plan exercises the graphical user interface, internal functions, stochastic processes, contaminant transport code, and result displays for the purpose of demonstrating that the software performs its numerical, logical, and input/output operations correctly.

The vendor's software verification plan consists of over 250 tests that cover the program's capabilities, including the user interface, user-defined expressions, internal functions, and distributed processing capabilities. These tests include:

- 93 Basic Functional Tests
- 23 Time and Monte Carlo Tests
- 130 Contaminant Transport Tests
- 17 Reliability Module Tests.

Specific tests from the vendor's verification plan are independently rerun as part of the Sandia National Labs (SNL) Quality Assurance (QA) procedure, IM-PRO-004, *Qualification of Software,* that demonstrates that the TSPA-identified functional requirements listed in *Requirements Document for: GoldSim v9.60* (DOE 2007 [DIRS 181106]) are satisfactorily implemented. For added confidence, key functions and capabilities of the simulation software are combined into four TSPA-developed tests and the results are compared to independently generated results. The independent tests are described in the *Design Document for: GoldSim v9.60* (DOE 2007 [DIRS 181107], Section 7.2.1) and the results are shown in *Software Validation Report for: GoldSim v9.60 on Windows 2000* (DOE 2007 [DIRS 181109], Sections 4.2.34 through 4.2.37).

The integrated system software (GoldSim) was qualified in accordance with IM-PRO-004. It was obtained from Software Configuration Management in accordance with IM-PRO-003, *Software Management*, and was installed in accordance with installation test instructions listed in Section 3.1 of *User Information Document for: GoldSim Version 9.60* (DOE 2007

[DIRS 181108]). GoldSim was used to develop the analyses for the TSPA-LA Model within the limitations and the range of verification guidance presented in Appendix G of the *User's Guide, GoldSim Probabilistic Simulation Environment* (GoldSim Technology Group 2007 [DIRS 181727]). Additional information regarding the GoldSim software is discussed in Section 3.8 and in the documents listed in Table 3-8.

7.2.2 Verification of Dynamically Linked Libraries in an Integrated System

This section describes the verification of DLLs in the integrated TSPA-LA Model. The DLLs that implement model abstractions are listed in Table 7.2-1 along with the section where the verification of these DLLs is discussed. The verification analyses for the implementation of the DLLs, the abstractions used from the analysis and/or model reports, and the coupling between TSPA-LA Model components are discussed in Sections 7.2.4.1 and 7.2.5. A roadmap of the verification analyses is provided in Table 7.2-2 along with the analysis description, the status of the verification, and the document section where the analysis is described.

The general approach to verifying the implementation of a DLL or other abstraction within an integrated model is described as follows. A validation test example reported in an analysis and/or model report, or a validation test report with known results, is first run on the stand-alone implementation of a DLL or other model abstraction to verify that the answer reported in the analysis and/or model report can be reproduced. The answer is then compared with the results of the implementation in the TSPA-LA Model. In some instances, small differences resulting from uncertainty and differences in calculation schemes between the two model implementations (e.g., discretization, timesteps, and numerical solutions as compared to analytical solutions) may be observed between the results reported in the analysis and/or model report and those calculated by the stand-alone implementation. Knowing these small variations were likely to occur, a screening criterion against which the importance of these variations could be evaluated was established. In many cases, the results calculated from the single realization of the TSPA-LA Model should be exactly equal to those calculated by the stand-alone implementation of the DLL.

7.2.3 Verification of Inputs in Total System Performance Assessment Database

Parameters used in the analyses for the TSPA-LA Model are documented in the TSPA Input Database described in Section 4.7. The TSPA Input Database supports the TSPA-LA Model by providing the parameter values and distributions necessary for performance assessment analysis of the repository. The TSPA Input Database categorizes, stores, and retrieves both fixed and distributed values of the TSPA-LA Model's parameters and allows qualified/authorized analysts to view and update values in the database.

Each TSPA-LA Model simulation accesses the database in order to obtain values for the model's parameters. Parameter values are obtained from the sources listed in Table 4-1 and manually entered into the database. Parameter values are maintained as originally entered. There is no transformation or post-processing of these parameter values. Parameter values are entered into the database using a number of forms. These forms include the Parameter Identification Form (PIF) that serves as the primary means to enter parameters into the TSPA Input Database. The PIF is linked by parameter identification to a Parameter Documentation Form (PDF) that

documents the source of the parameter information. The PDF is linked by value identification to a Parameter Value Entry Form that passes to the TSPA-LA Model the type of information to expect (i.e., distribution type, maximum, minimum, and parameter code). Figure 4-3 shows the structural framework of the database that is described in Section 4.8.

Before using parameter values in the TSPA-LA Model for the performance assessment analysis, each parameter undergoes a check of the PIF to verify that the information has been entered correctly. During development of the TSPA-LA Model, identified inconsistencies in parameter values were documented, revised values were entered into the TSPA-LA Model database, and the calculations affected by the inconsistencies were rerun. The parameter verification is documented on the Parameter Verification Form (Section 4.8). Only users with access to the TSPA-LA Model's controlled access input database can verify parameter values. The verification process includes recording the checker's name along with the date and time to identify the last user who changed any one of the parameter categories using a PIF, a PDF, a Parameter Value Entry Form, or a Parameter Verification Form. Strict control of access and the documentation trail increases the confidence in the security, integrity, and traceability of information entered into, or downloaded from, the TSPA Input Database.

7.2.4 Verification of Single Model Components

The TSPA-LA Model is composed primarily of submodels that are derived from abstraction models documented in various analysis and/or model reports. One technique used to improve confidence in a numerical model is to calibrate or compare model results with known results under a set of controlled conditions. Such confidence building activities may be divided into verification and validation activities. Validation activities test the applicability of the model to simulate an event or a process, and may be described as a process to establish model accuracy. On the other hand, verification activities are designed to establish model precision (i.e., they determine whether the model can calculate results with a satisfactory degree of confidence under a given set of controlled inputs). A discussion of verification activities of various submodels in the TSPA-LA Model is given in the following sections.

The approach used to verify the submodels implemented in the TSPA-LA Model was based on the type of information provided in the supporting analysis and/or model reports. In general, the information from the analysis and/or model reports used in verification of the submodels was in the following form:

- Look-up tables
- Abstraction equations with ranges of input values
- A qualified stand-alone implementation of the abstraction or DLL with a GoldSim-based model file.

When inputs or results used from an analysis and/or model report are in the form of a look-up table, a verification subroutine is implemented in the TSPA-LA Model file that is triggered by a verification switch. After the verification switch is triggered, input values corresponding to the independent variables in the look-up table are fed into the appropriate submodel in the TSPA-LA Model file. The verification switch is set so that the simulation can be run deterministically with no uncertain parameters. The verification results are values that have been retrieved from

look-up tables with appropriate interpolations. Because the results have no built-in uncertain parameters, these values should equal the values presented in the look-up tables or equal the linearly interpolated values exactly. The expected results for a given set of inputs are stored in a TSPA-LA Model file results element. Values that are calculated by the submodel implemented in the TSPA-LA Model file are also stored in a TSPA-LA Model file results element. The expected values and the estimated values in the TSPA-LA Model file are compared to determine the verification outcome.

The same approach is used when the analysis and/or model report presents results in the form of an abstraction equation. The verification subroutine calculates results for a range of input values under which the abstraction equation is valid. Results from the TSPA-LA Model file calculations are compared with values estimated from the equations presented in the analysis and/or model reports. A good match between the expected values and TSPA-LA Model file-calculated values indicates that the abstracted model has been verified. As with the earlier case of model verification using look-up tables, the TSPA-LA Model file calculations are run deterministically with no uncertainty.

In some instances, the feed to the TSPA-LA Model may not be in the form of a table or equation presented in an analysis and/or model report. Such TSPA-LA submodels or components may be receiving inputs from qualified DLLs or may be retrieving information from qualified external databases. Furthermore, under certain circumstances, the TSPA-LA Model may be using a simple equation with no values provided for verification testing in the associated analysis and/or model report. Under these conditions, the verification process involves checking to ensure that the TSPA-LA Model is correctly linked to the TSPA Input Database and the correct values are returned. In addition, checking also verifies that equations were implemented correctly.

Finally, in some instances where an external DLL is used to do calculations or when a simple implementation within a GoldSim-based model is available in the analysis and/or model report, the verification process involves conducting test runs presented in the analysis and/or model report or in DLL software qualification documents. Verification runs in the TSPA-LA Model are set to simulate the runs presented in the validation documentation (i.e., the TSPA-LA Model is run with the same set of inputs as those presented in the DLL validation). Outputs of the TSPA-LA Model are compared to results presented in the DLL validation.

As discussed earlier, the approach to verification is to compare TSPA-LA Model file results with results of stand-alone implementations reported in analysis and/or model reports or validation test reports, where applicable. Therefore, the input values for a validation run are taken from a validation test report or analysis and/or model report and used in the TSPA-LA Model. In some instances, the input values may be truncated for ease of reporting in a table. As an illustration, a value of 2.61364 may be truncated to 2.61. Therefore, in a verification realization, an error is introduced with the use of a truncated input value. Consequently, a small difference occurs between expected and calculated results. In some submodels, where the calculated values are strongly dependent upon inputs, such as the solubility submodels, the error can be potentially higher depending upon the input values used. In some cases, the supporting analysis and/or model report utilizes a separate GoldSim-based model file. A comparison is made whereby the separate model file is run deterministically for a set of inputs described in the analysis and/or

model report. Then, the TSPA-LA Model is run with the same set of inputs, and the results of the two runs are compared.

7.2.4.1 Verification Results

The variety of methods by which the various submodel abstractions were implemented within the TSPA-LA Model yielded some implementations that were of limited modeling complexity and thus were considered verified by checking activities conducted during the model development phase. Examples of these types of submodel abstractions would include the Infiltration Submodel, the Climate Submodel, the Radionuclide Inventory Submodel, and the Human Intrusion Submodel. For the Infiltration Submodel, the selection of the infiltration percentage was a simple probability selection. For the Climate Submodel, the change in the climate scenario was a function of time. The Radionuclide Inventory Submodel was verified by ensuring that the inventory elements in the TSPA-LA Model file were correctly linked to the database. The Human Intrusion Submodel included defined parameters and simple model implementation. Therefore, a verification description for each submodel listed in Table 6-1 is not presented.

Results for the submodel verifications that were conducted for the TSPA-LA Model are presented in the following sections. All submodel verifications were performed using GoldSim V9.60.100 [DIRS 181903]. The supporting documentation, which consists of electronic versions of the TSPA-LA Model output files and results, is provided in the supporting material (output DTN: MO0708TSPAPOST.000 [DIRS 182986]). The submodel verifications were performed during the TSPA-LA Model development for those submodels that were no longer subject to development changes. As a result, the verification simulations were, in many cases, performed with earlier versions of the TSPA-LA Model that are labeled by specific version numbers found in the relevant records package. A brief description of the analyses described below is presented in Table 7.2-2 along with the status of the verification and identification of the section that contains the discussion of the verification.

7.2.4.1.1 Drift Seepage

The Drift Seepage Submodel, as implemented in the TSPA-LA Model, is defined in *Abstraction of Drift Seepage* (SNL 2007 [DIRS 181244]). The verification of the Drift Seepage Submodel was conducted to ensure the proper implementation of the submodel within the TSPA-LA Model (v5.000) via the SEEPAGEDLL_LA V.1.3 [DIRS 181058] DLL. The verification focused on the flow of information into and the results out of the SEEPAGEDLL_LA DLL.

A stand-alone GoldSim-based model file that contained the implementation of the SEEPAGEDLL_LA validation test case TC-24 (*User Information Document for: SEEPAGEDLL_LA V1.3* (DOE 2006 [DIRS 181133])) was selected for use in the verification of the TSPA-LA Model implementation. This test case is identified as the stand-alone model file.

The verification process was initiated by running a single realization of the TSPA-LA Model (v5.000) and saving the values of the SEEPAGEDLL_LA input parameters. This input parameter set was then fed into the parameter elements of the stand-alone TC-24 implementation to develop a set of verification results. Table 7.2-3 lists the results from the outputs generated by

the SEEPAGEDLL_LA for both the TSPA-LA Model and the stand-alone model. The verification results shown in Table 7.2-3 are identical for the TSPA-LA Model single realization and the stand-alone model. Therefore, the implementation of the Drift Seepage Submodel, including the seepage DLL, is considered verified (output DTN: MO0708TSPAPOST.000 [DIRS 182986]).

7.2.4.1.2 Drift Wall Condensation Submodel Verification

The Drift Wall Condensation Submodel and Abstraction (Table 6-1) is defined in *In-Drift Natural Convection and Condensation* (SNL 2007 [DIRS 181648], Sections 8.3 and 8.0[a]). The abstraction calculates a probability of condensation occurrence on the drift walls at a WP location. If condensation occurs, its rate is calculated.

The implementation of the Drift Wall Condensation Submodel was verified using version 4.042 of the TSPA-LA Model. The model was modified to verify the implementation of the Drift Wall Condensation Submodel by comparing the simulated model results to a set of drift-wall condensation rates independently calculated in a Microsoft Excel spreadsheet. The Excel spreadsheet calculations were based on *In-Drift Natural Convection and Condensation* (SNL 2007 [DIRS 181648], Sections 8.3 and 8.0[a]). A set of known inputs were defined for both the TSPA-LA Model (v4.042) and the Excel spreadsheet (output DTN: MO0708TSPAPOST.000 [DIRS 182986]). Then simulation and calculated condensation rates were compared to verify the implementation of the abstraction in the TSPA-LA Model (output DTN: MO0708TSPAPOST.000 [DIRS 182986]).

The abstraction is implemented such that the independent variables of time, percolation rate, invert transport condition (high or low), dispersivity condition (high or low) for axial transport, and the ventilation condition of the DS (ventilated or unventilated) are sampled. Then, based on a set of correlation tables using these independent variables, the correlation of the fraction of locations where condensation occurs (probability) is determined. If the probability is such that condensation will occur, then another set of correlation tables is utilized to determine the actual condensation rate. For the verification task, the values for the independent variables were specified at each timestep for a simulation time of 3,000 years. The timestep length was set equal to 75 years, yielding a total of 40 parameter sets. The specified simulation duration of 3,000 years was due to no condensation occurring after a simulation time of 3,000 years as defined in the abstraction.

Table 7.2-4 shows the comparison of the drift-wall condensation rates simulated by the TSPA-LA Model (v4.042) and calculated by the Excel spreadsheet (output DTN: MO0708TSPAPOST.000 [DIRS 182986]). The percent differences in the condensation rates indicate that the values are identical and thus the implementation of the Drift Wall Condensation Submodel and Abstraction in the TSPA-LA Model is considered verified.

7.2.4.1.3 Engineered Barrier System Chemical Environment

Verification of the Engineered Barrier System (EBS) Chemical Environment Submodel (Table 6-1) was conducted in a version of the TSPA-LA Model that was modified to allow the use of a controlled set of input parameters. The goal of the verification process was to determine

the ability of the TSPA-LA Model file to satisfactorily estimate, under both evaporative and condensation conditions, the Pco_2, pH, and ionic strength for a set of controlled inputs. Verification consists of comparing expected Pco_2, pH, and ionic strength values against those calculated by the TSPA-LA Model file. The implementation of the EBS Chemical Environment Submodel is defined in *Engineered Barrier System: Physical and Chemical Environment* (SNL 2007 [DIRS 177412], Section 6.15.1).

The verification of the Pco_2 calculation was conducted separately from the pH and ionic strength calculations. The implementation of the Pco_2 calculation within the TSPA-LA Model was based on determining the bounding values for a range in Pco_2 from look-up tables as a function of seepage water type, water-rock interaction parameter, temperature, and relative humidity. Next a Pco_2 uncertainty parameter was sampled that defined the relative location of a single Pco_2 value within the determined range. The verification process developed a set of known input parameter combinations. This input set was used to calculate the Pco_2 values in the TSPA-LA Model (v4.043) and in an independent calculation within a Microsoft Excel worksheet (output DTN: MO0708TSPAPOST.000 [DIRS 182986]). A single realization of the TSPA-LA Model (v4.043) was simulated with a different set of input parameter values at each timestep, with a total of 44 input parameter combinations. Table 7.2-5 lists the values of the water-rock interaction parameter, temperature, and relative humidity input parameters and the calculated Pco_2 values. The calculation was conducted for seepage water type number 2, which was randomly chosen from the three seepage water types. The values presented in Table 7.2-5 indicate that the calculated Pco_2 values are essentially the same. Therefore, the implementation of the EBS Chemical Environment Submodel Pco_2 determination process in the TSPA-LA Model is considered verified.

The verification of the pH and ionic strength implementation within the TSPA-LA Model was conducted in a similar manner as the Pco_2 verification. The pH and ionic strength is obtained from a series of look-up tables as a function of seepage water type, Pco_2, temperature, and relative humidity at the WP surface, and the water-rock interaction parameter. A total of 396 combinations of constant-value input parameters were specified and the pH and ionic strength values calculated for each input set. Table 7.2-6 lists the range of the input parameters used in developing the input sets. A comparison of the pH and ionic strength values calculated in the TSPA-LA Model (v4.043) and in an independent Microsoft Excel worksheet (output DTN: MO0708TSPAPOST.000 [DIRS 182986]) were used for the verification. Figures 7.2-1 and 7.2-2 present the comparison plots for the pH and ionic strength values, respectively, calculated for each of the 396 input sets. An examination of the data indicates that the difference in the pH and ionic strength values between the two calculation methods is essentially zero. Therefore, the implementation of the pH and ionic strength calculation in the EBS Chemical Environment Submodel within the TSPA-LA Model is considered verified.

7.2.4.1.4 Waste Package and Drip Shield Degradation

An integrated WP and DS Degradation Submodel is implemented in the TSPA-LA Model and contains a set of external DLLs that operate in series. The DLLs are WAPDEG V 4.07 [DIRS 181064]; CWD V2.0 [DIRS 181037]; and SCCD V2.01 [DIRS 181054].

The verification process uses a previously defined stand-alone GoldSim-based model test case, documented in *WAPDEG Analysis of Waste Package and Drip Shield Degradation* (BSC 2004 [DIRS 169996], Section 7.1 and Appendix I), as the basis for comparison to the implementation within the TSPA-LA Model (v4.042). The original stand-alone model files are located in DTN: MO0310MWDWAPAN.002_R0 [DIRS 165800]. The stand-alone model configuration was updated in the current version of the GoldSim software (v9.60) for direct comparison to the TSPA-LA Model (v5.000) results (output DTN: MO0708TSPAPOST.000 [DIRS 182986]).

An identical set of constant input parameter values were specified for the stochastic parameters in both the stand-alone model file and the TSPA-LA Model (v5.000) (Table 7.2-7). Examination of the Failure_Opening output table values verify that the DS and WP breaches occur in the correct time bins consistent with the input (i.e., supplied general corrosion rates and microbially influenced corrosion factor) and that stress corrosion cracking (SCC) is taking place. Figure 7.2-3 presents a comparison of results for two parameters from the Failure_Opening output tables. These are the average number of patch failures and average number of crack failures on the side of a failed waste package. The results from the output table which are not presented in Figure 7.2-3 are identical for both cases. The comparison verifies implementation of the WP and DS Degradation Submodel in the TSPA-LA Model.

7.2.4.1.5 Waste Form Degradation and Mobilization

Verification of the Waste Form Degradation and Mobilization submodels (Table 6-1) involved testing of the rind volume and rind mass calculations for the co-disposed waste packages (CDSP WPs) and commercial spent nuclear fuel (CSNF) WPs, the waste form degradation calculations for the CSNF, the in-package chemistry, and the dissolved concentration limits. The following discusses the results of the Waste Form Degradation Submodel verifications (Table 6-1).

CSNF Rind Volume and Mass—The ability of the Waste Form Degradation and Mobilization Submodels (Table 6-1) to satisfactorily estimate the volume and mass of the CSNF WP rind was verified for the TSPA-LA Model. Inputs for verification were taken from values given in *Cladding Degradation Summary for LA* (SNL 2007 [DIRS 180616], Table 6-3). The values of rind porosity, fraction of failed rods, and the fraction of total WP inventory that was corroded were varied over a range of values for a total of 12 input sets. The degradation values to be used in the TSPA-LA Model are given in *Cladding Degradation Summary for LA* (SNL 2007 [DIRS 180616], Table 7-1) and were used to calculate the rind volume and mass in a CSNF WP using the parameters and equations in *Cladding Degradation Summary for LA* (SNL 2007 [DIRS 180616], Tables 6-3 and 6-4, Equations 6-3, 6-4, 6-5, and 6-12). The estimated values of the CSNF WP rind volume and mass were calculated using a Microsoft Excel spreadsheet (output DTN: MO0708TSPAPOST.000 [DIRS 182986]). Modification of the TSPA-LA Model (v4.041) was made to allow for the use of the same input values as in the spreadsheet calculations. Details of the verification module implementation are given in the supporting information (output DTN: MO0708TSPAPOST.000 [DIRS 182986]). The results of the rind volume and mass calculations from the TSPA-LA Model (v4.041) were compared against those calculated in the spreadsheet (Table 7.2-8). The percent difference between the calculation methods was found to be essentially zero. Therefore, the ability of the submodel implementation

within the TSPA-LA Model to estimate the rind volume and mass in the failed CSNF WPs has been verified.

CDSP Rind Volume and Mass—The ability of the Waste Form Degradation and Mobilization Submodels (Table 6-1) to satisfactorily estimate the HLW rind volume and mass in the CDSP WPs was verified for the TSPA-LA Model. In addition, the ability to estimate HLW rind thickness was also verified.

A Microsoft Excel spreadsheet was used to calculate the HLW rind properties using the equations given in *Defense HLW Glass Degradation Model* (BSC 2004 [DIRS 169988], Section 8.1). Input parameters, such as the initial radius and length of the glass log, were also obtained from *Defense HLW Glass Degradation Model* (BSC 2004 [DIRS 169988], Section 8.1). The fraction of the waste form degraded varied between 0.01 and 0.99, resulting in a total of 12 separate verification calculations.

The details of the verification module implementation in v4.041 of the TSPA-LA Model are given in the supporting document (output DTN: MO0708TSPAPOST.000 [DIRS 182986]). The main input change to the model was the specification of the 12 values of the fraction of waste form degraded. A single realization of the TSPA-LA Model (v4.041) was simulated with these input changes. The values of the HLW rind thickness, volume, and mass estimated in the Microsoft Excel spreadsheet (output DTN: MO0708TSPAPOST.000 [DIRS 182986]) were compared to the TSPA-LA Model file-estimated values (Table 7.2-9). The percent difference in the values was found to be essentially zero. Therefore, the ability of the submodel implementation within the TSPA-LA Model to estimate the HLW rind thickness, volume, and mass in the failed CDSP WPs has been verified.

CSNF Waste Form Degradation—The ability of the CSNF Waste Form Degradation Abstraction (Table 6-1) to satisfactorily estimate the waste form degradation rate was verified for the TSPA-LA Model. The variables controlling the waste form degradation rate under acidic and alkaline conditions are pH, temperature, pO_2, and pCO_3, as defined in *CSNF Waste Form Degradation*: *Summary Abstraction* (BSC 2004 [DIRS 169987], Sections 6.4.1.3 and 6.4.1.2). A Microsoft Excel spreadsheet was used to calculate values of the waste form degradation rate under both acidic and alkaline conditions (output DTN: MO0708TSPAPOST.000 [DIRS 182986). The Microsoft Excel-calculated values of the logarithm of the waste form degradation rate were compared with values estimated by implementation of the CSNF Waste Form Degradation Abstraction in the TSPA-LA Model (v4.041).

The results of the verification under both acidic and alkaline conditions are summarized in Table 7.2-10. These results indicate that the ability of the CSNF Waste Form Degradation Abstraction (Table 6-1) to calculate the waste form degradation rates under both acidic and alkaline conditions with a satisfactory degree of confidence (maximum percent difference of less than 0.1 percent).

HLW Glass Degradation—The ability of the HLW Glass Degradation Abstraction (Table 6-1) to satisfactorily estimate the waste form degradation rate was verified for the TSPA-LA Model. The variables controlling the HLW glass degradation rate are pH, temperature, and relative humidity, as defined in *Defense HLW Glass Degradation Model* (BSC 2004 [DIRS 169988],

Section 6.7). Microsoft Excel was used to calculate verification values of the glass degradation rate under both acidic and alkaline conditions (output DTN: MO0708TSPAPOST.000 [DIRS 182986]). The glass degradation rates were calculated for relative humidity conditions less than and greater than 0.44 even though *Defense HLW Glass Degradation Model* (BSC 2004 [DIRS 169988], Section 6.7) stipulates that no glass degradation occurs if relative humidity is less than 0.44. The Microsoft Excel-calculated verification values of the glass degradation rate were compared with values estimated by the implementation of the HLW Glass Degradation Abstraction in the TSPA-LA Model (v4.041) as shown in Table 7.2-11. The comparison indicates that the percent difference is essentially zero and that this verifies the ability of the HLW Glass Degradation Abstraction to satisfactorily calculate glass degradation rates under both acidic and alkaline conditions.

In-Package Chemistry—The ability of the In-Package Chemistry Submodel and Abstraction (Table 6-1), implemented in the TSPA-LA Model, to satisfactorily estimate values of pH, ionic strength, and total carbonate was verified. The submodel and abstraction are defined in *In-Package Chemistry Abstraction* (SNL 2007 [DIRS 180506]). The goal of verification was to determine the ability of the TSPA-LA Model file to satisfactorily estimate ionic strength, pH, and total carbonate values inside the WP based on a set of known inputs. The main inputs included temperature, relative humidity, Pco_2, seepage flow rate, and bin number. Verification consisted of comparing the values of pH and ionic strength calculated from the TSPA-LA Model to those calculated independently in a Microsoft Excel spreadsheet (output DTN: MO0708TSPAPOST.000 [DIRS 182986]).

The implementation within the TSPA-LA Model calculated the ionic strength and pH parameters under two seepage conditions and the total carbonate parameter. A series of look-up tables that define these parameters, based on a set of known inputs, are presented in DTN: SN0702PAIPC1CA.001_R2 [DIRS 180451] along with the steps required to implement the abstraction. Each parameter was calculated for the TSPA-LA Model cells that represent the CSNF WP, the HLW canister portion of the CDSP WP, and the multi canister over pack canister portion of the CDSP WP.

The ionic strength is determined inside a WP only if the relative humidity is greater than or equal to 95 percent. If the relative humidity is greater than or equal to 95 percent, the ionic strength is then determined from a series of look-up tables based on the seepage condition. If the seepage flow rate at the location of the WP is less than or equal to 0.1 L/yr, then the vapor influx abstraction tables are used, else the liquid influx abstraction tables are used (DTN: SN0702PAIPC1CA.001_R2 [DIRS 180451]). Once the appropriate table has been selected, the ionic strength value is determined for the liquid influx case as a function of seepage flow rate and time since the WP failure, or for the vapor influx case as a function of relative humidity. The implementation of the ionic strength calculation within the TSPA-LA Model (v4.043) was verified against an independent calculation in a Microsoft Excel spreadsheet (output DTN: MO0708TSPAPOST.000 [DIRS 182986]). The calculation developed in the spreadsheet was based on the identical abstraction and look-up tables as presented in DTN: SN0702PAIPC1CA.001_R2 [DIRS 180451].

Table 7.2-12 presents the range of values for the defined input parameters of time since WP failure and seepage flow rate, along with a random stochastic parameter used in incorporating

uncertainty into the final ionic strength value (Section 6.3.7). Figure 7.2-4 presents a comparison plot of the TSPA-LA Model (v4.043), and calculated verification ionic strength values for both the non-seeping and seeping cases. The percent differences between the two sets of calculations were essentially zero.

The pH is determined inside the CSNF and DHLW WPs for relative humidity values less than 95 percent. The CSNF pH is uniformly sampled between 6 and 7. The DHLW pH is set to 10. The implementation of these two pH calculations was not verified in this section. For relative humidity values greater than or equal to 95 percent, the pH is determined as function of the ionic strength and the Pco_2 using a series of look-up tables (DTN: SN0702PAIPC1CA.001_R2 [DIRS 180451]). The ionic strength selected is based on either the vapor influx or liquid influx conditions as defined previously. If the liquid influx case is determined, then the minimum of the liquid influx or the vapor influx ionic strength is selected. If the vapor influx case is determined, then the ionic strength is based on the vapor influx. The implementation of the pH calculation within the TSPA-LA Model (v4.043) was verified against an independent calculation in a Microsoft Excel spreadsheet (output DTN: MO0708TSPAPOST.000 [DIRS 182986]). The calculation developed in the spreadsheet was based on the identical abstraction and look-up tables as presented in DTN: SN0702PAIPC1CA.001_R2 [DIRS 180451]. Table 7.2-12 presents the range of values for the constant input parameters of ionic strength and Pco_2, along with a random stochastic parameter used in incorporating uncertainty into the pH calculation (Section 6.3.7). Figure 7.2-5 presents a comparison plot of the TSPA-LA Model (v4.043), and Excel calculated verification pH values for both the non-seeping and seeping cases. The percent differences between the two sets of calculations were essentially zero.

The total carbonate is determined as function of the Pco_2, pH, and temperature using an equation. The equation along with a set of calculated total carbonate values is given in DTN: SN0702PAIPC1CA.001_R2 [DIRS 180451]. These calculated values were used as the verification calculations with which the TSPA-LA Model (v4.043) was verified against (output DTN: MO0708TSPAPOST.000 [DIRS 182986]). Table 7.2-12 presents the range of values for the constant input parameters of P_{CO2}, pH, and temperature. Figure 7.2-6 presents a comparison plot of the TSPA-LA Model (v4.043) and DTN calculated total carbonate values. The percent differences between the two sets of calculations were essentially zero.

Based on these verification results, the In-Package Chemistry Submodel and Abstraction implementation within the TSPA-LA Model is considered verified.

Dissolved Concentration Limits: Nominal Scenario—Verification of the Dissolved Concentration Limits Submodel (Table 6-1), as implemented within the TSPA-LA Model based on *Dissolved Concentration Limits of Elements with Radioactive Isotopes* (SNL 2007 [DIRS 177418]), was divided into two segments. This section discusses that solubility of americium, neptunium, protactinium, plutonium, tin, thorium, and uranium were verified for the Nominal Scenario Class Modeling Case. The solubility model for uranium was independently verified for the Igneous Scenario Class (Igneous Intrusion Modeling Case only), as described below.

Modeling of dissolved concentration limits (also referred to as solubility limits) of elements with radioactive isotopes has been implemented within the TSPA-LA Model. These dissolved

concentration limits calculations are needed to determine radionuclide solubilities–an important component in calculating releases from the EBS. Three key parameters to the calculation of the dissolved concentration limits are pH, ionic strength, and the Pco_2. Values for these parameters are calculated elsewhere within the TSPA-LA Model but for this verification, a set of parameter ranges was defined. The ranges were a pH of 5.5 to 10.5, an ionic strength of 0.1 to 10 mol/kg, and a Pco_2 of 1×10^{-5} to 1×10^{-1} bars. Using the defined parameter ranges, a total of 471 data input sets were developed to use in the calculation of the dissolved concentration limits. With these data sets, a single realization of the TSPA-LA Model (v5.000) was conducted. The dissolved concentration limits results for americium, neptunium, protactinium, plutonium, tin, thorium, and uranium were extracted from this model simulation.

An independent calculation of the expected dissolved concentration limits was developed within a Microsoft Excel spreadsheet for use as verification data to the TSPA-LA Model results. This calculation was based on the methods provided by three DTNs and the *Dissolved Concentration Limits of Elements with Radioactive Isotopes* (SNL 2007 [DIRS 177418]). The three DTNs were MO0702PADISCON.001_R0 [DIRS 179358], MO0702PAFLUORI.000_R1 [DIRS 181219], and MO0704PASOLCAP.000_R0 [DIRS 180389]. The input parameters utilized in the verification calculation included the same parameter ranges for pH, ionic strength, and Pco_2. In addition, the epistemic sampled parameter values from the TSPA-LA Model single realization run were exported and utilized in the verification calculation.

The calculation of the dissolved concentration limits values by the TSPA-LA Model and the verification calculation for americium, neptunium, and uranium are presented on Figure 7.2-7. The remaining four elements were not presented on the figure for easier viewing of the comparison results. However, the percent differences between the stand-alone and the TSPA-LA Model calculations for all seven elements for each of the input parameter sets were essentially zero. Based on these results, the Dissolved Concentration Limits Submodel is considered to be verified as implemented within the TSPA-LA Model. The results of this verification are presented in output DTN: MO0708TSPAPOST.000 [DIRS 182986].

Dissolved Concentration Limits: Uranium in the Igneous Scenario—The calculation of uranium-dissolved concentration limits in the Igneous Intrusion Modeling Case for the Igneous Scenario Class, were performed using the same approach as presented above. The difference to the modeling approaches was not extensive and mainly required the sampling of variables from a larger number of tables, based on the calculated conditions.

These various tables provide for solubility control of uranium by three solids, whereas the solubilities of all other radionuclides were controlled by only one or two solids. The three solids controlling uranium solubilities are schoepite ($UO_3{\cdot}2H_2O$), Na-boltwoodite ($NaUO_2SiO_3OH{\cdot}1.5H_2O$), and the solid $Na_4UO_2(CO_3)_3$, as described within *Dissolved Concentration Limits of Elements with Radioactive Isotopes* (SNL 2007 [DIRS 177418]). Based on the variables and the conditions, values were either sampled from one table or interpolated between multiple tables.

The same approach to verification used for the other dissolved concentration limits calculations was used for verifying uranium in the Igneous Intrusion Modeling Case. The independent verification calculations were modified appropriately. The initial verification of the TSPA-LA

Model (v5.000) failed. The cause of the failure was found to be two TSPA-LA Model file elements being linked to incorrect tables. When the CSNF WPs were subjected to high ionic strength (greater than 3 mol/kg) and solubilities were controlled by the schoepite mineral phase, the model read the incorrect look-up tables for low ionic strength conditions, using Na-boltwoodite-controlled solubilities. The discrepancy was documented in the TSPA-LA Model file, and it's impact was assessed as described in Appendix P. The incorrect element links were corrected in the TSPA-LA Model (v5.000) for verification purposes only, and the verification analysis was conducted again. Using the revised values, the model results were within the acceptable verification range. The results of the updated verification are provided on Figure 7.2-8. The verification calculations are described in greater detail in the output DTN: MO0708TSPAPOST.000 [DIRS 182986]. Based on the results of this verification analysis, the dissolved concentration limits calculations for uranium in the Igneous Intrusion Modeling Case are considered to be not verified due to the noted incorrect element linkages. However, when these linkages are corrected, the verification results show that the remainder of the dissolved concentration limits calculations for uranium in the Igneous Intrusion Modeling Case, are properly implemented within the TSPA-LA compliance model.

7.2.4.1.6 Engineered Barrier System Transport

The EBS Flow Submodel and the EBS Transport Submodel are defined in *EBS Radionuclide Transport Abstraction* (SNL 2007 [DIRS 177407]). This section describes the verification of both the EBS Flow Submodel and the EBS Transport Submodel as implemented in the TSPA-LA Model.

The EBS Flow Submodel, as described in *EBS Radionuclide Transport Abstraction* (SNL 2007 [DIRS 177407]) and in Section 6.3.6 of this document, does not directly calculate the flow of water through the various components of the EBS (i.e., DS, WP, invert) but takes flow rates from the Drift Seepage and Drift Wall Condensation Submodels as inputs and applies a series of conditional statements to determine the amount and rate of water available for transport within and out of the EBS. Based on this method by which the EBS Flow Submodel was implemented within the TSPA-LA Model, it was considered that the checking conducted during the model development process, and documented in the relevant records package was sufficient for verification purposes.

The implementation of the EBS Transport Submodel within the TSPA-LA Model (v4.042) was verified by comparing the results of dissolved radionuclide transport and colloid-facilitated radionuclide transport within the EBS from the TSPA-LA Model and a finite-difference approximation of the governing mass balance equations implemented in a Microsoft Excel spreadsheet (*Transport_Calc_Appendix_B.xls* in output DTN: SN0703PAEBSRTA.001_R3 [DIRS 183217]). The mass balance equations describe the transport of radionuclides (^{239}Pu) and associated colloids with irreversible sorption onto iron oxyhydroxide colloids and the stationary corrosion products, as well as reversible sorption onto both waste form and groundwater colloids within the WP.

Two verification cases were conducted. The first includes both advective and diffusive transport and the second includes only diffusive transport. The input parameter values for both the TSPA-LA Model and the Excel spreadsheet implementation were set to the same values,

including a specified constant flow rate. Figure 7.2-9 is a comparison of the results for the case that includes both advection and diffusion. This case shows good agreement between the TSPA-LA Model (v4.042) results and those based on the finite-difference approximation of the sample calculation, except for the initial timesteps where the difference is approximately 10 percent based on examination of the numerical values. The comparison for the case with only diffusive transport is shown on Figure 7.2-10. This case shows good agreement for the dissolved ^{239}Pu and ^{239}Pu reversibly sorbed onto groundwater and waste form colloids as well as for the ^{239}Pu irreversibly sorbed onto the stationary corrosion products, with some slight deviation for the initial timesteps. The agreement is not as good for ^{239}Pu irreversibly sorbed to the FeOH colloids. In this case, the differences at the initial timesteps between the TSPA-LA Model (v4.042) results and those based on the finite-difference approximation range from 50 to 100 percent based on examination of the numerical values. The differences decrease rapidly with time and by the time the system reaches a steady state there is only a two percent difference in value. Given the different solution methods used in the TSPA-LA Model and in the Excel spreadsheet calculations, some differences in the simulation results were expected. If identical solution techniques with identical timesteps were used in the comparison, then the expectation would be that the results should be identical and thus would be held to a more stringent degree of comparison. Therefore, the agreement is still considered good and contributes to increasing the level of confidence in the model. The implementation of the EBS Transport Submodel in the TSPA-LA Model can be considered verified.

7.2.4.1.7 Unsaturated Zone Transport

The verification of the UZ Transport Submodel (Table 6-1), as implemented within the TSPA-LA Model, was conducted by verifying that the implementation of the FEHM_V2.24-01 DLL (STN: 10086-2.24-01 [DIRS 179419]) provided the expected results based on a set of known inputs. The implementation of the UZ Transport Submodel within the TSPA-LA Model was verified against a stand-alone test-case model developed with the glacial-transition climate with the 10th percentile flow field with the water table raised to 850 meters above mean sea level. The stand-alone test case was derived from the base-case UZ Transport model that utilized the FEHM (FEHM V2.24-01 [DIRS 179419]) numerical model as defined in *Particle Tracking Model and Abstraction of Transport Processes* (SNL 2008 [DIRS 184748]).

The verification activities simulated the decay chain of ^{241}Am→^{237}Np→^{233}U→^{229}Th in both the stand-alone model and in the TSPA-LA Model (v5.000). The source term consisted of prescribing 1.0 g/yr of ^{241}Am to the inflow connection for the UZ fractures. With ^{241}Am as the only source, the other radionuclides in the decay chain were produced only by in-growth. The files associated with both the stand-alone test case and the TSPA-LA Model (v5.000) are contained in output DTN: MO0708TSPAPOST.000 [DIRS 182986].

A comparison plot showing the mass breakthrough of ^{237}Np and ^{233}U at the base of the UZ is presented on Figure 7.2-11. The mass breakthrough for ^{229}Th was essentially zero so it was not included in Figure 7.2-11. The plot shows excellent agreement for the ^{237}Np mass breakthrough between the stand-alone model and the TSPA-LA Model (v5.000). For ^{233}U, both curves show oscillations in the breakthrough curves with a slight shift in the oscillations during the middle of the simulation timeframe. This shift is due to a different number of particles being tracked between the two FEHM simulations and thus differences in randomly generated seed numbers.

However, the overall match between the two simulation cases is considered valid. Therefore, the implementation of the UZ Transport Submodel within the TSPA-LA Model is considered verified.

7.2.4.1.8 Saturated Zone Flow and Transport

The SZ Flow and Transport Model, as implemented in the TSPA-LA Model, is defined in *Saturated Zone Flow and Transport Model Abstraction* (SNL 2008 [DIRS 183750]). Verification of the SZ Flow and Transport Submodel was conducted by verifying the implementations of both the 1-D and the 3-D SZ Flow and Transport Abstractions within the TSPA-LA Model.

The implementation of the 3-D SZ Flow and Transport Abstraction, including the SZ_Convolute V3.1 DLL (STN: 10207-3.10.01-00 [DIRS 181060]), in the TSPA-LA Model (v4.042) was verified. The result from a base-case transport simulation developed in *Site-Scale Saturated Zone Transport* (SNL 2007 [DIRS 177392]; DTN: LA0306SK831231.001_R0 [DIRS 164362]) was utilized for comparison to the TSPA-LA Model (v4.042) results. The input parameters that defined the realization 1 for the base-case transport simulation (DTN: LA0306SK831231.001_R0 [DIRS 164362]) were also implemented into the TSPA-LA Model (v4.042) with some modifications, as defined in the output DTN: MO0708TSPAPOST.000 [DIRS 182986]. The SZ source term was defined by assigning a unit mass flux (1.0 g/yr) for a sorbing radionuclide (^{237}Np) that includes radioactive decay (output DTN: MO0708TSPAPOST.000 [DIRS 182986). This source term was assigned to the UZ Transport Submodel output element that feeds mass out of the UZ and into the SZ at Source Region 1. The mass input into this region was then input into the SZ_Convolute DLL in the TSPA-LA Model (v4.042). The ^{237}Np mass flux output from the SZ_Convolute DLL was passed into the model elements, which sums all mass flux out of the 3-D SZ Transport Submodel. The results of the TSPA-LA Model (v4.042) simulation were then compared to the single-realization transport median case breakthrough curve provided by the SZ Site-Scale Transport Model (DTN: LA0306SK831231.001_R0 [DIRS 164362]). The mass fluxes from the two simulations are plotted on Figure 7.2-12 and indicate good overall agreement. There is a slight deviation at early times due to an increase in the timestep size for the TSPA-LA Model.

It should be noted that when the modifications to the TSPA-LA Model were conducted for the verification activities, a documented test case simulation which utilized the updated 3-D SZ Flow and Transport breakthrough curves within the SZ_Convolute DLL had not been developed and thus an older set of breakthrough curve files were utilized. The purpose of the verification activities was to ensure that the 3-D SZ Flow and Transport Abstraction had been implemented correctly and that the flow of information into and out of the submodel was correct. Therefore, the use of the older external breakthrough curve files is justified as long as the correct inputs are implemented and the flow of information through the submodel yields the expected results.

The 1-D SZ Flow and Transport Abstraction, as defined in *Saturated Zone Flow and Transport Model Abstraction* (SNL 2008 [DIRS 183750]), consists of a one-dimensional pathway model that is used to simulate the transport of daughter products through the SZ. The 1-D SZ Flow and Transport Abstraction was developed as a separate stand-alone GoldSim-based model file which was qualified prior to implementation within the TSPA-LA Model

(DTN: SN0702PASZFTMA.002_R1 [DIRS 183471]). The transport results from this stand-alone model were used as the verification data for comparison to the implementation of the 1-D SZ Flow and Transport Abstraction within the TSPA-LA Model. The verification of the abstraction in the TSPA-LA Model (v4.042) was performed by taking the fixed input parameters as defined in the stand-alone model and implementing them in the TSPA-LA Model. In addition, a unit mass flux (1.0 g/yr) was assigned for each radionuclide as cumulative input into each of the four SZ source zone regions, resulting in a total source mass flux of 4.0 g/yr. The calculated total SZ mass flux outflows for ^{14}C and ^{237}Np are shown on Figure 7.2-13 for both the stand-alone and the TSPA-LA Model. The curves indicate good agreement between the two model simulations.

The verification results for the implementation of both the 1-D SZ Flow and Transport Abstraction and the 3-D SZ Flow and Transport Abstraction indicate that both are considered verified and thus the overall implementation of the SZ Flow and Transport Model Component is verified. The verification of the 3-D SZ Flow and Transport Abstraction also demonstrates proper implementation of the UZ-SZ interface.

7.2.4.1.9 Biosphere

Verification of the Biosphere Model Component involved checking of the groundwater exposure case of the Biosphere Submodel (Table 6-1) in the TSPA-LA Model (v4.041). The main parameters controlling the annual dose calculation are the climate state, biosphere dose conversion factors (BDCF), and the concentration of the radionuclides from the SZ. A single realization of the TSPA-LA Model (v4.041) was simulated to calculate the SZ radionuclide concentrations and the corresponding annual dose. The SZ radionuclide concentrations were subsequently exported to provide for an independent calculation of the annual dose for verification purposes.

BDCFs based on three climate states (Present-Day, Monsoon, and Glacial Transition) were developed and documented in *Biosphere Model Report* (SNL 2007 [DIRS 177399], Section 6.4.10.4). The capabilities to utilize the BDCFs for multiple climates states were incorporated into the TSPA-LA Model. However, the TSPA-LA Model, currently only utilizes the Present-Day BDCFs, as discussed in Section 6.3.11.

The verification simulation of the TSPA-LA Model tested the groundwater source term to annual dose. The BDCF values, per radionuclide and climate state, were taken from data tables provided in DTN: MO0702PAGBDCFS.001_R0 [DIRS 179327]. The SZ radionuclide concentrations exported from the TSPA-LA Model (v4.041) (output DTN: MO0708TSPAPOST.000 [DIRS 182986]) were used along with the BDCFs as inputs to independently calculate the annual dose, as defined in the *Biosphere Model Report* (SNL 2007 [DIRS 177399], Section 6.4.10.4). The independent annual dose calculations were developed using a Microsoft Excel spreadsheet (output DTN: MO0708TSPAPOST.000 [DIRS 182986]).

The annual dose calculated by the TSPA-LA Model (v4.041) model file was compared to that calculated using Microsoft Excel (output DTN: MO0708TSPAPOST.000) [DIRS 182986]. This comparison is shown on Figure 7.2-14 along with the percent difference in the two calculations. The maximum percent difference between the calculated annual doses is approximately 0.043

percent with the differences in the dose calculations likely due to round-off in the calculation of the specific activities for each radionuclide. The verification results indicate a good match and thus the groundwater source term to dose submodel is considered verified. Similar verification results would be expected if the present-day BDCF's were used for the entire simulation duration, as is used in the current TSPA-LA Model.

7.2.4.1.10 Igneous Scenario Class Modeling Cases

Verification of the Igneous Scenario Class Modeling Cases includes verification of the ASHPLUME_DLL_LA V2.1 (STN: 11117-2.1-01 [DIRS 180147]) and the FAR V1.2 DLL (STN: 11190-1.2-00 [DIRS 182225]) for the Volcanic Eruption Modeling Case. In addition, the impact on the physical-chemical environment of the EBS, and the input parameters controlling the probability of an igneous intrusion event, are analyzed for the Igneous Intrusion Modeling Case.

Volcanic Eruption Modeling Case (ASHPLUME)—The ability of the Volcanic Eruption Modeling Case to estimate values of ash and fuel concentrations using ASHPLUME_DLL_LA V2.1 [DIRS 180147] was verified in the Volcanic Eruption TSPA-LA Model (vE1.003). The approach for the verification was to compare the results from the Volcanic Eruption TSPA-LA Model (vE1.003) to the results developed in stand-alone GoldSim-based model files used as installation tests for the ASHPLUME V2.1 DLL as in *User Information Document for*: *ASHPLUME_DLL_LA Version 2.1*, (DOE 2006 [DIRS 181076]), based on a consistent set of fixed input values as defined in the installation test files. The details and associated documentation in terms of the input files and the model files used in the verification are presented in output DTN: MO0708TSPAPOST.000 [DIRS 182986].

The comparison of results between the stand-alone file and the Volcanic Eruption TSPA-LA Model (vE1.003) file, as shown in Table 7.2-13, shows exactly the same values for the parameters X_ash and X_fuel. Because of the identical match in the results reported, the implementation of the ASHPLUME_DLL_LA V2.1 is considered verified in the Volcanic Eruption Modeling Case.

Volcanic Eruption Modeling Case (FAR)—A verification test for the implementation of the FAR 1.2 DLL in the Volcanic Eruption TSPA-LA Model (vE1.003) was performed. The approach for the verification was to compare the results from the Volcanic Eruption TSPA-LA Model (vE1.003) to the results developed in stand-alone GoldSim-based model files used as installation tests for the FAR 1.2 DLL as in *User Information Document for*: FAR Version 1.2 (DOE 2007 [DIRS 183116]), based on a consistent set of fixed input values as defined in the installation test files. The details of the input parameters, installation test case, and the output results are included in the output DTN: MO0708TSPAPOST.000 [DIRS 182986].

A single realization was conducted and a comparison of the output results at 10 years after a volcanic eruption was presented in Table 7.2-14. The results are identical for all four output parameters (Table 7.2-14). A comparison of the model results calculated at each timestep by each model file shows the same values for each parameter (output DTN: MO0708TSPAPOST.000 [DIRS 182986]) and thus the implementation of the FAR V1.2 DLL is considered verified in the Volcanic Eruption Modeling Case.

Igneous Intrusion Modeling Case—As defined in *Dike/Drift Interactions* (SNL 2007 [DIRS 177430], Table 8-2, Section 8.2.2) and DTN: LA0702PADE01EG.001_R0 [DIRS 179495], when an igneous intrusion event that intersects the repository is simulated within the TSPA-LA Model, the intrusion of magma into the repository causes a perturbation in the EBS thermal-hydrologic (TH) properties for approximately 100 years. The global timestep size in the TSPA-LA Model is set at 250 years and thus the perturbation in the EBS TH properties would not be accurately reflected. Therefore, conditional logic was incorporated into the TSPA-LA Model to force a five-year timestep for approximately 100 years following the initiation of a single igneous intrusion event to accurately calculate the change in the TH properties of the EBS TH Environment Submodel (Section 6.5.1.3).

The verification process for the Igneous Intrusion Modeling Case captured the temperature within the CDSP WPs at each of the forced five-year timesteps as simulated in the TSPA-LA Model (v4.042). For verification comparison, a stand-alone GoldSim-based model file was developed with a global timestep increment of five years and with the same pre-event thermal-hydrological properties as the TSPA-LA Model (v4.042) (output DTN: MO0708TSPAPOST.000 [DIRS 182986]). The comparison of the CDSP WP temperatures calculated for both model files are shown on Figure 7.2-15. A comparison of the actual temperature values indicates that the maximum difference in the temperatures was significantly less than one percent and a result of round off. This comparison verifies the ability of the model to accurately calculate the impact on the TH properties of the EBS TH Environment Submodel as a result of an igneous-intrusion event.

7.2.4.1.11 Seismic Scenario Class Modeling Cases

The Seismic Damage Abstraction implementation was verified against two separate stand-alone GoldSim-based models. One stand-alone model was used to verify the implementation of the Ground Motion Submodel, whereas the second verified the Fault Displacement Submodel. The Seismic Damage Abstraction as defined in *Seismic Consequence Abstraction* (SNL 2007 [DIRS 176828]) is implemented in the TSPA-LA Model and was also used to develop the two stand-alone verification models.

In the TSPA-LA Model (v4.046), modifications were made to force a set of input values to be used in the place of inputs and feeds associated with any uncertainty or variability. For example, the exceedance frequency, which controls the peak ground velocity (PGV) during a ground motion event, was set to 1×10^{-8} yr^{-1}. There were 29 variable inputs identified and changed. The same set of inputs was used in both verification stand-alone models (output DTN: MO0708TSPAPOST.000 [DIRS 182986]). For simplification, these inputs were set to static values (i.e., the values remain unchanged over time). Therefore, most of the results did not change over time.

A set of 13 outputs was created from the Seismic Damage Abstraction implemented in the TSPA-LA Model. These outputs were compared to those from the two stand-alone verifications model (output DTN: MO0708TSPAPOST.000 [DIRS 182986]). The comparison of the Seismic Ground Motion Submodel results is shown in Table 7.2-15. The comparison of the Fault Displacement Submodel results is shown in Table 7.2-16. Based on these results, the Seismic Damage Abstraction implementation within the TSPA-LA Model is considered verified.

7.2.5 Verification of Coupling Among Submodels and Model Components

Verification of the coupling of submodels and TSPA-LA Model components within the TSPA-LA Model was accomplished through checking the model implementation during development of the TSPA-LA Model. Verification of coupling among other model components includes verification of the DLLs and the single model components described in Section 7.2.4.

Coupling among TSPA-LA Model components includes flow and transport through the EBS, coupling at the EBS-UZ interface (Section 7.2.5.1), and coupling at the UZ-SZ interface (Section 7.2.4.1.8). Verification of the single components of the TSPA-LA Model, which is discussed in Section 7.2.4, is also important for verification of coupling across model interfaces. After development, the verification of coupling among TSPA-LA Model components is primarily accomplished through auxiliary analyses, discussed in Section 7.7, in order to demonstrate that the TSPA-LA Model yields results that would be expected.

7.2.5.1 Placement of an Effective Zero-Concentration Boundary in the Engineered Barrier System-Unsaturated Zone Interface Domain

The EBS-UZ Interface domain is included beneath the invert domain for modeling EBS radionuclide transport in the TSPA-LA Model. The primary purpose of the EBS-UZ Interface domain is to establish an effective zero-concentration boundary condition at some distance away from the base of the invert in order to compute the diffusive flux from the invert to the UZ and the fraction of total mass flux that goes into the UZ fracture and matrix continua (Section 6.3.8). For this purpose, the EBS-UZ Interface domain is discretized into four layers and the zero-concentration boundary is applied at the base of the fourth layer, approximately 17 m below the invert (Figure 6.3.8-9). The dual continuum of overlapping matrix and fracture continua is represented by cell pathways. The thickness of the first (top) layer of cells is chosen to be 0.6567 m, which is 10 percent greater than the average invert thickness (0.597 m). The thickness of the second layer is set to be double that of the first layer, or 1.3134 m. The third and fourth layers are given a thickness of 5 m and 10 m, respectively. Grid sizes are more refined near the base of the invert to accurately capture the higher concentration gradient in the region. A collector cell is placed beneath the fourth layer and is given a very large water volume to simulate an effective zero-concentration boundary. This collector cell acts as a sink for all the mass flux from the UZ cells. For more details on the implementation, refer to Section 6.3.8.3.

An analysis is performed to evaluate the appropriateness of the location of the effective zero-concentration boundary for the diffusive flux calculation from the invert. The TSPA-LA Model (v5.000) was used for the analysis. In this study, the effective zero-concentration boundary is applied at the base of the invert and then moved down one layer at a time. The effect of the placement of this boundary is evaluated in terms of the diffusive flux from the invert. It is expected that, as the distance to the zero-concentration boundary increases, the diffusive flux from the invert will decrease and converge to a true value. Because analytical solutions do not exist for a dual-continuum representation, the convergence of the invert diffusive flux with increasing distance to the zero-concentration boundary is deemed adequate for evaluating the appropriateness of the location of the effective zero-concentration boundary.

The study is performed for a nonsorbing radionuclide such as ^{99}Tc. The radionuclide mass is injected in the invert cell at 100 years, and the concentration is held constant in the invert at 100 mg/L. The simulation is performed for 20,000 years using the TSPA-LA Model optimal timesteps. The study is only performed for a non-dripping environment for Percolation Subregion 3 for CSNF WPs, where the release from the invert is primarily diffusive (a small advective component is also present due to imbibition flux from the host rock into the invert). A total number of 300 realizations is run in order to sample the epistemic uncertainty in the hydrologic properties of the invert and the UZ. The results of the study are shown on Figure 7.2-16 to compare the total mean diffusive mass flux of ^{99}Tc from the invert for varying placement of the zero-concentration boundary (output DTN: MO0708TSPAPOST.000 [DIRS 182986]). Almost all of the diffusive mass flux from the invert goes into the matrix continuum, as the effective diffusive area for the matrix continuum is much greater than that for the fracture continuum. As would be expected, the diffusive flux decreases as the zero-concentration boundary is moved farther down from the invert. The diffusive flux at 10,000 years for the case where the zero concentration is applied at the base of the invert is about 7.4 g/yr, but reduces to about 0.62 g/yr when the boundary is placed at the base of the first layer (a distance of about 0.66 m from the base of invert). The diffusive flux reduces further to about 0.55 g/yr when the zero-concentration boundary is placed at the base of the second layer (a total distance of about 1.97 m from the base of invert) and then to about 0.54 g/yr when the zero-concentration boundary is applied to the base of the third and fourth layers (at total respective distances of 6.97 m and 16.97 m).

This analysis shows that it is important to properly locate the zero-concentration boundary when the dominant flux from the invert is diffusive. The analysis further shows that the diffusive flux converges when the zero-concentration boundary is applied at the base of the third and fourth layers, indicating that placement of the zero-concentration boundary at further distances is not going to appreciably affect the diffusive mass flux from the invert. This analysis also shows that the discretization chosen for the EBS-UZ Interface domain is adequate for the purpose of computing the diffusive flux from the invert.

7.2.6 Verification of Range of Applicability of Submodels and Model Components

The verification of the range of applicability of submodels and model components is another important aspect of TSPA-LA Model confidence building. When provided by the supporting analysis and/or model reports, the range of applicability of inputs to submodels implemented in the TSPA-LA Model are verified as part of the checking of the TSPA-LA Model. The records that document the implementation and checking of the TSPA-LA Model are located in the relevant records package.

The type of verification performed to ensure that the range of applicability was properly defined within the TSPA-LA Model depends on the nature of the implementation. In some cases, logic has been built into the TSPA-LA Model to verify that the inputs are within the appropriate range. If an input is outside its valid range, a flag is set. In other cases, logic has been built into the TSPA-LA Model such that if a parameter value is selected outside the valid range, the value is reset to the bounding value depending on if the value is greater than or less than that of the range.

An example of this logic implemented within the TSPA-LA Model can be seen in the implementation of the Drift Seepage Submodel (Section 6.3.3.1). First, the drift-wall temperature must be below 100°C for seepage to occur into no-collapsed drifts. Logic is built into the model such that if the temperature is greater than or equal to 100°C, then a flag is set that turns off the presence of drift seepage (Section 6.3.3.1.3). Second, the range of percolation flux over which the Drift Seepage Submodel is valid is from 0.01 to 5,000 mm/yr. If a percolation flux that is input into the Drift Seepage Submodel is less than 0.01 mm/yr or greater than 5,000 mm/yr, the value is reset to the bounding value of 0.01 mm/yr or 5,000 mm/yr, respectively (Section 6.3.3.1.3).

Table 7.2-1. Verification of TSPA-LA Model Dynamically Linked Libraries

DLL (Version)	Type of Verification	Where Described
SEEPAGEDLL_LA (v1.3)	Verification analysis	Section 7.2.4.1.1
WAPDEG (v4.07)	Verification analysis	Section 7.2.4.1.4
CWD (v2.0)	Verification analysis	Section 7.2.4.1.4
SCCD (v2.01)	Verification analysis	Section 7.2.4.1.4
FEHM_V2_24-01 (v2.24)	Verification analysis	Section 7.2.4.1.7
SZ_CONV_3.10 (v3.1)	Verification analysis	Section 7.2.4.1.8
ASHPLUME_DLL_LA (v2.1)	Verification analysis	Section 7.2.4.1.10
FAR (v1.2)	Verification analysis	Section 7.2.4.1.10

NOTE: Comparison with Table 3-1 shows that the versions used for verification of the TSPA-LA Model DLLs match those used in the final version of the TSPA-LA Model.

Table 7.2-2. Verification of Dynamically Linked Libraries and Model Abstractions Used in the TSPA-LA Model

Model Component/Submodel	Analysis Description	Status	Section Described
Drift Seepage			
Drift Seepage Implementation	Verification of Seepage DLL by comparison of the TSPA-LA Model results with a stand-alone GoldSim-based implementation	Verified	Section 7.2.4.1.1
Drift Wall Condensation			
Verification of the Drift Wall Condensation Submodel	Comparison of drift-wall condensation rates and probability data to that supplied in supporting DTNs	Verified	Section 7.2.4.1.2
Engineered Barrier System Chemical Environment			
Physical and Chemical Environment Submodel	Verification of TSPA-LA Model file to accurately estimate (under both evaporative and condensation conditions) pH and ionic strength for a set of controlled inputs of temperature, relative humidity, Pco_2, and percolation bin number	Verified	Section 7.2.4.1.3
Waste Package and Drip Shield Degradation			
Integrated Waste Package and Drip Shield Degradation	Verification of the WAPDEG, CWD, and SCCD DLLs through comparison of the results of TSPA-LA Model implementation with the results of a stand-alone implementation	Verified	Section 7.2.4.1.4
Waste Form Degradation and Mobilization			
Verification of Waste Rind Degradation	Comparison of the rind volume and thickness in a CSNF WP using a Microsoft Excel spreadsheet and the TSPA-LA Model file	Verified	Section 7.2.4.1.5
	Comparison of the rind volume and thickness in a CDSP WP using a Microsoft Excel spreadsheet and the TSPA-LA Model file	Verified	Section 7.2.4.1.5
Verification of CSNF Waste Form Degradation	Comparison of waste form degradation rate in a CSNF WP using a Microsoft Excel spreadsheet and the TSPA-LA Model file	Verified	Section 7.2.4.1.5
Verification of HLW Glass Degradation	Comparison of TSPA-LA Model file results with a spreadsheet implementing the source analysis model report equations for acidic and alkaline conditions with relative humidity less and greater than 0.44	Verified	Section 7.2.4.1.5
Verification of Dissolved Concentration Limits	Nominal Scenario: Comparison of TSPA-LA Model file results with a spreadsheet implementing the calculation of radionuclide solubilities using look-up tables and applying epistemic uncertainty	Verified	Section 7.2.4.1.5
	Igneous Scenario (Igneous Intrusion Modeling Case): Comparison of TSPA-LA Model file results with a spreadsheet implementing the calculation of uranium solubilities using look-up tables and applying epistemic uncertainty	Impact Analysis Conducted using TSPA-LA Model	Section 7.2.4.1.5
Verification of the In-Package Chemistry Submodel	Comparison of pH, ionic strength, and total carbonate in the WPs using a Microsoft Excel spreadsheet and the TSPA-LA Model file	Verified	Section 7.2.4.1.5

Table 7.2-2. Verification of Dynamically Linked Libraries and Model Abstractions Used in the TSPA-LA Model (Continued)

Model Component/Submodel	Analysis Description	Status	Section Described
Engineered Barrier System Transport			
Verification of EBS Transport Submodel	Comparison of results of plutonium transport and colloidal transport for both reversible and irreversible sorption on iron oxyhydroxide colloids using a Microsoft Excel implemented finite-difference approximation and the TSPA-LA Model file transport submodel	Verified	Section 7.2.4.1.6
Unsaturated Zone Transport			
Verification of FEHM Particle Tracking for the UZ Transport Submodel	Comparison of results from the TSPA-LA Model (FEHM DLL) with that of a test case developed from the base case FEHM model	Verified	Section 7.2.4.1.7
Saturated Zone Flow and Transport			
Verification of SZ Flow and Transport	Comparison of TSPA-LA Model results with the site-scale SZ transport base case for ^{99}Tc	Verified	Section 7.2.4.1.8
	Comparison of a 1-D stand-alone model that was used for validation of the site-scale model with the TSPA-LA Model for ^{14}C	Verified	Section 7.2.4.1.8
Biosphere			
Verification of the Groundwater Source Term to Dose Submodel	Comparison of calculated dose using a Microsoft Excel spreadsheet and the TSPA-LA Model file	Verified	Section 7.2.4.1.9
Igneous Scenario Class Modeling Cases			
Volcanic Eruption Modeling Case	Comparison of TSPA-LA Model results with the stand-alone model used for validation of the ASHPLUME DLL	Verified	Section 7.2.4.1.10
	Comparison of TSPA-LA Model results with a Microsoft Excel spreadsheet based on the FAR model	Verified	Section 7.2.4.1.10
Igneous Intrusion Modeling Case	Comparison of TSPA-LA Model with a stand-alone GoldSim-based model file showing the impact of an igneous intrusion event on the EBS thermal-hydrologic properties	Verified	Section 7.2.4.1.10
Seismic Scenario Class Modeling Cases			
Verification of Seismic Damage Abstraction	Comparison of TSPA-LA Model calculated ground motion and fault displacement damage with that of stand-along GoldSim-based models developed based on the source analysis model report	Verified	Section 7.2.4.1.11

Table 7.2-2. Verification of Dynamically Linked Libraries and Model Abstractions Used in the TSPA-LA Model (Continued)

Model Component/Submodel	Analysis Description	Status	Section Described
Verification of Coupling Between Model Components			
EBS Transport and EBS-UZ Interface	Transport through the EBS-UZ interface to demonstrate proper placement of the Effective Zero-Concentration Boundary	Verified	Section 7.2.5.1
UZ-SZ Interface	Included in results presented for Verification of SZ Flow and Transport in which a radionuclide source term was specified at the base of the UZ Submodel domain and passed across the interface for use in the SZ Submodel.	Verified	Section and 7.2.4.1.8

Table 7.2-3. Verification Summary of the Drift Seepage Dynamically Linked Library

	Stand-Alone Verification Model			TSPA-LA Model (v5.000)		
Percolation Subregion	**Seepage Rate (m^3/yr) at 10,000 years**	**Seepage Fraction**	**Non-Lithophysal Fraction**	**Seepage Rate (m^3/yr) at 10,000 years**	**Seepage Fraction**	**Non-Lithophysal Fraction**
CDSP 1	0.030	0.021	0.319	0.030	0.021	0.319
CDSP 2	0.070	0.108	0.237	0.070	0.108	0.237
CDSP 3	0.103	0.163	0.173	0.103	0.163	0.173
CDSP 4	0.125	0.135	0.041	0.125	0.135	0.041
CDSP 5	0.140	0.171	0.110	0.140	0.171	0.110
CSNF 1	0.019	0.015	0.319	0.019	0.015	0.319
CSNF 2	0.076	0.103	0.237	0.076	0.103	0.237
CSNF 3	0.108	0.160	0.173	0.108	0.160	0.173
CSNF 4	0.120	0.154	0.041	0.120	0.154	0.041
CSNF 5	0.159	0.206	0.110	0.159	0.206	0.110

Source: Stand-alone and TSPA-LA Model results are contained in output DTN: MO0708TSPAPOST.000 [DIRS 182986].

Table 7.2-4. Comparison of the Drift-Wall Condensation Rates Verification Calculations

Time (yr)	Condensation Rate [m^3/yr], Verification	Condensation Rate [m^3/yr], TSPA-LA Model (v4.042)
0 to 600	0	0
675	0	0
750	0	0
825	5.92E-06	5.92E-06
900	0	0
975	1.25E-05	1.25E-05
1,050	0	0
1,125	1.79E-05	1.79E-05
1,200	0	0
1,275	2.76E-05	2.76E-05
1,350	0	0
1,425	6.32E-06	6.32E-06
1,500	0	0
1,575	1.08E-06	1.08E-06
1,650	0	0
1,725	6.07E-06	6.07E-06
1,800	0	0
1,875	4.53E-06	4.53E-06
1,950	0	0
2,025	0	0
2,100 to 3,000	0	0

Source: Output DTN: MO0708TSPAPOST.000 [DIRS 182986].

Table 7.2-5. Summary of the Verification Inputs and Outputs for Calculation of the P_{CO2} Values in the EBS Physical and Chemical Environment Abstraction

Input Set	Water:Rock Interaction Parameter	Temperature (°C)	Relative Humidity (%)	P_{CO2} (bar) Verification	P_{CO2} (bar) TSPA-LA Model(v4.043)
1	0.0002	0	0	1.000E-03	1.000E-03
2	0.1932	23	0	1.000E-03	1.000E-03
3	0.1046	40	0	1.000E-03	1.000E-03
4	0.0585	55	0	1.000E-03	1.000E-03
5	0.0378	70	0	1.000E-03	1.000E-03
6	0.0278	85	0	1.000E-03	1.000E-03
7	0.0222	96	0	1.000E-03	1.000E-03
8	0.0166	23	0.2	1.000E-03	1.000E-03
9	0.0111	40	0.2	1.000E-03	1.000E-03
10	0.0077	55	0.2	9.996E-04	9.996E-04
11	0.0077	70	0.2	9.955E-04	9.955E-04
12	0.0077	85	0.2	9.886E-04	9.886E-04
13	0.0077	96	0.2	9.807E-04	9.807E-04
14	0.0077	23	0.4	1.000E-03	1.000E-03
15	0.0077	40	0.4	9.998E-04	9.998E-04
16	0.0077	55	0.4	9.954E-04	9.954E-04
17	0.0077	70	0.4	9.874E-04	9.874E-04
18	0.0077	85	0.4	9.734E-04	9.734E-04
19	0.0077	96	0.4	9.577E-04	9.577E-04
20	0.0077	23	0.65	1.000E-03	1.000E-03
21	0.0077	40	0.65	9.974E-04	9.974E-04
22	0.0077	55	0.65	9.903E-04	9.903E-04
23	0.0072	70	0.65	9.772E-04	9.772E-04
24	0.0063	85	0.65	9.544E-04	9.544E-04
25	0.0054	96	0.65	9.289E-04	9.289E-04
26	0.0045	23	0.75	1.000E-03	1.000E-03
27	0.0036	40	0.75	9.964E-04	9.964E-04
28	0.0028	55	0.75	9.882E-04	9.882E-04
29	0.0019	70	0.75	9.731E-04	9.731E-04
30	0.0010	85	0.75	9.468E-04	9.468E-04
31	0.0001	96	0.75	9.174E-04	9.174E-04
32	10	23	0.85	1.000E-03	1.000E-03
33	10	40	0.85	9.955E-04	9.955E-04
34	10	55	0.85	9.862E-04	9.862E-04
35	10	70	0.85	9.690E-04	9.690E-04
36	10	85	0.85	9.393E-04	9.392E-04
37	10	96	0.85	9.059E-04	9.059E-04

Table 7.2-5. Summary of the Verification Inputs and Outputs for Calculation of the P_{CO2} Values in the EBS Physical and Chemical Environment Abstraction (Continued)

Input Set	Water:Rock Interaction Parameter	Temperature (°C)	Relative Humidity (%)	P_{CO2} (bar), Verification	P_{CO2} (bar), TSPA-LA Model (v4.043)
38	10	23	1	1.000E-03	1.000E-03
39	10	40	1	9.940E-04	9.940E-04
40	10	55	1	9.831E-04	9.831E-04
41	10	70	1	9.629E-04	9.628E-04
42	10	85	1	9.279E-04	9.278E-04
43	10	96	1	8.886E-04	8.886E-04
44	10	150	1	8.886E-04	8.886E-04

Source: Output DTN: MO0708TSPAPOST.000 [DIRS 182986].

Table 7.2-6. Summary of Input Values Used in EBS Physical and Chemical Environment Verifications of pH and Ionic Strength

Parameter	Range
Seepage Water Type	1, 2, 3, or 4
P_{CO2} (bar)	0.0001 to 0.01
Temperature on Waste-Package Surface (^{o}C)	30, 70, or 100
Relative Humidity at Waste-Package Surface	0.99
WRIP	0 to 10

Source: Output DTN: MO0708TSPAPOST.000 [DIRS 182986].

Table 7.2-7. Values Used in the WAPDEG Dynamically Linked Library for Verifying the TSPA-LA Model

Element Name	Value	Comment
C1_GenCorr_A22	3,116.47	Slope term for the WP outer shell general corrosion temperature dependence (K^{-1})
WDDSAggrGC	2.0×10^{-3}	DS general corrosion rate under aggressive conditions (mm/yr)
WDDSBenignGC	2.0×10^{-3}	DS general corrosion rate under benign conditions (mm/yr)
MIC_RHThresh	0.825	Microbially influenced corrosion (MIC) relative humidity threshold
Stress_Thress_SCC	342.225	Stress threshold for SCC
n_SCC	1.165	SCC model parameter
WDSeed	123456789	WAPDEG random seed value
z_OL	0	Outer lid uncertainty
GC_ULevel_A22	2.0	Uncertainty level for Alloy 22 general corrosion
Defect Count	4.02997×10^{-7}	Defect count (mm^{-3})
Defect Size	0.220472	Defect size (mm^{-1})

Source: Output DTN: MO0506MWDTLMPI.001 [DIRS 174808].

Table 7.2-8. Summary of Input/Output Values and GoldSim Verification Checks for the CSNF Rind Volume and Mass Calculations

Input Set No.	Porosity	Fraction of Failed Rods	Fraction of Corroded WPs	CSNF Rind Volume (cm^3) Verification	CSNF Rind Volume (cm^3), TSPA-LA Model (v4.041)	CSNF Rind Mass (g) Verification	CSNF Rind Mass (g) TSPA-LA Model (v4.041)
1	0.05	0.01	0.005	15243.9	15243.9	69946.4	69946.4
2	0.3	0.01	0.005	20688.1	20688.1	69946.4	69946.4
3	0.05	0.01	0.01	30487.7	30487.7	139892.9	139892.9
4	0.3	0.01	0.01	41376.2	41376.2	139892.9	139892.9
5	0.05	0.05	0.005	15243.9	15243.9	69946.4	69946.4
6	0.3	0.05	0.005	20688.1	20688.1	69946.4	69946.4
7	0.05	0.05	0.05	152438.6	152438.6	699464.4	699464.4
8	0.3	0.05	0.05	206880.9	206880.9	699464.4	699464.4
9	0.05	0.1	0.005	15243.9	15243.9	69946.4	69946.4
10	0.3	0.1	0.005	20688.1	20688.1	69946.4	69946.4
11	0.05	0.1	0.1	304877.1	304877.1	1398928.7	1398928.7
12	0.3	0.1	0.1	413761.8	413761.8	1398928.7	1398928.7

Sources: Parameters in Table 6-3 and Equations 6-3, 6-4, 6-5, and 6-12 in Table 6-4 of *Cladding Degradation Summary for LA* (SNL 2007 [DIRS 180616]) were used to calculate the CSNF rind volume and mass.

Output DTN: MO0708TSPAPOST.000 [DIRS 182986].

Table 7.2-9. Summary of Input/Output Values and GoldSim Verification Checks for the CDSP WPs HLW Rind Thickness and Mass

Input Set No.	Fraction Degraded	HLW Rind Thickness (cm) Verification	HLW Rind Thickness (cm) TSPA-LA Model (v4.041)	HLW Rind Mass (g) Verification	HLW Rind Mass (g) TSPA-LA Model (v4.041)
1	0.01	0.15	0.15	123.6	123.6
2	0.02	0.30	0.30	247.1	247.1
3	0.05	0.76	0.76	617.8	617.8
4	0.1	1.54	1.54	1235.6	1235.6
5	0.2	3.17	3.17	2471.1	2471.1
6	0.3	4.90	4.90	3706.7	3706.7
7	0.4	6.76	6.76	4942.3	4942.3
8	0.5	8.79	8.79	6177.9	6177.9
9	0.6	11.03	11.03	7413.4	7413.4
10	0.8	16.58	16.58	9884.6	9884.6
11	0.9	20.51	20.51	11120.2	11120.2
12	0.99	27.00	27.00	12232.2	12232.2

Sources: Parameters and equations in Section 8-1 and Table 8-1 of *Defense HLW Glass Degradation Model* (BSC 2004 [DIRS 169988]) were used to calculate CDSP rind thickness and water volume.

Output DTN: MO0708TSPAPOST.000 [DIRS 182986].

Table 7.2-10. Summary of Verification Checks for the CSNF Waste Form Degradation Submodel

Acidic Verifications		
pH	**Degradation Rate (yr^{-1}) Verification**	**Degradation Rate (yr^{-1}) TSPA-LA Model (v4.041)**
2.00	1.448E-02	1.449E-02
3.00	6.619E-03	6.624E-03
4.00	3.026E-03	3.028E-03
5.00	1.383E-03	1.384E-03
6.00	6.321E-04	6.326E-04
6.50	4.274E-04	4.277E-04
Alkaline Verifications		
pco_3	**Degradation Rate (yr^{-1}) Verification**	**Degradation Rate (yr^{-1}) TSPA-LA Model (v4.041)**
0.0002	3.703E-04	3.705E-04
0.0005	4.065E-04	4.068E-04
0.001	4.363E-04	4.366E-04
0.005	5.142E-04	5.145E-04
0.01	5.518E-04	5.522E-04
0.02	5.923E-04	5.926E-04

Sources: *CSNF Waste Form Degradation: Summary Abstraction* (BSC 2004 [DIRS 169987], Sections 6.4.1.2 and 6.4.1.3).

Output DTN: MO0708TSPAPOST.000 [DIRS 182986].

Table 7.2-11a. Summary of Verification Checks for the HLW Glass Degradation Submodel

HLW Degradation Verification at Relative Humidity Conditions Less Than 0.44				
Temperature (°C)	pH	Relative Humidity	Degradation Rate (yr^{-1}) Verification	Degradation Rate (yr^{-1}) TSPA-LA Model (v4.041)
50	4	0.2	0	0
50	5	0.2	0	0
50	6	0.2	0	0
50	7	0.2	0	0
50	8	0.2	0	0
50	9	0.2	0	0
50	10	0.2	0	0
75	4	0.2	0	0
75	5	0.2	0	0
75	6	0.2	0	0
75	7	0.2	0	0
75	8	0.2	0	0
75	9	0.2	0	0
75	10	0.2	0	0
100	4	0.2	0	0
100	5	0.2	0	0
100	6	0.2	0	0
100	7	0.2	0	0
100	8	0.2	0	0
100	9	0.2	0	0
100	10	0.2	0	0
125	4	0.2	0	0
125	5	0.2	0	0
125	6	0.2	0	0
125	7	0.2	0	0
125	8	0.2	0	0
125	9	0.2	0	0
125	10	0.2	0	0
150	4	0.2	0	0
150	5	0.2	0	0
150	6	0.2	0	0
150	7	0.2	0	0
150	8	0.2	0	0
150	9	0.2	0	0
150	10	0.2	0	0

Source: Output DTN: MO0708TSPAPOST.000 [DIRS 182986].

Table 7.2-11b. Summary of Verification Checks for the HLW Glass Degradation Submodel

HLW Degradation Verification at Relative Humidity Conditions Greater Than 0.44				
Temperature (°C)	**pH**	**Relative Humidity**	**Degradation Rate (yr^{-1}) Verification**	**Degradation Rate (yr^{-1}) TSPA-LA Model (v4.041)**
50	4	0.8	1.17E-05	1.17E-05
50	5	0.8	3.80E-06	3.80E-06
50	6	0.8	1.23E-06	1.23E-06
50	7	0.8	3.98E-07	3.98E-07
50	8	0.8	1.29E-07	1.29E-07
50	9	0.8	6.65E-08	6.65E-08
50	10	0.8	2.05E-07	2.05E-07
75	4	0.8	2.69E-05	2.69E-05
75	5	0.8	8.70E-06	8.70E-06
75	6	0.8	2.81E-06	2.81E-06
75	7	0.8	9.11E-07	9.11E-07
75	8	0.8	2.95E-07	2.95E-07
75	9	0.8	4.20E-07	4.20E-07
75	10	0.8	1.30E-06	1.30E-06
100	4	0.8	5.51E-05	5.51E-05
100	5	0.8	1.78E-05	1.78E-05
100	6	0.8	5.77E-06	5.77E-06
100	7	0.8	1.87E-06	1.87E-06
100	8	0.8	6.72E-07	6.72E-07
100	9	0.8	2.08E-06	2.08E-06
100	10	0.8	6.42E-06	6.42E-06
125	4	0.8	2.59E-05	2.59E-05
125	5	0.8	2.59E-05	2.59E-05
125	6	0.8	2.59E-05	2.59E-05
125	7	0.8	2.59E-05	2.59E-05
125	8	0.8	2.59E-05	2.59E-05
125	9	0.8	2.59E-05	2.59E-05
125	10	0.8	2.59E-05	2.59E-05
150	4	0.8	8.88E-05	8.88E-05
150	5	0.8	8.88E-05	8.88E-05
150	6	0.8	8.88E-05	8.88E-05
150	7	0.8	8.88E-05	8.88E-05
150	8	0.8	8.88E-05	8.88E-05
150	9	0.8	8.88E-05	8.88E-05
150	10	0.8	8.88E-05	8.88E-05

Source: Output DTN: MO0708TSPAPOST.000 [DIRS 182986].

Table 7.2-12. Summary of Parameter Ranges Used in Developing the Input Data Sets for the In-Package Chemistry Submodel Verifications of Ionic Strength, pH, and Total Carbonate

Parameter	Range
Ionic Strength (Seepage)	
Time Since Waste Package Failure (years)	5,250 to 42,500
Seepage Flow Rate (L/yr)	0.1 to 1,000
Random Number	0.5
Ionic Strength (Non-Seepage)	
pH	0.95 to 1.0
Random Number	0, 0.3, and 1.0
pH (Seepage and Non-Seepage)	
Ionic Strength (molality)	0.003 to 10
P_{CO2} (bar)	1.5, 2, 3, and 4
Random Number	0.5
Total Carbonate (Seepage and Non-Seepage)	
Temperature (°C)	25, 40, and 100
pH	2, 4, 6, 8, and 10
P_{CO2} (bar)	0.001 and 0.01

Source: Output DTN: MO0708TSPAPOST.000 [DIRS 182986].

Table 7.2-13. Comparison of Results for the ASHPLUME Verification

TSPA-LA Model Output Element Name	Description	Value (g/cm^2) Verification	Value (g/cm^2) TSPA-LA Model (vE1.003)
X_Ash	Ash concentration on gridded area	0.126	0.126
X_Fuel	Fuel concentration on gridded area	2.03E-07	2.03E-07

Source: Output DTN: MO0708TSPAPOST.000 [DIRS 182986].

Table 7.2-14. Comparison of Results for the FAR Verification

Output Parameter Description	Verification Model	TSPA-LA Model (vE1.003)
Concentration at surface channels (g/cm^3)	3.05E-07	3.05E-07
Depth Integrated concentration in channels (g/cm^2)	6.10E-06	6.10E-06
Concentration at surface along divides (g/cm^3)	9.75E-07	9.75E-07
Depth Integrated concentration along divides (g/cm^2)	1.00E-06	1.00E-06

Source: Output DTN: MO0708TSPAPOST.000 [DIRS 182986].

Table 7.2-15. Comparison of the Seismic Damage Abstraction Ground Motion Submodel Verification Calculations

TSPA-LA Model Parameter Element Name	Parameter Description	Value Verification	Value TSPA-LA Model (v4.046)
Seismic_Rubble_Fill_time [years]	Time that the drift fills with rubble as a consequence of a seismic event	2.0×10^6	2.0×10^6
F_DS_Patch_Damage_Seismic	Fraction of the DS surface open to advective flow	1.0	1.0
Event_Time_Seismic_CDSP [years]	Initiation time of the seismic event for CDSP WPs	451.64	451.64
Event_Time_Seismic [years]	Initiation time of the seismic event	451.64	451.64
Event_Time_Seismic_TAD [years]	Initiation time of the seismic event for TAD WPs	451.64	451.64
F_WP_Crk_Damage_Seismic	Fraction of WP surface failed by ground motion	0.003977	0.003977
WP_Failure_Fraction_Seismic	Fraction of WPs failed following a seismic event	1.0	1.0
F_WP_Patch_Damage_Seismic	Fraction of WP surface failed by ruptures or fault displacement	0.002973	0.002973
Cum_Event_Occurs	Cumulative discrete change signals indicating a seismic event has been triggered	446	446
Rubble_Vol_Accum_Li_max [m^3/m]	Maximum lithophysal rubble volume required to fill drift, per length of drift	22.3(1)	0(1)
Rubble_Vol_Accum_NoLi_max [m^3/m]	Maximum non-lithophysal rubble volume required to fill drift, per length of drift	22.3(1)	0(1)
Rubble_Vol_Accum_Li [m^3/m]	Calculated lithophysal rubble volume required to fill drift, per length of drift	0	0
Rubble_Vol_Accum_NoLi [m^3/m]	Calculated non-lithophysal rubble volume required to fill drift, per length of drift	0	0

NOTE: (1) The TSPA-LA Model (v4.046) has a switch that does not allow the calculation of the maximum rubble volume parameters if no rock fall occurs. This switch was not included in the stand-alone verification model and thus a value was determined even though no rock fall occurred.

Source: Output DTN: MO0708TSPAPOST.000 [DIRS 182986].

Table 7.2-16. Comparison of the Seismic Damage Abstraction Fault Displacement Submodel Verification Calculations

TSPA-LA Model Parameter Element Name	Parameter Description	Value Verification	Value TSPA-LA Model (v4.046)
Seismic_Rubble_Fill_time [years]	Time that the drift fills with rubble as a consequence of a seismic event	250	250
F_DS_Patch_Damage_Seismic	Fraction of the DS surface open to advective flow	1	1
Event_Time_Seismic_CDSP [years]	Initiation time of the seismic event for CDSP WPs	250	250
Event_Time_Seismic [years]	Initiation time of the seismic event	250	250
Event_Time_Seismic_TAD [years]	Initiation time of the seismic event for TAD WPs	250	250
F_WP_Crk_Damage_Seismic	Fraction of WP surface failed by ground motion	0	0
WP_Failure_Fraction_Seismic	Fraction of WPs failed following a seismic event	1	1
F_WP_Patch_Damage_Seismic	Fraction of WP surface failed by ruptures or fault displacement	0.05	0.05
Cum_Event_Occurs	Cumulative discrete change signals indicating a seismic event has been triggered	0	0
Rubble_Vol_Accum_Li_max [m^3/m]	Maximum lithophysal rubble volume required to fill drift, per length of drift	112	112
Rubble_Vol_Accum_NoLi_max [m^3/m]	Maximum non-lithophysal rubble volume required to fill drift, per length of drift	2.9	2.9
Rubble_Vol_Accum_Li [m^3/m]	Calculated lithophysal rubble volume required to fill drift, per length of drift	112	112
Rubble_Vol_Accum_NoLi [m^3/m]	Calculated non-lithophysal rubble volume required to fill drift, per length of drift	2.9	2.9

Source: Output DTN: MO0708TSPAPOST.000 [DIRS 182986].

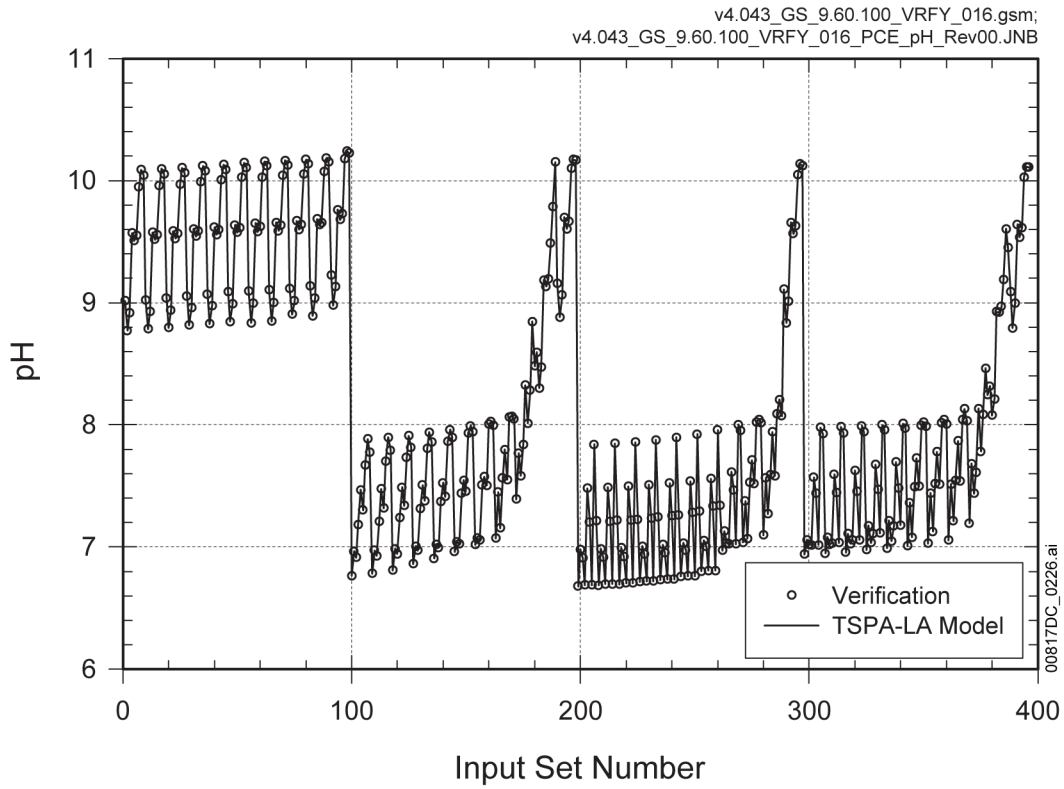

Source: Output DTN: MO0708TSPAPOST.000 [DIRS 182986].

Figure 7.2-1. Comparison of EBS Physical and Chemical Environment pH Calculations between a Stand-Alone Verification Calculation and the TSPA-LA Model

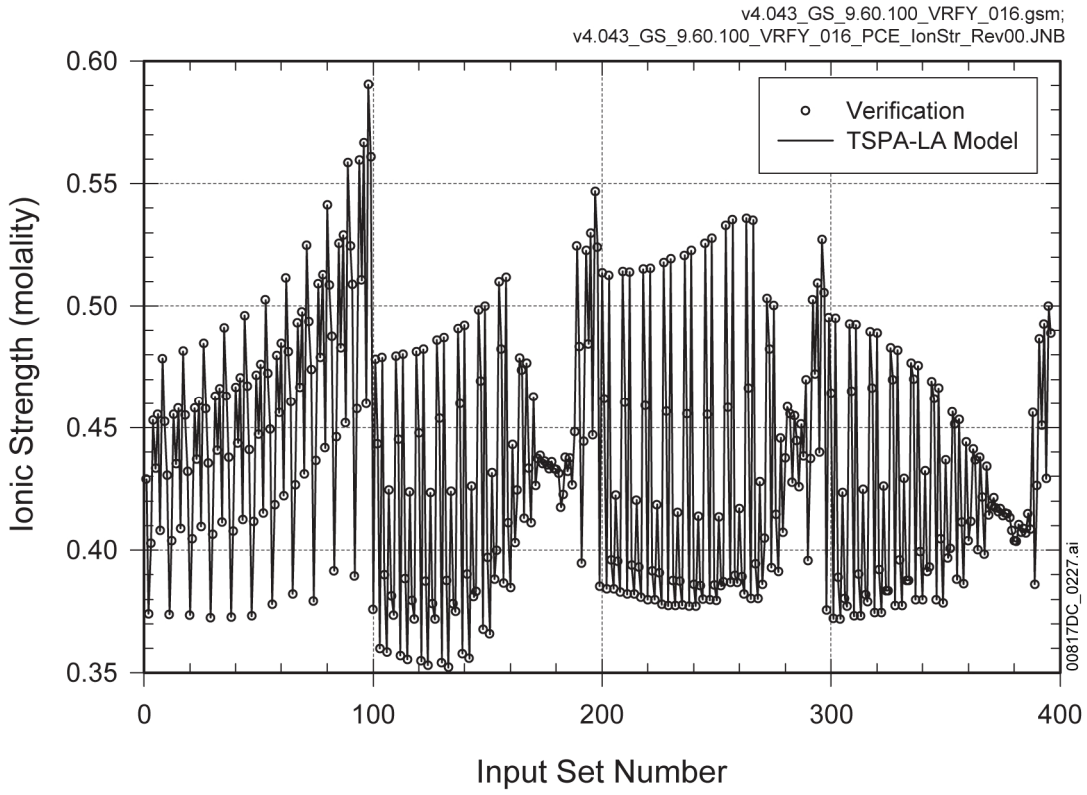

Source: Output DTN: MO0708TSPAPOST.000 [DIRS 182986].

Figure 7.2-2. Comparison of EBS Physical and Chemical Environment Ionic Strength Calculations between a Stand-Alone Verification Calculation and the TSPA-LA Model

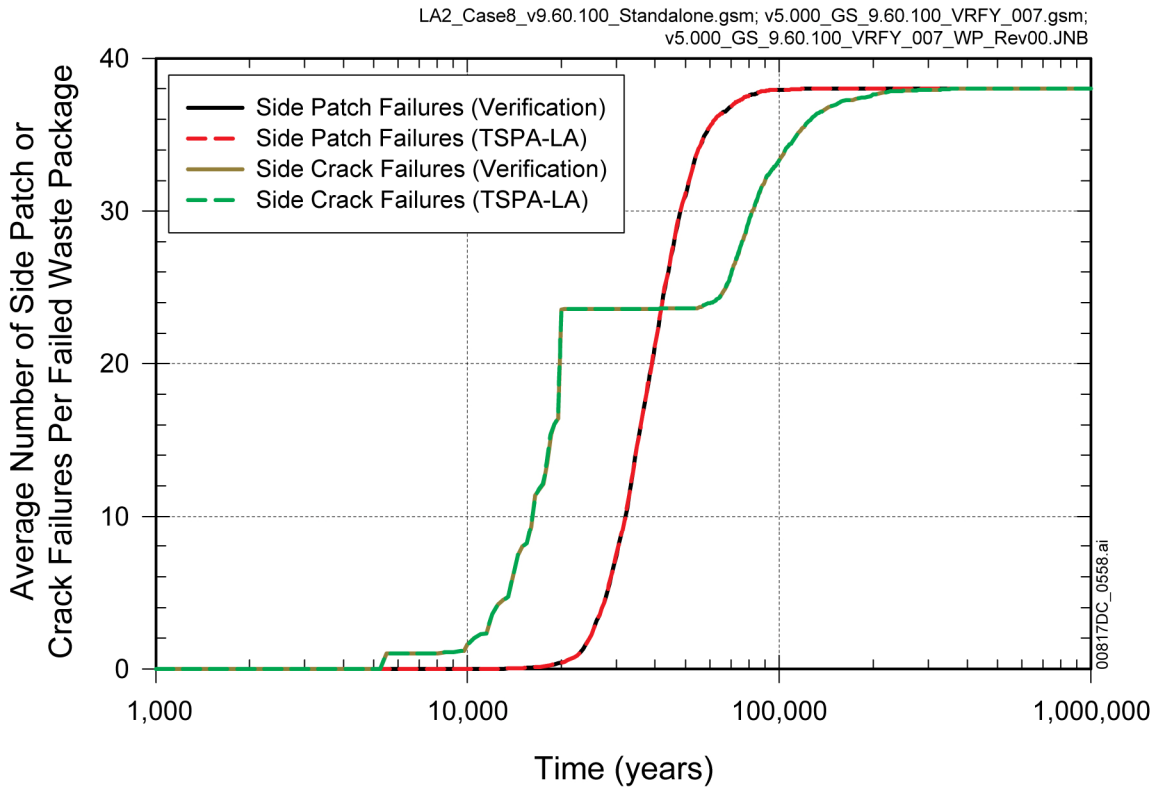

Source: Output DTN: MO0708TSPAPOST.000 [DIRS 182986].

Figure 7.2-3. Comparison of the Average Number of Waste Package Side Patch and Crack Failures between a Stand-Alone Verification Calculation and the TSPA-LA Model

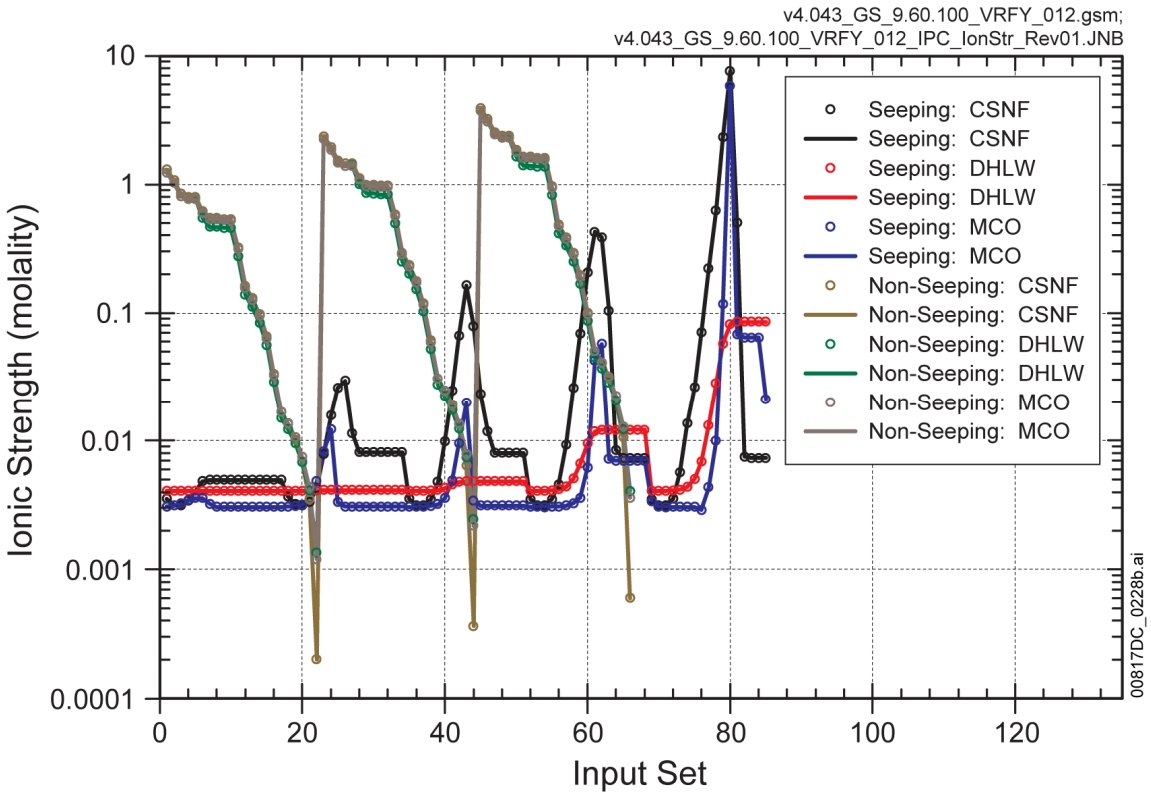

Source: Output DTN: MO0708TSPAPOST.000 [DIRS 182986].

NOTE: The verification data and the TSPA-LA Model results are represented by the open circles and solid lines, respectively. Some of the No Seepage data lines cannot be seen due to being obscured by other data lines.

Figure 7.2-4. Comparison of In-Package Chemistry Ionic Strength Calculations between a Stand-Alone Verification Calculation and the TSPA-LA Model

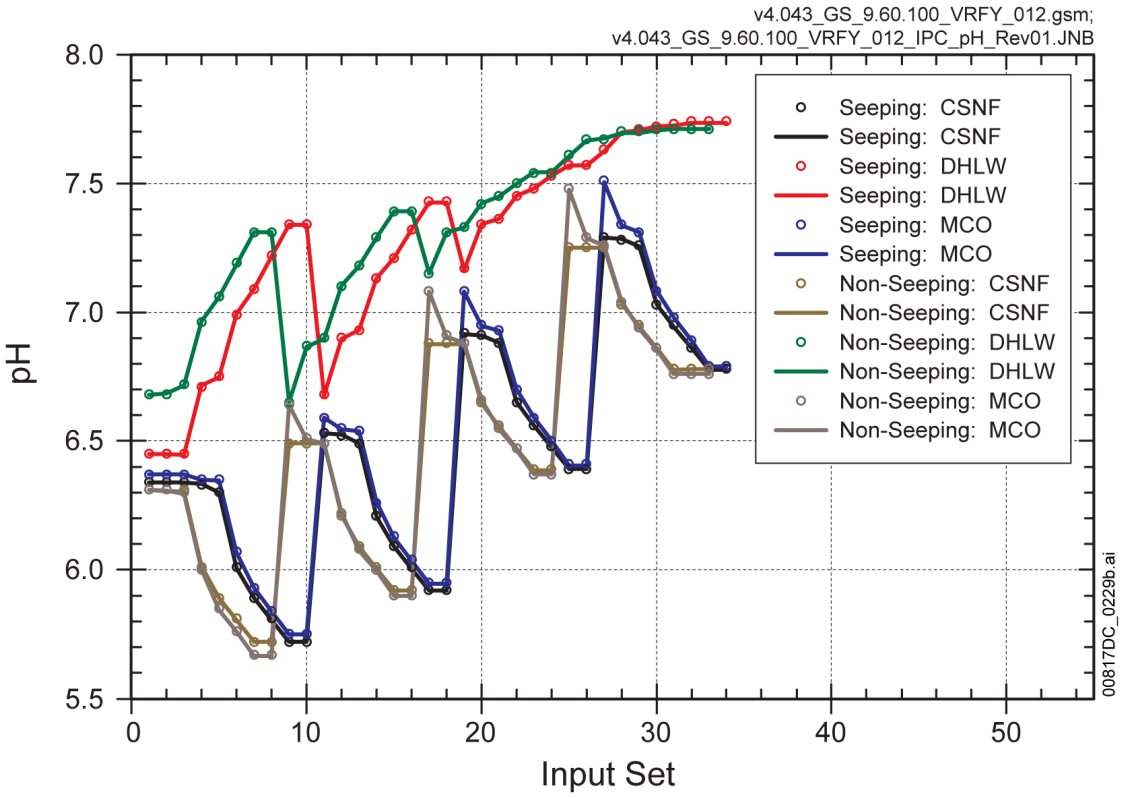

Source: Output DTN: MO0708TSPAPOST.000 [DIRS 182986].

NOTE: The verification data and the TSPA-LA Model results are represented by the open circles and solid lines, respectively. Some of the No Seepage data lines cannot be seen due to being obscured by other data lines.

Figure 7.2-5. Comparison of In-Package Chemistry pH Calculations between a Stand-Alone Verification Calculation and the TSPA-LA Model

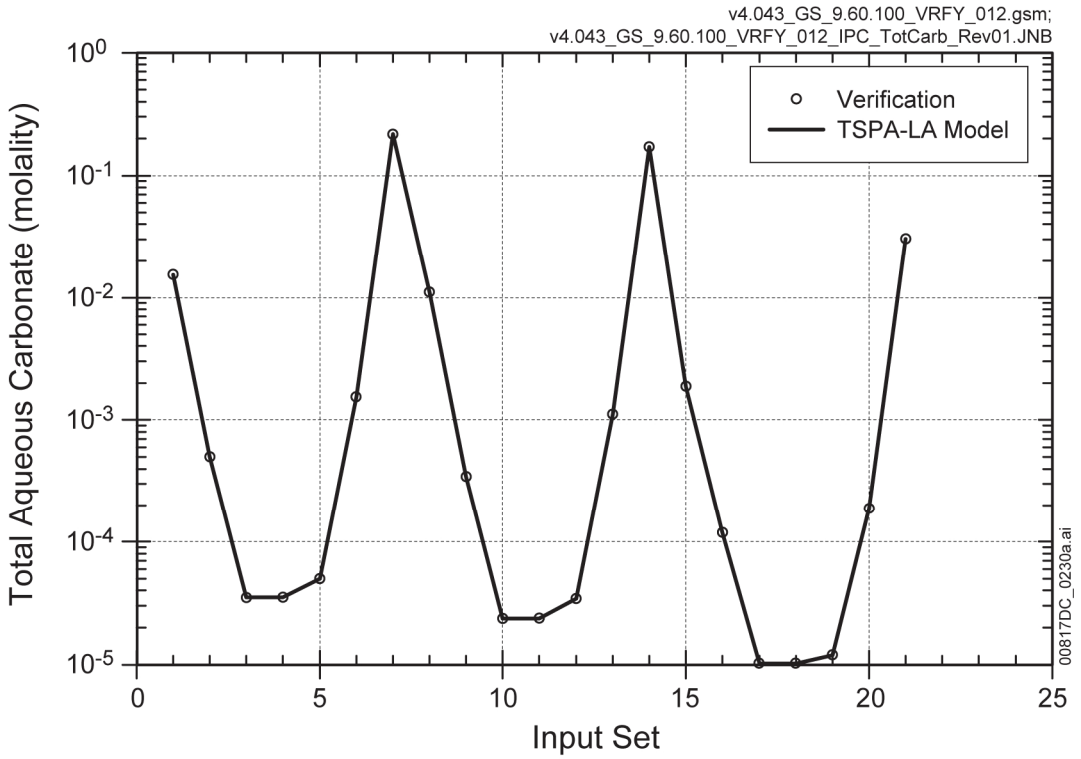

Source: Output DTN: MO0708TSPAPOST.000 [DIRS 182986].

Figure 7.2-6. Comparison of In-Package Chemistry Total Carbonate Calculations between a Stand-Alone Verification Calculation and the TSPA-LA Model

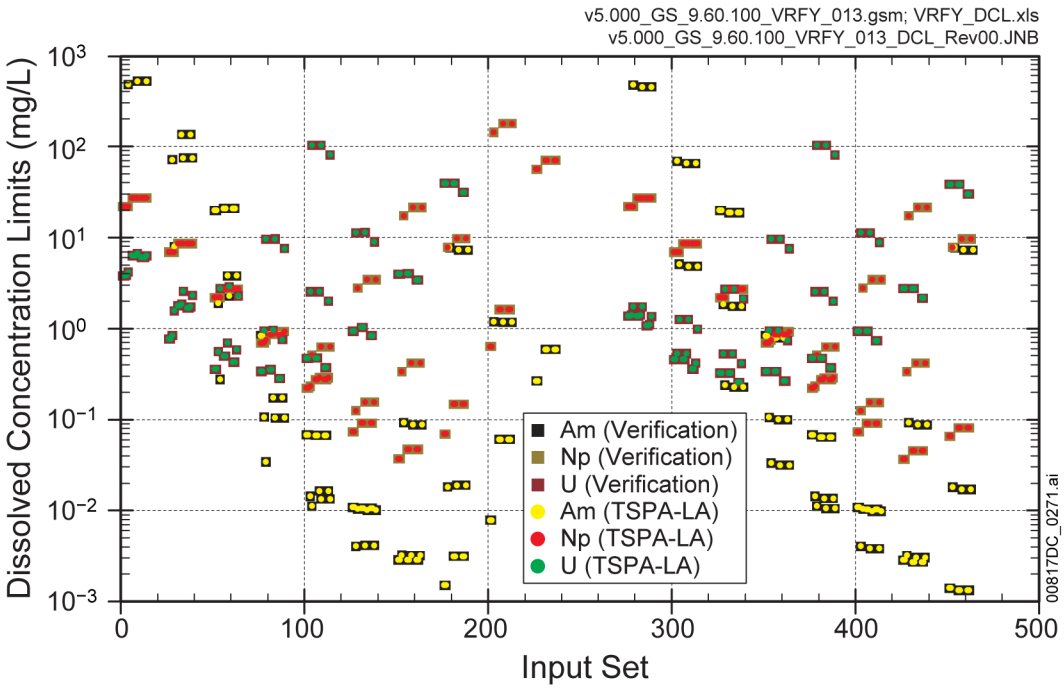

Source: Output DTN: MO0708TSPAPOST.000 [DIRS 182986].

Figure 7.2-7. Comparison of the Calculated Solubility of Americium (Am), Neptunium (Np), and Uranium (U) from the Verification of the Dissolved Concentrations Limits Submodel for the Nominal and Seismic Scenario Classes

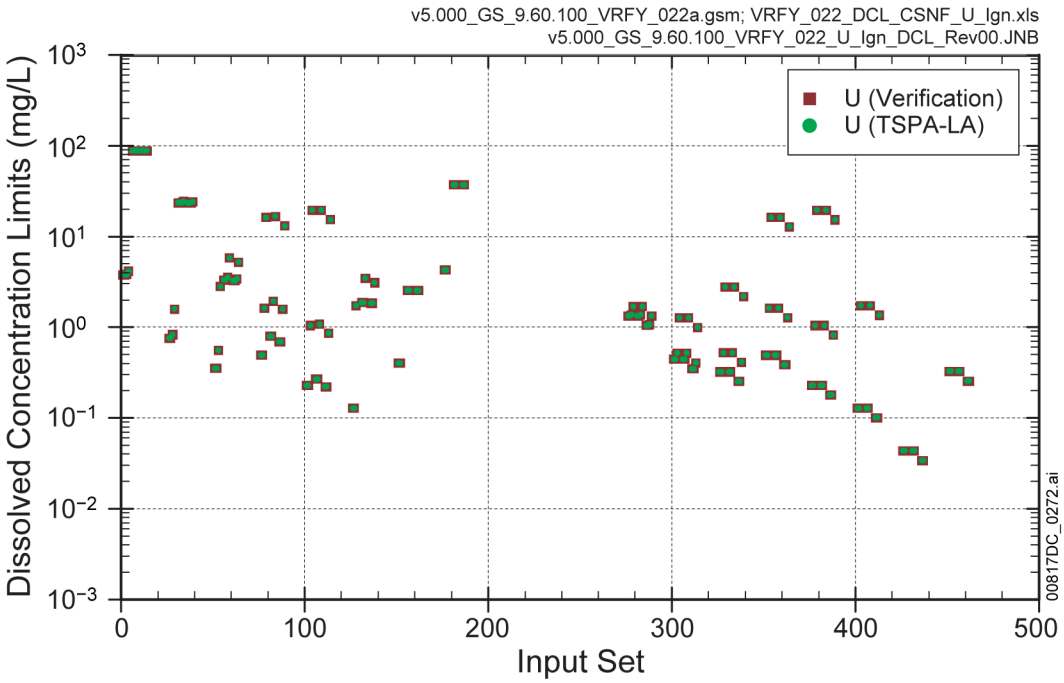

Source: Output DTN: MO0708TSPAPOST.000 [DIRS 182986].

Figure 7.2-8. Comparison of the Calculated Solubility of Uranium (U) from the Verification of the Dissolved Concentrations Limits Submodel for the Igneous Intrusion Modeling Case

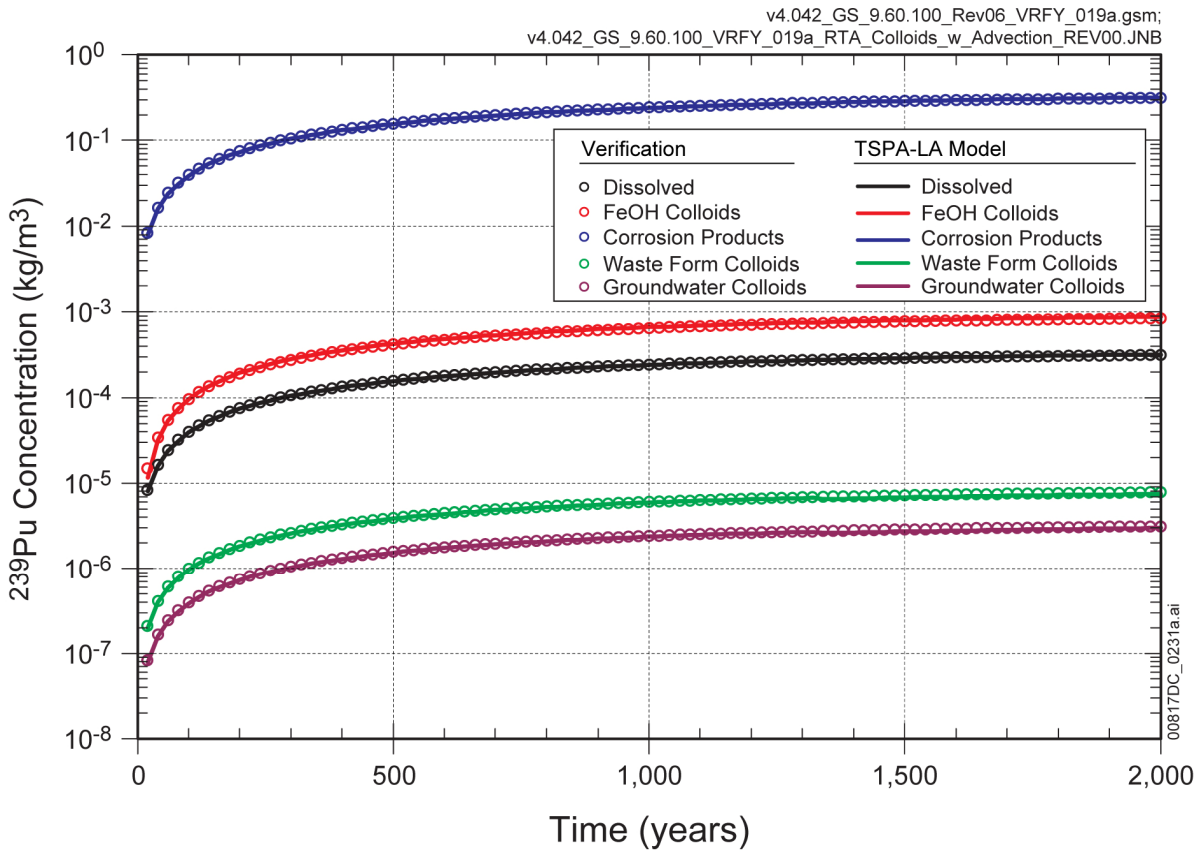

Source: Output DTN: MO0708TSPAPOST.000 [DIRS 182986].

NOTE: The verification data and the TSPA-LA Model results are represented by the open circles and solid lines, respectively.

Figure 7.2-9. Verification of the Dissolved and Colloidal Radionuclide Transport within the EBS Transport Submodel for the Case with Advection and Diffusion

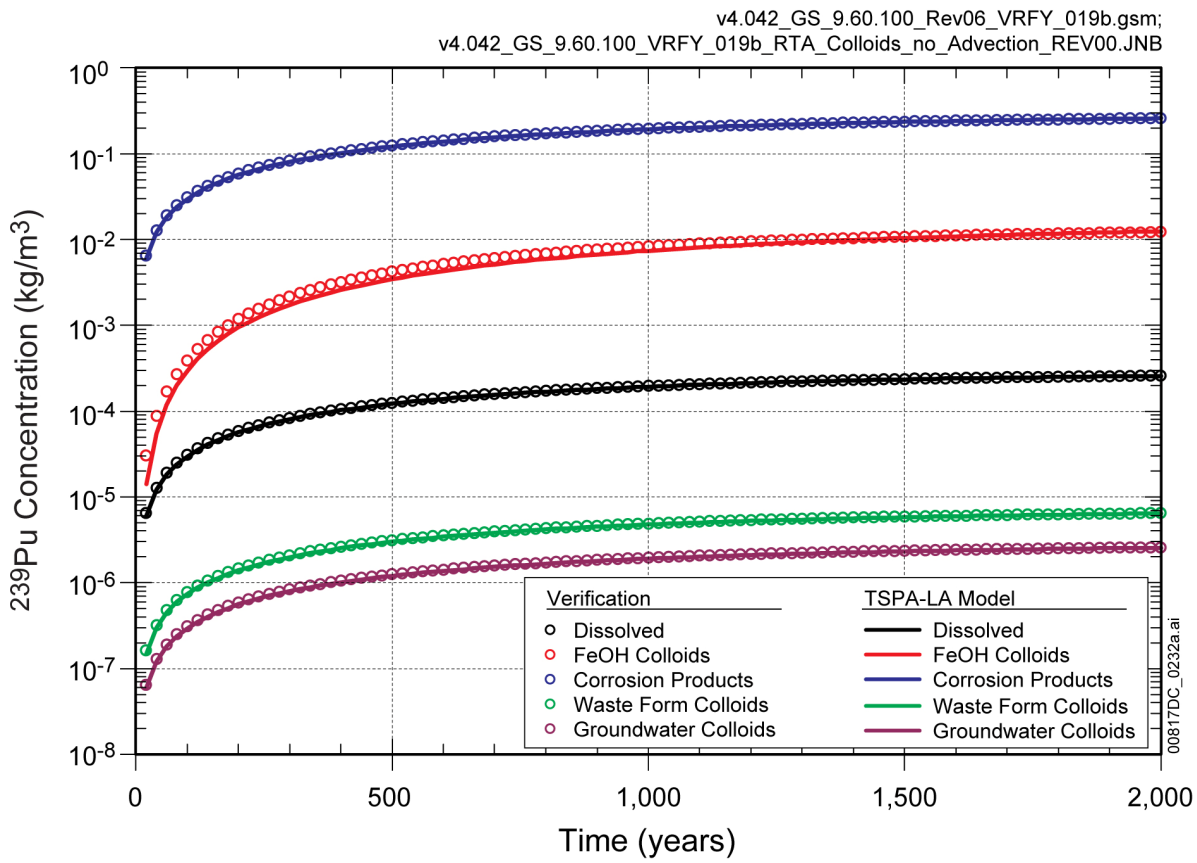

Source: Output DTN: MO0708TSPAPOST.000 [DIRS 182986].

NOTE: The verification data and the TSPA-LA Model results are represented by the open circles and solid lines, respectively.

Figure 7.2-10. Verification of the Dissolved and Colloidal Radionuclide Transport within the EBS Transport Submodel for the Case with Diffusion Only

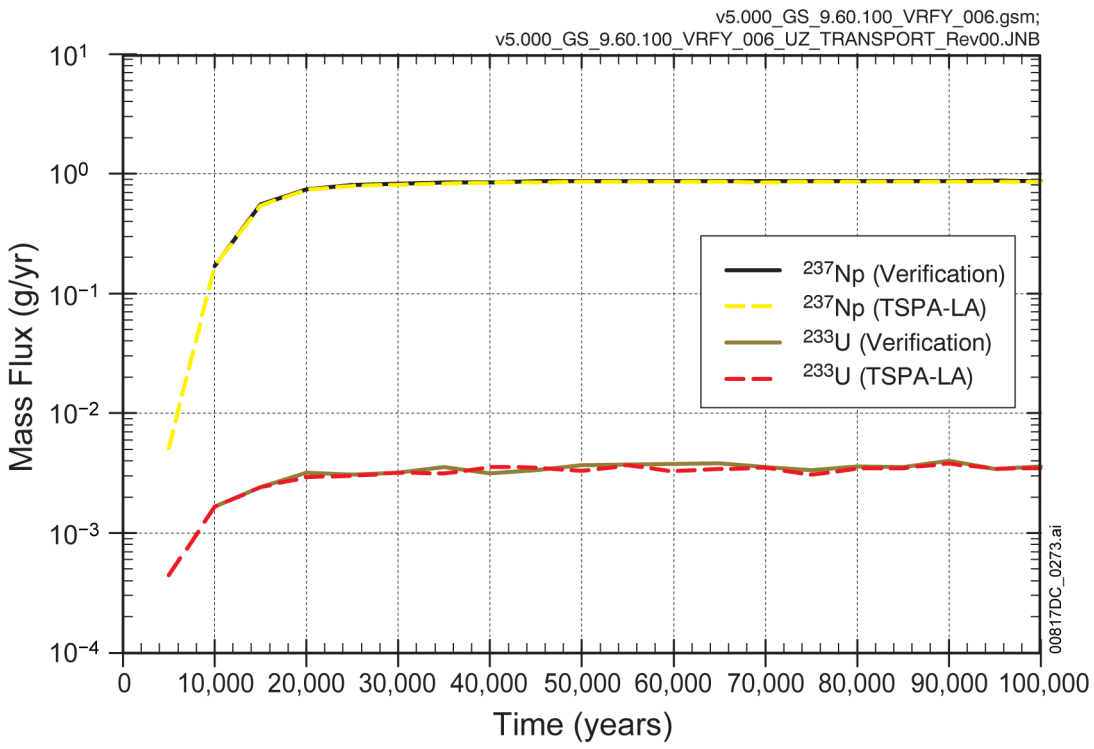

Source: Output DTN: MO0708TSPAPOST.000 [DIRS 182986].

Figure 7.2-11. Comparison of the ^{237}Np and ^{233}U Breakthrough Curves for the Verification of the Unsaturated Zone Transport Submodel

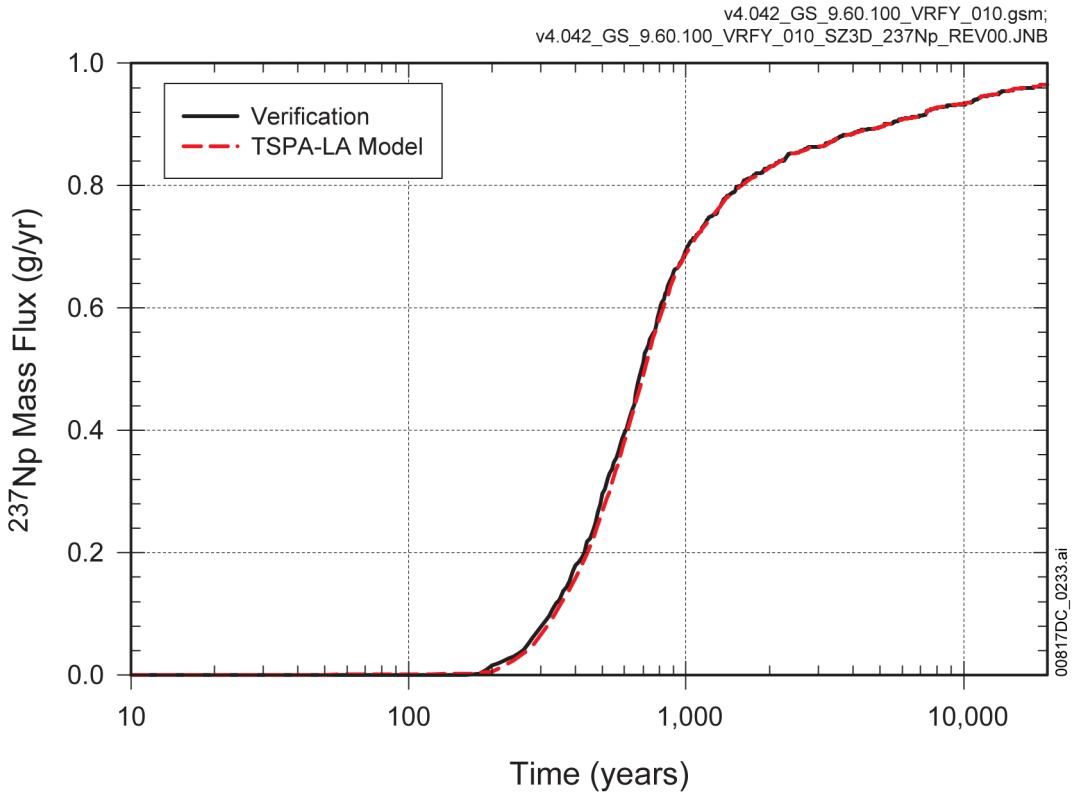

Source: Output DTN: MO0708TSPAPOST.000 [DIRS 182986].

Figure 7.2-12. Comparison of the ^{237}Np Breakthrough Curve Using the SZ_Convolute DLL in the Verification of the 3-D Saturated Zone Flow and Transport Abstraction

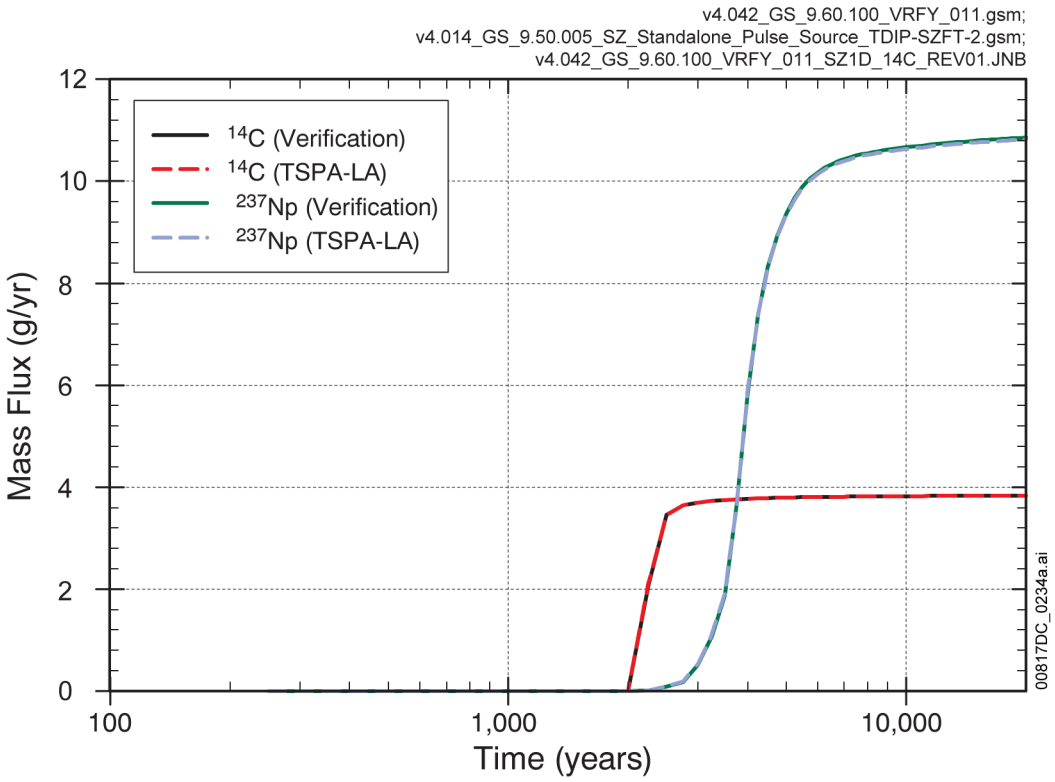

Source: Output DTN: MO0708TSPAPOST.000 [DIRS 182986].

Figure 7.2-13. Comparison of the Breakthrough Curves for ^{14}C and ^{237}Np from the Verification of the 1-D Saturated Zone Flow and Transport Abstraction

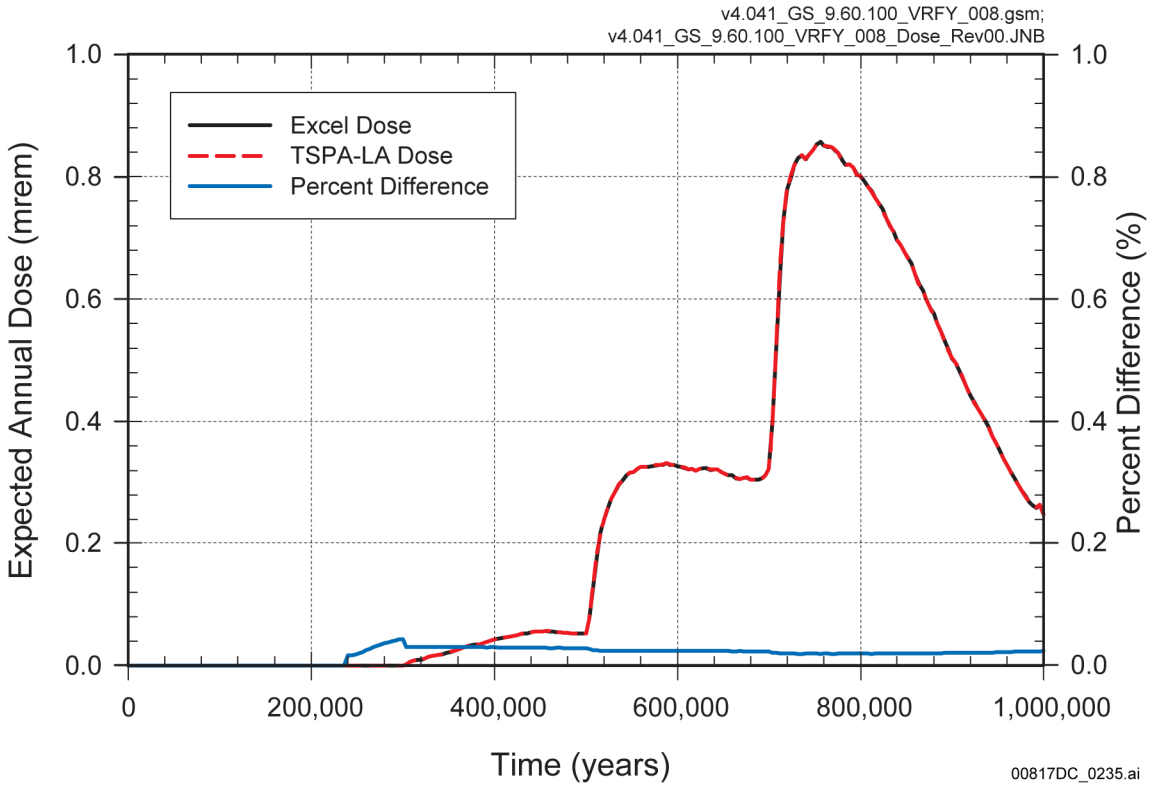

Source: Output DTN: MO0708TSPAPOST.000 [DIRS 182986].

Figure 7.2-14. Comparison of Expected Annual Dose Calculations from the Verification of the Biosphere Submodel

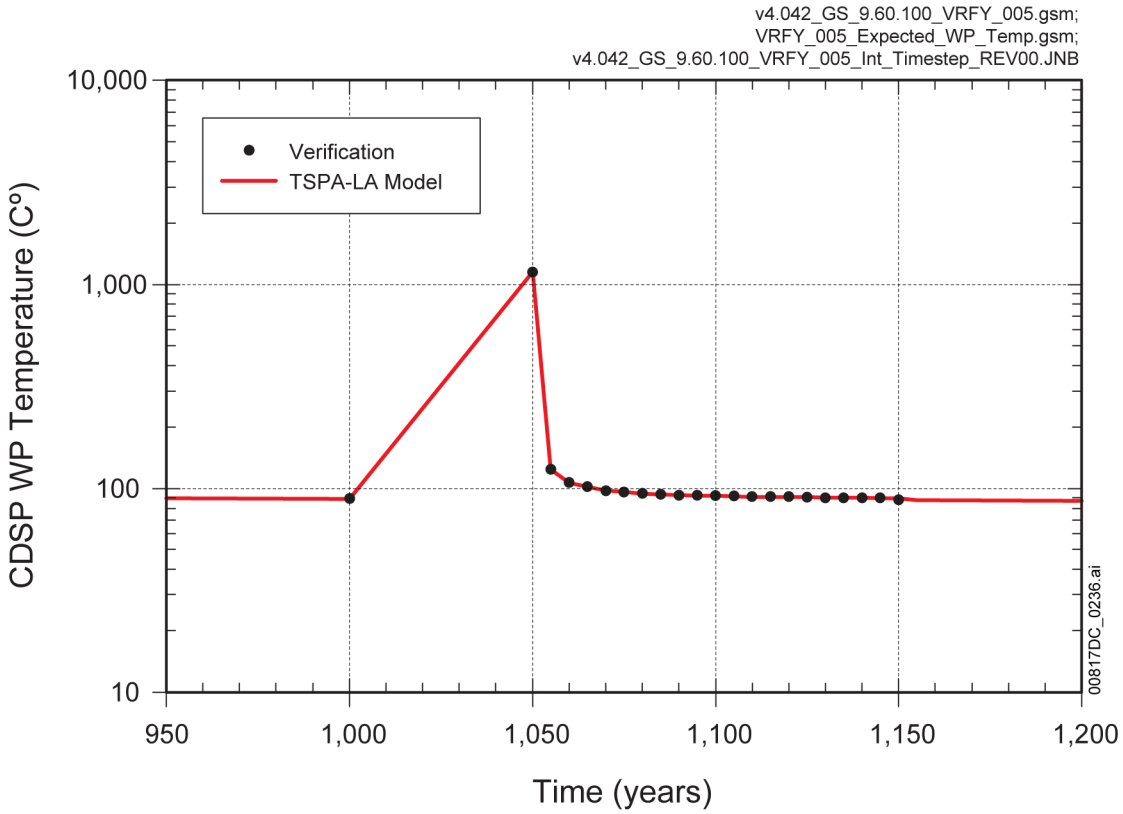

Source: Output DTN: MO0708TSPAPOST.000 [DIRS 182986].

Figure 7.2-15. Verification of the Impact on the EBS Thermal-Hydrologic Properties, as Represented by the CDSP WP Temperature, Resulting from an Igneous Intrusion Event

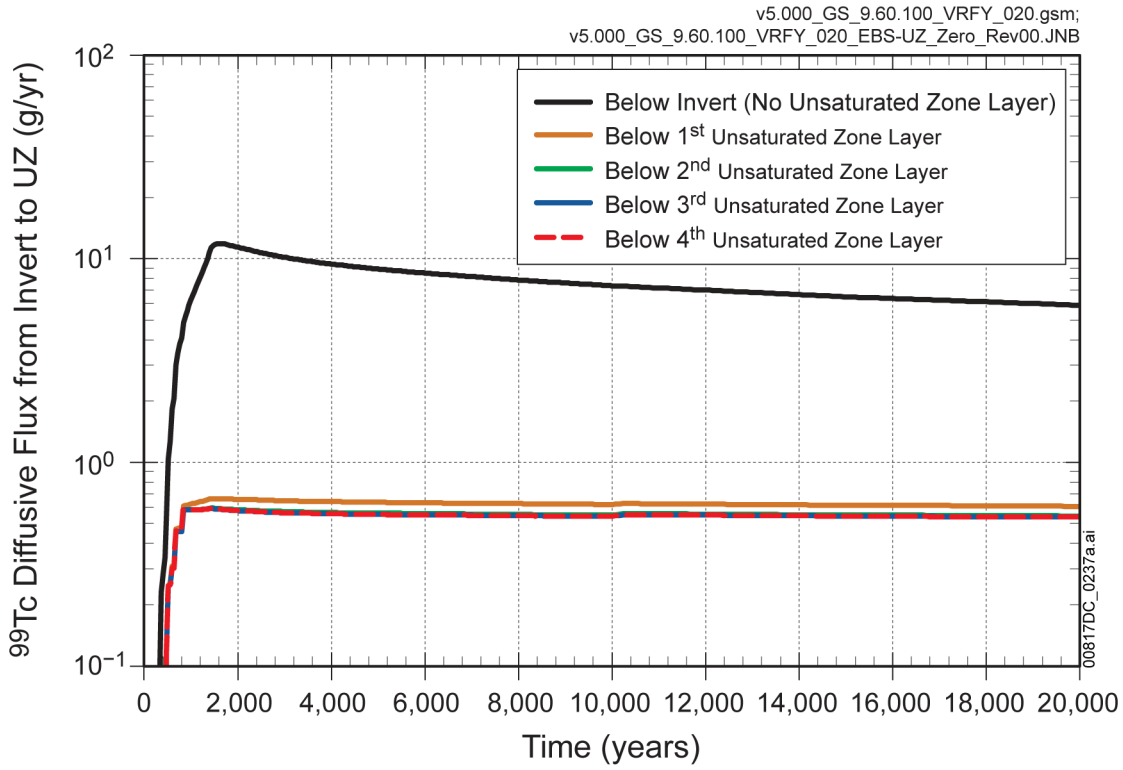

Source: Output DTN: MO0708TSPAPOST.000 [DIRS 182986].

Figure 7.2-16. Comparison of the Diffusive Flux of ^{99}Tc across the EBS-UZ Interface for Different Placement Locations of an Effective Zero-Concentration Boundary below the Invert

7.3 MODEL STABILITY

Yucca Mountain Review Plan, Final Report (NRC 2003 [DIRS 163274], Section 2.2.1.4.1.3) specifically mentions the stability of the TSPA-LA Model results as an acceptance criterion, stating:

> "A sufficient number of realizations has been obtained, for each scenario class, using the total system performance assessment code, to ensure that the results of the calculations are statistically stable."

The TSPA-LA Model is statistically stable if the mean annual dose computed by the model is stable. Demonstrating stability of the mean annual dose requires evaluation of the sufficiency of the sample size for uncertain parameters, the accuracy of numerical integration employed, and the stability of the models for physical processes with regards to discretizations of temporal and spatial variables. Stability is generally determined by demonstrating that the estimate of the mean annual dose does not depend on the sample size, the numerical integration, or on the discretizations in models for physical processes. The stability of the TSPA-LA Model results is discussed in this section.

The TSPA-LA Model computes total mean annual dose $\bar{\bar{D}}(\tau)$ at time τ by numerically evaluating

$$\begin{aligned}\bar{\bar{D}}(\tau) &= \int_{\mathcal{E}} \bar{D}(\tau|\mathbf{e})\, d_E(\mathbf{e})\, dE \\ &= \int_{\mathcal{E}} \left[\int_{\mathcal{A}} D(\tau|\mathbf{a},\mathbf{e})\, d_A(\mathbf{a})\, dA \right] d_E(\mathbf{e})\, dE\end{aligned} \qquad \text{(Eq. 7.3-1)}$$

where E is a probability space comprising the epistemic uncertain parameters, A is a probability space comprising the aleatory uncertainties that describe possible future states of the repository, and $D(\tau|\mathbf{a},\mathbf{e})$ is a function that computes the annual dose at time τ for a given element $\mathbf{e}$ in E, and $\mathbf{a}$ in A. The intermediate quantity $\bar{D}(\tau|\mathbf{e})$ is termed expected annual dose, and is more formally defined as the expectation of annual dose over aleatory uncertainty, conditional on epistemic uncertainty. Section 6.1.2 outlines the calculation of total mean annual dose, the scenario classes and modeling cases employed in this calculation, and the calculation methods used for each modeling case.

Numerical evaluation of Equation 7.3-1 involves four steps:

1. Selection of values for epistemic parameters $\mathbf{e}$ and aleatory uncertainties $\mathbf{a}$
2. Evaluation of the function $D(\tau|\mathbf{a},\mathbf{e})$ by numerically solving a complex, coupled system of differential equations describing radionuclide decay, flow, transport and other physical processes
3. Integration over aleatory uncertainty, carried out either by quadrature or Monte Carlo techniques, depending on the modeling case (see Section 6.1.2.4 for details)

4. Integration over epistemic uncertainty, conducted by a Monte Carlo technique due to the large number of epistemic parameters that define the probability space E.

These steps are carried out for each modeling case defined in Section 6.1. The results of the modeling cases are summed to compute total mean annual dose, which is the overall measure of repository compliance with the individual protection standard within 10,000 years of disposal as specified in the NRC Proposed Rule 10 CFR 63.303(a) [DIRS 178394]. The results are also used to calculate the median annual dose as the measure of compliance for the period 10,000 years after disposal through the period of geologic stability as required by NRC Proposed Rule 10 CFR 63.303(b) [DIRS 178394]. The individual protection standards for these measures of compliance are specified in 10 CFR 63.311 [DIRS 178394]. The stability of each of these three steps is examined in this section, in the reverse order listed above.

The integration over epistemic uncertainty employs Latin hypercube sampling (McKay et al. 1979 [DIRS 127905]) to sample the distributions of epistemic uncertain parameters. This sampling technique was selected, as in past TSPAs, because of the efficient manner in which it stratifies the sampling of values across the range of each uncertain variable, and the stability it provides for uncertainty and sensitivity analysis results in performance assessments of complex systems (McKay et al. 1979 [DIRS 127905]; Iman and Helton 1991 [DIRS 159039]; Helton 1999 [DIRS 159042]). Here, stability relates to how much variability takes place in the outcome of interest as model results are repeatedly calculated with different samples. Theoretical results indicate that, under certain conditions, Latin hypercube sampling does indeed exhibit better statistical convergence properties than random sampling (McKay et al. 1979 [DIRS 127905]; Stein 1987 [DIRS 159060]). However, due to the complexity of the TSPA-LA Model, it is not possible to prove that these conditions are respected. As a result, a practical method of assessing the stability of the results obtained with Latin hypercube sampling is used. Section 7.3.1 compares mean annual dose and uncertainty in the underlying distribution of expected annual dose for three independent LHSs, each of size 300. Using these three independent LHSs, confidence intervals are computed and shown. The analysis concludes that the sample size of 300 is adequate to estimate mean annual dose for each modeling case as well as to estimate total mean annual dose (summed over all modeling cases).

Section 7.3.2 discusses the numerical accuracy of the integration over aleatory uncertainty. These calculations evaluate the expected annual dose

$$\bar{D}\left(\tau\left|\mathbf{e}\right.\right) = \int_{\mathcal{A}} D\left(\tau\left|\mathbf{a},\mathbf{e}\right.\right) d_A\left(\mathbf{a}\right) dA \qquad \text{(Eq. 7.3-2)}$$

for each modeling case. Expected dose is computed either by quadrature techniques or by Monte Carlo techniques, depending on the modeling case. Quadrature integration is implemented in EXDOC_LA V2.0 (STN: 11193-2.0-00 [DIRS 182102]); Monte Carlo integration is done with GoldSim V9.60.100 (STN: 10344-9.60-01 [DIRS 181903]). Section 7.3.2 presents analyses that conclude that the discretization used for the quadrature techniques is adequate, and that the sample sizes used for the Monte Carlo techniques are sufficient.

The evaluation of annual dose, $D\left(\tau\left|\mathbf{a},\mathbf{e}\right.\right)$, involves numerical solution of a complex, couple systems of differential equations. Some of these equations are evaluated in model abstractions

provided as input to the TSPA-LA Model (as outlined in Section 6.3). The various analysis and/or model reports that document model abstractions also discuss the stability of these abstractions. Other equations are evaluated within the TSPA-LA Model, using techniques that discretize the temporal and spatial domains within which the equations are applied. Section 7.3.3 discusses the temporal discretization within the TSPA-LA Model and shows that temporal discretization is sufficient to adequately evaluate annual dose. Section 7.3.4 describes the spatial discretization employed in the TSPA-LA Model and its component abstractions and evaluates the adequacy of the percolation subregions to represent spatial variability in the TSPA-LA Model. Section 7.3.5 investigates the stability of the UZ Transport Model, which employs a particle tracking technique, by showing that a sufficient number of particles are used to obtain stable transport results.

INTENTIONALLY LEFT BLANK

7.3.1 Statistical Stability

As outlined in Section 7.3, mean annual dose is calculated as the expected value over epistemic uncertainty and aleatory uncertainty of the estimates of annual dose (Equation 7.3-1). The expectation of annual dose over aleatory uncertainty is evaluated first, the result of which is termed (for brevity) expected annual dose. The accuracy of the integral over aleatory uncertainty is discussed in Section 7.3.2. The integral of expected annual dose over epistemic uncertainty is referred to as the mean annual dose and is evaluated numerically using a Monte Carlo technique. The mean annual dose is statistically stable if the sample employed in the Monte Carlo technique produces an adequate estimate of the mean annual dose.

This section describes the replicated sampling procedure used to determine statistical stability and to compute the confidence intervals for the mean annual dose. Results are presented for each modeling case and for total mean annual dose (summed over all modeling cases). The analysis concludes that the sample size used in the Monte Carlo technique is adequate to estimate mean annual dose in each modeling case as well as to estimate the total mean annual dose. Moreover, the analysis demonstrates that the three independent replicates produce similar estimates of repository performance by comparing the mean annual dose and the distribution of uncertainty in expected annual dose among the three replicates. Therefore, the results of the TSPA-LA Model are statistically stable, and the repository performance can be evaluated by examining any one of the three generated replicates.

7.3.1.1 Replicated Sampling Procedure

As outlined in Section 6.1.3, values for epistemic parameters are selected using an LHS technique. In the TSPA-LA Model, the LHS includes 300 epistemic uncertain parameters in the groundwater model (comprising all modeling cases except the Volcanic Eruption Modeling Case) and 87 epistemic uncertain parameters in the model for the Volcanic Eruption Modeling Case. The parameters are listed in Table K.3-1. Section 7.4 describes review efforts undertaken to ensure that uncertainty in important parameters is appropriately characterized. The base sample size for the LHS is 300 for all modeling cases.

A replicated sampling procedure developed in the NRC HLW program at SNL provides an effective approach to estimating the potential sampling error in quantities derived from LHS (Iman 1982 [DIRS 146012]). With this procedure, the LHS is repeatedly generated with different random seeds. Each LHS is used to produce an estimate of the mean annual dose. The ensemble of estimates of the mean annual dose is used to compute an overall mean and standard error. Confidence intervals for the mean annual dose can then be estimated by means of the *t*-distribution. Appendix J, Section J.4.10, provides details on the replicated sampling procedure and the application of the *t*-distribution. The appropriate value for the number of replicates cannot be known with assurance before an analysis. In practice, a reasonable computational strategy is to start with a small number of replicates (e.g., three to five) and then add additional replicates if additional refinement of the confidence interval is desired.

7.3.1.2 Stability Analysis Results for Modeling Cases

The stability analysis was conducted by generating three replicates for each modeling case. The mean annual dose and statistics for the underlying distribution of uncertainty in the expected annual dose are compared for the three replicates. The three sample means are used to compute an overall mean and a 95 percent confidence interval about the overall mean. The confidence interval is displayed as an upper and lower bound. At each point in time, the true mean annual dose is less than the upper bound of the confidence interval (and greater than the lower bound) with probability 0.95.

Nominal Modeling Case—Figure 7.3.1-1(a) shows the mean annual dose for each of the three replicates of the Nominal Modeling Case, along with the median and the 5th and 95th percentiles of the distribution of uncertainty in the expected annual dose. The similarity of the median and the 5th and 95th percentiles indicates that the distributions of expected annual dose are similar in all three replicates. The means differ somewhat before 200,000 years because the mean is being determined by a very few realizations (less than 5 percent) that have corrosion failures before 200,000 years.

Figure 7.3.1-1(b) shows the mean annual dose for each of the three replicates, the overall mean, and the upper and lower bounds for the 95 percent confidence interval about the overall mean. The interval indicates that, with probability 0.975, there is no numerically significant dose from nominal processes before 100,000 years. Between 100,000 years and 300,000 years, when relatively few realizations have corrosion failures, the confidence intervals are wider than after 300,000 years, when corrosion failures are observed in many realizations. The confidence interval narrows at around 500,000 years because at that time most realizations have experienced SCC failures of WPs. Because the uncertainty in occurrence of SCC is reduced, the variability in expected dose between realizations decreases, resulting in more precise estimates of the mean and consequently narrow confidence interval about the mean. The confidence interval widens after 500,000 years because general corrosion failures begin to occur in some realizations. The uncertainty in the occurrence of general corrosion failures increases the variability in expected dose between realizations and contributes variability to the estimated mean and results in a wider confidence interval. The lower bound of the confidence interval is somewhat visually unappealing at early times because a logarithmic scale is used for display in keeping with the convention for displaying dose. However, for most of the 1,000,000-year period, the mean of each replicate is within an order of magnitude of the upper confidence interval, indicating that the true mean annual dose is estimated adequately by each of the three replicates. The similarity evident among the three replicates and the relatively small width of the confidence interval demonstrate that the sample size of 300 is adequate.

Early Failure Modeling Cases—Figure 7.3.1-2(a), shows the mean annual dose for each of the three replicates of the Waste Package EF Modeling Case for 20,000 years, along with the median and the 5th and 95th percentiles of the distribution of the expected annual dose. Figure 7.3.1-2(b) displays the confidence interval for the Waste Package EF Modeling Case for 20,000 years. Again, the lower bound of the confidence interval is visually distorted by the logarithmic scale used for dose. The similarity evident among the three replicates and the relatively small width of the confidence interval demonstrates that the mean annual dose is estimated with sufficient accuracy with the sample size of 300.

Figure 7.3.1-3(a) shows the mean annual dose for each of the three replicates of the Waste Package EF Modeling Case for 1,000,000 years, along with the median and the 5th and 95th percentiles of the distribution of uncertainty in the expected annual dose. Figure 7.3.1-3(b) displays the confidence interval for the Waste Package EF Modeling Case for 1,000,000 years. The figures indicate that the sample size for 300 is adequate to estimate the mean annual dose.

Figure 7.3.1-4(a), Figure 7.3.1-4(b), Figure 7.3.1-5(a) and Figure 7.3.1-5(b) display the mean annual dose along with the median and the 5th and 95th percentiles of expected annual dose, for each of the three replicates of the Drip Shield EF Modeling Case, and the confidence intervals for the Drip Shield EF Modeling Case, for both 20,000 years and 1,000,000 years. The figures indicate that the sample size for 300 is adequate for the Drip Shield EF Modeling Cases.

Igneous Modeling Cases—Figure 7.3.1-6(a) shows the mean annual dose for each of the three replicates of the Igneous Intrusion Modeling Case for 20,000 years, along with the median and the 5th and 95th percentiles of the distribution of the expected annual dose. Figure 7.3.1-6(b) displays the confidence interval for this modeling case. The high degree of similarity among replicates and the overall narrow confidence interval indicates that the mean annual dose for this modeling case is estimated accurately, and the sample size of 300 is adequate.

Figure 7.3.1-7(a) shows the mean annual dose for each of the three replicates of the Igneous Intrusion Modeling Case for 1,000,000 years, along with the median and the 5th and 95th percentiles of the distribution of the expected annual dose. Figure 7.3.1-7(b) displays the confidence interval for this modeling case. As in the 20,000-year calculation, the high degree of similarity among replicates and the overall narrow confidence interval indicates that the mean annual dose for this modeling case is estimated accurately, and the sample size of 300 is adequate. The confidence interval in Figure 7.3.1-7(b) narrows at 200,000 years because the means of Replicate 1 and Replicate 3 cross over, however, this narrowing of the confidence interval is an artifact of the intersection of the means, and may not represent an actual reduction in the uncertainty in the results at 200,000 years.

Figure 7.3.1-8(a), Figure 7.3.1-8(b), Figure 7.3.1-9(a), and Figure 7.3.1-9(b) display the mean annual dose along with the median and the 5th and 95th percentiles of expected annual dose, for each of the three replicates of the Volcanic Eruption Modeling Case, and the confidence intervals for this modeling case, for both 20,000 years and 1,000,000 years. The figures indicate that the sample size of 300 is adequate to estimate mean annual dose for the Volcanic Eruption Modeling Cases.

Seismic Modeling Cases—Figure 7.3.1-10(a) shows the mean annual dose for each of the three replicates of the Seismic GM Modeling Case for 20,000 years, along with the median and the 5th and 95th percentiles of the distribution of the expected annual dose. Figure 7.3.1-10(b) displays the confidence interval for this modeling case. The high degree of similarity among replicates and the very narrow confidence interval indicates that the mean annual dose for this modeling case is estimated accurately, and the sample size of 300 is adequate.

Figure 7.3.1-11(a) shows the mean annual dose for each of the three replicates of the Seismic GM Modeling Case for 1,000,000 years, along with the median and the 5th and 95th percentiles of the distribution of the expected annual dose. Figure 7.3.1-11(b) displays the confidence

interval for this modeling case. Because the Seismic GM Modeling Case employs a Monte Carlo technique for 1,000,000 years and a quadrature technique for 20,000 years (Section 6.1.2.4), the 1,000,000-year results are not as smooth as the 20,000 year results. However, the distribution of expected annual dose compares very well between the three replicates, and the confidence interval indicates that the mean annual dose is estimated well within an order of magnitude. Therefore, the sample size of 300 is adequate for estimating mean annual dose in this modeling case.

Figure 7.3.1-12(a) shows the mean annual dose for each of the three replicates of the Seismic FD Modeling Case for 20,000 years, along with the median and the 5th and 95th percentiles of the distribution of the expected annual dose. Figure 7.3.1-12(b) displays the confidence interval for this modeling case. The high degree of similarity among replicates and the very narrow confidence interval indicates that the mean annual dose for this modeling case is estimated accurately, and the sample size of 300 is adequate.

Figure 7.3.1-13(a) and Figure 7.3.1-13(b) display the distributions of expected annual dose and the confidence interval for the Seismic FD Modeling Case for 1,000,000 years. The figures indicate that the sample size of 300 is adequate to estimate mean annual dose for this modeling case.

Human Intrusion Modeling Case—Figure 7.3.1-14(a) shows the mean annual dose for each of the three replicates of the Human Intrusion Modeling Case, along with the median and the 5th and 95th percentiles of the distribution of the expected annual dose. Figure 7.3.1-14(b) displays the confidence interval for this modeling case. The high degree of similarity among replicates and the very narrow confidence interval indicates that the mean annual dose for this modeling case is estimated accurately, and the sample size of 300 is adequate.

7.3.1.3 Stability Analysis Results for Total Mean Annual Dose

Total mean annual dose is computed by summing the results of each modeling case, except for the Human Intrusion Modeling Case. The distribution of total expected annual dose is first obtained by summing the expected annual doses for each modeling case by epistemic sample element, resulting in one total expected annual dose history for each sample element. The mean of the distribution of total expected annual dose is the total mean annual dose.

Stability of the total mean annual dose is determined by computing the distribution of total expected annual dose for each of the three replicated LHS samples, and by computing the confidence interval using the total mean annual doses for the three replicates. Figure 7.3.1-15(a) shows the total mean annual dose for the three replicates for 20,000 years, along with the median and the 5th and 95th percentiles of the distribution of the total expected annual dose. Figure 7.3.1-15(a) indicates that the means from each replicate differ by approximately a factor of 2. These differences are attributable to the differences in the sampling of parameters for each replicate, and could be reduced if the sample size was increased. Figure 7.3.1-15(b) displays the confidence interval for total mean annual dose for 20,000 years, and shows that, with probability 0.975, the true mean is estimated to lie more than an order of magnitude below the regulatory standard specified in 10 CFR 63.311 [DIRS 178394]. Therefore, the high degree of similarity among replicates, the very narrow confidence interval, and the large separation between the

confidence interval and the regulatory limit relative to the width of the confidence interval indicates that total mean annual dose is estimated with sufficient accuracy, and the sample size of 300 is adequate. The stability evident in the total mean annual dose for 20,000 years is primarily due to the stability of the mean annual dose results for the Seismic GM Modeling Case for 20,000 years (Figure 7.3.1-10b) and for the Igneous Intrusion Modeling Case for 20,000 years (Figure 7.3.1-6b) because these two modeling cases constitute almost all of the total mean annual dose (Figure 8.1-3a).

Figure 7.3.1-16(a) and Figure 7.3.1-16(b) display the distributions of total expected annual dose and the confidence interval for total mean annual dose for 1,000,000 years. The figures indicate that the total mean annual dose is estimated with sufficient accuracy, and that the sample size of 300 is adequate. The stability evident in the total mean annual dose for 1,000,000 years is primarily due to the stability of the mean annual dose results for the Seismic GM Modeling Case for 1,000,000 years (Figure 7.3.1-11b) and for the Igneous Intrusion Modeling Case for 1,000,000 years (Figure 7.3.1-7b) because these two modeling cases constitute almost all of the total mean annual dose (Figure 8.1-3b).

7.3.1.4 Conclusion

Statistical stability of the total mean annual dose was evaluated by means of a replicated sampling procedure. Three independent LHSs of epistemic uncertain parameters were generated, and with these LHSs, three estimates of total mean annual dose were computed using the TSPA-LA Model. Comparison of these three estimates of total mean annual dose and the associated distributions of uncertainty in expected annual dose showed that the three independent LHSs produced statistically similar values of the total mean annual dose, as well as similar distributions of uncertainty in expected annual dose. The analysis concludes that the results of the TSPA-LA Model are statistically stable. Moreover, the similarity between replicates demonstrates that repository performance can be evaluated using any one of the three replicates. Consequently, Replicate 1 was selected for analysis and evaluation. The model results presented in this report are all taken from Replicate 1.

INTENTIONALLY LEFT BLANK

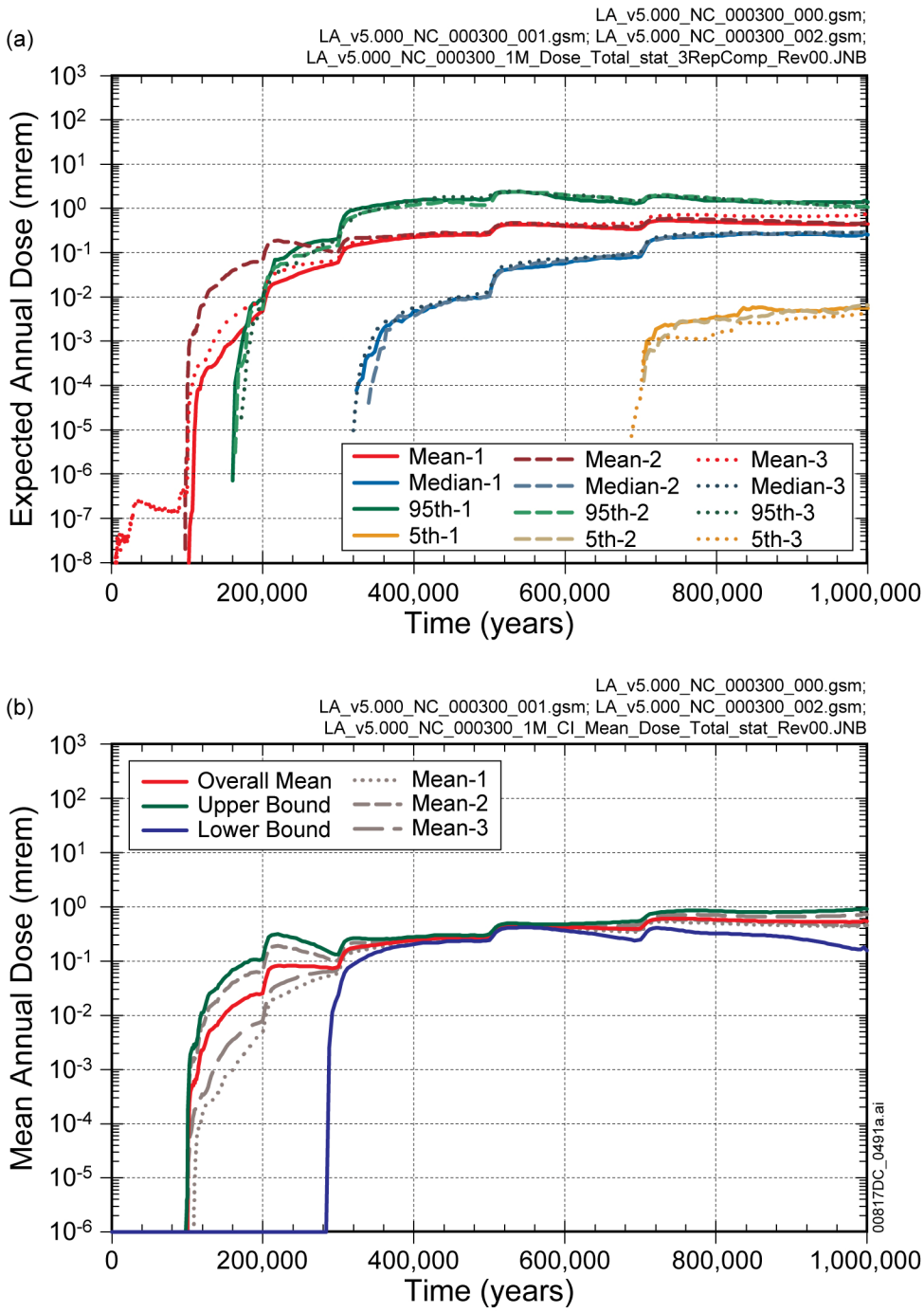

Source: Output DTNs: MO0709TSPASTAB.000 [DIRS 182983]; and MO0709TSPAREGS.000 [DIRS 182976].

Figure 7.3.1-1. Stability of Nominal Modeling Case: (a) Comparison of Expected Annual Dose for Three Replicates and (b) Confidence Interval around Mean Annual Dose

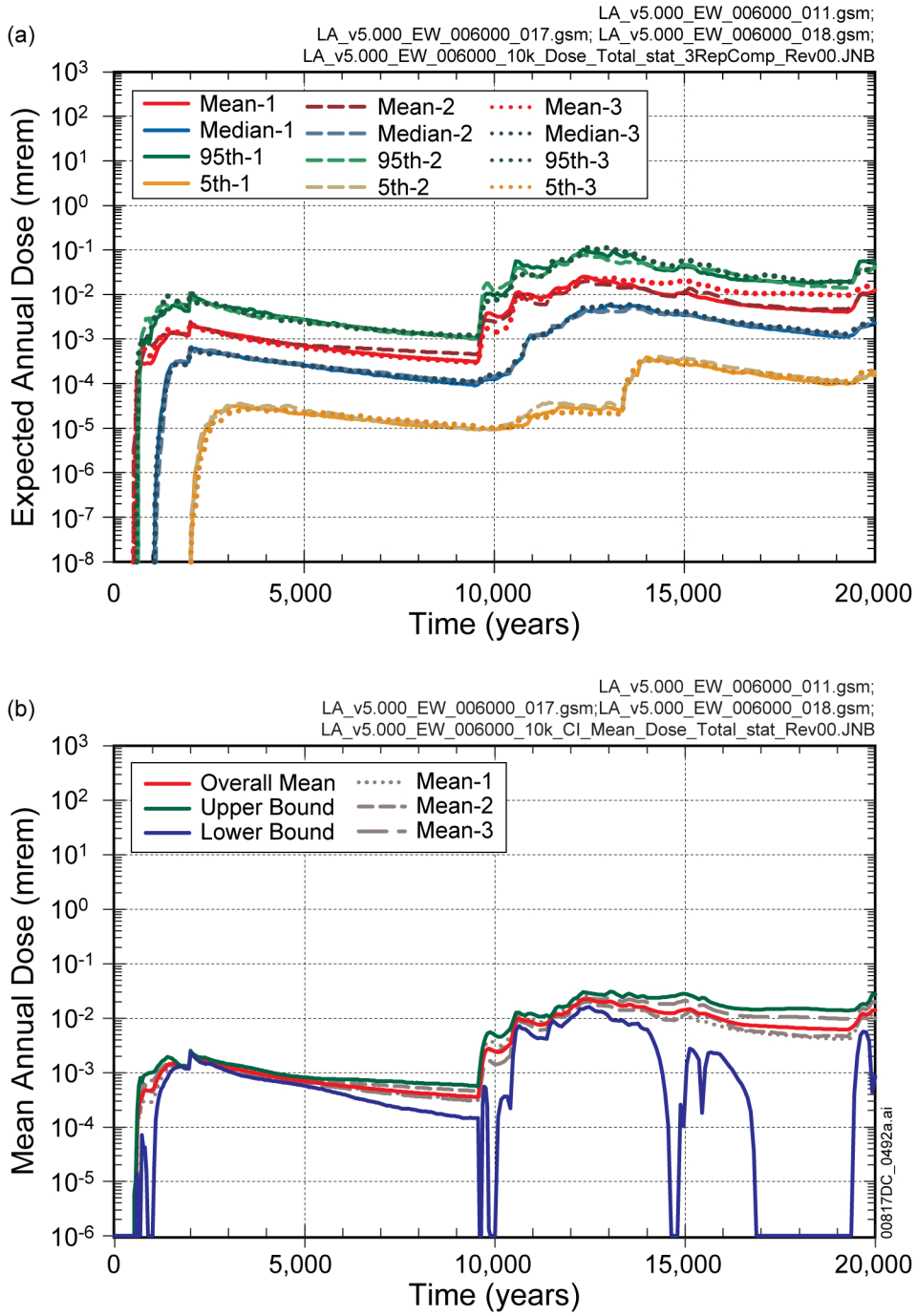

Source: Output DTNs: MO0709TSPASTAB.000 [DIRS 182983]; and MO0709TSPAREGS.000 [DIRS 182976].

Figure 7.3.1-2. Stability of Waste Package Early Failure Modeling Case for 20,000 Years: (a) Comparison of Expected Annual Dose for Three Replicates and (b) Confidence Interval around Mean Annual Dose

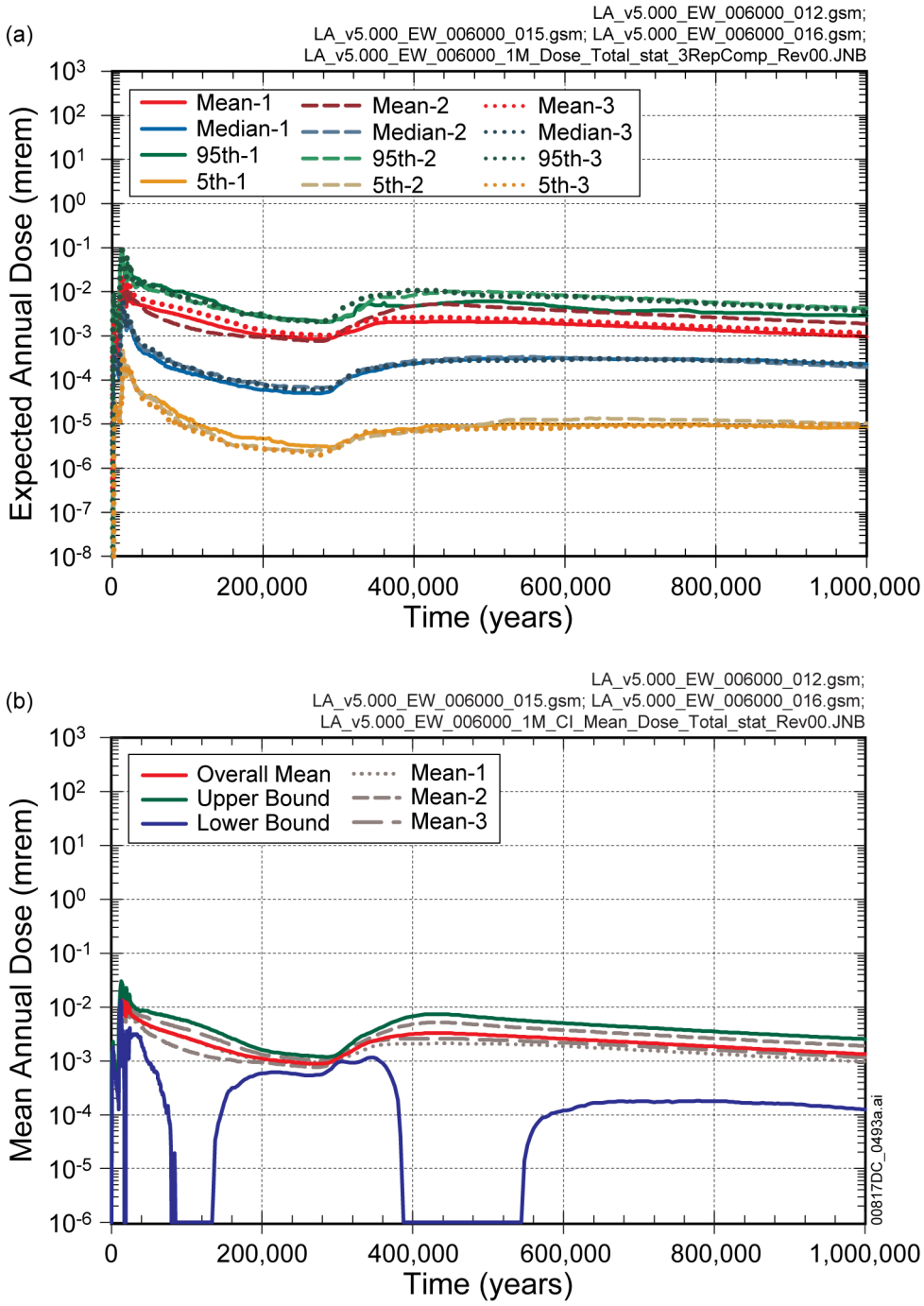

Source: Output DTNs: MO0709TSPASTAB.000 [DIRS 182983]; and MO0709TSPAREGS.000 [DIRS 182976].

Figure 7.3.1-3. Stability of Waste Package Early Failure Modeling Case for 1,000,000 Years: (a) Comparison of Expected Annual Dose for Three Replicates and (b) Confidence Interval around Mean Annual Dose

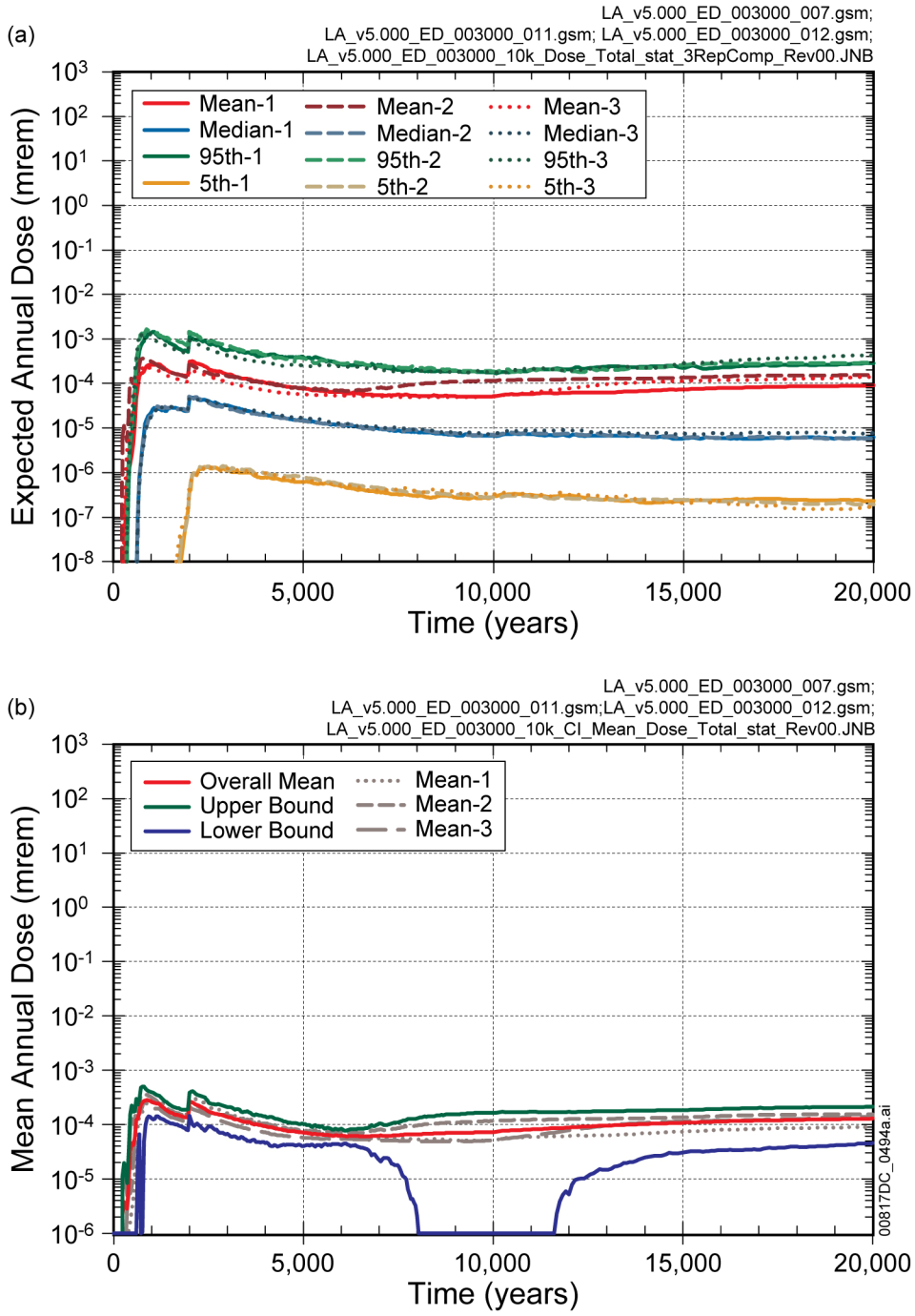

Source: Output DTNs: MO0709TSPASTAB.000 [DIRS 182983]; and MO0709TSPAREGS.000 [DIRS 182976].

Figure 7.3.1-4. Stability of Drip Shield Early Failure Modeling Case for 20,000 Years: (a) Comparison of Expected Annual Dose for Three Replicates and (b) Confidence Interval around Mean Annual Dose

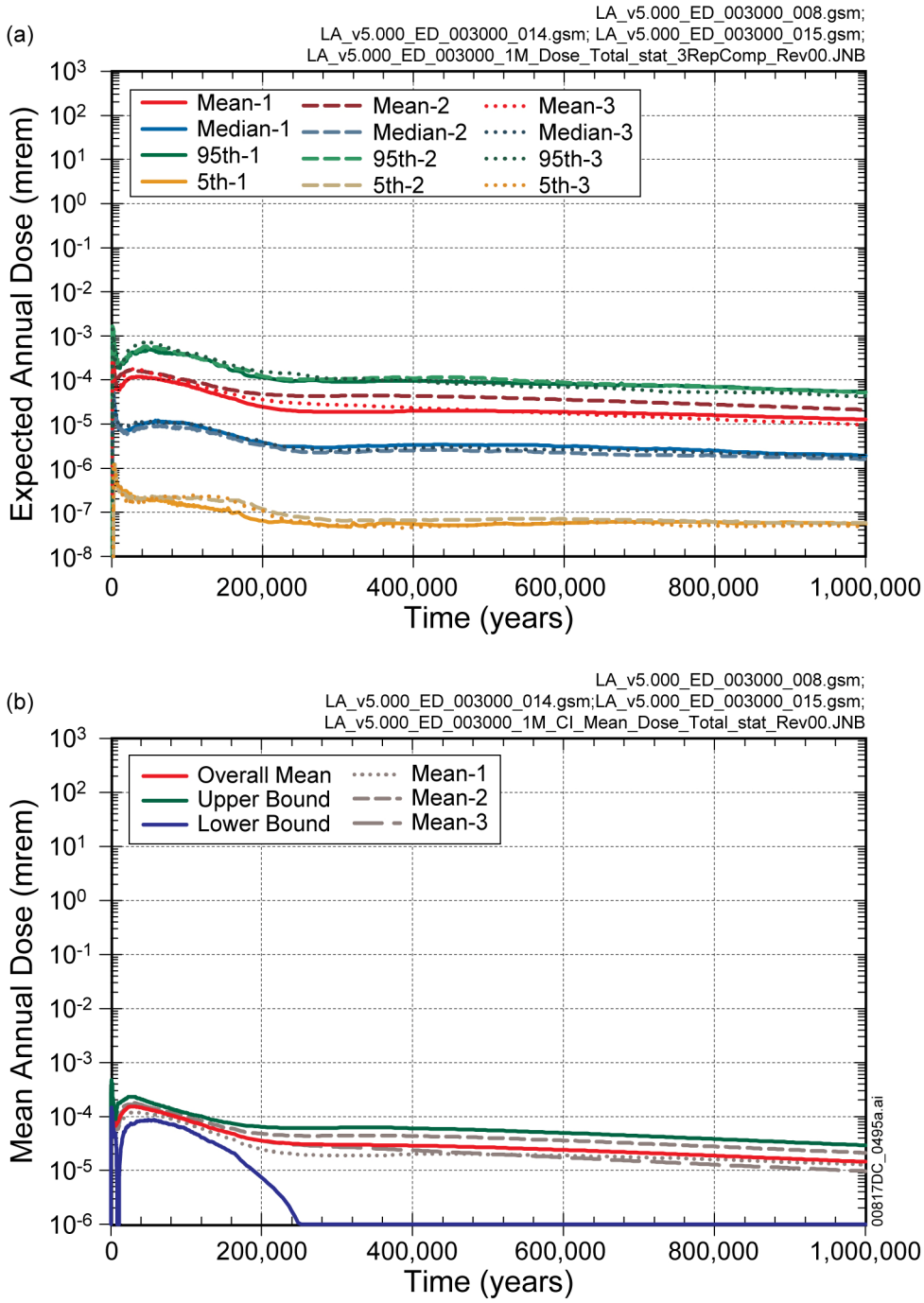

Source: Output DTNs: MO0709TSPASTAB.000 [DIRS 182983]; and MO0709TSPAREGS.000 [DIRS 182976].

Figure 7.3.1-5. Stability of Drip Shield Early Failure Modeling Case for 1,000,000 Years: (a) Comparison of Expected Annual Dose for Three Replicates and (b) Confidence Interval around Mean Annual Dose

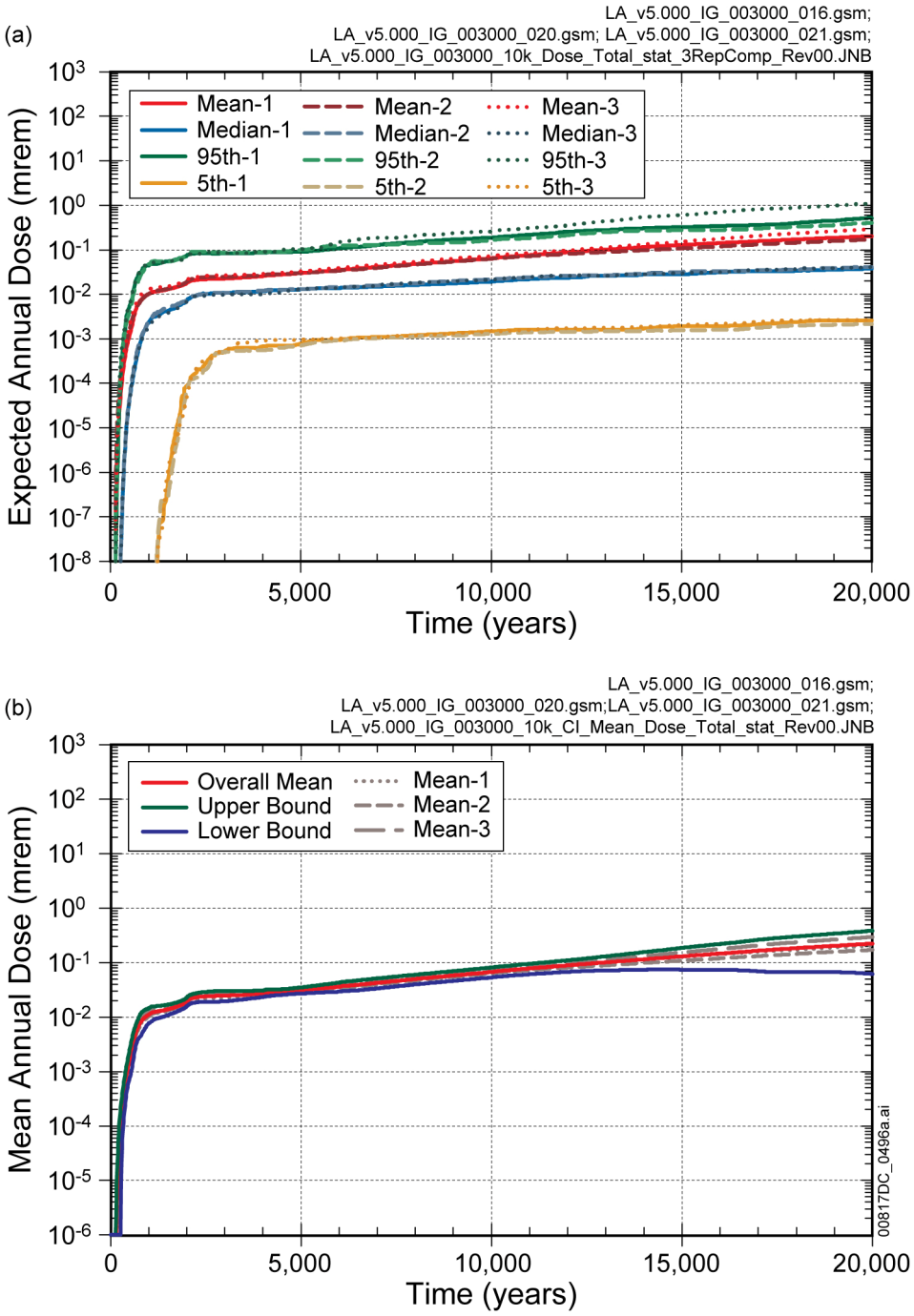

Source: Output DTNs: MO0709TSPASTAB.000 [DIRS 182983]; and MO0709TSPAREGS.000 [DIRS 182976].

Figure 7.3.1-6. Stability of Igneous Intrusion Modeling Case for 20,000 Years: (a) Comparison of Expected Annual Dose for Three Replicates and (b) Confidence Interval around Mean Annual Dose

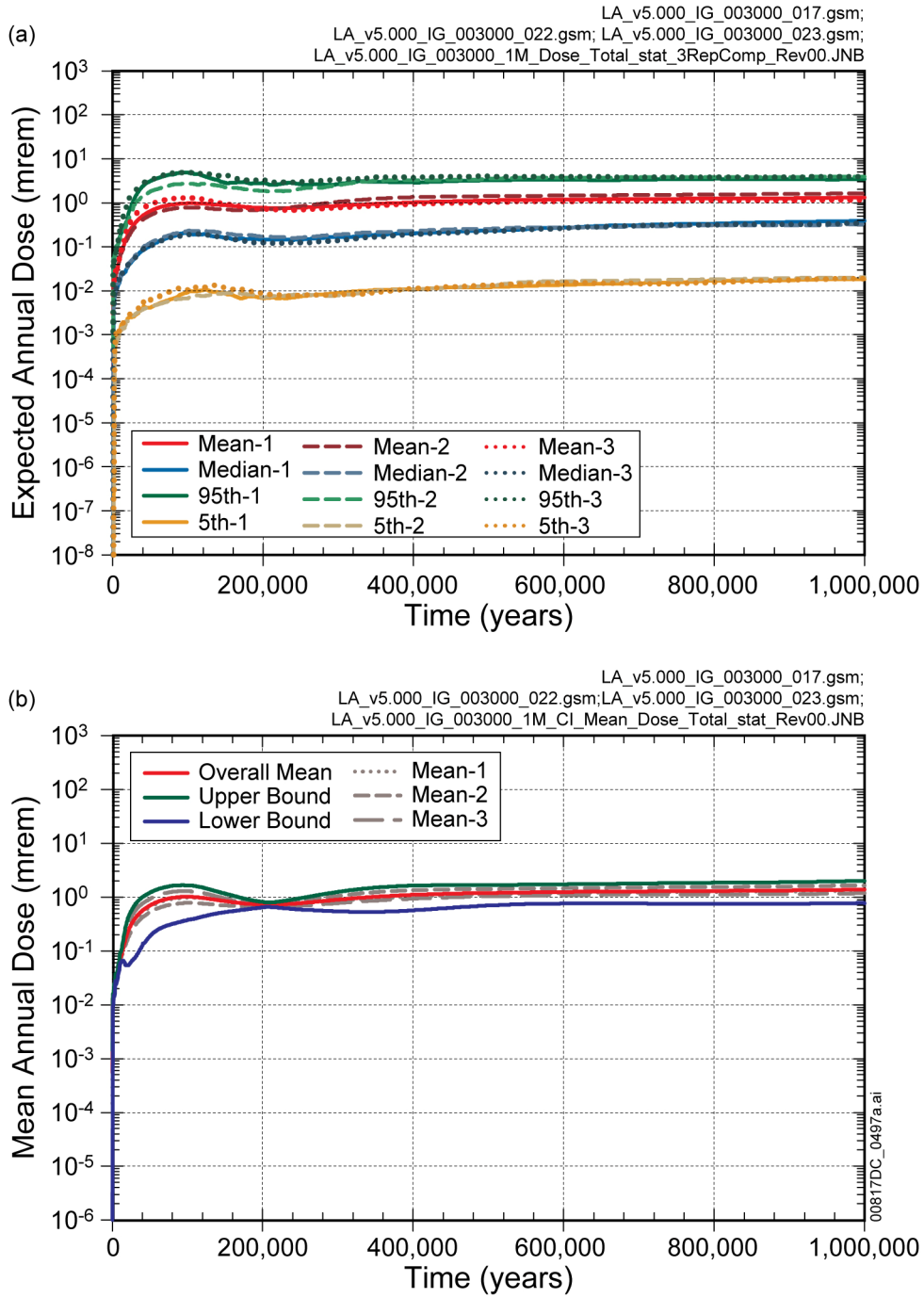

Source: Output DTNs: MO0709TSPASTAB.000 [DIRS 182983]; and MO0709TSPAREGS.000 [DIRS 182976].

Figure 7.3.1-7. Stability of Igneous Intrusion Modeling Case for 1,000,000 Years: (a) Comparison of Expected Annual Dose for Three Replicates and (b) Confidence Interval around Mean Annual Dose

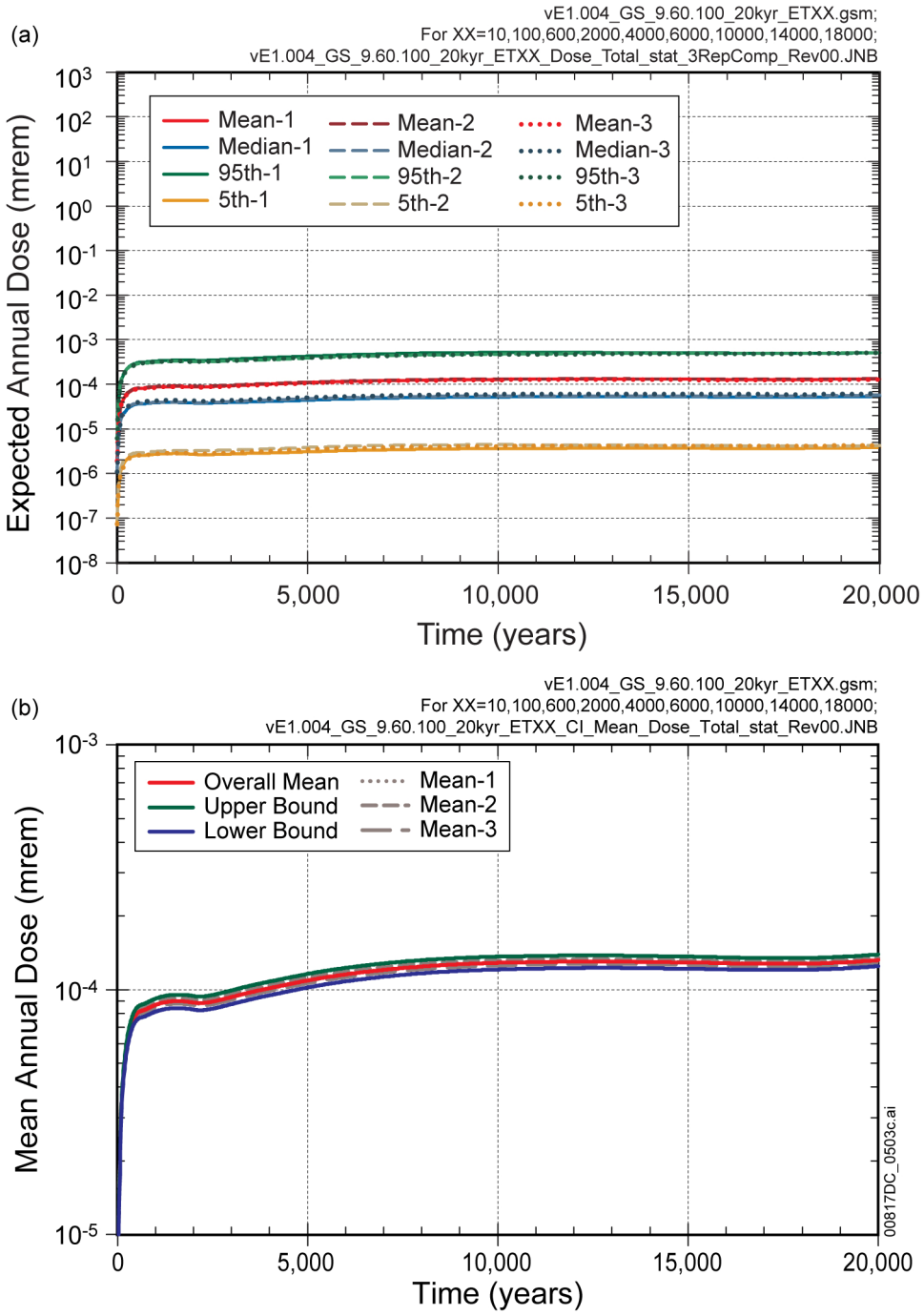

Source: Output DTN: MO0709TSPAREGS.000 [DIRS 182976].

Figure 7.3.1-8. Stability of Volcanic Eruption Modeling Case for 20,000 Years: (a) Comparison of Expected Annual Dose for Three Replicates and (b) Confidence Interval around Mean Annual Dose

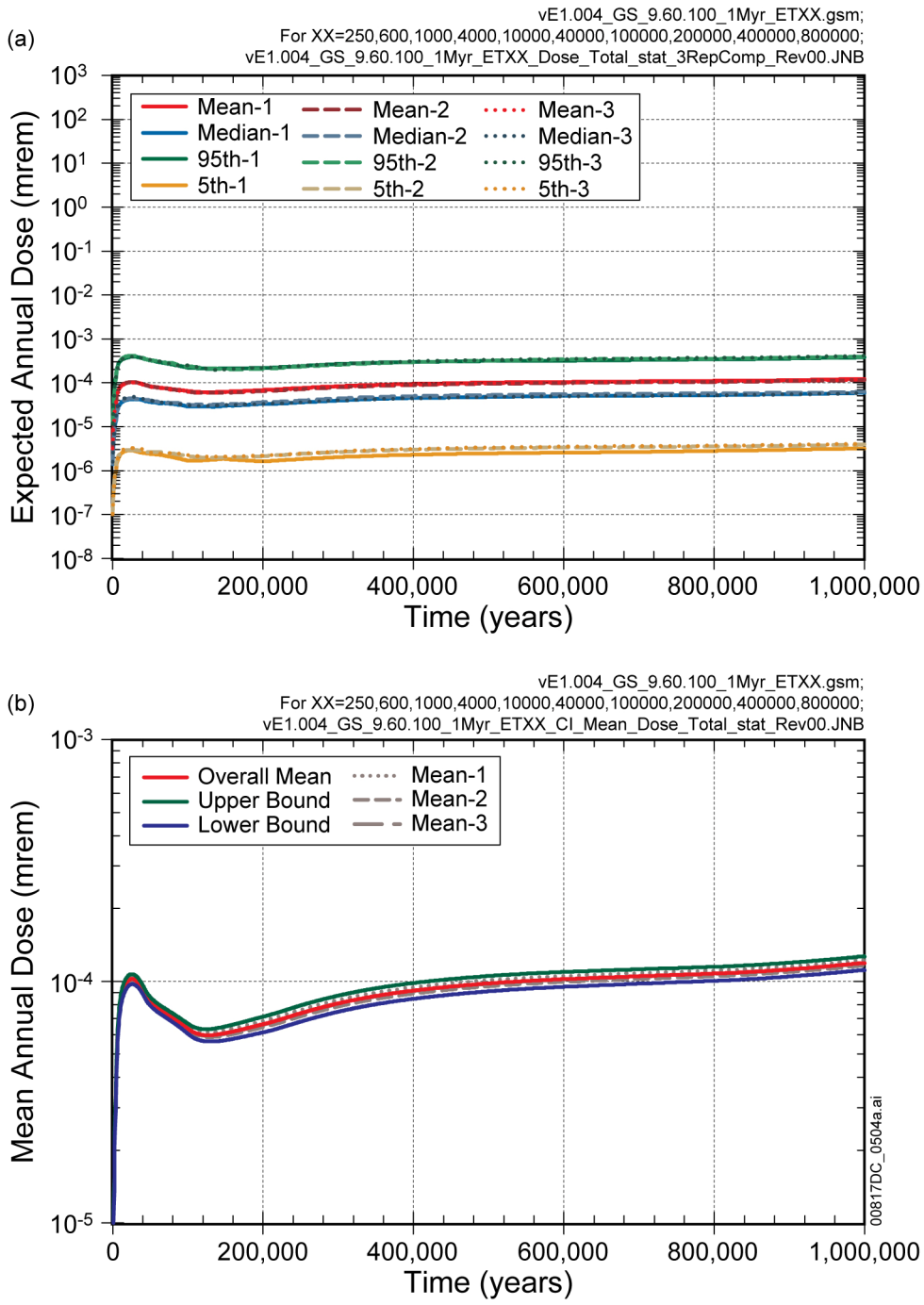

Source: Output DTN: MO0709TSPAREGS.000 [DIRS 182976].

Figure 7.3.1-9. Stability of Volcanic Eruption Modeling Case for 1,000,000 Years: (a) Comparison of Expected Annual Dose for Three Replicates and (b) Confidence Interval around Mean Annual Dose

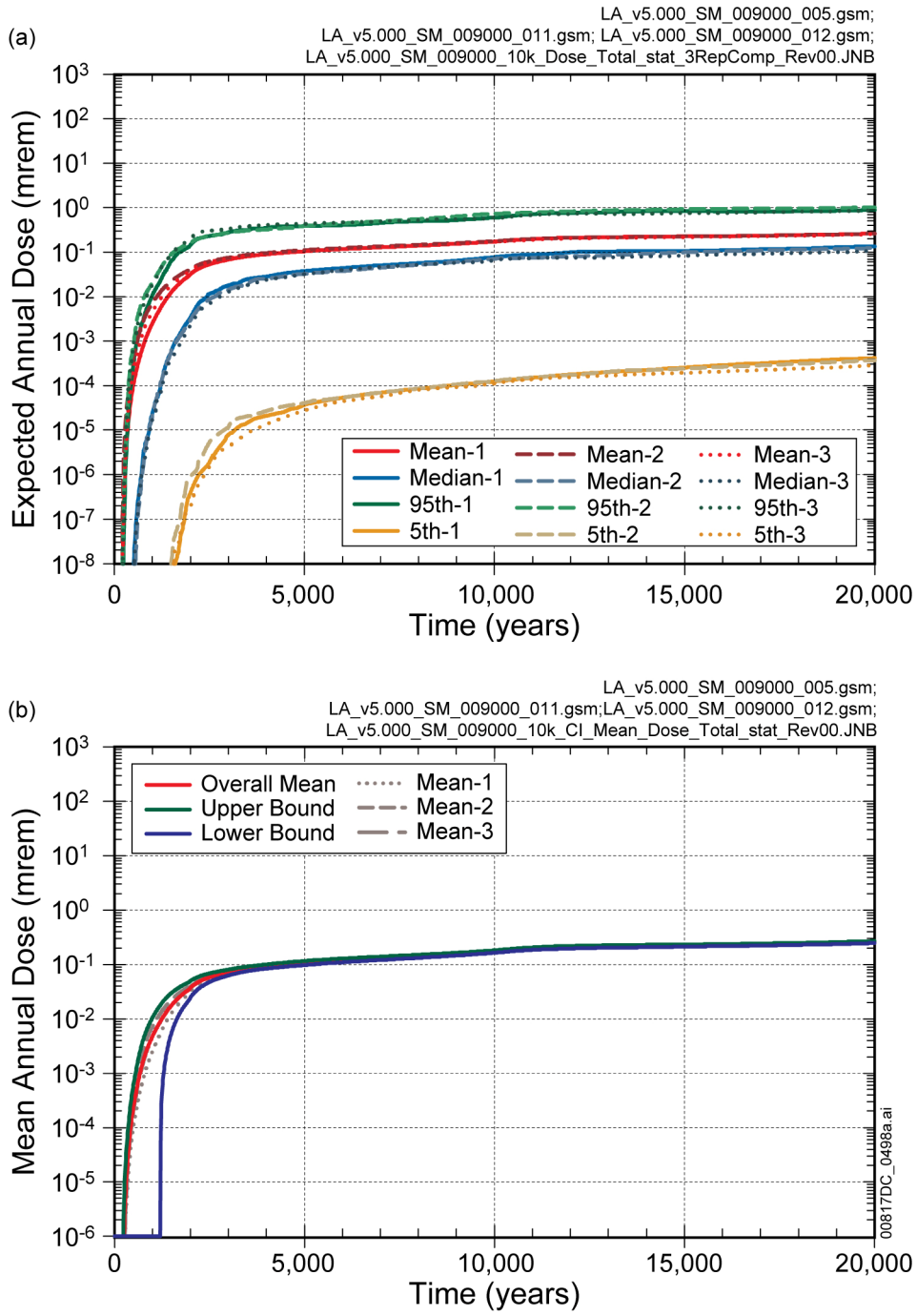

Source: Output DTNs: MO0709TSPASTAB.000 [DIRS 182983]; and MO0709TSPAREGS.000 [DIRS 182976].

Figure 7.3.1-10. Stability of Seismic Ground Motion Modeling Case for 20,000 Years: (a) Comparison of Expected Annual Dose for Three Replicates and (b) Confidence Interval around Mean Annual Dose

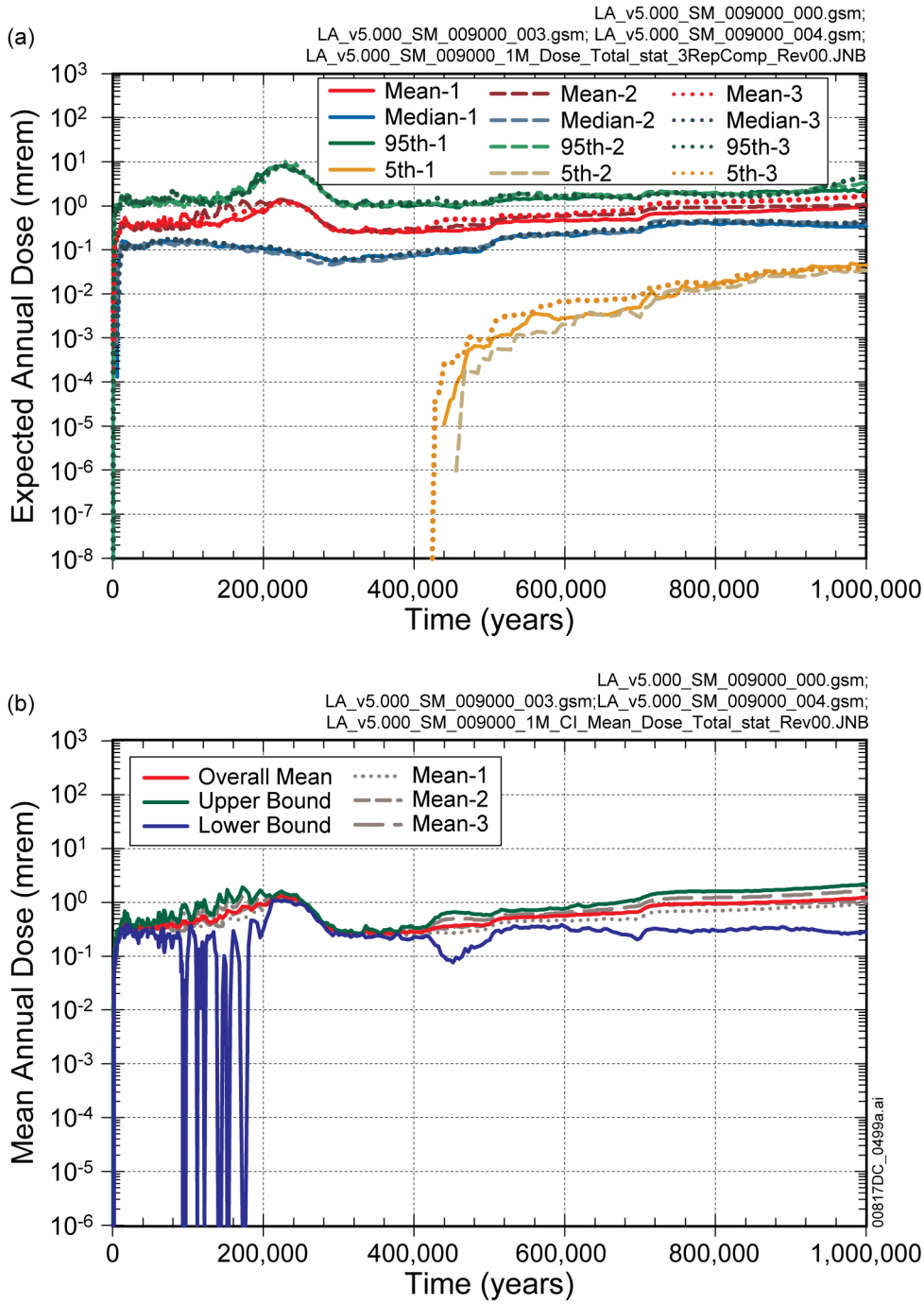

Source: Output DTNs: MO0709TSPASTAB.000 [DIRS 182983]; and MO0709TSPAREGS.000 [DIRS 182976].

Figure 7.3.1-11. Stability of Seismic Ground Motion Modeling Case for 1,000,000 Years: (a) Comparison of Expected Annual Dose for Three Replicates and (b) Confidence Interval around Mean Annual Dose

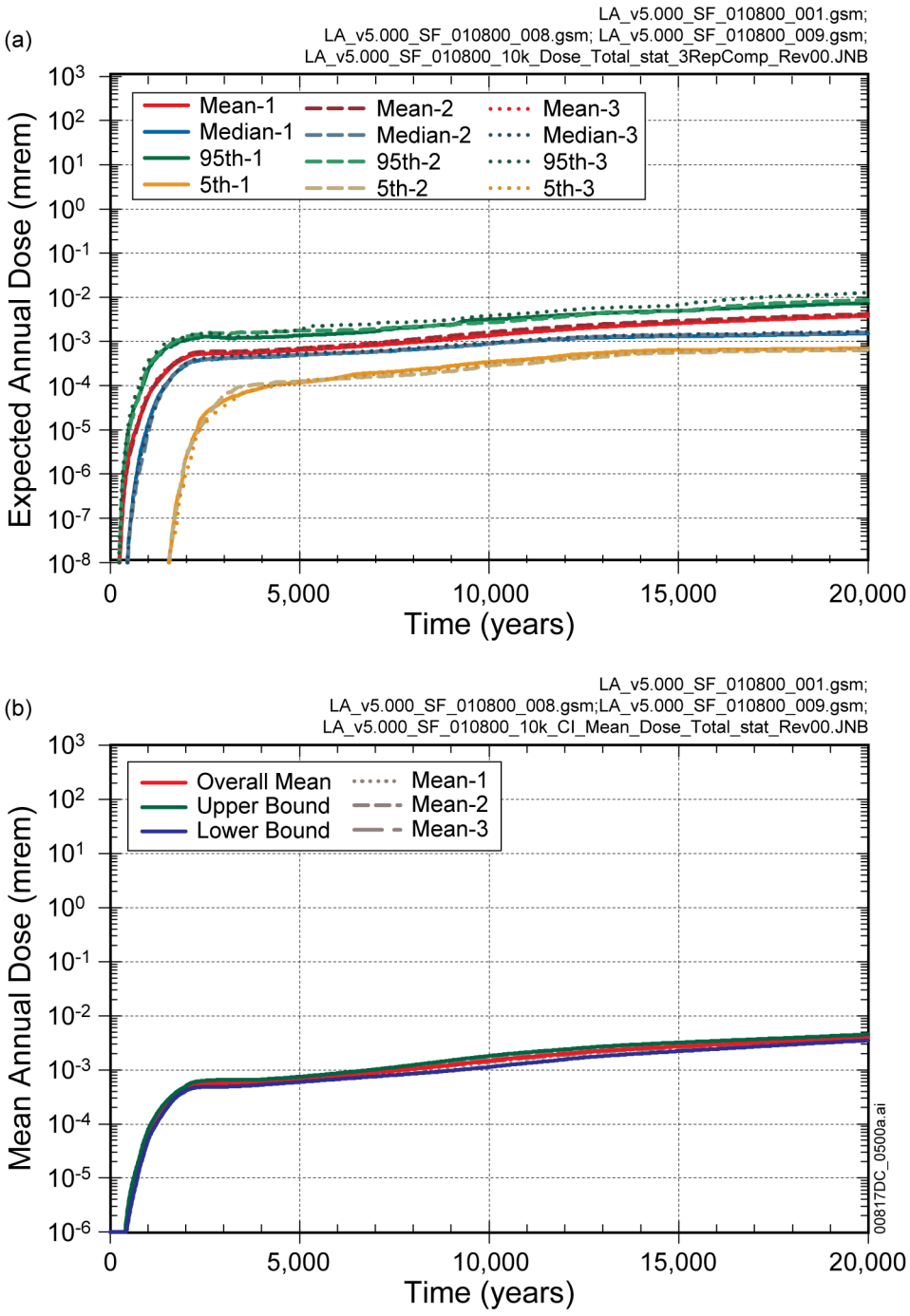

Source: Output DTNs: MO0709TSPASTAB.000 [DIRS 182983]; and MO0709TSPAREGS.000 [DIRS 182976].

Figure 7.3.1-12. Stability of Seismic Fault Displacement Modeling Case for 20,000 Years: (a) Comparison of Expected Annual Dose for Three Replicates and (b) Confidence Interval around Mean Annual Dose

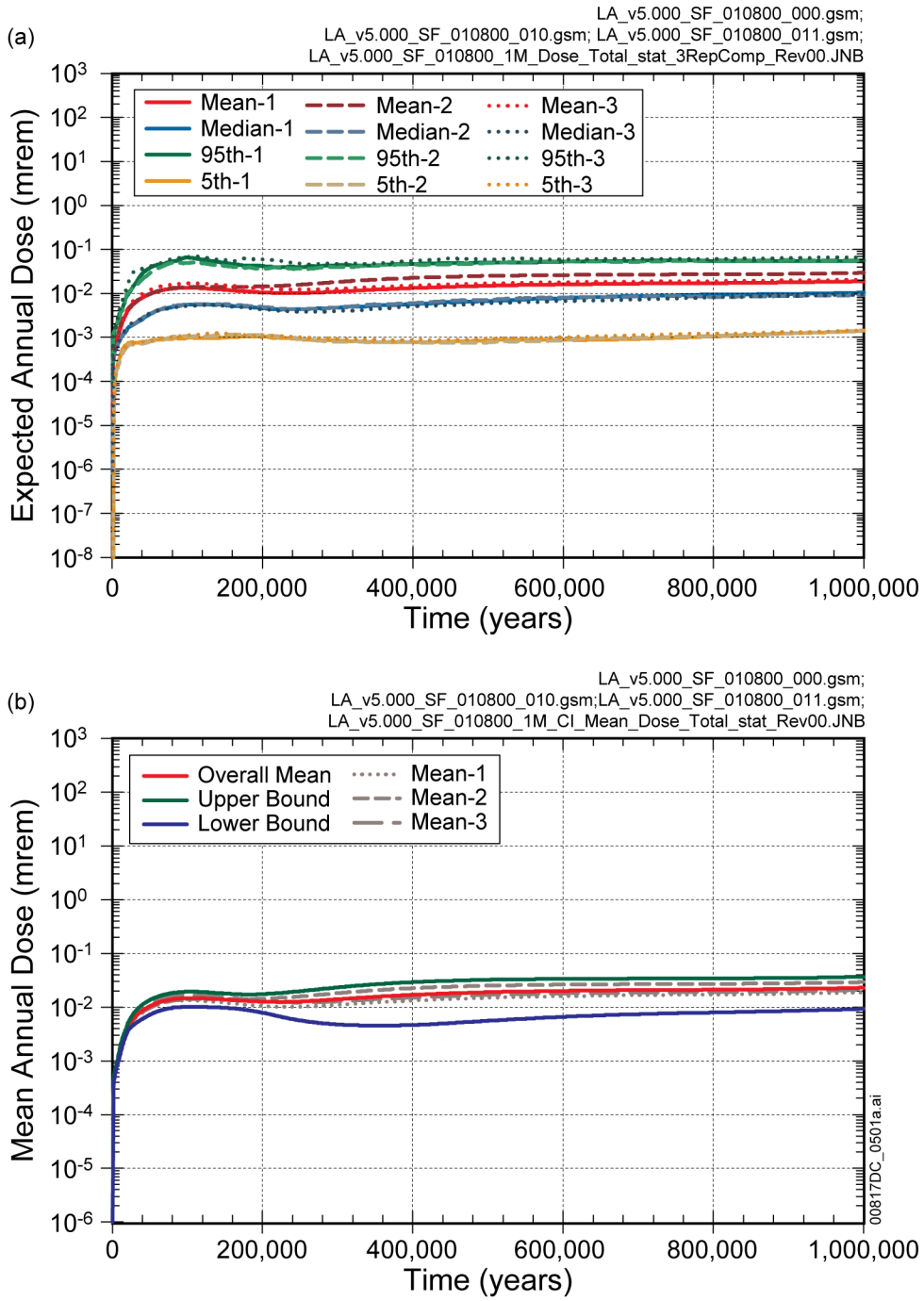

Source: Output DTNs: MO0709TSPASTAB.000 [DIRS 182983]; and MO0709TSPAREGS.000 [DIRS 182976].

Figure 7.3.1-13. Stability of Seismic Fault Displacement Modeling Case for 1,000,000 Years: (a) Comparison of Expected Annual Dose for Three Replicates and (b) Confidence Interval around Mean Annual Dose

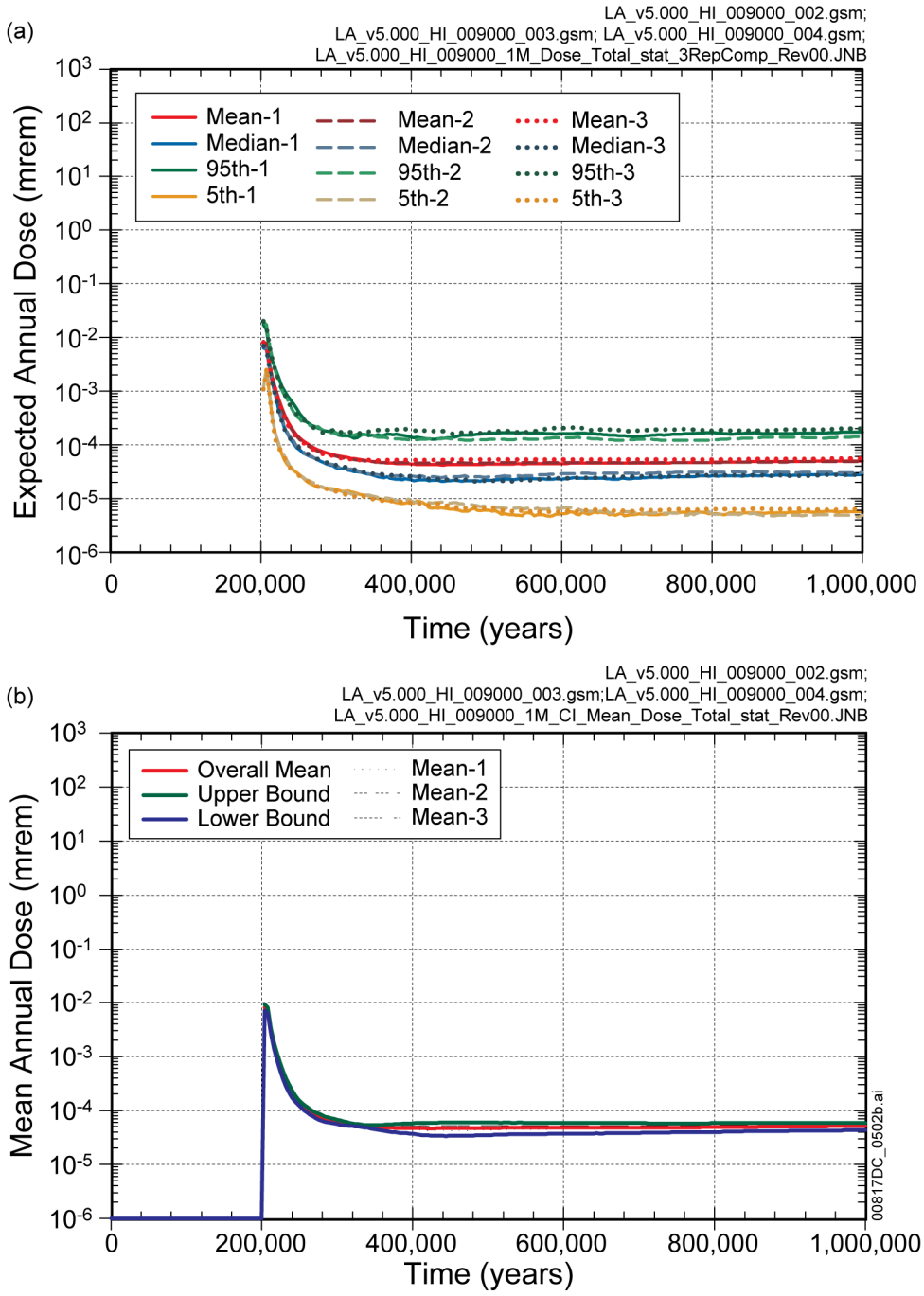

Source: Output DTNs: MO0709TSPASTAB.000 [DIRS 182983]; MO0709TSPAREGS.000 [DIRS 182976].

Figure 7.3.1-14. Stability of Human Intrusion Scenario: (a) Comparison of Expected Annual Dose for Three Replicates and (b) Confidence Interval around Mean Annual Dose

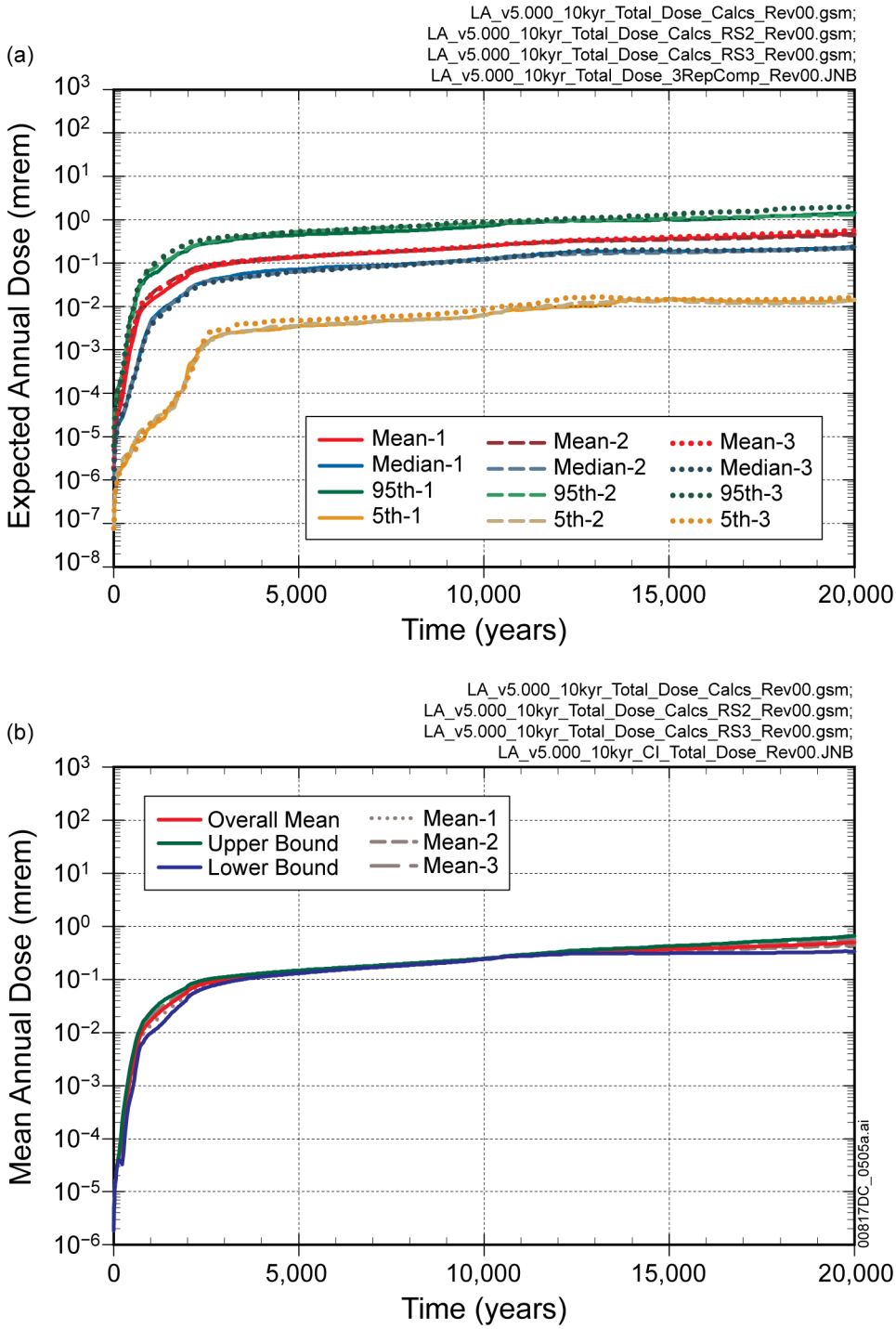

Source: Output DTN: MO0709TSPAPLOT.000 [DIRS 183010].

Figure 7.3.1-15. Stability of Total Mean Annual Dose 20,000 Years: (a) Comparison of Expected Annual Dose for Three Replicates and (b) Confidence Interval around Mean Annual Dose

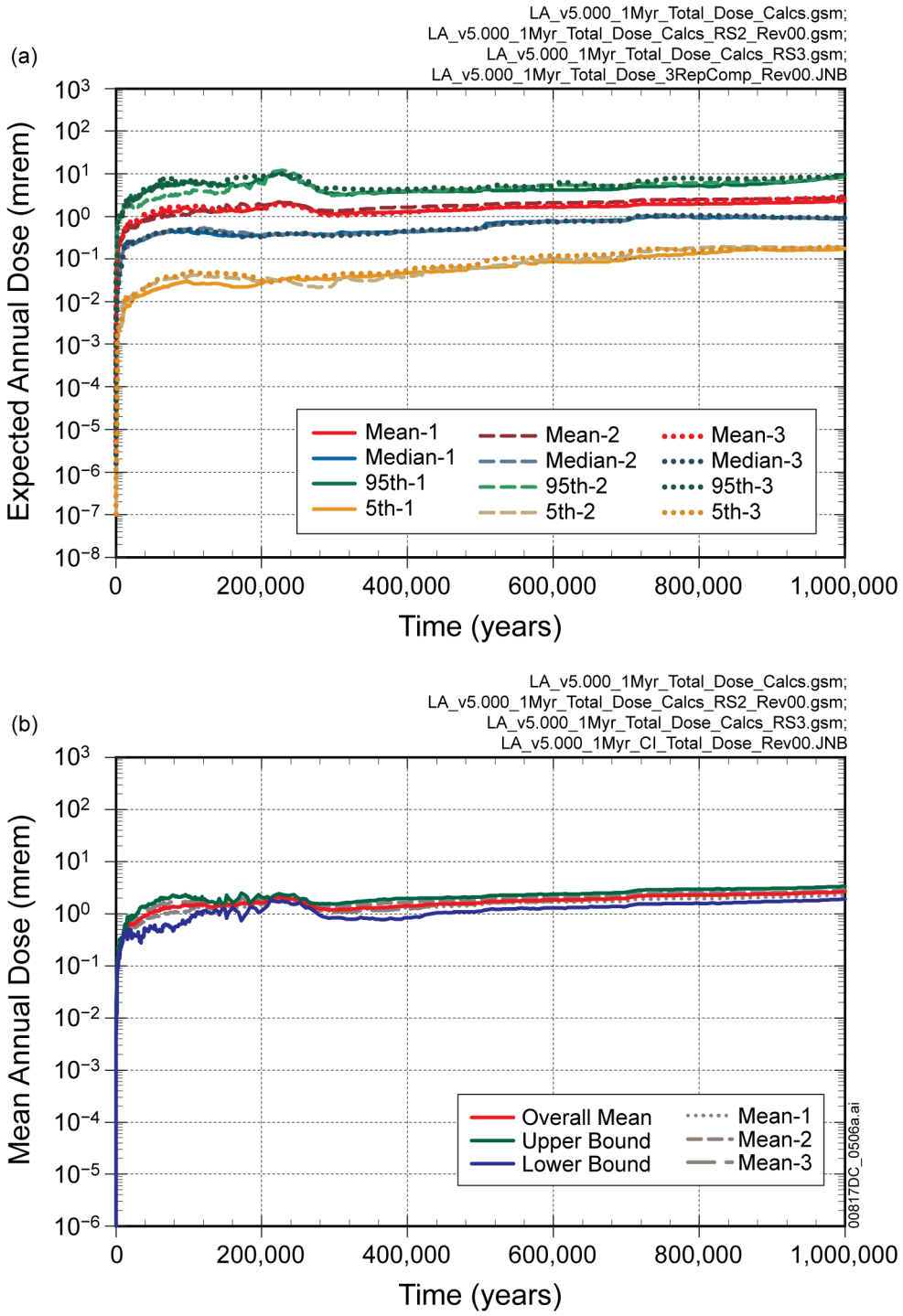

Source: Output DTN: MO0709TSPAPLOT.000 [DIRS 183010].

Figure 7.3.1-16. Stability of Total Mean Annual Dose for 1,000,000 Years: (a) Comparison of Expected Annual Dose for Three Replicates and (b) Confidence Interval around Mean Annual Dose

7.3.2 Numerical Accuracy of Expected Annual Dose

The TSPA-LA Model calculates expected annual dose $\overline{D}(\tau|\mathbf{e})$ for each epistemic realization. As a reminder, the term expected annual dose refers to the expectation of dose over aleatory uncertainty but conditional on epistemic uncertainty. Section 6.1.2.4 describes the calculation of expected annual dose for each modeling case. In general, the calculation involves numerical evaluation of one or more integrals. Because each modeling case addresses different aleatory uncertainties, the methods of calculating expected annual dose differ for each modeling case. This section examines the numerical accuracy of these calculations for each modeling case. In general, numerical accuracy is determined by refining the discretization employed in the numerical evaluation of each integral and showing that the results of the evaluation do not significantly change with improved discretization.

7.3.2.1 Nominal Modeling Case

Because the aleatory uncertain variables in the Nominal Modeling Case are sampled with the epistemic uncertain variables, the expected annual dose is the same as the annual dose calculated directly by GoldSim. For each element of the LHS of epistemic parameters, the GoldSim component of the TSPA-LA Model calculates the expected annual dose. The ensemble of expected annual doses is averaged to obtain the mean annual dose for the Nominal Modeling Case.

The numerical accuracy of the mean annual dose for the Nominal Modeling Case is confirmed by increasing the size of the LHS and comparing the mean annual doses. Figure 7.3.2-1 shows the expected annual dose for the Nominal Modeling Case for (a) an LHS of size 300 and (b) an LHS of size 1,000. Increasing the LHS size to 1,000 samples ensures that more extreme values for epistemic parameters are represented, and increases the probability that combinations of extreme values for different epistemic parameters are also represented. Increasing the LHS size to 1,000 resulted in corrosion failures before 100,000 years in six realizations, which did not occur in the smaller LHS size of 300. Additionally, increasing the LHS size resulted in a greater expected annual dose for the realizations with the largest expected annual dose after 800,000 years. Figure 7.3.2-2 shows the mean, median, 95th percentile, and 5th percentile of expected annual dose for both LHS sizes. The mean annual dose for LHS size of 1,000 is larger at very early times than the mean dose for LHS size of 300, due to the six realizations with very early corrosion failures. However, the magnitude of the mean dose at early times for either LHS size is small ($<10^{-5}$ mrem) compared to the long-term mean dose (~0.4 mrem), and the uncertainty in expected annual dose (as depicted by the median, 95th, and 5th percentiles) is nearly identical. Moreover, despite greater expected annual dose in some realizations after 800,000 years, the 95th percentile is essentially the same after 800,000 years, demonstrating that increasing the sample size only changes the extremes of the distribution of expected annual dose. Consequently, the mean annual dose computed using a LHS of size 300 is sufficiently accurate.

7.3.2.2 Waste Package Early Failure Modeling Case

Expected annual dose for the Waste Package EF Modeling Case is calculated as described by Equation 6.1.2-13. Because Equation 6.1.2-13 involves only sums rather than numeric integration, the calculation of expected annual dose is exact and does not require an estimate of

numerical accuracy. The EXDOC calculation of expected annual dose for the Waste Package EF Modeling Case was verified by reproducing the EXDOC results using Mathcad (output DTN: MO0708TSPAVALI.000 [DIRS 182985]).

7.3.2.3 Drip Shield Early Failure Modeling Case

Expected annual dose for the Drip Shield EF Modeling Case is calculated as described by Equation 6.1.2-14. Because Equation 6.1.2-14 involves only sums rather than numeric integration, the calculation of expected annual dose is exact and does not require an estimate of numerical accuracy. The EXDOC calculation of expected annual dose for the Drip Shield EF Modeling Case was verified by reproducing the EXDOC results using Mathcad (output DTN: MO0708TSPAVALI.000 [DIRS 182985]).

7.3.2.4 Igneous Intrusion Modeling Case

Expected annual dose for the Igneous Intrusion Modeling Case is calculated as described by Equation 6.1.2-16. Equation 6.1.2-16 is numerically evaluated as indicated in Equation 6.1.2-17 in two steps. First, for each of a sequence $[t_0, t_2, \ldots, t_N]$ of times for igneous intrusions, annual dose at time τ from an intrusion occurring at time, t_j, $D_{II}\left(\tau \middle| [1, t_j], \mathbf{e}_i\right)$, is calculated using the GoldSim component of the TSPA-LA Model. Second, the GoldSim results are used by the EXDOC component of the TSPA-LA Model to calculate expected annual dose.

The accuracy of the numerical evaluation of Equation 6.1.2-16 was examined by increasing the number of times of igneous intrusions for which GoldSim results are calculated from 10 to 50. Table 7.3.2-1 lists the 10 intrusion times considered in the base case for 20,000 years and for 1,000,000 years, and the 50 intrusion times considered in the stability analysis.

Figure 7.3.2-3 shows the annual dose resulting from each intrusion in the base case, and the annual dose resulting from the additional intrusions modeled in the stability analysis, for epistemic realization 2, for 20,000 years. In terms of Equation 6.1.2-16, Figure 7.3.2-3 shows the quantities $D_{II}\left(\tau \middle| [1, t_j], \mathbf{e}_2\right)$ for t_j as listed in Table 7.3.2-1. Each dose history's shape is similar for different times of intrusion within the same climate period, indicating that the interpolation techniques within the EXDOC software are justified. When the climate changes (at 2,000 and 10,000 years) the percolation rates increase in each percolation bin, resulting in more rapid transport of radionuclides through the UZ, and correspondingly, higher concentrations of radionuclides in the SZ and a larger maximum annual dose after the intrusion. Since UZ flow is modeled as steady (Section 6.3.1), when a climate change occurs, the UZ flow rates change instantaneously from one set of constant rates to another set, resulting in an abrupt change in the maximum annual dose.

Figure 7.3.2-4 compares the expected annual dose over 20,000 years for five epistemic realizations calculated using the 10 intrusion times and again using the 50 intrusion times listed in Table 7.3.2-1. The comparison shows that 10 intrusion times are sufficient to obtain a numerically accurate calculation of expected annual dose over 20,000 years. Using more intrusion times provides better resolution of the abrupt change in dose coincident with a climate

change. However, the abrupt change in dose is a result of modeling UZ flow as steady (Section 6.3.1) and the difference between the two cases is small enough that a better resolution of this change is not warranted. Figure 7.3.2-5 compares the expected annual dose over 1,000,000 years for five epistemic realizations calculated using the 10 intrusion times, and again using the 50 intrusion times listed in Table 7.3.2-1. Figure 7.3.2-5 shows that 10 intrusion times are sufficient to obtain a numerically accurate calculation of expected annual dose over 1,000,000 years.

7.3.2.5 Volcanic Eruption Modeling Case

Expected annual dose for the Volcanic Eruption Modeling Case is calculated as described by Equation 6.1.2-18. Equation 6.1.2-18 is numerically evaluated as indicated in Equation 6.1.2-19 in two steps. First, for each of a sequence $[t_1, t_2, \ldots, t_N]$ of times for eruption events and a LHS of uncertain aleatory parameters describing an eruption event $[\mathbf{u}_1, \mathbf{u}_2, \ldots, \mathbf{u}_M]$, annual dose at time τ from an eruption event occurring at time t_j and described by parameters $\mathbf{u}_k$ and affecting one WP, $D_{VE}\left(\tau \middle\| [1, t_j, 1, \mathbf{u}_k], \mathbf{e}_i\right)$, is calculated using the GoldSim component of the TSPA-LA Model. Second, the GoldSim results are used by the EXDOC component of the TSPA-LA Model to calculate expected annual dose.

Validation of the calculation of expected annual dose involved two steps: (1) demonstration that the size of the LHS of aleatory parameters is sufficient, and (2) demonstration that the integration over time of the eruption event is numerically accurate. Sufficiency of the size of the LHS for aleatory parameters is demonstrated by increasing the LHS size from 40 to 80. Numerical accuracy of the integration over time is demonstrated by increasing the number of specified times for volcanic eruption events. The aleatory parameters included in the LHS described by $[\mathbf{u}_1, \mathbf{u}_2, \ldots, \mathbf{u}_M]$ are eruptive power, eruptive velocity, eruptive duration, wind speed, and wind direction. Table 7.3.2-2 lists the times of eruption events considered in the base case and the additional times used to demonstrate numerical accuracy.

Figure 7.3.2-6 shows the expected annual dose resulting from the two different LHS sizes (40 vs. 80) for five realizations of epistemic parameters. The expected annual dose curves shown on Figure 7.3.2-6, use the eruption times for the base case. The expected annual dose is generally greater for the larger LHS, but the difference is no more than 10 percent, and is relatively constant throughout the 1,000,000-year period. Moreover, the mean annual dose from the Volcanic Eruption Modeling Case is very small relative to the compliance limits of 15 mrem and 300 mrem. Consequently, a difference of 10 percent due to numerical accuracy is acceptable, and the LHS size of 40 used in the base case is adequate to estimate expected annual dose.

Because the mean annual dose from volcanic eruption constitutes most of the total mean annual dose during the first 1,000 years (Figure 8.1-3(a)), the evaluation of the numerical accuracy of the expected annual dose from volcanic eruption focuses on this time period. Additional event times were added primarily during the first 1,000 years, as listed in Table 7.3.2-2. Figure 7.3.2-7(a) shows the expected annual dose for 20,000 years calculated using the specified eruption times for the base case and again using the additional times listed in Table 7.3.2-2, for the first five epistemic realizations. Figure 7.3.2-7(b) focuses on the expected annual dose for

the first 1,000 years. The expected annual dose curves shown on Figure 7.3.2-7 use the LHS of size 40 for aleatory parameters describing eruptive power, eruptive velocity, eruptive duration, wind speed, and wind direction. The expected annual dose does not change when more event times are used, either during the first 1,000 years or throughout the 20,000 year period. Consequently, the ten specified eruption times listed in Table 7.3.2-2 for the base case provide a sufficiently accurate calculation of expected annual dose. Because the expected annual dose is stable and relatively constant throughout the 20,000 year period, it is reasonable to presume that the expected annual dose calculation for 1,000,000 years is also numerically stable.

7.3.2.6 Seismic Ground Motion Modeling Case

Validation of the calculation of expected annual dose for the Seismic GM Modeling Case differs for the 10,000-year and 1,000,000-year time periods because of the different numerical techniques employed.

7.3.2.6.1 Seismic Ground Motion Modeling Case for 10,000 years

Expected annual dose for the Seismic GM Modeling Case is calculated as described by Equation 6.1.2-21. Equation 6.1.2-21 is numerically evaluated as indicated in Equation 6.1.2-22 in two steps. First, for each of a sequence $[t_1, t_2, \ldots, t_N]$ of times for seismic events and a set of damage fractions $[A_1, A_2, \ldots, A_M]$, annual dose at time τ from a seismic event occurring at time t_j and resulting in damage fraction A_k, $D_{SG}\left(\tau \middle\| [1, t_j, A_k], \mathbf{e}_i\right)$, is calculated using the GoldSim component of the TSPA-LA Model. Second, the GoldSim results are used by the EXDOC component of the TSPA-LA Model to calculate expected annual dose. The term "damage fraction" is used for brevity; this quantity is more precisely defined as the fraction of WP surface area that consists of open cracks.

For the 10,000-year period, validation of the calculation of expected annual dose involved three separate steps:

1. Demonstration that expected annual dose calculations are numerically accurate
2. Justification of assumption about linearity in damage fraction
3. Justification of simplifications to the Seismic Consequences Abstraction.

7.3.2.6.1.1 Accuracy of Expected Annual Dose Calculations

To demonstrate that the expected annual dose calculations conducted by EXDOC are numerically accurate, the number of times of seismic events was increased from 6 to 12, and the number of damage fractions was increased from 5 to 8. Table 7.3.2-3 lists the times of seismic events and the damage fractions considered in the base case and in the expanded case for numerical accuracy.

Figure 7.3.2-8 shows the annual dose resulting from each seismic event in the base case, and the annual dose resulting from the additional seismic events in the expanded case, for the damage fraction of 1.0×10^{-6}, for epistemic realization 1. In terms of Equation 6.1.2-21, Figure 7.3.2-8

shows the quantities $D_{SG}\left(\tau \middle| \left[1, t_j, 1.0\times10^{-6}\right], \mathbf{e}_1\right)$ for t_j as listed in Table 7.3.2-3. Each dose history's shape is similar for different times of the seismic event. Since UZ flow is modeled as steady (Section 6.3.1) when a climate change occurs, the UZ flow rates change instantaneously from one set of constant rates to another set, resulting in a small change in the annual dose at 10,000 years. The dose histories for an event at 200 years (base case) and at 100 years (expanded case) coincide on Figure 7.3.2-8, as do the dose histories for events at 1,000 years (base case) and at 1,600 years (expanded case). These dose histories coincide because, before about 2,000 years, the time that radionuclides are released from the WP is determined by the time that diffusive transport begins rather than the time that the damage occurred. Diffusive transport begins when relative humidity inside the WP reaches 95 percent (Section 5.1.4). The TSPA-LA Model does not model the dynamics of water transport through cracks in the WP in computing relative humidity inside the waste package. When damage to the WP consists of cracks, as in the Seismic GM Modeling Case, the relative humidity inside the WP is assumed to be in equilibrium with the relative humidity in the drift (Section 6.3.7.2.1). Thus, the time that diffusion begins depends only on the environmental conditions external to the WP, and is not affected by the time that the damage occurred to the WP.

Figure 7.3.2-9 shows the annual dose resulting from a seismic event at 100 years for each of the different damage fractions for epistemic realization 1. In terms of Equation 6.1.2-21, Figure 7.3.2-9 shows the quantities $D_{SG}\left(\tau \middle| \left[1, 100, A_k\right], \mathbf{e}_1\right)$ for A_k as listed in Table 7.3.2-3. Each dose history's shape is similar for different damage fractions. As discussed in detail in the next section, the magnitude of annual dose increases proportionally with increasing damage fraction up to damage fraction of 1.0×10^{-5}. The effect of the climate changes at 2,000 years and at 10,000 years can be observed. Figure 7.3.2-10 shows the annual dose resulting from a seismic event at 11,200 years for each of the different damage fractions, for epistemic realization 1, and shows that the shape of dose history does not significantly change for events occurring at later times. The curves for damage fractions of 1×10^{-3} and 5×10^{-3} coincide on Figure 7.3.2-9 and Figure 7.3.2-10.

EXDOC computes expected annual dose by interpolating between single dose histories for different event times and damage fractions, similar to those illustrated on Figure 7.3.2-8 and Figure 7.3.2-9, and performing numerical integration using the interpolated dose histories. Because the dose histories maintain similar shapes as the event time and damage fraction change, the interpolation scheme implemented in EXDOC is justified.

Figure 7.3.2-11 compares the expected annual dose over 20,000 years calculated for the base case and the expanded case for five epistemic realizations (identified as #1 through #5 on the figure), using the times of seismic events and damage fractions listed in Table 7.3.2-3 in the calculation of expected dose for each realization. Figure 7.3.2-11 shows that increasing the number of event times and the number of damage fractions does not change the expected annual dose calculation for any realization. Therefore, the discretization used to calculate expected annual dose is adequate and the calculation of expected annual dose is numerically accurate.

7.3.2.6.1.2 Linearity in Damage Fraction

As noted in Section 6.1.2.4.3, Equation 6.1.2-22 is based on the assumption that the annual dose from two or more events causing cumulative damage to WPs is reasonably approximated by the sum of the annual doses from the events modeled independently. Figure 7.3.2-12 illustrates the change in annual dose at 10,000 years due to changes in damage fraction, after an event at 100 years, for epistemic realization 1. The change in annual dose is proportional to changes in damage fraction, up to the damage fraction of about 10^{-5}. Beyond damage fraction of 10^{-5}, annual dose does not increase proportionally with increasing damage fraction. Thus, when two or more seismic events cause cumulative damage fraction exceeding 10^{-5}, the linearity assumption results in an overestimate of the annual dose resulting from seismic events. The dose resulting from a single event causing damage fraction exceeding 10^{-5} is not overestimated, since this quantity is computed by interpolation between the level curves shown on Figure 7.3.2-9.

To estimate the degree of conservatism incurred by this linearity assumption, expected annual dose from one seismic event was calculated, by evaluating the first integral term in Equation 6.1.2-22:

$$\bar{D}_{SG}\left(\tau\middle|1,\mathbf{e}_i\right)=\int_0^{\tau}\left(\lambda_1\left(\mathbf{e}_i\right)e^{-\lambda_1(\mathbf{e}_i)t}\left(\int_{A_{\min}}^{A_{\max}}D_{SG}\left(\tau\middle|[1,t,A],\mathbf{e}_i\right)d_{A1}\left(A\middle|\mathbf{e}_i\right)dA\right)\right)dt \quad \text{(Eq. 7.3.2-1)}$$

The integral displayed in Equation 7.3.2-1 computes the expected annual dose from the first seismic event that damages CDSP WPs. The second integral in Equation 6.1.2-22 computes the additional expected annual dose from the second and subsequent seismic events. Figure 7.3.2-13 shows the expected annual dose from the first damaging seismic event; Figure 7.3.2-14 shows the expected annual dose from all damaging seismic events for all 300 epistemic realizations. Comparison of the expected annual dose from the first damaging event to the expected annual dose from all damaging events shows that the second and subsequent damaging events add somewhat to the magnitude of the expected annual dose, but do not change the magnitude or range of uncertainty to any great extent. Consequently, the assumption that seismic consequences are linear in damage fraction, while conservative, does not result in a significant overestimate of the expected annual dose.

7.3.2.6.1.3 Simplifications to the Seismic Consequences Abstraction

For 10,000 years, the consequences of seismic ground motion events are approximated by examining only the occurrence of SCC damage to CDSP WPs with the DS intact and without significant rockfall, and without considering the effects of corrosion processes. Figure 7.3.2-14 shows expected annual dose for the Seismic GM Modeling Case for 10,000 years. Corrosion processes do not appreciably thin the WP in 10,000 years; hence, it is reasonable to omit these processes. The probability of DS plate or framework failure within 10,000 years is low enough that these failures are omitted from the calculation. The expected volume of rockfall within 10,000 years is small enough that it is reasonable to omit the changes in thermal and flow modeling caused by rockfall. Rupture and puncture of CDSP WPs are not considered because the probability that these events occur within 10,000 years is low enough that the expected annual dose from these events is also low. Finally, damage to CSNF WPs is omitted because the

low probability of seismic damage to the transportation, aging, and disposal (TAD)-bearing WPs results in low estimate of the expected annual dose from CSNF WPs. Each of these approximations is justified in the following discussion.

7.3.2.6.1.3.1 General Corrosion of Waste Package

General corrosion reduces the thickness of the WP outer corrosion barrier (OCB) and the DS, and this reduction in thickness alters the probability and extent of seismic damage to WPs and DSs. General corrosion of WP is modeled by time-dependent rates, calculated using several uncertain parameters, that vary spatially among WP locations and over a WP surface. The seismic consequences abstraction uses the spatially-averaged WP OCB thickness to calculate the probability and extent of seismic damage. The WP outer barrier initial thickness is 25 mm (SNL 2007 [DIRS 179394], Table 4-1). Seismic consequence calculations are performed for WP thickness of 23 mm and are used while WP thickness exceeds 23 mm. Figure 7.3.2-15 shows the spatially-averaged WP thickness for each realization for 1,000,000 years for (a) CSNF WPs and (b) CDSP WPs. No realization shows thickness reduced below 23 mm before about 200,000 years. Consequently, WP thicknesses below 23 mm are not considered in seismic calculations for 10,000 years.

7.3.2.6.1.3.2 Drip Shield Plate Failure

Section 6.6.1.3.3 outlines the mechanisms leading to DS plate failure. The probability of plate failure depends on the uncertainties describing DS corrosion and accumulated rockfall. DS corrosion is determined by two independent epistemic parameters: an aggressive corrosion rate for the upper surface, which is exposed to seepage, and a benign rate for the lower surface. One additional epistemic uncertainty describes the volume of intact lithophysal rock that must collapse to fill the drift.

Figure 7.3.2-16 shows the probability of DS plate failure for (a) 250,000 years and (b) 10,000 years, conditional on DS corrosion rates above the 99.99th percentile of the joint distribution for corrosion rate and the minimal value for the volume of intact lithophysal rock that must collapse to fill the drift (30 m^3/m). Because DS plate failure becomes less likely for lower rates of DS corrosion and for larger values of the volume of intact lithophysal rock that must collapse to fill the drift, the probability of DS plate failure shown on Figure 7.3.2-16 is bounding. The calculations included on Figure 7.3.2-16 are averaged over 100,000 sequences of seismic events and thus account for uncertainty in seismic event magnitude and amount of rockfall from each event. The probability of DS plate failure before 10,000 years is thus estimated to be less than 3.4×10^{-4} for all epistemic realizations.

If DS plate failure occurs, then all DSs fail as a barrier to seepage. After DS failure, radionuclide release depends on the condition of the WPs underneath failed DS. WP condition falls into one of three categories:

1. WPs are ruptured from seismic events. In this case, the consequence in terms of expected annual dose to the RMEI is discussed in Section 7.3.2.6.1.3.5 and is shown to be small.

2. WPs are damaged from seismic events and localized corrosion does not occur. In this case, the damage to WPs consists of cracks in the WP outer barrier. Failure of the DS does not alter the condition of the WP outer barrier. Dissolved radionuclides and radionuclides sorbed to colloids can diffuse out of the waste, through the cracks in the WP outer barrier, and into the invert. Transport of radionuclides out of the invert is not changed by DS failure because the volume of seepage flowing into the invert is unchanged. While the DS is intact, the seepage entering the drift diverts around the DS and flows into the invert. After the DS fails, the same volume of seepage flows through the DS, around the WP (since only cracks are present in the WP outer barrier), and into the invert. Because radionuclide transport through the WP outer barrier and the invert are not affected by the failure of the DS, the expected annual dose to the RMEI is unchanged in this case.

3. WPs are intact or damaged from seismic events and localized corrosion can occur. In this case, failure of the DS can lead to additional radionuclide releases because seepage that was diverted around the DS now falls onto the WP and localized corrosion breaches or enlarges existing breaches in WPs. The consequences of this case are analyzed below.

The expected annual dose to the RMEI at time τ, from seismic events that cause DS failure, and in circumstances in which localized corrosion causes WP failure, $\bar{D}_{DS}\left(\tau\middle|\mathbf{e}_i\right)$, is estimated by:

$$\bar{D}_{DS}\left(\tau\middle|\mathbf{e}_i\right)=\sum_{p=1}^{2}\sum_{b=1}^{5}E\left(n_{LC}\left(p,b,\mathbf{e}_i\right)\right)\times D_{ED}\left(\tau-t_{LC}\middle|1,p,b,\mathbf{e}_i\right) \qquad \text{(Eq. 7.3.2-2)}$$

where

$E\left(n_{LC}\left(p,b,\mathbf{e}_i\right)\right)$ is the expected number of WPs of type p in bin b that fail due to DS failure and localized corrosion, in epistemic realization $\mathbf{e}_i$.

$D_{ED}\left(\tau\middle|1,p,b,\mathbf{e}_i\right)$ is the annual dose at time τ from a failed DS co-located with a failed WP of type p, in dripping conditions in bin b, in epistemic realization $\mathbf{e}_i$.

$t_{LC}=t_{LC}\left(p,b,\mathbf{e}_i\right)$ is the earliest time that localized corrosion is possible on a WP of type p in bin b in epistemic realization $\mathbf{e}_i$.

The quantities $D_{ED}\left(\tau\middle|1,p,b,\mathbf{e}_i\right)$ are computed by the Drip Shield EF Modeling Case. The Drip Shield EF Modeling Case computes the dose that results following complete failure of a DS and the outer barrier of the underlying WP. Use of the Drip Shield EF Modeling Case in this estimate is conservative, because the modeling case assumes that the entire outer barrier of a WP is compromised, and that all of the impinging seepage flows through the waste.

The term t_{LC} is included because localized corrosion requires seepage to be present, which may not occur until some time after repository closure. The inclusion of t_{LC} in

$D_{ED}\left(\tau - t_{LC} \middle| 1, p, b, \mathbf{e}_i\right)$ shifts the beginning of radionuclide transport to the earliest time that localized corrosion could result in WP failure.

The term $E\left(n_{LC}\left(p, b, \mathbf{e}_i\right)\right)$ is estimated by

$$E\left(n_{LC}\left(p, b, \mathbf{e}_i\right)\right) = \lambda_F \times T_{LC}\left(p, b, \mathbf{e}_i\right) \times \left(f_p \times f_b \times N\right) \times f_{LC}\left(p, b, \mathbf{e}_i\right) \quad \text{(Eq. 7.3.2-3)}$$

where

λ_F	is the frequency of DS failure due to seismic events
$T_{LC}\left(p, b, \mathbf{e}_i\right)$	is the latest time that localized corrosion could occur on a WP of type p in bin b, in epistemic realization $\mathbf{e}_i$
$\left(f_p \times f_b \times N\right)$	is the total number of WP of type p in percolation subregion b
f_p	is the fraction of WPs of type p (CDSP WP or CSNF WP)
f_b	is the fraction of WPs in percolation subregion b
N	is the total number of WP in the repository
$f_{LC}\left(p, b, \mathbf{e}_i\right)$	is the maximum fraction of WPs of type p in bin b, on which localized corrosion may occur, in epistemic realization $\mathbf{e}_i$.

The frequency of DS failure due to seismic events is not larger than $3.4\times10^{-4}/10^{4}$ yr $= 3.4\times10^{-8}$ yr^{-1} (Figure 7.3.2-16). Figure 7.3.2-17 displays the expected annual dose computed by Equation 7.3.2-2. The expected annual dose considering DS failure is substantially less than the expected annual dose calculated in the Seismic GM Modeling Case (compare Figures 7.3.2-17 and 7.3.2-14). Moreover, the mean annual dose considering DS failures is less than 5×10^{-3} mrem during 10,000 years, which is numerically insignificant compared to the mean annual dose in the Seismic GM Modeling Case. Thus, the omission of DS failure from the Seismic GM Modeling Case is justified.

The estimate of expected annual dose considering DS failure is very conservative. The frequency of DS failure (3.4×10^{-8} yr^{-1}) is computed using extreme values for DS corrosion and for the volume of lithophysal rockfall required to fill the drift. If the analysis was repeated to include the uncertainty in DS corrosion and rockfall, the frequency of DS failure would decrease, and lead to lower expected annual dose from DS failure. Additionally, the use of the Drip Shield EF Modeling Case as a surrogate for the dose resulting from DS failure from seismic events is very conservative. For simplicity, the Drip Shield EF Modeling Case assumes that DS early failure results in compromise of the entire outer barrier of the underlying WP. This assumption overestimates the extent of localized corrosion damage, and consequently overestimates the volume of seepage that flows through the waste, and the amount of radionuclides mobilized and transported from the WP.

7.3.2.6.1.3.3 Drip Shield Framework Failure

The omission of framework failure from the Seismic GM Modeling Case for 10,000 years conservatively overestimates the occurrence of seismic damage, as outlined in the following sections. If DS framework failure occurs, the DS continues to prevent seepage from contacting the WPs; however, framework failure alters the probability of damage to WP from seismic events (Section 6.6.1.2.2.1). In general, the probability for damage to CDSP WP is reduced but the probability for damage to CSNF WP is increased. This change in the probability of damage is not accounted for the in Seismic GM Modeling Case for 10,000 years. The modeling case calculates damage to WPs as if the DS framework was intact.

Figure 7.3.2-18 shows the probability of DS framework failure over (a) 250,000 years and (b) 20,000 years, conditional on DS corrosion rates above the 99.99th percentile of the joint distribution for corrosion rate and the minimal value for the volume of intact lithophysal rock that must collapse to fill the drift, per unit length of drift (30 m^3/m). DS framework corrosion rates are scaled from the sampled values for DS plate corrosion rates. Because DS framework failure becomes less likely for lower rates of DS corrosion and for larger values for the value for the volume of intact lithophysal rock that must collapse to fill the drift, the probability of DS framework failure shown on Figure 7.3.2-18 is bounding. From a simulation of 100,000 sequences of seismic events, the probability of DS framework failure before 10,000 years is approximately 3×10^{-3}. Consequently, the frequency of DS framework failure is less than 3×10^{-7} yr^{-1}.

After DS framework failure, the mechanical response of WPs to seismic events is a function of the state of the internals. If the internals are degraded (i.e., the WP has already been damaged), the kinematic damage abstraction for a WP under intact DS plates but with degraded internals applies. If the internals are intact, the abstraction for a WP surrounded by rubble applies (Section 6.6.1.2.2.2).

The Seismic GM Modeling Case accounts for the radionuclides released from CDSP WPs for all seismic events that damage the WP while DS plates are intact. The first damaging event is assumed to occur while the DS framework is intact. The effects of any subsequent damaging events are computed using the appropriate abstraction. Consequently, the omission of DS framework failure only affects the probability of occurrence for the first damaging event. For RST=90, the frequency of damage to CDSP WPs with intact internals and intact DS framework is 2.181×10^{-5} (output DTN: MO0708CDSPSEIS.000 [DIRS 183007], *FreqDamageCDSP_v5.pdf*). In contrast, the frequency of damage to CDSP WP with intact internals and failed DS framework (described by the abstraction for a WP surrounded by rubble) is 3.923×10^{-8} (output DTN: MO0708FREQCALC.000 [DIRS 183006], *Rubble_Damage.pdf*). Because the probability of first damage to CDSP WPs decreases significantly after DS framework failure, omitting DS framework failure is conservative. However, because DS framework failure is unlikely before 10,000 years, the conservatism has a small, if any, effect on the results of the modeling case.

The Seismic GM Modeling Case does not account for the radionuclides released from CSNF WPs because, as discussed in Section 7.3.2.6.1.3.7, the probability of damage to intact TAD-bearing WPs is less than 1.575×10^{-8} yr^{-1} and the expected annual dose considering

damage to CSNF WPs is less than 0.036 mrem. If the DS framework fails before the CSNF WPs are damaged, the frequency of damage to CSNF WPs with intact internals increases, from 1.575×10^{-8} yr^{-1} (for RST=90) to 3.923×10^{-8} (for RST=90), due to the switch from the abstraction for WPs under an intact DS to WPs surrounded by rubble. Although the frequency of damage to CSNF WPs increases by a factor of 2.5, the increase is offset by the low probability of DS framework failure. Expected annual dose considering DS framework failure is estimated by

$$\begin{aligned} &\left(\text{prob DS framework failure}\right)\times\left(\text{prob damage TAD}\right) \\ &\quad\times\left(\text{num TAD}\right)\times\max_{t}\left(\text{Dose}(t\,|\,\text{1 TAD})\right) \\ &\leq\left(3\times10^{-3}\right)\times\left(3.923\times10^{-4}\right)\times8213\times\left(0.028\right) \\ &= 2.7\times10^{-4}\ \text{mrem/yr} \end{aligned} \qquad \text{(Eq. 7.3.2-4)}$$

Thus, expected annual dose from CSNF considering DS framework failure is numerically small, and consequently, omission of DS framework failure from the Seismic GM Modeling Case is justified.

7.3.2.6.1.3.4 Rockfall

Besides contributing to the possibility of DS failure, as discussed in Section 7.3.2.6.1.3.2, rockfall caused by seismic events also alters the seepage entering the drift. Section 6.6.1.2.1 describes the model for rockfall; Section 6.6.2.1 describes the changes to drift seepage that may occur as a consequence of rockfall.

Figure 7.3.2-19(a) shows the volume of lithophysal rockfall that may accumulate during 20,000 years, determined by simulating 10,000 possible sequences of seismic events. The threshold volume of lithophysal rockfall per meter of drift length, that causes a change to the seepage model, is 5 m^3/m. When rockfall exceeds this threshold, seepage increases, as described in Section 6.3.3.1.3. At 10,000 years, approximately 11 percent of realizations have lithophysal rockfall at or above the threshold of 5 m^3/m, and approximately 1 percent of the realizations have lithophysal rockfall exceeding the 60 m^3/m volume that identifies a fully collapsed drift. When rockfall exceeds the threshold of 5 m^3/m, the volume of seepage flowing into the drift is increased. However, as long as the DS remains intact, there is no change in the radionuclides released from a WP, because the diffusion of radionuclides through the WP outer barrier does not depend on the volume of seepage in the invert. Transport of radionuclides through the invert would be somewhat faster if seepage increases, resulting in an increase in the rate of mass entering the UZ, and possibly an increase the rate of mass arriving at the RMEI location through the SZ. However, because seepage does not increase by as much as a factor of 5 from intact to fully collapsed drift (SNL 2007 [DIRS 181244], Table 6-7[a]), it is reasonable to expect that any increase in dose would not be more than a factor of 5, and likely would be much smaller, as uncertainty and variability in travel time through the UZ and SZ would tend to ameliorate any increase in mass flux from the invert. Moreover, any increase in dose would be observed in only 11 percent of realizations, and thus would not significantly alter the mean annual dose to the RMEI.

Figure 7.3.2-19(b) shows the volume of nonlithophysal rockfall that may accumulate during 20,000 years, determined by simulating 10,000 possible sequences of seismic events. The threshold volume of nonlithophysal rockfall per unit length of drift for change to the seepage model is 0.5 m^3/m. When rockfall exceeds this threshold, seepage increases, as described in Section 6.3.3.1.3. At 10,000 years, less than 1 percent of realizations have nonlithophysal rockfall at or above the threshold. When nonlithophysal rockfall exceeds the threshold, the rate of percolation rather than seepage is used. Percolation rates tend to be approximately 10 times greater than seepage rates (SNL 2007 [DIRS 181244], Table 6-6[a]). However, only approximately 20 percent of WPs are located in nonlithophysal zones, and few realizations have nonlithophysal rockfall at or above the threshold of 0.5 m^3/m, so seepage changes due to nonlithophysal rockfall have little effect on mean annual dose. Thus, the omission of rockfall effects from the Seismic GM Modeling Case for 10,000 years is justified.

7.3.2.6.1.3.5 Rupture

Rupture is conceptualized to occur when extreme deformation of the WP outer barrier accumulates as a result of package-to-pallet impacts during seismic events (Section 6.6.1.2.2.2). Rupture can only occur after package internals are degraded and when the packages can move freely beneath the DS (Section 6.6.1.2.2.2). Hence, rupture requires that a damaging seismic event has already occurred, and that the DS plates are still intact. After the DS plates have failed, the WPs are surrounded by rubble from rockfall, and rupture is not considered possible.

A seismic event may result in immediate rupture of a WP. Alternatively, the event may cause an incipient rupture, meaning that the event caused damage that increases the probability of rupture from a subsequent event. After an incipient rupture occurs, any subsequent event that would cause either incipient rupture or immediate rupture causes a rupture. Figure 7.3.2-20 diagrams the transition from an intact WP to a ruptured WP. The probabilities of immediate rupture ($p_{imm}(v)$) and incipient rupture ($p_{inc}(v)$) are conditional on the occurrence of a seismic event after WP internals have degraded, and are functions of the PGV v of the seismic event (DTN: MO0703PASEISDA.002_R4 [DIRS 183156], Eq. 1-12, Eq. 1-13, Eq. 1-17, Eq. 1-18, and Table 1-17).

If rupture occurs, the rupture creates an opening in the WP OCB sampled uniformly between 0 m^2 and the cross-sectional area of the WP (Section 6.6.1.2.2.2), 2.78 m^2 and 3.28 m^2 for CSNF and CDSP WPs, respectively (DTN: MO0703PASEISDA.002_R4 [DIRS 183156], Table 1-17). The opening allows both advection and diffusion of radionuclides out of the WP. A fault displacement event creates a similar opening in the WP OCB (Section 6.6.1.2.3). The Seismic FD Modeling Case calculates the annual dose $D_{SFr}\left(\tau \middle| [1, t, 100, A_r], \mathbf{e}_i\right)$ at time τ resulting from a fault displacement occurring at time t, which damages 100 WPs of type r, causing an opening with an area equal to A_r on each WP, where $\mathbf{e}_i$ is a realization of epistemic parameters. Because a fault displacement causes damage similar to a WP rupture, the Seismic FD Modeling Case results can be used to approximate the dose resulting from a rupture event occurring at time t that affects $nWP(r)$ WPs of type r and causing a damage fraction equal to A_r on each WP. This dose from rupture is denoted by $D_R\left(\tau \middle| [1, t, nWP(r), A_r], \mathbf{e}_i\right)$, and the relationship between the dose from rupture and the results of the Seismic FD Modeling Case is

$$D_R\left(\tau\left|[1,t,nWP(r),A_r],\mathbf{e}_i\right.\right)\approx\frac{nWP(r)}{100}D_{SFr}\left(\tau\left|[1,t,100,A_r],\mathbf{e}_i\right.\right) \qquad \text{(Eq. 7.3.2-5)}$$

Divide the interval $[0,\tau]$ into n intervals of width Δt. The probability that the first damaging event occurs within an interval $[t_i,t_i+\Delta t]$ is $e^{-\lambda_D(\mathbf{e}_i)t_i}\lambda_D(\mathbf{e}_i)\Delta t$, where $\lambda_D(\mathbf{e}_i)$ is the frequency of events that cause damage to a WP with intact internals, calculated as

$$\lambda_D(\mathbf{e}_i)=\int_{\lambda_{\min}}^{\lambda_{\max}} pD\left(r,v(\lambda)\left|\mathbf{e}_i\right.\right)d\lambda \qquad \text{(Eq. 7.3.2-6)}$$

where

$\lambda_{\min}$ and $\lambda_{\max}$ are the minimum and maximum frequencies of seismic events included in the seismic hazard curve (10^{-8} and 4.287×10^{-4}, respectively) (DTN: MO0703PASEISDA.002_R4 [DIRS 183156], Table 1-15)

$pD\left(r,v(\lambda)\left|\mathbf{e}_i\right.\right)$ is the probability of damage occurring to a WP of type r with intact internals and residual stress threshold (RST) given by an element *RST* in $\mathbf{e}_i$, given that a seismic event with PGV v occurs (DTN: MO0703PASEISDA.002_R4 [DIRS 183156], Table 1-4 and Table 1-6).

The probability of one or more events that causes rupture occurring in the interval $[t_i+\Delta t,\tau]$ is $1-e^{-\lambda_R(\tau-t_i-\Delta t)}$, where λ_R is the frequency of events that cause rupture to packages with degraded internals, calculated as

$$\lambda_R(r)=\int_{\lambda_{\min}}^{\lambda_{\max}} p_R\left(r,v(\lambda)\right)d\lambda \qquad \text{(Eq. 7.3.2-7)}$$

where

$p_R\left(r,v(\lambda)\right)$ is the probability of immediate rupture occurring to a WP of type r with degraded internals given that a seismic event with PGV v occurs (DTN: MO0703PASEISDA.002_R4 [DIRS 183156], Eq. 1-12, Eq. 1-13, Eq. 1-17, Eq. 1-18, and Table 1-17).

Evaluation of Equation 7.3.2-7, yields frequencies of rupture of 8.327×10^{-9} yr^{-1}, for CDSP WP and 1.378×10^{-8} yr^{-1} for CSNF WP (output DTN: MO0708FREQCALC.000 [DIRS 183006], *FreqRupture.pdf*). Equation 7.3.2-7 is simplified by considering only events that cause immediate rupture. The frequency of events that cause immediate rupture can be expressed as $P\left(\text{Imm.}\left|\text{seismic event}\right.\right)\times\lambda_S$ where $P\left(\text{Imm.}\left|\text{seismic event}\right.\right)$ is the probability of immediate rupture conditional on a seismic event occurring, and λ_S is the frequency (yr^{-1}) of seismic events

(10^{-4} yr^{-1}). In contrast, the frequency of rupture occurring from the sequence of an incipient rupture followed by an incipient or immediate rupture can be expressed as

$$\left[P\left(\text{Imm.}\middle|\text{seismic event}\right)\times\lambda_S\right]\times\left[\left(P\left(\text{Inc.}\middle|\text{seismic event}\right)+P\left(\text{Imm.}\middle|\text{seismic event}\right)\right)\times\lambda_S\right]$$
$$=\left(P^2\left(\text{Inc.}\middle|\text{seismic event}\right)+P\left(\text{Inc.}\middle|\text{seismic event}\right)P\left(\text{Imm.}\middle|\text{seismic event}\right)\right)\times\lambda_S^2$$

where $P\left(\text{Inc.}\middle|\text{seismic event}\right)$ is the probability of an incipient rupture conditional on a seismic event occurring. Since $P\left(\text{Inc.}\middle|\text{seismic event}\right)$ is of the same order of magnitude as $P\left(\text{Imm.}\middle|\text{seismic event}\right)$, the frequency of rupture from the sequence of an incipient rupture followed by a second event is several orders of magnitude less than the frequency of immediate rupture.

The expected annual dose at time τ from events that cause rupture to WP of type r can be estimated by

$$\bar{D}_R\left(\tau\middle|r,\mathbf{e}_i\right)\approx\sum_{j=0}^{n}e^{-\lambda_D(\mathbf{e}_i)t_j}\lambda_D\left(\mathbf{e}_i\right)\Delta t\left(1-e^{-\lambda_R\left(\tau-t_j-\Delta t\right)}\right)\left\{\int_0^{A_{\max}}D_R\left(\tau\middle|\left[1,t_j,nWP(r),A\right],\mathbf{e}_i\right)dA\right\}$$
$$\cong\int_0^{\tau}e^{-\lambda_D(\mathbf{e}_i)t}\lambda_D\left(\mathbf{e}_i\right)\left(1-e^{-\lambda_R(\tau-t)}\right)\left\{\int_0^{A_{\max}}D_R\left(\tau\middle|\left[1,t,nWP(r),A\right],\mathbf{e}_i\right)dA\right\}dt$$

(Eq. 7.3.2-8)

Figure 7.3.2-21 displays the expected annual dose from events that cause rupture, estimated by Equation 7.3.2-8. Except for one realization, the expected annual dose at 10,000 years is less than 4×10^{-3} mrem/yr. In contrast, the expected annual dose at 10,000 years in the Seismic GM Modeling Case exceeds 4×10^{-3} mrem in approximately 70 percent of the realizations (Figure 7.3.2-14). Moreover, the mean annual dose at 10,000 years in the Seismic GM Modeling Case is approximately 0.2 mrem, whereas the mean dose at 10,000 years due to events that cause rupture is about 3×10^{-4} mrem. Thus, the expected annual dose from rupture events is small enough that its exclusion from the dose for the Seismic GM Modeling Case for 10,000 years is justified.

Moreover, using the Seismic FD Modeling Case results to estimate bounds on the dose due to rupture over-estimates the dose from rupture in two ways. First, the dose resulting from fault displacement assumes that DSs fail at the time of the fault displacement event, allowing advective transport through the affected WPs. In contrast, the probability of DS failure is not accounted for in Equation 7.3.2-8. If the DS plates remained intact after a rupture event, radionuclide transport from the underlying package would occur by diffusion, which tends to be slower than transport by advection, and would result in lower annual doses. Additionally, the Seismic FD Modeling Case considers only the effects of fault displacement events. Thus, using these results to estimate rupture neglects the effects of the damaging events that precede rupture,

and overcounts the released radionuclides because the content of the WPs is not reduced by any radionuclides that would be released prior to a rupture occurring.

7.3.2.6.1.3.6 Puncture

Puncture is conceptualized to be possible after the DS plates have failed, rubble from rockfall surrounds the WP, and the outer corrosion barrier collapses around the degraded internal contents of the WP. Although the internal components of the WP are conceptualized to degrade structurally after the OCB is breached, large fragments of the stainless steel inner vessel and parts of the waste assembly may persist for long periods of time. Puncture may result when a severely deformed outer corrosion barrier is loaded down by rubble from rockfall and thus impinges on the edges or corners of fragments of the degraded internal structure. Puncture can only occur after package internals are degraded and the rubble from rockfall surrounds the WP; hence, puncture requires that a damaging seismic event has already occurred and that the drift has fully degraded.

When puncture occurs, the resulting puncture area allows both advection and diffusion of radionuclides out of the WP. The puncture area for the TSPA-LA ranges between 0 m^2 and 0.1 m^2 (DTN: MO0703PASEISDA.002_R4 [DIRS 183156], Table 1-17), generally smaller than the area considered for rupture, which ranges between 0 m^2 and 2.78 m^2 (3.28 m^2) for CSNF (CDSP) WPs (DTN: MO0703PASEISDA.002_R4 [DIRS 183156], Table 1-17).

For 10,000 years, corrosion of the WP outer barrier does not reduce the spatially averaged outer barrier thickness below 23 mm. Thus, the calculation of the frequency of puncture does not consider the outer barrier thickness changing with time. The frequency of events that cause puncture to a WP with degraded internals and which is surrounded by rubble, λ_P, is calculated as

$$\lambda_P = \int_{\lambda_{\min}}^{\lambda_{\max}} p_P\left(v(\lambda)\right) d\lambda = 1.453 \times 10^{-8} \qquad \text{(Eq. 7.3.2-9)}$$

where

$p_P\left(v(\lambda)\right)$ is the probability of puncture occurring to a WP with degraded internals, surrounded by rubble, with 23 mm thick OCB, given that a seismic event with PGV v occurs (DTN: MO0703PASEISDA.002_R4 [DIRS 183156], Eqs. 1-22 and 1-23 and Table 1-17)).

Equation 7.3.2-9 is evaluated and reported in output DTN: MO0708FREQCALC.000 [DIRS 183006], *FreqPuncture.pdf*. Figure 7.3.2-16 shows the bounding probability of DS plate failure as a function of time for each realization. Over all realizations, at 10,000 years, the probability of DS plate failure does not exceed 3.4×10^{-4}. Thus, the probability of rubble surrounding the WPs within 10,000 years is also less than 3.4×10^{-4}, and the frequency of events that cause puncture is less than

$$3.4\times10^{-4}\times\lambda_P=\left(3.4\times10^{-4}\right)\times\left(1.453\times10^{-8}\right)=5.2\times10^{-12}. \qquad \text{(Eq. 7.3.2-10)}$$

As expressed by Equation 7.3.2-10, the frequency of puncture is much less than the frequency of rupture (Equation 7.3.2-7). Since the area opened by a puncture is smaller than the area opened by rupture, the expected annual dose from seismic events that puncture WPs would not be larger than the expected annual dose from seismic events that rupture WPs. Hence, the expected annual dose from puncture would be much less, than the expected annual dose from rupture, and the exclusion of puncture from the expected annual dose for the Seismic GM Modeling Case for 10,000 years is also justified.

7.3.2.6.1.3.7 Damage to CSNF Waste Packages

The frequency of seismic events that cause SCC damage to a CSNF WP with intact internals and 23 mm thick OCB is estimated by Equation 7.3.2-6. The maximum frequency corresponds to RST=90 and is calculated to be 1.575×10^{-8} (output DTN: MO0708FREQCALC.000 [DIRS 183006], *FreqDamageTAD.pdf*). In contrast, the maximum frequency of events that cause SCC damage to a CDSP WP is estimated to be 2.181×10^{-5} (output DTN: MO0708CDSPSEIS.000 [DIRS 183007], *FreqDamageCDSP_v5.pdf*). The expected annual dose from seismic events that damage CSNF WPs is estimated by comparing the dose resulting from CSNF and CDSP WPs in the Waste Package EF Modeling Case. This modeling case calculates the annual dose from a single WP with a completely compromised WP outer barrier (Section 6.4). Figure 7.3.2-22 shows the mean annual dose resulting from (a) one CSNF WP and (b) one CDSP WP, as modeling in the Waste Package EF Modeling Case, considering all locations within the repository and all realizations of epistemic parameters. The maximum mean annual dose from CSNF WPs with SCC damage is estimated by

$$\begin{aligned}&\left(\text{prob damage CSNF in 10,000 yrs}\right)\times\left(\text{num CSNF}\right)\times\max_t\left(\text{Dose}(t\,|\,\text{1 CSNF})\right)\\&=\left(1.575\times10^{-4}\right)\times8213\times\left(0.028\right)\\&=0.036\text{ mrem}\end{aligned} \qquad \text{(Eq. 7.3.2-11)}$$

Because the quantity, $\max_t\left(\text{Dose}(t\,|\,\text{1 CSNF})\right)$, is estimated from the results of the Waste Package EF Modeling Case for CSNF WPs, in which the entire WP outer barrier is assumed to fail, the estimate of this quantity effectively assumes that the entire surface area of each CSNF WP consists of cracks. Consequently, the quantity 0.036 mrem estimated by Equation 7.3.2-11 should not be compared to the mean annual dose from CDSP WPs from the Seismic GM Modeling Case, but rather to the comparable quantity for CDSP WPs using the results of the Waste Package EF Modeling Case for CDSP WPs:

$$\begin{aligned}&\left(\text{prob damage CDSP in 10,000 yrs}\right)\times\left(\text{num CDSP}\right)\times\max_{t}\left(\text{Dose}(t\,|1\text{ CDSP})\right)\\&=\left(2.181\times10^{-1}\right)\times3416\times\left(0.008\right)\\&=5.96\text{ mrem/yr}\end{aligned}$$

(Eq. 7.3.2-12)

Comparison of the results of Equation 7.3.2-11 and Equation 7.3.2-12 shows that the maximum mean annual dose associated with seismic damage to CSNF WPs is expected to be less than 1 percent of the maximum mean annual dose associated with seismic damage to CDSP WPs. Thus, the omission of damage to TADs from the Seismic GM Modeling Case for 10,000 years is justified.

7.3.2.6.2 Seismic Ground Motion Modeling Case for 1,000,000 Years

Expected annual dose for the Seismic GM Modeling Case for 1,000,000 years is calculated as described by Equation 6.1.2-23, using a Monte Carlo technique. First, a LHS of size 300 is generated for epistemic parameters. Next, for each vector $\mathbf{e}_i$ in the epistemic LHS, an aleatory sample is randomly generated, consisting of 30 independent sequences $\left\{\mathbf{a}_{ij}\right\}_{j=1,30}$ of seismic events and corrosion failures, and annual dose at time τ from the combination of corrosion processes and seismic ground motion events, $D_{N+G}\left(\tau\left|\mathbf{a}_{ij},\mathbf{e}_i\right.\right)$, is calculated. For each vector $\mathbf{e}_i$ in the epistemic LHS, expected annual dose $\bar{D}_{SG}\left(\tau\left|\mathbf{e}_i\right.\right)$ is computed as

$$\bar{D}_{SG}\left(\tau\left|\mathbf{e}_i\right.\right)=\sum_{j=1}^{30}D_{N+G}\left(\tau\left|\mathbf{a}_{ij},\mathbf{e}_i\right.\right)\Big/30 \qquad \text{(Eq. 7.3.2-13)}$$

Mean annual dose $\bar{\bar{D}}_{GM}\left(\tau\right)$ is computed as

$$\begin{aligned}\bar{\bar{D}}_{SG}\left(\tau\right)&=\sum_{i=1}^{300}\bar{D}_{SG}\left(\tau\left|\mathbf{e}_i\right.\right)\Big/300\\&=\sum_{i=1}^{300}\left(\sum_{j=1}^{30}D_{N+G}\left(\tau\left|\mathbf{a}_{ij},\mathbf{e}_i\right.\right)\Big/30\right)\Big/300\end{aligned} \qquad \text{(Eq. 7.3.2-14)}$$

Because of the Monte Carlo technique used in the Seismic GM Modeling Case for 1,000,000 years, the relatively small size (30) of the aleatory sample, and the wide variability in the effects of a seismic event (Section 6.6), it is not reasonable to presume that the expected annual dose would be numerically stable for each individual epistemic vector $\mathbf{e}_i$. Moreover, due to the computational requirements of this modeling case, it is not practical to dramatically increase the aleatory sample size. Figure 7.3.2-23 compares expected annual dose for an aleatory sample size of 30 to expected annual dose for an aleatory sample size of 90, for epistemic realization 2, in which the sampled value of RST is low (93.5) and thus the frequency of seismic events that cause damage is relatively high. The similarity in the two expected annual dose results indicates

that increasing the aleatory sample size does not produce a qualitatively different expected annual dose, although at any particular time τ the expected annual dose may vary significantly.

Section 7.3.1.2 demonstrates that the mean annual dose calculated by Equation 7.3.2-14 is statistically stable by means of replicated sampling. Moreover, the quantiles of the distribution of expected annual dose are also reasonably stable. The mean annual dose is calculated for each of three independent epistemic LHSs, and the overall mean annual dose for the pooled set of 900 LHS elements is computed by averaging the three independent mean dose histories. Confidence intervals around the overall mean are computed by applying a *t*-test to the sample of three independent means. The overall mean, three independent means, and the confidence intervals are shown on Figure 7.3.1-11. The confidence intervals follow the overall mean quite closely, and the upper confidence interval is consistently about twice the magnitude of the overall mean, indicating that the overall mean annual dose is statistically stable.

7.3.2.7 Seismic Fault Displacement Modeling Case

Expected annual dose for the Seismic FD Modeling Case is calculated as described by Equation 6.1.2-25. Equation 6.1.2-25 is numerically evaluated in two steps. First, for each of a sequence $[t_1, t_2, \ldots, t_N]$ of times for fault displacement events, each WP type r, and each of a set of damage areas $[A_1, A_2, \ldots, A_M]$, annual dose at time τ from a fault displacement event occurring at time t_j resulting in damage area A_k to 100 WPs of type r, $D_{SFr}\left(\tau \middle\| \left[1, t_j, 100, A_k\right], \mathbf{e}_i\right)$, is calculated using the GoldSim component of the TSPA-LA Model. The 100 WPs are placed proportionally into each percolation bin, and within each bin, proportionally into dripping and non-dripping locations. Second, the GoldSim results are used by the EXDOC component of the TSPA-LA Model to calculate expected annual dose.

To determine if the expected annual dose calculations conducted by EXDOC are numerically accurate, the number of times of fault displacement events was increased from 6 to 12, and the number of damage areas was increased from 3 to 5. Table 7.3.2-4 lists the times of seismic events and the damage fractions considered in the base case and in the expanded case for numerical accuracy.

Figure 7.3.2-24 shows the annual dose resulting from each fault displacement event in the base case, and the annual dose resulting from the additional fault displacement events in the expanded case, for a damage area of 1/3 of the cross-sectional area, for both CDSP and CSNF WPs, for epistemic realization 1. In terms of Equation 6.1.2-25, Figure 7.3.2-24 shows the quantities $D_{SFr}\left(\tau \middle\| \left[1, t_j, 100, \frac{1}{3} A_r\right], \mathbf{e}_i\right)$ for t_j as listed in Table 7.3.2-4. For each type of WP, each dose history's shape is similar for different times of the fault displacement event, although the dose history has a different shape for the different WP types since the radionuclide inventory and the temperature of different WP types are different.

Figure 7.3.2-25 shows the annual dose resulting from a fault displacement event at 200 years for each of the different damage areas, for (a) CDSP and (b) CSNF WPs, for epistemic realization 1.

In terms of Equation 6.1.2-25, Figure 7.3.2-25 shows the quantities $D_{SFr}\left(\tau \left| [1, 200, 100, A_k], \mathbf{e}_i \right.\right)$ for A_k as listed in Table 7.3.2-4. For each type of WP, the shape of each dose history is similar for different damage areas, for all but the smallest damage areas on CDSP WPs. For most damage areas, the area is large enough that it does not limit the rate of radionuclide transport through the WP OCB. For CDSP WPs, Figure 7.3.2-25 indicates that dose is proportional to damage area when damage area is quite small. When the damage area increases to approximately 5 percent of the WP cylindrical surface area, essentially all of the seepage that contacts the WP is captured by the openings in the WP. In the Seismic FD Modeling Case, water flux into the WP is modeled with the EBS Flow Submodel described in Section 6.3.6. For this modeling case, the application of the EBS Flow Submodel obviates the need to explicitly consider the geometry of openings in the WP caused by fault displacement. As a consequence of this simplification, the maximum influx of water is achieved at relatively low damage areas from fault displacement events. The effect is observed for CDSP WPs because the annual dose from CDSP WPs between 10,000 and 20,000 years is largely due to ^{239}Pu sorbed to colloids, which transport primarily by advection. In contrast, the annual dose from CSNF WPs is primarily from ^{99}Tc and ^{129}I, which transport rapidly through very small openings in the WPs, as discussed in Section 7.3.2.6.1 for the Seismic GM Modeling Case for 10,000 years.

EXDOC computes expected annual dose by interpolating between single dose histories for different event times and damage areas, similar to those illustrated on Figure 7.3.2-24 and 7.3.2-25, and performing numerical integration using the interpolated dose histories. Because the dose histories maintain similar shapes as the event time and damage fraction change, the interpolation scheme implemented in EXDOC is justified.

Figure 7.3.2-26 compares the expected annual dose over 20,000 years for five epistemic realizations calculated for the base case and the expanded case, using the times of seismic events and damage fractions listed in Table 7.3.2-3. Using additional event times and damage areas increases the expected annual dose by approximately 30 percent in all 5 realizations. Because the dose histories are not different for different damage areas, the change in expected annual dose is due to the additional event times included in the numerical integration. Inclusion of these additional event times in the baseline expected annual dose calculation would improve the accuracy of the baseline results, by approximately 30 percent, as indicated by Figure 7.3.2-26. However, because the contribution to total mean annual dose from the Seismic FD Modeling Case is small compared to other modeling cases (for example, compare Figure 7.3.1-12 for the Seismic FD Modeling Case and Figure 7.3.1-10 for the Seismic GM Modeling Case), the improvement in the accuracy of this modeling case does not justify the additional computational burden imposed by the additional event times.

The analysis of the calculation of expected annual dose for the Seismic FD Modeling Case for 20,000 years showed that, although improvements are possible, the expected annual dose is estimated with sufficient accuracy for 20,000 years. In addition, because the computation of expected annual dose for the Seismic FD Modeling Case for 1,000,000 years is carried out using the same numerical technique, it is reasonable to presume that the expected annual dose for 1,000,000 years is also estimated with sufficient accuracy.

7.3.2.8 Human Intrusion Modeling Case

Expected annual dose for the Human Intrusion Modeling Case is calculated as described by Equation 6.1.2-26. Equation 6.1.2-26 is numerically evaluated using a Monte Carlo technique. One intrusion is modeled, and the time of intrusion is fixed at 200,000 years. For each epistemic realization $\mathbf{e}_i$, a sample of aleatory realizations $\{r_j, q_j, SR_j\}$ is generated, describing the type of WP r_j, the percolation rate q_j, and the SZ source region SR_j at the location of the intrusion. For each combination of epistemic and aleatory realization, annual dose at time τ from an intrusion, $D_{HI}\left(\tau \middle\| [1, r_j, q_j, SR_j], \mathbf{e}_i\right)$, is calculated using the GoldSim component of the TSPA-LA Model and is used in Equation 6.1.2-26 to compute expected annual dose.

To demonstrate that expected annual dose calculations are numerically stable, the size of the aleatory sample was increased from 30 to 90, and expected annual dose was calculated for the first five epistemic realizations. Figure 7.3.2-27 compares expected annual dose for the two aleatory sample sizes. Increasing aleatory sample size has no significant effect on the expected annual dose. Hence, an aleatory sample size of 30 is adequate to obtain a numerically stable estimate of expected annual dose.

Table 7.3.2-1. Times for Igneous Intrusions in the Base Case and the Expanded Case

Calculation Period	Base Case	Expanded Case
20,000 yr	10, 100, 600, 1000, 2000, 4000, 6000, 10000, 14000, 18000	10, 400, 800, 1200, 1600 2000, 2400, 2800, 3200, 3600 4000, 4400, 4800, 5200, 5600 6000, 6400, 6800, 7200, 7600 8000, 8400, 8800, 9200, 9600 10000, 10400, 10800, 11200, 11600 12000, 12400, 12800, 13200, 13600 14000, 14400, 14800, 15200, 15600 16000, 16400, 16800, 17200, 17600 18000, 18400, 18800, 19200, 19600
1,000,000 yr	250, 600, 1000, 4000, 10000, 40000, 100000, 200000, 400000, 800000	250, 20000, 40000, 60000, 80000 100000, 120000, 140000, 160000, 180000 200000, 220000, 240000, 260000, 280000 300000, 320000, 340000, 360000, 380000 400000, 420000, 440000, 460000, 480000 500000, 520000, 540000, 560000, 580000 600000, 620000, 640000, 660000, 680000 700000, 720000, 740000, 760000, 780000 800000, 820000, 840000, 860000, 880000 900000, 920000, 940000, 960000, 980000

Source: Output DTNs: MO0709TSPAREGS.000 [DIRS 182976] for Base Case and MO0708TSPAVALI_000 [DIRS 182985 for Expanded Case.

Table 7.3.2-2. Event Times in the Volcanic Eruption Modeling Case for 20,000 Years

Base Case	Expanded Case
0, 10, 100, 600, 2000, 4000 6000, 10000, 14000, 18000	0, 10, 40, 100, 240, 400, 600 800, 1000, 2000, 4000, 6000 10000, 14000, 18000

Source: Output DTN: MO0709TSPAREGS.000 [DIRS 182976] for Base Case and MO0708TSPAVALI_000 [DIRS 182985] for Expanded Case.

Table 7.3.2-3. Event Times and Damage Fractions in the Seismic Ground Motion Modeling Case for 20,000 Years

	Base Case	Expanded Case
Event Times (yrs)	200, 1000, 3000, 6000, 12000, 18000	100, 1600, 3200, 4800, 6400, 8000, 9600, 11200, 12800, 14400, 16000, 19200
Damage Fractions	10^{-7}, 10^{-6}, 10^{-5}, 10^{-4}, 10^{-3}	10^{-9}, 10^{-8}, 10^{-7}, 10^{-6}, 10^{-5}, 10^{-4}, 10^{-3}, $5x10^{-3}$

Source: Output DTN: MO0709TSPAREGS.000 [DIRS 182976] for Base Case and MO0708TSPAVALI_000 [DIRS 182985] for Expanded Case.

Table 7.3.2-4. Event Times and Damage Areas in the Seismic Fault Displacement Modeling Case for 20,000 Years

	Base Case	Expanded Case
Event Times (yrs)	200, 800, 2000, 4000, 8000, 18000	200, 1600, 3200, 4800 6400, 8000, 9600, 11200 12800, 14400, 16000, 19200
Damage Areas (fraction of cross section area)	1/3, 2/3, 1	1/12, 1/6, 1/3, 2/3, 1

Source: Output DTN: MO0709TSPAREGS.000 [DIRS 182976] for Base Case and MO0708TSPAVALI_000 [DIRS 182985] for Expanded Case

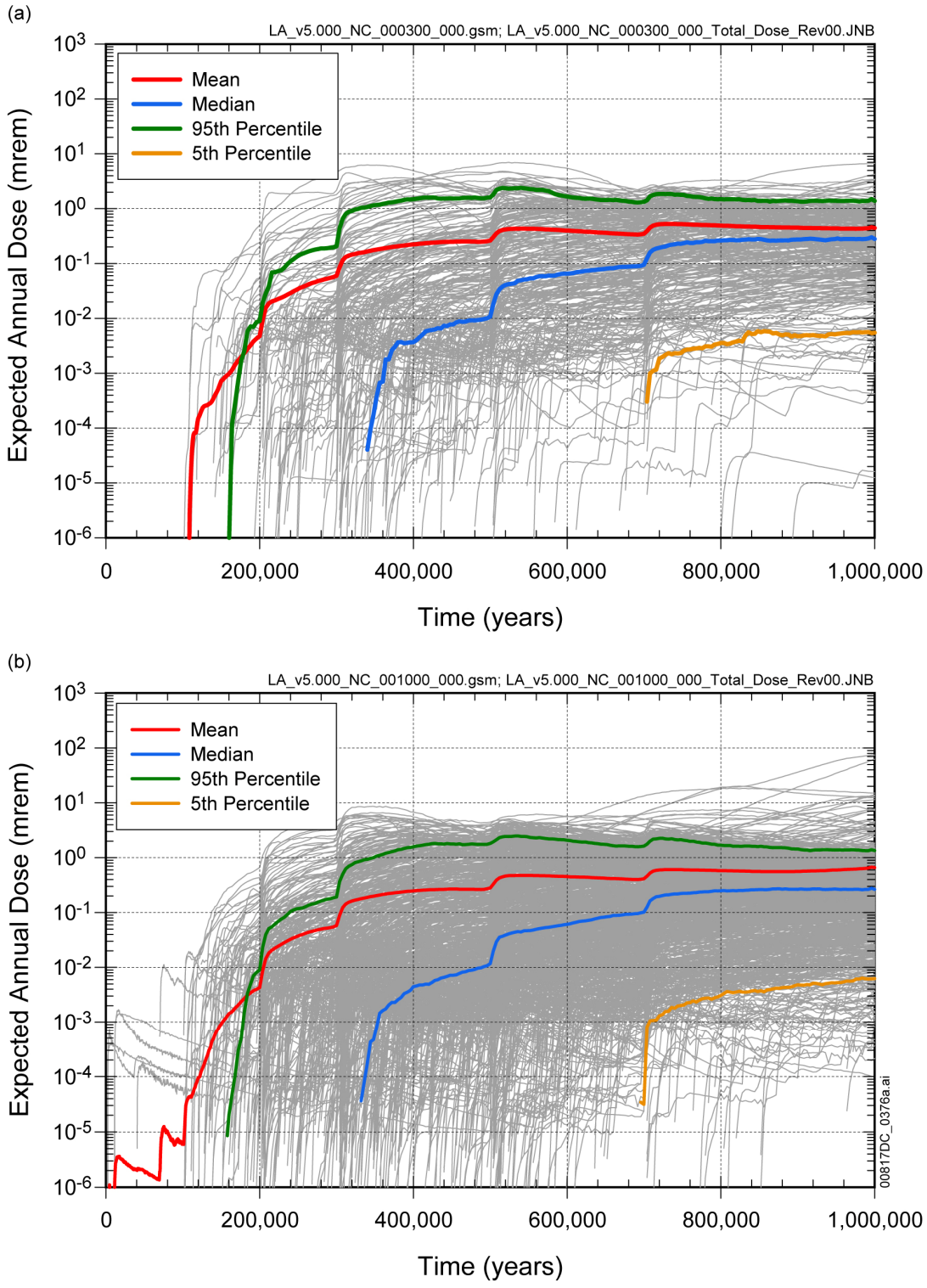

Source: Output DTNs: MO0709TSPASTAB.000 [DIRS 182983] and MO0709TSPAREGS.000 [DIRS 182976].

Figure 7.3.2-1. Expected Annual Dose for the Nominal Modeling Case: (a) Latin Hypercube Sampling Size of 300 and (b) Latin Hypercube Sampling Size of 1,000

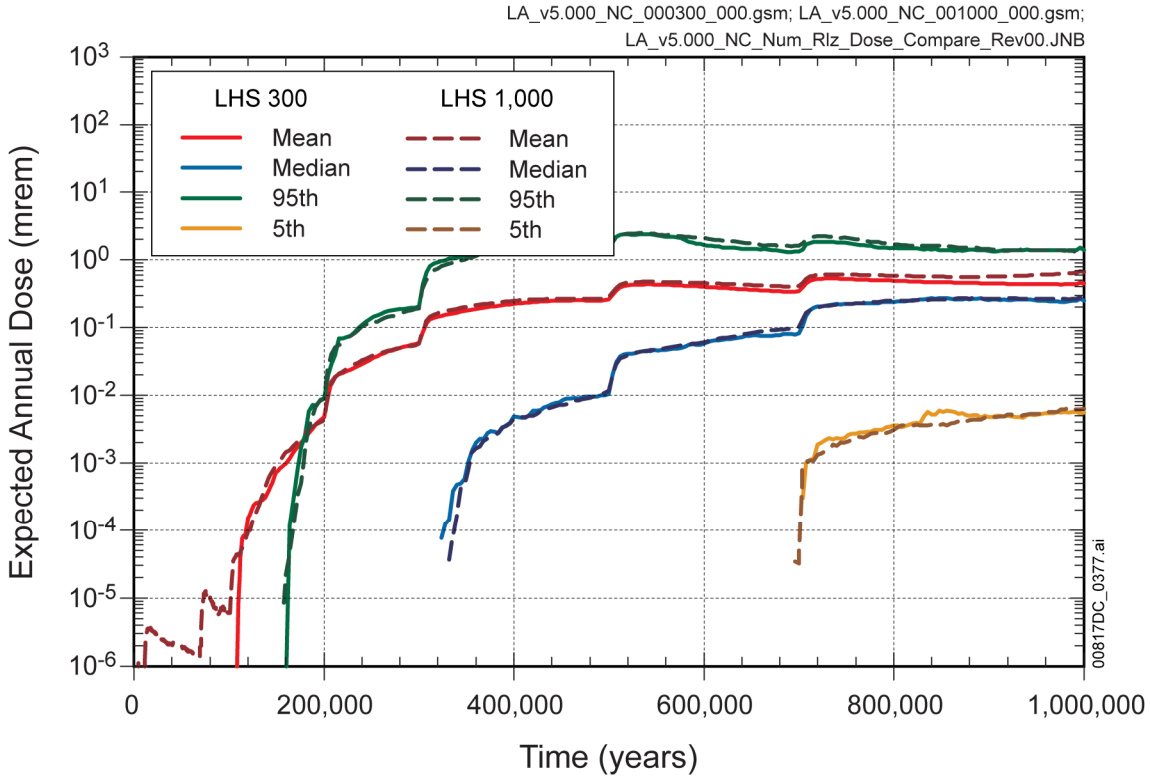

Source: Output DTNs: MO0709TSPASTAB.000 [DIRS 182983] and MO0709TSPAREGS.000 [DIRS 182976].

Figure 7.3.2-2. Uncertainty in Expected Annual Dose for the Nominal Modeling Case using Latin Hypercube Sampling Sizes of 300 and 1,000

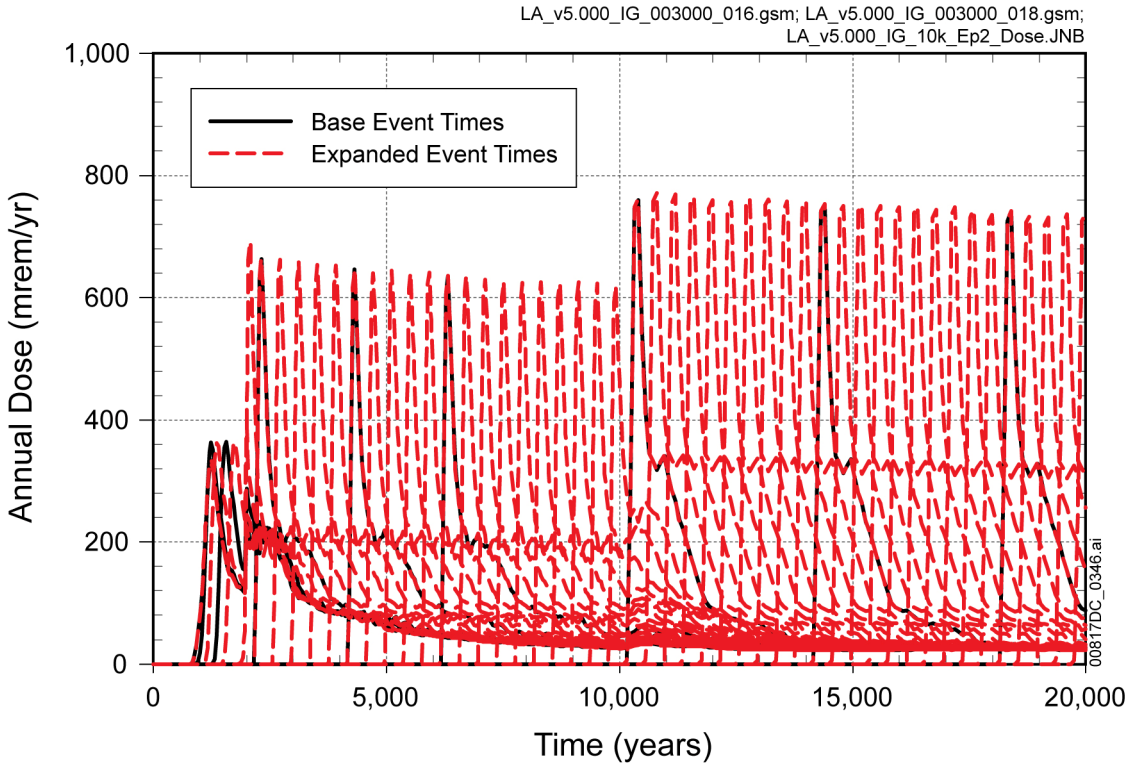

Source: Output DTNs: MO0709TSPASTAB.000 [DIRS 182983] and MO0709TSPAREGS.000 [DIRS 182976].

Figure 7.3.2-3. Annual Dose Over 20,000 Years for the Igneous Intrusion Modeling Case Considering Additional Specified Event Times for Epistemic Realization 2

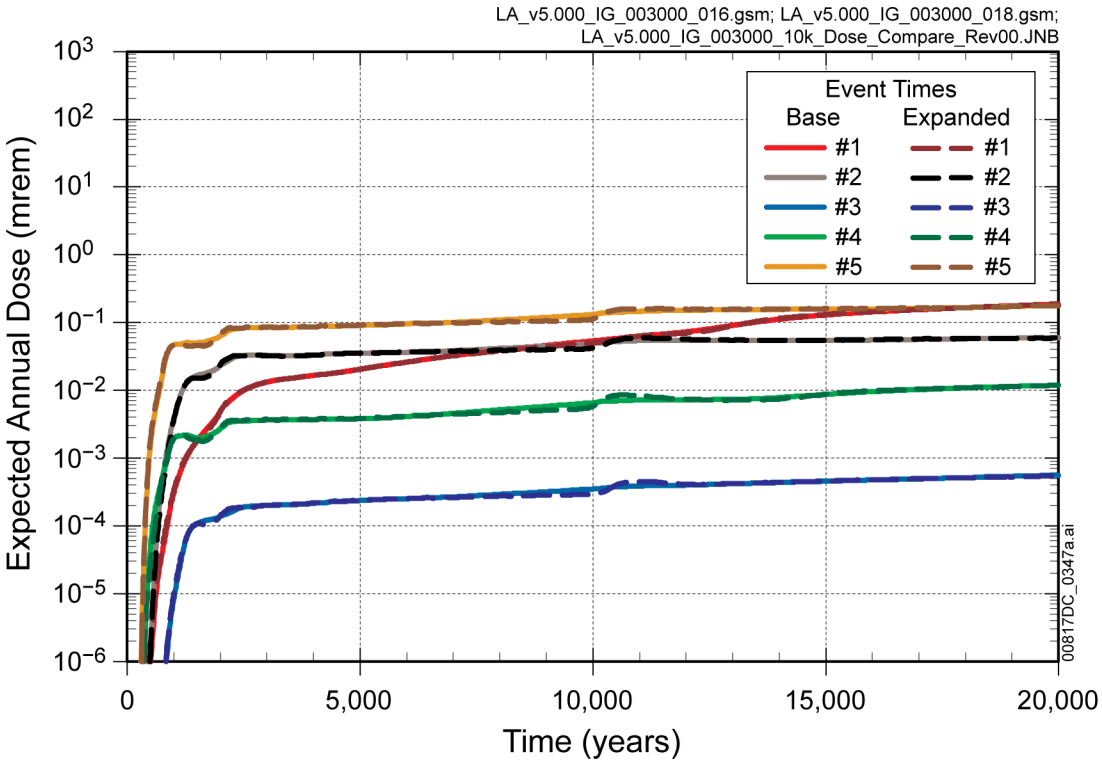

Source: Output DTNs: MO0709TSPASTAB.000 [DIRS 182983] and MO0709TSPAREGS.000 [DIRS 182976].

Figure 7.3.2-4. Expected Annual Dose Over 20,000 Years for the Igneous Intrusion Modeling Case Considering Additional Specified Event Times

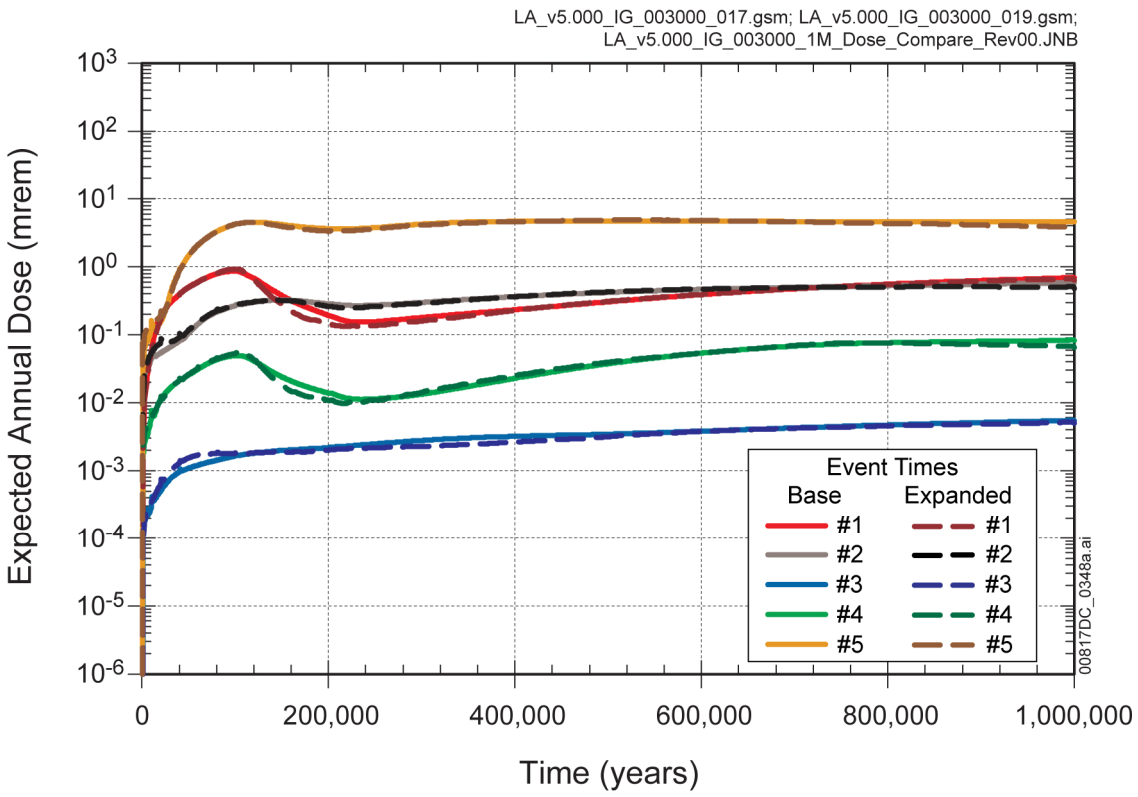

Source: Output DTNs: MO0709TSPASTAB.000 [DIRS 182983] and MO0709TSPAREGS.000 [DIRS 182976].

Figure 7.3.2-5. Expected Annual Dose Over 1,000,000 Years for Igneous Intrusion Modeling Case Considering Additional Specified Event Times

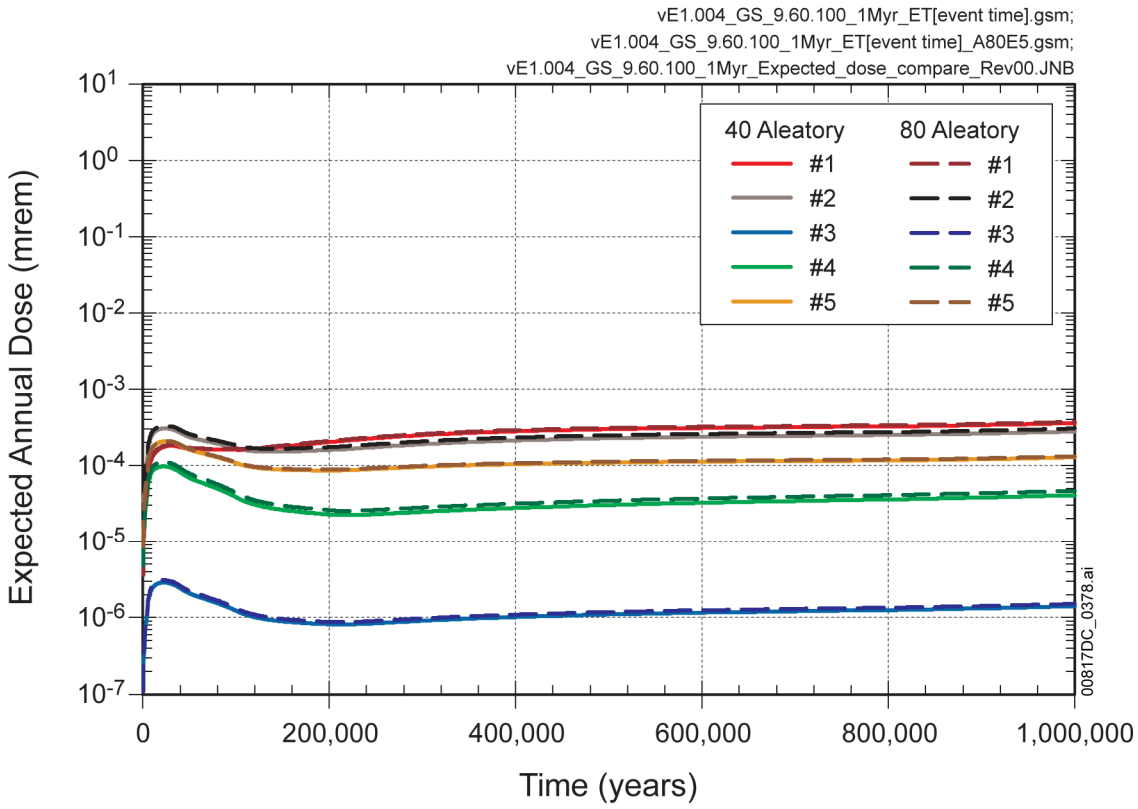

Source: Output DTNs: MO0709TSPASTAB.000 [DIRS 182983] and MO0709TSPAREGS.000 [DIRS 182976].

Figure 7.3.2-6. Expected Annual Dose Over 1,000,000 Years for Volcanic Eruption Modeling Case Using Aleatory Latin Hypercube Sampling Sizes of 40 and 80

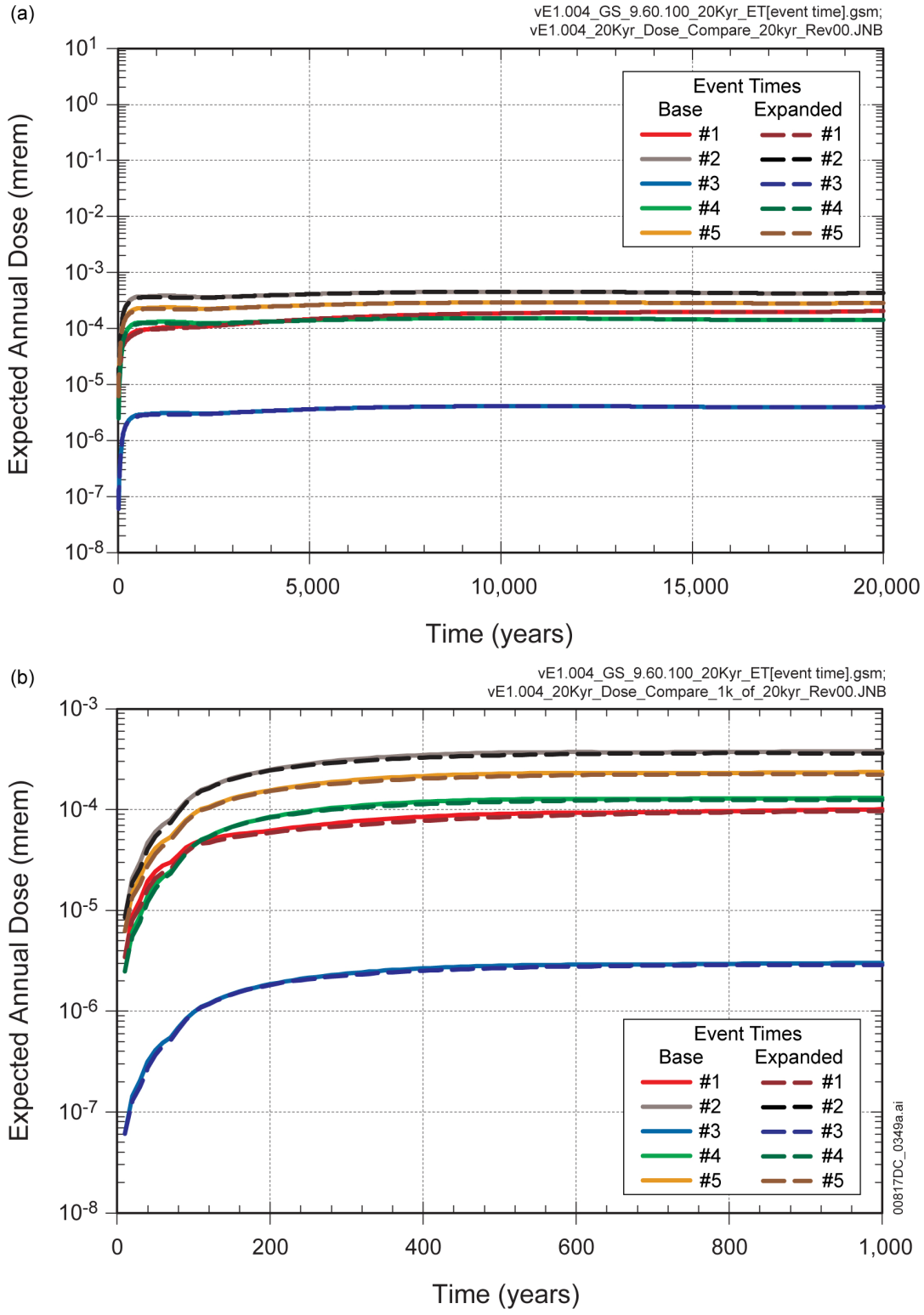

Source: Output DTNs: MO0709TSPASTAB.000 [DIRS 182983] and MO0709TSPAREGS.000 [DIRS 182976].

Figure 7.3.2-7. Expected Annual Dose for Volcanic Eruption Modeling Case Considering Additional Specified Event Times Over (a) 20,000 Years and (b) 1,000 Years

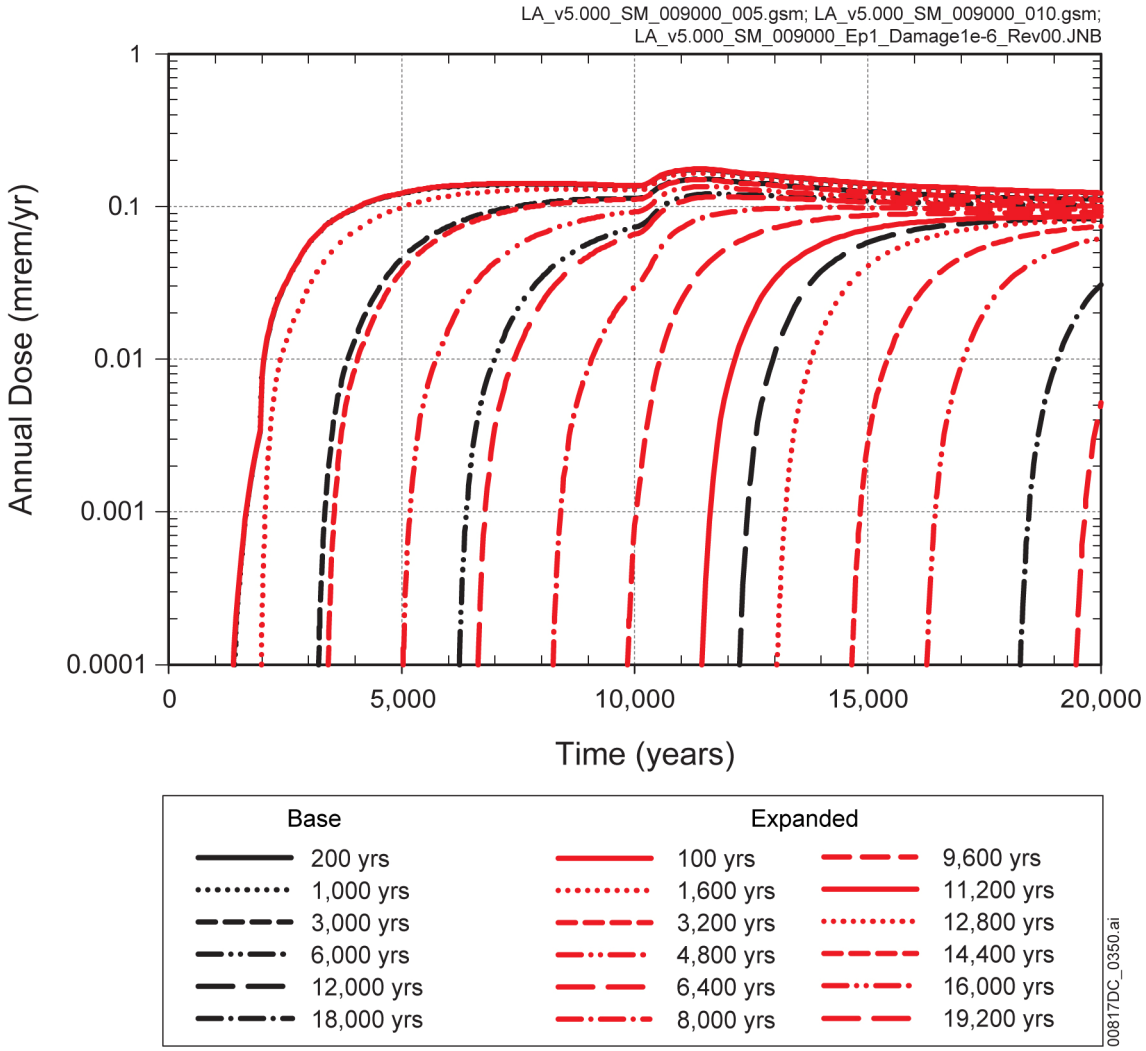

Source: Output DTNs: MO0709TSPASTAB.000 [DIRS 182983] and MO0709TSPAREGS.000 [DIRS 182976].

Figure 7.3.2-8. Annual Dose Over 20,000 Years for the Seismic Ground Motion Modeling Case Considering Additional Specified Event Times with Constant Damage Fraction 10^{-6} for Epistemic Realization 1

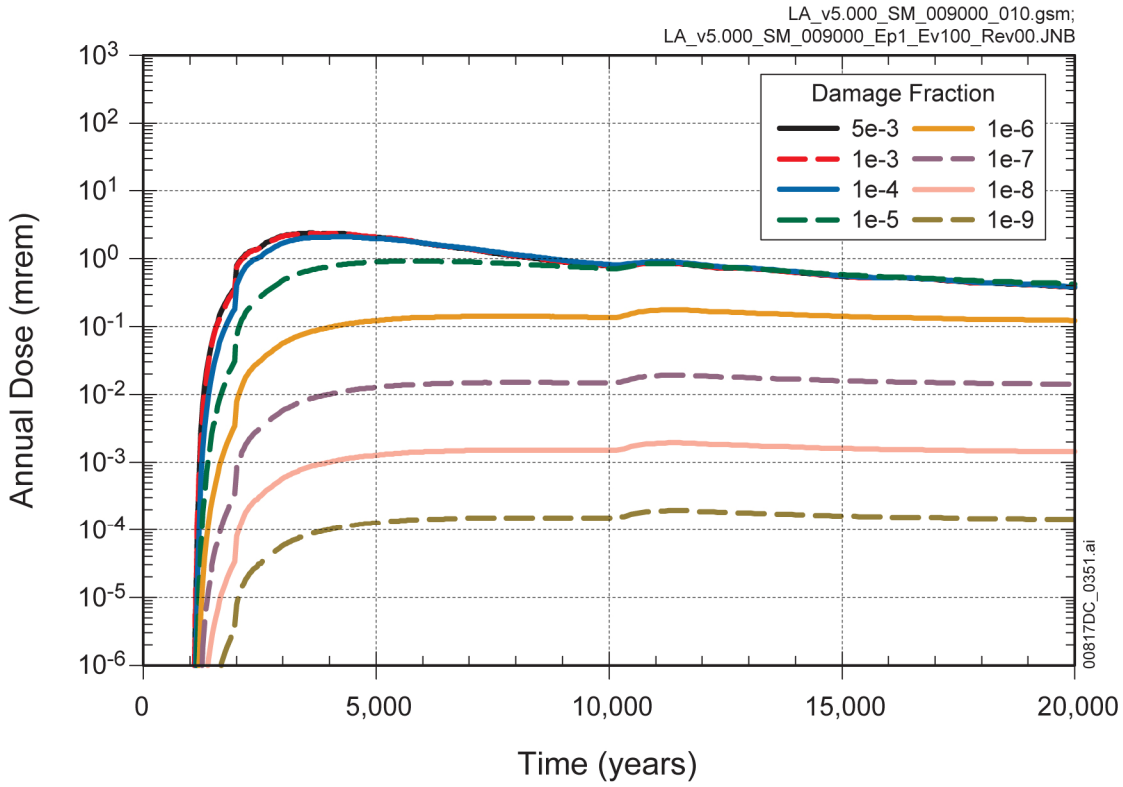

Source: Output DTN: MO0709TSPASTAB.000 [DIRS 182983].

Figure 7.3.2-9. Annual Dose Over 20,000 Years for Seismic Ground Motion Modeling Case Considering Additional Specified Damage Fractions from a Seismic Event at 100 Years for Epistemic Realization 1

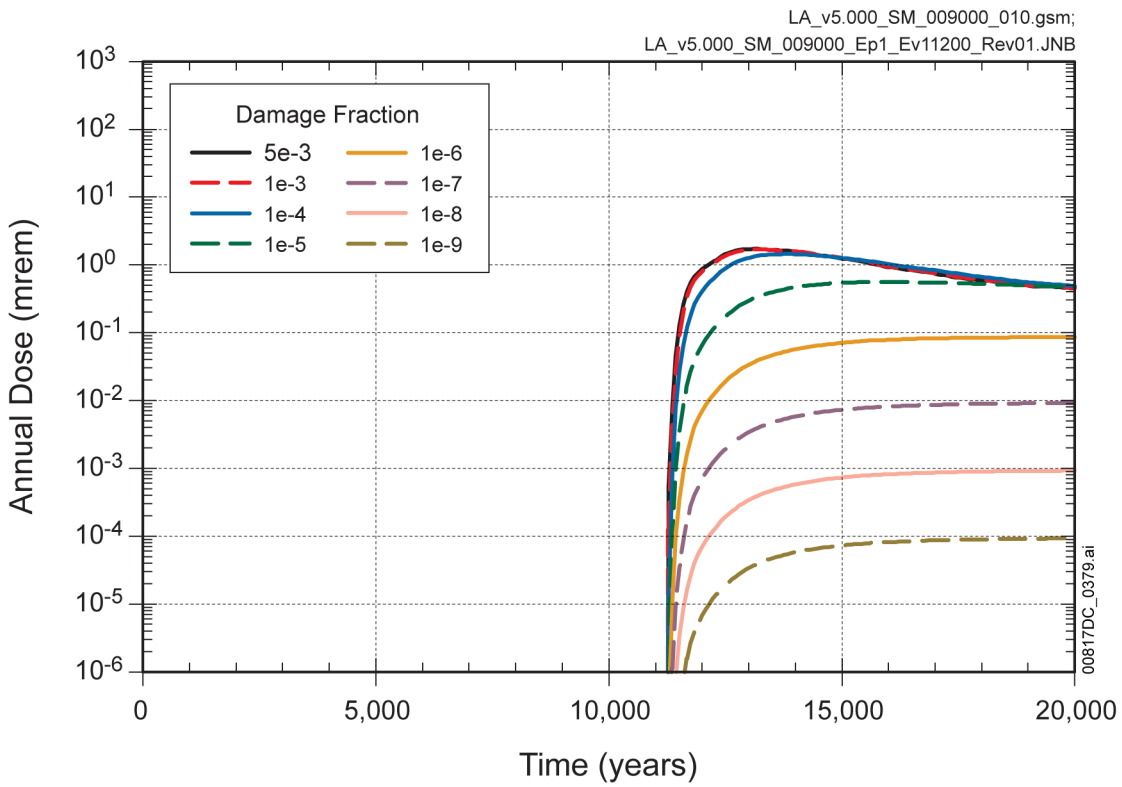

Source: Output DTN: MO0709TSPASTAB.000 [DIRS 182983].

Figure 7.3.2-10. Annual Dose Over 20,000 Years for Seismic Ground Motion Modeling Case Considering Additional Specified Damage Fractions from a Seismic Event at 11,200 Years for Epistemic Realization 1

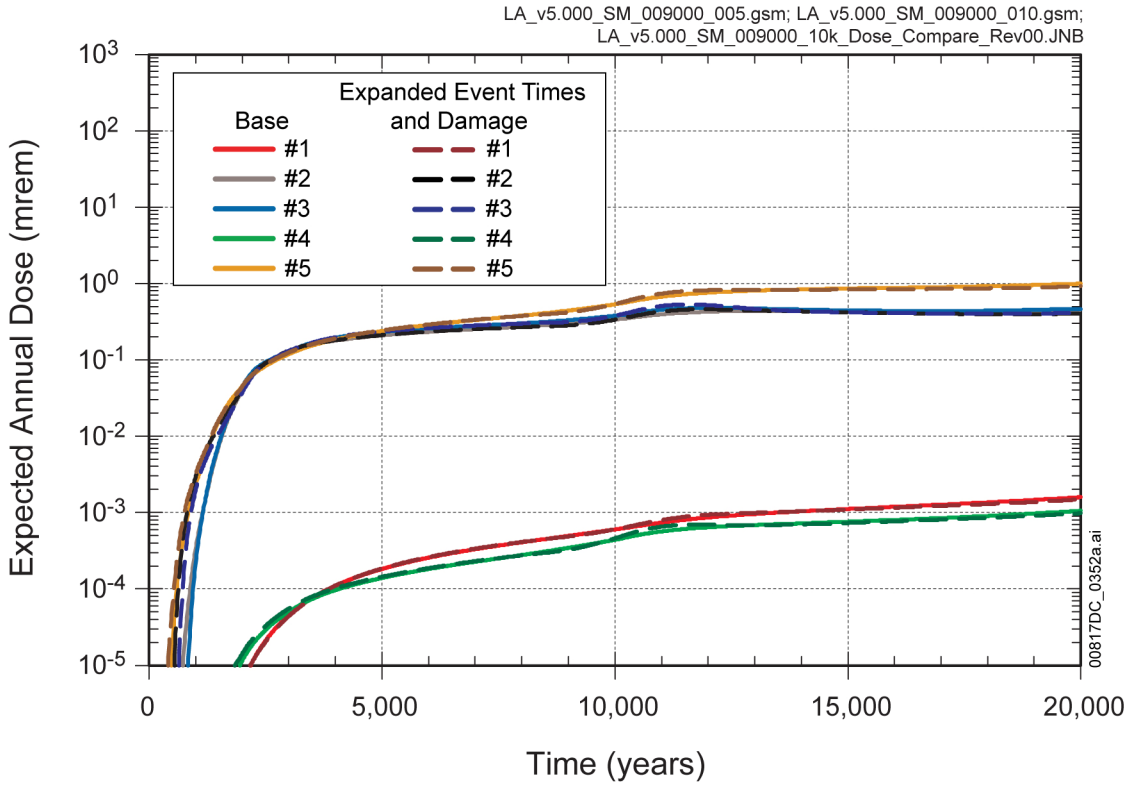

Source: Output DTNs: MO0709TSPASTAB.000 [DIRS 182983] and MO0709TSPAREGS.000 [DIRS 182976].

Figure 7.3.2-11. Expected Annual Dose Over 20,000 Years for Seismic Ground Motion Modeling Case Considering Additional Specified Event Times and Damage Fractions

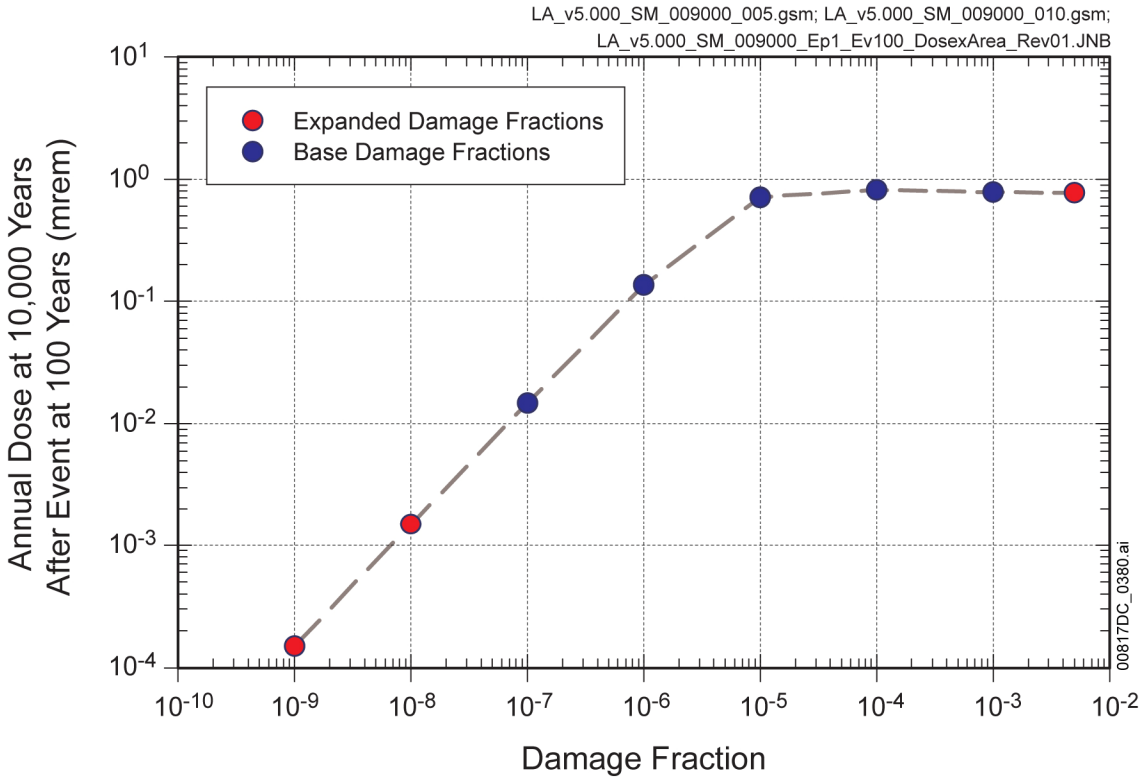

Source: Output DTNs: MO0709TSPASTAB.000 [DIRS 182983] and MO0709TSPAREGS.000 [DIRS 182976].

Figure 7.3.2-12. Annual Dose vs. Damage Fraction for a Seismic Ground Motion Event at 100 Years for Epistemic Realization 1

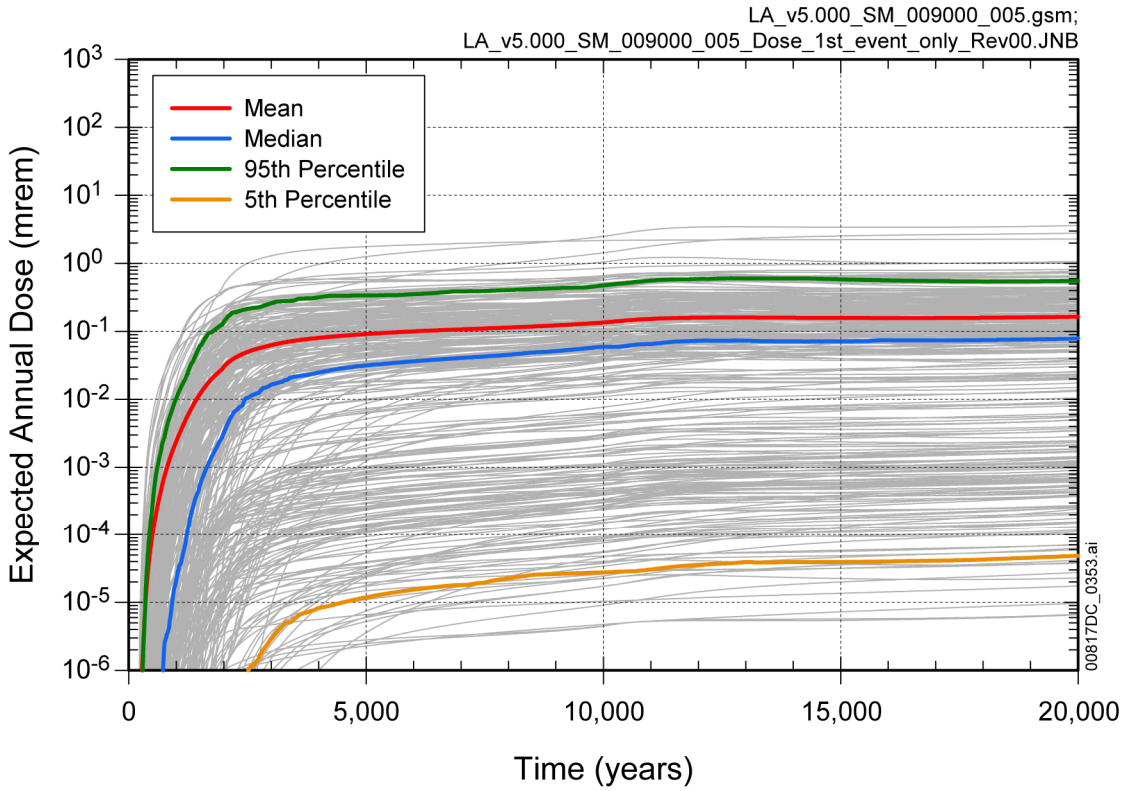

Source: Output DTN: MO0709TSPAREGS.000 [DIRS 182976].

Figure 7.3.2-13. Expected Annual Dose Over 20,000 Years from First Damaging Seismic Ground Motion Event

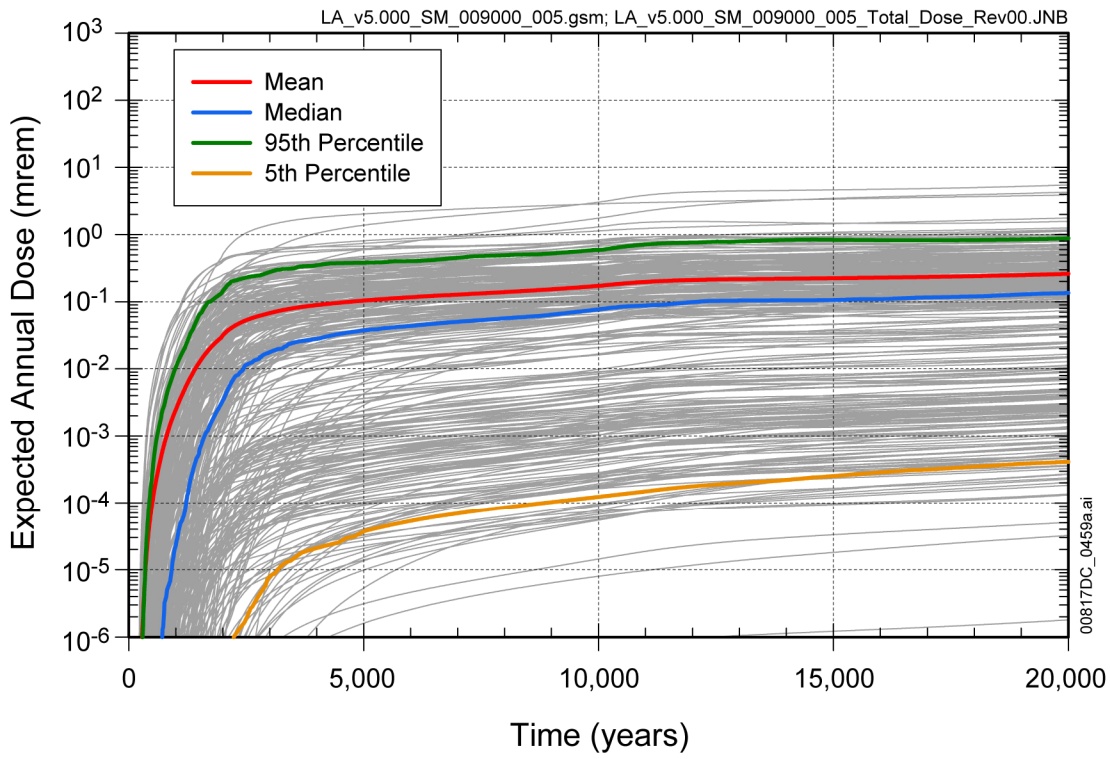

Source: Output DTN: MO0709TSPAREGS.000 [DIRS 182976].

Figure 7.3.2-14. Expected Annual Dose Over 20,000 Years from All Damaging Seismic Ground Motion Events

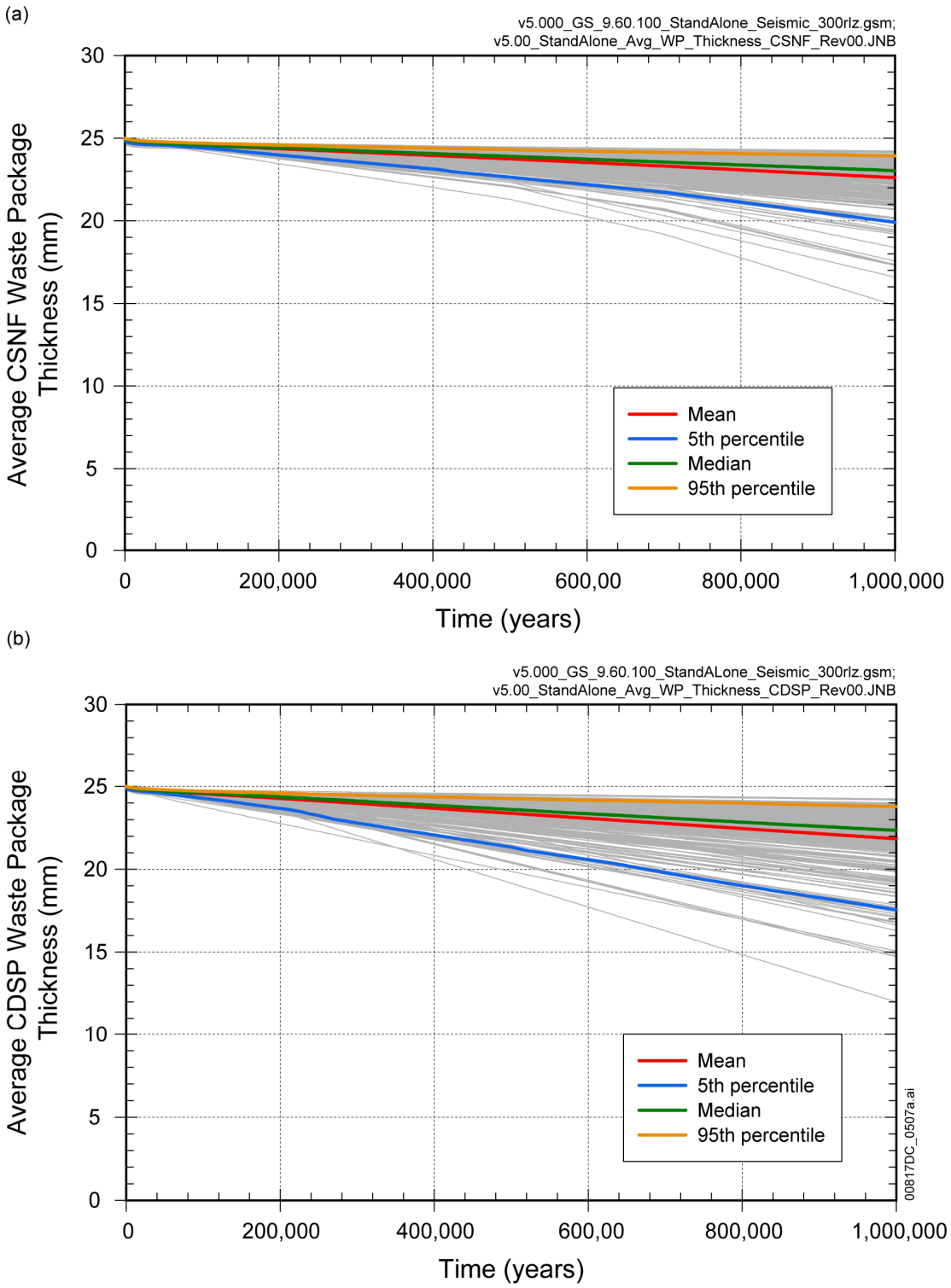

Source: Output DTN: MO0709TSPAWPDS.000 [DIRS 183170].

Figure 7.3.2-15. Spatially-Averaged Waste Package Thickness for 1,000,000 Years for (a) CSNF WPs and (b) CDSP WPs

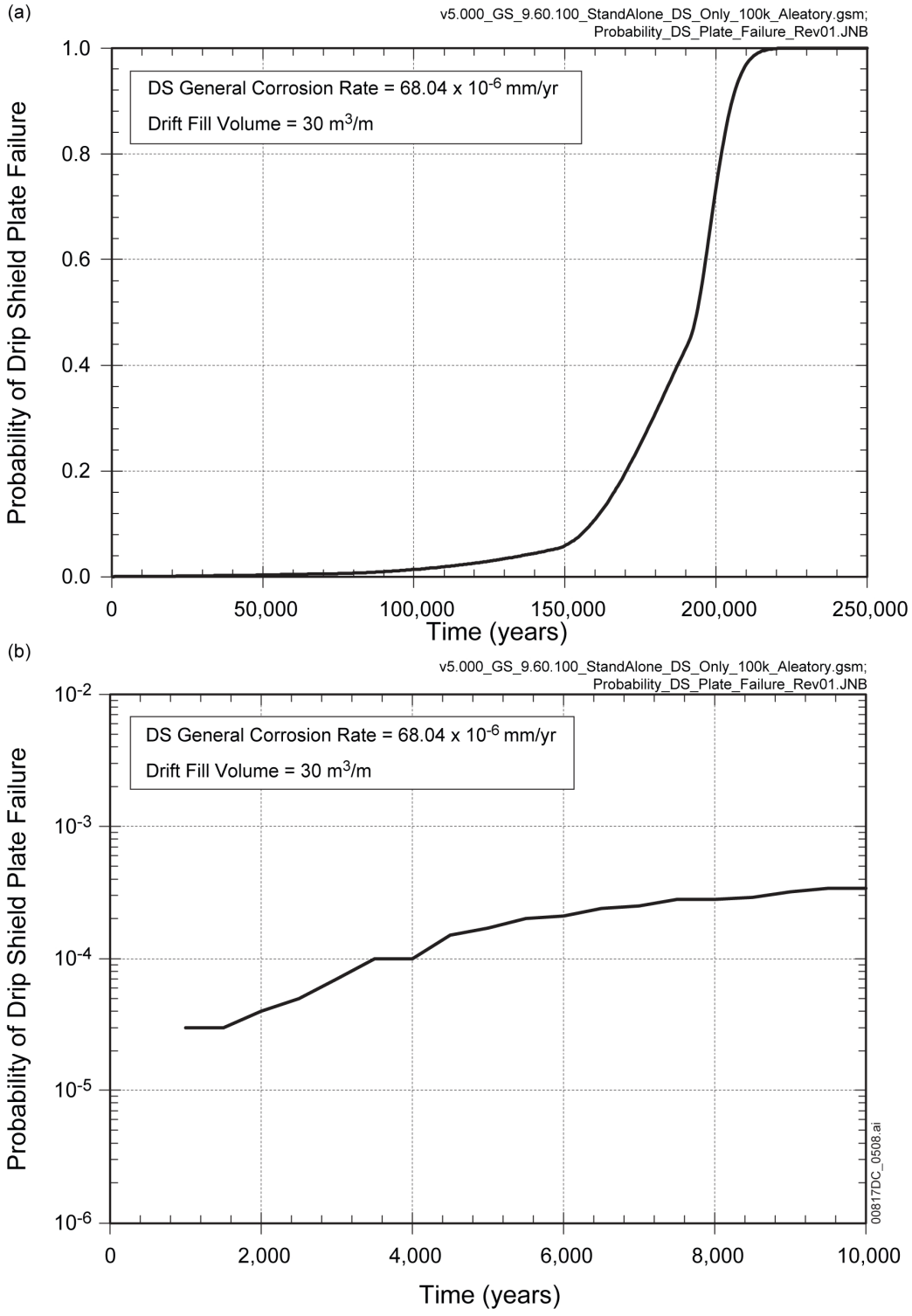

Source: Output DTN: MO0709TSPAWPDS.000 [DIRS 183170].

Figure 7.3.2-16. Bounding Probability of Drip Shield Plate Failure for (a) 250,000 Years and (b) 10,000 Years

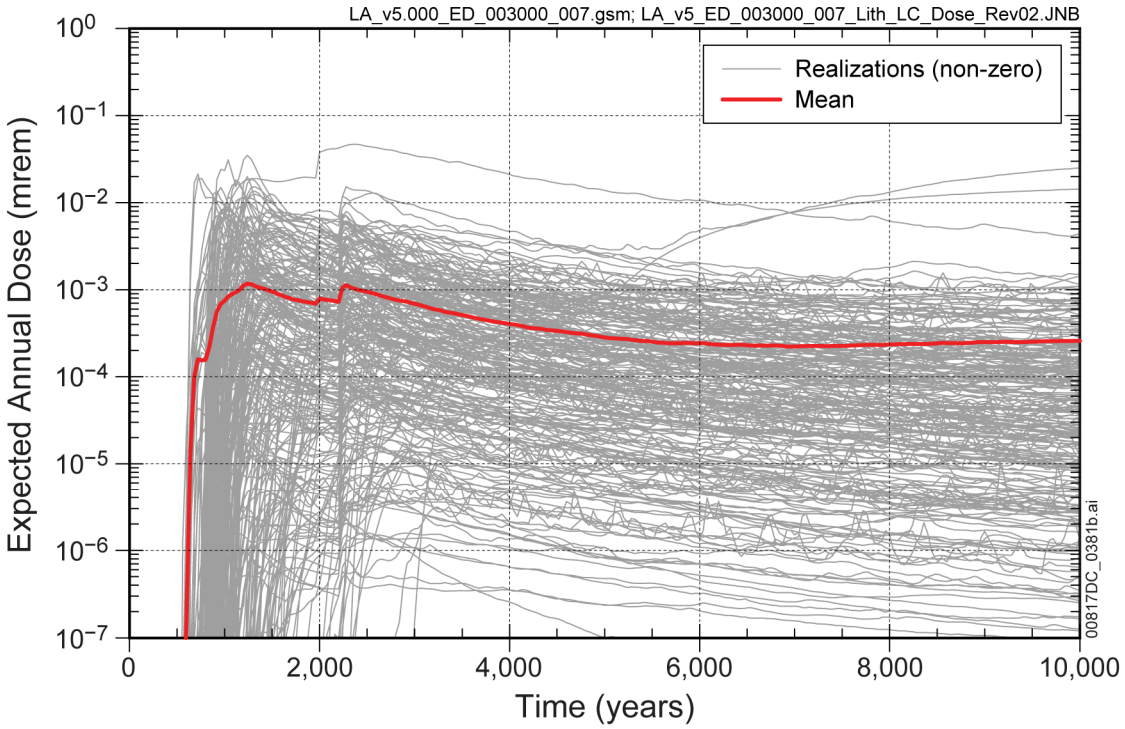

Source: Output DTNs: MO0709TSPAREGS.000 [DIRS 182976] and MO708FREQCALC.000 [DIRS 183006].

Figure 7.3.2-17. Expected Annual Dose Over 10,000 Years from Seismic Ground Motion Events that Result in Drip Shield Plate Failure

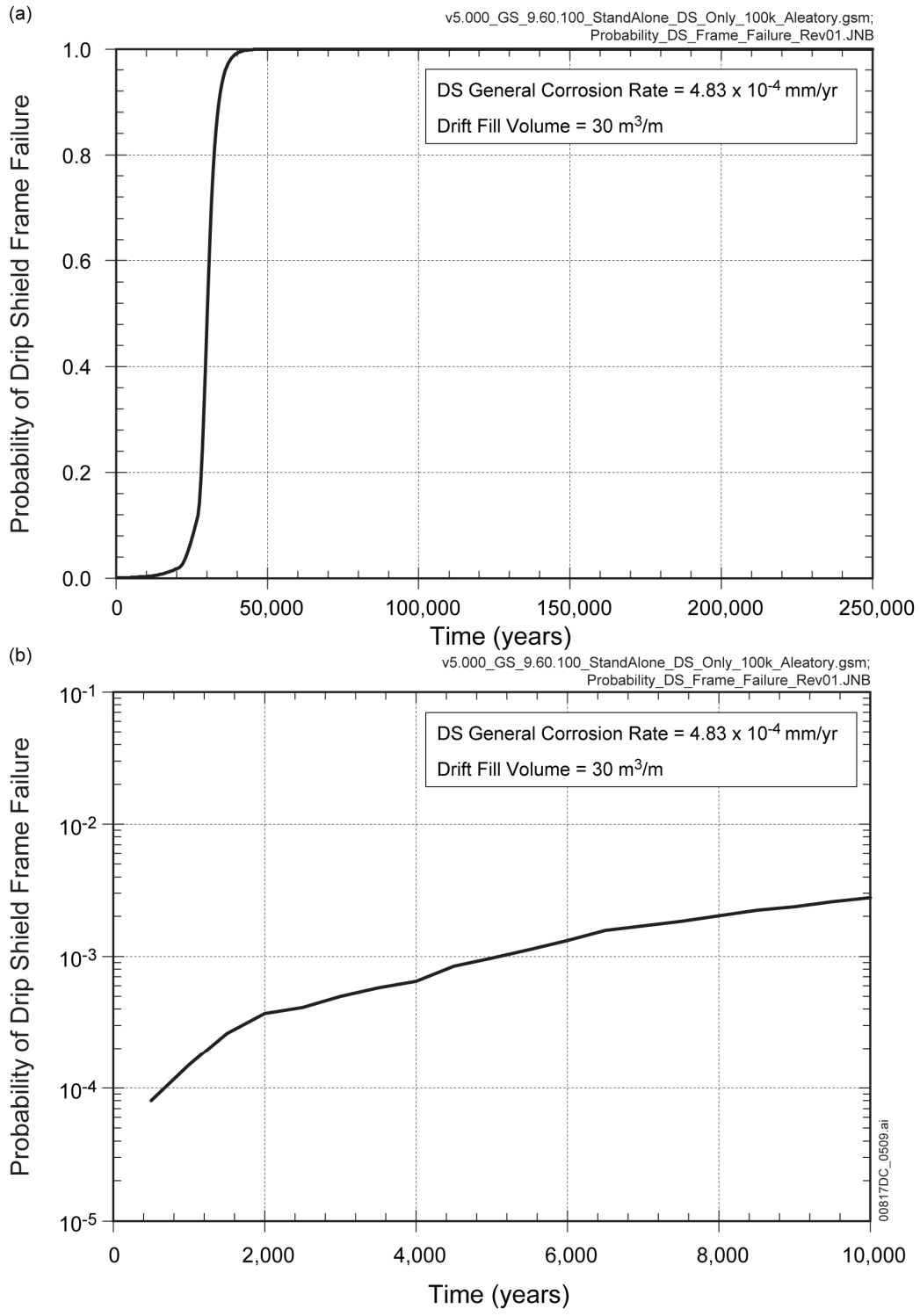

Source: Output DTN: MO0709TSPAWPDS.000 [DIRS 183170].

Figure 7.3.2-18. Bounding Probability of Drip Shield Framework Failure for (a) 250,000 Years and (b) 10,000 Years

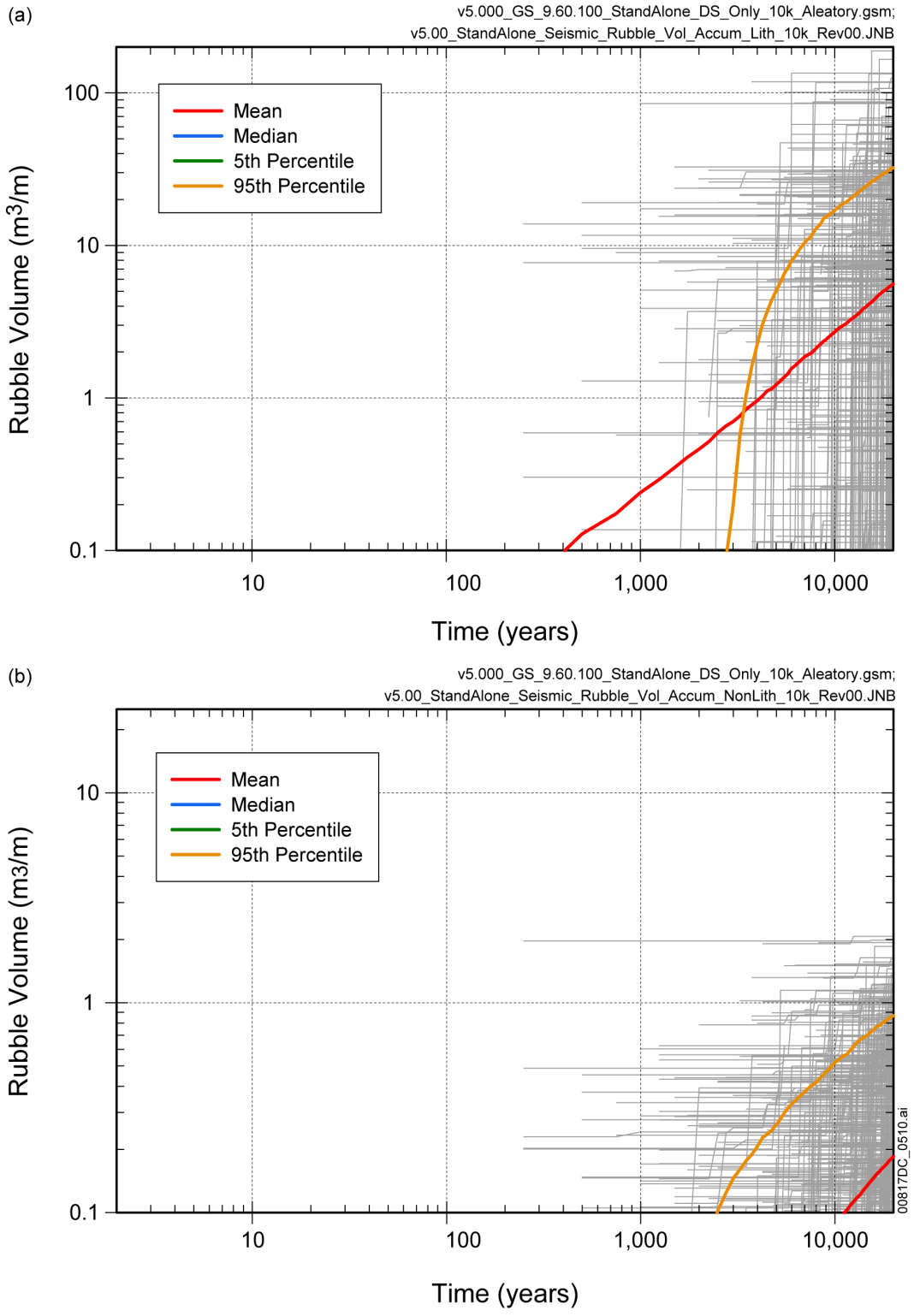

Source: Output DTN: MO0709TSPAWPDS.000 [DIRS 183170].

Figure 7.3.2-19. Volume of (a) Lithophysal and (b) Nonlithophysal Rockfall Over 20,000 Years

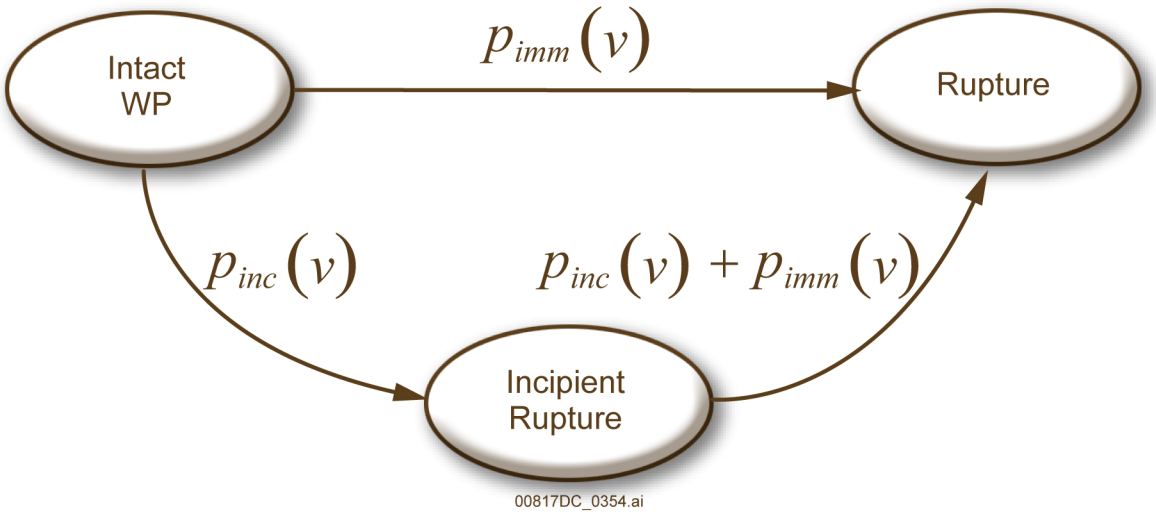

Figure 7.3.2-20. State Diagram for Waste Package Rupture in the Seismic Consequences Abstraction

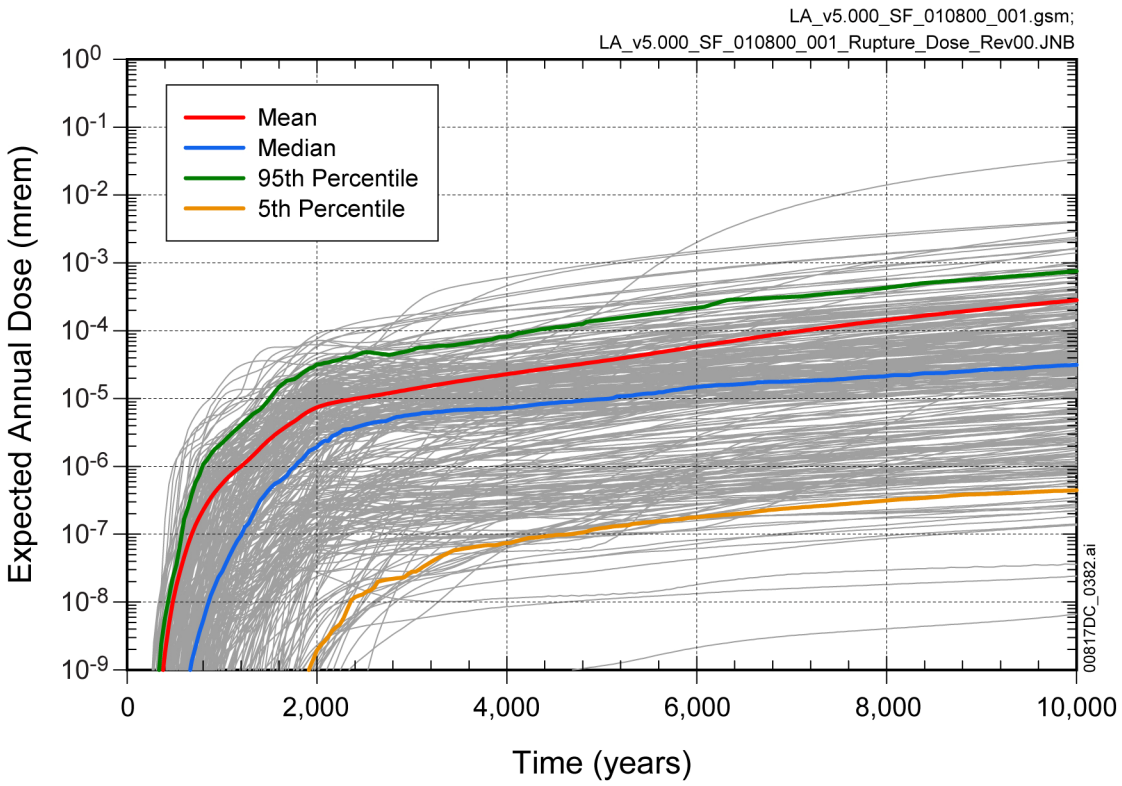

Source: Output DTN: MO0709TSPAREGS.000 [DIRS 182976].

Figure 7.3.2-21. Estimated Expected Annual Dose Over 10,000 Years from Seismic Ground Motion Events that Result in Rupture

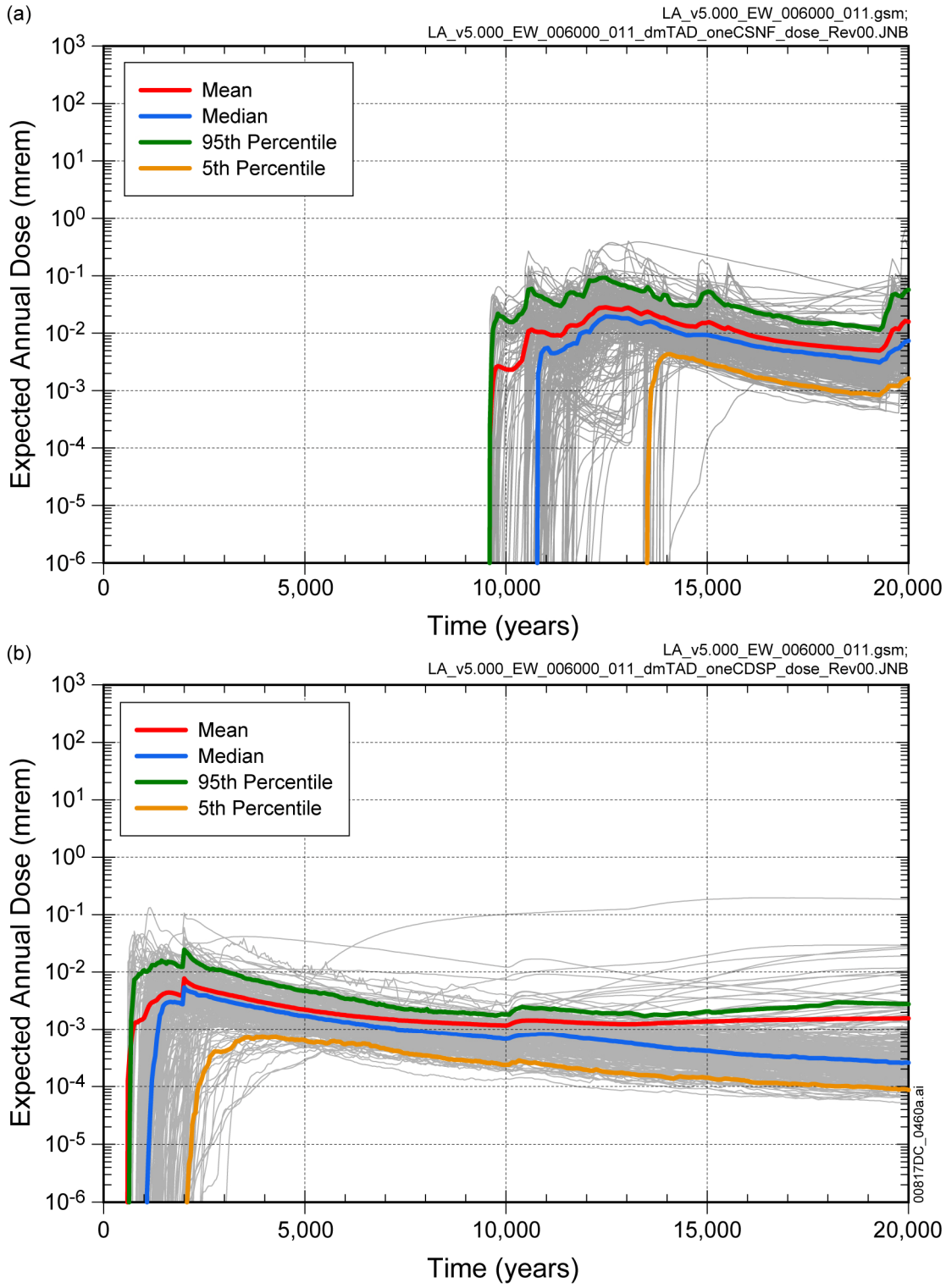

Source: Output DTN: MO0709TSPAREGS.000 [DIRS 182976].

Figure 7.3.2-22. Annual Dose from (a) One Early Failure CSNF WP and (b) One Early Failure CDSP WP Considering All Five Percolation Bins and 300 Epistemic Realizations

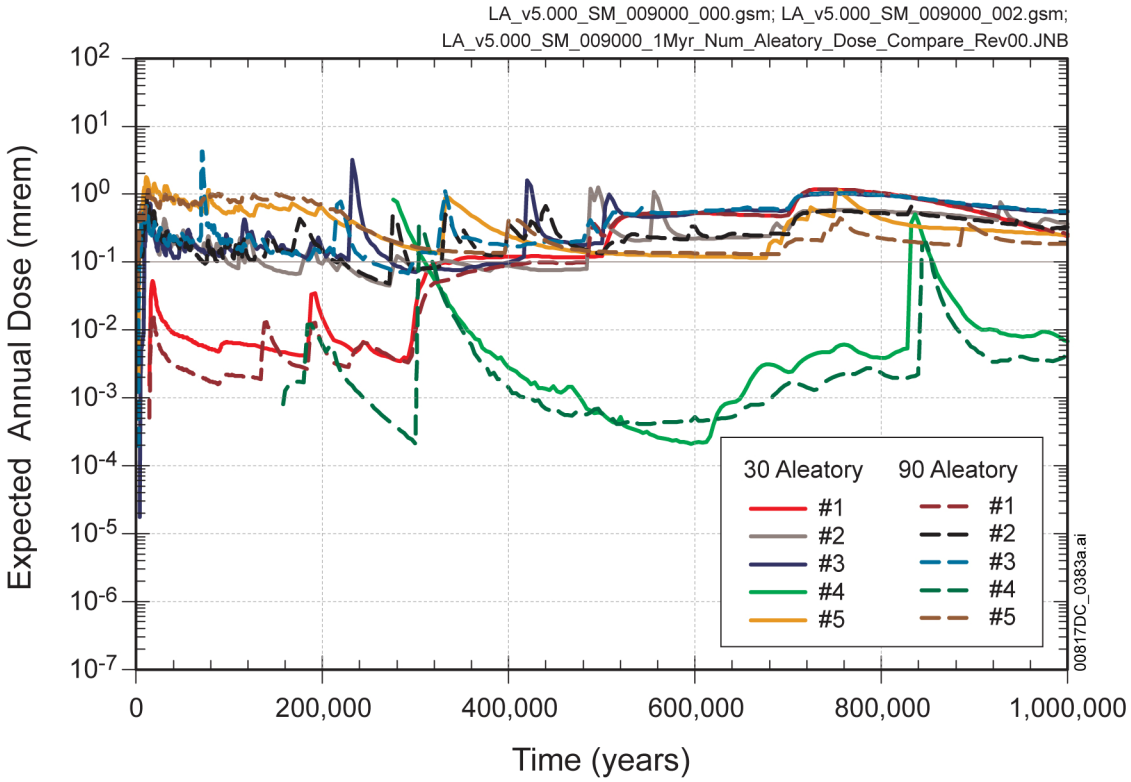

Source: Output DTNs: MO0709TSPASTAB.000 [DIRS 182983] and MO0709TSPAREGS.000 [DIRS 182976].

Figure 7.3.2-23. Expected Annual Dose for 1,000,000 Years from Seismic Ground Motion for Epistemic Realization 2 for Aleatory Sample Size of 30 and 90

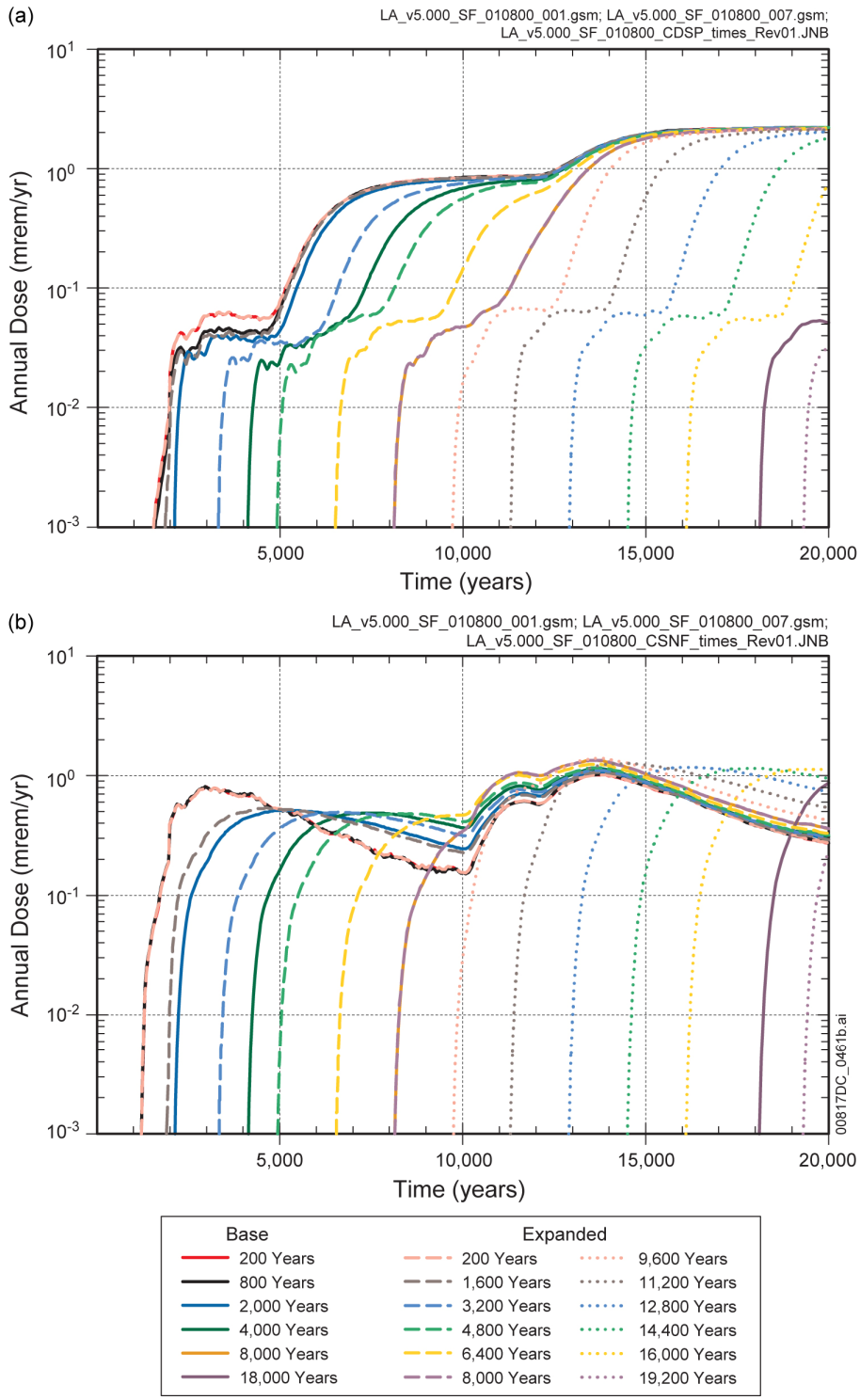

Source: Output DTNs: MO0709TSPASTAB.000 [DIRS 182983] and MO0709TSPAREGS.000 [DIRS 182976].

Figure 7.3.2-24. Annual Dose Over 20,000 Years for Seismic Fault Displacement Modeling Case for (a) CDSP WPs and (b) CSNF WPs Considering Additional Specified Event Times with Constant Damage Area for Epistemic Realization 1

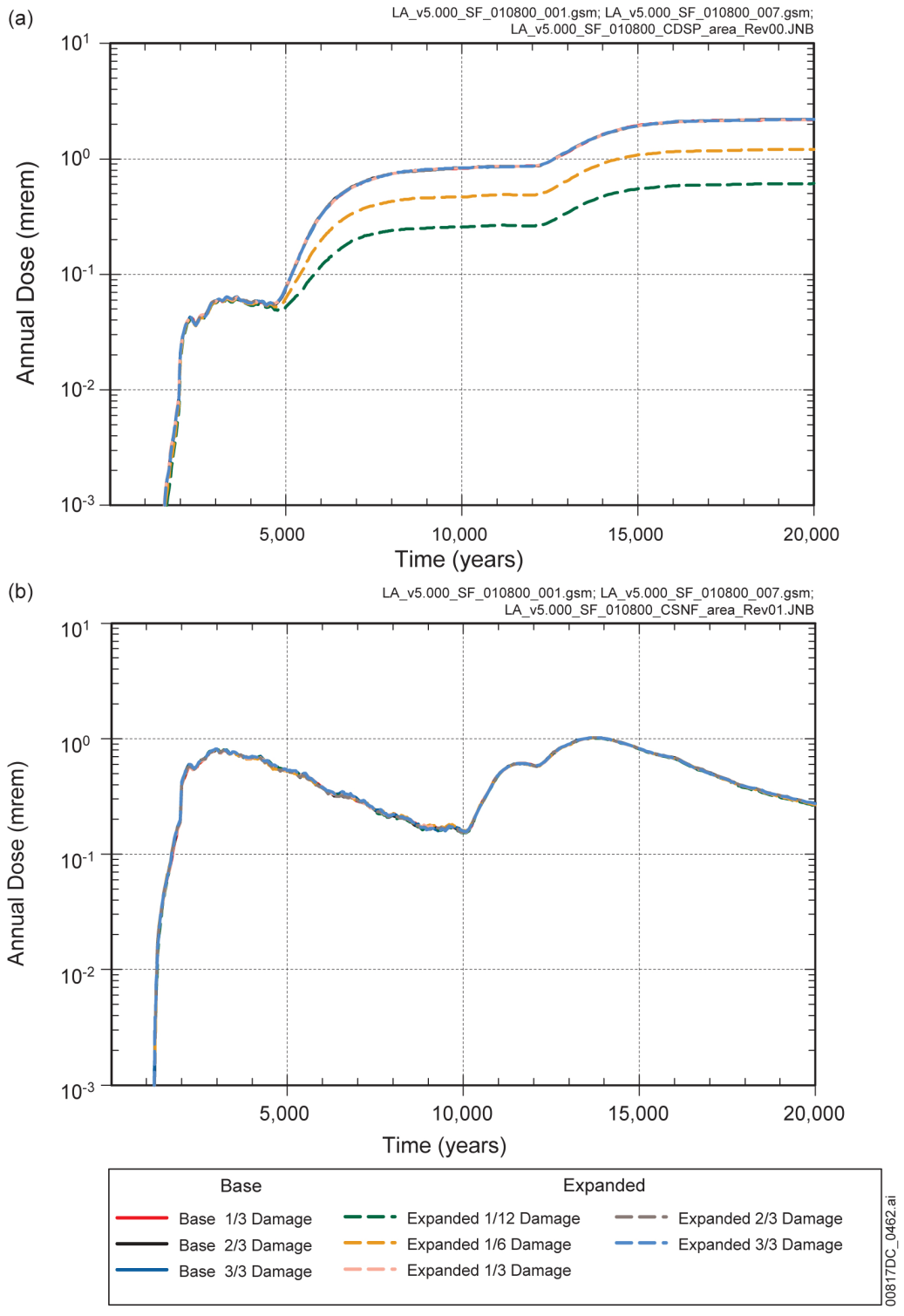

Source: Output DTNs: MO0709TSPASTAB.000 [DIRS 182983] and MO0709TSPAREGS.000 [DIRS 182976].

Figure 7.3.2-25. Annual Dose over 20,000 Years for a Fault Displacement Event at 200 Years Considering Additional Damage Areas for Epistemic Realization 1 for (a) CDSP WPs and (b) CSNF WPs

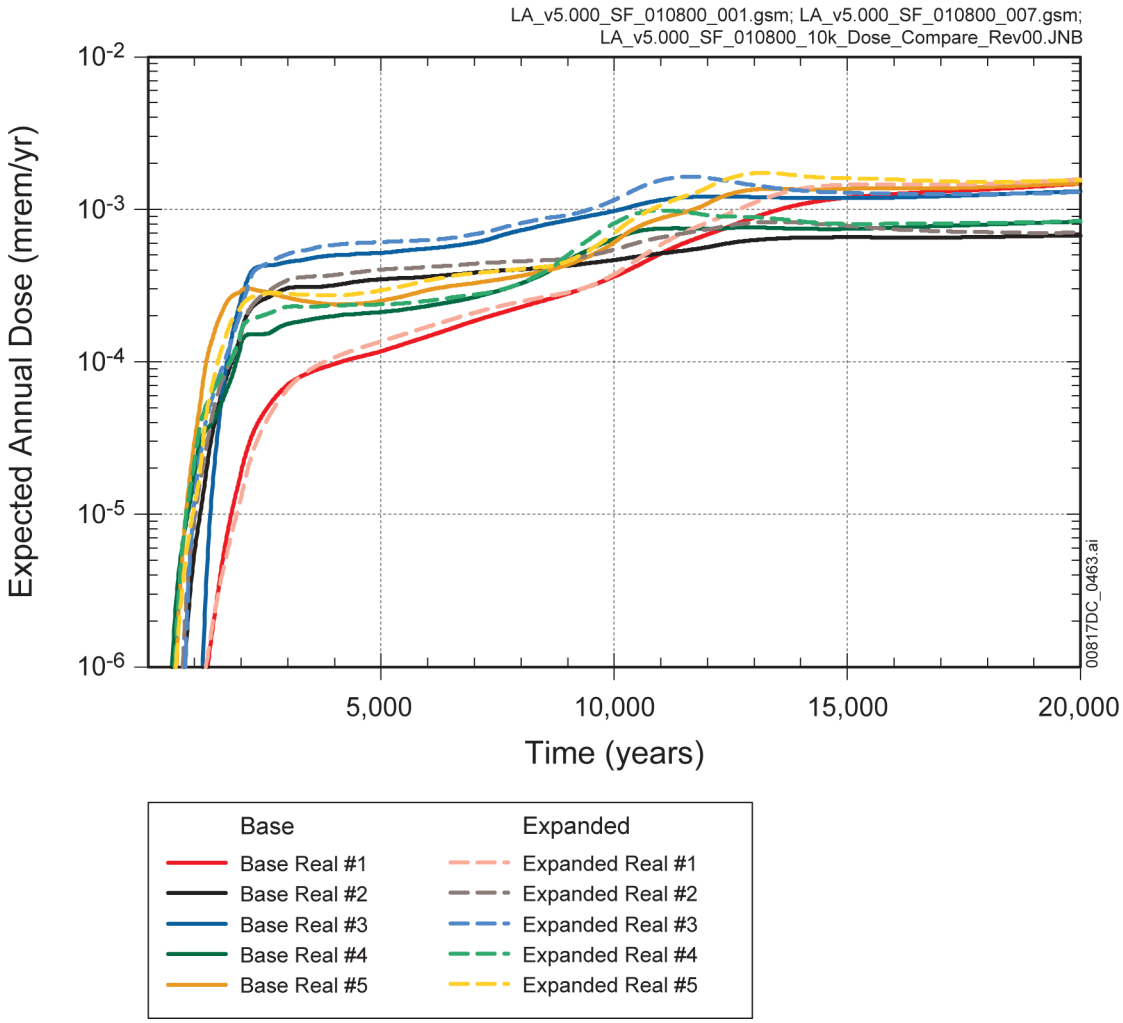

Source: Output DTNs: MO0709TSPASTAB.000 [DIRS 182983] and MO0709TSPAREGS.000 [DIRS 182976].

Figure 7.3.2-26. Expected Annual Dose Over 20,000 Years for Seismic Fault Displacement Modeling Case Considering Additional Specified Event Times and Damage Areas

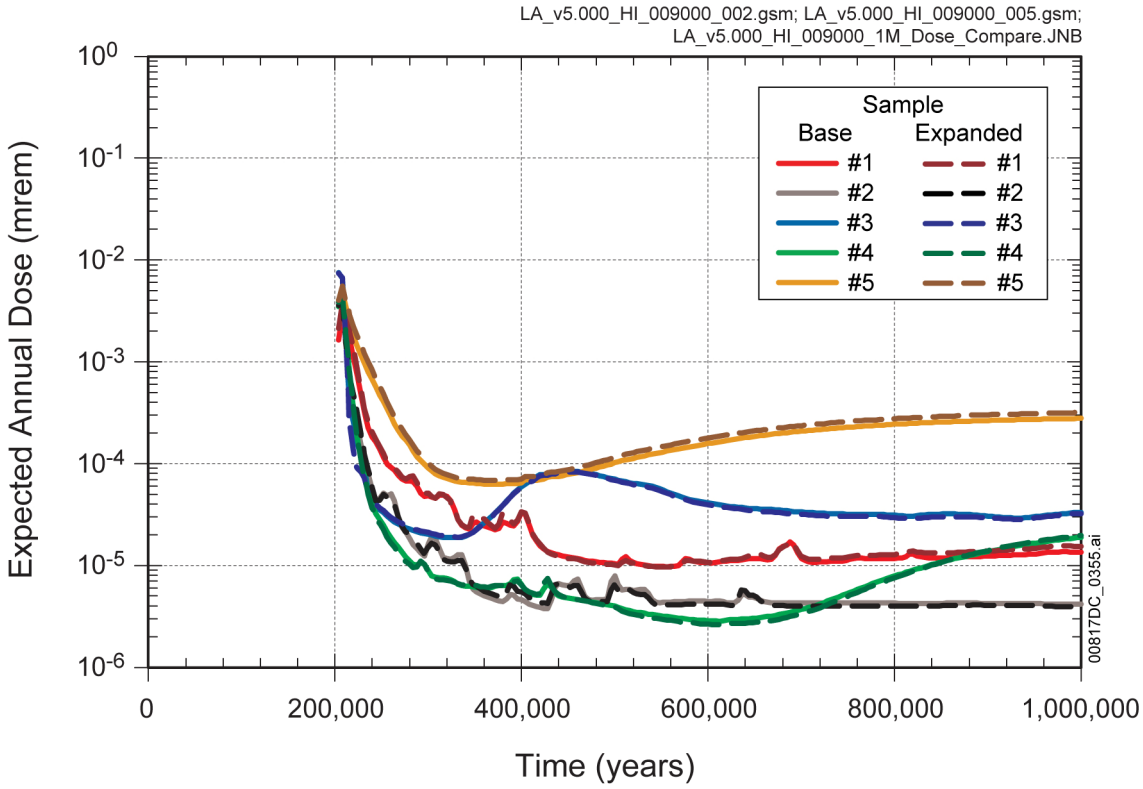

Source: Output DTNs: MO0709TSPAREGS.000 [DIRS 182976]; and MO0709TSPASTAB.000 [DIRS 182983].

Figure 7.3.2-27. Expected Annual Dose Over 1,000,000 Years for Human Intrusion Modeling Case Considering Increased Aleatory Sample Size

INTENTIONALLY LEFT BLANK

7.3.3 Temporal Stability

Another issue related to the stability of the TSPA-LA Model results is temporal discretization of the model. In order to estimate the movement of radionuclides, the TSPA-LA Model solves partial differential equations numerically in various submodels (e.g., FEHM for UZ transport) and model abstractions (e.g., EBS Chemical Environment Submodel). The numerical solution involves computations with discrete timesteps, referred to as temporal discretization. The temporal discretization may affect the accuracy of the solution to the differential equations, and thus affect the outputs of TSPA-LA Model. Several different TSPA-LA Model runs are performed to evaluate the potential for variability in model output due to timestep size. The analysis demonstrates that the output of the TSPA-LA Model is not significantly affected by refining the temporal discretization. Thus, the analysis concludes that the temporal discretization used in the TSPA-LA Model is adequate.

7.3.3.1 Selection of Modeling Cases

The TSPA-LA Model describes repository performance by analyzing the complex system of FEPs; natural disruptive events, such as igneous intrusion, volcanic eruption, seismic ground motion, and fault displacement; and a human-intrusion scenario that could occur at the Yucca Mountain repository after closure during the first 10,000 years and up to the period of geologic stability (1,000,000 years) (NRC Proposed Rule 10 CFR 63.342(c) [DIRS 178394]). The screening and scenario development of FEPs for the TSPA-LA Model are discussed in Section 6.1.1. The modeling cases to address the scenario classes are discussed in Section 6.1.2 and include:

- Nominal Modeling Case
- Drip Shield EF Modeling Case
- Waste Package EF Modeling Case
- Igneous Intrusion Modeling Case
- Volcanic Eruption Modeling Case
- Seismic GM Modeling Case
- Seismic FD Modeling Case
- Human Intrusion Modeling Case.

For each modeling case, separate calculations are performed for two time periods: up to 20,000 years and up to 1,000,000 years.

The Waste Package EF, Igneous Intrusion, Seismic GM, and Human Intrusion Modeling Cases were selected for the temporal stability analysis. These modeling cases are the most influential on repository system performance, and encompass the range of events and processes that result in radionuclide transport. Each modeling case describes repository performance subsequent to failure of parts of the engineered barrier, although the time and nature of the failures varies between modeling cases. When failure occurs, the initial mobilization of radionuclides out of the WP generates an impulse of mass into the models for transport, resolution of which may be dependent upon the timesteps used in the TSPA-LA GoldSim model file.

The Waste Package EF Modeling Case calculation for 20,000 years models the diffusive release of radionuclides from an initial WP failure under an intact DS. During the first 20,000 years, diffusive releases from the WP can vary greatly with time as temperature and relative humidity change (Section 7.7.1.3). The timestep analysis for this modeling case examines both types of WP (CDSP and TAD) in one of the 10 possible environments (percolation bin and dripping conditions). The effect of timesteps on diffusive releases across the environments is examined in the Seismic GM Modeling Case calculation for 20,000 years, which models the diffusive releases that result from seismic events that affect all CDSP WPs in all environments. The Igneous Intrusion Modeling Case for 20,000 years models the release of radionuclides primarily by advection and includes all WPs in all environments.

For the time period of 1,000,000 years, only the Igneous Intrusion Modeling Case is analyzed because this modeling case represents the extreme transient effect of an event that completely compromises the engineered barrier at a single time. In contrast, the Seismic GM Modeling Case describes degrees of degradation and failure of the components of the engineered barrier through time, resulting from corrosion processes and seismic events. The Seismic GM Modeling Case essentially models a series of less extreme events. If the timestep scheme for 1,000,000 years is adequate for the Igneous Intrusion Modeling Case, it is reasonable to expect that this same timestep scheme would be adequate for the Seismic GM Modeling Case.

The Human Intrusion Modeling Case was examined separately because this modeling case uses a different model for transport through the UZ.

The Nominal, Drip Shield EF, and Seismic FD Modeling Cases use the same timestep scheme as is used in the Waste Package EF, Seismic GM, and Igneous Intrusion Modeling Cases. The submodels included in the Nominal, Drip Shield EF, and Seismic FD Modeling Cases differ from the Waste Package EF, Seismic GM, and Igneous Intrusion Modeling Cases primarily in the characterization of failure of parts of the EBS. Radionuclide mobilization and transport are computed with a similar set of sub-models in all of these modeling cases. Therefore, if the timestep scheme is shown to be adequate for the Waste Package EF, Seismic GM, and Igneous Intrusion Modeling Cases, the temporal stability analysis need not be conducted for the remaining modeling cases.

The Igneous Eruption Modeling Case uses a different timestep scheme than the other modeling cases because of the highly-transient nature of the eruptive processes. This timestep scheme employs 1-year timesteps after an eruption. Because the quantity computed by the modeling case is the annual dose (i.e., dose averaged over a year), reducing the timestep below one year is not warranted. No temporal stability analysis was performed for the Igneous Eruption Modeling Case.

7.3.3.2 Methodology

Separate calculations are performed for each of two time periods: 20,000 years and 1,000,000 years following repository closure. For each time period, one base timestep scheme is used for all modeling cases. The base timestep scheme uses shorter timesteps during the period of time immediately following repository closure, when environmental variables such as

temperature and relative humidity are changing more rapidly. As repository environmental conditions become stable, longer timesteps are employed.

The temporal stability of the selected modeling cases was examined by introducing additional, shorter timesteps immediately following the events that fail components of the engineered barrier. For each modeling case, two additional simulations were constructed and run, varying the timestep scheme from the baseline TSPA-LA Model. The baseline TSPA-LA Model timestep scheme and the two alternative timestep schemes used in the modeling cases are presented in Table 7.3.3-1. Each simulation calculated repository performance for the first five of 300 epistemic realizations of the baseline TSPA-LA Model. The timestep analysis was conducted for five epistemic realizations rather than the full set of 300 to reduce the computational burden. It was anticipated that examining five realizations would be sufficient to expose any systematic effect on model results of varying the timesteps. TSPA-LA Model runs with different timestep sizes were compared graphically to determine the effect of refining the timesteps. Due to the high degree of stability evident in the graphical comparison of model results, statistical comparison of model results for different timesteps was not deemed necessary.

7.3.3.3 Waste Package EF Modeling Case

The TSPA-LA models early failures as occurring at repository closure. However, since the DS remains functional in this modeling case, seepage does not contact the early failed WPs, so radionuclides transport out of the WP by diffusion only. Diffusion does not begin until sufficient water is present inside the WP, and the rate of water accumulation depends on temperature and relative humidity within the drift. Consequently, diffusive transport begins at different times for different WPs.

The base-case timestep scheme uses 10-year timesteps until 120 years, followed by 40-year timesteps until 10,000 years, and then 80-year timesteps until 20,000 years. Temporal stability was tested by considering an alternate timestep scheme, which begins with the 10-year timesteps until 120 years and then switches to 20-year timesteps for the remaining duration of the simulation. Because the onset of transport can occur at different times, the alternate timestep scheme uses additional, shorter timesteps throughout the calculation year period.

The Waste Package EF Modeling Case considers a total of twenty possible combinations of aleatory variables: five different percolation subregions, two WP types, and either dripping or non-dripping conditions. Two aleatory combinations were chosen for analysis: CSNF and CDSP WPs, in percolation bin three, with dripping conditions. For each of five epistemic realizations and the timestep schemes listed in Table 7.3.3-1, the annual dose from one early failed WP was calculated. Figure 7.3.3-1 shows the results for both CSNF and CDSP WPs. In both cases, the annual dose is very similar for the two-timestep schemes.

Annual dose for the other eighteen aleatory combinations was computed for both timestep schemes, and the ensemble of twenty dose histories was used to compute expected annual dose as described by Equation 6.1.2-13. Figure 7.3.3-2 shows the expected annual dose for each of five epistemic realizations for the timestep schemes listed in Table 7.3.3-1. The similarity in expected annual dose for the two-timestep schemes confirms that the Waste Package EF Modeling Case is stable with respect to temporal discretization.

7.3.3.4 Igneous Intrusion Modeling Case

In the Igneous Intrusion Modeling Case, annual dose is computed by the GoldSim component of the TSPA-LA Model at each of a set of specified intrusion times (Table 7.3.2-1). For each epistemic realization, the ensemble of dose histories (one for each intrusion time) is used to compute expected annual dose, as described by Equation 6.1.2-16. At the time of an intrusion, the DS and WP cease to isolate the waste from seepage waters. Immediately after an intrusion, relatively large quantities of radionuclides enter the natural system over a few timesteps. Temporal stability was tested for the 1,000,000-year and 20,000-year calculations by considering the alternate timestep schemes listed in Table 7.3.3-1. The alternate timestep schemes add additional, shorter timesteps immediately after the modeled intrusions to provide better resolution of the effects of each intrusion.

For the 1,000,000 year calculation, the intrusion is fixed at 400,000 years. The base-case timesteps are used up to the time of the intrusion. After the intrusion, the first alternate timestep scheme uses 250-year timesteps until 640,000 years and then reverts back to the base-case timestep of 4,000 years until 1,000,000 years. The second alternate scheme uses 25-year timesteps until 424,000 years, then uses the base-case timestep of 4,000 years until 1,000,000 years. Figure 7.3.3-3 shows the annual dose for the second epistemic realization and the three-timestep schemes. The overall shape of the dose history for each epistemic realization is similar for all timestep schemes. Thus, better resolution of the short-term effects of an intrusion, provided by the alternate timestep schemes, does not alter the estimates of the long-term effects of the intrusion.

To examine the short-term effects, Figure 7.3.3-4 focuses on the period immediately after 400,000 years and shows that the alternate timestep schemes result in higher dose that occur earlier than in the base-case timestep scheme. Although radionuclides are released at the same intrusion time in all timestep schemes, the first dose cannot occur until the next time GoldSim timestep (404,000 years in the base case, compared to 400,250 years and 400,025 years in the alternate timestep schemes.)

The dose shown on Figure 7.3.3-4 is the annual dose conditional on the occurrence of an intrusion at 400,000 years. In contrast, the quantities compared to the individual protection standards specified in 10 CFR 63.311 [DIRS 178394] to determine compliance is the total mean annual dose, as defined in Section 6.1.2.2, for the first 10,000 years post closure (10 CFR 63.303(a) [DIRS 178394]); and the median of the projected doses for the period 10,000 years after disposal through the period of geologic stability (10 CFR 63.303(b) [DIRS 178394]). The median annual dose is calculated for each modeling case by first calculating expected annual dose (average over aleatory uncertainty) as described in Section 6.1.2.2 for each realization of epistemic parameters, and then by averaging over the ensemble of expected annual doses. Thus, if the differences shown on Figure 7.3.3-4 do not affect expected annual dose, they also would not affect mean annual dose, and thus would not be important.

To determine if the higher dose values for the alternate timestep schemes affect expected annual dose, expected annual dose was computed for each of five epistemic realizations using an increased timestep scheme similar to that illustrated on Figure 7.3.3-4. One dose history is computed for each epistemic realization and four of the ten specified igneous event times listed

for the base case in Table 7.3.2-1. However, to avoid having to create 10 unique GoldSim files, regardless of a dose history's specified igneous event time, one alternate timestep scheme was used. This alternate timestep scheme used 50-year timesteps for the 4,000-year period immediately following each of the ten specified event times.

Figure 7.3.3-5 shows the expected annual dose results for the five epistemic realizations. Although small variations can be observed for the two timestep schemes, each expected annual dose history's shape and magnitude are similar. Thus, the timestep scheme used in the Igneous Intrusion Modeling Case for 1,000,000 years is adequate. The similarity in expected annual dose occurs because expected annual dose at time τ involves averaging over the dose at time τ from all possible events that could occur prior to time τ. Because the dose that follows an event appears as a pulse, both the magnitude and duration of each pulse influence the expected annual dose. When the alternate scheme with shorter timesteps is used, the pulse of dose that immediately follows an event is larger in magnitude but shorter in duration. Consequently, with the alternate timesteps, the expected annual dose at time τ is determined by fewer, larger pulses of dose prior to τ. However, similar values of expected annual dose result in the base-case timestep scheme, which produces dose pulses of lower magnitude and longer duration. The similarity in expected annual dose shows that the timestep scheme provides sufficient resolution of the annual dose to obtain a stable value for the integral defining expected annual dose.

For the 20,000-year calculation, the intrusion is fixed at 1,000 years. The base-case timesteps are used up to the time of the intrusion. After the intrusion, the first alternate timestep scheme uses ten-year timesteps until 10,000 years and then reverts back to the base-case timesteps until 20,000 years. The second alternate scheme uses one-year timesteps for 1,000 years following the intrusion and then reverts back to the base-case timesteps until 20,000 years. Figure 7.3.3-6 shows the annual dose for each of five epistemic realizations and the three-timestep schemes. The overall shape of the dose history for each epistemic realization is very similar for all three timestep schemes. Figure 7.3.3-7 focuses on the period immediately following the intrusion and shows that, similar to the 1,000,000 year calculation, the finer timestep schemes result in a higher dose that occurs earlier. However, the analysis of the 1,000,000 year calculation showed that the earlier, higher dose observed in the finer timestep scheme did not affect the expected annual dose for 1,000,000 years. Because the differences in dose shown on Figure 7.3.3-7 due to finer timesteps in the 20,000-year calculation are qualitatively similar to those observed on Figure 7.3.3-4 for the 1,000,000-year calculation, the differences in annual dose shown on Figure 7.3.3-7 should not significantly affect the expected annual dose, and the timestep scheme used in the 20,000-year calculation is adequate.

7.3.3.5 Seismic Ground Motion Modeling Case

In the Seismic Ground Motion Modeling Case for 20,000 years, annual dose is computed by the GoldSim component of the TSPA-LA Model at each combination of a specified event time and specified damage fraction (Table 7.3.2-3). For each epistemic realization, the ensemble of dose histories (one for each combination of event time and damage fraction) is used to compute expected annual dose, as described by Equation 6.1.2-22. At the time of a seismic event, damage to the WP allows water to build inside the WP and, when sufficient water is present, radionuclides begin to diffuse out of the WP and into the natural system. The time required for diffusion to begin depends on the area of the WP that is damaged, as well as temperature and

relative humidity in the drift. It is possible that relatively large quantities of radionuclides would enter the natural system over a few timesteps following a seismic event. Temporal stability was tested for the 20,000-year calculation by considering the alternate timestep schemes listed in Table 7.3.3-1. The alternate timestep schemes add additional, shorter timesteps immediately after the modeled seismic event to provide better resolution of the effects of the event.

The event time was fixed at 1,000 years and the damage fraction at 10^{-6}. The base-case timesteps were used up to the time of the event. After the event, the first alternate timestep scheme uses 10-year timesteps until 10,000 years and then reverts to the base-case timestep for the remainder of the calculation. The second alternate scheme uses one-year timesteps until 2,000 years, followed by the base-case timesteps until 20,000 years. Although a fixed combination of event time and damage fraction are investigated in the analysis of timesteps, the results for other combinations of event times and damage fractions would be similar. Figure 7.3.2-9 and Figure 7.3.2-10 illustrate the annual dose resulting from seismic events at two different fixed times for varying damage fractions, and show that the doses resulting from the combinations of event times and damage fractions have different magnitudes but retain similar shape.

Figure 7.3.3-8 shows the annual dose for each of five epistemic realizations and the three timestep schemes. The overall shape of the dose history for each epistemic realization is similar for all timestep schemes. Figure 7.3.3-9 focuses on the annual dose immediately after the seismic event at 1,000 years and shows variations in dose between timestep schemes. The abrupt change in dose just before 2,000 years is due to the change in climate and is not an important feature in the computation of expected annual dose. The dose following the seismic event generally occurs sooner after the event when using the alternate timestep schemes. However, unlike the Igneous Intrusion Modeling Case, the dose does not exhibit a large peak followed by rapid decline but, rather, reaches and maintains a steady state. In the Igneous Intrusion Modeling Case, the engineered barrier does not restrict radionuclide transport after the intrusion; whereas in the Seismic GM Modeling Case, only a small fraction of WP surface is damaged, which in turn constrains the rate of radionuclide transport. The expected annual dose for the Seismic GM Modeling Case will be determined by the magnitude of the steady state dose after the seismic event. Because the magnitude of the steady state dose is similar for the base case and the alternate timestep schemes, the differences in annual dose shown on Figure 7.3.3-9 will have no significant effect on expected annual dose. Therefore, the timestep scheme used in the 20,000-year calculation is adequate.

7.3.3.6 Human Intrusion Modeling Case

In the Human Intrusion Modeling Case, a single stylized intrusion occurs at 200,000 years. Annual dose is computed by the GoldSim component of the TSPA-LA Model for each combination of a sampled intrusion location (characterized by percolation rate and entry point into the SZ) and epistemic realization. For each epistemic realization, the ensemble of dose histories is averaged to compute expected annual dose, as described by Equation 6.1.2-26. At the time of the intrusion, percolation waters begin to flow through the waste, entrain mobilized radionuclides, and transport the radionuclides down the borehole to the SZ. Thus, the dose following an intrusion has a large initial value that rapidly decreases as radionuclide inventory is depleted or decays.

Temporal stability was tested by considering the alternate timestep scheme listed in Table 7.3.3-1. The alternate timestep schemes add additional, shorter timesteps immediately after the drilling intrusion to provide better resolution of the effects of the event. Figure 7.3.3-10 compares the expected annual dose that results from the two timestep schemes and shows that both timestep schemes result in similar long-term doses. Figure 7.3.3-11 focuses on the expected annual dose immediately after the intrusion and shows that the alternate timestep scheme provides better resolution of the dose immediately following the intrusion. Because the expected annual doses are many orders of magnitude below the limit specified in NRC Proposed Rule 10 CFR 63.321 [DIRS 178394], the coarse resolution of expected annual dose provided by the base-case timestep is adequate.

INTENTIONALLY LEFT BLANK

Table 7.3.3-1. Timestep Schemes Used in Temporal Stability Analysis

Modeling Case	Base Case Timestep Scheme	First Alternate Timestep Scheme	Second Alternate Timestep Scheme
Waste Package Early Failure	10 yr from 0 yr to 120 yr 40 yr from 120 yr to 10k yr 80 yr from 10k yr to 20k yr	10 yr from 0 yr to 120 yr 20 yr from 120 yr to 20,000 yr	NA
Igneous Intrusion 1M yr (intrusion occurs at 400,000 yr)	250 yr from 0 to 10k yr 500 yr from 10k to 100k yr 1,000 yr from 100k to 120k yr 2,000 yr from 120k to 160k yr 4,000 yr from 160k to 1M yr	250 yr from 0 to 10k yr 500 yr from 10k to 100k yr 1,000 yr from 100k to 120k yr 2,000 yr from 120k to 160k yr 4,000 yr from 160k to 400k yr 250 yr from 400k to 640k yr 4,000 from 640k yr to 1M yr	250 yr from 0 to 10k yr 500 yr from 10k to 100k yr 1,000 yr from 100k to 120k yr 2,000 yr from 120k to 160k yr 4,000 yr from 160k to 400k yr 25 yr from 400k to 424k yr 4,000 from 424k yr to 1M yr
Igneous Intrusion 20k yr (intrusion occurs at 1,000 yr)	10 yr from 0 yr to 120 yr 40 yr from 120 yr to 10k yr 80 yr from 10k yr to 20k yr	10 yr from 0 yr to 120 yr 40 yr from 120 yr to 1k yr 10 yr from 1k yr to 10k yr 80 yr from 10k yr to 20k yr	10 yr from 0 yr to 120 yr 40 yr from 120 yr to 1k yr 1 yr from 1k yr to 2k yr 40 yr from 2k yr to 10k yr 80 yr from 10k yr to 20k yr
Seismic GM 20k yr (seismic event occurs at 1,000 yr)	10 yr from 0 yr to 120 yr 40 yr from 120 yr to 10k yr 80 yr from 10k yr to 20k yr	10 yr from 0 yr to 120 yr 40 yr from 120 yr to 1k yr 10 yr from 1k yr to 10k yr 80 yr from 10k yr to 20k yr	10 yr from 0 yr to 120 yr 40 yr from 120 yr to 1k yr 1 yr from 1k yr to 2k yr 40 yr from 2k yr to 10k yr 80 yr from 10k yr to 20k yr
Human Intrusion (intrusion occurs at 200,000 yr)	250 yr from 0 to 10k yr 500 yr from 10k to 100k yr 1,000 yr from 100k to 120k yr 2,000 yr from 120k to 160k yr 4,000 yr from 160k to 1M yr	250 yr from 0 to 10k yr 500 yr from 10k to 100k yr 1,000 yr from 100k to 120k yr 2,000 yr from 120k to 160k yr 4,000 yr from 160k to 200k yr 40 yr from 200k to 204k yr 400 yr from 204k to 212k yr 4,000 yr from 212k to 1M yr	NA

Source: Output DTN: MO0709TSPAREGS.000_R0 [DIRS 182976] (for Base Case); and MO0708TSPAVALI.000_R0 [DIRS 182985] (for Alternates).

INTENTIONALLY LEFT BLANK

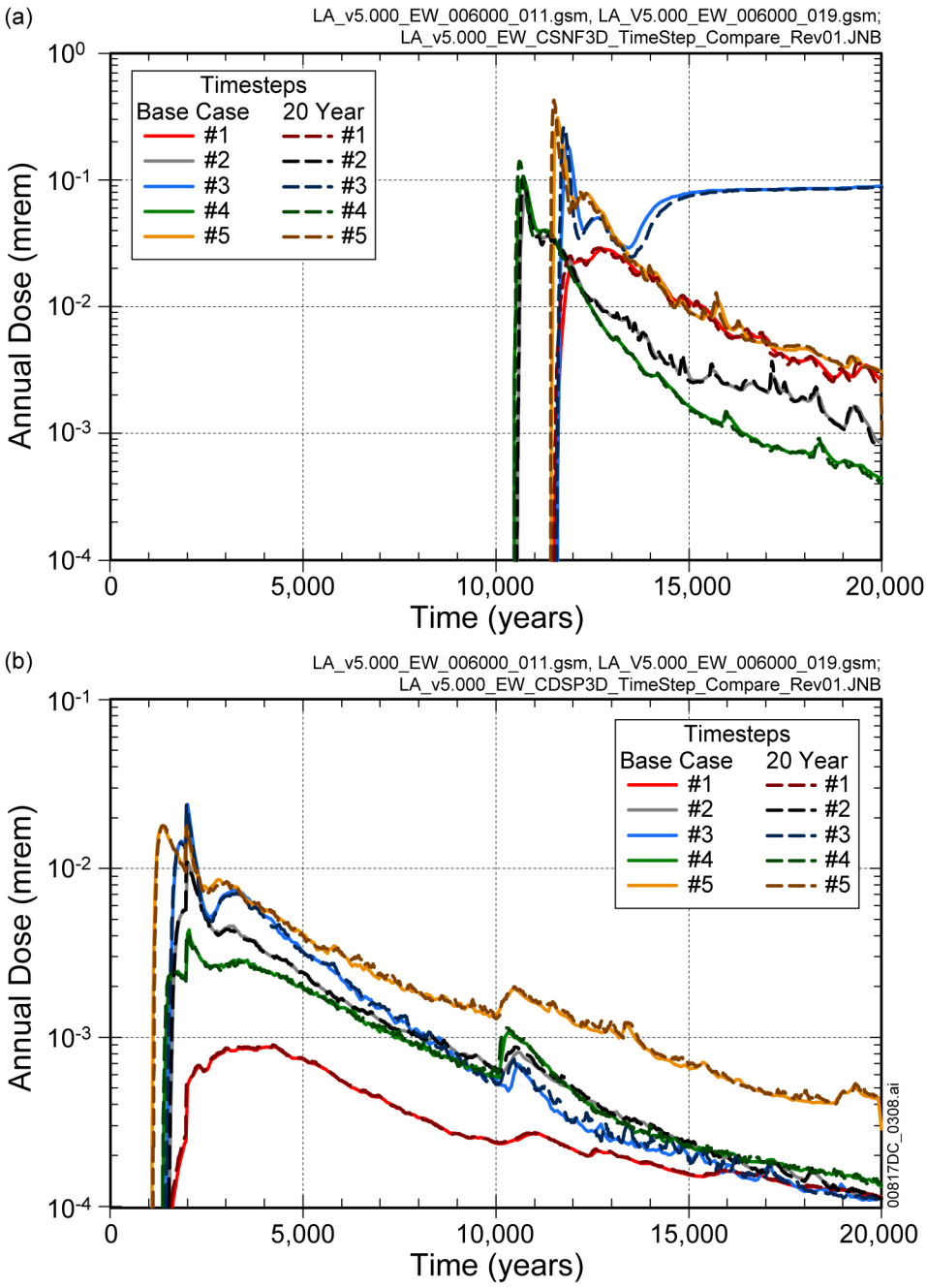

Source: Output DTNs: MO0708TSPAVALI.000 [DIRS 182985]; and MO0709TSPAREGS.000 [DIRS 182976].

Figure 7.3.3-1. Annual Dose from One Early Failed Waste Package for (a) CSNF WP and (b) CDSP WP

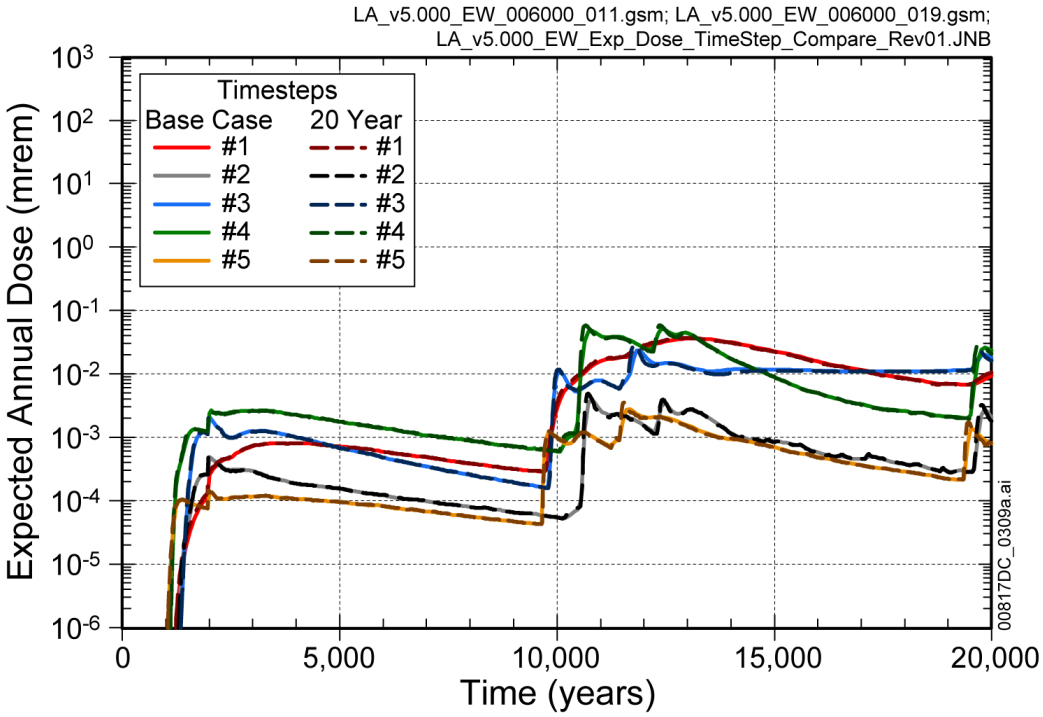

Source: Output DTNs: MO0708TSPAVALI.000 [DIRS 182985]; and MO0709TSPAREGS.000 [DIRS 182976].

Figure 7.3.3-2. Expected Annual Dose from Early Failed Waste Packages for Base Case and 20-Year Timestep Schemes

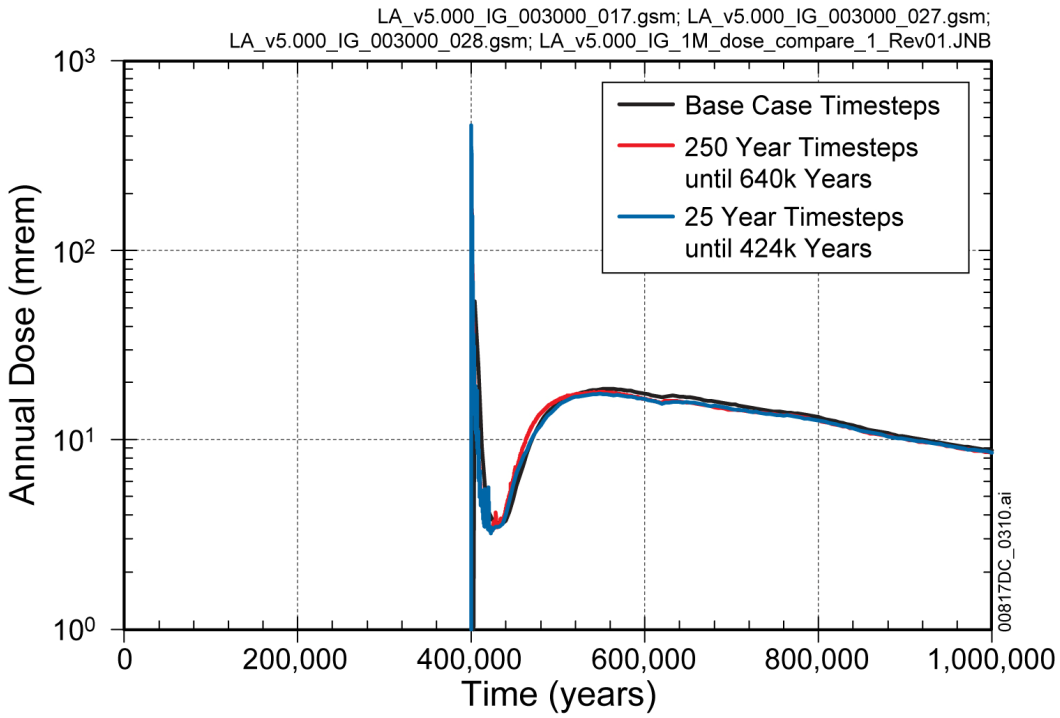

Source: Output DTNs: MO0708TSPAVALI.000 [DIRS 182985]; and MO0709TSPAREGS.000 [DIRS 182976].

Figure 7.3.3-3. Annual Dose from an Igneous Intrusion at 400,000 Years for Three Timestep Schemes for Epistemic Realization 2

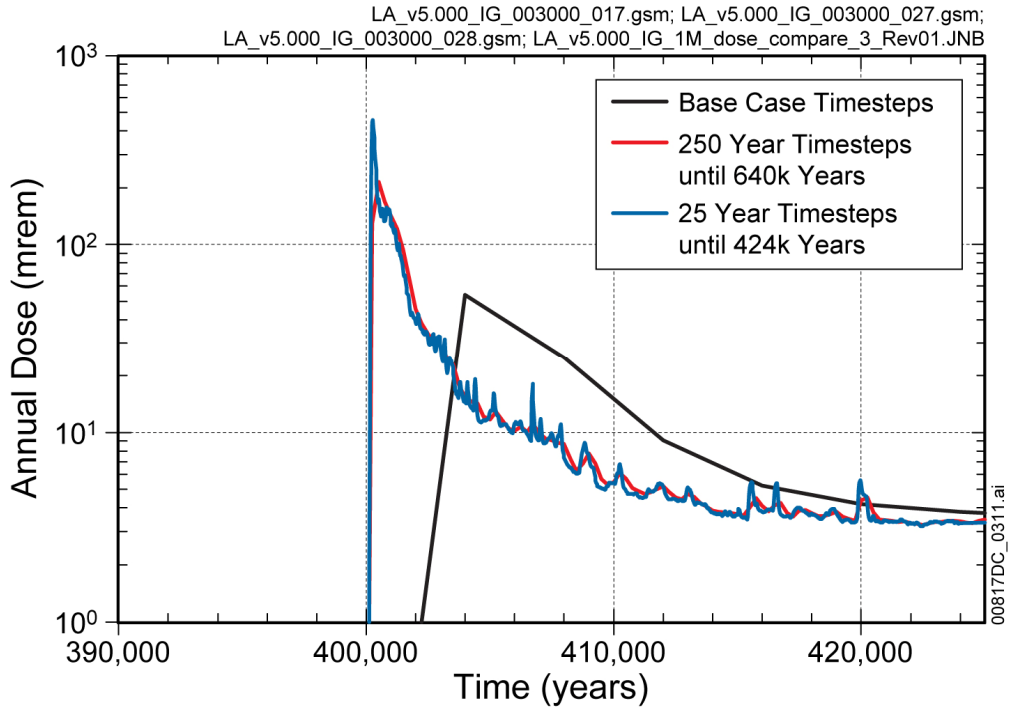

Source: Output DTNs: MO0708TSPAVALI.000 [DIRS 182985]; and MO0709TSPAREGS.000 [DIRS 182976].

Figure 7.3.3-4. Detail of Annual Dose from an Igneous Intrusion at 400,000 Years for Three Timestep Schemes for Epistemic Realization 2

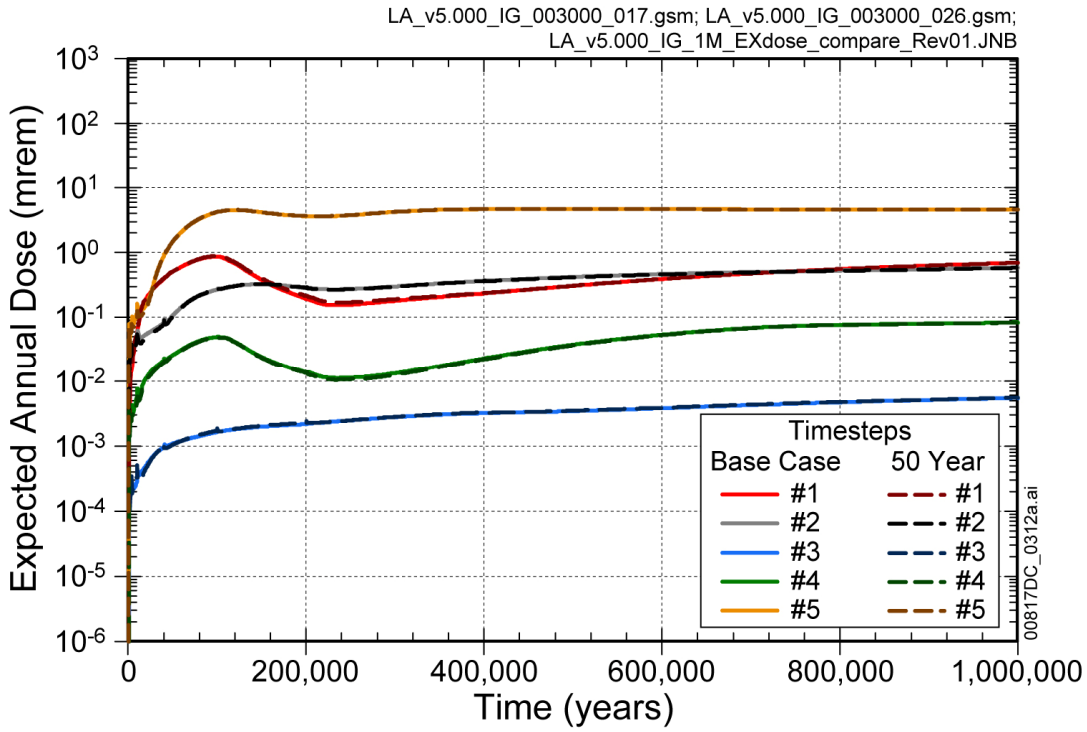

Source: Output DTNs: MO0708TSPAVALI.000 [DIRS 182985]; and MO0709TSPAREGS.000 [DIRS 182976].

Figure 7.3.3-5. Expected Annual Dose from Igneous Intrusion for Base Case and Alternate Timestep Schemes for Five Epistemic Realizations

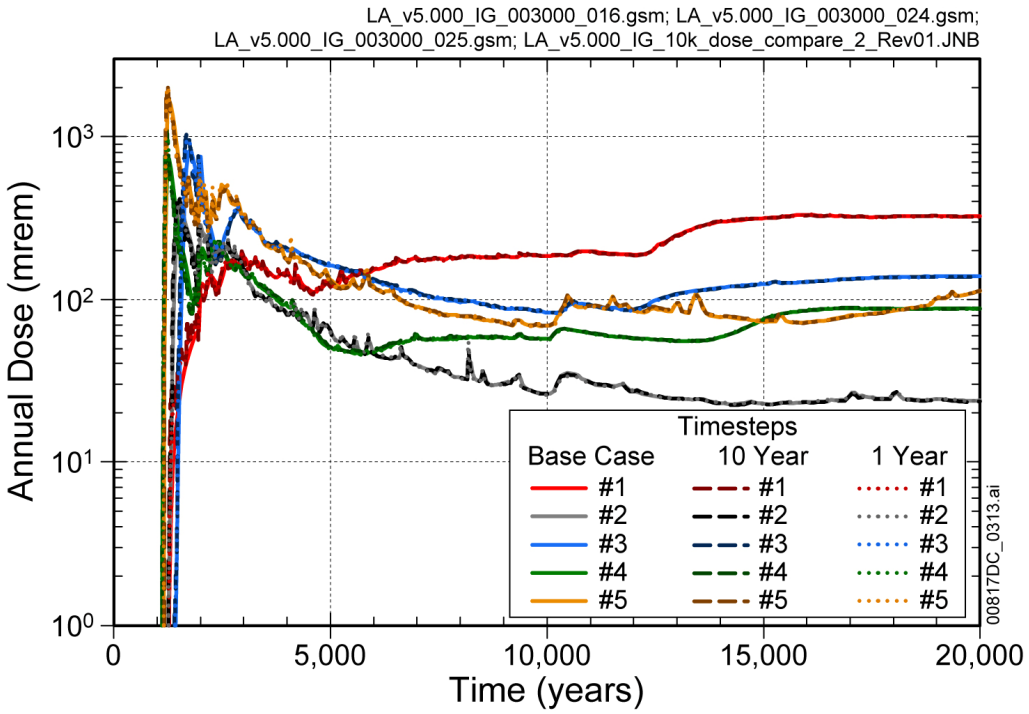

Source: Output DTNs: MO0708TSPAVALI.000 [DIRS 182985]; and MO0709TSPAREGS.000 [DIRS 182976].

Figure 7.3.3-6. Annual Dose from an Igneous Intrusion at 1,000 Years for Three Timestep Schemes

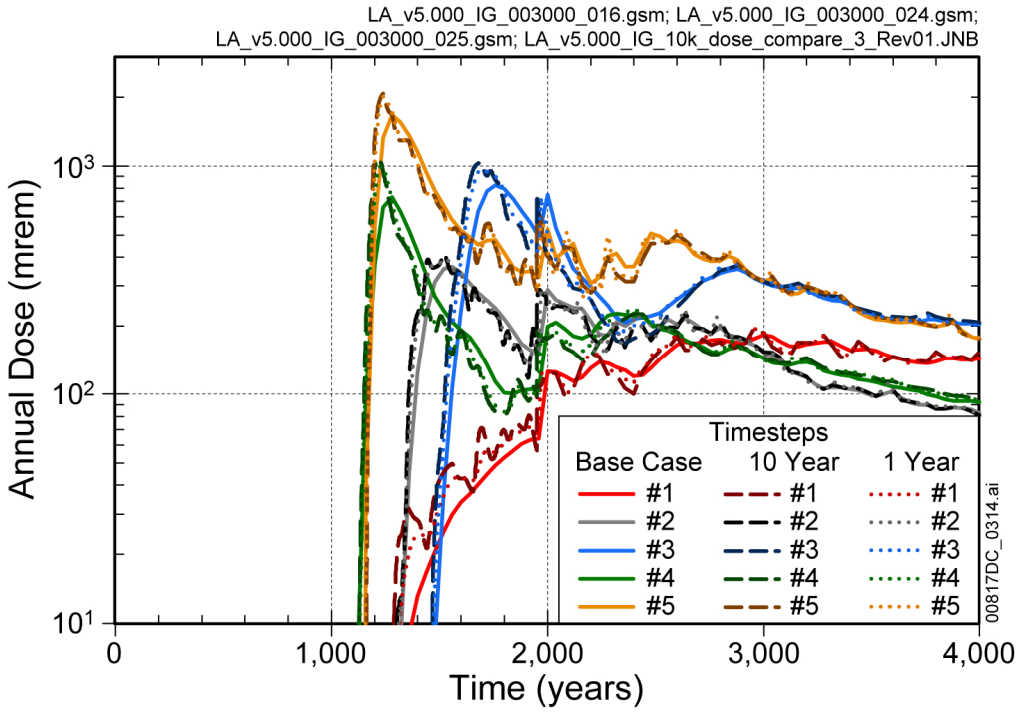

Source: Output DTNs: MO0708TSPAVALI.000 [DIRS 182985]; and MO0709TSPAREGS.000 [DIRS 182976].

Figure 7.3.3-7. Detail of Annual Dose from an Igneous Intrusion at 1,000 Years for Three Timestep Schemes

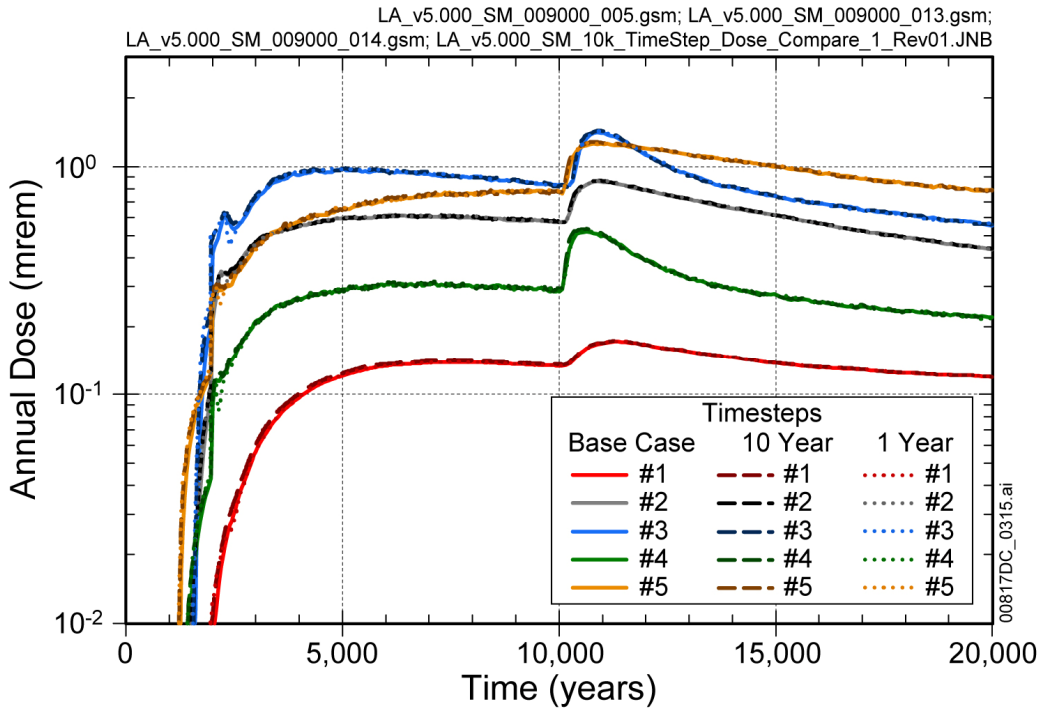

Source: Output DTNs: MO0708TSPAVALI.000 [DIRS 182985]; and MO0709TSPAREGS.000 [DIRS 182976].

Figure 7.3.3-8. Annual Dose from a Seismic Ground Motion Event at 1,000 Years with Damage Fraction 10^{-6} for Three Timestep Schemes

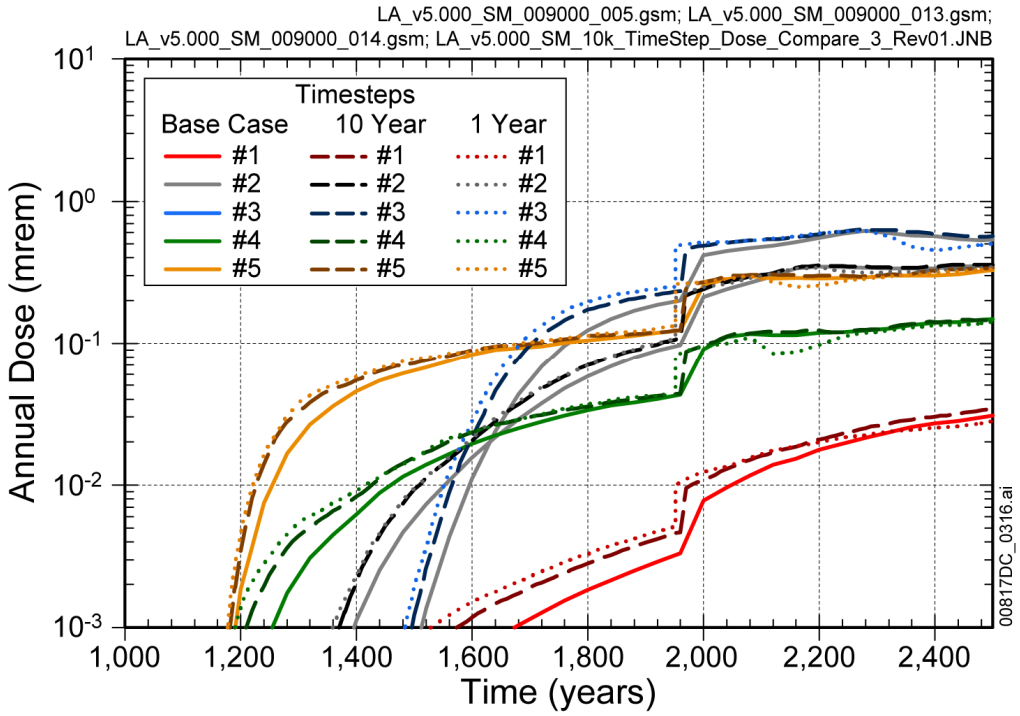

Source: Output DTNs: MO0708TSPAVALI.000 [DIRS 182985]; and MO0709TSPAREGS.000 [DIRS 182976].

Figure 7.3.3-9. Detail of Annual Dose from a Seismic Ground Motion Event at 1,000 Years with Damage Fraction 10^{-6} for Three Timestep Schemes

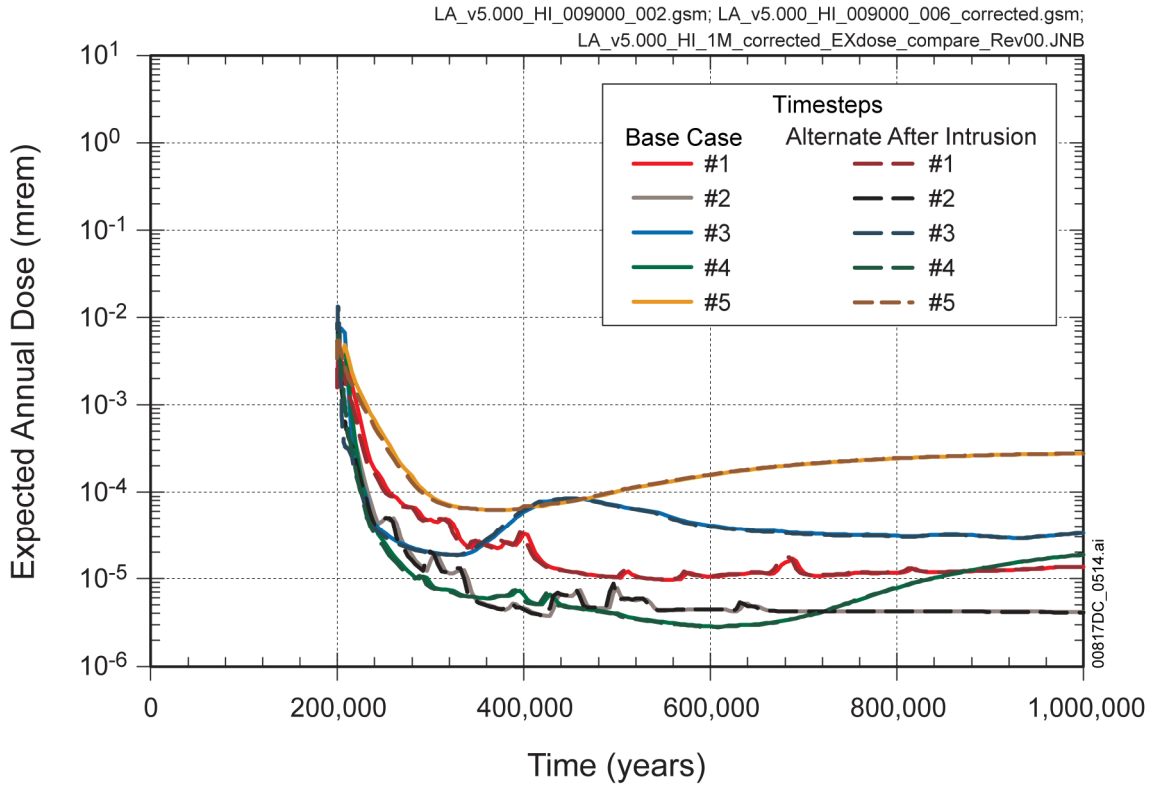

Source: Output DTNs: MO0708TSPAVALI.000 [DIRS 182985]; and MO0709TSPAREGS.000 [DIRS 182976].

Figure 7.3.3-10. Expected Annual Dose from a Human Intrusion Event at 200,000 Years for Two Timestep Schemes

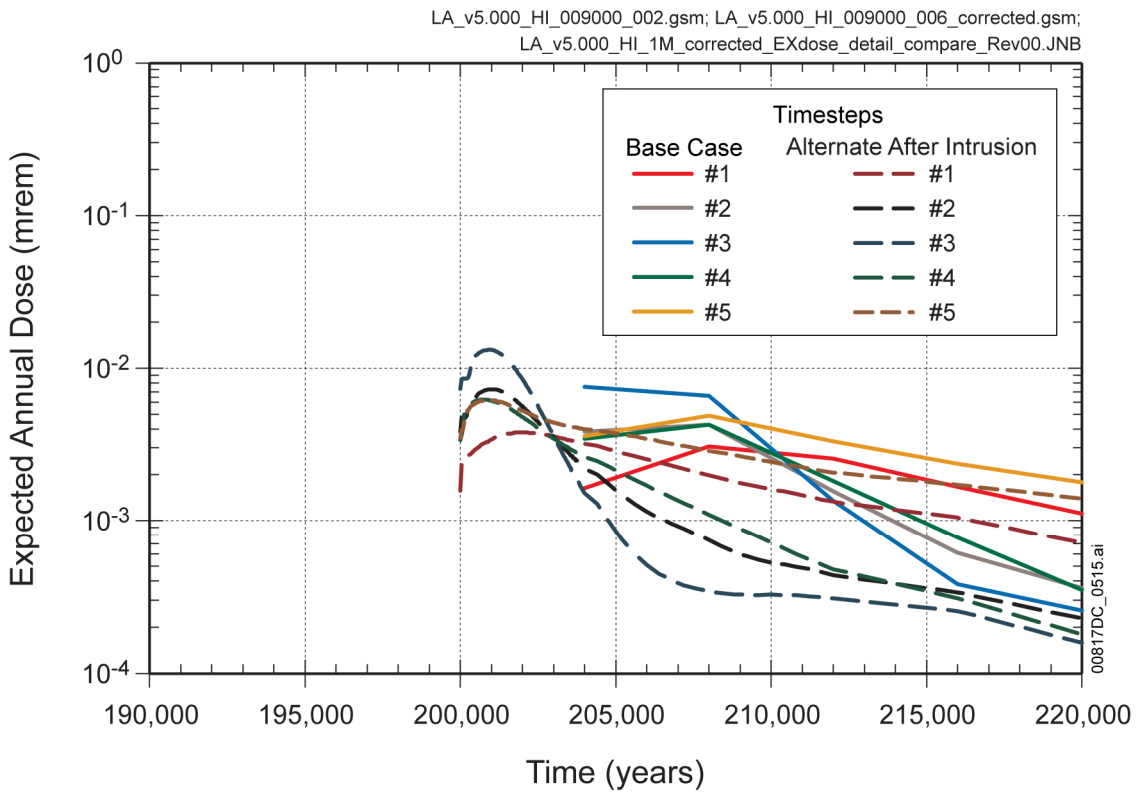

Source: Output DTNs: MO0708TSPAVALI.000 [DIRS 182985]; and MO0709TSPAREGS.000 [DIRS 182976].

Figure 7.3.3-11. Detail of Expected Annual Dose from a Human Intrusion Event at 200,000 Years for Two Timestep Schemes

INTENTIONALLY LEFT BLANK

7.3.4 Analysis of Spatial Discretization

Part of the uncertainty addressed by the TSPA-LA Model deals with the variability associated with spatial discretization of the various model domains. Different scales exist within the TSPA-LA Model relative to how spatially dependent information is used. Spatially discrete information used at one scale (e.g., the Mountain-Scale UZ Flow Submodel, Table 6-1 and Section 6.3.1) may be combined or averaged in order to be used at a different scale (e.g., the Drift Seepage Submodel, Table 6-1 and Section 6.3.3.1, and the Drift Wall Condensation Submodel, Table 6-1 and Section 6.3.3.2). The TSPA-LA Model inherits these different spatial scales from the process models that feed it, namely the Mountain-Scale UZ Flow, EBS TH Environment, UZ Transport, and SZ Flow and Transport abstractions. The spatial discretization and scales of these abstractions are investigated and validated for their intended use in the TSPA-LA within each abstraction's respective model report.

The TSPA-LA Model adds its own spatial domain by subdividing the repository into percolation subregions at the EBS Submodel level. Furthermore, the EBS thermal-hydrologic environment within a percolation subregion is characterized using a subset of the comprehensive TH dataset provided by the Multiscale Thermohydrologic Model (MSTHM) process model and is meant to be representative of the all different TH histories bounded by that particular percolation subregion. The purpose of this spatial discretization within the TSPA-LA is to reduce the model's computational overhead.

The primary purposes of this section are to: (1) summarize the inherited spatial discretization schemes of the process model abstractions that feed the TSPA-LA, (2) describe how the TSPA-LA discretizes the repository domain into percolation subregions, (3) describe and validate the use of representative TH histories within the percolation subregions in-lieu of using the comprehensive TH dataset, and (4) determine what impact, if any, this spatial discretization has on the results of the EBS releases that feed the UZ. The impacts to the TSPA-LA in terms of dose to the RMEI, if any, of the spatial discretization of the EBS releases to the nodes of the UZ within each percolation subregion, and the subsequent discretization of the UZ releases to the SZ, were not considered.

7.3.4.1 Inherited Spatial Discretization within the TSPA-LA

The areas within the TSPA-LA Model where the spatial discretization has been inherited from the upstream process model abstractions include the Mountain-Scale UZ Flow Submodel (Section 6.3.1), EBS TH Environment Submodel (Table 6-1 and Section 6.3.2), UZ Transport Submodel (Table 6-1 and Section 6.3.9), and SZ Flow and Transport Submodel (Section 6.3.10). The TSPA-LA Model implementation of the UZ transport calculations is achieved through the use of the FEHM DLL (Section 6.3.9). The UZ Transport Submodel is directly coupled (i.e., dynamically linked) with the TSPA-LA Model using an external pathway element within the GoldSim software (GoldSim V. 9.60.100 [DIRS 181903]) to link with the UZ transport code, FEHM. The FEHM particle-tracking code transports particles with the same dual-permeability spatial domain used in the Mountain-Scale UZ Flow Submodel (Section 6.3.1) and, therefore, the UZ Transport Submodel uses the same spatial discretization as the underlying Site-Scale UZ Flow Process Model and, hence, the variabilities associated with these spatial domains are coincident.

The SZ Flow and Transport Model Component of the TSPA-LA Model is used to evaluate the transport of radionuclides from their introduction, at the water table, to the accessible environment that is approximately 18 km downgradient from the repository (Section 6.3.10). A 3-D SZ Flow and Transport Process Model was developed to calculate the flow and transport of radionuclides through the SZ to the accessible environment. The output from the 3-D SZ Flow and Transport Process Model is provided to the TSPA-LA Model as 200 breakthrough curves for each of the four source saturated zone source regions and 12 radionuclide groups. This results in 9,600 spatially discretized unit-source radionuclide breakthrough curves (as discussed in Section 6.3.10.2). Within the TSPA-LA Model, a convolution integral technique combines these randomly sampled radionuclide breakthrough curves with the time-varying radionuclide sources from the UZ to quantify radionuclide transport to the accessible environment (as discussed in Section 6.3.10.3). This approach has been validated for the 3-D SZ Flow and Transport Abstraction, as documented in *Saturated Zone Flow and Transport Model Abstraction* (SNL 2008 [DIRS 183750], Section 7.1.1).

The EBS TH Environment Submodel implements the TH environment in and around an emplacement drift from the MSTHM Abstraction (Table 6-1 and Section 6.3.2). The MSTHM Process Model Abstraction results include the spatial discretization of TH conditions of the EBS and its components, as well as the variability of these results due to uncertainties with the percolation flux and the host-rock thermal conductivity inherited from the Site-Scale UZ Flow Process Model. These spatially discretized inputs to the TSPA-LA are provided by the MSTHM Process Model Abstraction at two scales, a fine-scale or comprehensive data set which is appropriate for determining WP failure histories due to general or localized corrosion, and a coarse-scale or representative data set, which is sufficient for capturing waste-form mobilization and transport processes. This scheme involves the discretization of the repository domain into a specified number of subregions based upon percolation flux, and each subregion's TH conditions are characterized by a subset of the comprehensive TH dataset that is meant to be representative of the TH conditions everywhere within that specific percolation subregion. This spatial discretization scheme, and the appropriateness of its use in the TSPA-LA to measure repository performance, is discussed in the following sections.

7.3.4.2 Spatial Discretization of the TSPA-LA into Percolation Subregions

Spatially discretizing the repository into subregions is a balance between a minimum number of subregions that would adequately capture the variability of the EBS TH environment across the footprint and the increased computational burden associated with each additional subregion. As described in Section 6.3.2, five percolation subregions were used. These five repository percolation subregions were selected in order to maximize the ability of the TSPA-LA Model to include spatial effects when sensitivity analyses and alternative scenarios were analyzed.

7.3.4.2.1 Percolation Flux as a Basis for Discretizing the Repository

Percolation flux at the base of the PTn has a primary role in determining the long-term in-drift TH environment (SNL 2007 [DIRS 181383], Section 6.3.2.1). Subregions in the repository footprint with similar percolation fluxes have similar long-term TH conditions, such as WP temperature or drift-wall temperature. However, using the percolation flux to determine the in-drift TH environment may not capture the short-term TH behavior like WP peak temperature,

which occurs within the first few decades after repository closure. Percolation flux, for use as a subregion selection parameter, has a temporal advantage over parameters, such as WP temperature or drift-wall temperature. Parameters such as WP or drift-wall temperature could have similar peaks from one subdomain location to another but have much different temperature histories over the course of time. TH environment variables, such as invert flux, that are used in EBS Transport Model Components (e.g., the EBS-UZ Interface Submodel, Table 6-1) have a short dry-out period at the beginning of the postclosure period (during the ramp up of heat in the repository), followed by long rewetting periods as the heat pulse decays (SNL 2007 [DIRS 181383], Section 6.3.3). The use of percolation flux as a parameter to define subregions in the repository footprint can be more predictive of the availability of liquid at a subdomain location than either the WP or drift-wall temperature because it remains constant during the duration of each climate period. In addition, percolation flux at the base of the PTn is used directly as input to the Drift Seepage Submodel and the Drift Wall Condensation Submodel and is abstracted from the UZ flow fields to be used as a direct input to the UZ Transport Submodel. In summary, percolation flux at the base of the PTn was selected as the primary parameter to discretize the repository into subdomains because:

- TH response in the emplacement drifts is sensitive to percolation flux (SNL 2007 [DIRS 181383], Section 6.3.2)
- Chemical environment for radionuclide mobility is driven by TH conditions (Section 6.3.4)
- Percolation flux is the boundary condition for the Drift Seepage Submodel (Table 6-1), and variability in drift seepage is the primary cause of variability in advective radionuclide releases from the EBS (Section 6.3.3).

7.3.4.2.2 Binning the Percolation Subregions by Quantiles

The process used to assign or bin each of the 3,264 MSTHM Process Model subdomains to each of the five repository percolation subregions is described in DTN: LA0702PANS02BR.001_R1 [DIRS 180322] and SNL 2008 [DIRS 184748], Section 6.5.15[a]. Note that only the first three climate states were considered in the analysis used to find a single zone file with five sets of source nodes that best represents all the infiltration/climate combinations. The subdomains comprising each of the five repository percolation subregions were chosen based on the cumulative probability of percolation for the 12 flow fields (three different climates: present-day, monsoon, and glacial-transition; each climate is categorized with 4 infiltration scenarios: 10^{th} percentile, 30^{th} percentile, 50^{th} percentile, and 90^{th} percentile). A four-step binning process was applied to each of the twelve flow fields, resulting in a list of repository subdomains divided into five percolation subregions that share common percolation fluxranges, based on the cumulative probability intervals for these subregions (SNL 2008 [DIRS 184748], Section 6.5.15[a]). The cumulative probability intervals for these five subregions of percolation rates sorted in ascending order are 0.0-0.05, 0.05-0.30, 0.30-0.70, 0.70-0.95, and 0.95-1.00 (SNL 2008 [DIRS 184748], Section 6.5.15[a]). The quantiles are shown in Table 6.3.2-2. An analysis of the degree of similarity or difference of the results of the binning process depending on which flow field is considered was performed. The results indicated that the bins for the 12 flow fields are quite similar to one another. As noted in *Particle Tracking Model and*

Abstraction of Transport Processes (SNL 2008 [DIRS 184748], Section 6.5.15[a]), if a subregion is identified for a particular subdomain in the glacial-transition, 10th percentile flow field, it is very often identified as the same subregion for the other flow fields. When they are different, they almost always differ by only one subregion; that is, a 3 in one flow field becomes a 4 in another flow field, or a 2 becomes a 1. Based upon this result, it was considered acceptable to use subregions from one flow field to approximate all infiltration scenarios and climate states. Therefore, the 10th percentile infiltration scenario for the glacial transition climate was used to define the five percolation subregions for all simulations including the post-10,000-year climate. The five percolation subregions are shown graphically on Figure 6.3.2-7. There are 163; 817; 1,300; 820; and 164 subdomains (i.e., different TH data sets) for Percolation Subregions 1, 2, 3, 4, and 5, respectively. The following points should be noted:

- The subregions are not completely contiguous in space but are located throughout the repository in different regions.
- Each subregion includes both edge and interior repository subdomain locations.
- The five selected subregions have a fixed set of repository subdomain locations for all realizations of the TSPA-LA Model, regardless of percolation flux, host-rock thermal conductivity, or climate state.
- The range of percolation flux values calculated for each percolation subregion will be different depending on the percolation flux and/or host-rock thermal conductivity scenario being considered and/or climate state.

7.3.4.3 Variability Analysis of the Engineered Barrier System Thermal-Hydrology within the TSPA-LA

To characterize the variability in repository TH conditions, the MSTHM Process Model subdivides the drifts in the repository footprint into 3,264 equal-area subdomains corresponding to 20-m repository drift segments (SNL 2007 [DIRS 181383], Section 6.2.12[a]). For each of the 12 percolation flux/host-rock thermal conductivity cases (Table 6.3.2-3), the MSTHM Abstraction includes the time-dependent TH variables, temperature, and relative humidity for six different possible CSNF WPs and two different possible CDSP WPs at each of the 3,264 repository subdomains (SNL 2007 [DIRS 181383], Tables 5.4-1 and 6.3-13, and Section 6.2.17[a]). In addition, the MSTHM Abstraction includes time-dependent values for DS temperature and relative humidity, average drift-wall temperature, the duration of boiling at the drift wall, the average invert temperature, the average invert saturation, and the average invert flux for each of the 3,264 repository subdomains. In all, that makes 19,584 different TH histories associated with CSNF WPs and 6,528 different TH histories associated with the CDSP WPs for each of the 12 infiltration/host-rock thermal conductivity cases. This comprehensive data set is used for the WAPDEG and seepage DLLs of the TSPA-LA. As for the TSPA-LA submodels that require TH inputs and feeds, the use of this comprehensive data set is not feasible with respect to computer simulation time and resources. Therefore, the MSHTM Process Model also provides an abstraction of the comprehensive TH data set by first grouping 3,264 repository subdomains into one of the five repository percolation subregions as described above. Next, the MSTHM Process Model determines a representative TH history associated with a single CSNF

WP and a single CDSP WP for each percolation subregion. These representative TH data are then used as input to the EBS Submodel and propagated throughout the rest of the TSPA-LA Model. The purpose of the TH variability analysis discussed in the following section is to demonstrate the appropriateness and validity of using the representative TH histories as inputs to the EBS Submodel of the TSPA-LA as opposed to using the comprehensive data set.

7.3.4.3.1 Use of Representative Thermal-Hydrology Histories Compared to the Comprehensive Thermal-Hydrology Histories

To conduct the analysis, the TSPA-LA Model was exercised over a range of percolation flux percentiles, host-rock thermal conductivities, and percolation subregions that represent the range of TH conditions from the driest and hottest, to the wettest and coolest, with appropriate conditions in between. Radionuclide releases from the EBS for a one million year compliance period were used as the benchmark for comparison between the two types of TH histories (i.e., representative versus comprehensive) invoked over the range of TH conditions described above. Since there is both a diffusive and an advective component to the release of radionuclides from the EBS, comparisons were made for both the Drip Shield EF (advection dominated transport) and the Waste Package EF (diffusion dominated transport) Modeling Cases.

For the runs using a representative TH data set, the TSPA-LA Model was run over a specified number of realizations corresponding to the number of subdomains for a specific percolation subregion but with the key epistemic and aleatory variables of infiltration and host-rock thermal conductivity fixed to be the same for each realization. By fixing these variables, the same representative TH history was used over the course of each respective run. For the Drip Shield EF Modeling Case, only a single DS over a CSNF WP and a single DS over a CDSP WP was allowed to fail during each realization. In similar manner, only a single CNSF WP and a single CDSP WP were allowed to fail for the Waste Package EF Modeling Cases.

For the runs using the comprehensive TH data set, a different implementation strategy was needed. This strategy involved the use of a single Monte Carlo realization coupled with the ability of the GoldSim software to loop over the number of subdomains associated with a specific percolation subregion. As was done for the runs using the representative TH data set, the key epistemic and aleatory variables of infiltration and host-rock thermal conductivity, and percolation subregion, were fixed for the single realization. In this case, however, the number of loops for that single realization, rather then the number of realizations, corresponded to the number of subdomains within the specified percolation subregion. To reduce the computational time of these runs to a more manageable quantity (days instead of weeks), only one of the six TH histories associated with the six CSNF WPs at each subdomain (or loop) was used, and only one of the two TH histories associated with the two CDSP WPs at each subdomain (or same loop) was used. These were chosen stochastically using discrete distributions each time the model looped to the next subdomain.

Table 7.3.4-1 outlines the TH variability cases that were run (output DTN: MO0708TSPAVALI.000 [DIRS 182985]). As an example, TH variability case LA_v5.000_ED_000300_002 represents the Drip Shield EF run where the representative TH was used that is associated with the 10th percentile infiltration, the low host-rock thermal conductivity value, and percolation subregion number one. This case was run for 163 Monte

Carlo realizations using the same set of representative TH data, where 163 represents the number of subdomains in percolation subregion one. For each realization, a single DS failure was forced to occur and, subsequently, a single WP was failed when conditions allowed. The TH variability comparison case, LA_v5.000_ED_000300_007, loops 163 times during a single Monte Carlo realization, failing a single DS and subsequent WP per loop. Each loop stochastically selects one of six CSNF TH histories and one of two CDSP TH histories for the subdomain associated with that loop, for a total of 163 different CSNF and CDSP TH histories. In the end, running 163 realizations with a single early failure is the same as running one realization with 163 early failures (one for each loop) but with the caveat that the single realization run uses 163 different TH histories per WP type versus one TH history per WP type for the multiple realization run.

7.3.4.3.2 Results of the Engineered Barrier System Thermal-Hydrology Variability Analysis

For each set of TH variability runs outlined in Table 7.3.4-1, a comparison of the means of the radionuclide cumulative releases of ^{99}Tc, ^{129}I, and ^{239}Pu from the EBS is the benchmark by which the appropriateness and validity of using a representative TH history over a comprehensive TH history is gauged. Figure 7.3.4-1(a) shows the EBS releases for the two cases described in the example above. That is, the case that used the representative TH data set compared to the case that used the comprehensive TH data for the Drip Shield EF Modeling Case, 10th percentile infiltration, low host-rock thermal conductivity, and Percolation Subregion 1. After about 1,000 years, the EBS cumulative release of these radionuclides is very similar for both the representative and comprehensive TH data sets. The same behavior is shown on Figures 7.3.4-2(a), 7.3.4-3(a), 7.3.4-4(a), and 7.3.4-5(a) for the other infiltration percentile, host-rock thermal conductivity, and percolation subregion cases.

The EBS releases that used the TH histories from the comprehensive data set generally begin earlier than the cases that used a representative TH history. The exception occurs for the cases that use the 90th percentile infiltration and high host-rock thermal conductivity where the releases from the EBS are initiated at about the same times. Figures 7.3.4-1(b) through 7.3.4-5(b) compare the CSNF WP temperature histories below 100°C for the representative and comprehensive TH data sets. The CSNF WP temperature histories for the representative TH data sets are similar to the means of the CSNF WP temperature histories associated with the comprehensive TH data set for each respective infiltration percentile, host-rock thermal conductivity, and percolation subregion case. This illustrates that the representative TH can be used as a surrogate for the comprehensive TH data set. The WP temperatures from the comprehensive TH data sets have lower and upper bounds. Since the TSPA-LA Model requires the WP temperature to drop below 100°C before transport from the EBS can be initiated, and since there is some spread between the lower bound and the mean CSNF WP temperatures from the comprehensive TH data set, the EBS releases from these cases start earlier than those that used the representative TH data.

Figures 7.3.4-6a through 7.3.4-10a show the EBS cumulative releases of ^{99}Tc, ^{129}I, and ^{239}Pu from the EBS for the Waste Package EF Modeling Case. The Waste Package EF Modeling Case is characterized by a relatively early EBS release from the CDSP WPs, followed later by an upward shift in cumulative release due to the failure of the CSNF WPs. The magnitudes of EBS releases from the cases that use the representative TH data is very similar to the releases from the

cases that use the comprehensive TH data sets after about 10,000 years. As was the situation with the Drip Shield EF Modeling case discussed previously, EBS releases from CDSP WPs occur sooner for the cases that use the comprehensive TH data set. This is again attributable to the times at which the WP temperatures drop below 100°C. EBS releases from the CSNF WPs also occur sooner for the cases that use the comprehensive TH data set. This is attributable to a 95 percent relative humidity threshold for EBS transport applied to CSNF WPs by the TSPA-LA Model for WP early failure cases. Figures 7.3.4-6b through 7.3.4-10b demonstrate this behavior by showing the representative relative humidity histories for CSNF WPs compared to the mean and lower and upper bounds of relative humidity histories from the comprehensive TH data sets.

In summary, in the Waste Package Early Failure Modeling Case, the EBS releases of ^{99}Tc, ^{129}I and ^{239}Pu tend to occur earlier in cases that use the comprehensive TH data sets than in cases that use the representative TH data, from either CDSP or CSNF WPs. However, the cumulative mass released from either type of WP is the same for both TH data sets. In particular, the equivalence in cumulative mass of these radionuclides released from CDSP WP can be observed in Figure 7.3.4-6(a) though Figure 7.3.4-10(a), for the time period before roughly 9,500 years. Before 9,500 years, radionuclides are diffusing only from CDSP WPs, because the relative humidity in CSNF WPs has not yet reached 95%, as shown in Figure 7.3.4-6(b) through Figure 7.3.4-10(b). The earlier release from CSNF WPs, and the equivalence in cumulative mass released from CSNF WPs, are also shown in Figure 7.3.4-6(a) though Figure 7.3.4-10(a), with the earlier release beginning at roughly 9,500 years and the equivalent cumulative releases being achieved at about 12,000 years.

The Drip Shield Early Failure Modeling Case, as modified for this analysis, demonstrates that the use of comprehensive or representative TH data results in equivalent cumulative releases from one WP. The Waste Package Early Failure Modeling Case, as modified for this analysis, demonstrates that the use of comprehensive or representative TH data results in equivalent cumulative releases from one WP, although the releases may occur earlier when using the comprehensive TH data. As demonstrated by Figure 8.1-3(a), total mean annual dose prior to 10,000 years is attributable primarily to radionuclides released due to igneous intrusion and seismic ground motion events. After an igneous intrusion, the EBS components (DS and WP) are destroyed, thus, radionuclide mobilization and transport is similar to that observed in the Drip Shield Early Failure Modeling Case. As demonstrated in Section 7.3.2.6, the mean annual dose from seismic ground motions events prior to 10,000 years is attributable to damage caused to CDSP WPs lying under functional drip shields. Because the damage consists of cracks, and the drip shield remains functional, radionuclide mobilization and transport in the Seismic Ground Motion Modeling Case is similar to that observed in the Waste Package Early Failure Modeling Case results for CDSP WPs. Because the mean annual dose at each time is determined by averaging over the dose resulting from all possible preceding events (as well as over uncertainty in input parameters), the mean annual dose is primarily determined by the cumulative release of radionculides, rather than the instantaneous release rates. Therefore, the use of either the comprehensive or representative TH data would produce equivalent estimates of mean annual dose, because the cumulative radionuclide releases from WPs are equivalent for the two data sets.

INTENTIONALLY LEFT BLANK

Table 7.3.4-1. Summary of the Thermal-Hydrologic Variability Cases Run to Validate the Use of Representative Thermal-Hydrologic Data Sets Over the Use of Computationally Expensive Comprehensive Thermal-Hydrologic Data Sets

Thermal –Hydrologic Variability Case ID	Modeling Case	Thermal-Hydrologic Data Set	Infiltration Percentile	Thermal Conductivity Case	Percolation Subregion	Number of Loops	Number of DS and/or WP Failures per Loop	Total Number of DS and/or WP Failures
LA_v5.000_ED_000300_002	DS EF	Representative	10^{th}	Low	1	1	163	163
LA_v5.000_ED_000300_007	DS EF	Comprehensive	10^{th}	Low	1	163	1	163
LA_v5.000_ED_000300_003	DS EF	Representative	10^{th}	Low	3	1	1,300	1,300
LA_v5.000_ED_000300_008	DS EF	Comprehensive	10^{th}	Low	3	1,300	1	1,300
LA_v5.000_ED_000300_004	DS EF	Representative	50^{th}	Mean	3	1	1,300	1,300
LA_v5.000_ED_000300_009	DS EF	Comprehensive	50^{th}	Mean	3	1,300	1	1,300
LA_v5.000_ED_000300_005	DS EF	Representative	90^{th}	High	3	1	1,300	1,300
LA_v5.000_ED_000300_010	DS EF	Comprehensive	90^{th}	High	3	1,300	1	1,300
LA_v5.000_ED_000300_006	DS EF	Representative	90^{th}	High	5	1	164	164
LA_v5.000_ED_000300_011	DS EF	Comprehensive	90^{th}	High	5	164	1	164
LA_v5.000_EW_000300_000	WP EF	Representative	10^{th}	Low	1	1	163	163
LA_v5.000_EW_000300_005	WP EF	Comprehensive	10^{th}	Low	1	163	1	163
LA_v5.000_EW_000300_001	WP EF	Representative	10^{th}	Low	3	1	1,300	1,300
LA_v5.000_EW_000300_006	WP EF	Comprehensive	10^{th}	Low	3	1,300	1	1,300
LA_v5.000_EW_000300_002	WP EF	Representative	50^{th}	Mean	3	1	1,300	1,300
LA_v5.000_EW_000300_007	WP EF	Comprehensive	50^{th}	Mean	3	1,300	1	1,300
LA_v5.000_EW_000300_010	WP EF	Representative	90^{th}	High	3	1	1,300	1,300
LA_v5.000_EW_000300_008	WP EF	Comprehensive	90^{th}	High	3	1,300	1	1,300
LA_v5.000_EW_000300_011	WP EF	Representative	90^{th}	High	5	1	164	164
LA_v5.000_EW_000300_009	WP EF	Comprehensive	90^{th}	High	5	164	1	164

Source: (Output DTN MO0708TSPAVALI.000 [DIRS 182985]).

INTENTIONALLY LEFT BLANK

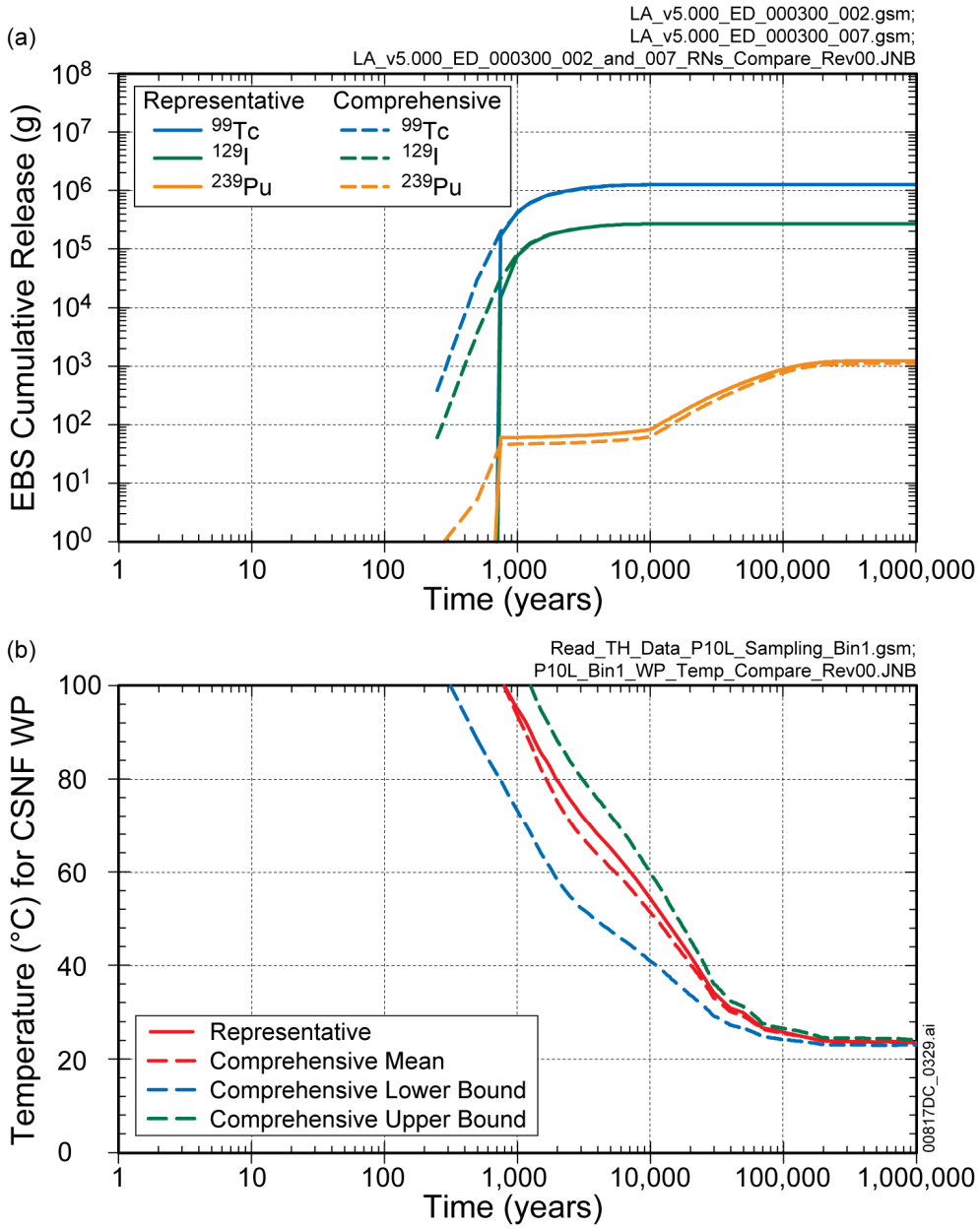

Source: Output DTN: MO0708TSPAVALI.000 [DIRS 182985].

Figure 7.3.4-1. Comparison of the Representative and Comprehensive Thermal Hydrologic Data Sets for (a) EBS Releases of ^{99}Tc, ^{129}I, and ^{239}Pu, and (b) Time when the CSNF WP Temperature Drops Below Boiling for the Drip Shield Early Failure Modeling Case, 10th Percentile Infiltration Flux, Low Host-Rock Thermal Conductivity, Percolation Subregion 1

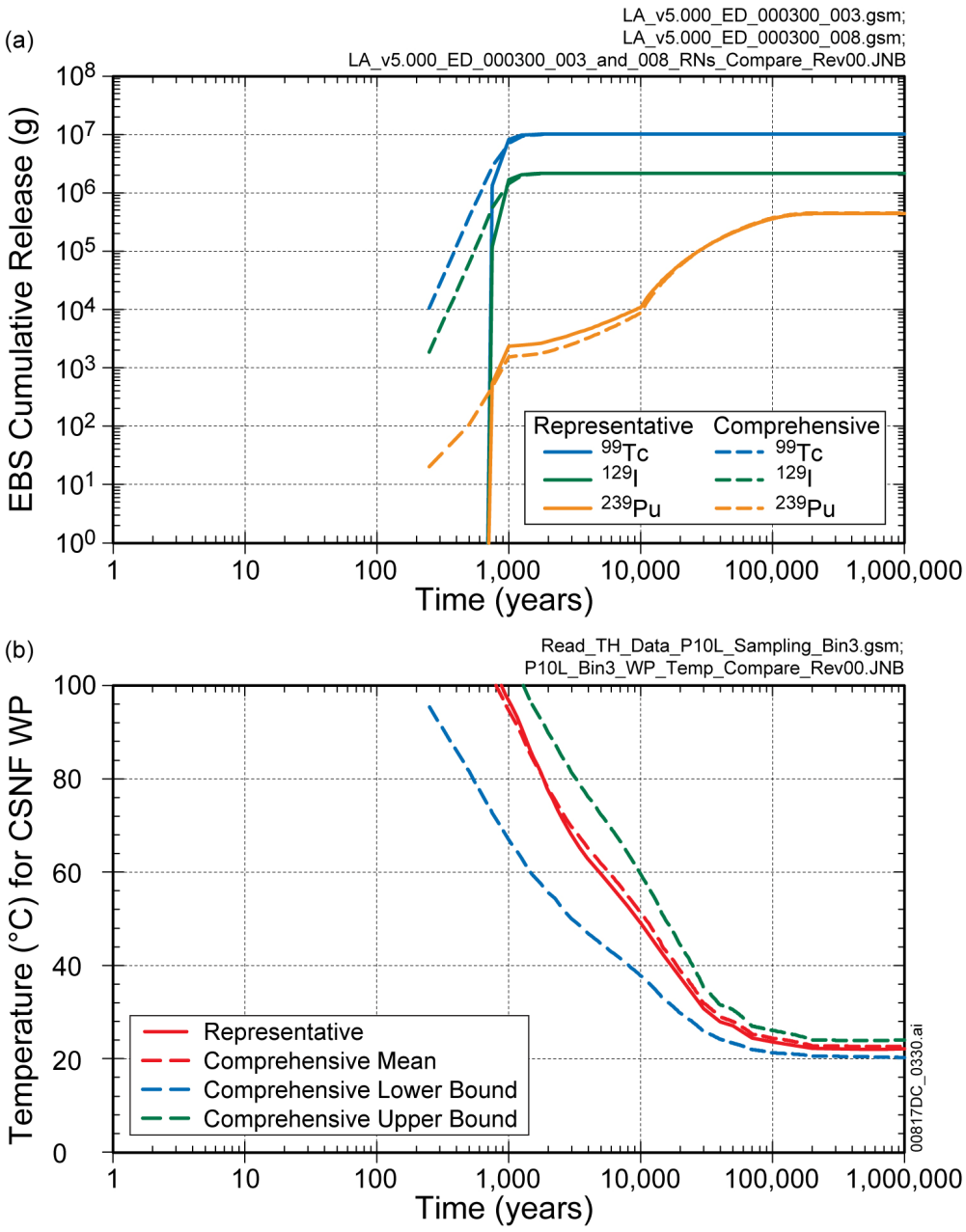

Source: Output DTN: MO0708TSPAVALI.000 [DIRS 182985].

Figure 7.3.4-2. Comparison of the Representative and Comprehensive Thermal Hydrologic Data Sets for (a) EBS Releases of ^{99}Tc, ^{129}I, and ^{239}Pu, and (b) Time when the CSNF WP Temperature Drops Below Boiling for the Drip Shield Early Failure Modeling Case, 10th Percentile Infiltration Flux, Low Host-Rock Thermal Conductivity, Percolation Subregion 3

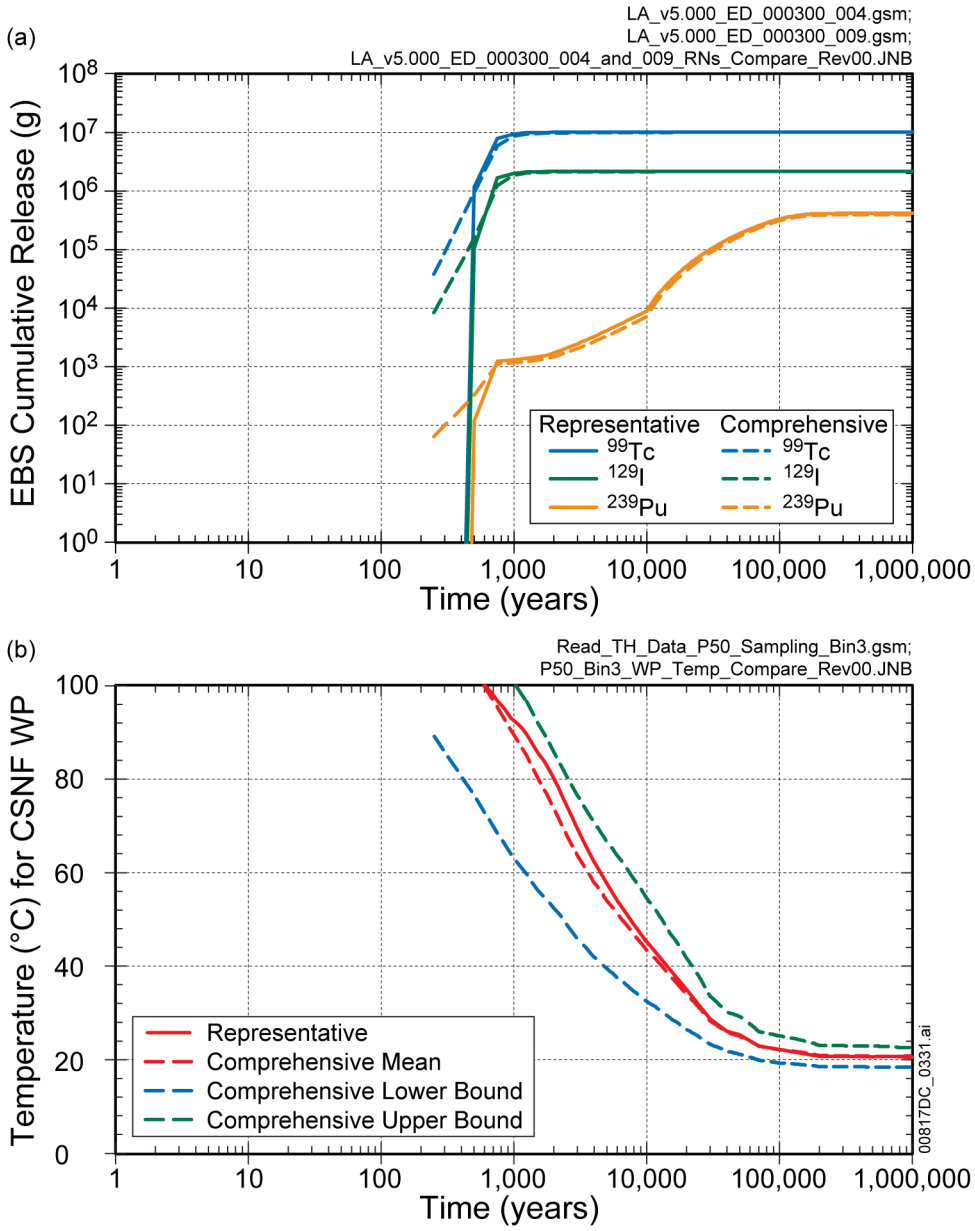

Source: Output DTN: MO0708TSPAVALI.000 [DIRS 182985].

Figure 7.3.4-3. Comparison of the Representative and Comprehensive Thermal Hydrologic Data Sets for (a) EBS Releases of ^{99}Tc, ^{129}I, and ^{239}Pu, and (b) Time when the CSNF WP Temperature Drops Below Boiling for Drip Shield Early Failure Modeling Case, 50th Percentile Infiltration Flux, Mean Host-Rock Thermal Conductivity, Percolation Subregion 3

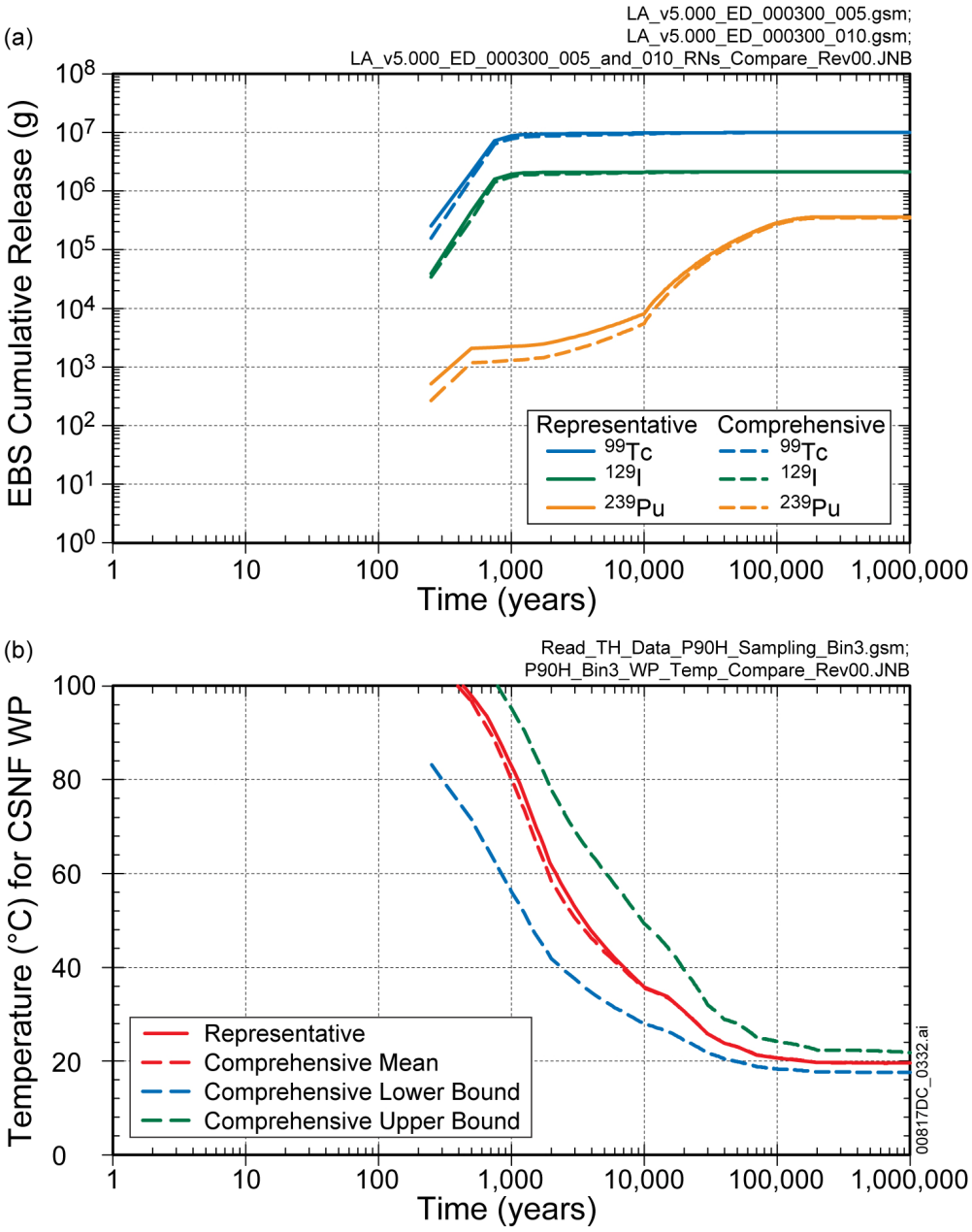

Source: Output DTN: MO0708TSPAVALI.000 [DIRS 182985].

Figure 7.3.4-4. Comparison of the Representative and Comprehensive Thermal Hydrologic Data Sets for (a) EBS Releases of ^{99}Tc, ^{129}I, and ^{239}Pu, and (b) Time when the CSNF WP Temperature Drops Below Boiling for the Drip Shield Early Failure Modeling Case, 90th Percentile Infiltration Flux, High Host-Rock Thermal Conductivity, Percolation Subregion 3

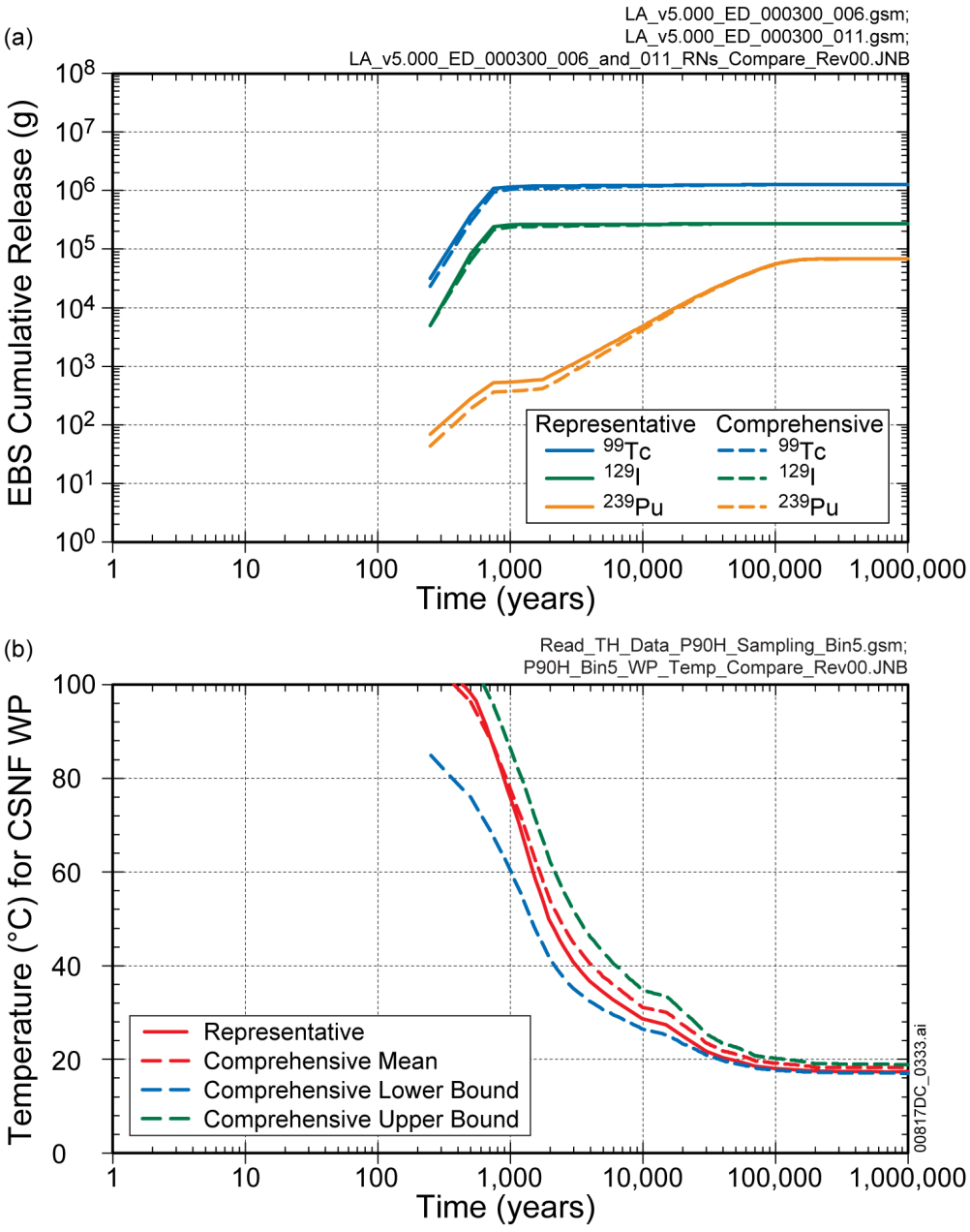

Source: Output DTN: MO0708TSPAVALI.000 [DIRS 182985].

Figure 7.3.4-5. Comparison of the Representative and Comprehensive Thermal Hydrologic Data Sets for (a) EBS Releases of ^{99}Tc, ^{129}I, and ^{239}Pu, and (b) Time when the CSNF WP Temperature Drops Below Boiling for the Drip Shield Early Failure Modeling Case, 90th Percentile Infiltration Flux, High Host-Rock Thermal Conductivity, Percolation Subregion 5

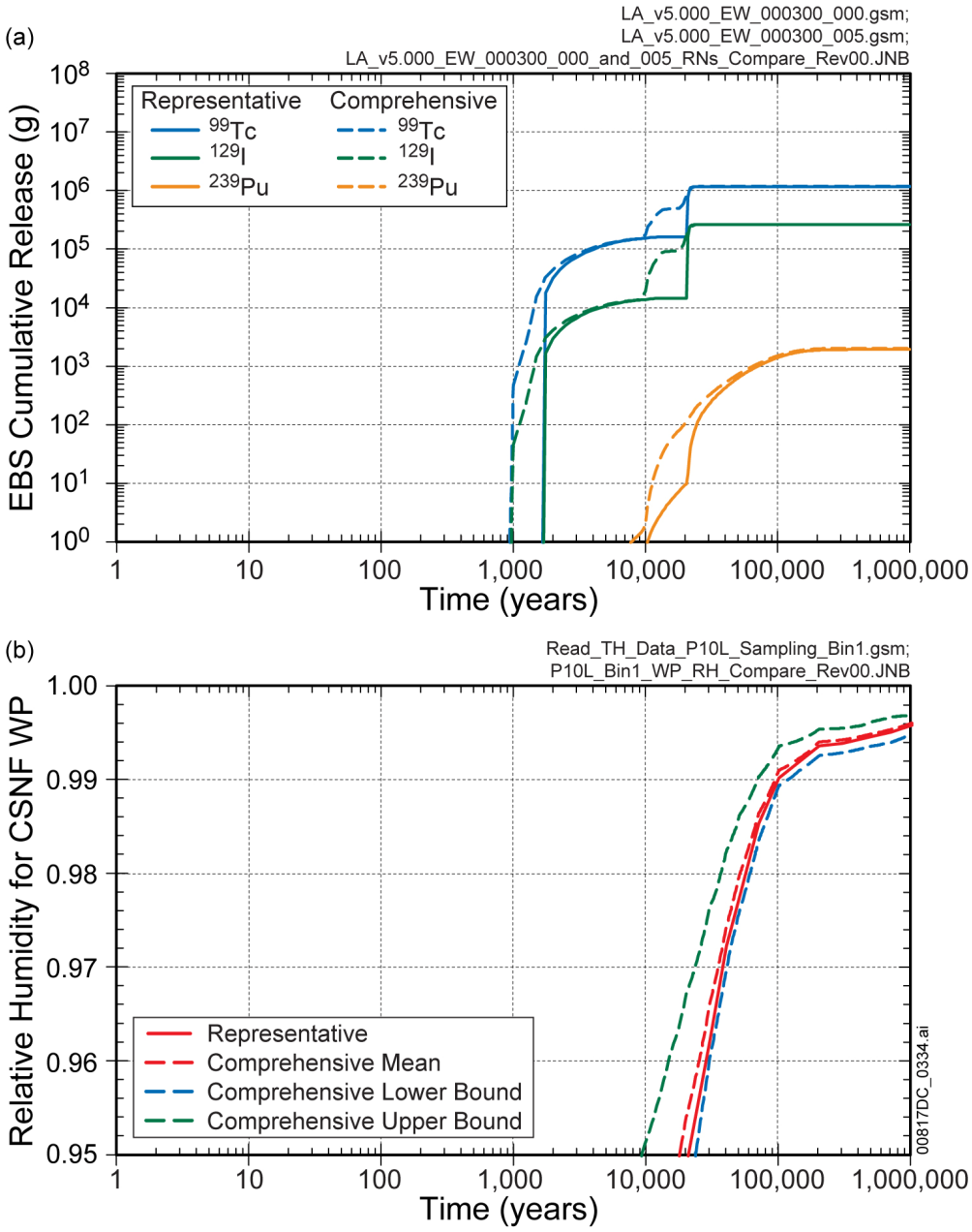

Source: Output DTN: MO0708TSPAVALI.000 [DIRS 182985].

Figure 7.3.4-6. Comparison of the Representative and Comprehensive Thermal Hydrologic Data Sets for (a) EBS Releases of ^{99}Tc, ^{129}I, and ^{239}Pu, and (b) Time when the WP Relative Humidity is above 95 Percent for the Waste Package Early Failure Modeling Case, 10th Percentile Infiltration Flux, Low Host-Rock Thermal Conductivity, Percolation Subregion 1

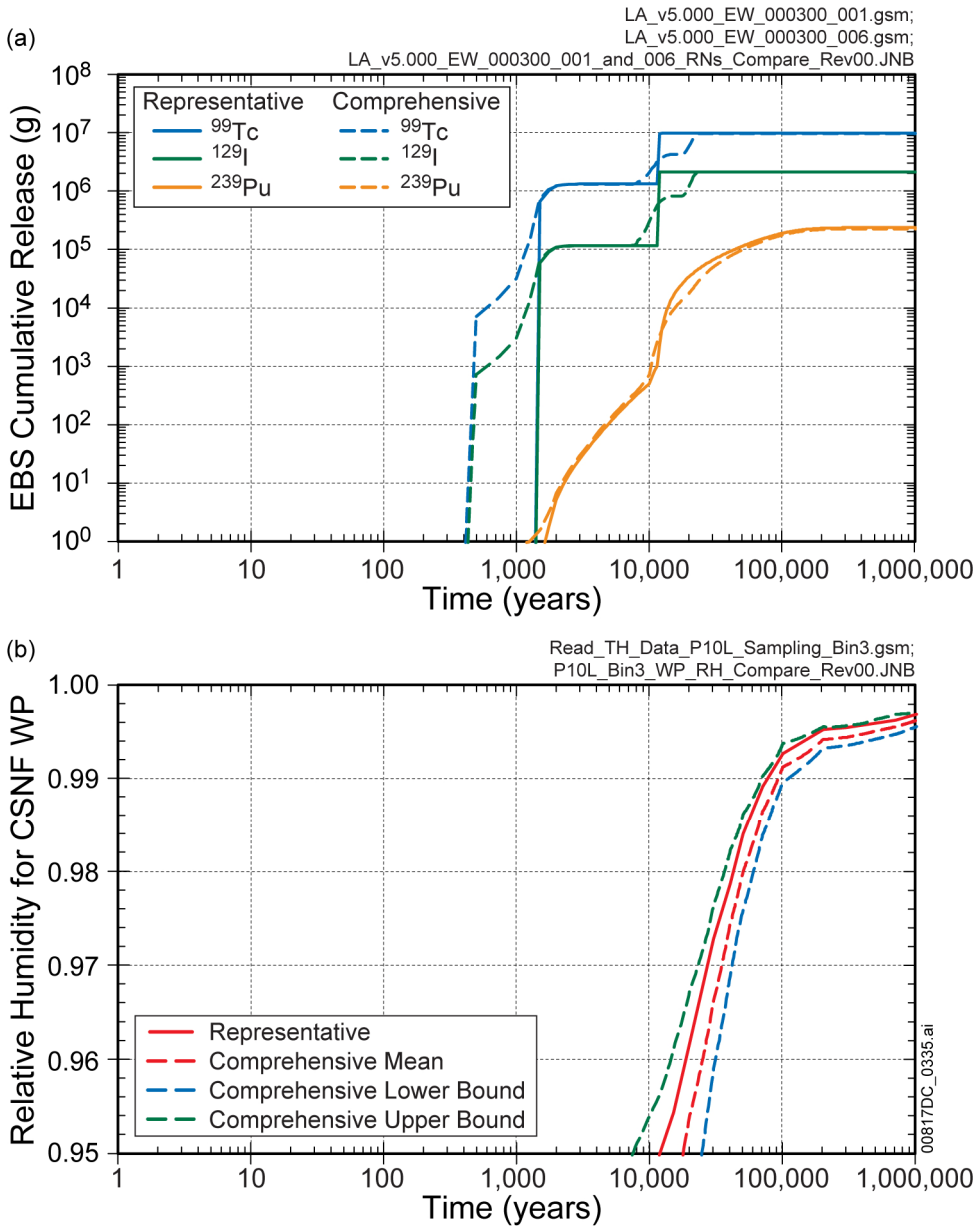

Source: Output DTN: MO0708TSPAVALI.000 [DIRS 182985].

Figure 7.3.4-7. Comparison of the Representative and Comprehensive Thermal Hydrologic Data Sets for (a) EBS Releases of ^{99}Tc, ^{129}I, and ^{239}Pu, and (b) Time when the WP Relative Humidity is above 95 Percent for the Waste Package Early Failure Modeling Case, 10th Percentile Infiltration Flux, Low Host-Rock Thermal Conductivity, Percolation Subregion 3

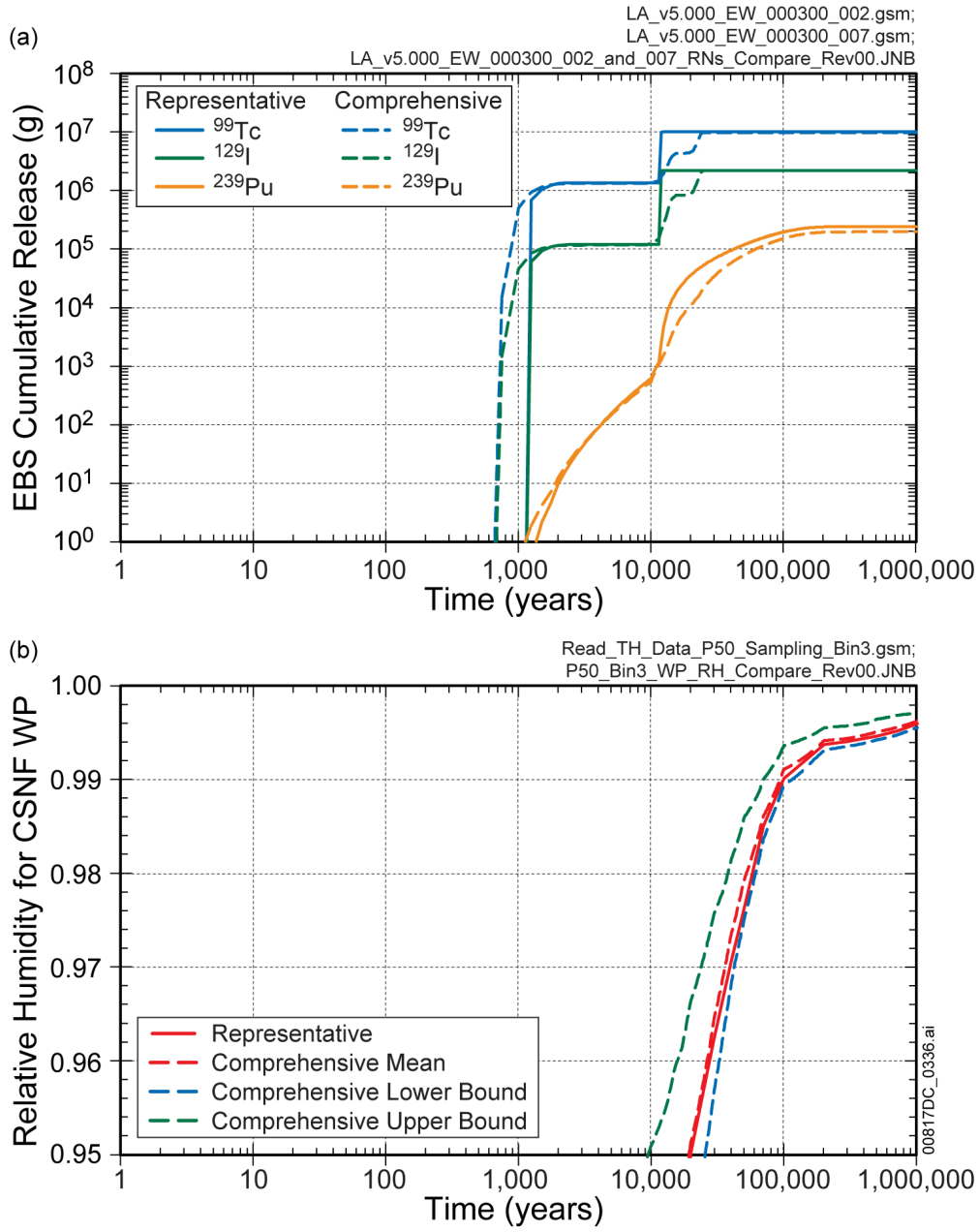

Source: Output DTN: MO0708TSPAVALI.000 [DIRS 182985].

Figure 7.3.4-8. Comparison of the Representative and Comprehensive Thermal Hydrologic Data Sets for (a) EBS Releases of ^{99}Tc, ^{129}I, and ^{239}Pu, and (b) Time when the WP Relative Humidity is above 95 Percent for the Waste Package Early Failure Modeling Case, 50th Percentile Infiltration Flux, Mean Host-Rock Thermal Conductivity, Percolation Subregion 3

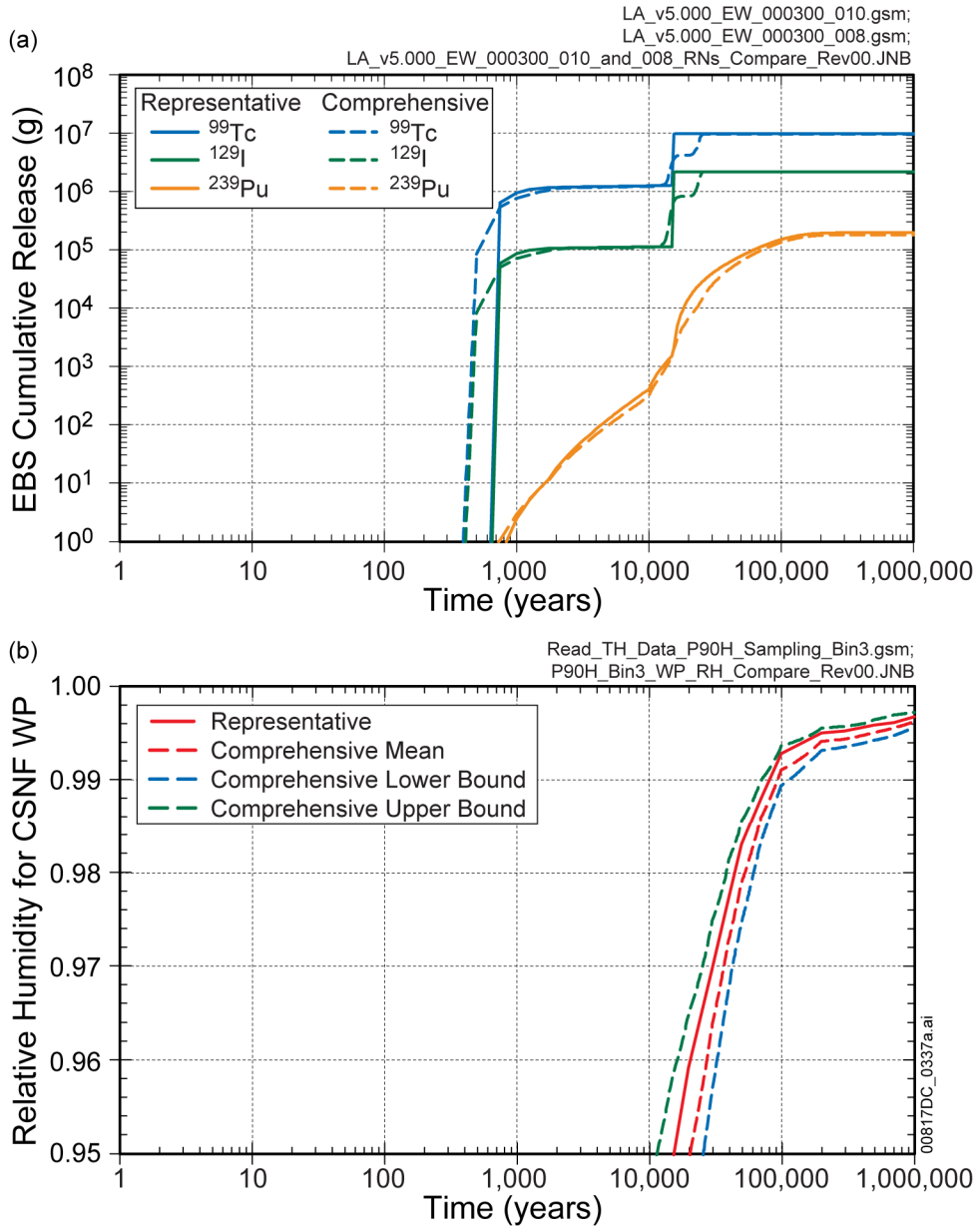

Source: Output DTN: MO0708TSPAVALI.000 [DIRS 182985].

Figure 7.3.4-9. Comparison of the Representative and Comprehensive Thermal Hydrologic Data Sets for (a) EBS Releases of ^{99}Tc, ^{129}I, and ^{239}Pu, and (b) Time when the WP Relative Humidity is above 95 Percent for the Waste Package Early Failure Modeling Case, 90th Percentile Infiltration Flux, High Host-Rock Thermal Conductivity, Percolation Subregion 3

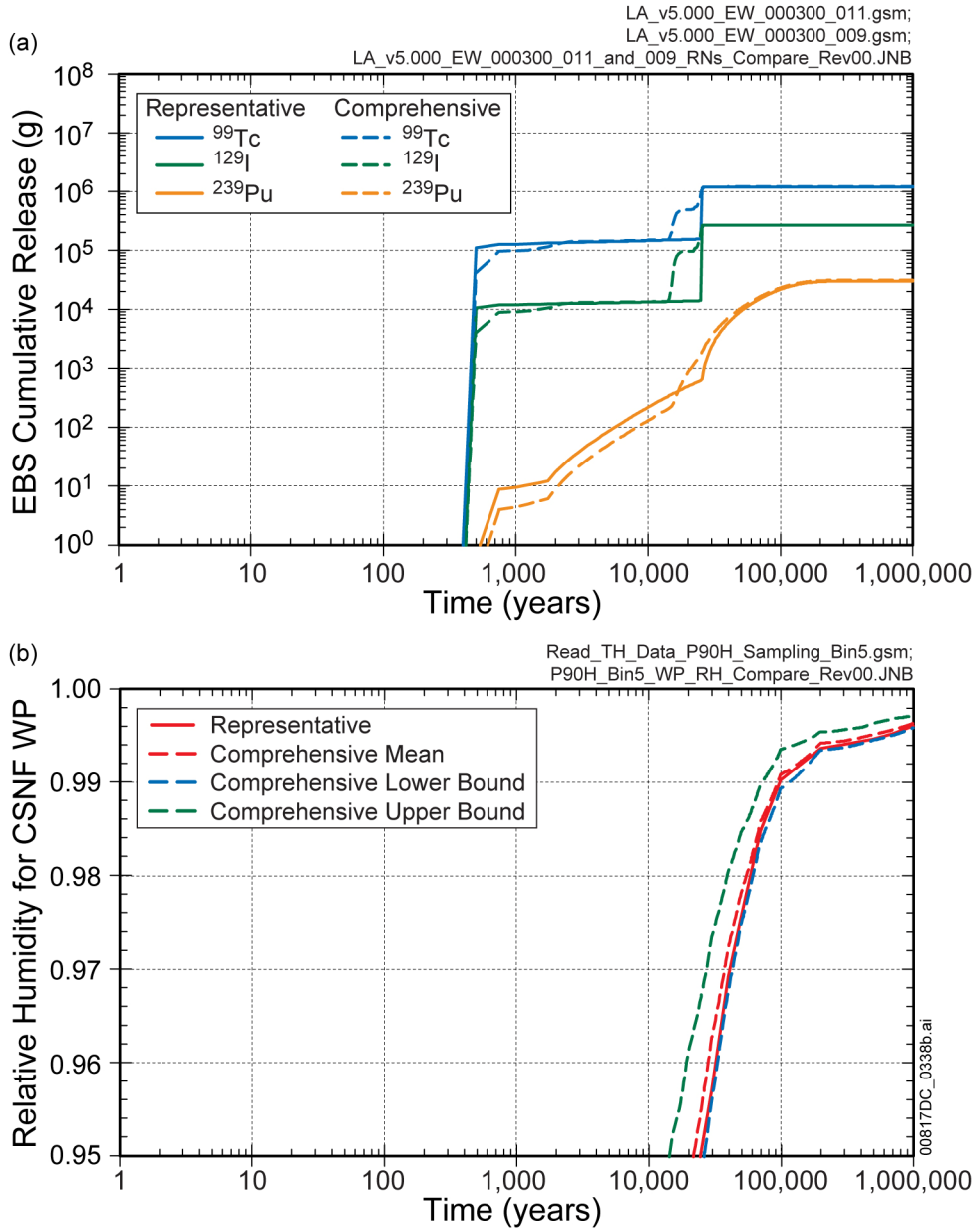

Source: Output DTN: MO0708TSPAVALI.000 [DIRS 182985].

Figure 7.3.4-10. Comparison of the Representative and Comprehensive Thermal Hydrologic Data Sets for (a) EBS Releases of ^{99}Tc, ^{129}I, and ^{239}Pu, and (b) Time when the WP Relative Humidity is above 95 Percent for the Waste Package Early Failure Modeling Case, 90th Percentile Infiltration Flux, High Host-Rock Thermal Conductivity, Percolation Subregion 5

7.3.5 Stability of FEHM Particle Tracking Model

In the TSPA-LA Model, radionuclide transport through the UZ is simulated using the FEHM (Zyvoloski et al. 1997 [DIRS 100615]) residence-time transfer-function particle-tracking technique, as described in *Particle Tracking Model and Abstraction of Transport Processes* (SNL 2008 [DIRS 184748], Section 6.4 and Appendix C). To have confidence in the results generated by the particle-tracking model, it is important to examine the stability of the TSPA-LA Model results relative to the number of particles being used. For particle-tracking models, the accuracy of the model is a function of the number of particles used to represent the source releases: the greater the number of particles, the greater the degree of stability (SNL 2008 [DIRS 184748], Section 6.6.2.1[a]) and accuracy. As the number of particles increases, a level will be reached where results stabilize and there will be little change in results associated with increasing the number of particles. In the TSPA-LA Model, the input for the maximum number of particles allowed in the TSPA-LA Model is 900,000 per species, which represents a near upper limit to the number of particles that can be used in conjunction with a three Gigabyte process limit on servers using the Windows 2000 and Windows Server 2003 operating systems. The memory needed for a FEHM multi-species particle-tracking simulation is a function of the number of particles used to represent the mass loading of each species, the number of species being tracked in the UZ (39 for the TSPA-LA Model), the number of timesteps simulated (the number of timesteps squared for daughter species), and the number of parents associated with daughter species. For each species, the maximum array length needed to store any timestep-dependent data, such as mass value of specific particles (this is a constant value for all particles of a specific species released at a specific timestep), is determined as follows:

$$ArrayLength_{\max} = \left[nts + \frac{nts}{2}(nts+1)\max_{dcl} \right] n_{bins} \qquad \text{(Eq. 7.3.5-1)}$$

where nts is the actual number of timesteps, max_{dcl} is the maximum number of parent species decaying into the specified species, and n is the number of source bins modeled (which is five for the TSPA-LA Model). Note that Equation 7.3.5-1 represents the maximum array length needed. There will be timesteps where no release of mass occurs and where no decay product is produced.

To test the stability of the results in reference to the number of particles used in the TSPA-LA Model, two supplemental simulations were performed with 500,000 and 750,000 particles as the maximum allowed. Note that the input to FEHM is the maximum number of particles allowed. The number of particles actually used by a specific species during a simulation is limited because FEHM saves part of the particle-based array length (a total length of 900,000 for the TSPA-LA Model) for any species that has mass introduced to the system from ingrowth. The saved space will be used to track particle-based data from particles that originally started as its parent species. The remainder of the particle-based array space is used to store data for particles representing mass released from the UZ. The maximum number of particles allowed per species covers both the particles representing releases from the EBS and the particles that will come from ingrowth.

To evaluate the particle-tracking model's stability, with reference to the number of particles used in the TSPA-LA Model, stability testing was performed using Version 5.000 of the TSPA-LA Model. LHS was utilized to generate TSPA-LA Model inputs for one aleatory realization of

base-case simulations that used 300 epistemic realizations. The base-case simulations considered in this study were the 3,000 realization (10 aleatory and 300 epistemic), 10,000-year duration Drip Shield EF Modeling Case; the 3,000 realization (10 aleatory and 300 epistemic), 1,000,000-year duration Igneous Intrusion Modeling Case; and the 9,000 realization (30 aleatory and 300 epistemic), 10,000-year duration Seismic GM Modeling Cases. The Drip Shield EF Modeling Case results used an aleatory realization comprised of percolation Bin 3 WPs and CSNF fuel type. The Igneous simulations used an aleatory realization with an event time of 250 years. The Seismic GM Modeling Case simulations used an aleatory realization comprised of a 10^{-6} damage fraction and an event time of 200 years. The base-case TSPA-LA Model simulations used for comparison in this analysis were LA_v5.000_ED_003000_007, LA_v5.000_IG_003000_017 output DTN: MO0709TSPAREGS.000 [DIRS 182976]), and LA_v5.000_SM_009000_008 (output DTN: MO0709TSPASENS.000 [DIRS 182982]). The simulations using a maximum of 500,000 particles to represent each species were LA_v5.000_ED_003000_018, LA_v5.000_IG_003000_029, and LA_v5.000_ SM_009000_006 (output DTN: MO0708TSPAVALI.000 [DIRS 182985]). The simulations using a maximum of 750,000 particles per species were LA_v5.000_ED_003000_019, LA_v5.000_IG_003000_030, and LA_v5.000_SM_009000_007 (output DTN: MO0708TSPAVALI.000 [DIRS 182985]). For each chosen modeling case, the results for five of the 300 epistemic realizations were examined closely to evaluate the effect of reducing the number of particles used in the simulations. Single realizations were examined because the averaging process would likely hide the differences. For igneous and seismic simulations, the choice of the single realizations is the first five epistemic realizations for the aleatory sample, making them random selections based on the epistemic sampling of the TSPA-LA Model. The choice of aleatory sample for the igneous and seismic simulations should have little influence on the results with the exception of allowing for the longest release time that would allow for the most complete evaluation. The DS early failure analysis uses a biased sampling of realizations chosen to allow for examination of how realizations with temporally oscillatory UZ ^{99}Tc releases are affected by the number of particles used to represent the releases. This choice of realizations was used to allow for an examination of the effect of the number of particles used on UZ releases that are not smooth over time and may be problematic because of it. As described later in this section, the results of simulations using 500,000 and 750,000 for the maximum number of particles were graphically compared to the TSPA-LA Compliance Model (900,000 particles) results in order to assess how much change in the annual doses occurs when the maximum number of particles is reduced. Although the doses are the output of concern in the TSPA-LA Model, the mass fluxes from the UZ for the Igneous Intrusion Modeling Case are also examined to show how the model is relatively insensitive to minor deviations in UZ transport results associated with the limit to the number of particles that are used.

7.3.5.1 Testing Procedure

As noted above, two supplemental simulations using different numbers of particles to represent the EBS releases were performed for each modeling case to test the stability of the TSPA-LA Model results relative to changes in the maximum number of particles (per species) used in the UZ particle-tracking analysis. These additional simulations used 500,000 and 750,000 as the maximum number of particles. For each chosen modeling case, the results for five of 300 epistemic realizations (for a chosen aleatory realization) were examined closely and compared to compliance model results to evaluate the effect of reducing the number of particles used in the

simulations. All parameters, except for the maximum number of particles allowed (900,000; 750,000; or 500,000) per species and, where applicable, the FEHM input parameter defining the number of particles assigned per mole, were the same for each set of simulations. In general, for the UZ submodel particle tracking analysis, particles are assigned on a per timestep basis. An exception has been made for the Igneous and Early Failure Modeling Cases where ^{99}Tc and ^{129}I particles are assigned on a particle per mole basis. The inputted ratio of particles allowed per mole is based on the maximum total release possible for the modeling case. This value is based on the inventories with all uncertainties included and the maximum possible WPs in the release (11,629 for igneous and one for the DS early failure analysis). This allows for a more accurate depiction of the spike-like portion of their EBS releases to the UZ. This technique more accurately simulates the portions of the release that are large contributors to dose. The major radionuclides considered in this analysis include ^{99}Tc, ^{233}U, ^{234}U, ^{237}Np, and Total ^{239}Pu (combined reversible and slow and fast irreversible colloids) (Section 6.3.7.1). The above species cover a range of transport behavior and are large contributors to dose. The Total ^{239}Pu includes the combined dissolved and reversibly sorbed colloidal phases and are summed with the (fast and slow fraction) irreversibly sorbed colloidal phases.

Note that the realization numbers for compliance runs and their associated stability analysis runs may differ because 300 realization subsets (based on the choice of a single aleatory event) of the full 3,000 and 9,000 realizations compliance runs (900,000 maximum particles) are utilized in the stability runs (500,000 and 750,000 maximum particles). The TSPA-LA Model allows for running subsets based on a single aleatory realization, but the realizations in the 300 realization subsets are numbered 1 to 300, where realizations in a compliance run with 3,000 realizations are numbered 1 to 3,000. To avoid confusion, realization references used in comparisons will be given in the form *a/b* where *a* is the realization number for a compliance run and *b* is a realization number for the stability run. The relationship between *a* and *b* is as follows:

$$a = N_{aleatory}(b-1) + I_{aleatory} \qquad \text{(Eq. 7.3.5-2)}$$

where, $N_{aleatory}$ is the number of aleatory realizations and $I_{aleatory}$ is the chosen aleatory realization. For cases where the compliance realization number is the same as the stability run realization, a subset run was performed for the compliance model, and the data from that subset was used in the comparison.

7.3.5.2 Simulation Results

7.3.5.2.1 Dose Calculations

The examination of the annual doses for the major radionuclides showed only minor differences between annual-dose results for simulations with different maximum particle allocations as depicted for each of the three chosen modeling cases (Drip Shield EF Modeling Case, Igneous Intrusion Modeling Case, and Seismic GM Modeling Case) on Figures 7.3.5-1, 7.3.5-2, and 7.3.5-3, respectively. The curves for the stability runs overlaid the curves for the compliance runs, indicating that the number of particles is unlikely to affect the timing and magnitude of peak dose values. Note that all figures referred to in this section can be found in output DTN: MO0709TSPAPLOT.000 [DIRS 183010]. To show the limited effects of reducing the number of particles on the TSPA-LA peak-dose analysis, the peak dose results for each

representative realization for each modeling case are presented in Table 7.3.5-1. The results presented in Table 7.3.5-1 indicate that peak doses for individual realizations are relatively insensitive to the reduction of maximum number of particles allowed to represent the mass of each radionuclide in the particle tracking analysis, from 900,000 to 750,000 or 500,000. Note that the oscillatory nature of the results for the Drip Shield EF Modeling Case presented on Figure 7.3.5-1 is a function of the release pattern of ^{99}Tc. Most of the large ^{99}Tc releases from the EBS is over a very short period of time. A large component of the mass following the most likely pathway reaches the water table relatively early. This mass release at the 18 km boundary is followed by smaller mass releases following other stochastically determined pathways.

7.3.5.2.2 Radionuclide Contributions to Dose

Because the annual dose results are summations of annual dose contributions from 39 different radionuclide species (or phases of species) with varied transport behavior in the UZ, a representative group of radionuclides (^{237}Np, ^{99}Tc, ^{233}U, ^{234}U, and Total ^{239}Pu) was chosen to evaluate how much influence the changes in maximum particle assignment has on the dose contributions from the different radionuclides.

For the Drip Shield EF Modeling Case analysis, annual dose plots were drawn for each of the radionuclides ^{237}Np, ^{99}Tc, ^{233}U, ^{234}U, and Total ^{239}Pu. Each plot contains the 900,000; 750,000; and 500,000 maximum particle simulation results for five realizations. As can be seen on Figure 7.3.5-4, the ^{237}Np annual dose results show negligible differences except for low values found in realization 1166/117. The ^{99}Tc results (Figure 7.3.5-5) show a little more difference associated with the changes in maximum particle assignments, but differences are still minor. Results for the ^{233}U (Figure 7.3.5-6) annual doses show minor differences for realization 266/27 and negligible differences for the other four realizations. Figure 7.3.5-7 shows negligible differences in annual doses for the ^{234}U results. Results for the Total ^{239}Pu (Figure 7.3.5-8a) annual doses also show only minor differences. Note that Total ^{239}Pu is the sum of ^{239}Pu on reversible colloids, ^{239}Pu on retarded irreversible colloids, and ^{239}Pu on unretarded colloids. Total ^{239}Pu represents the dose contribution due to ^{239}Pu release. For the Drip Shield EF Modeling Case, the dose contributions for the individual phases, ^{239}Pu on reversible colloids, ^{239}Pu on retarded irreversible colloids, and ^{239}Pu on unretarded colloids are also presented on Figure 7.3.5-8b, Figure 7.3.5-8c, and Figure 7.3.5-8d, respectively, so that the influence of particle number on the stability of the different phases can also be seen.

The Igneous Intrusion Modeling Case simulations also show only minor differences in results for different maximum particle allocations, with the exception of the ^{99}Tc annual doses. As can be seen on Figure 7.3.5-9, the ^{237}Np annual dose results show minor differences. The ^{99}Tc results (Figure 7.3.5-10a) show that the peak values that exert a strong influence on total dose show a negligible difference associated with the change in maximum particles allowed. Figure 7.3.5-10b, which portrays the time axis on a log scale, shows that at lower annual dose values a larger discrepancy between results can be found. This larger discrepancy is associated with the use of FEHM's mass based particle assignment, which more accurately describes larger releases over time at the price of less accurately simulating lower mass-flux releases. Results for

the ^{233}U (Figure 7.3.5-11) annual doses show some minor differences for realization 21/3 and negligible differences for the other four realizations. Figure 7.3.5-12 shows some early differences in annual doses for the ^{234}U results but negligible differences through most of the simulation. Note that FEHM's timestep based particle assignment logic, as used for ^{234}U, assigns a smaller number of particles per timestep during the smaller early timesteps. Results for the Total ^{239}Pu (Figure 7.3.5-13) annual doses also show some differences early on, which are reduced with time and are minimal at the larger annual dose values.

For the Seismic GM Modeling Case analysis, the annual dose plots showed very little difference between 900,000; 750,000; and 500,000 maximum particle simulation results. As can be seen on Figure 7.3.5-14, the ^{237}Np annual dose results show negligible differences for all five realizations. The ^{99}Tc results (Figure 7.3.5-15) showed minor differences. Results for the ^{233}U (Figure 7.3.5-16) annual doses show negligible differences in annual dose between 900,000; 750,000; and 500,000 maximum particle simulation results. Figure 7.3.5-17 shows very minor changes in annual dose contributions from ^{234}U when the maximum particle numbers are changed. Results for the Total ^{239}Pu (Figure 7.3.5-18) annual doses also show only minor differences.

7.3.5.2.3 Comparison of Radionuclide Contributions to Dose Results to Unsaturated Zone Release Results

For the Igneous Intrusion Modeling Case, the annual mass release from the UZ for individual radionuclides were examined and compared to the annual dose results. This analysis was performed to show that expected differences in UZ mass releases associated with the nature of particle tracking in a dual permeability system are not reflected in the annual dose results. For individual realizations, a change in the number of particles representing mass releases will have some effect on the mass releases from the system. This is especially true at times where there are a number of particles representing parts of larger masses released from the EBS that are slowly being released from storage in the rock matrix a few particles at a time. It is also common when particles are being assigned by mass at times when relatively small masses are being released from the EBS. The UZ mass releases represent boundary conditions in the SZ Flow and Transport Submodel. Differences in the smoothness of the mass of the time-dependent boundary conditions are offset by dispersive processes as the mass travels 18 km downgradient.

A comparison of the ^{237}Np releases from the UZ shown on Figure 7.3.5-19 to the annual dose plot for ^{237}Np presented on Figure 7.3.5-9 shows that the differences in the shapes of UZ mass release source terms associated with using 900,000; 750,000; or 500,000 as the maximum number of particles representing a radionuclides mass in the UZ do not matter once the mass has moved 18 km through the SZ. The ^{99}Tc UZ mass release results presented on Figure 7.3.5-20 show large differences at the lower release rates. As previously noted, these differences are associated with the decision to more accurately depict the large, relatively short-term releases from the EBS that control the peak doses at early time. By the time the mass has traveled 18 km, the differences caused by changing the maximum particles allowed has mainly dissipated except at values six orders of magnitude less than the peak values (Figure 7.3.5-10a). UZ mass release

results for ^{233}U (Figure 7.3.5-21), when compared to the annual dose curves for ^{233}U (Figure 7.3.5-11), again show that differences in UZ mass releases associated with using 900,000; 750,000; or 500,000 as the maximum number of particles representing a radionuclides mass in the UZ are small enough that negligible differences in annual doses occur. Comparisons of Figure 7.3.5-12 with Figure 7.3.5-22 for ^{234}U and Figure 7.3.5-13 with Figure 7.3.5-23 for Total ^{239}Pu show similar dissipation of source term differences with downgradient transport in the SZ.

7.3.5.3 Conclusions

This stability test indicates that the use of 900,000 particles in the TSPA-LA Model analyses provides a stable result with respect to the number of particles used in all three of the modeling cases (Drip Shield EF Modeling Case, Igneous Intrusion Modeling Case, and Seismic GM Modeling Case). A reduction of the maximum number of particles to 750,000 or 500,000 is shown to have little effect on the annual dose results. Likewise, peak dose results showed that the reductions in the maximum number of particles used to represent the EBS releases had little influence on the TSPA-LA Model results. A more detailed comparison of annual doses for representative radionuclide species and UZ mass flux releases showed that slight differences in particle tracking results associated with the reductions to the number of particles representing source releases (and ingrowth contributions) represent differences in the refinement of source terms to the SZ. This difference in the source terms is dampened by the time mass has been transported 18 km.

Table 7.3.5-1. Peak Dose Values for Drip Shield Early Failure, Igneous, and Seismic Ground Motion Modeling Cases Evaluated for Particle Stability

		Peak Dose in mrems for Stability Based on the Maximum Number of Particles Per Species		
	Realization	**900,000**	**750,000**	**500,000**
Igneous – 1 Million years	1/1	364.8	357.7	358.7
	11/2	320.7	328.0	317.1
	21/3	671.3	668.7	656.6
	31/4	552.1	534.9	535.6
	41/5	1,310	1,303	1,308
Drip Shield Early Failure – 10,000 years	266/27	0.04533	0.04437	0.04533
	686/69	0.1030	0.1052	0.1055
	756/76	0.03040	0.02960	0.03052
	956/96	0.07744	0.07434	0.07509
	1,166/117	0.009840	0.009535	0.009815
Seismic Ground Motion – 10,000 years	2/1	0.1749	0.1752	0.1726
	32/2	0.9198	0.9236	0.9032
	62/3	1.473	1.476	1.478
	92/4	0.5553	0.5595	0.5558
	122/5	1.351	1.355	1.346

From output DTN: MO0709TSPAPLOT.000 [DIRS 183010] Files:
LA_v5.000_ED_003000_007_Total_Dose_Wt_300rlza.txt
From output DTN: MO0709TSPAVALI.000 [DIRS 182985] Files:
LA_v5.000_ED_003000_018_Total_Dose_Wt.txt
LA_v5.000_ED_003000_019_Total_Dose_Wt.txt
LA_v5.000_IG_003000_029_Total_Dose_UnWt.txt
LA_v5.000_IG_003000_030_Total_Dose_UnWt.txt
LA_v5.000_SM_009000_006_Total_Dose_UnWt.txt
LA_v5.000_SM_009000_007_Total_Dose_UnWt.txt
From output DTN: MO0709TSPAREGS.000 [DIRS 182976] Files:
LA_v5.000_IG_003000_017_Total_Dose_UnWt.txt
LA_v5.000_SM_009000_005_Total_Dose_UnWt.txt

INTENTIONALLY LEFT BLANK

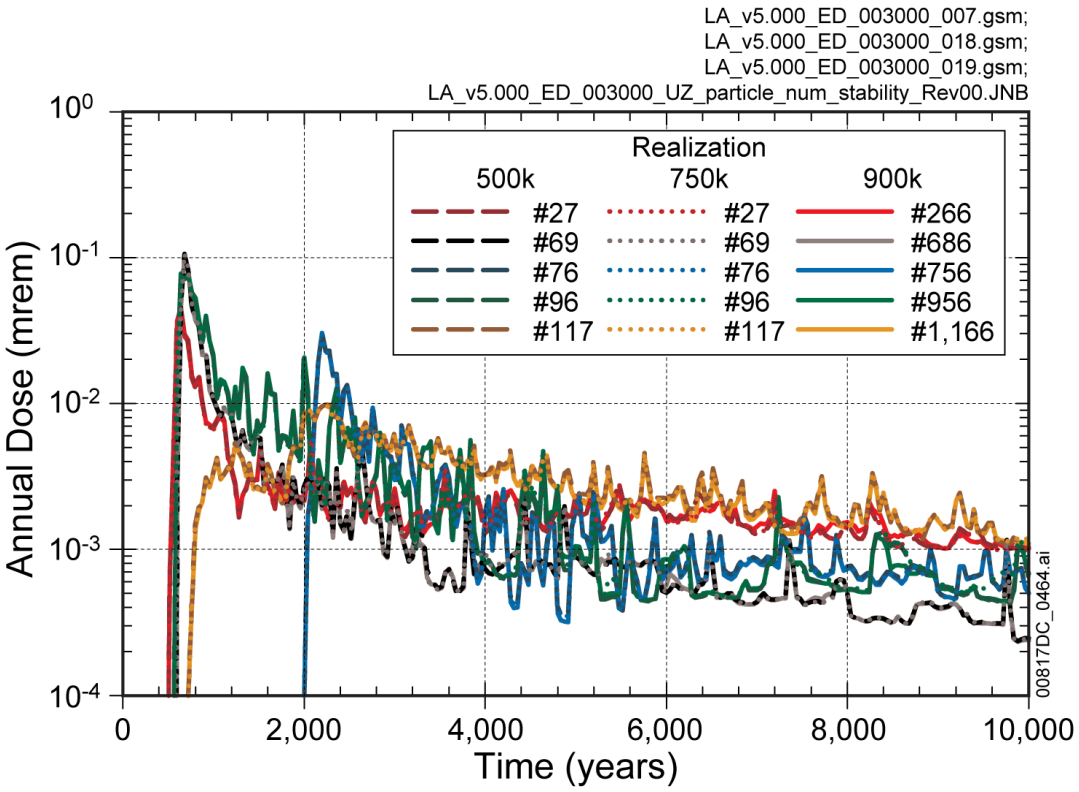

Source: Output DTNs: MO0708TSPAVALI.000 [DIRS 182985]; and MO0709TSPAREGS.000 [DIRS 182976].

Figure 7.3.5-1. Annual Dose for the Drip Shield Early Failure Modeling Case Simulations using a Maximum of 500,000; 750,000; and 900,000 Particles in the Unsaturated Zone Transport Submodel

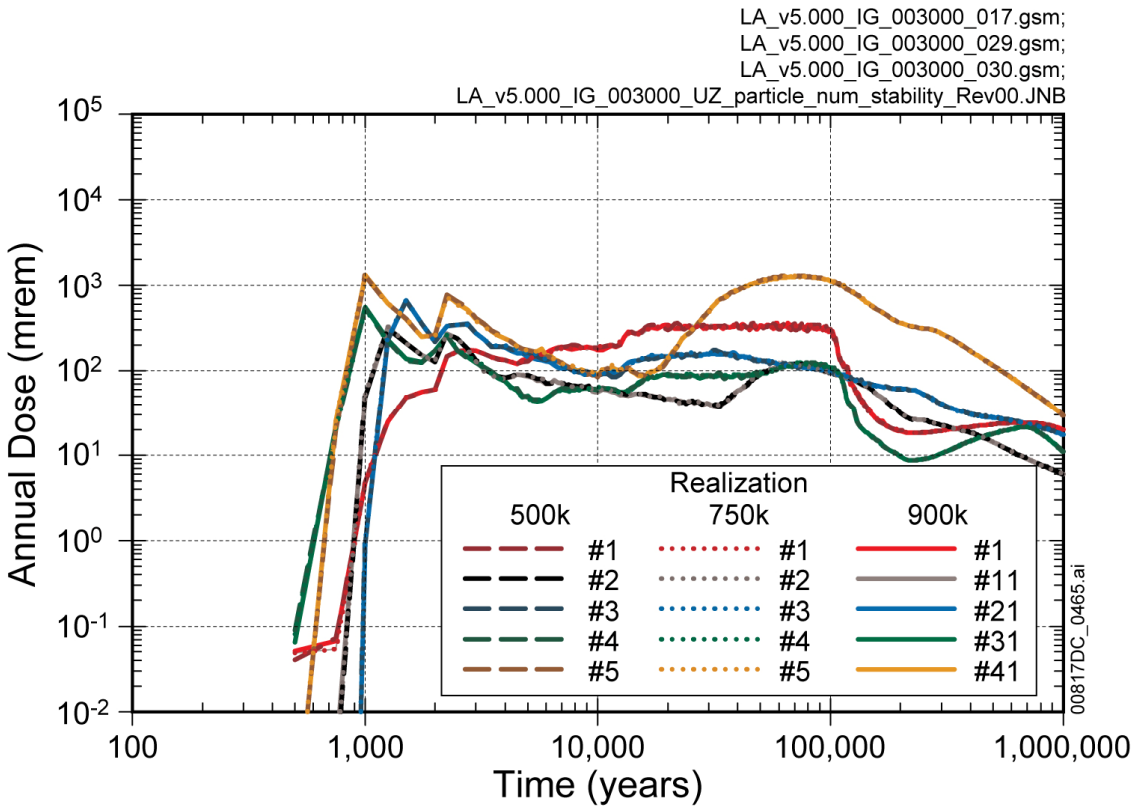

Source: Output DTNs: MO0708TSPAVALI.000 [DIRS 182985]; and MO0709TSPAREGS.000 [DIRS 182976].

Figure 7.3.5-2. Annual Dose for the Igneous Intrusion Modeling Case Simulations Using a Maximum of 500,000; 750,000; and 900,000 Particles in the Unsaturated Zone Transport Submodel

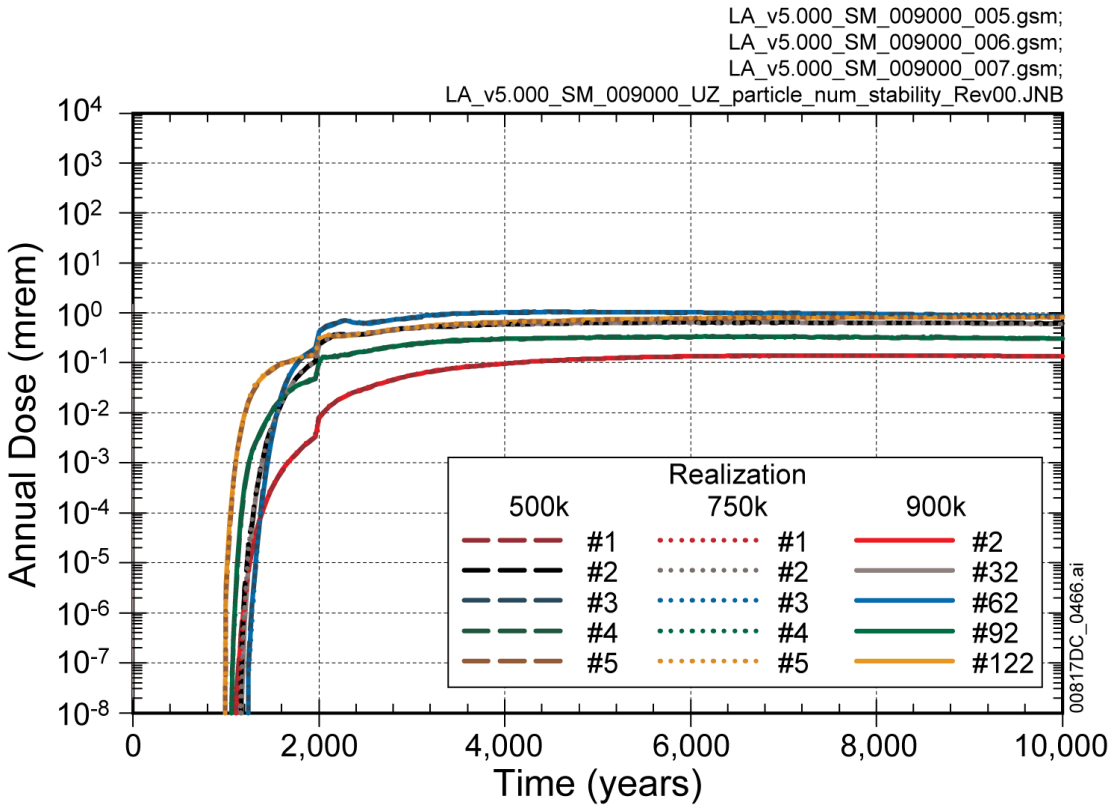

Source: Output DTNs: MO0708TSPAVALI.000 [DIRS 182985]; and MO0709TSPAREGS.000 [DIRS 182976].

Figure 7.3.5-3. Annual Dose for the Seismic Ground Motion Modeling Case Simulations Using a Maximum of 500,000; 750,000; and 900,000 Particles in the Unsaturated Zone Transport Submodel

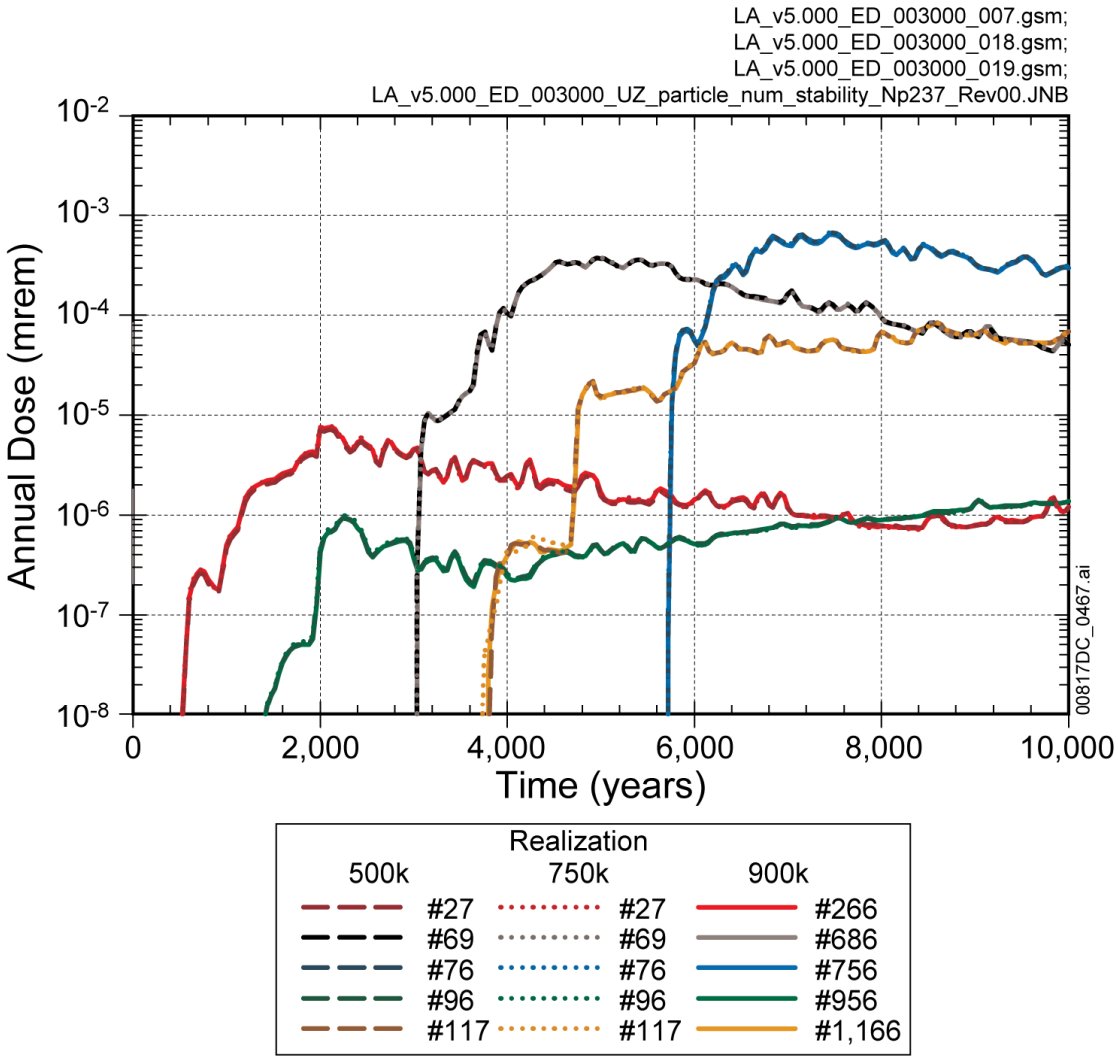

Source: Output DTNs: MO0708TSPAVALI.000 [DIRS 182985]; and MO0709TSPAREGS.000 [DIRS 182976].

Figure 7.3.5-4. Annual Dose Contribution from ^{237}Np for the Drip Shield Early Failure Modeling Case Simulations Using a Maximum of 500,000; 750,000; and 900,000 Particles in the Unsaturated Zone Transport Submodel

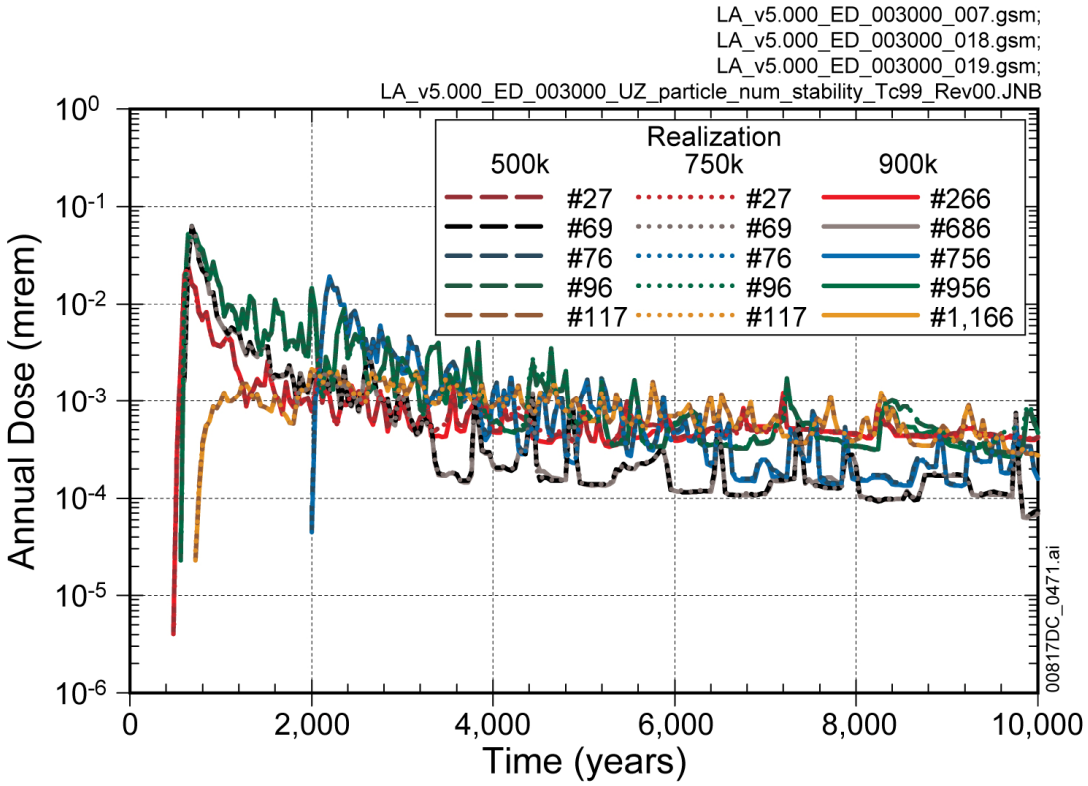

Source: Output DTNs: MO0708TSPAVALI.000 [DIRS 182985], and MO0709TSPAREGS.000 [DIRS 182976].

Figure 7.3.5-5. Annual Dose Contribution from ^{99}Tc for the Drip Shield Early Failure Modeling Case Simulations Using a Maximum of 500,000; 750,000; and 900,000 Particles in the Unsaturated Zone Transport Submodel

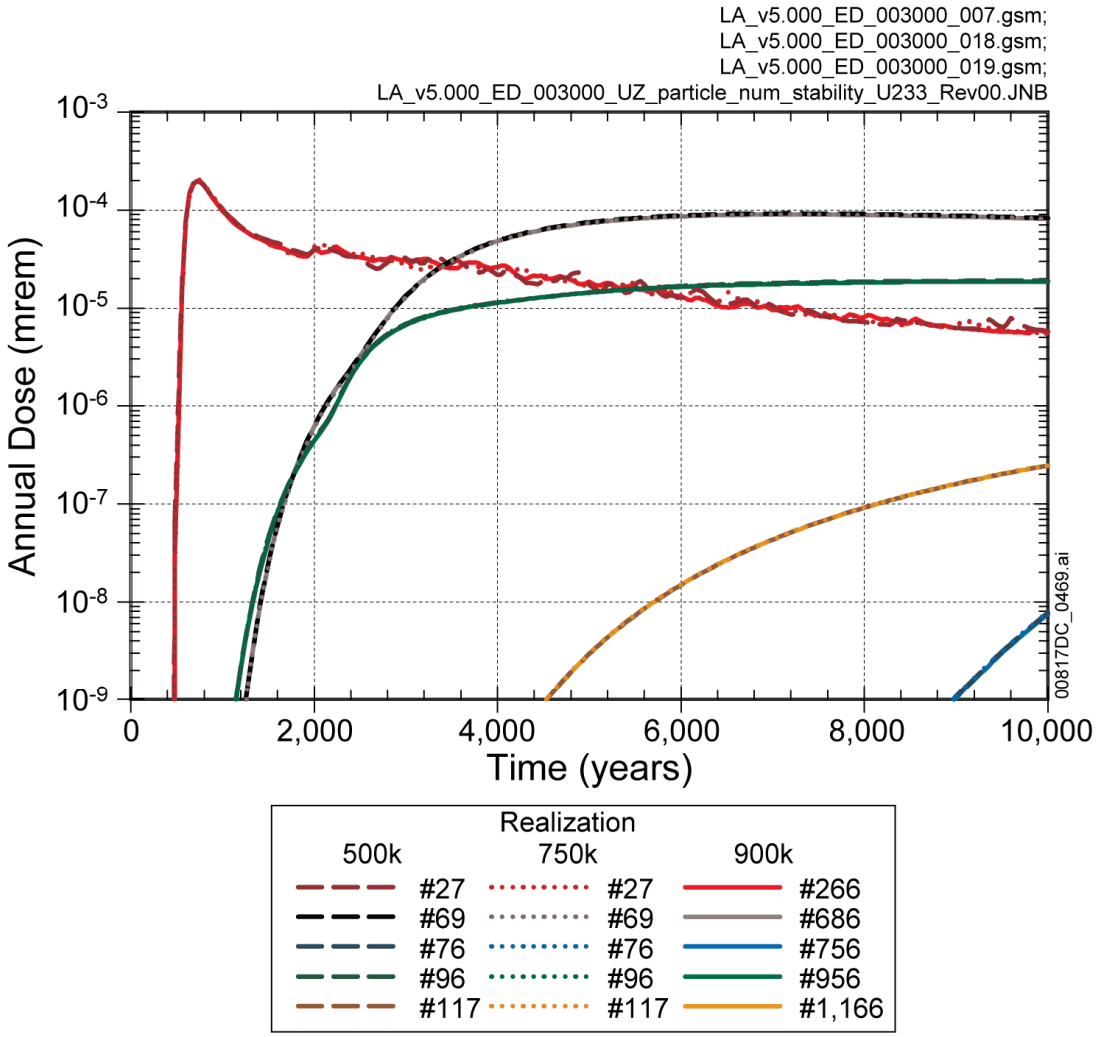

Source: Output DTNs: MO0708TSPAVALI.000 [DIRS 182985]; and MO0709TSPAREGS.000 [DIRS 182976].

Figure 7.3.5-6. Annual Dose Contribution from ^{233}U for the Drip Shield Early Failure Modeling Case Simulations Using a Maximum of 500,000; 750,000; and 900,000 Particles in the Unsaturated Zone Transport Submodel

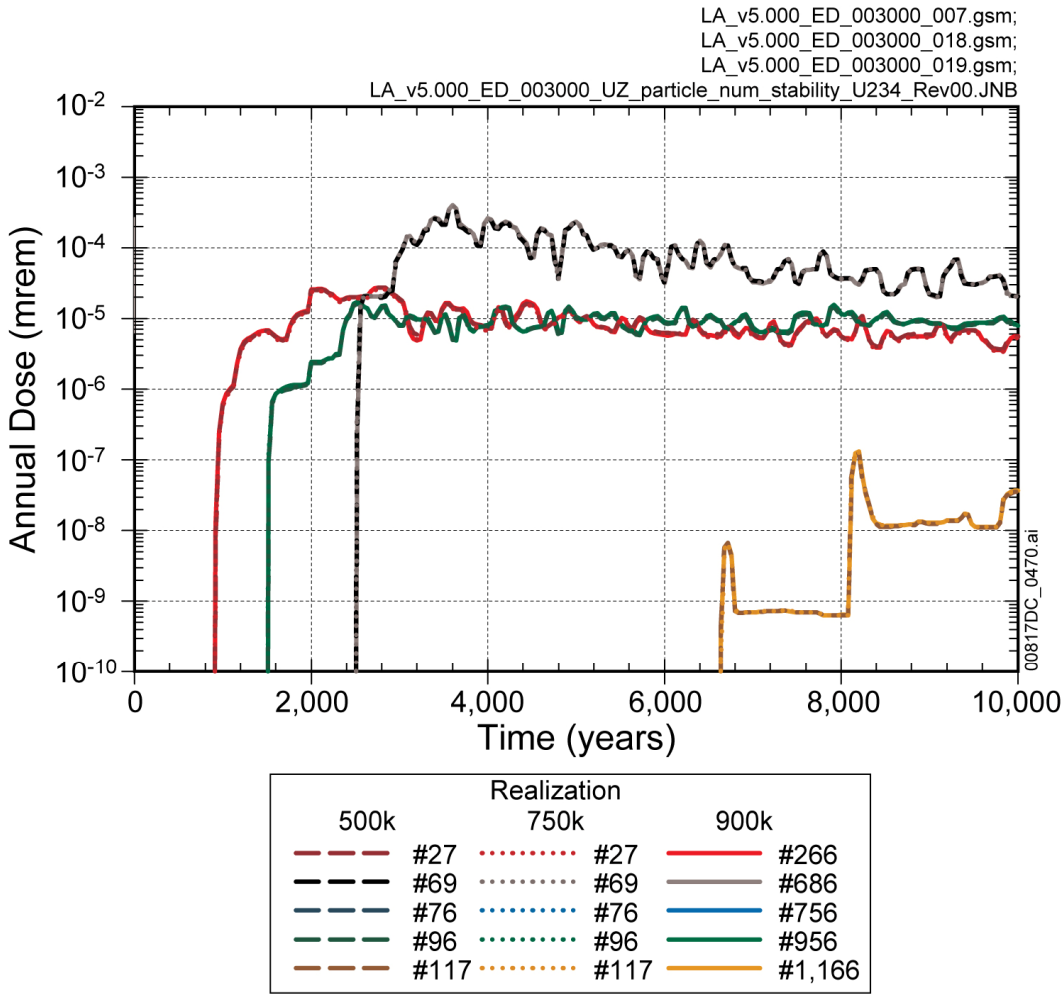

Source: Output DTNs: MO0708TSPAVALI.000 [DIRS 182985], MO0709TSPAREGS.000 [DIRS 182976].

Figure 7.3.5-7. Annual Dose Contribution from ^{234}U for the Drip Shield Early Failure Modeling Case Simulations Using a Maximum of 500,000; 750,000; and 900,000 Particles in the Unsaturated Zone Transport Submodel

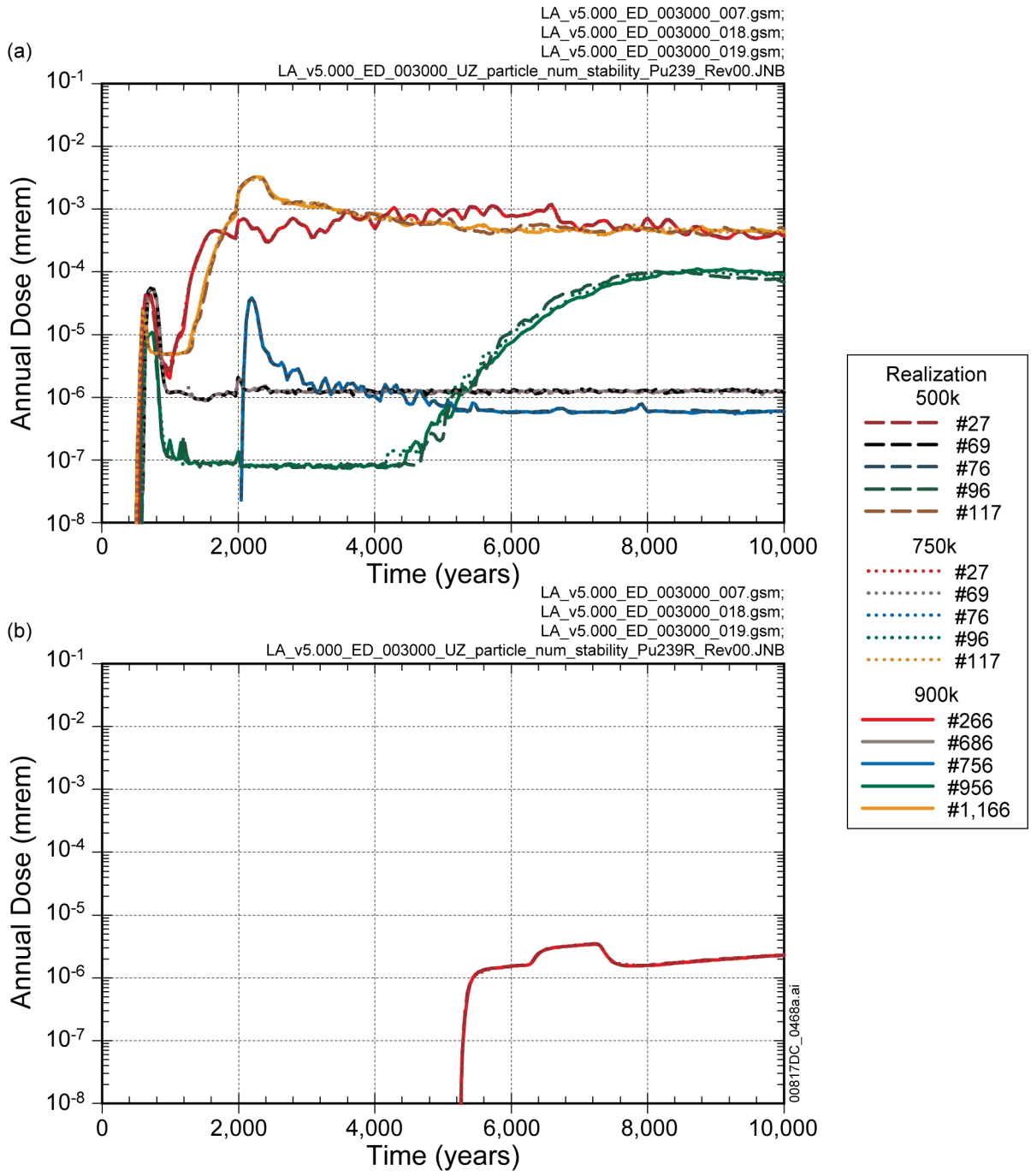

Source: Output DTNs: MO0708TSPAVALI.000 [DIRS 182985], MO0709TSPAREGS.000 [DIRS 182976].

Figure 7.3.5-8. Annual Dose Contribution from (a) ^{239}Pu Total, (b) ^{239}Pu on Reversible Colloids, (c) ^{239}Pu on Retarded Irreversible Colloids, and (d) ^{239}Pu on Unretarded Irreversible Colloids for the Drip Shield Early Failure Modeling Case Simulations Using a Maximum of 500,000, 750,000; and 900,000 Particles in the Unsaturated Zone Transport Submodel

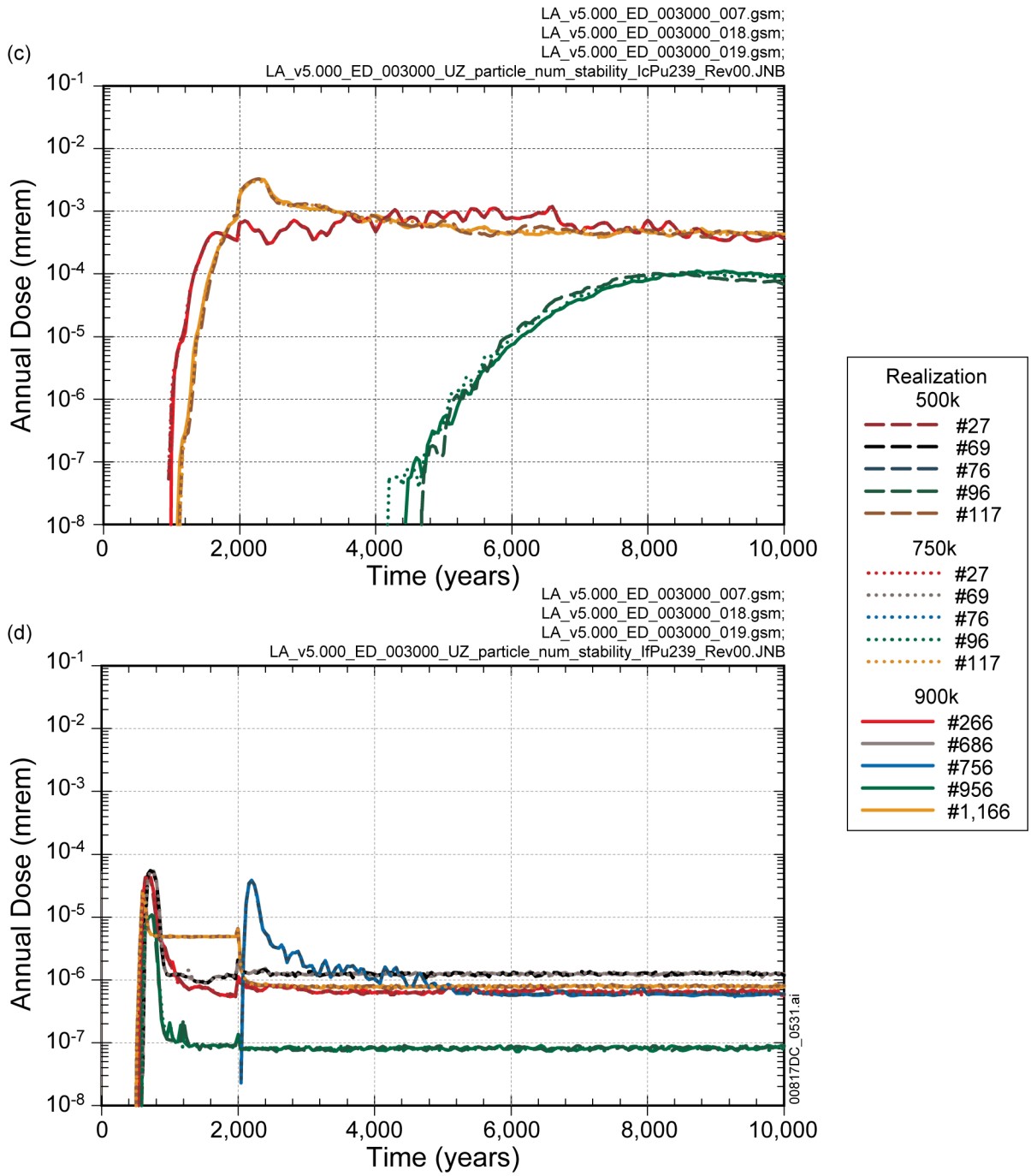

Source: Output DTNs: MO0708TSPAVALI.000 [DIRS 182985], and MO0709TSPAREGS.000 [DIRS 182976].

Figure 7.3.5-8. Annual Dose Contribution from (a) ^{239}Pu Total, (b) ^{239}Pu on Reversible Colloids, (c) ^{239}Pu on Retarded Irreversible Colloids, and (d) ^{239}Pu on Unretarded Irreversible Colloids for the Drip Shield Early Failure Modeling Case Simulations Using a Maximum of 500,000; 750,000; and 900,000 Particles in the Unsaturated Zone Transport Submodel (Continued)

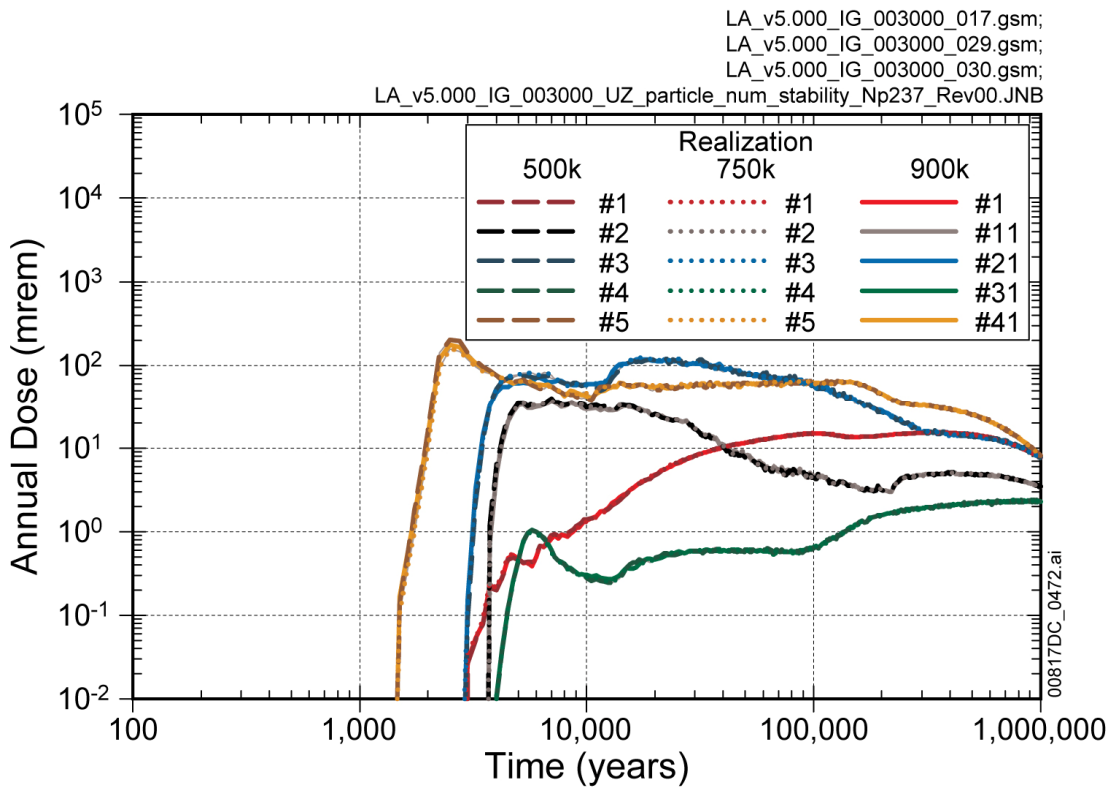

Source: Output DTNs: MO0708TSPAVALI.000 [DIRS 182985]; and MO0709TSPAREGS.000 [DIRS 182976].

Figure 7.3.5-9. Annual Dose Contribution from ^{237}Np for the Igneous Intrusion Modeling Case Simulations Using a Maximum of 500,000; 750,000; and 900,000 Particles in the Unsaturated Zone Transport Submodel

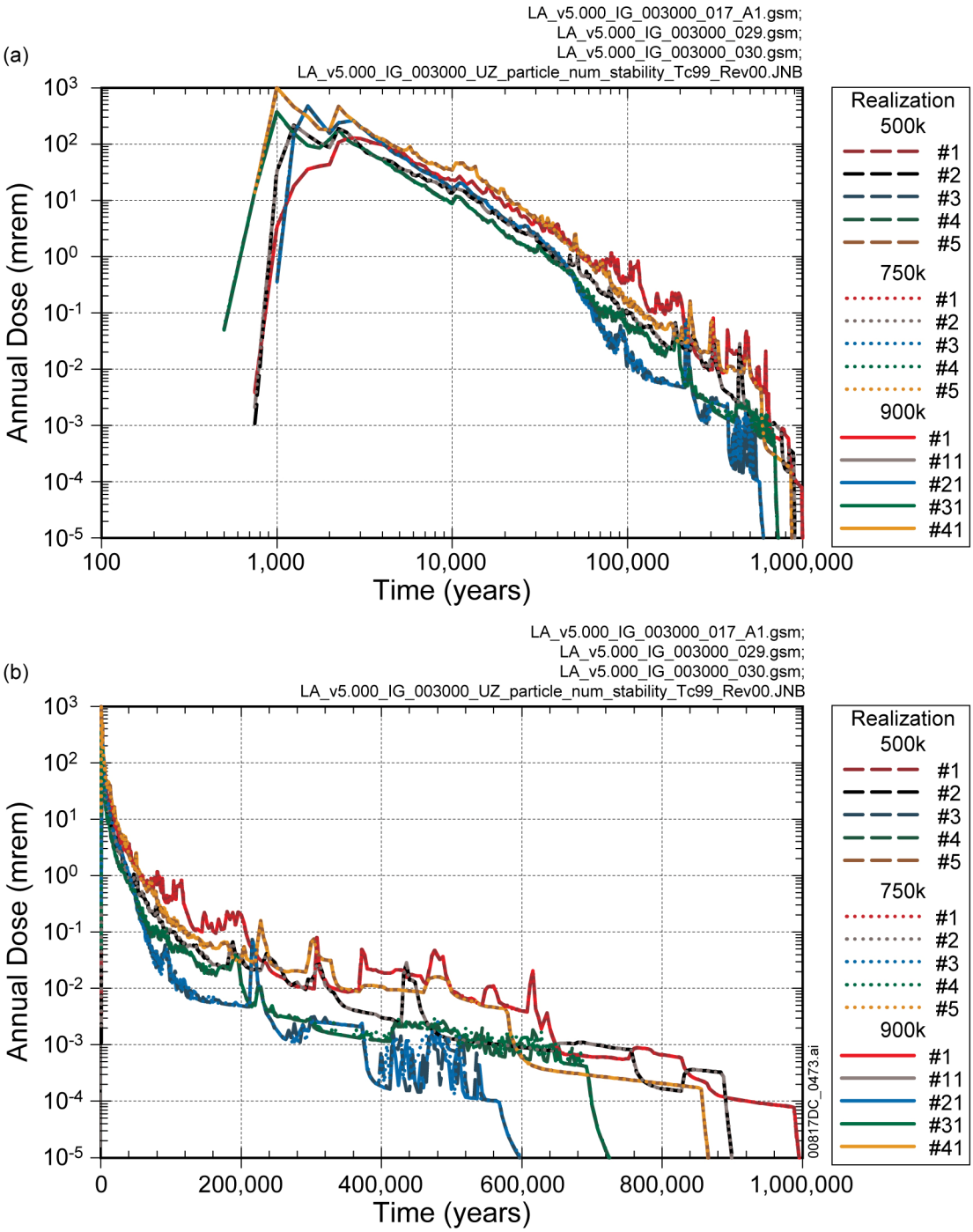

Source: Output DTNs: MO0708TSPAVALI.000 [DIRS 182985]; MO0709TSPAREGS.000 [DIRS 182976].

Figure 7.3.5-10. Annual Dose Contribution from ^{99}Tc for the Igneous Intrusion Modeling Case Simulations Using a Maximum of 500,000; 750,000; and 900,000 Particles in the Unsaturated Zone Transport Submodel

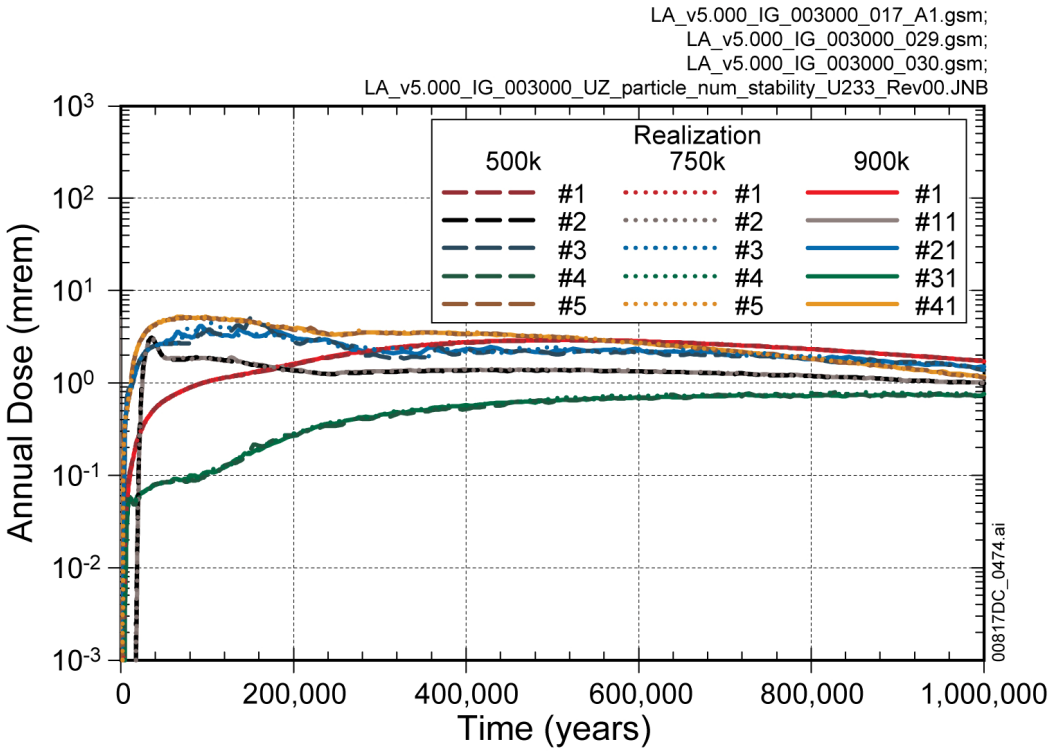

Source: Output DTNs: MO0708TSPAVALI.000 [DIRS 182985], MO0709TSPAREGS.000 [DIRS 182976].

Figure 7.3.5-11. Annual Dose Contribution from ^{233}U for the Igneous Intrusion Modeling Case Simulations Using a Maximum of 500,000; 750,000; and 900,000 Particles in the Unsaturated Zone Transport Submodel

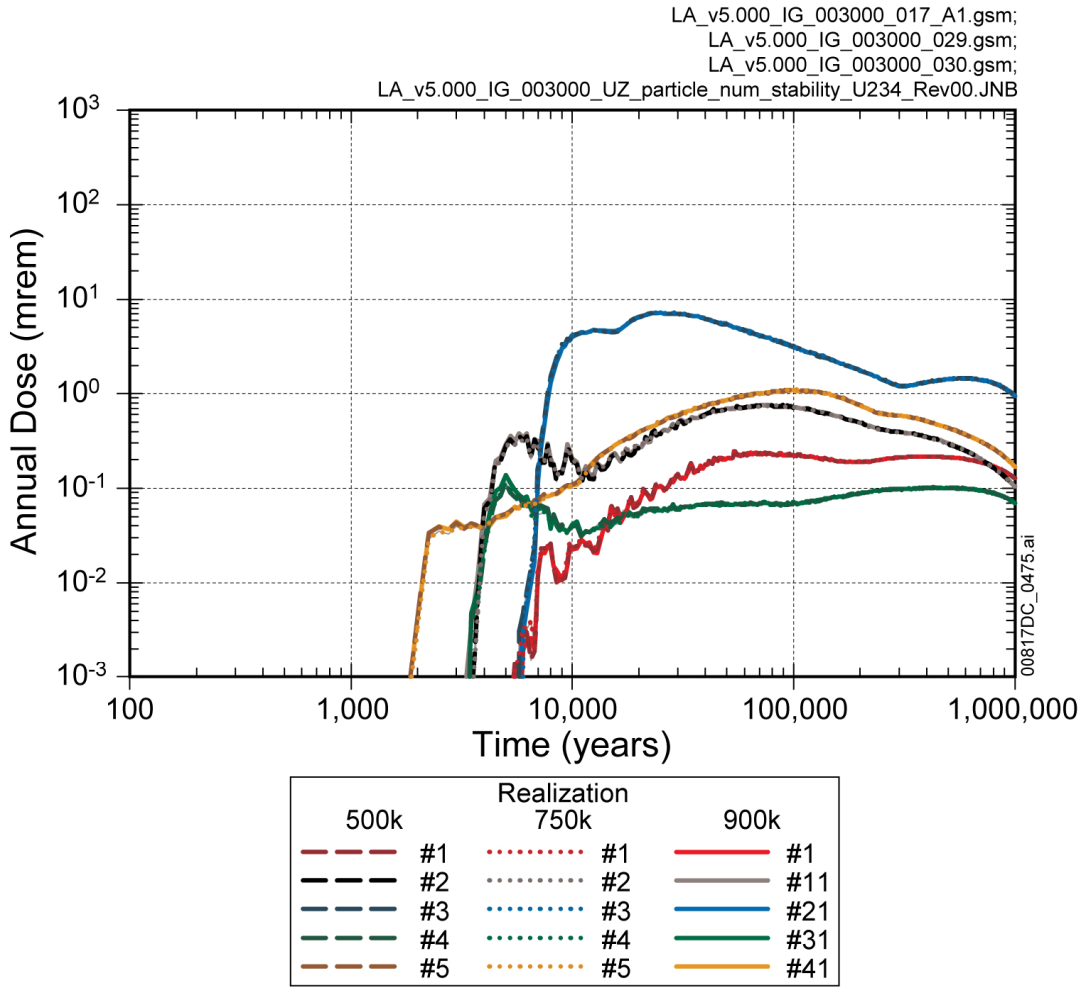

Source: Output DTNs: MO0708TSPAVALI.000 [DIRS 182985]; and MO0709TSPAREGS.000 [DIRS 182976].

Figure 7.3.5-12. Annual Dose Contribution from ^{234}U for the Igneous Intrusion Modeling Case Simulations Using a Maximum of 500,000; 750,000; and 900,000 Particles in the Unsaturated Zone Transport Submodel

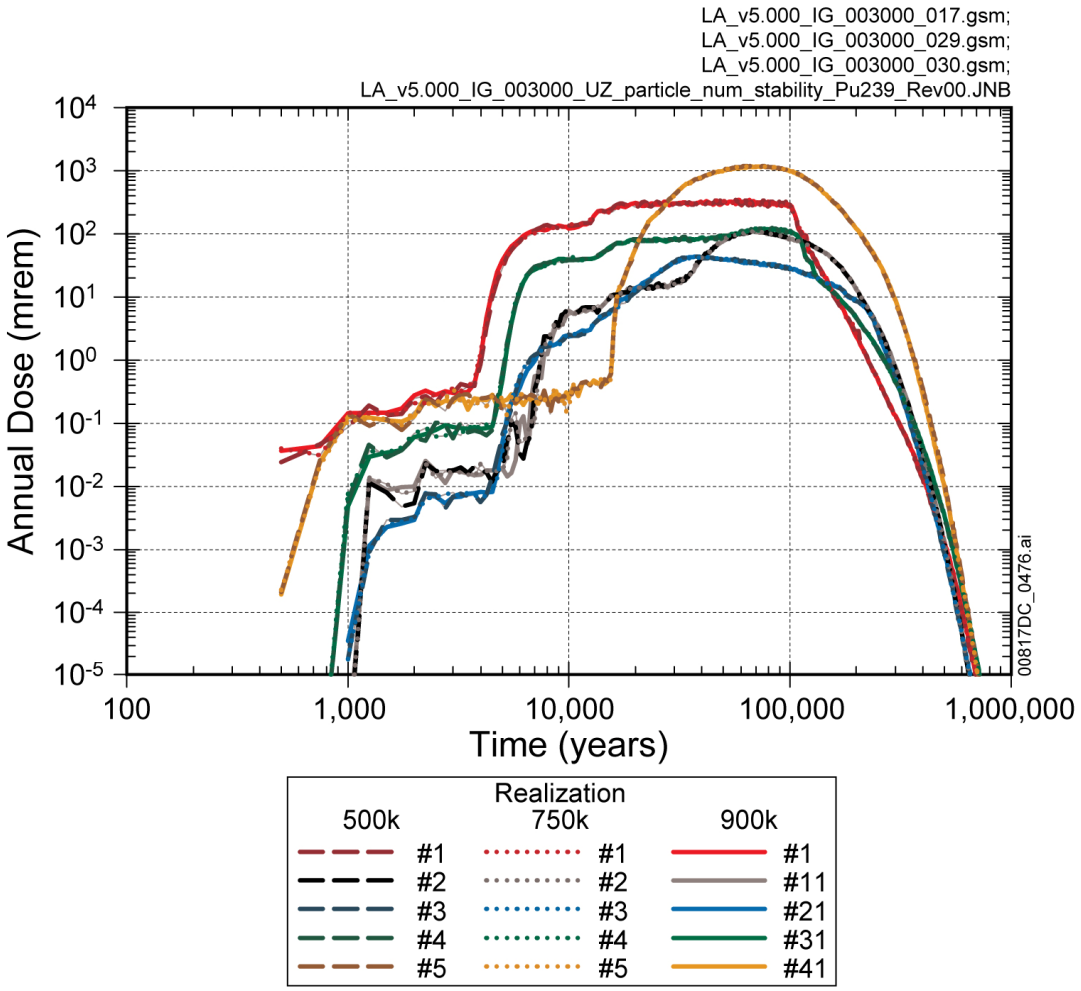

Source: Output DTNs: MO0708TSPAVALI.000 [DIRS 182985]; MO0709TSPAREGS.000 [DIRS 182976].

Figure 7.3.5-13. Annual Dose Contribution from ^{239}Pu for the Igneous Intrusion Modeling Case Simulations Using a Maximum of 500,000; 750,000; and 900,000 Particles in the Unsaturated Zone Transport Submodel

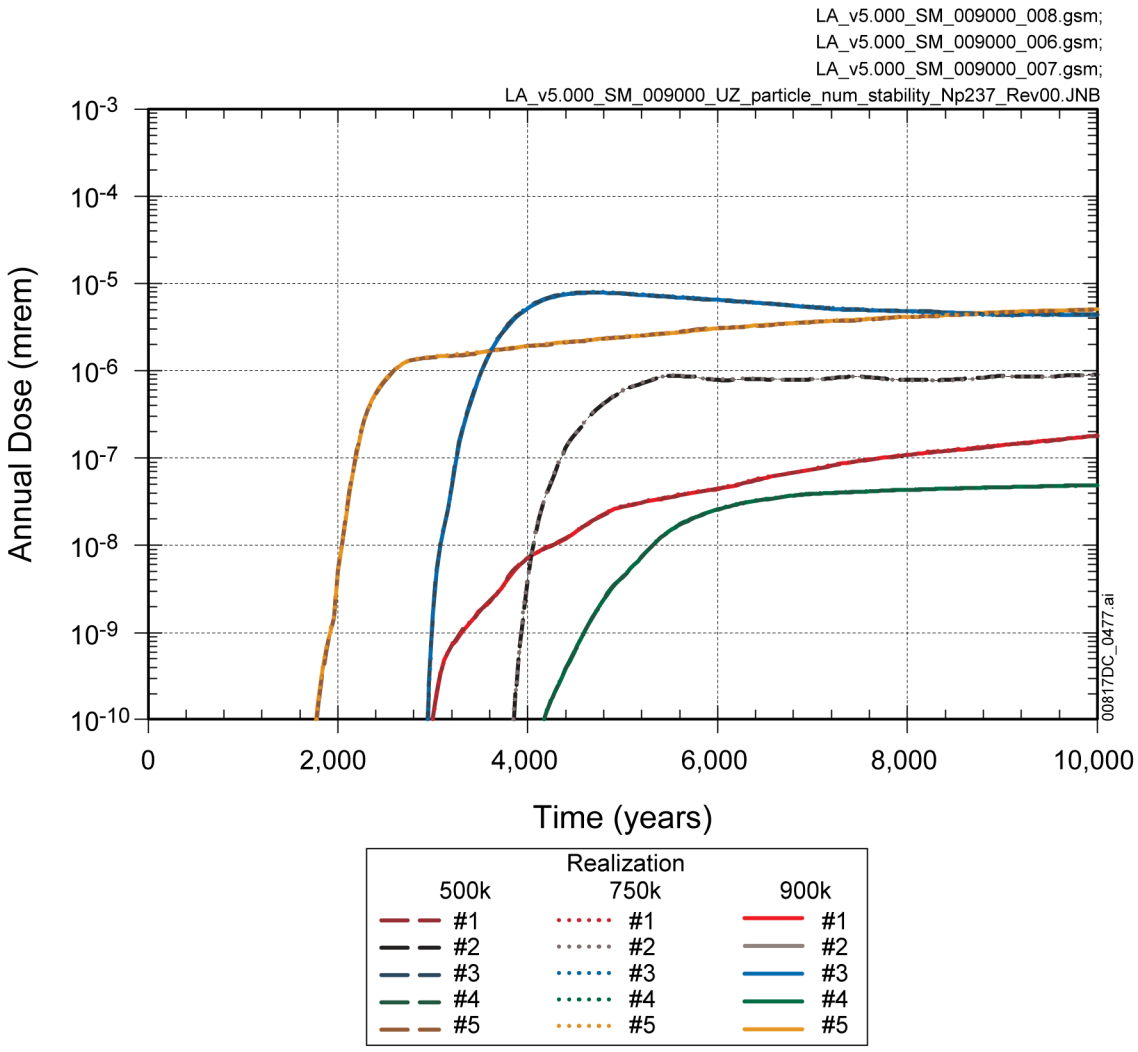

Source: Output DTNs: MO0708TSPAVALI.000 [DIRS 182985]; and MO0709TSPASENS.000 [DIRS 182982].

Figure 7.3.5-14. Annual Dose Contribution from ^{237}Np for the Seismic Ground Motion Modeling Case Simulations Using a Maximum of 500,000; 750,000; and 900,000 Particles in the Unsaturated Zone Transport Submodel

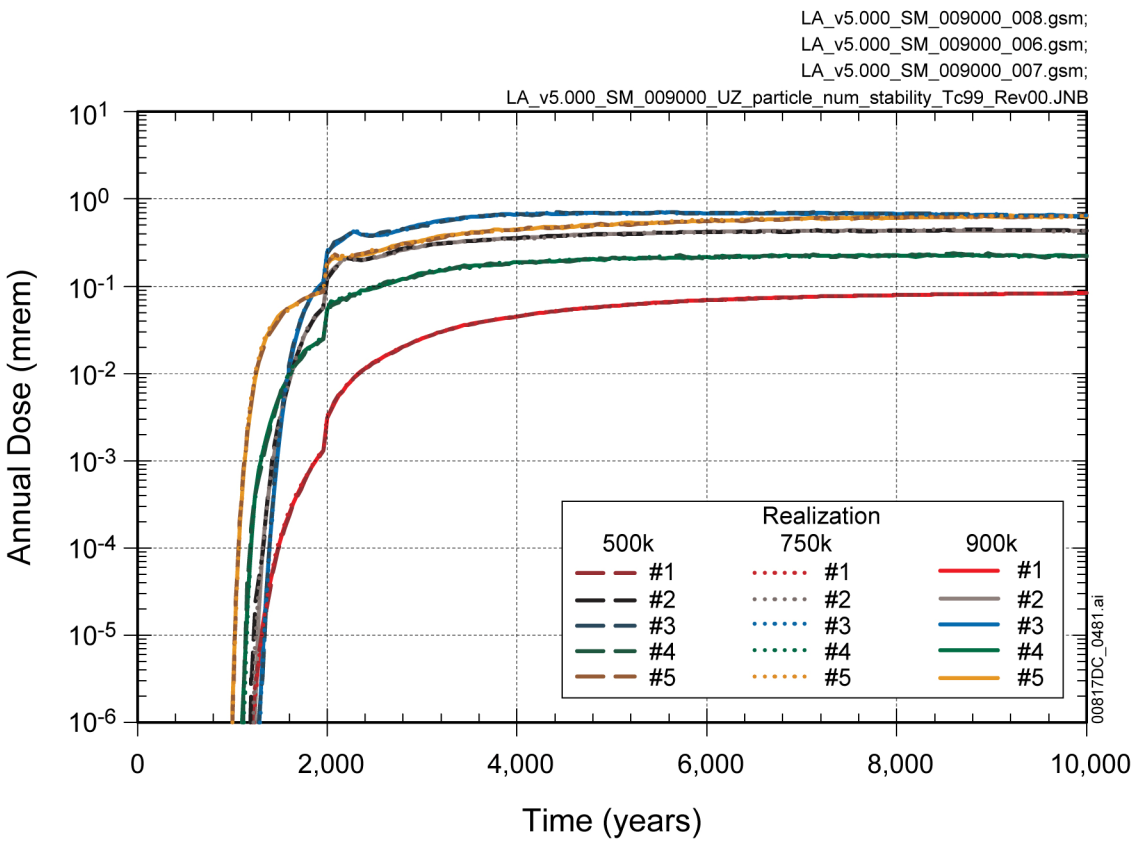

Source: Output DTNs: MO0708TSPAVALI.000 [DIRS 182985]; and MO0709TSPASENS.000 [DIRS 182982].

Figure 7.3.5-15. Annual Dose Contribution from ^{99}Tc for the Seismic Ground Motion Modeling Case Simulations Using a Maximum of 500,000; 750,000; and 900,000 Particles in the Unsaturated Zone Transport Submodel

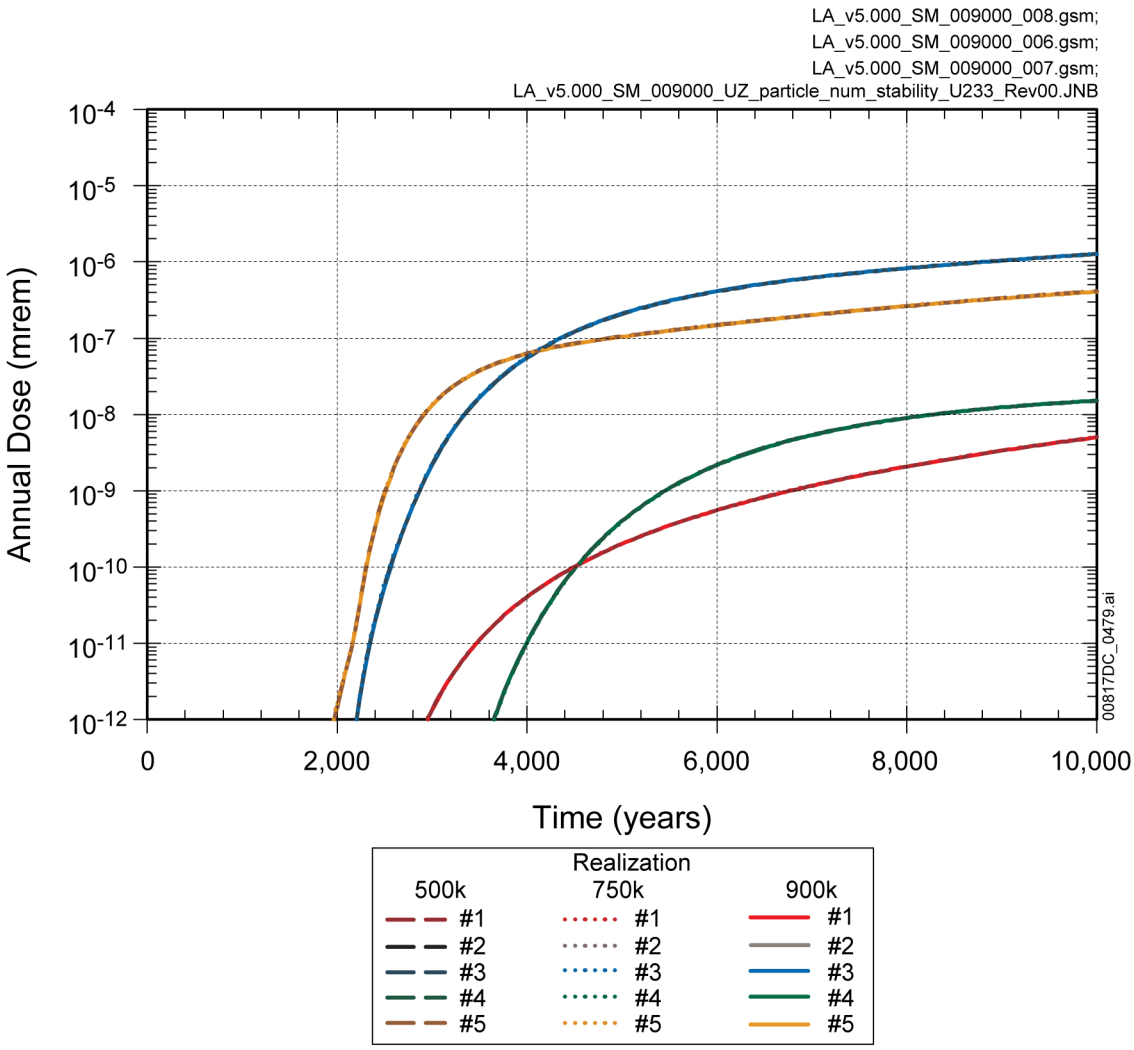

Source: Output DTNs: MO0708TSPAVALI.000 [DIRS 182985]; and MO0709TSPASENS.000 [DIRS 182982].

Figure 7.3.5-16. Annual Dose Contribution from ^{233}U for the Seismic Ground Motion Modeling Case Simulations Using a Maximum of 500,000; 750,000; and 900,000 Particles in the Unsaturated Zone Transport Submodel

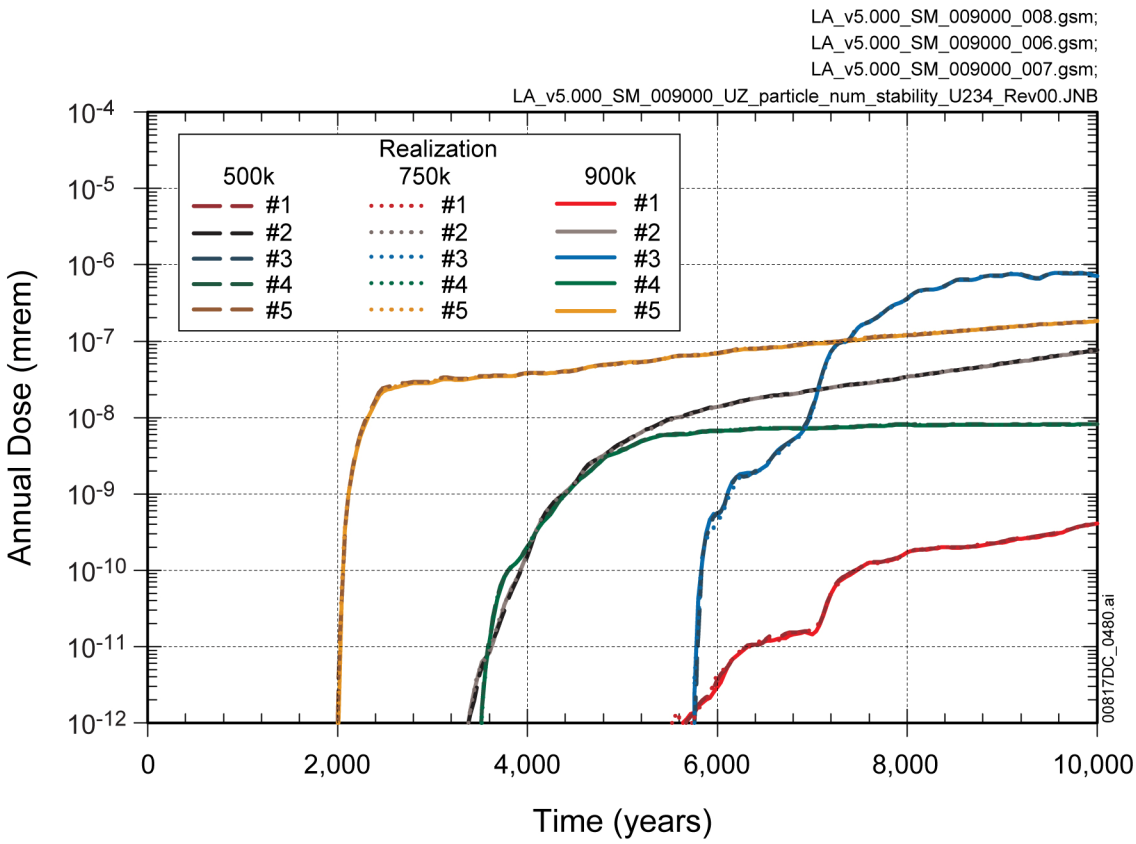

Source: Output DTNs: MO0708TSPAVALI.000 [DIRS 182985]; and MO0709TSPASENS.000 [DIRS 182982].

Figure 7.3.5-17. Annual Dose Contribution from ^{234}U in for the Seismic Ground Motion Modeling Case Simulations Using a Maximum of 500,000; 750,000; and 900,000 Particles in the Unsaturated Zone Transport Submodel

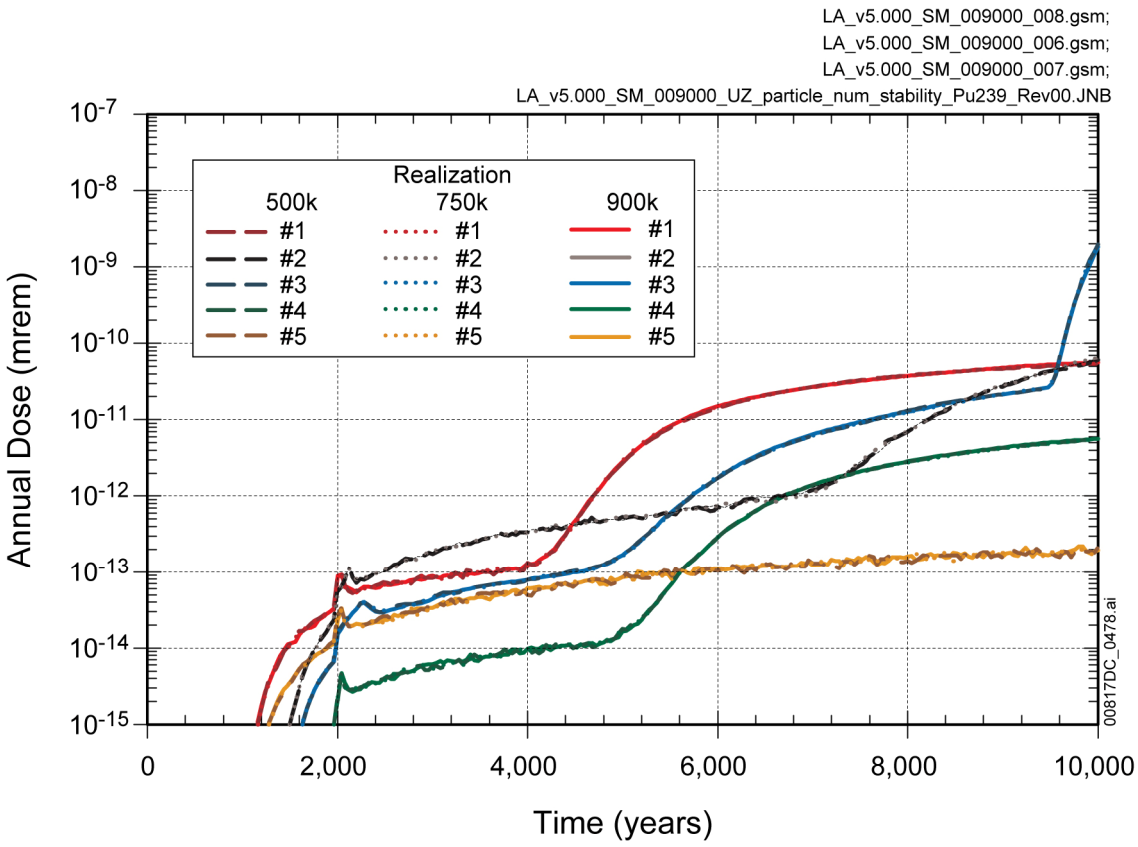

Source: Output DTNs: MO0708TSPAVALI.000 [DIRS 182985]; and MO0709TSPASENS.000 [DIRS 182982].

Figure 7.3.5-18. Annual Dose Contribution from ^{239}Pu for the Seismic Ground Motion Modeling Case Simulations Using a Maximum of 500,000; 750,000; and 900,000 Particles in the Unsaturated Zone Transport Submodel

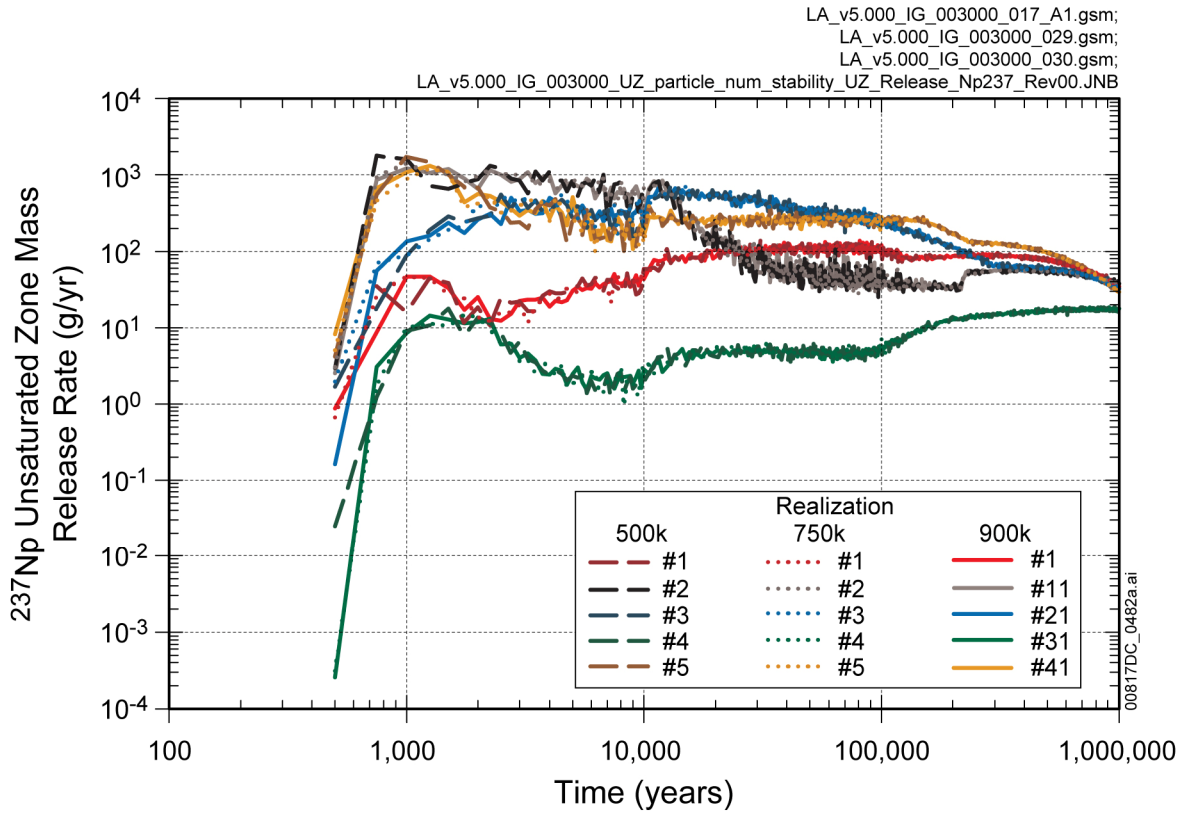

Source: Output DTNs: MO0708TSPAVALI.000 [DIRS 182985]; and MO0709TSPAREGS.000 [DIRS 182976].

Figure 7.3.5-19. Annual Unsaturated Zone Mass Release of ^{237}Np for the Igneous Intrusion Modeling Case Simulations Using a Maximum of 500,000; 750,000; and 900,000 Particles in the Unsaturated Zone Transport Submodel

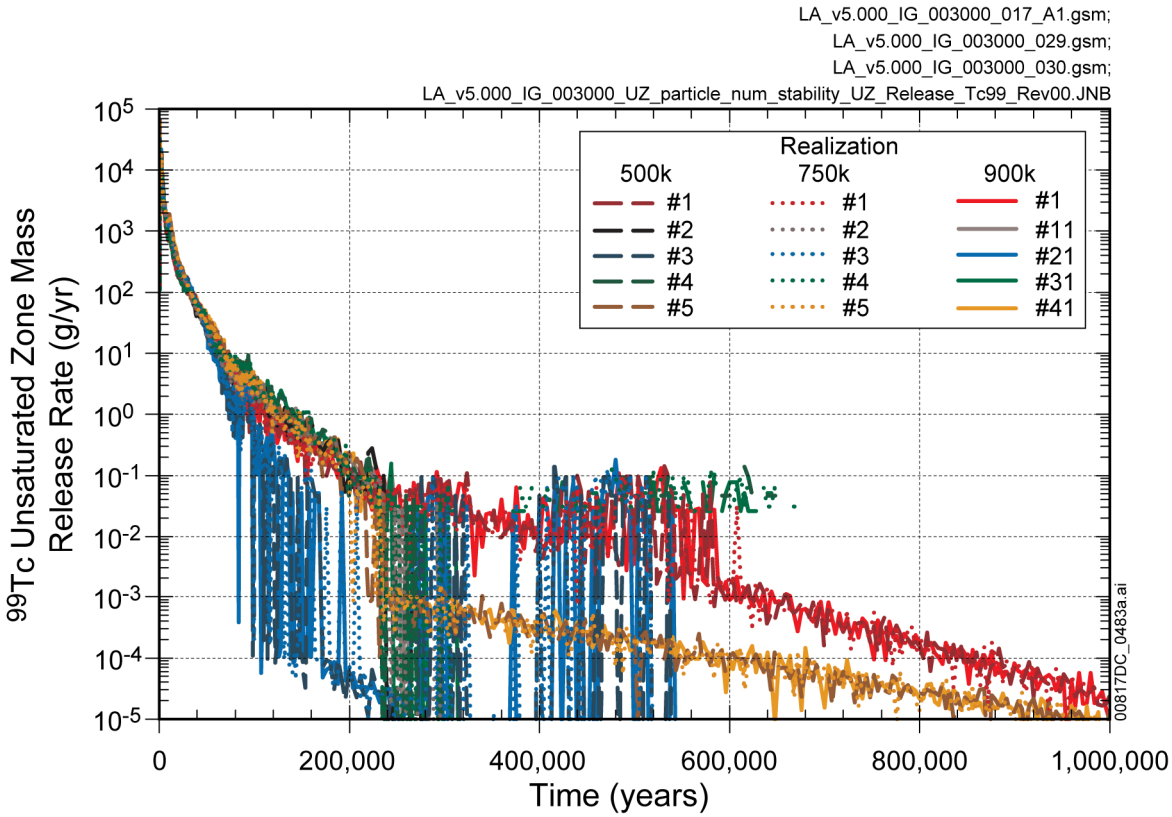

Source: Output DTNs: MO0708TSPAVALI.000 [DIRS 182985]; and MO0709TSPAREGS.000 [DIRS 182976].

Figure 7.3.5-20. Annual Unsaturated Zone Mass Release of ^{99}Tc for the Igneous Intrusion Modeling Case Simulations Using a Maximum of 500,000; 750,000; and 900,000 Particles in the Unsaturated Zone Transport Submodel

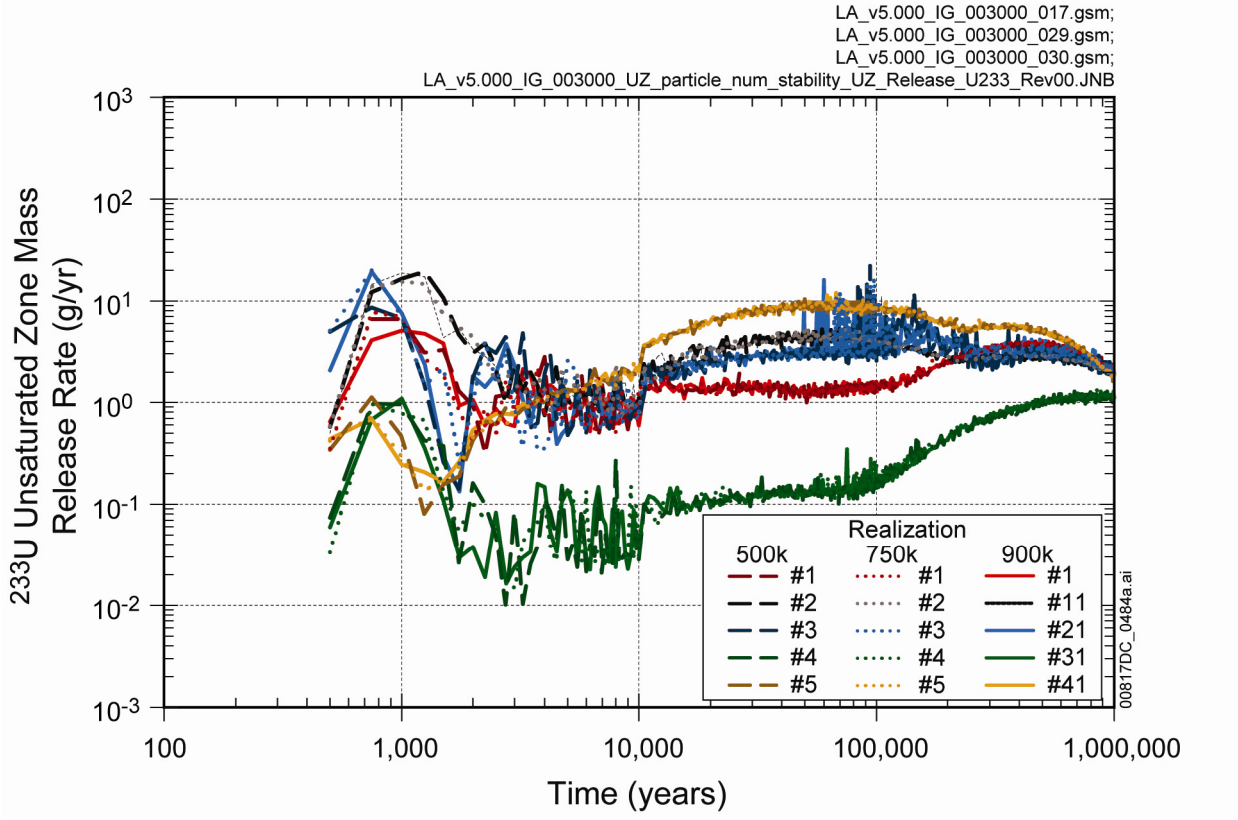

Source: Output DTNs: MO0708TSPAVALI.000 [DIRS 182985]; and MO0709TSPAREGS.000 [DIRS 182976].

Figure 7.3.5-21. Annual Unsaturated Zone Mass Release of ^{233}U for the Igneous Intrusion Modeling Case Simulations Using a Maximum of 500,000; 750,000; and 900,000 Particles in the Unsaturated Zone Transport Submodel

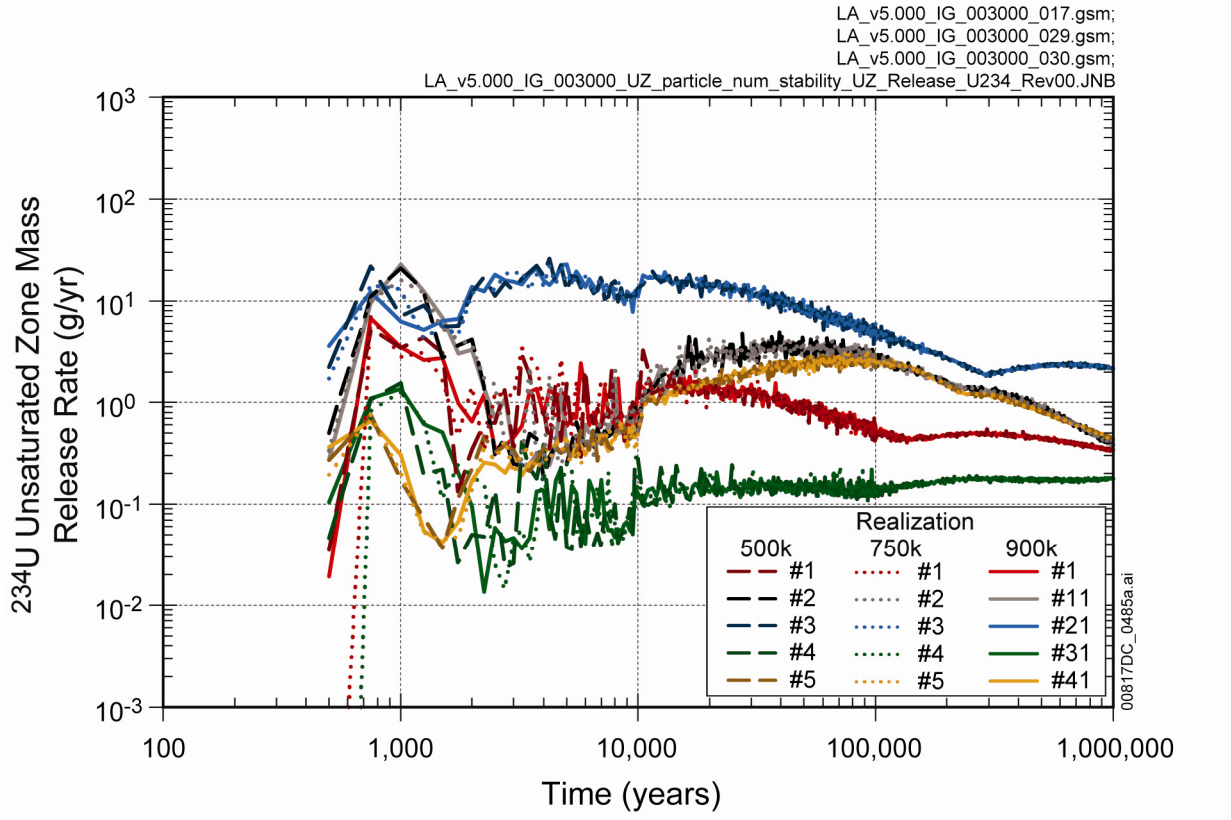

Source: Output DTNs: MO0708TSPAVALI.000 [DIRS 182985]; and MO0709TSPAREGS.000 [DIRS 182976].

Figure 7.3.5-22. Annual Unsaturated Zone Mass Release of ^{234}U for the Igneous Intrusion Modeling Case Simulations Using a Maximum of 500,000; 750,000; and 900,000 Particles in the Unsaturated Zone Transport Submodel

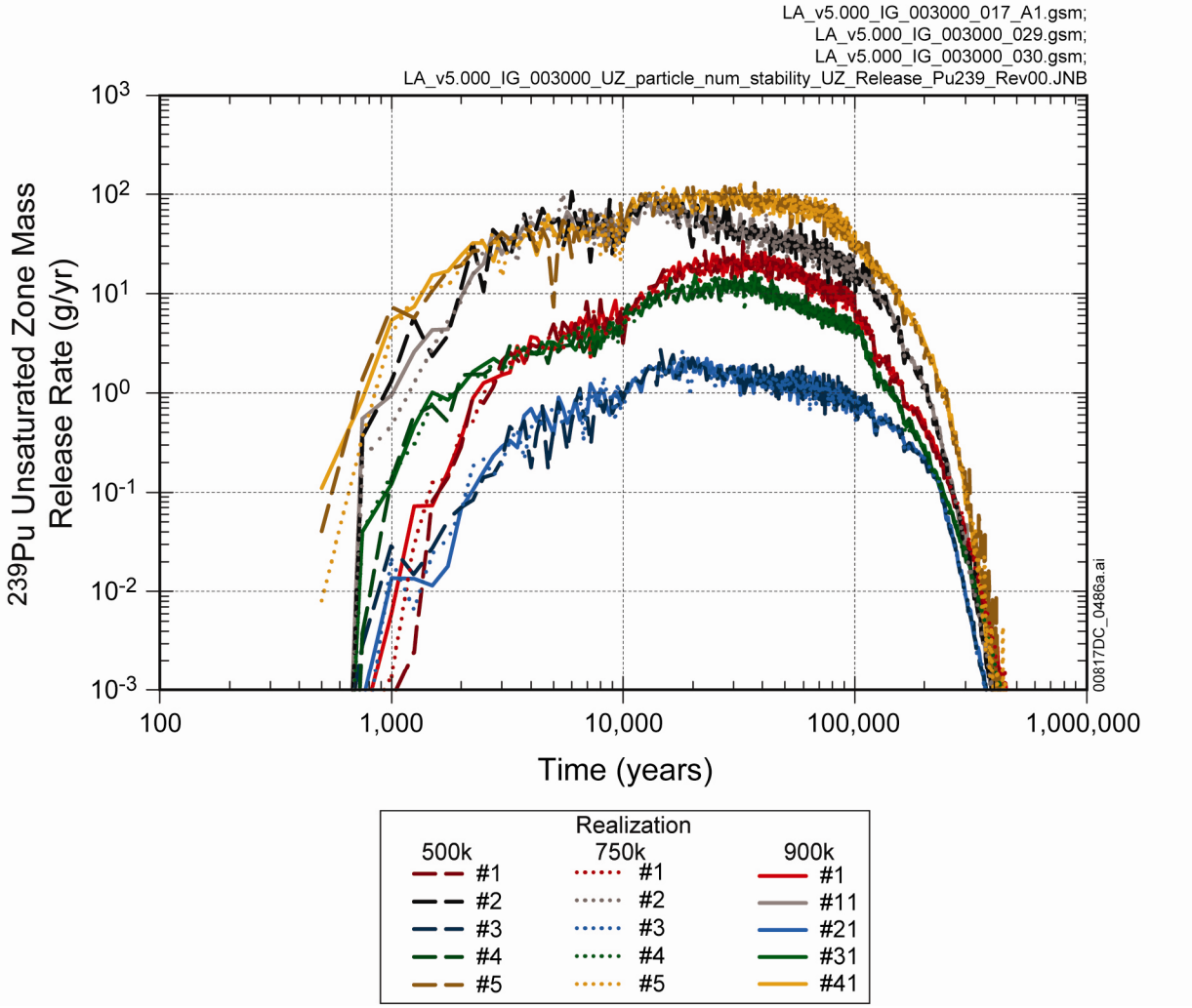

Source: Output DTNs: MO0708TSPAVALI.000 [DIRS 182985]; and MO0709TSPAREGS.000 [DIRS 182976].

Figure 7.3.5-23. Annual Unsaturated Zone Mass Release of ^{239}Pu for the Igneous Intrusion Modeling Case Simulations Using a Maximum of 500,000; 750,000; and 900,000 Particles in the Unsaturated Zone Transport Submodel

7.4 Uncertainty and Variability Characterization Reviews

One of the basic NRC requirements for a repository performance assessment is that it includes an appropriate treatment of parameter uncertainty and variability (10 CFR 63.114(a)(2) [DIRS 178394]). Specific details on how the NRC determines conformance with this requirement are given in *Yucca Mountain Review Plan, Final Report* (NRC 2003 [DIRS 163274], Section 2.2.1.3). To ensure compliance with this basic requirement and to build confidence in this aspect of the TSPA-LA Model, the Lead Laboratory conducted a risk informed review of the TSPA-LA uncertainty and variability characterizations for consistency, defensibility, and traceability of the direct-input parameters to the TSPA-LA Model. A special review team was formed to carefully examine stochastic parameter representations and correct or modify them as necessary. In addition, uncertainty and sensitivity analyses were performed during the development of the TSPA-LA Model based on the direct-input parameters in order to ensure that the parameter uncertainties are accurately propagated during the model development. After the model development, a final sensitivity analysis was conducted in order to identify the dominant sources of uncertainty in total expected dose to the RMEI and the errors that might have occurred during the TSPA-LA Model development. The results of the uncertainty characterization reviews on the direct-input parameters together with the uncertainty and sensitivity analyses performed during and after the TSPA-LA Model development built the foundation of confidence in the results of the model and ensured that supporting documentation was ready for regulatory review. The subsequent sections describe the overall review process, specific parameters and abstractions reviewed, and the actions taken to ensure that the treatment of parameter uncertainty and variability was of suitable quality for the LA, and summarizes the performed uncertainty and sensitivity analyses with the details of the analyses presented in Appendix K.

7.4.1 Approach

The technical reviews performed focused on: (1) confirming that the stochastic parameter representations appropriately reflect the major sources of uncertainty and/or variability, (2) verifying that the probability distributions were derived using sound statistical methods and interpretations, and (3) ensuring model parameter representations (i.e., probability distributions) are reasonable and defensible, as opposed to depicting extreme variations that could potentially introduce risk dilution (i.e., underestimation of dose risk). The reviews provided a risk informed or risk based evaluation of parameters important to dose in the TSPA-LA Model. A total of 15 formal reviews were performed to scrutinize the uncertainty characterizations of some 40 key TSPA input parameters (Table 7.4-1 through 7.4-3) and their associated abstractions.

A core team of several senior staff members of the Yucca Mountain Project (YMP) was formed with special expertise in probability and statistics, uncertainty analysis, TSPA modeling, and knowledge of the regulatory guidance regarding consistent treatment of uncertainty and variability. In addition, selected YMP subject matter experts (SMEs) provided support on an as-needed basis and facilitated the reviews of data, parameters, and model abstractions. This approach is based on, but not as formalized as the guidelines for uncertainty characterization and propagation presented in *Guidelines for Developing and Documenting Alternative Conceptual Models, Model Abstractions, and Parameter Uncertainty in the Total System Performance Assessment for the License Application* (BSC 2002 [DIRS 158794]).

The general work scope of the review team included:

- Familiarizing YMP SMEs with methodologies for analyzing data uncertainties and variabilities as well as use of statistical techniques to derive probability distributions, (i.e., probability density functions (pdfs) and cumulative density functions (CDFs))
- Performing independent statistical analyses and interpretations of laboratory and field data
- Checking the appropriateness of probability distributions chosen to fit data and ensuring consistency with respect to the quantity of available data
- Deriving probability distributions using advanced statistical techniques, including subjective methods such as Bayesian updating
- Ensuring parameter values are representative of component model scale (i.e., up-scaling data from small-scale samples and tests to the physical scale of the model)
- Examining subjective probability distributions to ensure that informal professional judgments were reasonable and consistent.

Potential inadequacies or problems in the uncertainty or variability treatment were generally resolved through review team collaborations with data collectors, TSPA data input package and analysis and model report authors, and TSPA component model leads. Inconsistencies or issues that could not be resolved through collegial interactions were presented to the Performance Assessment Systems Integration Management Team (a senior technical team) for resolution (Figure 7.4-1). Final resolution of parameter uncertainty team review comments were incorporated into the appropriate analysis and/or model reports.

7.4.2 Risk Informed Ranking of Scenario Classes and Modeling Cases

A risk-based ranking of TSPA-LA scenario classes and modeling cases was focused on the uncertainty/variability characterization reviews on the most important component model abstractions. Simulation results from past TSPA scoping studies were used to rank the major scenario classes and modeling cases according to their contribution to overall risk. It is important to note that past TSPA analyses have been largely limited to a 10,000-year time period. For simplicity, it was assumed that the ranking was also valid for post-10,000-year time periods.

There are four major scenario classes (Section 1.5) that are analyzed in demonstrating compliance with the individual protection standard (10 CFR 63.311(a) (1) and (2) [DIRS 178394]). Specific TSPA-LA scenario classes that are considered include:

- Nominal Scenario Class (i.e., expected evolution of the natural environment and degradation of the WPs and DSs, excluding early failures and disruptive processes and events)

- Early Failure Scenario Class (i.e., early failure of WPs and DSs due to material defects, process failures, and human errors)

- Igneous Scenario Class (includes Igneous Intrusion and Volcanic Eruption Modeling Cases)

- Seismic Scenario Class (includes Ground Motion and Fault Displacement Modeling Cases).

The Human Intrusion Scenario was excluded from the ranking because the relevant model parameters (for release, flow, and transport) are addressed in the Nominal Scenario.

Based on comparison of past TSPA dose projections (Gibson 2007 [DIRS 181099], Section 8.2), the following ranking (from highest to lowest) of the Scenario Classes and Modeling Cases were obtained:

1. Seismic Scenario Class, Seismic GM Modeling Case
2. Igneous Scenario Class, Igneous Intrusion Modeling Case
3. Igneous Scenario Class, Volcanic Eruption Modeling Case
4. Early Failure Scenario Class, Waste Package and Drip Shield EF Modeling Cases
5. Seismic Scenario Class, Seismic FD Modeling Case
6. Nominal Scenario Class, Nominal Modeling Case.

The magnitudes of the projected mean annual doses indicated that the first three modeling cases by far dominated the projected total mean annual dose for 10,000 years. As a result of this ranking and selection, the uncertainty/variability characterization reviews were focused on the top three modeling cases. However, because many component models of the Nominal Scenario Class are actually used in the Seismic and Igneous Modeling Cases, it was included in the selected set of modeling cases.

7.4.3 Risk Informed Identification of Stochastic Parameters Important to Dose

Because of the relatively large number of stochastic parameters used in the TSPA-LA simulation model (see Table K.3-2 in Appendix K for a detailed list), it was necessary to use a risk informed approach to prioritize the parameters associated with the Seismic, Igneous, and Nominal Modeling Cases. This approach builds confidence in the TSPA-LA Model, as it provides the review and consideration of the parameters that most impact the expected annual dose.

The risk informed selection of TSPA parameters was based on both importance rankings from preliminary TSPA scoping studies (Gibson 2007 [DIRS 181099], Appendix M) and recommendations provided by model abstraction developers and experienced TSPA analysts. The list of parameters was considered a candidate set appropriate for setting review priorities. The set of parameters was grouped into three of the four scenario classes. For each of the modeling cases selected, a cross-walk between the model abstractions and their associated key parameters was developed. The following sections briefly describe the relevant model abstractions and their associated key parameter sets.

7.4.3.1 Seismic Scenario Class—Key Abstractions and Parameters

The Seismic GM Modeling Case simulates the damage of WPs and DSs resulting from kinematic motion and rockfall for a range of seismic conditions. For the Seismic GM Modeling Case, seven major categories of parameters were identified as potentially having high importance. Within this parameter set, the seismic hazard curve was expected to dominate the importance ranking; this expectation is based on the previous TSPA scoping calculations (Gibson 2007 [DIRS 181099], Section 8.2.1.7), which indicated that the Seismic GM Modeling Case was an important contributor to the projected total mean annual dose. The seismic hazard curve defines the annualized probability of a given magnitude of PGV; WP damage abstractions are a function of PGV.

The set of key parameters identified for the Seismic GM Modeling Case, and the rationale for their selection, is presented in Table 7.4-1. The model abstractions for the Seismic GM Modeling Case are substantially more detailed than those used in past TSPA scoping calculations. The more detailed process and damage abstractions introduced several new parameters; the set of parameters considered to be important to simulation of repository system performance are included in Table 7.4-1. Detailed descriptions of these parameters and their uncertainty/variability characterizations are documented in *Seismic Consequence Abstraction* (SNL 2007 [DIRS 176828], Tables 6-88 through 6-93).

A number of Nominal Scenario parameters are also used in the Seismic Scenario Modeling Cases. For example, DS general corrosion rate is used in the damage seismic abstraction; this abstraction simulates the structural behavior of the DS as a function of plate thickness, which is a function of corrosion rate.

7.4.3.2 Igneous Scenario Class—Key Abstractions and Parameters

The Igneous Scenario Class consists of two modeling cases, Igneous Intrusion and Volcanic Eruption. Previous TSPA scoping calculations, performed for a 10,000-year time frame, have indicated that the annual frequency or occurrence rate is of high importance to both modeling cases. Similarly, the number of WPs hit parameter was also considered by the TSPA analysts to be important for both modeling cases. These and other key parameters for the Igneous Scenario Class are presented in Table 7.4-2.

For the Igneous Intrusion Modeling Case, it is important to clarify that at the time of the uncertainty/variability characterization reviews, the number of WPs hit was a stochastic parameter; subsequent to the review, however, it was decided to assign a constant value to the number of WPs hit. For the TSPA-LA compliance analysis (presented in Section 8), it was conservatively assumed that all the CDSP and CSNF WPs in the repository are damaged for any realization in which a main, drift, turnout, or other extension is intersected by an igneous intrusion (SNL 2007 [DIRS 177432], Section 5.1).

In the Volcanic Eruption Modeling Case, there are two basic and potentially important parameters, namely wind speed and direction. These stochastic parameters determine the characteristics of atmospheric dispersion and deposition of ash and contaminants produced by a hypothetical eruption through the repository. The scour depth parameter represents the depth to

which tephra and channel sediments are mixed and its tephra redistribution abstraction (i.e., simulates the transport of deposited ash to the location of the RMEI). Detailed descriptions of these parameters and their uncertainty/variability characterizations are documented in *Atmospheric Dispersal and Deposition of Tephra from a Potential Volcanic Eruption at Yucca Mountain, Nevada* (SNL 2007 [DIRS 177431], Tables 8-2 through 8-4) and in *Redistribution of Tephra and Waste by Geomorphic Processes Following a Potential Volcanic Eruption at Yucca Mountain, Nevada* (SNL 2007 [DIRS 179347], Table 6.4-1).

7.4.3.3 Nominal Scenario Class—Key Abstractions and Parameters

The Nominal Scenario Class represents the changes of the repository system that are expected to occur over a regulatory time frame. A total of eight component models have been developed to describe the isolation characteristics of the three primary barriers (i.e., upper natural barrier, engineered barrier, and lower natural barrier). As described in Section 6.3, the model components for the Nominal Modeling Case consist of: (1) UZ Flow, (2) EBS Environment, (3) WP and DS Degradation, (4) Waste Form Degradation and Mobilization, (5) EBS Flow and Transport, (6) UZ Transport, (7) SZ Flow and Transport, and (8) Biosphere.

Of the eight model components, five have abstractions that are likely to play a dominant role in the calculation of postclosure performance, even with the added effects of disruptive events. The model components are:

- UZ Flow (climate-induced infiltration, UZ flow fields, and drift seepage)
- WP and DS Degradation (general corrosion, localized corrosion, and SCC of WP outer barrier, and general corrosion of DS)
- Waste Form Degradation and Mobilization (radionuclide solubilities and waste form colloids)
- EBS Radionuclide Transport (corrosion products and colloids)
- SZ Flow and Transport (breakthrough curves and transport).

The key TSPA parameters for this scenario class are listed in Table 7.4-3. Based on sensitivity analyses carried out with preliminary TSPA scoping calculations (Gibson 2007 [DIRS 181099], Section 8.2), several of these probabilistic parameters have been shown to have a strong influence on the calculated distribution of expected annual dose.

In the UZ Flow Model Component, the parameter of fundamental importance is the net infiltration rate. This rate or flux is computed for pre-10,000-years from infiltration maps for the three climate states (i.e., present-day, monsoon, and glacial-transition) using a probabilistic approach that uses weighting factors. The uncertainty range for the post-10,000-years percolation rates has been specified in the NRC proposed regulation (10 CFR 63.342(c)(2) [DIRS 178394]). Two other important UZ parameters are the effective soil thickness of the soil cover and permeability of the lithophysal rock of the emplacement horizon. The effective soil

thickness is used in the process-level model for infiltration, while the permeability is used in the drift seepage abstraction.

The WP and DS degradation component models simulate the effects of various degradation processes and mechanisms as a function of the drip seepage, geochemical, and thermal conditions. The WP outer barrier, which is fabricated of Alloy 22 (UNS N06022), is degraded by general corrosion, localized corrosion, and SCC. The DSs are manufactured with Titanium Grade 7 metal plates and frame. The Titanium Grade 7 is relatively corrosion resistant and degrades only by general corrosion.

Of the six submodels that make up the Waste Form Degradation and Mobilization Model Component, the key parameters are the radionuclide solubility uncertainty factor in the Dissolved Concentration submodel (accounts for uncertainty in the thermodynamic coefficients) and the concentration of plutonium irreversibly attached to the waste form colloids in the EBS colloids submodel.

In the EBS Flow and Transport Model Component, the key parameters are corrosion rates for stainless and carbon steel, which determines the accumulation of corrosion products, and the specific surface and site density of the iron oxide mineral goethite. The importance of these parameters is associated with their influence on the sorption of dissolved and colloidal phase radionuclides and, thereby, affects the rate of release from the EBS.

In the SZ Flow and Transport Model Component, the two key parameters for groundwater flow are groundwater-specific discharge and the flowing interval spacing of the volcanic units. Parameters particularly important to dissolved and colloidal phase radionuclide transport are the radionuclide sorption coefficients and colloid retardation factor for the alluvium.

Detailed descriptions of these parameters and their statistical representations are documented in the following documents:

1. *Simulation of Net Infiltration for Present-Day and Potential Future Climates* (SNL 2007 [DIRS 182145], Section 6.5.5); *UZ Flow Models and Submodels* (SNL 2007 [DIRS 184614], Sections 6.10 and 6.8.5); and *Abstraction of Drift Seepage* (SNL 2007 [DIRS 181244], Section 6.6);

2. *General Corrosion and Localized Corrosion of the Drip Shield* (SNL 2007 [DIRS 180778], Section 8.1[a]); *General Corrosion and Localized Corrosion of Waste Package Outer Barrier* (SNL 2007 [DIRS 178519], Section 8.4); *Stress Corrosion Cracking of Waste Package Outer Barrier and Drip Shield Materials* (SNL 2007 [DIRS 181953], Section 8.4); *Analysis of Mechanisms for Early WP/DS Failure* (SNL 2007 [DIRS 178765], Section 7.1);

3. *Waste Form and In-Drift Colloids-Associated Radionuclide Concentrations: Abstraction and Summary* (SNL 2007 [DIRS 177423], Section 6); *Dissolved Concentration Limits of Elements with Radioactive Isotopes* (SNL 2007 [DIRS 177418], Section 8.1);

4. *EBS Radionuclide Transport Abstraction* (SNL 2007 [DIRS 177407], Section 8.2); and

5. *Saturated Zone Flow and Transport Abstraction* (SNL 2008 [DIRS 183750], Section 6.5.2).

7.4.4 Review Team

As noted above, a multi-disciplinary team of scientists and engineers was formed to conduct the parameter uncertainty/variability reviews. The skill composition of the review team was chosen to ensure a large breadth of expertise, experience, and knowledge. The review team selected brought together technical expertise spanning:

- Modeling of physical and chemical processes with inherent aleatory and epistemic uncertainty
- Statistical analysis and interpretation of data
- Analysis of probabilistic modeling results (via sensitivity and uncertainty analyses) to identify parameter importance ranking
- Conceptual and calculational structure of the TSPA-LA Model for the proposed Yucca Mountain repository system
- Encoding professional judgment to formulate subjective representations of uncertainty or variability.

In addition, the core members chosen were required to have an in-depth knowledge of the proposed NRC and U.S. Environmental Protection Agency (EPA) regulations for deep geologic repositories, regulatory guidance on consistent and adequate treatment of uncertainties, and the NRC review methods and guidance presented in *Yucca Mountain Review Plan, Final Report* (NRC 2003 [DIRS 163274]). The core review team that was formed consisted of five senior YMP staff members. The technical backgrounds of the core team members included: (1) TSPA modeling of deep geologic repositories, (2) statistical analysis of field and laboratory data, (3) application of probabilistic modeling and uncertainty propagation, (4) sensitivity and uncertainty analysis, and (5) seismic and volcanic hazard analysis.

A group of SMEs was also selected to provide support to the review activities. The SMEs were primarily used to perform independent evaluations of data, as well as facilitate in-depth reviews of the technical basis of model abstractions. These SMEs had specialized knowledge in: (1) hydrogeology and groundwater transport, (2) material science (e.g., WP and DS corrosion), (3) soil physics, soil chemistry, and groundwater geochemistry, and (4) reliability analysis and human factors engineering, and (5) elicitation methods for encoding professional judgment.

7.4.4.1 Review Scope, Process, and Criteria

For the most part, the scope of the uncertainty/variability characterization reviews was limited to a total of 15 formal reviews. Collectively, these reviews examined in detail the uncertainty/variability characterizations for the 40 plus TSPA input parameters listed in Tables 7.4-1 through 7.4-3. While the reviews primarily focused on scrutinizing the technical basis, they also included consistency aspects of the NRC Review Method for data uncertainty

described in *Yucca Mountain Review Plan, Final Report* (NRC 2003 [DIRS 163274]) for the 14 abstraction topics. In addition, the supporting documentation was reviewed and critiqued with respect to clarity and transparency. Verifying the traceability of data was outside the scope of these reviews; however, such reviews were performed separately in accordance with the YMP QA procedures for document review.

Each uncertainty/variability characterization review involved: (1) reviewing the relevant source documents (i.e., draft TSPA Data Input Packages and analysis and/or model reports); (2) meetings with the authors, data collectors, SMEs, and TSPA analysts to gain additional information and clarification; (3) developing recommendations and/or independent probabilistic representations; and (4) presenting the findings and recommendations to the authors and the Performance Assessment Systems Integration Team.

Parameter uncertainty/variability characterizations were judged appropriately, based on the criteria consistent with the NRC Acceptance Criterion for data uncertainty. More specifically, the criteria consisted of: (1) must be technically defensible and reasonably account for major sources of uncertainties and variabilities, and (2) will not introduce inappropriate risk dilution when propagated through the TSPA-LA Model. A review finding with respect to the first criterion was ascertained by addressing fundamental questions such as:

- What are the sources of uncertainty (i.e., aleatory and epistemic) and spatial variability?
- Is the parameter distribution consistent with the level of knowledge (i.e., maximum informational entropy) and/or quantity of data?
- Is there an underlying physical or mechanistic basis for the type of probability distribution used?
- Was the probability distribution evaluated for goodness-of-fit?
- Have potential correlations to other parameters been evaluated?

Similarly, the finding for the second criterion focused on questions such as:

- Are the bounds of the distribution reasonable and supported by data or other technical information?
- Have extreme conservatisms been embedded in the choice of location and scale parameters of the distribution (i.e., to skew the distribution)?
- What informal professional judgments have been made in uncertainty characterization and have they been peer reviewed?

The general review process is outlined in the flowchart shown on Figure 7.4-1. It is important to note the pivotal role of the Performance Assessment Systems Integration Team in this process, which was to evaluate the review team's findings and recommend an appropriate implementation, based on a risk-informed perspective.

7.4.5 Review Findings and Implementations

As explained in Section 7.4.2, a risk informed evaluation was conducted of the major scenario classes and their associated modeling cases to rank them according to their potential contribution to the overall dose-risk. This section gives highlights from selected reviews, principal findings, and recommended revisions to the uncertainty or variability characterizations.

7.4.5.1 Seismic Scenario Class—Ground Motion Modeling Case

The Seismic GM Modeling Case is one component of the seismic consequences model. The ground motion component evaluates the likelihood and consequences of both kinematic motion and rockfall on the WPs and DSs. The key probabilistic parameters for the Seismic GM Modeling Case can be grouped into the following three categories:

- Mean seismic hazard curve
- Fragility curves for the DSs
- Damage abstractions for kinematic motion and rockfall.

The model theory and stochastic parameter representations for the Seismic GM Modeling Case are documented in *Seismic Consequences Abstraction* (SNL 2007 [DIRS 176828], Section 6). The formal review of the Seismic GM Modeling Case examined six key parameter representations, which are listed in Table 7.4-1. Significant findings and recommendations are summarized below.

Seismic Hazard Curve—The ground motion component of the seismic consequences model uses the mean seismic hazard curve (Section 6.6.1.2) for the repository location, which is the product of several years of study conducted by the YMP under the *Probabilistic Seismic Hazards Analysis for Fault Displacement and Vibratory Ground Motion at Yucca Mountain, Nevada* (PSHA) (CRWMS M&O 1998 [DIRS 103731]). The mean hazard curve, which is defined as the mean estimate or average of the distribution of hazard curves derived by the PSHA expert elicitation (Budnitz et al. 1997 [DIRS 103635]), lies above the 80th percentile of the distribution for high intensity ground motions (i.e., at low annual exceedance frequencies) because the average is dominated by the larger PGV values of the distribution.

The review team noted that use of the mean hazard curve does not explicitly propagate the available distribution of epistemic uncertainty in the hazard curve to the estimate of the distribution of expected annual dose. Moreover, the use of a mean hazard curve is inconsistent with the probabilistic framework outlined in Section 6.1.3. Because the uncertainty distribution in the hazard curve could contribute significantly to the uncertainty distribution of the expected annual dose curves, the review team recommended projecting the annual dose for the Seismic GM Modeling Case using the distribution of hazard curves. The Performance Assessment Systems Integration Team elected not to adopt the review team recommendation because of a letter agreement between DOE and NRC on the approach to postclosure seismic analyses. That letter agreement states: “As the objective of the probabilistic risk assessment will be to determine mean risk, the mean ground motion hazard curve will be used” (Brocoum 2001 [DIRS 159576], enclosure, Section 3.2).

Fragility Curves and Damage Abstractions—Most of the key parameters for the Seismic GM Modeling Case are associated with the fragility curves and damage abstractions. Those curves and abstractions are based on detailed simulations of structural response to seismic histories. Two concerns were noted by the review team with regard to sources of uncertainty not included in the ground motion model:

1. The curves and abstractions are based on a relatively small number (i.e., 17) of representative ground motion histories.

2. The number of simulated structural response outcomes for these histories typically produced data sets with small sample sizes.

The first concern is that the number of histories used was arbitrary and not shown to adequately capture the spectrum of seismic conditions. The second and related concern is that the uncertainties in the functional fits (to the structural response data) were not quantified.

Bulking Factor for Rockfall—The bulking factor for rockfall (i.e., ratio of free volume in drift to volume of rock corresponding to complete drift collapse) is assumed as specified to range from 0.1 to 0.4. Correspondingly, given a value of 12 m^3 per meter as the value for the unfilled drift volume, the volume of rockfall per meter of rock is estimated to be between 30 (i.e., 12/0.4) and 120 (i.e., 12/0.1) m^3, and a uniform distribution is assigned to this range. This assumption implied that the PDF for the bulking factor (which is the primary uncertain variable) has to be a monotonically decreasing distribution, with its mode corresponding to the minimum value. The use of uniform distribution for both bulking factor and rock volume was found to be an inconsistent representation of uncertainty in the bulking factor (because of the reciprocal nature of the relationship). This inconsistency was corrected as a result of review comments.

7.4.5.2 Igneous Scenario Class—Igneous Intrusion and Volcanic Eruption Modeling Cases

The Igneous Intrusion and Volcanic Eruption Modeling Cases evaluate the likelihood and consequences of magma flow penetrating the repository footprint. Two types of penetrations are analyzed consisting of: (1) intrusive vertical tabular igneous dike, and (2) extrusive volcanic conduit. Component models for these modeling cases simulate the igneous penetrations in order to calculate the number of WPs damaged during hypothetical events. The total number of WPs damaged, in turn, provides a means to calculate the quantity of radionuclides released to the groundwater or atmosphere.

The key stochastic parameters for these two igneous modeling cases are:

- Annual frequency for an igneous event intersecting the repository footprint
- Number of WPs hit by an intrusive dike (resulting in release of radionuclides to the groundwater pathway)
- Number of WPs hit by an extrusive volcanic conduit (resulting in radionuclides dispersed into the atmosphere pathway)

- Eruptive center probability (i.e., percentage of intrusive penetrations with extrusive conduits).

The model theory and stochastic parameter representations for these igneous modeling cases are documented in *Number of Waste Packages Hit by Igneous Events* (SNL 2007 [DIRS 177432], Sections 6 and 7). The formal review of the Igneous Intrusion Modeling Case examined the key parameter representations, which are listed in Table 7.4-2. Significant findings and recommendations are summarized below.

Annual Frequency of Igneous Event—The probability distribution for the annual frequency of igneous event intersecting the repository footprint is the product of several years of work conducted under the YMP's ongoing *Probabilistic Volcanic Hazards Analysis* (CRWMS M&O 1996 [DIRS 100116]) study. The probability distribution accounts for both the aleatory and epistemic uncertainty in the occurrence of igneous events. The technical basis for this probability distribution has been extensively and independently peer reviewed. The review team concluded that the uncertainty representation of the annual frequency accounts for the major sources of aleatory and epistemic uncertainty and is suitable for its intended use.

Number of Waste Packages Hit—The probability distributions for the number of WPs hit are computed via computer simulations of igneous intrusive and extrusive events. As discussed in *Number of Waste Packages Hit By Igneous Events* (SNL 2007 [DIRS 177432]), the DIRECT code is used to simulate these processes using the distribution of annual frequency of igneous events, along with probability distributions for the dimensional, geometric, and spatial variability of the igneous events. The computed CDFs for WPs hit are provided as tabular data to the TSPA-LA Model.

Although the probabilistic inputs (e.g., dike spacing, dike length, and conduit diameter) to the DIRECT code are evidence supported, these inputs do not currently account for epistemic uncertainty. The review team concluded that the absence of these epistemic uncertainties is most likely to be offset by conservatism in the igneous component model. For example, subsequent to this review, the YMP opted to treat the number of WPs hit by intrusion events as a fixed conservative value. More specifically, any intrusive dike intersecting an emplacement drift is assumed to fail all the WPs.

Eruptive Center Probability—This parameter is represented by a point probability value (i.e., P = 0.28) and not by a probability distribution. Thus, there is no epistemic uncertainty included in the representation of this parameter. The review team concluded, however, that the eruptive center probability will most likely play a small role in the probabilistic outcomes of this modeling case because of the embedded conservatisms.

7.4.5.3 Igneous Scenario Class—Volcanic Eruption Modeling Case

This Volcanic Eruption Modeling Case is simulated using two coupled models, ASHPLUME and Fortymile Wash Ash Redistribution (FAR). These computer models simulate the atmospheric transport, deposition, and redistribution of ash through the Fortymile Wash watershed for a hypothetical volcanic eruption intersecting the repository footprint.

Two key probabilistic parameters and one abstraction were reviewed for the Volcanic Eruption Modeling Case, namely:

- Wind speed (functions of altitude)
- Wind direction (functions of altitude)
- Tephra redistribution abstraction.

The model theory and parameter representations for this modeling case are documented in *Atmospheric Dispersal and Deposition of Tephra from a Potential Volcanic Eruption at Yucca Mountain, Nevada* (SNL 2007 [DIRS 177431], Sections 5, 6, and 8, and Tables 8-2 through 8-4) and in *Redistribution of Tephra and Waste by Geomorphic Processes Following a Potential Volcanic Eruption at Yucca Mountain, Nevada* (SNL 2007 [DIRS 179347], Sections 5 and 6 and Table 6.4-1). Significant findings and recommendations are summarized below.

Wind Speed and Direction—The ASHPLUME model uses CDFs for wind speed and wind direction data for 13 altitude bins, ranging from 0 to 13 km. The CDFs for wind speed and wind direction are based on an analysis of a large data set for the Desert Rock weather station. The review team concluded that the uncertainty characterization for these parameters was appropriate. However, it noted that the parameters are treated as independent stochastic variables. Moreover, no statistical tests had been performed to evaluate potential correlation between wind speed and wind direction. A review of the literature on statistical analyses of wind data was performed to ascertain if statistical correlations were commonly observed; no such correlations were noted in the available literature, suggesting that assumption-independent random variables may be appropriate.

Tephra Redistribution Abstraction—The FAR model uses the spatial distribution of ash (computed by the ASHPLUME model) as input and then simulates the transport of tephra and waste from the Fortymile Wash drainage basin to the RMEI location. The FAR Model simulates mass transport by hill slope and fluvial processes and basically assumes that there is no significant redistribution by aeolian processes. The review team raised a concern regarding conceptual model uncertainty associated with the assumption of aeolian processes being unimportant.

The review team noted that the ASHPLUME calculations indicate tephra ranging from 0.0001-cm diameter particles (clay size) to about 0.2-cm diameter particles (coarse sand). The sampled particle size mode is 0.0013-cm diameter particles corresponding to fine silt-size class. Thus, the sand-sized tephra particles would be susceptible to redistribution by wind within the Fortymile Wash. The finer silt- and clay-sized particles could potentially be picked up and transported for miles from the source area by strong, sustained winds. Therefore, the FAR Model could be ignoring a relevant redistribution and/or removal process.

The review team concluded that this uncertainty in the conceptual model was most likely offset by the very conservative modeling assumption that the redistribution of ash and waste particles occurs instantaneously. In actuality, the time scale of the redistribution of material could take many thousands of years.

7.4.5.4 Nominal Scenario Class

The TSPA-LA Model is based on the Nominal Scenario Class, which incorporates all expected FEPs to describe the most likely fundamental processes that would persist under ambient conditions, as well as possible changes to those processes after repository closure. The Nominal Scenario Class includes a single modeling case that addresses FEPs that describe the natural degradation of the EBS (i.e., DSs and WPs).

7.4.5.4.1 Unsaturated Zone Flow

The UZ Flow Model Component consists of five submodels that collectively model water flow, beginning with climate-induced precipitation at the land surface, net infiltration into the soil cover, deep percolation through the geologic strata and to the repository horizon, seepage into the drifts, moisture condensation on drift walls, and subsequent flow into the underlying water table.

The uncertainty/variability characterization review examined key stochastic parameters of the Infiltration (SNL 2007 [DIRS 182145]), UZ Flow (SNL 2007 [DIRS 184614], Section 6.8) and Drift Seepage (SNL 2007 [DIRS 181244]) submodels. Three key parameters that were reviewed in depth were:

- Effective soil depth for surface infiltration
- Weighting factors for net infiltration
- Permeability of lithophysal rock units.

The importance of these parameters was identified from sensitivity analyses of preliminary TSPA scoping calculations. For brevity, only the review findings and recommendations for the effective soil depth and weighting factors for net infiltration are presented here.

Effective Soil Depth—While effective soil depth is not a parameter in the TSPA Model, it is an important parameter used in the analysis of infiltration in the surface soils. This parameter has a strong effect on the net infiltration into the UZ. The infiltration model considers a range of soils that were divided into five classes: (1) very deep, (2) moderately deep, (3) intermediate, (4) shallow soils, and (5) bedrock (no soil cover). Sensitivity analyses described in *Simulation of Net Infiltration for Present-Day and Potential Future Climates* (SNL 2007 [DIRS 182145]) showed that the effective thickness for soil class 4 was shown to be a very dominant parameter in the calculations of net infiltration.

The uncertainty/variability characterization reviews identified a concern with the method used to calculate upscaled effective soil depth (i.e., thickness). To address this concern, an analytic relationship was developed for properly upscaling the probability distribution for soil thickness that ensured that the average water flux was preserved. The new approach was implemented in the infiltration model and is documented in *Simulation of Net Infiltration for Present-Day and Potential Future Climates* (SNL 2007 [DIRS 182145]).

Weighting Factors—The UZ Flow Field weighting factors are used in the TSPA for stochastic sampling of the flow field uncertainty scenarios. These scenarios are characterized by the

10th percentile, 30th percentile, 50th percentile, and 90th percentile infiltration maps. For a given TSPA simulation, one of the four uncertainty scenarios is randomly selected based on the weighting factors and the selected flow field used through the climate states (present-day, monsoon, glacial-transition, and post-10,000-year) simulated.

The UZ Flow Field weighting factors were developed using the generalized likelihood uncertainty estimation (GLUE) method (Beven et al. 2000 [DIRS 179825] and SNL 2007 [DIRS 184614], Section 6.8.5.1). The GLUE approach takes into account prior information from the infiltration model for the probability of the infiltration maps, as well as the relative agreement between the flow model results corresponding to each infiltration map and corresponding field observations. The methodology uses a Bayesian framework to produce posterior probabilities (weighting factors) for the infiltration maps.

The review team questioned the appropriateness of the non-standard application of the GLUE methodology, as well as the lack of a rationale for the selection of likelihood functions. The review team questioned the use of a suite of likelihood functions and then averaging the results. In checking the GLUE calculations, the review team noted that the results from some of the likelihood functions lacked consistency. The review team proposed that likelihood functions be screened on the basis of consistency with the field data and only one be used in the GLUE method.

After several meetings, the review team and authors, with the concurrence from the Performance Assessment Systems Integration Team, decided to proceed forward with the original weighting factors. However, it was recommended that the documentation of the GLUE methodology show weighting factor calculations obtained by eliminating the likelihood functions that appeared to overweight or underweight selected model comparisons. The recommendation was implemented in *UZ Flow Models and Submodels* (SNL 2007 [DIRS 184614], Section 6.8.6.3).

7.4.5.4.2 Waste Package and Drip Shield

The WP and DS Degradation Model Component accounts for the following degradation processes: general corrosion of the DSs, general corrosion and localized corrosion of the outer surfaces of the WPs, and SCC of the WPs.

The uncertainty/variability characterization reviews examined the following key parameters of the DSs (SNL 2007 [DIRS 180778], Sections 6.1.5[a] through 6.1.7[a]) and WPs (SNL 2007 [DIRS 181031], Table 1-1; SNL 2007 [DIRS 181953], Table 1-1):

- DS (Titanium Grade 7) general corrosion rate
- WP outer barrier (Alloy 22) general corrosion rate and temperature dependence
- WP outer barrier SCC growth rate (repassivation rate)
- WP outer barrier material yield strength.

For brevity, only the review findings and recommendations for the review of DS general corrosion are presented here. The review team confirmed that the bases for the parameter uncertainty characterizations for the other parameters listed above were appropriate and defensible.

The original probabilistic model developed to simulate general corrosion of the DS was based on 1-year corrosion rate data for Titanium Grade 16 (SNL 2007 [DIRS 180778], Section 6.5.3.1). The YMP Corrosion team opted to develop a new probabilistic model using more relevant corrosion data (i.e., 2.5-year data for Titanium Grade 7). The review team provided direct assistance to the SMEs with performing statistical analyses of the laboratory data and development of a new probabilistic model that addressed both variability and epistemic uncertainty.

Weight-loss data for corrosion of Titanium Grade 7 consisted of tests in groundwater compositions for three groups: aggressive, intermediate, and benign conditions. The data subsets for aggressive and benign conditions were chosen to develop bounding models for general corrosion. A normal distribution was fit to the aggressive conditions data, while a gamma distribution was fit to the data set for the benign conditions. These probability distributions were used to describe variability in the DS general corrosion rate. Statistical relationships were also developed to estimate the uncertainty in the mean corrosion rates. The development of these statistical models included testing for normality, goodness-of-fit, and fitting with alternative distributions (SNL 2007 [DIRS 180778], Sections 6.1.5[a] through 6.1.7[a]).

7.4.5.4.3 Waste Form Degradation and Mobilization

The Waste Form Degradation and Mobilization Model Component consists of six submodels. Collectively, these submodels account for the following processes and conditions: in-package water chemistry; waste form cladding degradation; matrix degradation rates for CSNF, DSNF, and HLW waste forms; radionuclide solubilities; and the types and concentrations of waste form and in-drift colloids.

The uncertainty/variability characterization reviews focused on two key stochastic parameters used in the dissolved concentration (SNL 2007 [DIRS 177418], Tables 6.6-11) and EBS colloid transport (SNL 2007 [DIRS 177423], Table 6-24) submodels, namely:

- Radionuclide solubility uncertainty factor, low and high ionic strength
- Concentration of irreversibly attached plutonium on colloids.

For brevity, only the review findings and recommendations for the review of key colloids parameters for the colloids are presented here.

Concentration of Irreversibly Attached Plutonium on Colloids—The uncertainty/variability characterization review focused on examining the probability distributions for two colloid parameters: (1) $C_{RNcoll,DHLWG,embed,\ sampled}$ (concentration of irreversibly attached plutonium associated with defense HLW glass colloids), and (2) $C_{coll,DHLWG,\ triangular}$ (concentration of irreversibly attached plutonium per concentration of colloids). The draft documentation available for these parameters was initially found to be unclear or insufficient to lead to an unambiguous understanding of the technical basis.

Written comments were provided to the SMEs for improving the documentation, which were subsequently addressed and documented (SNL 2007 [DIRS 177423]). The review team

confirmed that the basis for the parameter uncertainty characterizations was appropriate and defensible.

7.4.5.4.4 Engineered Barrier System Radionuclide Transport

The Radionuclide Transport Abstraction, which is part of the EBS Flow and Transport Model Component, defines the water flow pathways in the EBS and simulates the advective and diffusive mass transport from a breached WP. The model considers radionuclide transport in both dissolved and colloidal phases. In addition, the model accounts for irreversible sorption of radionuclides onto corrosion products that builds up with time in the breached WP.

The uncertainty/variability characterization review of this component model focused on the stochastic parameters associated with the corrosion product generation and sorption. The relevant key parameters are:

- Stainless steel corrosion rate
- Carbon steel corrosion rate
- Specific surface area of Fe_2O_3 and FeOOH corrosion products
- Goethite site density.

Because of the important effect of corrosion products on radionuclide releases from the EBS, the formal review focused on the stainless steel and carbon steel corrosion rates, as documented in *EBS Radionuclide Transport Abstraction* (SNL 2007 [DIRS 177407], Section 6.3.4.3.4.3, and Appendix F, and Table 8.2-4). Review findings and recommendations for these parameters are summarized here.

Stainless Steel Corrosion Rate—The original uncertainty representation for Stainless Steel Type 316L corrosion rate consisted of an empirical CDF; that representation had been constructed from available short-term data from laboratory tests in a fresh water environment for temperatures ranging from 50°C to 100°C. With assistance from SMEs, the available laboratory measurements were reviewed to confirm their appropriateness. Some of the low values in the data were considered to be of questionable accuracy. As a result, the minimum value was set to a reasonable bound (i.e., set to the mean of the Alloy 22 corrosion rate, which has a much lower corrosion rate than stainless steel).

After review of the corrosion data, a rigorous statistical analysis was performed. A Bayesian updating procedure was then used to derive a truncated lognormal distribution. From the analytic probability curve, it was possible to also quantify the uncertainty in the median corrosion rate. A new CDF distribution was developed and used in place of the original empirical CDF. In addition to providing an excellent fit to the data, the new continuous distribution facilitated the implementation LHS in the TSPA-LA Model.

Carbon Steel Corrosion Rate—The original uncertainty representation for Carbon Steel Type A516 corrosion rate consisted of an empirical CDF. This CDF was based on data from short-term laboratory tests using simulated dilute J-13 well water (10 times the normal concentration of J-13 water) at 60°C and 90°C; the 10-times concentration in the simulated dilute J-13 well water was considered representative of the small potential degree of concentration that

might occur inside a breached WP. The corrosion rate data were obtained from laboratory tests of 0.5 year and 1.0 year in duration. The review team assisted the SME with development of the new carbon steel corrosion rate CDF.

A statistical analysis of the data was performed and a new probability distribution developed using a Bayesian updating method. A truncated lognormal distribution was derived and shown to provide an excellent fit to the data points. In addition, a statistical relationship was developed to quantify the uncertainty in the median corrosion rate.

7.4.5.4.5 Saturated Zone Flow and Transport

The SZ Flow and Transport Model Component simulates the transport of radionuclides from their introduction at the water table below the repository to the regulatory boundary at approximately 18 km. The uncertainty/variability characterization review of the SZ submodel (SNL 2008 [DIRS 183750], Table 6-8; SNL 2007 [DIRS 177392], Section 6.7.1) examined the following stochastic parameters:

- Groundwater-specific discharge multiplier
- Flowing interval spacing for volcanic units
- Radionuclide sorption coefficients.

For brevity, only the review findings and recommendations for groundwater-specific discharge and flowing interval spacing are presented here.

Groundwater Specific Discharge—Preliminary TSPA scoping studies have shown that the groundwater specific discharge multiplier is a dominant parameter for both Seismic GM and Igneous Intrusion Modeling Cases. Its high importance ranking is derived from the fact that groundwater specific discharge is a stochastic scale factor, which is applied to all values of permeability and boundary fluxes in the SZ Flow Model. The uncertainty characterization for groundwater specific discharge had been previously developed based on elicitation of expert judgment (CRWMS M&O 1998 [DIRS 100353]), and supplemented by tracer test results from the Alluvium Testing Complex (SNL 2007 [DIRS 177394]). The end points of the distribution and certain quantiles were subjectively selected, and a piecewise log uniform distribution was assumed between these point values.

The review team assisted the SME with revising the subjective probability distribution using a Bayesian updating procedure. Such a procedure provides a formal and systematic basis for combining prior information with new data to produce an updated distribution. Analytical expressions for Bayesian updating (SNL 2008 [DIRS 183750], Section 6.5.2.1[a]), appropriate for the specific distributional form (i.e., log-normal), were applied to characterize the uncertainty in groundwater specific discharge. The resulting new CDF for groundwater specific discharge is more defensible in that it is based on a formal statistical procedure for combining old information (i.e., expert elicitation) with new data (i.e., tracer test results), as opposed to a subjective integration of information.

Flowing Interval Spacing—The flowing interval spacing of volcanic units parameter is used in defining the effective flow in the fractured volcanic units. Previous TSPA scoping studies have

indicated that flowing interval spacing of volcanic units is one of the dominant SZ parameters. An empirical CDF (BSC 2004 [DIRS 170024], Section 6.3-6.4) for this parameter was originally developed from flow meter survey data obtained for various hydrogeologic units. The SZ SME requested that the review team perform an independent statistical analysis of the field data and derive the new CDF.

In examining the data, the review team noted that data had not been corrected for the dip angle of the fractures in the original analysis. After making this adjustment to the data, the review team used a Bayesian updating procedure (SNL 2008 [DIRS 183750], Section 6.5.2.3[a]) to develop a new CDF. Statistical tests indicated that the new distribution provided a very good fit to the field data. The new CDF for flowing interval spacing of volcanic units is more defensible in that it accounts for both variability in the data and epistemic uncertainty.

7.4.6 Summary of Sensitivity Analyses

Sensitivity analyses identify the contribution of uncertain model inputs to the uncertainty in model output. During development of the TSPA-LA Model, sensitivity analyses were performed using output from developmental versions of the TSPA-LA Model to investigate the propagation of uncertainty through the system model and to identify uncertain inputs that may be significant to the uncertainty in the results of the final TSPA-LA Model. These during-development analyses followed the analysis scheme presented in Appendix K, which documents results from the final sensitivity analysis completed after model development. The during-development sensitivity analyses generally confirmed that the uncertainty reviews had covered all key uncertain inputs. In addition, the during-development analyses provided a measure of confirmation that important uncertain inputs are propagated appropriately through the process models and that the effects of these uncertainties are consistent with physical principles underlying the models. The during-development sensitivity analyses also uncovered a number of implementation errors in developmental versions of the model, which were subsequently corrected before the TSPA-LA Model became final.

After model development, a final sensitivity analysis was conducted and is documented in Appendix K. This analysis identifies the dominant sources of uncertainty in total expected dose to the RMEI. For each modeling case, the analyses also investigate the sources of uncertainty in expected dose to the RMEI and in the movement of several key radionuclides (i.e., ^{239}Pu, both dissolved and sorbed to colloids, ^{237}Np, and ^{99}Tc). These radionuclides were chosen to illustrate a range of radionuclide behavior, including colloid-facilitated transport. In addition, for a few modeling cases, the analyses investigate uncertainty in other process model results such as the time of drip shield failure and the chemical environment in the drifts. Table 7.4-4 summarizes sensitivity analysis results for total expected annual dose and expected annual dose by modeling case by listing the key uncertain inputs identified by the analysis. The key uncertain inputs identified by the analyses that were also subjects of uncertainty reviews are indicated by **bold** font.

As presented in the discussion accompanying the sensitivity analysis results in Appendix K, the final sensitivity analysis confirms that the uncertainty in some high profile (or statistically significant) inputs are propagated through the TSPA-LA Model and that the effects of uncertainty in these inputs is consistent with physical principles. The confirmation is

demonstrated through causal explanations of the relationships between input and output variables. For example, where the analysis indicates a positive correlation between the input and output variables, the causal explanation illustrates the reasons why a positive correlation should be observed.

The final sensitivity analysis also identified a relatively small number of implementation errors present in the final version of the TSPA-LA Model (v5.000). These errors, along with others identified by check and review activities, are documented in Appendix P along with impact assessments investigating the effect of each error on the TSPA-LA Model v5.000 results. Although the errors do not significantly affect the output from the TSPA-LA Model, the errors influence the selection of uncertain input variables correlated to uncertainty in the transport of plutonium sorbed to certain colloids. As a consequence, the affected results were removed from the final version of Appendix K. These analyses were removed, rather than corrected, because the results of the analyses are not significant in determining the key uncertain inputs to the TSPA-LA Model.

INTENTIONALLY LEFT BLANK

Table 7.4-1. Key TSPA Parameters for Seismic Scenario Class for the Ground Motion and Rockfall Abstractions

Model Abstractions	Parameter Description	Basis for Selection
Ground Motion and Rockfall	Mean Seismic Hazard Curve	Identified in previous sensitivity and uncertainty analyses
	DS Plate and Frame fragility curves	Proposed by TSPA component model developer
	Damaged area of DS crown	Proposed by model abstraction developer
	Fraction of drift filled with lithophysal rock and accumulated volume of rock	Proposed by model abstraction developer
	Total damaged area for TAD and CDSP WPs	Proposed by model abstraction developer
	Probability of rupture for TAD and CDSP WPs	Proposed by model abstraction developer

Table 7.4-2. Key TSPA Parameters for Igneous Scenario Class

Model Abstractions	Parameter Description	Basis for Selection
Intrusion and Eruption	Annual frequency of a volcanic event intersecting the repository footprint	Identified in previous sensitivity and uncertainty analyses
	Number of WPS hit during a hypothetical igneous intrusion	Proposed by TSPA component model lead
	Number of WPs hit during a hypothetical volcanic eruption	Proposed by TSPA component model lead
	Wind speed and direction	Proposed by TSPA component model lead
	Scour depth at alluvial fan apex	Proposed by TSPA component model lead

Table 7.4-3. Key TSPA Parameter Sets for the Nominal Scenario Class by Model Abstraction

Model Abstraction	Parameter Description (TSPA-LA Model Name)	Basis for Selection
UZ Flow	Weighting factors for calculating net percolation over the repository (Infiltration_Scenario_a)	Identified in previous sensitivity and uncertainty analyses
	Effective soil depth over repository (used in infiltration process model) (Soil_Density_a)	Proposed by TSPA component model lead
	Uncertainty in permeability of lithophysal rock units (Alpha_Uncert_Lith_a)	Identified in previous sensitivity and uncertainty analyses
WP and DS	WP outer barrier (Alloy 22) general corrosion rate (GC_ULevel_A22_a)	Proposed by TSPA component model lead
	General corrosion rate (Alloy 22) temperature dependence (C1_GenCorr_A22_a)	Proposed by TSPA component model lead
	WP outer barrier SCC growth rate (repassivation rate) (n_SCC_a)	Proposed by TSPA component model lead
	Stress threshold for SCC nucleation (Stress_Thresh_A22_a, Stress_Thresh_SCC_a)	Proposed by TSPA component model lead
	DS (Titanium Grade 7) general corrosion rate (WDDSAggrGC_Mean_a, WDDSBenignGC_Mean_a)	Proposed by TSPA component model lead
Waste Form Degradation and Mobilization	Radionuclide Solubility (U, Np, Th, Pu, Am) ε_1, low ionic strength (See Tables 6.3.7-41 through 6.3.7-46)	Identified in previous sensitivity and uncertainty analyses
	Radionuclide Solubility (U, Np, Th, Pu, Am) ε_1, high ionic strength (See Tables 6.3.7-41 through 6.3.7-46)	Identified in previous sensitivity and uncertainty analyses
	Actinide Solubility, maximum limit (See Section 6.3.7.5.2, Treatments of Solubility Model Out-Of-Bounds)	Proposed by TSPA component model lead
	Concentration of irreversibly attached plutonium, associated with DHLWG colloids (CPu_Col_Wf_Embed_Sampled_a, CPu_Per_WF_Embed_Col_a)	Proposed by TSPA component model lead
EBS Radionuclide Transport Abstraction	Stainless Steel (316L) corrosion rate (SS_Corrosion_rate_a)	Proposed by TSPA component model lead
	Carbon Steel (A516) corrosion rate (SS_Corrosion_rate_a)	Proposed by TSPA component model lead
	Goethite site density (Goethite_Site_Density_a)	Identified in previous sensitivity and uncertainty analyses
	Specific surface area of Fe_2O_3 and FeOOH corrosion products (HFO_SA_a)	Identified in previous sensitivity and uncertainty analyses

Table 7.4-3. Key TSPA Parameter Sets for the Nominal Scenario Class by Model Abstraction (Continued)

Model Abstraction	Parameter Description (TSPA-LA Model Name)	Basis for Selection
SZ Flow and Transport	Groundwater specific discharge (GWSPD)	Identified in previous sensitivity and uncertainty analyses
	Flowing interval spacing in volcanic units (FISVO)	Identified in previous sensitivity and uncertainty analyses
	Colloidal retardation factor for alluvium (CORAL)	Identified in previous sensitivity and uncertainty analyses

Table 7.4-4. Summary of Selected Sensitivity Analysis Results

Modeling Case	TSPA-LA Model Output	Key Uncertain Inputs[a]
Total System	Total expected dose over 20,000 years	**Residual stress threshold for SCC (SCCTHRP)** Frequency of occurrence of igneous events (IGRATE) **Scale factor in ground water specific discharge (SZGWSPDM)**
	Total expected dose over 1,000,000 years	Frequency of occurrence of igneous events (IGRATE) **Residual stress threshold for SCC (SCCTHRP)** **General corrosion rate (Alloy 22) temperature dependence (WDGCA22)** **Scale factor in ground water specific discharge (SZGWSPDM)**
Nominal	Expected dose resulting from corrosion processes	**General corrosion rate (Alloy 22) temperature dependence (WDGCA22)** Deviation from median yield strength range for outer lid (WDZOLID)
Early Failure Waste Package	Expected dose resulting from early failure of waste packages over 20,000 years	Probability of early failure per waste package (PROBWPEF) **Pointer variable for infiltration scenario (INFIL)** Selector for host-rock thermal conductivity scenario (THERMCON)
Early Failure Drip Shield	Expected dose resulting from early failure of drip shields over 20,000 years	Probability of early failure per drip shield (PROBDSEF) Uncertainty factor accounting for small-scale heterogeneity in fracture permeability (SEEPUNC) Flowing interval porosity in volcanic units (SZFIPOVO)
Igneous Intrusion	Expected dose resulting from igneous intrusion over 1,000,000 years	Frequency of occurrence of igneous events (IGRATE) **Scale factor in ground water specific discharge (SZGWSPDM)** **Pointer variable for infiltration scenario (INFIL)**
Volcanic Eruption	Expected dose resulting from volcanic eruption over 1,000,000 years	**Frequency of occurrence of volcanic eruptions (IGERATE)** Depth of soil within which radionuclides affect the biosphere (BTILLAGE)

Table 7.4-4. Summary of Selected Sensitivity Analysis Results (Continued)

Modeling Case	TSPA-LA Model Output	Key Uncertain Inputs[a]
Seismic Ground Motion	Expected dose resulting from seismic ground motion over 20,000 years	**Residual stress threshold for SCC (SCCTHRP)**
	Expected dose resulting from combination of seismic ground motion and corrosion processes over 1,000,000 years	**Residual stress threshold (SCCTHRP)** **General corrosion rate (Alloy 22) temperature dependence (WDGCA22)**
Seismic Fault Displacement	Expected dose resulting from fault displacement over 20,000 years	**Groundwater biosphere dose conversion factor (MICTC99)** **Scale factor in ground water specific discharge (SZGWSPDM)**
	Expected dose resulting from fault displacement over 1,000,000 years	**Scale factor in ground water specific discharge (SZGWSPDM)** **Pointer variable for infiltration scenario (INFIL)**

[a] Bold font indicates uncertain parameters that were subject to uncertainty reviews. Name (in parentheses) is the variable name used in the sensitivity analyses (see Table K3-1).

INTENTIONALLY LEFT BLANK

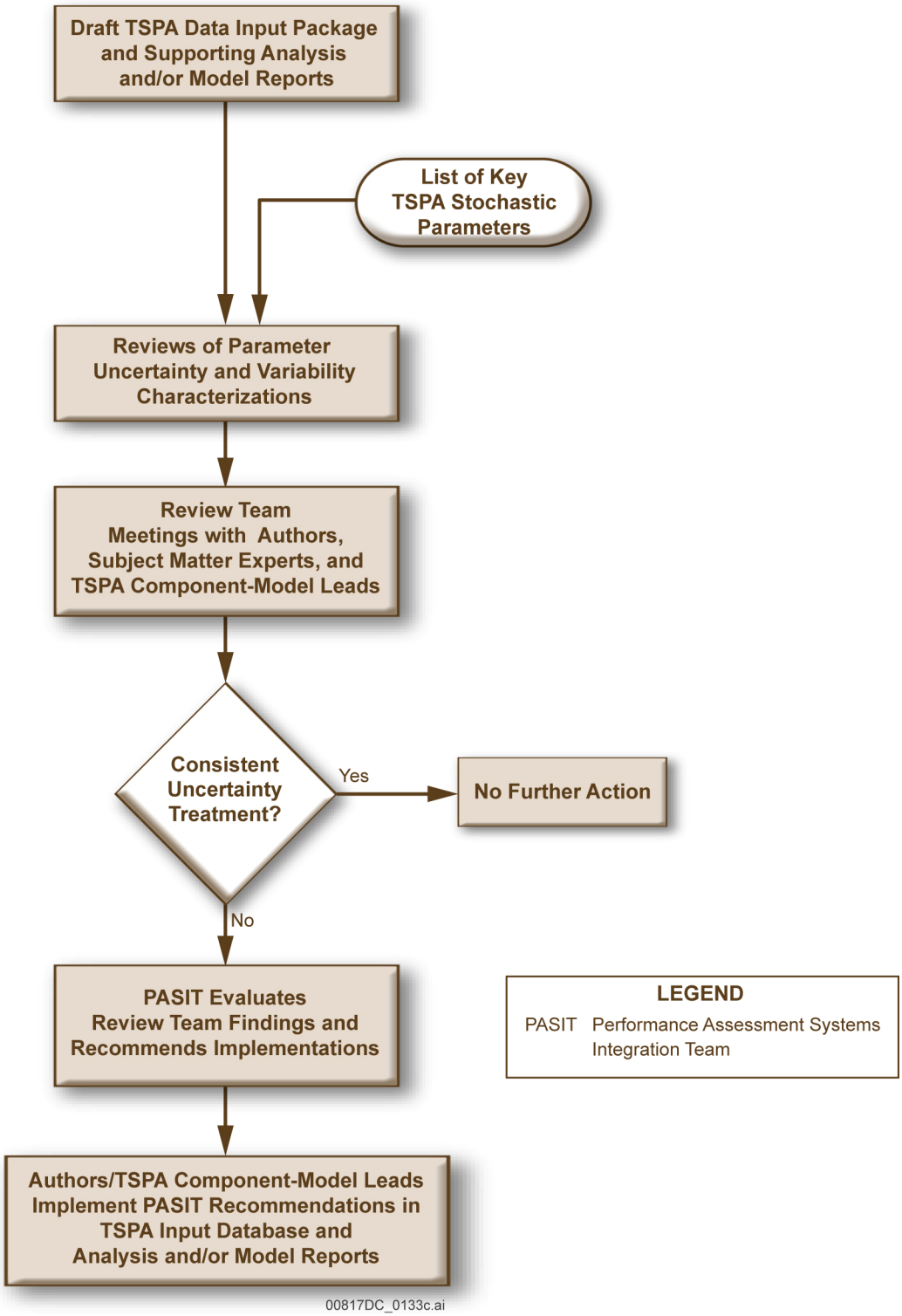

Figure 7.4-1. Uncertainty Characterization Review Process

INTENTIONALLY LEFT BLANK

7.5 SURROGATE WASTE FORM VALIDATION

The purpose of the analyses that follow is to show that the surrogate representation of naval spent fuel (Category 1 DSNF) and the DSNF surrogate, that is the average of DSNF Categories 2 through 11, are appropriate. The averaging of Categories 2 through 11 is related to the spatial averaging that is analyzed in Section 7.3.4.

The TSPA-LA Model represents Categories 2 through 11 of the DSNF using a surrogate fuel, as recommended by *DSNF and Other Waste Form Degradation Abstraction* (BSC 2004 [DIRS 172453], Sections 6.1.12 and 8.1). The abstraction represents each DSNF category with an instantaneous degradation and dissolution model. Therefore, for the analysis of DSNF, all of the radionuclides are available for release after WP failure (i.e., the instantaneous dissolution in the DSNF Waste Form Degradation Abstraction [Table 6-1]). The TSPA-LA Model uses the surrogate inventory for DSNF that is documented in *Initial Radionuclide Inventories* (SNL 2007 [DIRS 180472], Table 7-1[a]).

The analyses below confirm that it is appropriate to represent Categories 2 through 11 of the DSNF with a surrogate that has an average inventory and a bounding instantaneous degradation rate in the TSPA-LA Model. The analysis is conducted by using the TSPA-LA Model to simulate the performance of each of the individual DSNF categories and then comparing the results to the performance of the surrogate. The data used to model each of the individual fuel categories are from *Additional DOE Spent Nuclear Fuel Information in Support of TSPA-LA Analysis* (Loo et al. 2004 [DIRS 168999], Sections 6 and 7).

The analyses also confirm that Zircaloy-clad CSNF adequately represents Category 1 DSNF. Category 1 DSNF, naval spent fuel in the TSPA-LA Model, is represented as Zircaloy-clad CSNF. Section 7.5.3 discusses the analyses using the TSPA-LA Model where the naval source term replaced the CSNF source term for the Drip Shield EF and Igneous Intrusion Modeling Cases. The radionuclide release from naval spent fuel WPs would be expected to be lower than from CSNF WPs because of the robust nature of naval spent fuel, smaller inventory of key dose-producing radionuclides, and lower dissolution rate of naval spent fuel (Gisch 2004 [DIRS 171782]).

7.5.1 Methodology

In order to investigate the relative performance of the categories of DSNF versus the surrogate, the Drip Shield EF Modeling Case was chosen. This case fails one WP and DS at time zero and thus removes the variability of the engineered barrier. Only one DSNF inventory is needed per realization and a direct comparison between DSNF types is possible. This analysis tests whether the surrogate produces dose curves comparable to the sum of the doses from the individual DSNF types weighted by the fraction of WPs of each type.

The model file, v5.000_GS_9.60.100.gsm (output DTN: MO0707TSPADSNF.000 [DIRS 182992]), was modified to have no commercial or high-level waste glass inventory so that differences in dose due to DSNF would not be masked by the CSNF and HLW releases. To simplify the calculation and to focus on the variability due to DSNF, only the largest subregion, Subregion 3, was modeled. The dripping case was chosen because the doses from WPs with dripping are higher. Furthermore, the

aleatory uncertainty was removed because it should have little bearing on the relative performance of DSNF. The epistemic uncertainty was unmodified. The resulting analysis, LA_v5.000_ed_003300_002.gsm (output DTN: MO0707TSPADSNF.000 [DIRS 182992]), used 300 realizations for 11 inventories for one million years and thus required 3,300 simulations.

Figure 7.5-1 shows the results from a 300 realization run with the DSNF surrogate only, which serves as a base case for comparison. A series of analyses, based on the expected performance of each of the DSNF categories, provides confidence that the surrogate fuel used in the TSPA-LA Model is a reasonable representation of all of the DSNF that will be emplaced in the repository. The analyses include: (1) the comparison of the dose from the surrogate fuel with the weighted sum of the doses from the DSNF categories, (2) the comparison of the surrogate fuel with each DSNF fuel category, and (3) the evaluation of impacts from uncertainty parameters (e.g., degradation mechanisms, surface areas, number of WPs, radionuclide inventory, free inventory, and bounding radionuclide inventory). The analyses were conducted using the 300 realization DS early failure simulation (with DSNF inventories only) to compare the DSNF surrogate spent fuel and DSNF Categories 2 through 11 (output DTN: MO0707TSPADSNF.000 [DIRS 182992]).

For naval spent fuel, probabilistic analyses were conducted for the Drip Shield EF and Igneous Intrusion Modeling Cases. The results of failure for a single WP of CSNF were compared with the failure of a single WP of naval spent fuel. In addition, the Naval Nuclear Propulsion Project conducted seismic scenarios to evaluate the use of CSNF as a surrogate for navy spent fuel (Gisch 2004 [DIRS 171782]).

7.5.2 Spent Fuel Categories and Representation in Model

During the last four decades, the DOE and its predecessor agencies have generated approximately 250 varieties of spent fuel from weapons production, nuclear propulsion, and research missions. A method described by Fillmore (1998 [DIRS 104385], Section 2) allowed the grouping of these varieties of DSNF into 16 categories for the repository performance assessment. The 16 DSNF fuel categories were further reduced to 11 categories (DOE 2000 [DIRS 118968], Section 8). The reduction reflects a better understanding of the behavior of DOE fuels under expected repository conditions and allows the combining of some of the 16 DSNF categories. The reduced number of DSNF categories helps streamline repository analyses of the spent fuels. The grouping method used regulatory requirements to identify the parameters that affect the performance of DSNF in the repository and to meet analysis needs for the repository LA. Three fuel parameters (fuel matrix, fuel compound, and fuel-cladding condition) influence the performance of the DSNF in the repository. The grouping methodology categorizes the characteristics of a select number of fuel types by either a bound or by representing a particular characteristic of the whole category. Table 7.5-1 lists the DSNF categories and a typical fuel in the category that best fits the characteristics of the category.

A brief description of the fuel categories follows (DOE 2000 [DIRS 118968]):

Category 1—Classified Navy: NSNF was placed in its own category for several reasons: (1) the design of naval spent fuel is significantly different from other DSNF designs; (2) because of its robust design, naval spent fuel will remain virtually intact well beyond

10,000 years resulting in its impact on repository performance occurring much later than other DSNF designs; and (3) the design of naval spent fuels is classified.

Category 2—Plutonium/Uranium Alloy Fuel: The plutonium/uranium alloy fuels are grouped together because of the alloy microstructure and its effect on grain boundary attacks, stress fractures, and crazing (microcracking). For example, it is uncertain if there will be preferential attacks on the grain boundaries that could result in a large increase in the surface area of uranium-zirconium alloy fuel. However, the zirconium could also stabilize the uranium metal and, thus, this category could perform differently than the uranium-metal fuels. On the other hand, uranium alloyed with ten weight-percent molybdenum corrodes at only one percent of the rate of pure uranium. However, after corrosion starts, molybdenum causes stress fractures and crazing. This increases the matrix porosity and surface area and potentially increases the dissolution rate.

Category 3—Plutonium/Uranium-Carbide Fuel: This category consists primarily of fuels from the Fast Flux Test Facility. The Fast Flux Test Facility fuels are either UC_2 pellets or UC_2 spheres, with helium or sodium bonded between the fuels and cladding. The performance of the carbide particles is uncertain as compared to the Fort St. Vrain fuels (Category 5). Thus, this fuel was placed into its own category. The release rate of this category may be 100 times that from pure uranium-metal fuel. The effective enrichments (including the ^{239}Pu) vary from about 10 to 18 percent ^{235}U.

Category 4—Mixed Oxide Fuel (MOX): MOX fuels are composed of a mixture of uranium and plutonium oxides with various types of cladding. The uranium enrichment is low, but the plutonium content increases the effective enrichment above 15 percent ^{235}U. The Fast Flux Test Facility driver fuel assembly and test fuel assembly contributed to the large quantity of the fuel in this category. Because the fuels were fabricated using techniques similar to that of the commercial oxide fuels, performance of the MOX fuels should be very similar. Because of the high plutonium content, as compared to the uranium-oxide fuel, this fuel was placed into its own category.

Category 5—Uranium/Thorium-Carbide Fuel: This category primarily consists of fuel from the Fort St. Vrain Reactor and fuels from Core 1 and 2 of the Peach Bottom Reactor. Fuel from the General Atomic Gas-Cooled Reactor is also included in this category. The fuel in Category 5 is in the form of carbide particles coated with layers of pyrolytic carbon and it may also have a silicon carbide coating, bonded together by a carbonaceous matrix material. Two types of particles are used: fissile and fertile. The fissile particles contain thorium and approximately 93 percent enriched uranium. The fertile particles contain only thorium. One difference between the Fort St. Vrain and Peach Bottom fuels is that the Peach Bottom particles lack the silicon-carbide coating. The fuel particles in the Fort St. Vrain and Peach Bottom Core 2 fuel assemblies are in excellent condition; however, the fuel particles in the Peach Bottom Core 1 fuel assemblies are in poor condition. Some preliminary tests indicated that up to 60 percent of the particles may have been breached. Thus, the release rate of this category may be ten times the uranium-metal rate (Category 7) because of possible water or carbide reactions. The effective enrichment (including the ^{233}U) level at the end of life varies from about 78 to 83 percent ^{235}U.

Category 6—Uranium/Thorium-Oxide Fuel: Shippingport Light Water Breeder Reactor fuels make up the major inventory of the fuel in Category 6. The Shippingport Light Water Breeder Reactor fuel was used to demonstrate the production of fissile ^{233}U from thorium in a water-cooled reactor. The fuel is composed of uranium oxide, enriched up to 98 percent ^{233}U, mixed with thorium oxide in cylindrically-shaped ceramic pellets. These ceramic pellets are expected to dissolve at a different rate than the standard uranium-oxide fuel and, thus, this fuel was placed into its own category.

Category 7—Uranium-Metal Fuel: The majority of this category consists of zirconium-clad N-Reactor fuel with a small amount of aluminum-clad Single Pass Reactor fuel. Enrichments are less than 2 percent ^{235}U. The majority of the fuels have low burn up. Some uranium target materials are also included in this category.

Category 8—Uranium-Oxide Fuel: This category consists of the fuels removed from commercial reactors or test fuel with uranium-oxide matrices similar to CSNF. In addition, the fuels removed from commercial reactors or test fuels with uranium-oxide matrices that have failed cladding, or are declad, are also included in this category. This category is modeled as CSNF but with a potentially much higher fuel surface area due to the damage or the physical state (small pieces of disrupted fuel) of the fuel. Because enrichment should not alter the release rate for fuels with the same matrix, enrichments from about one to two percent (the commercial range, such as Three Mile Island Reactor fuels) to 93 percent ^{235}U fuel from the High Flux Isotope Reactor and Shippingport pressurized water reactor are included in this category.

Category 9—Aluminum-Based Fuel (Uranium-Aluminide Fuel, Uranium Silicide, and Uranium Oxide in Aluminum): This category consists of fuels with the: (1) uranium aluminide dispersed in a continuous aluminum phase, (2) uranium silicide dispersed in a continuous aluminum phase, and (3) uranium oxide dispersed in a continuous aluminum phase. This category should perform better than uranium-metal fuel (Category 7) depending upon the continuity of the primary aluminum phase and the release rate from each of the phases. Foreign Research Reactor fuels make up a large part of the aluminum-based fuel. The enrichment level varies from about 11 to 93 percent ^{235}U, with the majority of the silicide fuels having less than 20 percent ^{235}U.

Category 10—Miscellaneous Fuel: The DSNFs with unknown matrices are placed in this category. Because of the potential varying matrices, cladding, and condition of this category of fuel, the fuel properties need to be conservatively represented with a dissolution model that reasonably represents this category. Based on the category inventory, the uranium-metal dissolution model is most representative of the dissolution rate of DSNF in this category.

Category 11—Uranium-Zirconium Hydride Fuel: Category 11 contains fuel with the uranium/zirconium hydride matrix. Fuels from the Training Research Isotopes General Atomics reactors make up the majority of the fuel in this category. The uranium-zirconium hydride in this category provides the reactor with its built-in control and inherent safety. The fuel consists of uranium-metal particles dispersed in the zirconium hydride matrix, clad with aluminum, stainless steel, or Incoloy-800, with varying enrichment and weight percents of ^{235}U. Because of the unique uranium/zirconium hydride matrix, this fuel was placed in its own category. This fuel matrix is expected to perform better than the uranium-oxide fuel.

Table 7.5-2 shows the radionuclide inventory for each category (Categories 2 through 11) of DSNF (DOE 2004 [DIRS 169354], Appendix D). The inventory was developed from the total radionuclide inventory in each DSNF category divided by the number of WPs for that category. Table 7.5-2 also shows the DSNF surrogate inventory that is used in the TSPA-LA Model to represent Categories 2 through 11 DSNF.

The number of canisters by canister size for each DSNF category and the total number of WPs per category are presented in Table 7.5-3 (DOE 2004 [DIRS 169354], Appendix D). The primary canister lengths are 10 and 15 ft. The multicanister overpack is used for the N-Reactor DSNF. The multicanister overpack CDSP WP contains two multicanister overpacks and two canisters of HLW in a 15-ft WP. The other two CDSP WPs contain one DSNF canister and four or five canisters of HLW in 10- or 15-ft WPs. The CDSP WP with a 24-in. canister of DSNF contains four canisters of HLW (Table 7.5-3).

A degradation rate for each fuel category was developed and applied to the TSPA-LA Model in order to compare the results of individual categories of DSNF to the DSNF surrogate spent fuel from *Additional DOE Spent Nuclear Fuel Information in Support of TSPA-LA Analysis* (Loo et al. 2004 [DIRS 168999], Section 6). The degradation rate is the product of a dissolution rate times a fuel surface area. The dissolution rate equations and fuel surface areas for each DSNF category are shown in Table 7.5-4.

7.5.3 Naval Spent Fuel, Category 1

Analyses were performed to disposition the use of CSNF as a surrogate for NSNF. These analyses are outlined in Table 7.5-5 and in the following sections. They were performed out to 10,000 years, and a qualitative argument for the extension of the results beyond the 10,000-year compliance period is also presented. The TSPA-LA Model was exercised explicitly using NSNF inventories in place of the CSNF inventory for an early failure case and an igneous intrusion case. The dose results from these cases were compared to show that CSNF inventory bounds the NSNF inventory. Quantitative comparisons of NSNF and CSNF inventories for the major radionuclide contributors to dose for the Volcanic Eruption, Human Intrusion, and Seismic Modeling Cases were made to disposition the use of the CSNF as a surrogate for NSNF for these cases. The Nominal Modeling Case, as it relates to NSNF, is also discussed. The seismic modeling cases were also evaluated by the Naval Nuclear Propulsion Project (Gisch 2004 [DIRS 171782]), and confirmed to be valid as discussed in Section 7.5.3.7.

7.5.3.1 Comparison of the Naval Spent Nuclear Fuel and Commercial Spent Nuclear Fuel Inventories for 10,000 Years and 1,000,000 Years

Radionuclide release rates for an NSNF WP are provided for the first 10,000 years of the compliance period for the early failure case and out to 1,000,000 years for the igneous intrusion case. These release rates, in terms of activities, are plotted on Figures 7.5-2 and 7.5-3 for the radionuclides that are major contributors to the mean annual total dose. Figure 7.5-2 shows that for the early failure case, the activities of the NSNF inventory on a per WP basis are orders of magnitude lower than the activities of the CSNF inventory for the first 10,000 years. The only exception to this is for ^{229}Th for the first 200 years. An extrapolation of the NSNF activities out to 1,000,000 years would show the same behavior.

Figure 7.5-3 shows that for the Igneous Intrusion Modeling Case, the activities of the NSNF inventory on a per WP basis are again generally lower out to 1,000,000 years, although by not as much as was the case for the early failure source term. The activities for ^{229}Th and ^{233}U for the NSNF are higher for the first few thousand years but diverge below the CSNF source term over the majority (i.e. hundreds of thousands of years) of the compliance period. This is because initially the NSNF inventory, on a per WP basis, has more ^{229}Th and ^{233}U than the CSNF inventory (McKenzie 2007 [DIRS 182657]), but the ingrowth of ^{229}Th and ^{233}U from the decay of ^{237}Np is greater for the CSNF because there is more ^{237}Np in the CSNF inventory.

7.5.3.2 Disposition of Commercial Spent Nuclear Fuel as a Surrogate for Naval Spent Nuclear Fuel for the Early Failure Modeling Cases

NSNF was analyzed using inventories, or source terms, supplied by the Navy for radionuclides that are available for release from naval spent fuel. The source terms are based on a hypothetically failed WP of naval spent fuel for the Drip Shield EF and Igneous Intrusion Modeling Cases. These source terms were provided by the Naval Nuclear Provision Program (McKenzie 2007 [DIRS 182657]). The analyses of naval spent fuel are special cases developed to compare CSNF and naval spent fuel for the Drip Shield EF and Igneous Intrusion Modeling Cases. For these analyses, the NSNF source term (radionuclides available for release within a failed WP) was modeled in a failed CSNF WP, and the radionuclides were then subject to all of the transport processes that are applied to dissolved CSNF (e.g., solubility, sorption, and chemistry along the transport pathway from dissolved CSNF to the RMEI) in the TSPA-LA Model.

In the modeled repository, there are 8,213 WPs of CSNF, 417 of which represent naval spent fuel (SNL 2007 [DIRS 180472], Table 6-2[a]). The TSPA-LA Model does not explicitly include naval spent fuel, but bounds its behavior with 417 CSNF WPs that represent naval spent fuel. The special case analyses in this section were conducted to demonstrate that the annual dose from naval spent fuel is bounded by the annual dose from CSNF.

For the validation of CSNF as a surrogate for naval spent fuel for the nondisruptive event cases, the Drip Shield EF Modeling Case was chosen over the Waste Package EF Modeling Case because of the following considerations. First, the transport of radionuclides within the EBS for the Drip Shield EF Modeling Case is advection dominated with some diffusion. The transport of radionuclides within the EBS for the Waste Package EF Modeling Case is diffusion dominated since the DS stays intact. The Waste Package EF Modeling Case would produce lower radionuclide doses compared to the Drip Shield EF Modeling Case and, therefore, can be considered a subset of the Drip Shield EF Modeling Case for the NSNF analysis. In addition, in the TSPA-LA Model, the Waste Package EF Modeling Case applies not only a temperature threshold to transport, but a relative humidity threshold to transport radionuclides from the waste form to the WP outer barrier. Since the naval source term is a release from a failed WP, it is implemented in the TSPA-LA Model by applying the release to the WP transport cell and, therefore, bypasses the relative humidity threshold for transport from the waste form transport cell. The result of using the Waste Package EF Modeling Case for the analysis would be an early release of radionuclides to the accessible environment for the naval source term, which would be inconsistent with a later release of radionuclides for the CSNF source term. The delay in release from the waste form to the WP outer barrier due to the relative humidity threshold for

transport is not implemented in the Drip Shield EF Modeling Case. Therefore, for the Drip Shield EF Modeling Case, the timing of the release of radionuclides to the accessible environment from a failed WP with a CSNF source term is more consistent with the timing of the release from a failed WP where the naval source term has been substituted for the CSNF source term in the WP transport cell.

For the Drip Shield EF Modeling Case, a single DS failure was forced to occur at the first timestep of the simulation. Two simulations were run: one for a single CSNF WP and one for a single WP where the naval source term replaced the CSNF source term. The simulations were run for 10,000 years and used a unified sampling of epistemic and aleatory uncertainty over 300 model realizations. The results, in terms of a mean annual dose over the unified sampling of epistemic and aleatory uncertainty, are shown on Figure 7.5-4. The results show that over a 10,000-year period, the dose associated with the naval source term is less than that of the CSNF source term. At 10,000 years, the mean annual dose from a failed WP with a naval source term is about two orders of magnitude lower than the mean annual dose for a failed CSNF WP, justifying the use of a CSNF WP as a surrogate for a naval WP.

7.5.3.3 Disposition of Commercial Spent Nuclear Fuel as a Surrogate for Naval Spent Nuclear Fuel for the Igneous Intrusion Modeling Case

A similar analysis conducted for the Igneous Intrusion Modeling Case is used to disposition the use of CSNF as a surrogate for NSNF. For both the CSNF and naval source term scenarios, the time of the igneous intrusion was forced to occur at a specified timestep, and a single WP was failed. The simulations were run for 10,000 years and used a unified sampling of epistemic and aleatory uncertainty over 300 model realizations. The results, in terms of a mean annual dose over the unified sampling of epistemic and aleatory uncertainty, are shown on Figure 7.5-5. As was the case for the Drip Shield EF Modeling Case, the results for the Igneous Intrusion Modeling Case show that at over a 10,000-year period the dose associated with the naval source term is less than that of the CSNF source term, again justifying the use of a CSNF WP as a surrogate for a naval WP.

7.5.3.4 Disposition of Commercial Spent Nuclear Fuel as a Surrogate for Naval Spent Nuclear Fuel for the Volcanic Eruption Modeling Case

The disposition of CSNF as a surrogate for NSNF for the Volcanic Eruption Modeling Case is done by showing that the NSNF inventory for the radionuclides that are the major contributors to the mean annual dose is less than the CSNF inventory and by taking credit for the robustness of the naval WP. Figure 8.2-10 shows ^{239}Pu and ^{241}Am, early in time, and ^{226}Ra, ^{229}Th, ^{237}Np, ^{126}Sn, and ^{238}U, later in time, as the major contributors to the volcanic eruptive total mean annual dose. The inventory activities for these same radionuclides are plotted on Figure 7.5-6 using the igneous NSNF and CSNF source terms. With respect to when each of these radionuclides breakthrough in terms of the eruptive dose, each has a lower activity for the NSNF source term than for the CSNF. Therefore, the use of CSNF as a surrogate for NSNF for the Volcanic Eruption Modeling Case is justified.

7.5.3.5 Disposition of Commercial Spent Nuclear Fuel as a Surrogate for Naval Spent Nuclear Fuel for the Human Intrusion Modeling Case

The disposition of CSNF as a surrogate for NSNF for the Human Intrusion Modeling Case is done by showing that the NSNF inventory for the radionuclides that are the major contributors to the mean annual dose is lower than the CSNF inventory and by taking credit for the robustness of the naval WP. Figure 8.1-13 shows the ^{99}Tc; ^{129}I; ^{79}Se near the time of the event, and ^{242}Pu, ^{135}Cs, and ^{237}Np, later in time, as the major contributors to the human intrusive total mean annual dose. The inventory activities for these same radionuclides are plotted on Figure 7.5-7 using the igneous NSNF and CSNF source terms. With respect to when each of these radionuclides breaks through in terms of the human intrusion dose, each has a lower activity for the NSNF source term than for the CSNF. Therefore, in combination with the robustness of the naval WP, the use of CSNF as a surrogate for NSNF for the Human Intrusion Modeling Case is justified.

7.5.3.6 Disposition of Commercial Spent Nuclear Fuel as a Surrogate for Naval Spent Nuclear Fuel for the Nominal Modeling Case

The use of CSNF as a surrogate for NSNF for the first 10,000 years of the Nominal Modeling Case is justified because there are no WP failures during this time period, and because the naval WP is more robust than the commercial WP as discussed in the naval classified technical support document. The 1,000,000 year Nominal Modeling Case is a stylized case (see Section 8.2.1) where the WP fails by SCC and general corrosion sometime after the first 10,000 years. These effects are accounted for in the 1,000,000 year Seismic GM Modeling Case. The use of CSNF as a surrogate for NSNF for the 1,000,000 year Nominal Modeling Case is justified because of the NSNF is adequately represented by CSNF in the early failure cases, and again because the naval WP is more robust than the commercial WP.

7.5.3.7 Disposition of Commercial Spent Nuclear Fuel as a Surrogate for Naval Spent Nuclear Fuel for the Seismic Ground Motion Modeling Cases.

The disposition of CSNF as a surrogate for NSNF for the Seismic GM Modeling Case is done by showing that the NSNF inventory for the radionuclides that are the major contributors to the mean annual dose is lower than the CSNF inventory and by taking credit for the robustness of the naval WP. Figure 8.2-12 shows ^{129}I, ^{242}Pu, ^{237}Np, ^{226}Ra, and ^{135}Cs as the major contributors to the seismic ground motion total mean annual dose at 1,000,000 years. Figure 8.2-12 also shows ^{99}Tc, ^{129}I, and ^{79}Se as the major contributors to the seismic ground motion total peak mean annual dose around 225,000 years. The inventory activities for these same radionuclides are plotted on Figure 7.5-8 using the igneous NSNF and CSNF source terms. With respect to when each of these radionuclides breaks through in terms of the seismic ground motion dose, each has a lower activity for the NSNF source term than for the CSNF. Therefore, in combination with the robustness of the naval WP, the use of CSNF as a surrogate for NSNF for the Seismic GM Modeling Case is justified. In addition to the analyses presented here, three seismic scenario class cases were evaluated by the Naval Nuclear Propulsion Project (Gisch 2004 [DIRS 171782]). The three modeling cases are for a large seismic event: (1) without the formation of a rock blanket, (2) with the formation of a rock blanket, and (3) with faulting through a WP. For each modeling case, the release rate of the key isotopes from naval SNF is bounded by the release rate of the key isotopes from CSNF.

7.5.4 U.S. Department of Energy Spent Fuel, Categories 2 through 11

The analyses of DSNF are based on several 300 realization simulations of the Drip Shield EF Modeling Case. In these simulations, aleatory uncertainty is fixed on percolation Subregion 3 in a dripping environment, where a single CDSP WP and the overlying DS are failed, allowing advective and diffusive transport from the waste. One simulation is performed for each category of DSNF and for the DSNF surrogate, with each simulation including 300 realizations, one for each element of the LHS for epistemic parameters. The HLW in the CDSP WP is not included in the analyses, so the results show the annual dose from the DSNF only. The analysis computes a mean annual dose for each simulation, and compares the mean annual dose for each DSNF category to the mean annual dose for the DSNF surrogate. In these analyses, the term mean annual dose refers to the average dose at each time conditional on the fixed aleatory quantities; for brevity the term mean annual dose is used to describe this quantity.

The dose from each category is expected to differ from the surrogate because of differences in (1) the degradation rate of the matrix, (2) fraction of bound inventory, and (3) the inventory of key isotopes per WP. Some categories will yield lower doses and some will yield higher doses, but the weighted sum of the dose from all categories should be close to the dose from the surrogate. This analysis confirms that the dose from the surrogate adequately represents or bounds the weighted sum of the dose from all categories.

The degradation rate of the matrix for the surrogate is set to instantaneous, so early dose from the surrogate that is controlled by degradation rate should bound or be equal to the dose from individual categories. The effect of degradation rate is only expected to be seen for the categories that have degradation rates that are slow compared to the 250 year timestep. Figure 7.5-9 shows the degradation rates of the categories, and only categories 4 and 6 have rates slow enough to require multiple times steps to degrade all the fuel. These two categories are expected to have lower doses during early times before all the fuel has degraded. The fraction of bound inventory parameter is important only for the slowly degrading fuels.

There are three ways the inventory can influence dose: (1) for highly soluble, low sorbing isotopes, the early dose should be proportional to the inventory released per WP; (2) for solubility controlled elements, the isotopic abundance should determine the relative release of the isotope; and (3) for long-lived, low solubility isotopes, the inventory and flow rate will determine how long it takes to deplete the WP. Looking at the mean annual dose from surrogate DSNF (Figure 7.5-1), it can be seen that the low solubility, highly sorbing isotopes ^{239}Pu and ^{226}Ra dominate at late times. The peak mean dose comes from ^{239}Pu with only a minor contribution from ^{233}U. The late time ^{226}Ra comes from decay of ^{234}U and ^{230}Th. Doses from ^{233}U and ^{234}U do not go above 10^{-3} mrem because these isotopes share solubility with the abundant but long-lived ^{238}U. From this, we would expect that the fuel that is more highly burned than the surrogate would have higher doses because of increased inventory per WP of ^{99}Tc and ^{237}Np. Other fuels that are based on ^{239}Pu or ^{233}U instead of ^{235}U for fission are also expected to result in significantly different dose from these isotopes. Although it is difficult to see on a linear time scale, the highly soluble and low sorbing isotopes ^{14}C and ^{99}Tc dominate the early mean annual dose (less than 5,000 years), and the moderately soluble and sorbing ^{237}Np dominates at 10,000 years.

Figure 7.5-10 shows the comparison of one WP of Category 2 (plutonium/uranium alloy) DSNF with one WP of DSNF surrogate. The Category 2 DSNF has a higher mean annual dose curve because of a higher per WP inventory of ^{14}C and ^{99}Tc from higher burn-up. The mean annual dose at late times is higher because of the weight percent of ^{234}U (4 percent for Category 2, 0.06 percent for the surrogate, calculated from information in Table 7.5-2) results in higher release of ^{234}U and its daughters, ^{230}Th and ^{226}Ra.

Figure 7.5-11 shows the comparison of one WP of Category 3 (plutonium/uranium carbide) DSNF with one WP of DSNF surrogate. The Category 3 DSNF mean annual dose curve is slightly lower than the surrogate because of lower per WP inventories of key dose contributors. This is in part due to the small amount of Category 3 fuel per WP (1.5×10^4g versus 7.4×10^5g for the surrogate) (Table 7.5-2). Late time mean annual dose may also be lower than the surrogate because of lower ^{234}U weight percent (0.01 percent, calculated from information in Table 7.5-2) leading to lower ^{230}Th and ^{226}Ra release.

Figure 7.5-12 shows the comparison of one WP of Category 4 (mixed oxide) DSNF with one WP of DSNF surrogate. The Category 4 DSNF has a lower mean annual dose curve up to about 10,000 years because the calculated degradation rate for Category 4 is less than 1×10^{-4} per year compared to the instantaneous degradation rate of the DSNF surrogate. The Category 4 DSNF mean annual dose is slightly higher after 100,000 years because of higher per WP inventories of long-lived radionuclides such as ^{226}Ra, ^{237}Np, and ^{230}Th (Table 7.5-2). This is due in part to the higher percent of ^{234}U in the fuel (0.26% for Category 4, 0.06% for the surrogate, calculated from information in Table 7.5-2) leading to higher late time ^{230}Th and ^{226}Ra release.

Figure 7.5-13 shows the comparison of one WP of Category 5 (uranium/thorium carbide) DSNF with one WP of DSNF surrogate. The Category 5 DSNF has a lower mean annual dose curve after 20,000 years when compared to the DSNF surrogate. The mean annual dose curve is slightly higher for Category 5 DSNF between 3,000 years and 20,000 years because of ^{233}U. The per WP inventories of ^{234}U, ^{235}U, ^{236}U, and ^{238}U are lower in Category 5 than for the DSNF surrogate (Table 7.5-2). This allows much more ^{233}U to be dissolved and transported in the Category 5 case because all uranium species share the same solubility limit in proportion to their inventory.

Figure 7.5-14 shows the comparison of one WP of Category 6 (uranium/thorium oxide) DSNF with one WP of DSNF surrogate. The Category 6 DSNF has a higher mean annual dose curve because of a higher per WP inventory of ^{233}U. The inventory of ^{238}U is significantly lower (than the surrogate) for Category 6, allowing more of the other uranium species to be dissolved and transported. Category 6 DSNF has a significantly higher ^{233}U per WP inventory than the other nine categories of DSNF. Category 6 DSNF contains about 92 percent of the total ^{233}U for all 10 categories on a per-WP basis (calculated from information in Table 7.5-2). Thus, Category 6 DSNF has a significantly higher ^{233}U inventory than the DSNF surrogate. The initial inventory of ^{233}U for the DSNF surrogate is 538 g per WP. The initial inventory of ^{233}U for Category 6 DSNF is 31,600 g per WP (Table 7.5-2).

Figure 7.5-15 shows the comparison of one WP of Category 7 (uranium metal) DSNF with one WP of DSNF surrogate. The mean annual dose curve is higher for Category 7 DSNF after about 100,000 years because of higher per WP inventories of long-lived radionuclides such as ^{237}Np,

^{226}Ra, and ^{230}Th (which decays to ^{226}Ra). This per WP concentration is larger in part due to the much larger amount of Category 7 fuel in the WP than the other fuels. The total inventory of Category 7 is 9.7×10^6g per WP while the next largest amount is Category 6 with 9.5×10^5g per WP and the surrogate having 7.4×10^5g per WP (Table 7.5-2).

Figure 7.5-16 shows the comparison of one WP of Category 8 (uranium oxide) DSNF with one WP of DSNF surrogate. The Category 8 DSNF has a slightly lower mean annual dose curve than the surrogate, but it follows the surrogate very well.

Figure 7.5-17 shows the comparison of one WP of Category 9 (aluminum-based) DSNF with one WP of DSNF surrogate. The Category 9 DSNF has a lower mean annual dose curve than the surrogate during the first 10,000 years because of a lower per WP inventory of key contributors (i.e., ^{99}Tc, ^{129}I, and ^{14}C). The mean annual dose curve is lower for Category 9 DSNF after 10,000 years because of lower per WP inventories of long-lived radionuclides such as ^{226}Ra, ^{234}U, ^{237}Np, ^{239}Pu, ^{233}U, and ^{230}Th. Category 9 fuel has one of the lowest amounts of fuel per WP (1.6×10^4g) compared to the surrogate (7.4×10^5g) (Table 7.5-2).

Figure 7.5-18 shows the comparison of one WP of Category 10 (miscellaneous) DSNF with one WP of DSNF surrogate. The Category 10 DSNF has a slightly higher mean annual dose curve because of higher per WP inventories of key contributors (i.e., ^{99}Tc, ^{233}U, and ^{14}C).

Figure 7.5-19 shows the comparison of one WP of Category 11 (uranium-zirconium hydride) DSNF with one WP of DSNF surrogate. The Category 11 DSNF has a lower mean annual dose curve during the first 10,000 years because of lower per WP inventories of key contributors (i.e., ^{99}Tc, ^{129}I, and ^{14}C), and because the calculated degradation rate for Category 11 is less than 1.0 per year. The mean annual dose curve is lower than the surrogate after 10,000 years because of lower per WP inventories of ^{237}Np, ^{233}U, ^{234}U, ^{226}Ra, and ^{239}Pu. Category 11 fuel has a low amount of fuel per WP (2.2×10^4g) (Table 7.5-2).

The analyses of Categories 2 through 11 show that the DSNF surrogate is a reasonable representation of all categories except Categories 2, 6, and 7 where significant differences occur due to higher per WP inventories of key dose contributors. However, Category 2 DSNF only accounts for about 0.5 percent of the total WPs of DSNF, Category 6 DSNF fills only 1.6 percent of the WPs, and Category 7 DSNF fills 6.6 percent of the WPs (Table 7.5-3). When the weighted sum (based on the number of WPs) is taken of all the individual DSNF categories, the resulting weighted sum dose curve matches up reasonably well with the DSNF surrogate (Figure 7.5-20). The weighted sum dose curve is dominated by the contribution from the Category 7 fuel at early and late times, and by the contribution from the Category 6 fuel from about 2,500 to 268,000 years. The mean dose of the surrogate bounds that of the weighted sum from about 40,000 years to about 400,000 years. The peak mean dose from the surrogate has the same magnitude as the weighted sum, but occurs later in the simulation.

The results for DSNF have been shown for the Drip Shield EF Modeling Case because a direct comparison between releases from single WPs in the same thermohydrology subregion (bin) is possible. The relative performance of DSNF in other bins is expected to be similar because the factors limiting release, available per WP inventory and solubility, do not vary significantly within bins. In the other modeling cases, multiple WPs in several bins are breached at different

times (Section 6.1.2). However, in these modeling cases, an approximation is made that the mean annual dose history from *n* breached WPs in the same bin is equal to the mean annual dose history from one breached WP in that bin times *n*. Thus it would be expected that the mean annual dose history from a single DS early failure would be similar to 1/*n* times the mean annual dose history from either a seismic or igneous event that occurs at time 0. The relative performance of the DSNF surrogate versus the Categories 2 through 11 fuels in the igneous and seismic cases is thus expected to be similar to the Drip Shield EF Modeling Case.

7.5.5 Selected Sensitivity Analyses

Sensitivity analyses for selected DSNF categories were performed to further build confidence in the TSPA-LA Model and to investigate how changing uncertain parameters (e.g., degradation rate, fuel surface area, free inventory, bounding inventory, and number of WPs) would affect the results (output DTN: MO0707TSPADSNF.000 [DIRS 182992]). The categories selected include: (1) uranium-metal DSNF, because it consists of a majority of the fuel (about 87 percent by metric tons of heavy metal), it has a free inventory as the remaining cladding degrades, and it increases surface area as it degrades; (2) uranium/thorium-carbide DSNF because of its slow degradation rate; and (3) aluminum-based DSNF because of the uncertainty in the number of WPs needed for disposal. The major contributors to mean annual dose are also examined for three categories of DSNF.

Figure 7.5-9 shows a comparison of the mean degradation rates for Categories 2 through 11 DSNF (Table 7.5-4), for the air alteration rate for Categories 5 and 7, and for the bounding surface area for Category 7. Table 7.5-6 contains the air alteration rates for Category 5 DSNF (uranium/thorium-carbide DSNF) and Category 7 DSNF (uranium-metal DSNF). These were applied to the TSPA-LA Model to provide comparisons with the nominal dissolution models of the same categories (Figures 7.5-21 and 7.5-22). The air alteration rate refers to the air oxidation rate of the DSNF under the repository conditions from *Additional DOE Spent Nuclear Fuel Information in Support of TSPA-LA Analysis* (Loo et al. 2004 [DIRS 168999], Section 7.3). Here it is interesting to note that the air alteration rate of Category 5 DSNF is extremely low and would affect its release of ^{233}U. Sensitivity runs were conducted for Category 7 DSNF because it represents 87 percent of the total DSNF (by mass) and for Category 5 DSNF because of its low air alteration rate.

Two model runs were performed using the Category 7 DSNF inventory. One used the Category 7 air alteration dissolution rate and the other used instantaneous dissolution (Table 7.5-6). The results are shown on Figure 7.5-21. On Figure 7.5-21, the mean annual dose curves are stacked on top of one another. This occurs because the calculated nominal degradation rate for Category 7 starts out greater than 1.0 per year, which equates to instantaneous degradation. In addition, the calculated air alteration rate starts out at about 0.2 per year, which equates to instantaneous degradation when applied over the first 250-year timestep.

The same analysis was performed for Category 5 DSNF (Tables 7.5-4 and 7.5-6). On Figure 7.5-22, the nominal and instantaneous dissolution rates produce mean annual dose results that plot on top of each other. This occurs because the calculated nominal degradation rate for Category 5 starts out greater than 1.0 per year, which equates to instantaneous degradation. The mean annual dose curve for air alteration is much lower than the nominal degradation because

the calculated air alteration rate starts out at about 8×10^{-11} per year, causing the fuel to degrade slowly over time.

A bounding fuel surface area of 2.8×10^{-4} m^2/g for Category 7 DSNF (uranium-metal DSNF) was used to compare the degradation rate to results using the nominal fuel surface area, which is 7.0×10^{-5} m^2/g (Table 7.5-4). The results show that there is no effect from the uncertainty in the surface area of uranium-metal DSNF (Figure 7.5-23). This occurs because the calculated degradation rates for both the nominal and bounding surface areas for Category 7 start out greater than 1.0 per year, which equates to instantaneous degradation.

For Category 7 (uranium-metal DSNF), the nominal free inventory fraction is 0.001. This parameter was changed to a bounding value of 0.01 for comparison. The nominal free and bounding free inventories refer to the fraction of radionuclide inventory that may be available immediately for transport from the fuel when the WP is breached, as referenced from *Additional DOE Spent Nuclear Fuel Information in Support of TSPA-LA Analysis* (Loo et al. 2004 [DIRS 168999], Section 7.5). A comparison of the nominal and bounding free radionuclide inventory for Category 7 (uranium metal) DSNF is shown on Figure 7.5-24. The nominal and bounding curves plot on top of each other because the calculated degradation rate for Category 7 starts out greater than 1.0 per year.

A bounding number of WPs (i.e., 2,030) (DOE 2004 [DIRS 169354], Appendix F) for Category 9 DSNF (aluminum-based DSNF) was used in the TSPA-LA Model to compare results with the nominal number of WPs (i.e., 1,415) (Table 7.5-3). This sensitivity analysis was conducted due to the uncertain number of WPs for the aluminum-based DSNF. The results show that the mean annual dose decreases slightly as the number of WPs increases because the radionuclide inventory is spread over more WPs (Figure 7.5-25). A similar run was performed with the minimum number of WPs (i.e., 1,016) (DOE 2004 [DIRS 169354], Appendix F). The results show that the mean annual dose increases slightly as the number of WPs decreases because the radionuclide inventory is concentrated in fewer WPs.

A similar analysis was conducted for Category 7 DSNF due to the uncertainty in the radionuclide inventory. Table 7.5-7 contains the nominal and bounding radionuclide inventories for Category 7 DSNF (uranium-metal DSNF). A plot comparing the mean annual dose curves of these inventories is shown on Figure 7.5-26. The bounding inventory was developed with the intention of bounding the actual source term for Category 7 DSNF (DOE 2004 [DIRS 169354], Appendix D). The bounding mean annual dose curve increased slightly, reflecting an increase in radionuclide inventory.

Figure 7.5-27 shows a 1,000,000-year plot of the top dose producing radionuclides that contribute to mean annual dose from HLW only. Here it is seen that the five HLW canisters contribute about the same to the mean annual dose as one canister of DSNF surrogate (compare to Figure 7.5-1). The major contributor to mean annual dose during the first 3,000 years is ^{99}Tc, and then ^{239}Pu dominates the mean annual dose curve until about 300,000 years. After that, ^{226}Ra, ^{234}U, ^{237}Np, and ^{242}Pu dominate the mean annual dose. Note that ^{14}C does not contribute to mean annual dose because it has a zero inventory for HLW.

Figure 7.5-28 shows a 1,000,000-year plot of the top dose producing radionuclides that contribute to the mean annual dose from Category 7, uranium-metal DSNF. The key mean annual dose contributors from Category 7 DSNF are similar to the DSNF surrogate. The major contributor to mean annual dose is ^{14}C and ^{99}Tc until about 10,000 years, and then ^{237}Np, ^{239}Pu, and ^{226}Ra dominate the mean annual dose curve in the later years.

Figure 7.5-29 shows a 1,000,000-year plot of the top dose producing radionuclides that contribute to the mean annual dose from Category 5, uranium/thorium-carbide DSNF. The major contributors to mean annual dose during the first 1,000 years are ^{99}Tc and ^{129}I. After 1,000 years, ^{233}U and ^{226}Ra dominate the mean annual dose curve. As explained in Section 7.5.4, the mean annual dose for ^{233}U is much higher for Category 5 because the inventory of ^{238}U is about three orders of magnitude lower for Category 5 than it is for the surrogate. This allows much more ^{233}U to be dissolved and transported in the Category 5 case because all uranium species have the same solubility limit in proportion to their inventory.

Figure 7.5-30 shows a 1,000,000-year plot of the top dose producing radionuclides that contribute to mean annual dose from Category 6, uranium/thorium-oxide DSNF. The major contributors to mean annual dose during the first 1,000 years are ^{14}C and ^{99}Tc, and then ^{233}U dominates thereafter because of a much higher inventory of ^{233}U and a lower inventory of ^{238}U.

7.5.6 Summary of Results for U.S. Department of Energy Spent Fuel

The result for naval spent fuel in comparison to Zircaloy-clad CSNF shows that the CSNF bounds the results of naval spent fuel for both the nondisruptive and disruptive event modeling cases. Additional analyses performed by the Naval Nuclear Propulsion Project confirm the use of CSNF as a surrogate for naval spent fuel for the seismic scenarios (Gisch 2004 [DIRS 171782]). The representation of naval spent fuel by CSNF as its surrogate in the TSPA-LA Model adequately bounds the behavior of naval spent fuel (Section 7.5.3).

Figure 7.5-20 shows a comparison of a single WP of DSNF surrogate with the weighted sum of the mean annual dose from DSNF Categories 2 through 11. The weighting of the mean annual dose in each category is based on the number of WPs in the category (Table 7.5-3). The weighted-sum lines up well with the surrogate curve, and has about the same peak mean dose. The current DSNF surrogate radionuclide inventory is based on *Source Term Estimates for DOE Spent Nuclear Fuels* (DOE 2003 [DIRS 163377]). These inventories were updated in *Source Term Estimates for DOE Spent Nuclear Fuels* (DOE 2004 [DIRS 169354]). The DSNF surrogate based on Revision 1 inventories is also plotted on Figure 7.5-20 for comparison.

The weighted-sum of the mean annual dose curves from DSNF Categories 2 through 11 is slightly higher than the surrogate mean annual dose curve at about 10,000 years. This is primarily due to the influence of Category 6 DSNF (Figure 7.5-14) and to a lesser extent Category 5 DSNF (Figure 7.5-13) and their high contribution to mean annual dose from ^{233}U (Figures 7.5-30 and 7.5-29). However, it still results in a similar peak mean dose as the surrogate mean annual dose curve.

Although for some DSNF, such as Categories 2, 6, 7, and 10, where the mean annual dose history shows a higher mean annual dose as compared to the surrogate, the number of WPs in these categories is much lower than the total number of DSNF WPs. These categories make up about 9 percent of the total number of DSNF WPs (Table 7.5-3). Thus, the probability of a WP failure in one of these categories is lower when compared to the probability of WP failure in Categories 3, 4, 5, 8, 9, and 11, which make up about 91 percent of the total number of DSNF WPs. Overall, Figure 7.5-20 shows that the DSNF surrogate is a reasonable representation of the combination of the ten DSNF categories.

INTENTIONALLY LEFT BLANK

Table 7.5-1. U.S. Department of Energy Spent Fuel Categories Analyzed for the TSPA-LA Model[a,b]

Category	Fuel Category/Fuel Matrix	Typical Fuel in Category	Mass (MTHM)[c]	Percent of Total
1	Naval nuclear fuel	Naval Nuclear Fuel	70[b]	2.88
2	Plutonium/uranium alloy	Enrico Fermi Reactor (FERMI) Core 1 and 2 (standard fuel subassembly)	4.58	0.19
3	Plutonium/uranium carbide	Fast Flux Test Facility Test Fuel Assembly (FFTF-TFA-FC-1)	0.0765	0.003
4	Mixed oxide fuel (plutonium/ uranium oxide and plutonium oxide)	Fast Flux Test Facility Driver Fuel Assembly (FFTF-DFA/TDFA)	12.0	0.49
5	Uranium/thorium carbide	Fort St. Vrain Reactor	26.3	1.08
6	Uranium/thorium oxide	Shippingport Light Water Breeder Reactor (Reflect. IV)	50.2	2.06
7	Uranium metal	N-Reactor	2,110	86.77
8	Uranium oxide	Three Mile Island (TMI-2) Core Debris	134	5.51
9	Aluminum based (UAlx, U_3Si_2, uranium oxide in aluminum)	Foreign Research Reactor Pin Cluster (Canada)	22.3	0.92
10	Miscellaneous	Miscellaneous Radioactive Scrap Waste Facility Fuel	0.438	0.02
11	Uranium-zirconium hydride	Training Research Isotopes General Atomics (TRIGA)	1.95	0.08

[a] *Additional DOE Spent Nuclear Fuel Information in Support of TSPA-LA Analysis* (Loo et al. 2004 [DIRS 168999], Table 5-1).

[b] *DSNF and Other Waste Form Degradation Abstraction* (BSC 2004 [DIRS 172453], Section 6.2) states that naval spent fuel represents approximately one-tenth of one percent of the MTHM inventory in the repository. Based on *The Nuclear Waste Policy Act, as Amended, with Appropriations Acts Appended* (DOE 1995 [DIRS 122137], Section 114), the repository contains 70,000 MTHM and the approximate naval mass is 70 MTHM.

[c] MTHM from *Source Term Estimates for DOE Spent Nuclear Fuels* (DOE 2004 [DIRS 169354], Appendix D, pp. D-3 through D-567). Summed heavy metal mass end of life values from each worksheet for TSPA Categories 2 to 11, excluding bare fuel transfers.

NOTE: The total number of WPs is provided in Table 7.5-3.

Table 7.5-2. Radionuclide Inventory for Each U.S. Department of Energy Spent Fuel Category and the U.S. Department of Energy Surrogate Spent Fuel (grams/waste package)[a]

Radionuclide	Category 1 (g/WP)	Category 2 (g/WP)	Category 3 (g/WP)	Category 4 (g/WP)	Category 5 (g/WP)	Category 6 (g/WP)
^{227}Ac	NA	1.34E-05	1.47E-10	1.81E-05	8.94E-05	1.41E-02
^{241}Am	NA	2.42E+02	6.35E+01	1.60E+03	1.50E+00	4.28E+01
^{243}Am	NA	3.61E-01	9.02E-01	4.68E+01	3.73E-01	1.41E+00
^{14}C	NA	8.86E+00	9.78E-03	1.43E+01	8.37E-03	6.76E-01
^{36}Cl	NA	1.00E-02	1.74E-05	3.65E+01	5.23E-02	1.75E+00
^{245}Cm	NA	9.97E-05	1.72E-02	1.68E-01	3.78E-02	3.56E-03
^{135}Cs	NA	4.31E+02	6.95E+01	4.89E+02	3.47E+01	2.63E+02
^{137}Cs	NA	3.45E+02	2.67E+01	2.07E+02	2.23E+01	1.73E+02
^{129}I	NA	1.81E+02	1.22E+01	8.24E+01	9.25E+00	9.37E+01
^{237}Np	NA	3.12E+02	8.99E+00	1.59E+02	2.88E+01	5.64E+00
^{231}Pa	NA	3.34E-02	4.50E-07	3.20E-02	1.62E-01	2.63E+01
^{238}Pu	NA	1.04E+01	1.42E+00	5.08E+01	1.48E+01	3.22E+00
^{239}Pu	NA	1.21E+04	3.28E+03	1.90E+04	3.54E+00	1.19E+02
^{240}Pu	NA	1.29E+03	7.41E+02	3.87E+03	1.94E+00	2.27E+01
^{241}Pu	NA	1.18E+01	3.59E+01	3.10E+02	2.50E-01	8.20E+00
^{242}Pu	NA	1.82E+01	1.38E+01	2.60E+02	1.60E+00	1.07E+01
^{226}Ra	NA	1.05E-03	1.39E-08	5.38E-05	5.31E-06	2.36E-04
^{228}Ra	NA	1.54E-07	1.52E-15	1.16E-06	5.46E-06	1.75E-04
^{79}Se	NA	3.39E+01	1.11E+00	1.12E+01	2.22E+00	2.40E+01
^{126}Sn	NA	5.33E+01	6.49E+00	3.46E+01	3.16E+00	3.65E+01
^{90}Sr	NA	1.87E+02	6.00E+00	8.13E+01	1.33E+01	1.09E+02
^{99}Tc	NA	1.04E+03	3.90E+01	3.72E+02	3.18E+01	2.05E+02
^{229}Th	NA	1.14E-03	2.17E-08	5.37E-03	8.78E-02	3.23E+00
^{230}Th	NA	2.91E+00	8.71E-05	1.88E-01	1.59E-02	5.85E-01
^{232}Th	NA	3.82E+02	4.92E-06	2.88E+03	4.21E+04	9.07E+05
^{232}U	NA	1.51E-04	9.55E-05	5.41E-03	1.13E-01	1.73E+01
^{233}U	NA	3.34E+00	1.02E-04	1.97E+01	3.45E+02	3.16E+04
^{234}U	NA	1.33E+04	1.17E+00	1.09E+03	7.59E+01	1.39E+03
^{235}U	NA	5.20E+04	1.90E+01	1.42E+05	3.10E+03	4.88E+03
^{236}U	NA	1.54E+04	4.71E+00	1.93E+03	2.16E+02	8.31E+01
^{238}U	NA	2.20E+05	1.08E+04	2.37E+05	2.54E+02	6.03E+03
Totals:	NA	3.17E+05	1.51E+04	4.12E+05	4.63E+04	9.52E+05

Table 7.5-2. Radionuclide Inventory for Each U.S. Department of Energy Spent Fuel Category and the U.S. Department of Energy Surrogate Spent Fuel (grams/waste package)[a] (Continued)

Radionuclide	Category 7 (g/WP)	Category 8 (g/WP)	Category 9 (g/WP)	Category 10 (g/WP)	Category 11 (g/WP)	Surrogate[b] (g/WP)
^{227}Ac	6.71E-07	5.44E-07	5.72E-08	4.40E-05	8.57E-08	1.22E-03
^{241}Am	1.01E+03	1.29E+02	6.52E+00	2.01E+02	2.41E+00	2.18E+02
^{243}Am	8.72E+00	8.39E+00	1.36E-01	1.83E+01	6.16E-02	6.73E+00
^{14}C	3.17E+00	8.47E-01	2.42E-04	2.17E+00	3.81E-02	1.81E+00
^{36}Cl	5.17E+00	1.69E+00	3.13E-05	5.31E+00	1.09E-01	4.23E+00
^{245}Cm	3.50E-02	2.98E-01	6.05E-03	1.42E+00	8.90E-04	9.25E-02
^{135}Cs	3.12E+02	5.98E+01	1.31E+01	9.54E+02	3.51E+01	9.74E+01
^{137}Cs	3.46E+02	5.29E+01	8.76E+01	3.86E+02	2.86E+01	9.72E+01
^{129}I	1.73E+02	2.12E+01	1.60E+01	1.58E+02	5.83E+00	3.56E+01
^{237}Np	4.56E+02	5.36E+01	6.41E+01	1.34E+02	8.69E+00	8.14E+01
^{231}Pa	1.95E-03	1.32E-03	2.04E-04	1.16E-01	2.40E-04	2.14E+00
^{238}Pu	3.67E+01	1.13E+01	7.65E+00	9.87E+00	1.12E+00	1.25E+01
^{239}Pu	1.64E+04	8.16E+02	1.15E+02	8.37E+03	9.96E+01	2.21E+03
^{240}Pu	3.46E+03	2.12E+02	1.66E+01	2.10E+02	1.16E+01	4.35E+02
^{241}Pu	9.82E+01	1.65E+01	3.45E+00	1.40E+01	1.35E+00	2.92E+01
^{242}Pu	1.29E+02	4.49E+01	1.08E+00	4.54E+01	5.59E-01	3.02E+01
^{226}Ra	7.59E-05	2.27E-05	1.51E-06	1.28E-05	5.91E-09	4.57E-05
^{228}Ra	8.72E-09	9.33E-09	2.01E-11	2.86E-07	8.87E-10	1.51E-05
^{79}Se	2.61E+01	3.54E+00	3.20E+00	2.63E+01	1.19E+00	6.82E+00
^{126}Sn	3.70E+00	7.47E+00	3.84E+00	7.96E+01	1.51E+00	9.40E+00
^{90}Sr	1.55E+02	2.46E+01	5.19E+01	2.12E+02	1.68E+01	5.22E+01
^{99}Tc	7.81E+02	1.03E+02	9.48E+01	6.56E+02	3.58E+01	1.58E+02
^{229}Th	6.83E-05	6.11E-05	1.64E-07	3.59E-03	2.81E-06	3.24E-01
^{230}Th	2.29E-01	6.35E-02	7.82E-03	3.68E-02	2.98E-05	1.18E-01
^{232}Th	2.16E+01	2.31E+01	5.24E-02	6.21E+04	2.40E+00	2.17E+04
^{232}U	2.19E-05	8.08E-05	1.85E-05	1.07E-02	8.32E-06	1.28E+00
^{233}U	2.05E-01	1.80E-01	1.46E-03	2.24E+03	1.58E-02	5.38E+02
^{234}U	1.21E+03	2.96E+02	8.69E+01	1.77E+02	3.75E-01	4.73E+02
^{235}U	1.02E+05	5.84E+03	7.22E+03	2.42E+04	4.37E+03	2.51E+04
^{236}U	7.09E+03	8.14E+02	9.08E+02	4.86E+03	2.82E+02	1.25E+03
^{238}U	9.56E+06	1.69E+05	7.36E+03	6.40E+04	1.74E+04	6.84E+05
Totals:	9.69E+06	1.78E+05	1.61E+04	1.69E+05	2.23E+04	7.37E+05

[a] *Source Term Estimates for DOE Spent Nuclear Fuels* (DOE 2004 [DIRS 169354], Appendix D, pp. D-577 to D-586, excluding bare fuel transfers). The units of the radionuclide inventories in the document are in curies. The conversion from curies to grams required the half-life of each radionuclide from *Initial Radionuclide Inventories* (SNL 2007 [DIRS 180472], Table 4-12). Inventory values for ^{245}Cm are from *Radionuclide Inventory Calculation Checks, SFD Version 5.0.1* (DOE 2007 [DIRS 182943]).

[b] *Initial Radionuclide Inventories* (SNL 2007 [DIRS 180472]), Table 7-1[a]). The DSNF inventory from Table 7-1[a] is a surrogate inventory that represents the 10 categories of DSNF. In the analyses in Section 7.5, the entire DSNF inventory is referred to as DSNF surrogate to distinguish it from Categories 2 through 11 DSNF.

NOTE: N/A = not applicable; not available for public review.

Table 7.5-3. Number of Canisters by Size of Canister and Total Number of Waste Packages for Each DSNF Category[a]

Category, Group/Matrix	18-Inch × 10-Foot Canisters	18-Inch × 15-Foot Canisters[b]	24-Inch × 10-Foot Canisters	24-Inch × 15-Foot Canisters	Multicanister Overpack[c]	Total WPs[d]	Percent of Total WPs
1. Naval fuel	N/A	N/A	N/A	N/A	N/A	N/A	N/A
2. Plutonium/uranium alloy	10	8	0	0	0	18	0.5
3. Plutonium/uranium carbide	2	3	0	0	0	5	0.2
4. Mixed oxide	15	128	0	0	0	143	4.3
5. Uranium/thorium carbide	1	568	0	0	0	569	17.3
6. Uranium/thorium oxide	13	13	0	27	0	53	1.6
7. Uranium metal	15	2	0	0	401	218	6.6
8. Uranium oxide	277	489	0	0	18	775	23.6
9. Aluminum based	1,013	236	166	0	0	1,415	43.0
10. Miscellaneous	3	1	0	0	0	4	0.1
11. Uranium-zirconium hydride	89	0	0	0	0	89	2.7

[a] *Source Term Estimates for DOE Spent Nuclear Fuels* (DOE 2004 [DIRS 169354], Appendix F, Table F-1). The number of WPs is rounded up to a whole WP for this table. The number of WPs is used for the analysis of each category of DSNF.
[b] For the analysis of DSNF, the high-integrity cans are included in the 10-ft and 15-ft canisters.
[c] Two multicanister overpacks per WP.
[d] The total number of CDSP WPs (3,289) shown in this table is different than the total shown in Table 6.3.7-1 (3,416). This is due to the use of a multiplier in *Initial Radionuclide Inventories* (SNL 2007 [DIRS 180472]) used to fill the entire footprint of the repository. The sensitivity analysis in Section 7.5.5 (on the number of WPs) indicates that this difference does not have a significant effect on annual dose.

NOTE: N/A = not applicable to DSNF; Naval spent fuel does not use any of the DOE canisters.

Table 7.5-4. Dissolution Models and Fuel Surface Areas for Each DSNF Category[a]

Category, Group/Matrix	Dissolution Model[b]	Nominal Fuel Surface Area (m^2/g)
1. Naval fuel	N/A	N/A
2. Plutonium/uranium alloy	$k = 1.15\times10^{8}\exp\left[\frac{-66.5\,kJ/mol}{RT}\right] mg\,metal/cm^2h$	3.6E-4
3. Plutonium/uranium carbide	$k = 8.9\times10^{10}\exp\left[\frac{-17\,kJ/mol}{RT}\right] mg\,UC/m^2d$	2.6E-3
4. Mixed oxide	$k = 4.46\times10^{4}\exp\left[\frac{-39\,kJ/mol}{RT}\right] mg\,PuO_2/m^2d$	5.5E-4
5. Uranium/thorium carbide	$k = 5.37\times10^{11}\exp\left[\frac{-35\,kJ/mol}{RT}\right] mg\,UC_2/m^2d$	2.2E-2
6. Uranium/thorium oxide	$k_{alkaline} = 5\times10^{4}[CO_3]^{0.12}\times[O_2]^{0.32}\times\exp\left[\frac{-20.8\,kJ/mol}{RT}\right] mg\,UO_2/m^2d$ $k_{acidic} = 1.35\times10^{7}[H^+]^{0.41}\times[O_2]^{0.32}\times\exp\left[\frac{-20.8\,kJ/mol}{RT}\right] mg\,UO_2/m^2d$	3.6E-4
7. Uranium metal	$k = 5.03\times10^{9}\exp\left[\frac{-66.4\,kJ/mol}{RT}\right] mg\,U/cm^2h$	7.0E-5 (Bounding = 2.8E-4)
8. Uranium oxide	$k_{alkaline} = 5\times10^{4}[CO_3]^{0.12}\times[O_2]^{0.32}\times\exp\left[\frac{-20.8\,kJ/mol}{RT}\right] mg\,UO_2/m^2d$ $k_{acidic} = 1.35\times10^{7}[H^+]^{0.41}\times[O_2]^{0.32}\times\exp\left[\frac{-20.8\,kJ/mol}{RT}\right] mg\,UO_2/m^2d$	2.2E-2
9. Aluminum based	$k = 4.29\exp\left[\frac{-32.8\,kJ/mol}{RT}\right] mg\,metal/cm^2h$	6.5E-3
10. Miscellaneous	$k = 5.03\times10^{9}\exp\left[\frac{-66.4\,kJ/mol}{RT}\right] mg\,metal/cm^2h$	2.2E-2
11. Uranium-zirconium hydride	$k = 2\times10^{-6}\,g^2\,ZrH_2/cm^4h$	1.0E-4

[a] *Additional DOE Spent Nuclear Fuel Information in Support of TSPA-LA Analysis* (Loo et al. 2004 [DIRS 168999], Section 6 and Table 7-1).

[b] k is the dissolution rate, R is the universal gas constant (8.3145 J/K·mol); T is the temperature (K). In some cases, these dissolution models were used outside of their range of validity. This was done only to produce a comparison of a potential dissolution model for a specific spent fuel type to the dissolution model used in the TSPA-LA Model. It has no impact on the dose from the TSPA-LA Model that uses an instantaneous dissolution model as a reasonable surrogate.

NOTE: N/A = not applicable; not available for public review.

Table 7.5-5. Disposition of the Use of CSNF as a Surrogate for NSNF for the TSPA-LA Model

Modeling Case	Disposition	Documented
Early Failure	Advection + diffusion case (Drip Shield EF), and a subset with just diffusion (Waste Package EF). Modeled DS early failure explicitly with nominal naval source term replacing commercial source term. Qualitative arguments for WP early failure.	Section 7.5.3.2
Igneous Intrusion	Modeled explicitly with igneous naval source term replacing commercial source term.	Section 7.5.3.3
Volcanic Eruption	Quantitative comparison using igneous naval source term, naval WP percentage of the total inventory, and robustness of naval WP.	Section 7.5.3.4
Human Intrusion	Quantitative comparison using igneous naval source term, naval WP percentage of the total inventory, and robustness of naval WP.	Section 7.5.3.5
Nominal	Qualitative. Zero probability case. No WP failures in 10,000 years; generalized corrosion (i.e. patch) failures in 1,000,000 years. WP patch failures similar to an human intrusion WP failure.	Section 7.5.3.6
Seismic	Quantitative comparison using the naval source term and robustness of the naval WP.	Section 7.5.3.7

Table 7.5-6. Air Alteration Rate for DSNF Category 5, Uranium/Thorium Carbide, and Category 7, Uranium Metal[a]

Category, Group/Matrix	Air Alteration Dissolution Model[b]
5. Uranium/thorium carbide	$k = 3.12\times10^{9}\exp\left[\frac{-94.3\,kJ/mol}{RT}\right] mg^{2}\,SiC/m^{4}d$
7. Uranium metal	$k = 1.09\times10^{8}\exp\left[\frac{-71.3\,kJ/mol}{RT}\right] mgU/cm^{2}h$

[a] *Additional DOE Spent Nuclear Fuel Information in Support of TSPA-LA Analysis* (Loo et al. 2004 [DIRS 168999], Table 7-3).

[b] In some cases, these dissolution models were used outside of their range of validity. This was done only to produce a comparison of a potential dissolution model for a specific spent fuel type to the dissolution model used in the TSPA-LA Model. It has no impact on the dose from the TSPA-LA Model that uses an instantaneous dissolution model as a reasonable surrogate.

Table 7.5-7. Nominal and Bounding Inventories for Uranium-Metal Spent Fuel (Category 7)[a]

Radionuclide	Nominal Inventory (g/WP)	Bounding Inventory (g/WP)	Radionuclide	Nominal Inventory (g/WP)	Bounding Inventory (g/WP)
^{227}Ac	6.71E-07	1.07E-06	^{242}Pu	1.29E+02	2.56E+02
^{241}Am	1.01E+03	1.98E+03	^{226}Ra	7.59E-05	8.37E-05
^{243}Am	8.72E+00	1.73E+01	^{228}Ra	8.72E-09	8.73E-09
^{14}C	3.17E+00	3.85E+00	^{79}Se	2.61E+01	4.98E+01
^{36}Cl	5.17E+00	5.18E+00	^{126}Sn	3.70E+00	4.62E+00
^{245}Cm	3.50E-02	6.81E-02	^{90}Sr	1.55E+02	2.98E+02
^{135}Cs	3.12E+02	6.07E+02	^{99}Tc	7.81E+02	1.50E+03
^{137}Cs	3.46E+02	6.71E+02	^{229}Th	6.83E-05	6.90E-05
^{129}I	1.73E+02	3.36E+02	^{230}Th	2.29E-01	2.70E-01
^{237}Np	4.56E+02	8.84E+02	^{232}Th	2.16E+01	2.16E+01
^{231}Pa	1.95E-03	3.30E-03	^{232}U	2.19E-05	3.04E-05
^{238}Pu	3.67E+01	7.21E+01	^{233}U	2.05E-01	2.11E-01
^{239}Pu	1.64E+04	3.19E+04	^{234}U	1.21E+03	1.57E+03
^{240}Pu	3.46E+03	6.81E+03	^{235}U	1.02E+05	1.22E+05
^{241}Pu	9.82E+01	1.94E+02	^{236}U	7.09E+03	1.32E+04
			^{238}U	9.56E+06	9.59E+06

[a] *Source Term Estimates for DOE Spent Nuclear Fuels* (DOE 2004 [DIRS 169354], Appendix D, p. D-581, excluding bare fuel transfers). The units of the radionuclide inventories in the document (DOE 2004 [DIRS 169354]) are in curies. The conversion from curies to grams (presented above) required the half-life of each radionuclide from *Initial Radionuclide Inventories* (SNL 2007 [DIRS 180472], Table 4-12). Inventory values for ^{245}Cm are from *Inventory Values for Curium-245 for DOE SNF in the License Application* (DOE 2007 [DIRS 182943]).

INTENTIONALLY LEFT BLANK

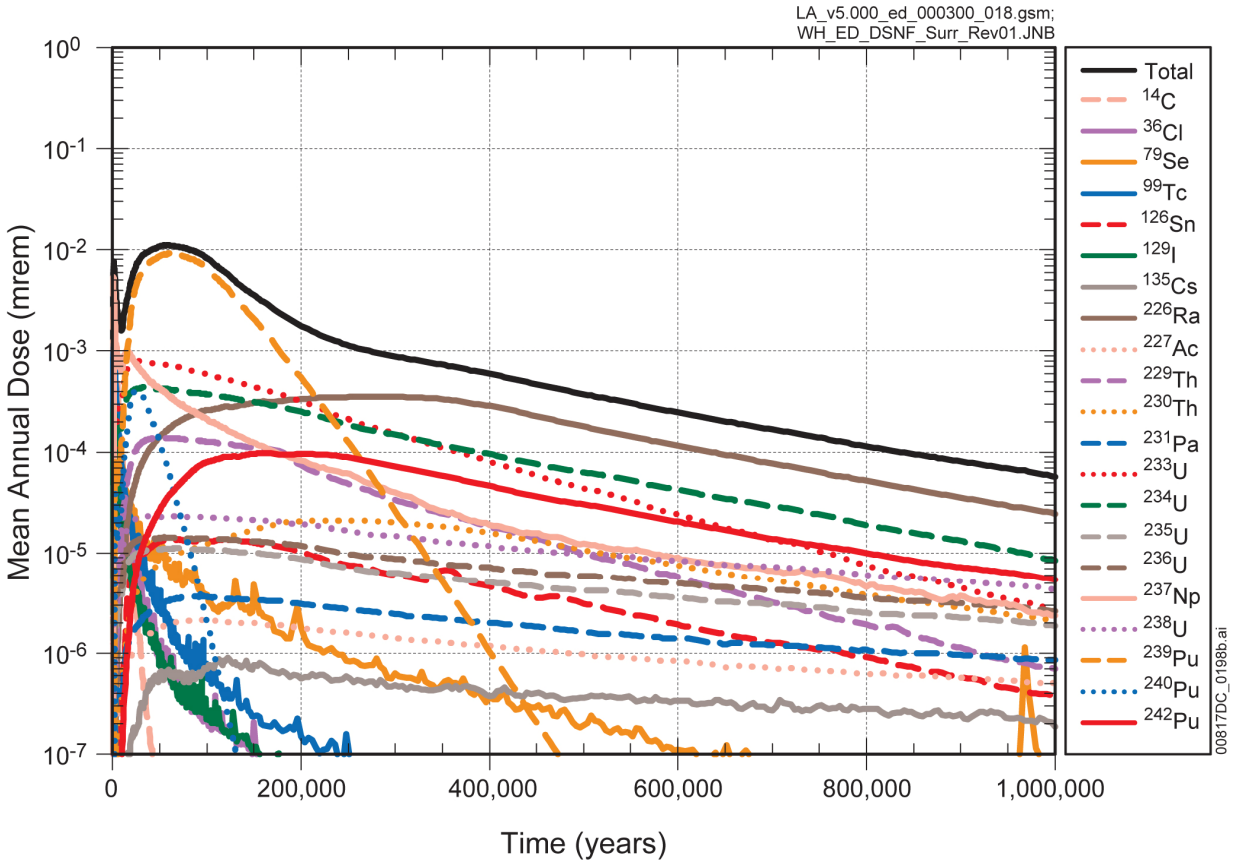

Source: Output DTN: MO0707TSPADSNF.000 [DIRS 182992].

NOTE: ^{226}Ra dose is the sum of ^{226}Ra and ^{210}Pb doses (secular equilibrium assumed).

Figure 7.5-1. Mean Annual Dose and Dose Contributors from DSNF Only Using Surrogate Inventory (One Waste Package Failure with no HLW)

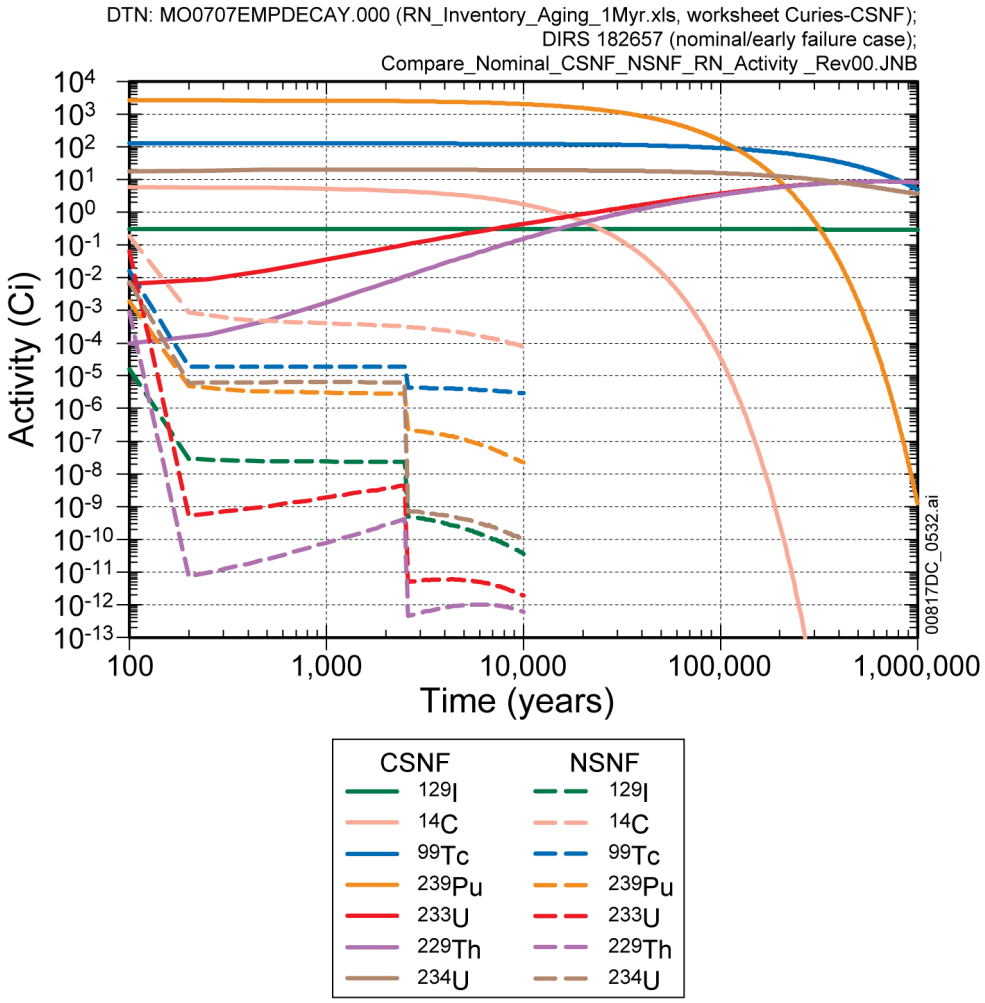

Sources: McKenzie 2007 [DIRS 182657] and Output DTN: MO0707EMPDECAY.000 [DIRS 183475], *FileRN_Inventory_Aging_1Myr.xls*, worksheet Curies-CSNF.

Figure 7.5-2. Comparison of Radionuclide Activities on a per Waste Package Basis for the Nominal/Early Failure NSNF and CSNF Inventories

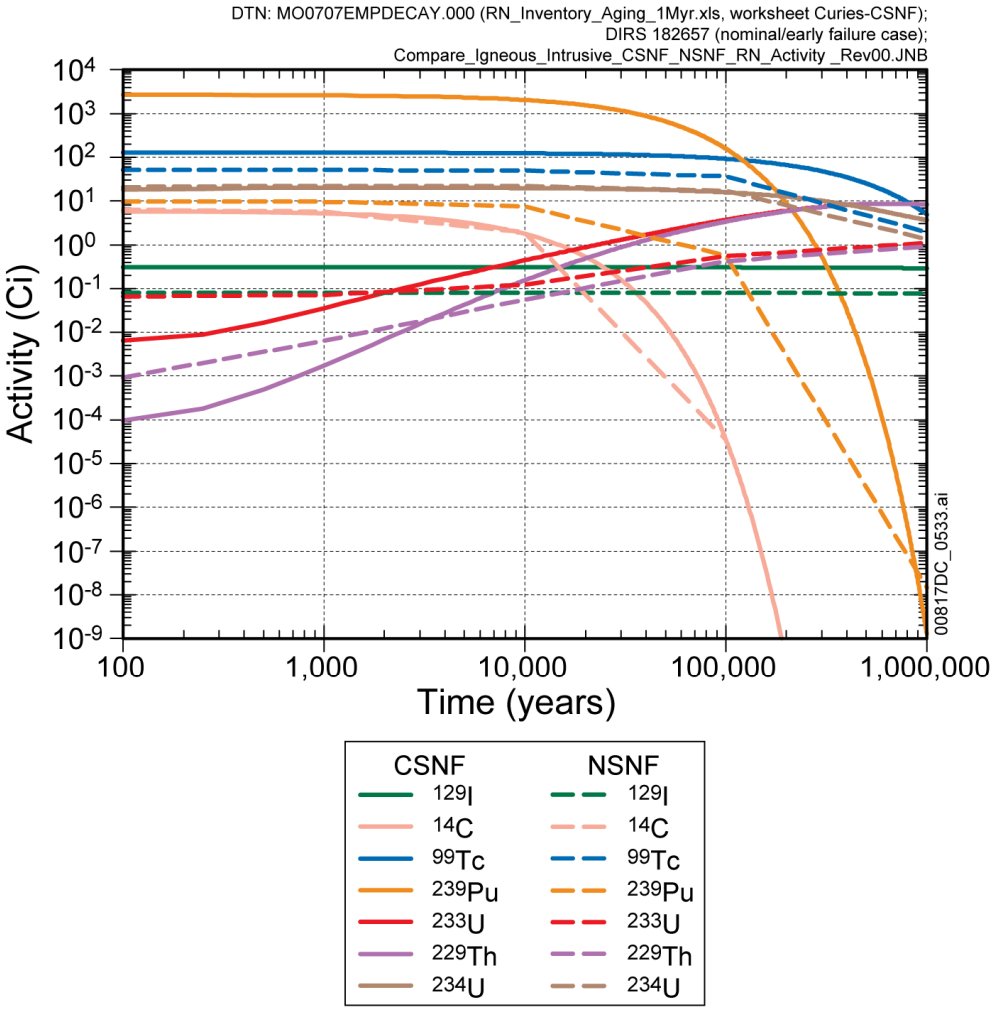

Sources: McKenzie 2007 [DIRS 182657] and Output DTN: MO0707EMPDECAY.000 [DIRS 183475], *FileRN_Inventory_Aging_1Myr.xls*, worksheet Curies-CSNF.

Figure 7.5-3. Comparison of Radionuclide Activities on a per Waste Package Basis for the Igneous Intrusion NSNF and CSNF Inventories

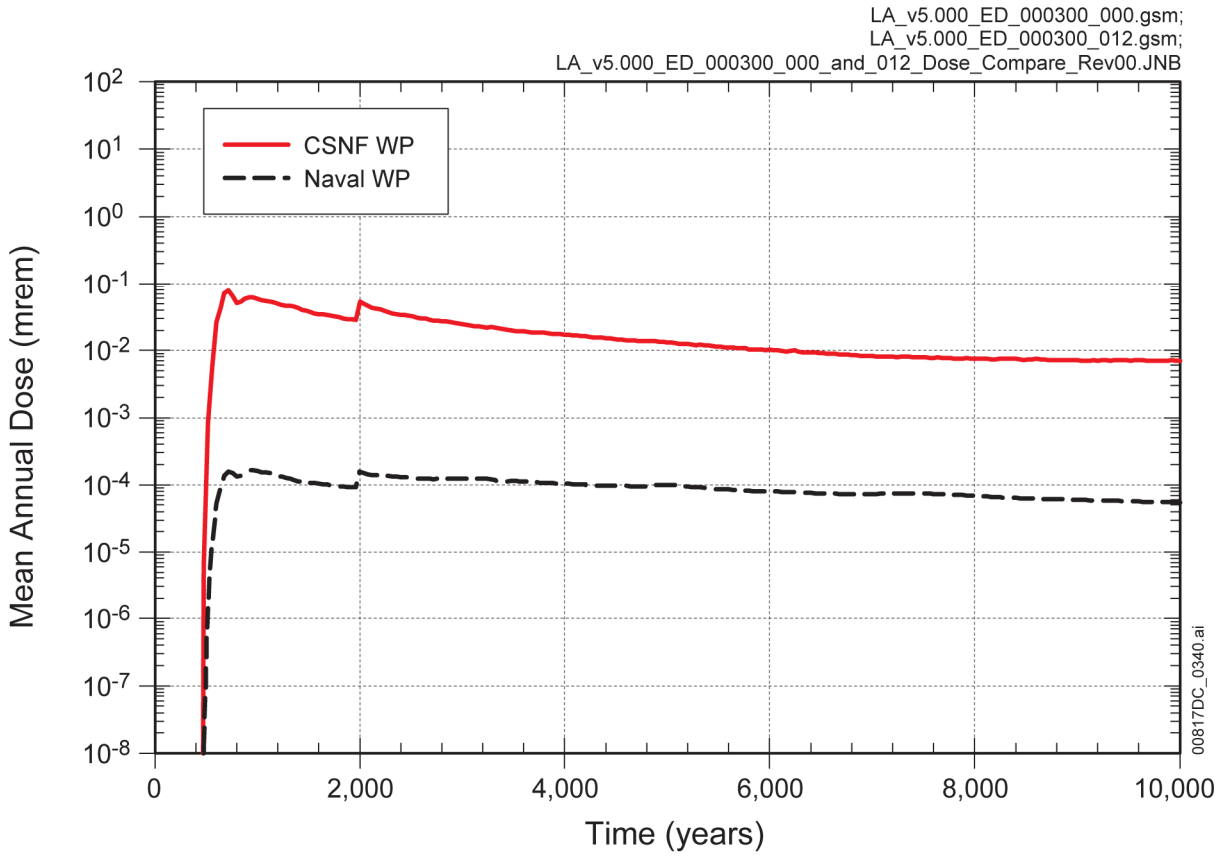

Source: Output DTN: MO0707NAVYFUEL.000 [DIRS 182991].

Figure 7.5-4. Comparison of Mean Annual Dose for a Single CSNF WP and a Single Waste Package with a Naval Source Term for the Drip Shield Early Failure Modeling Case

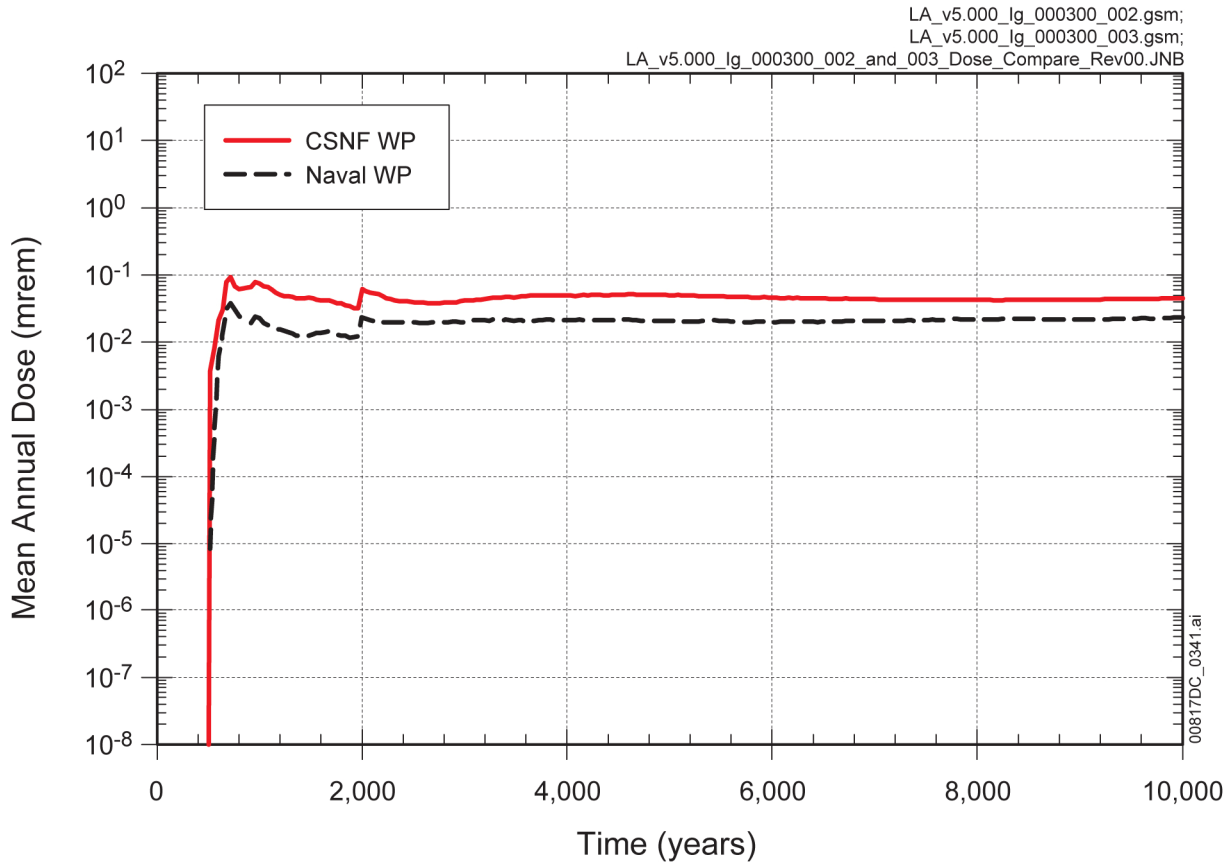

Source: Output DTN: MO0707NAVYFUEL.000 [DIRS 182991].

Figure 7.5-5. Comparison of Mean Annual Dose for a Single CSNF WP and Single Waste Package with a Naval Source Term for the Igneous Intrusion Modeling Case

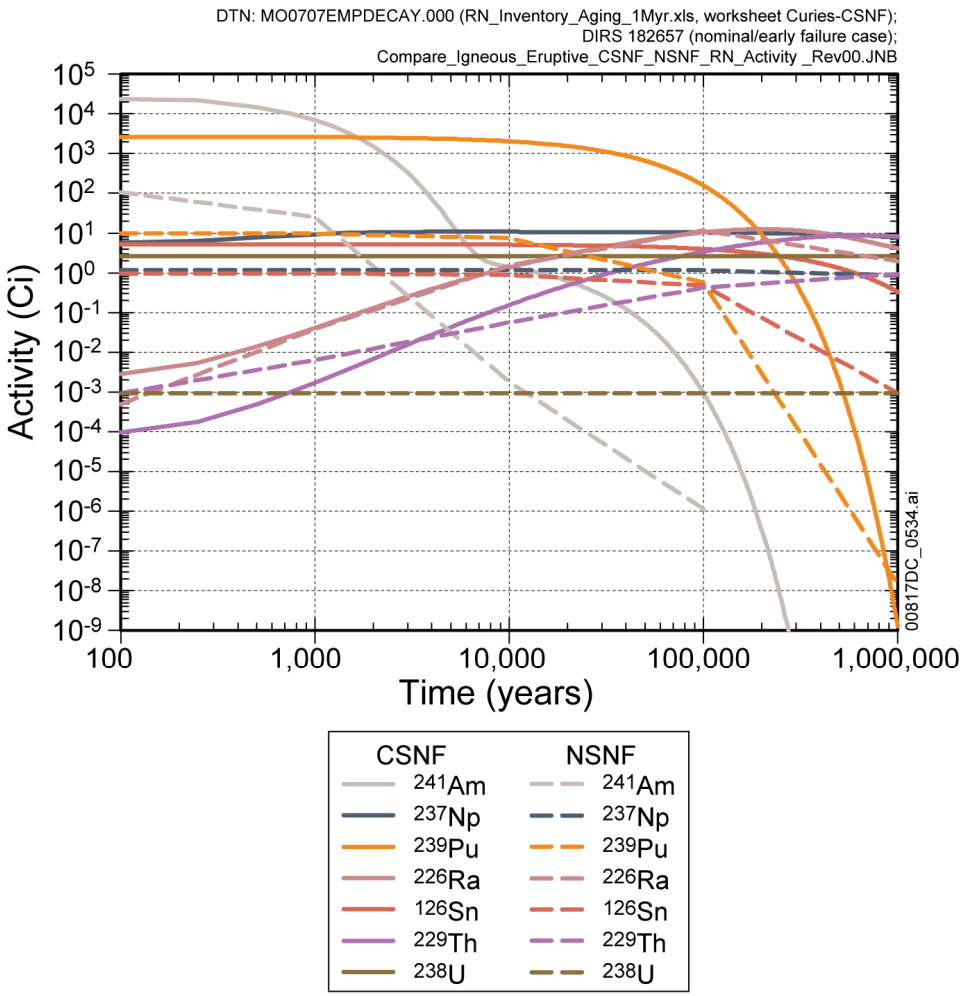

Sources: McKenzie 2007 [DIRS 182657] and Output DTN: MO0707EMPDECAY.000 [DIRS 183475], *FileRN_Inventory_Aging_1Myr.xls*, worksheet Curies-CSNF.

Figure 7.5-6. Comparison of Radionuclide Activities on a per Waste Package Basis for the Igneous NSNF and CSNF Inventories for the Radionuclides that are Major Contributors to the Volcanic Eruption Mean Annual Dose

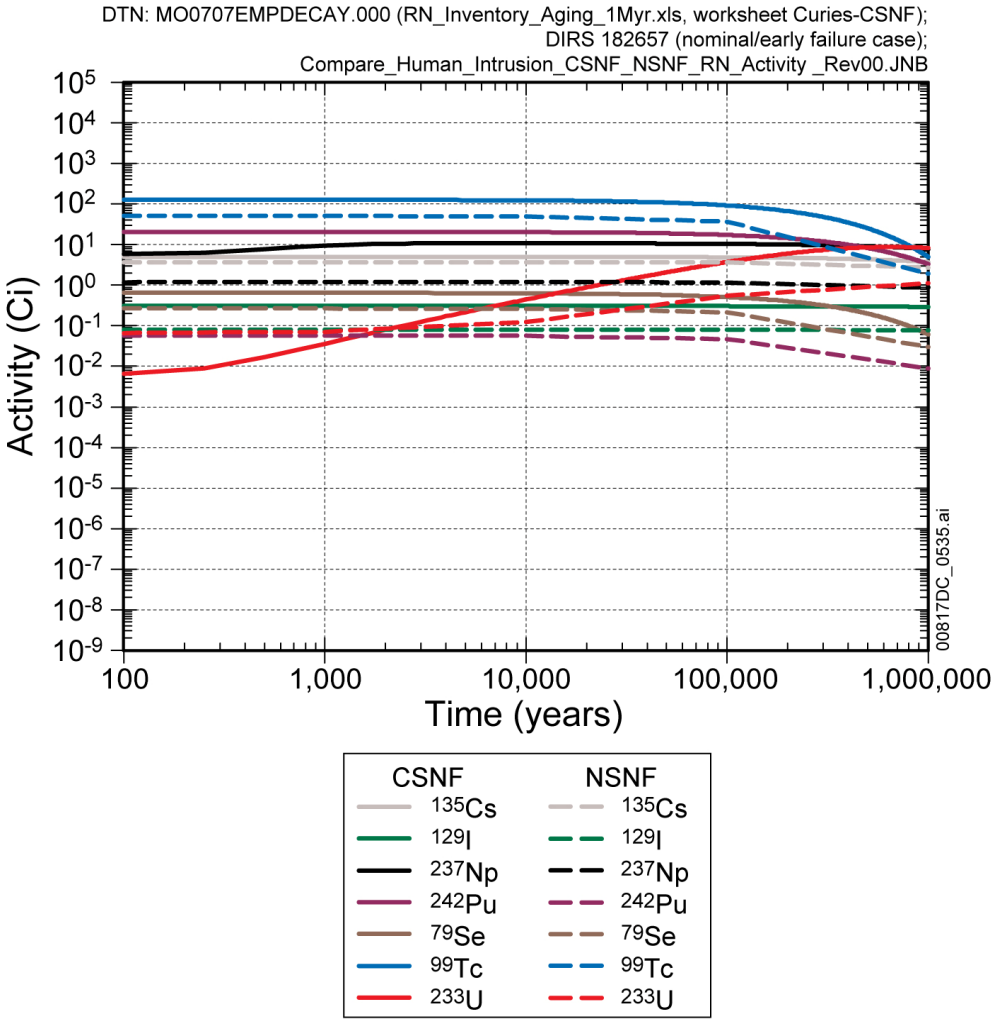

Sources: McKenzie 2007 [DIRS 182657] and Output DTN: MO0707EMPDECAY.000 [DIRS 183475], *FileRN_Inventory_Aging_1Myr.xls*, worksheet Curies-CSNF.

Figure 7.5-7. Comparison of Radionuclide Activities on a per Waste Package Basis for the Igneous NSNF and CSNF Inventories for the Radionuclides that are Major Contributors to the Human Intrusion Mean Annual Dose

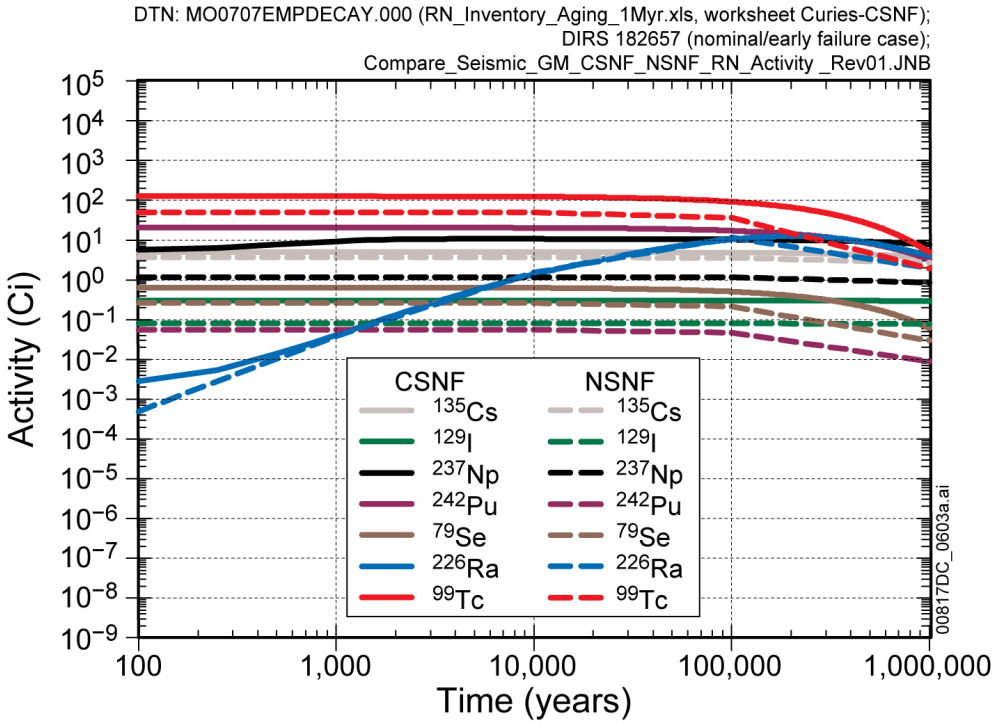

Sources: McKenzie 2007 [DIRS 182657] and Output DTN: MO0707EMPDECAY.000 [DIRS 183475], *FileRN_Inventory_Aging_1Myr.xls*, worksheet Curies-CSNF.

Figure 7.5-8. Comparison of Radionuclide Activities on a per Waste Package Basis for the Igneous NSNF and CSNF Inventories for the Radionuclides that are Major Contributors to the Seismic Ground Motion Mean Annual Dose

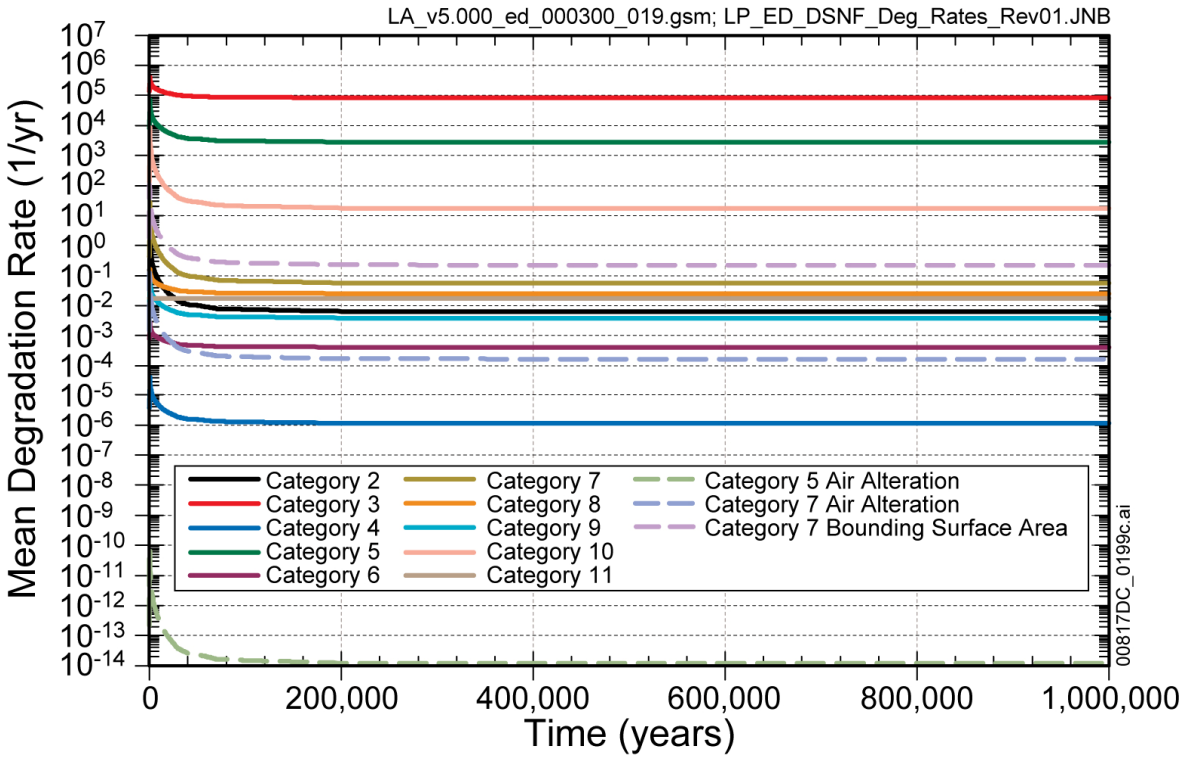

Source: Output DTN: MO0707TSPADSNF.000 [DIRS 182992].

Figure 7.5-9. Comparison of Mean Spent Fuel Degradation Rates for Categories 2 to 11, Air Alteration Rates for Categories 5 and 7, and Category 7 Bounding Surface Area of DSNF

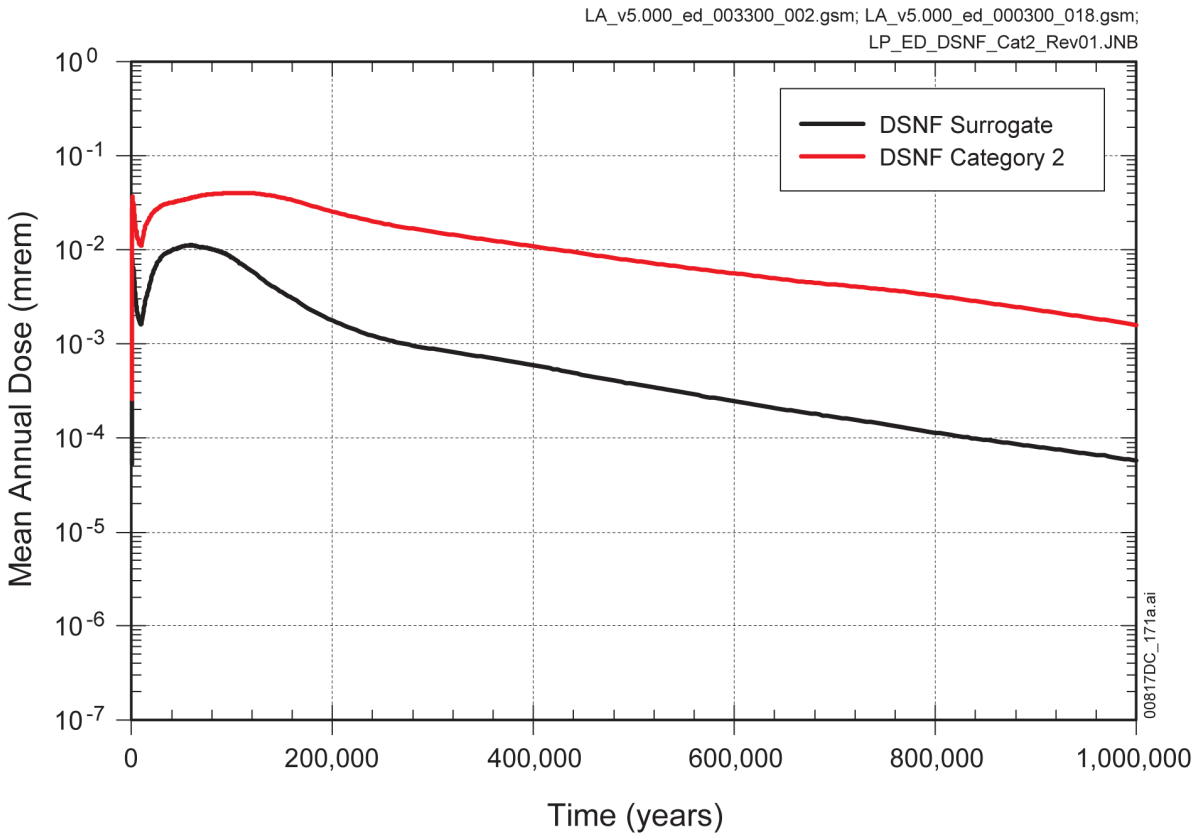

Source: Output DTN: MO0707TSPADSNF.000 [DIRS 182992].

Figure 7.5-10. Comparison of Mean Annual Dose from the Failure of One Waste Package of Plutonium/Uranium Alloy Spent Fuel (Category 2) with One Waste Package of DSNF Surrogate (with no HLW)

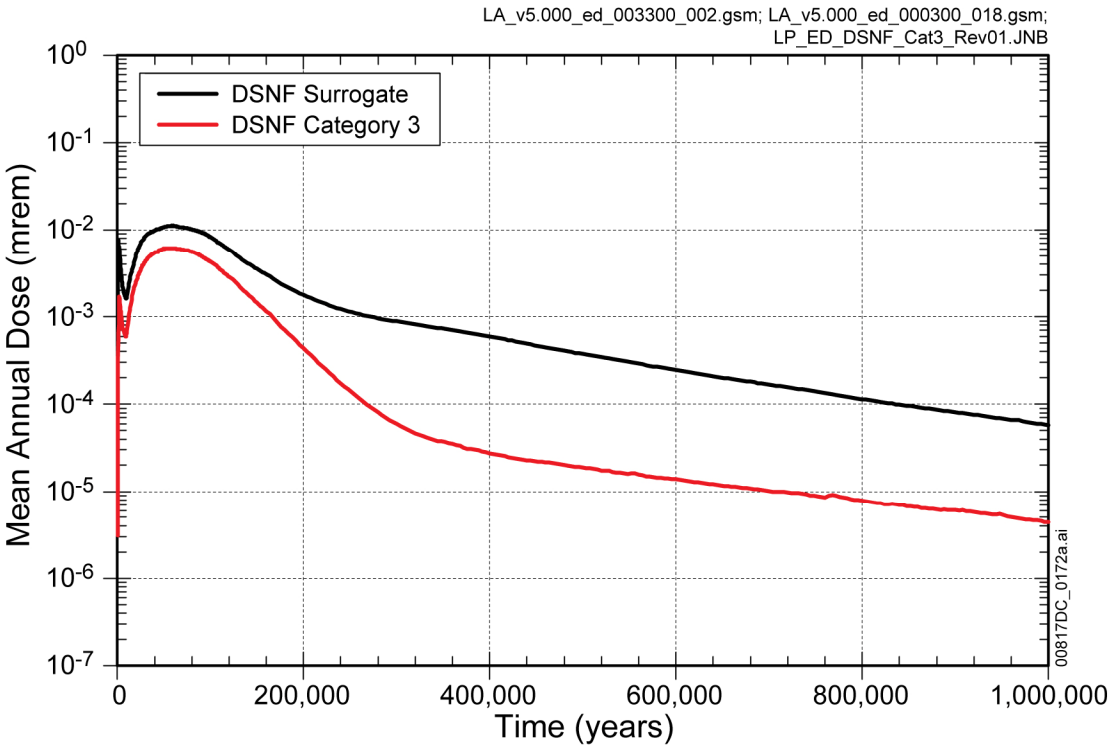

Source: Output DTN: MO0707TSPADSNF.000 [DIRS 182992].

Figure 7.5-11. Comparison of Mean Annual Dose from the Failure of One Waste Package of Plutonium/Uranium-Carbide Spent Fuel (Category 3) with One Waste Package of DSNF Surrogate (with no HLW)

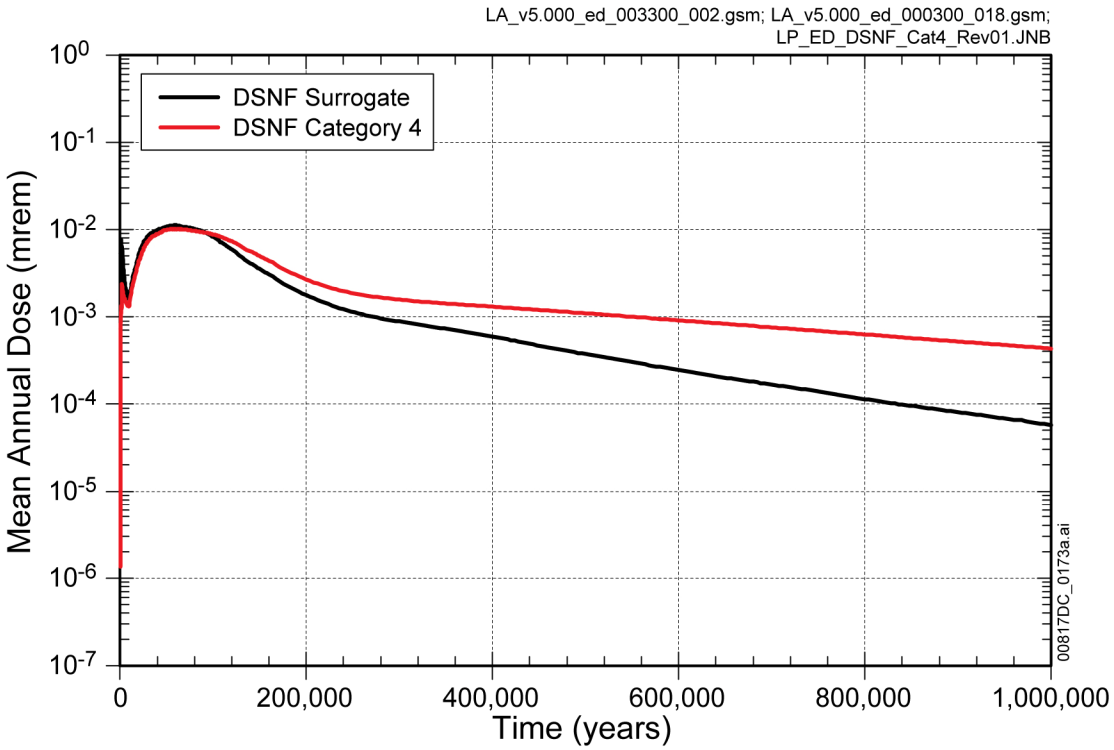

Source: Output DTN: MO0707TSPADSNF.000 [DIRS 182992].

Figure 7.5-12. Comparison of Mean Annual Dose from the Failure of One Waste Package of Mixed Oxide Spent Fuel (Category 4) with One Waste Package of DSNF Surrogate (with no HLW)

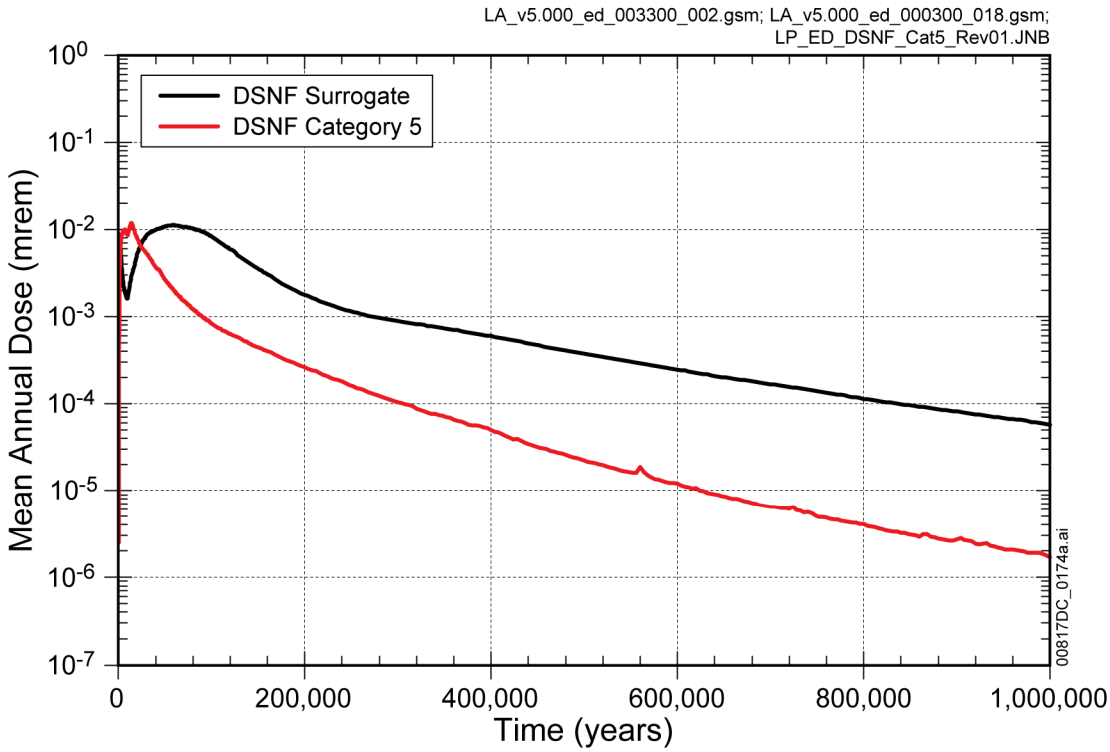

Source: Output DTN: MO0707TSPADSNF.000 [DIRS 182992].

Figure 7.5-13. Comparison of Mean Annual Dose from the Failure of One Waste Package of Uranium/Thorium-Carbide Spent Fuel (Category 5) with One Waste Package of DSNF Surrogate (with no HLW)

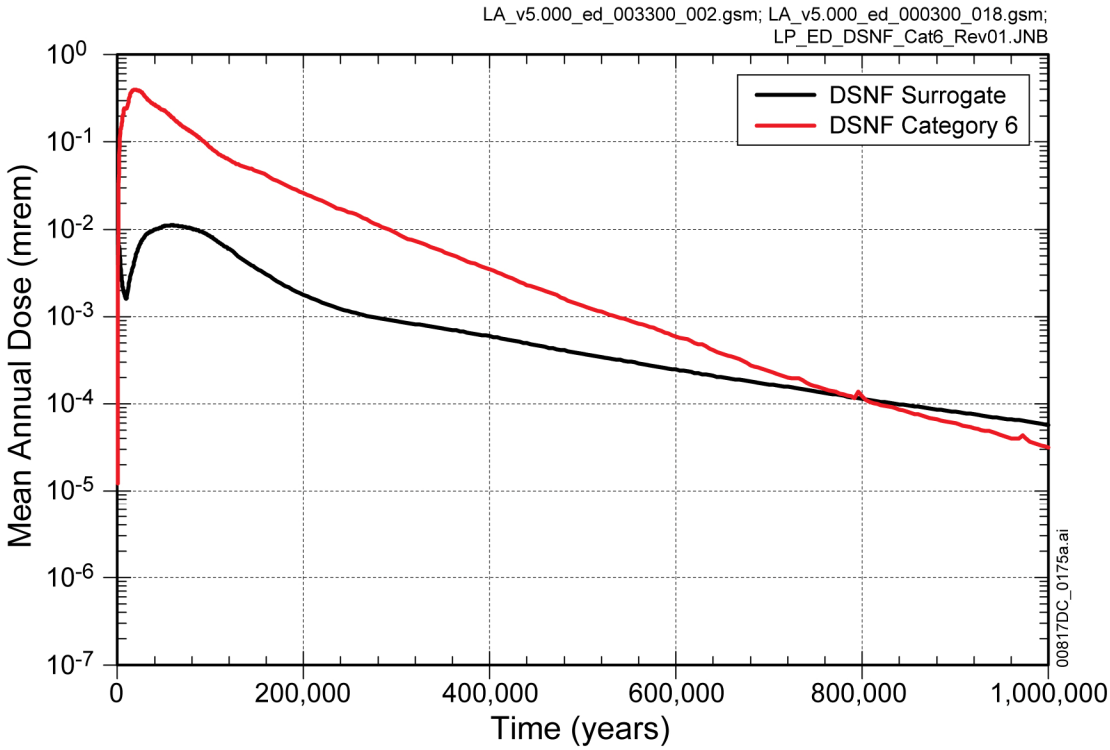

Source: Output DTN: MO0707TSPADSNF.000 [DIRS 182992].

Figure 7.5-14. Comparison of Mean Annual Dose from the Failure of One Waste Package of Uranium/Thorium-Oxide Spent Fuel (Category 6) with One Waste Package of DSNF Surrogate (with no HLW)

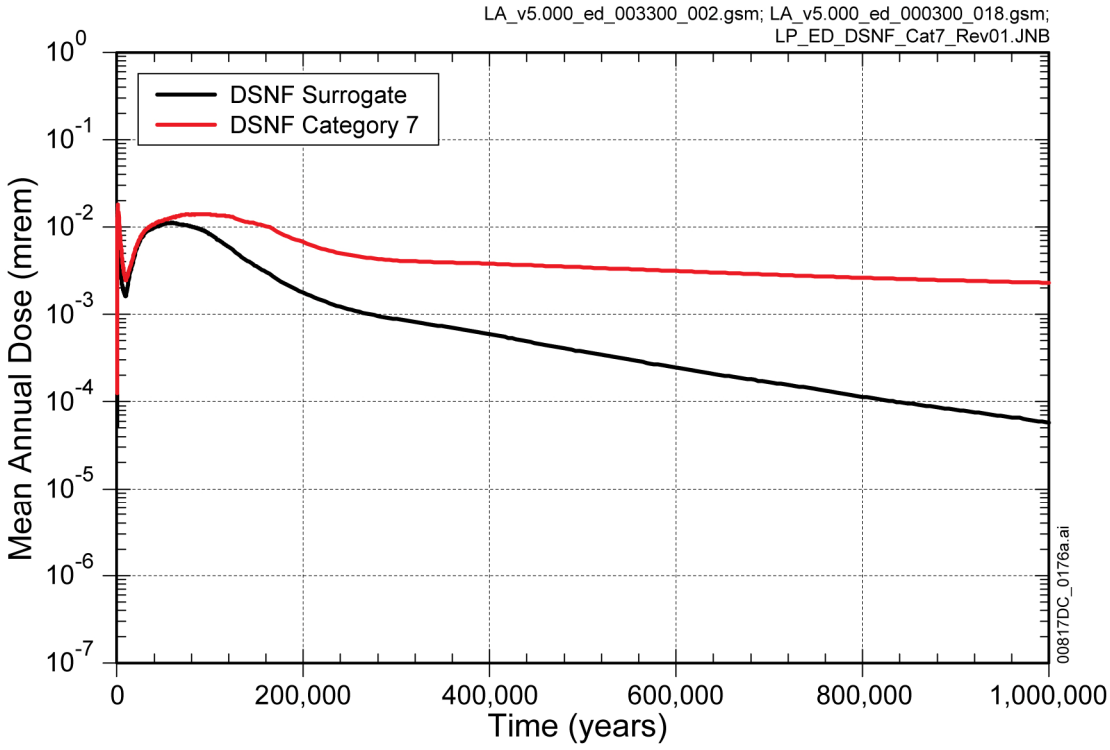

Source: Output DTN: MO0707TSPADSNF.000 [DIRS 182992].

Figure 7.5-15. Comparison of Mean Annual Dose from the Failure of One Waste Package of Uranium-Metal Spent Fuel (Category 7) with One Waste Package of DSNF Surrogate (with no HLW)

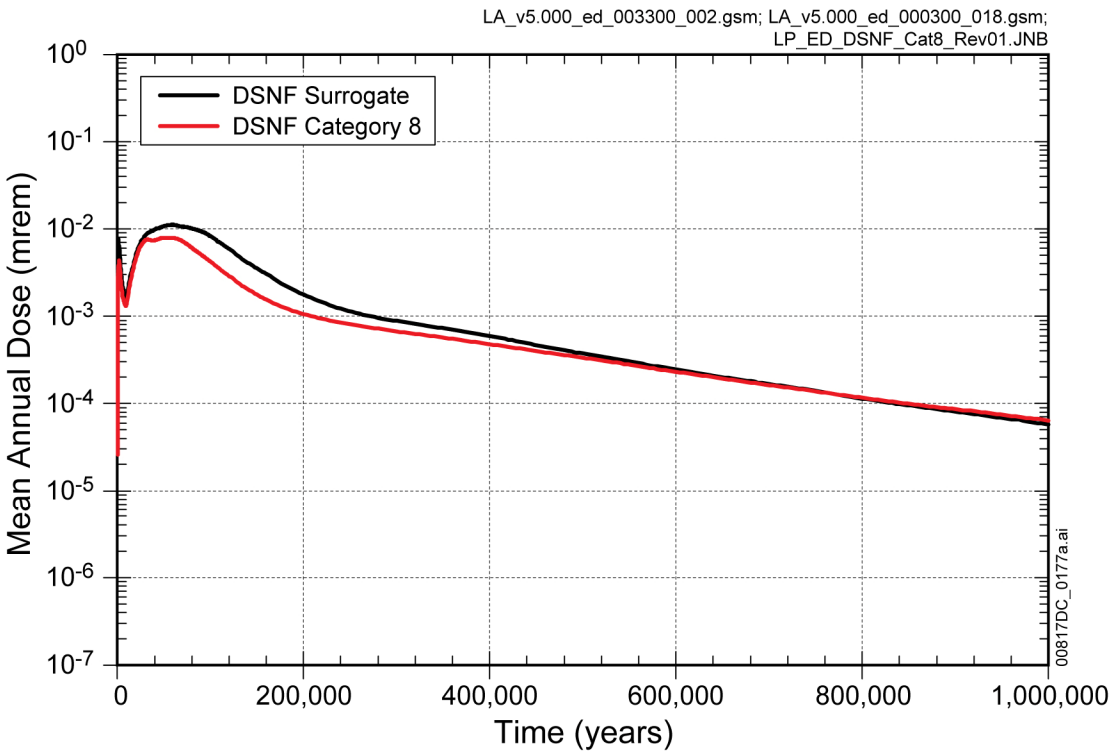

Source: Output DTN: MO0707TSPADSNF.000 [DIRS 182992].

Figure 7.5-16. Comparison of Mean Annual Dose from the Failure of One Waste Package of Uranium-Oxide Spent Fuel (Category 8) with One Waste Package of DSNF Surrogate (with no HLW)

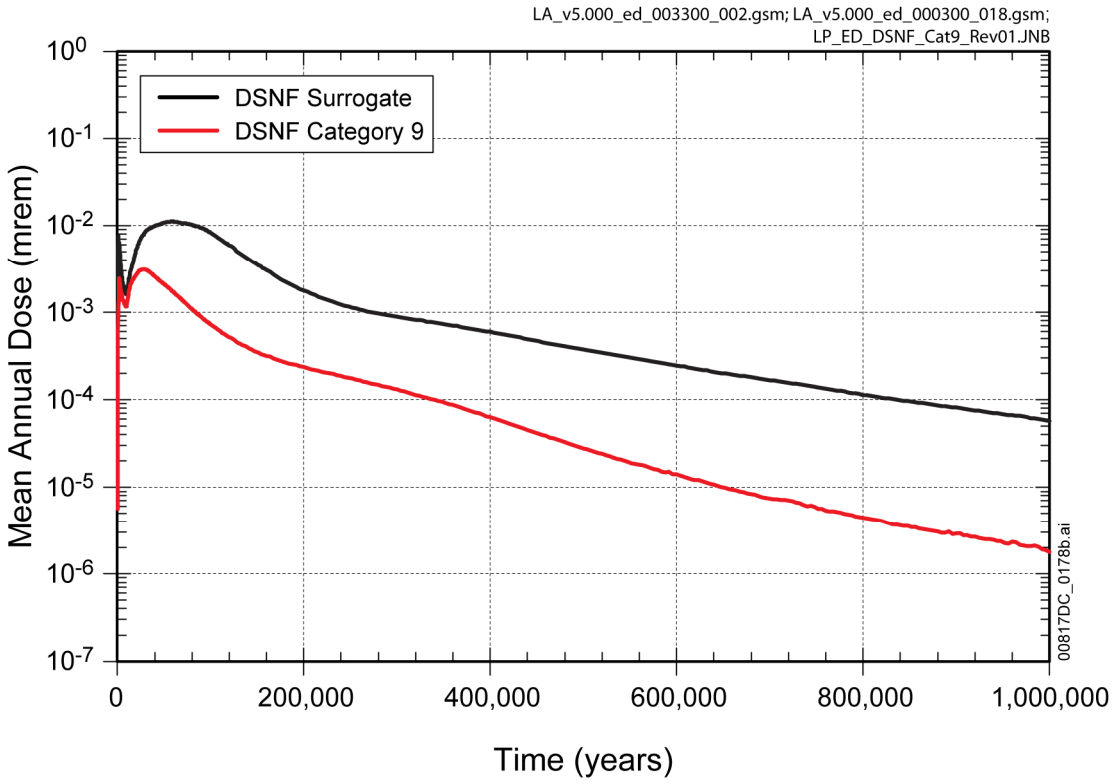

Source: Output DTN: MO0707TSPADSNF.000 [DIRS 182992].

Figure 7.5-17. Comparison of Mean Annual Dose from the Failure of One Waste Package of Aluminum-Based Spent Fuel (Category 9) with One Waste Package of DSNF Surrogate (with no HLW)

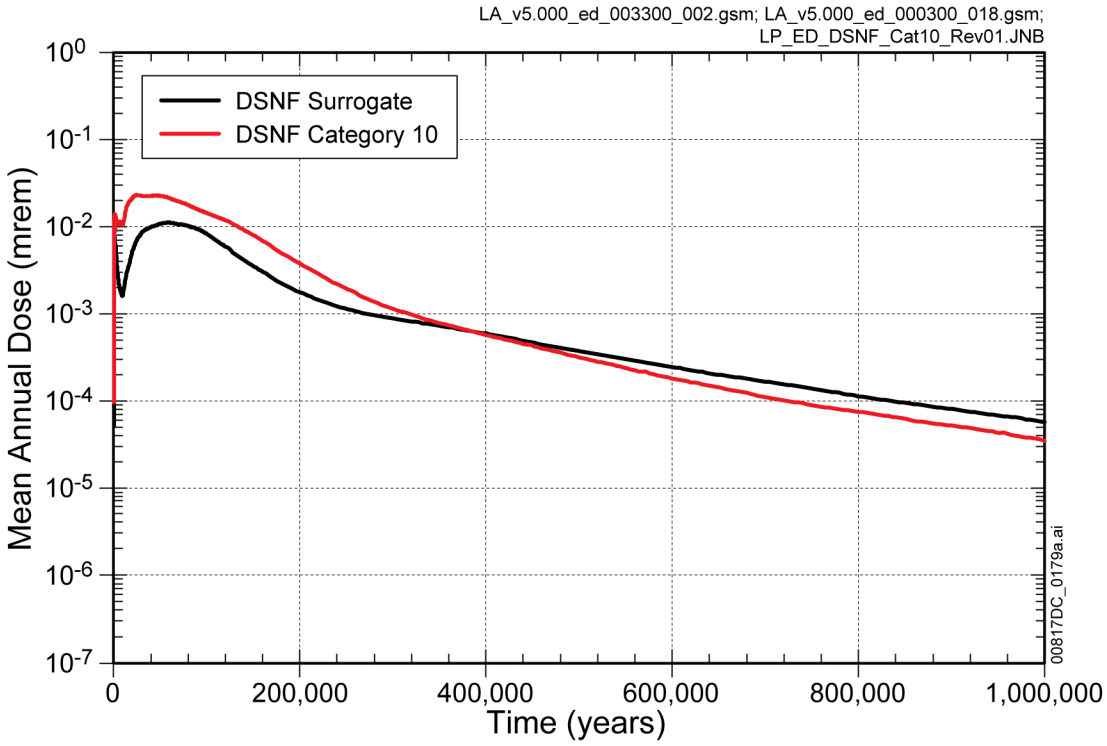

Source: Output DTN: MO0707TSPADSNF.000 [DIRS 182992].

Figure 7.5-18. Comparison of Mean Annual Dose from the Failure of One Waste Package of Miscellaneous Spent Fuel (Category 10) with One Waste Package of DSNF Surrogate (with no HLW)

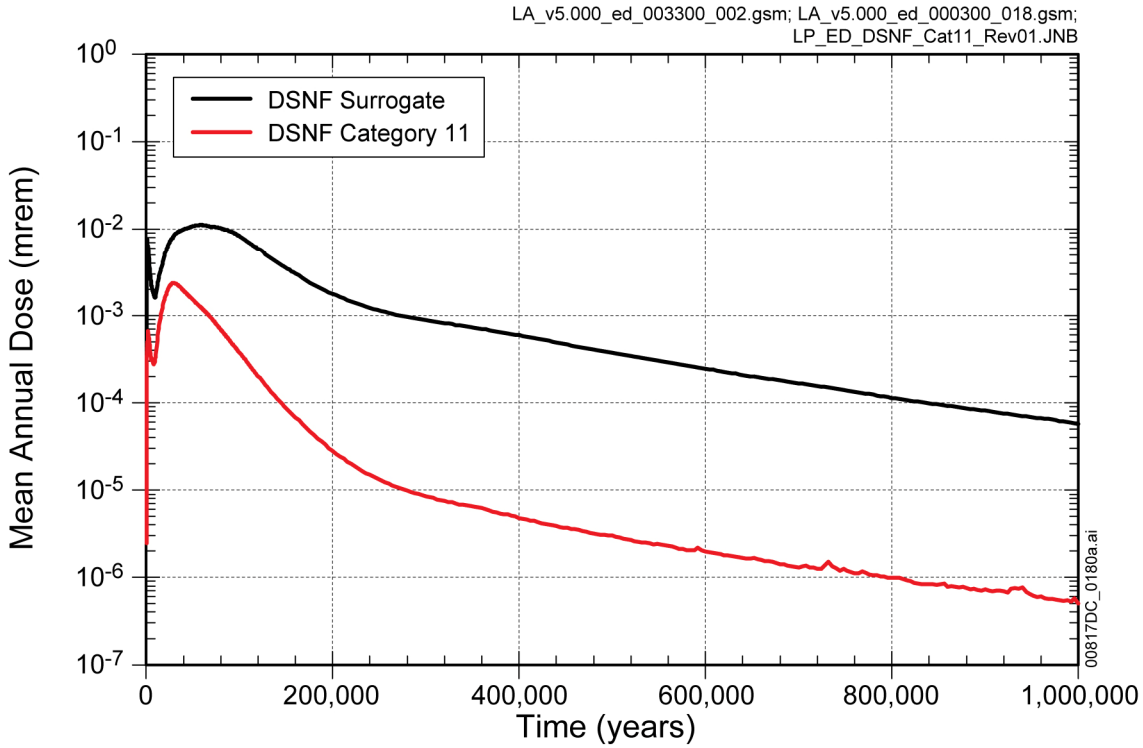

Source: Output DTN: MO0707TSPADSNF.000 [DIRS 182992].

Figure 7.5-19 Comparison of Mean Annual Dose from the Failure of One Waste Package of Uranium-Zirconium Hydride Spent Fuel (Category 11) with One Waste Package of DSNF Surrogate (with no HLW)

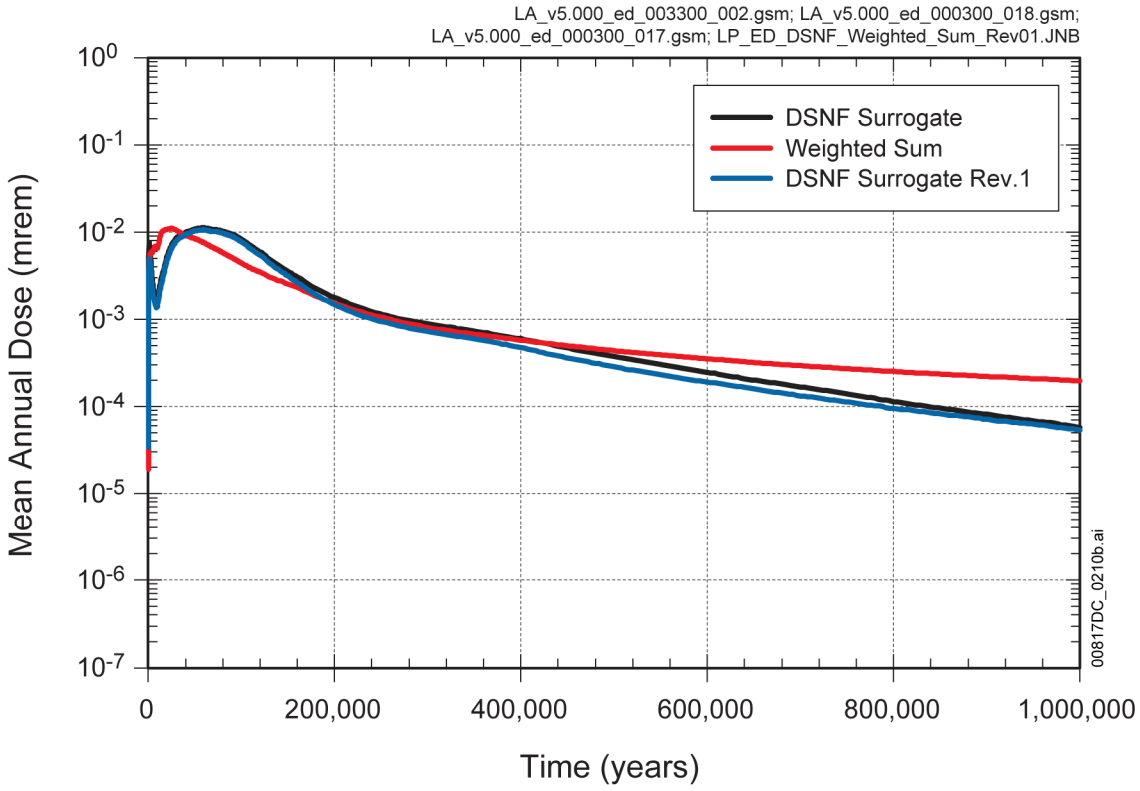

Source: Output DTN: MO0707TSPADSNF.000 [DIRS 182992].

Figure 7.5-20. Comparison of the Weighted Sum (weighted by the number of packages per category) of the Mean Annual Dose from One Waste Package Failure of Categories 2 to 11 DSNF with One Waste Package Failure of DSNF Surrogate and Revision 1 DSNF Surrogate

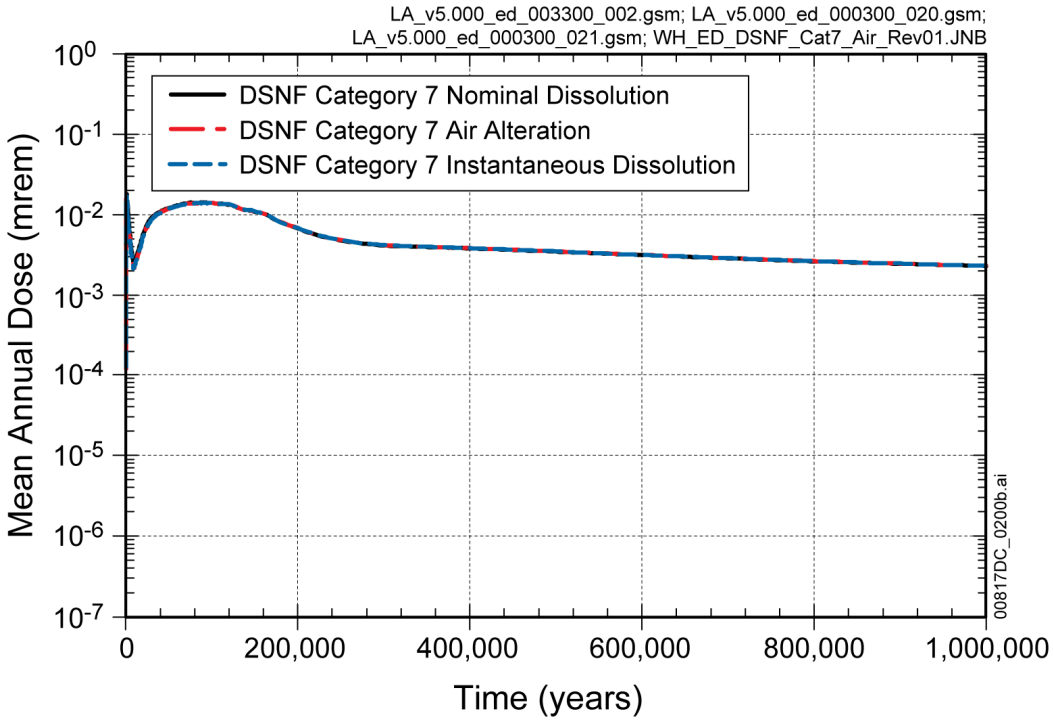

Source: Output DTN: MO0707TSPADSNF.000 [DIRS 182992].

NOTE: Lines plot on top of one another, making colors slightly indistinguishable.

Figure 7.5-21. Comparison of Mean Annual Dose from One Waste Package Failure of Uranium-Metal DSNF (Category 7) Using the Nominal Dissolution Model, Uranium-Metal Dissolution Model with Air Alteration, and Instantaneous Dissolution (with no HLW)

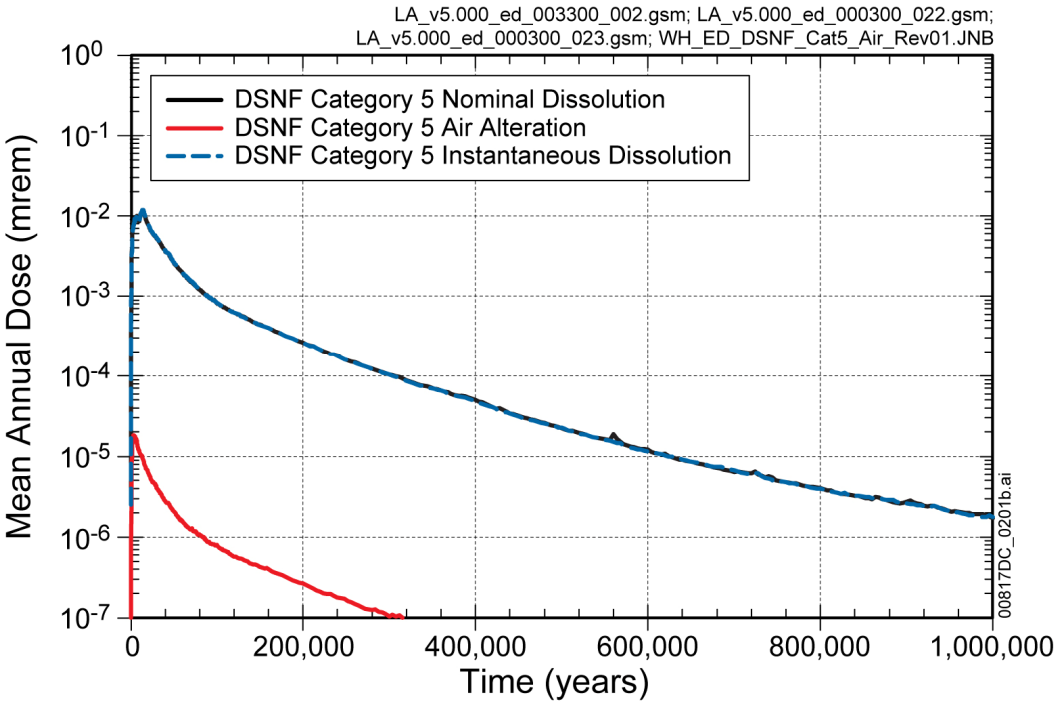

Source: Output DTN: MO0707TSPADSNF.000 [DIRS 182992].

NOTE: Lines plot on top of one another, making colors slightly indistinguishable.

Figure 7.5-22. Comparison of Mean Annual Dose from One Waste Package Failure of Uranium/Thorium-Carbide DSNF (Category 5) Using the Nominal Dissolution Model, Uranium/Thorium-Carbide Dissolution Model with Air Alteration, and Instantaneous Dissolution (with no HLW)

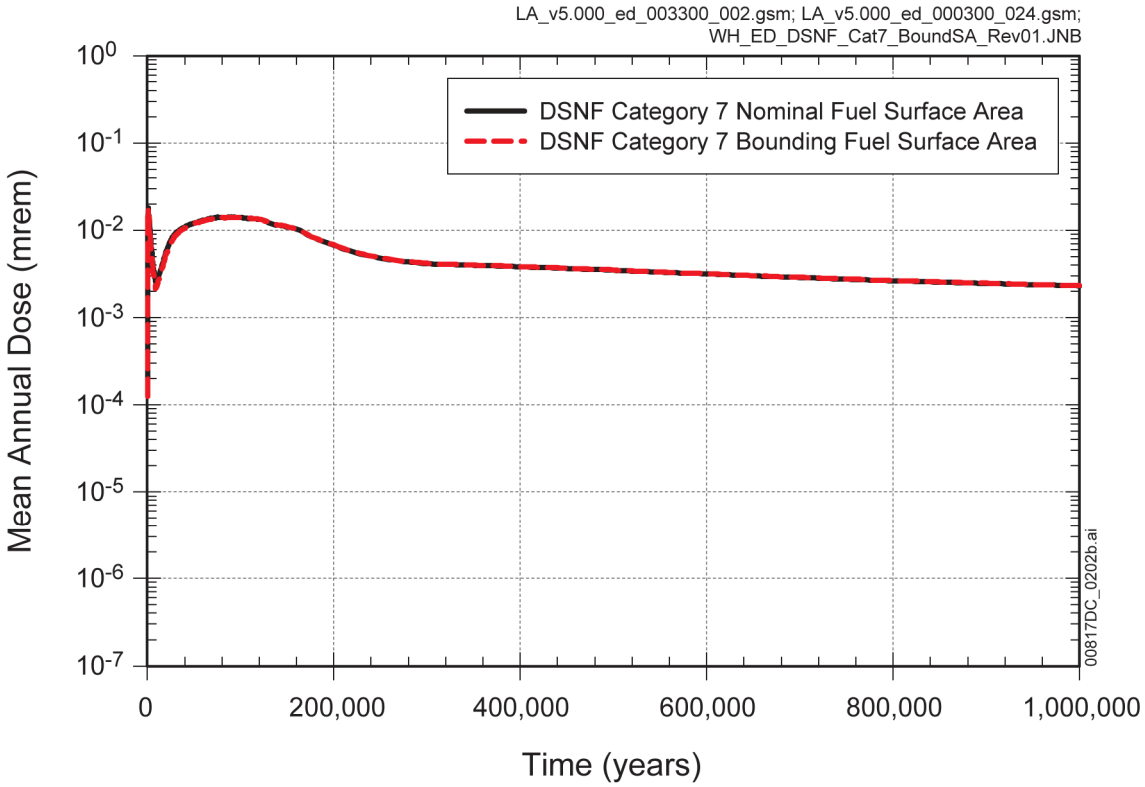

Source: Output DTN: MO0707TSPADSNF.000 [DIRS 182992].

NOTE: Lines plot on top of one another, making colors slightly indistinguishable.

Figure 7.5-23. Comparison of Mean Annual Dose from One Waste Package Failure of Uranium-Metal DSNF (Category 7) Using the Nominal Fuel Surface Area with the Bounding Fuel Surface Area (with no HLW)

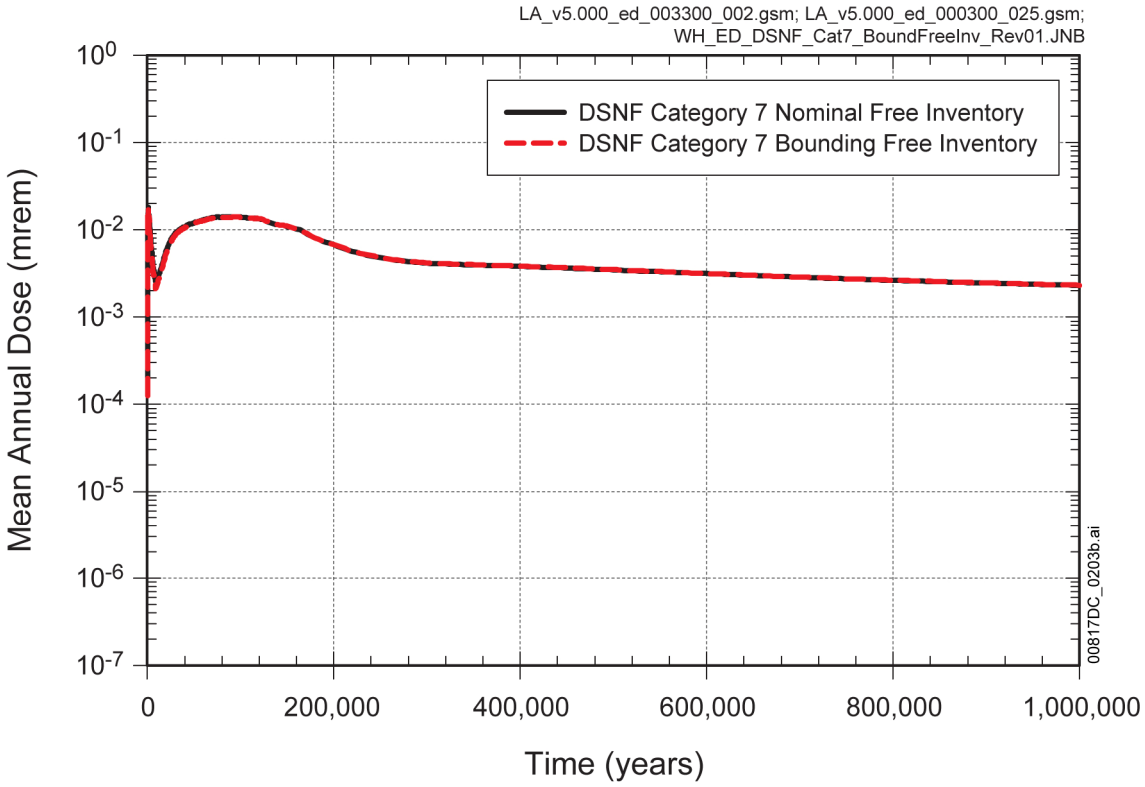

Source: Output DTN: MO0707TSPADSNF.000 [DIRS 182992].

NOTE: Lines plot on top of one another, making colors slightly indistinguishable.

Figure 7.5-24. Comparison of Mean Annual Dose from One Waste Package Failure of Uranium-Metal DSNF (Category 7) Using the Nominal Free Inventory with the Bounding Free Inventory (with no HLW)

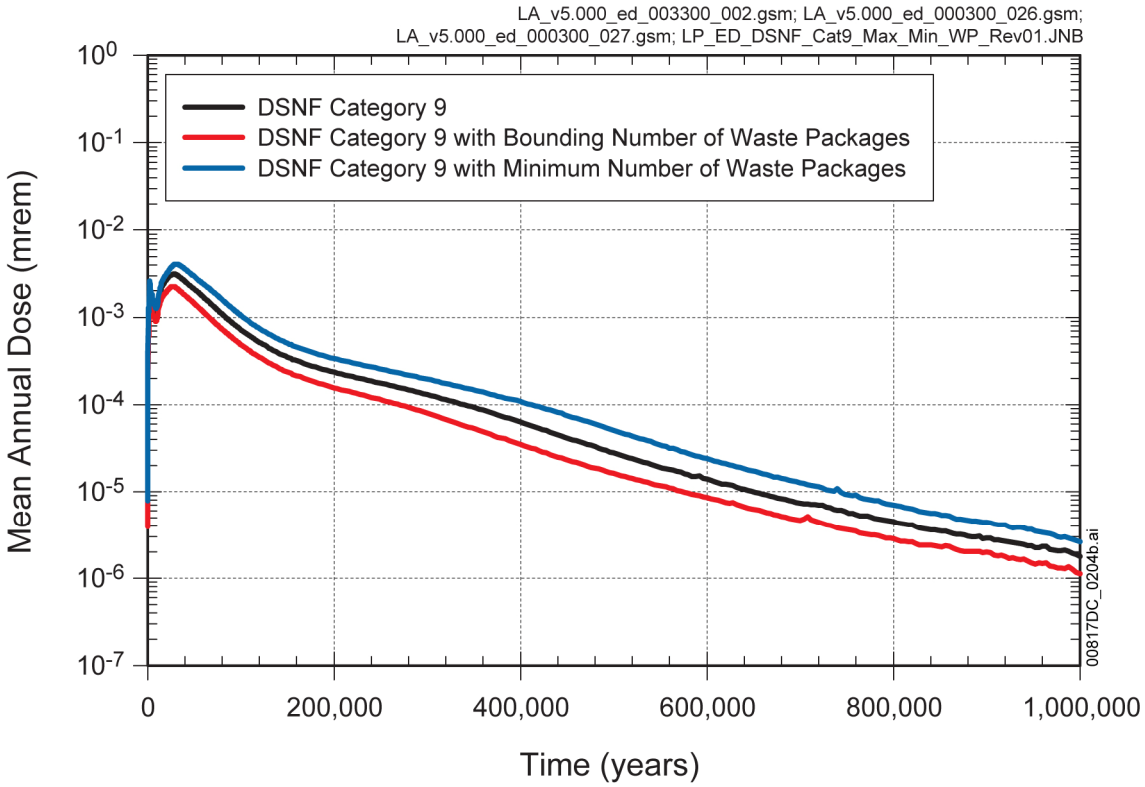

Source: Output DTN: MO0707TSPADSNF.000 [DIRS 182992].

Figure 7.5-25. Comparison of Mean Annual Dose from Aluminum-Based DSNF (Category 9) Minimum, Nominal, and Bounding Number of Waste Packages (with no HLW)

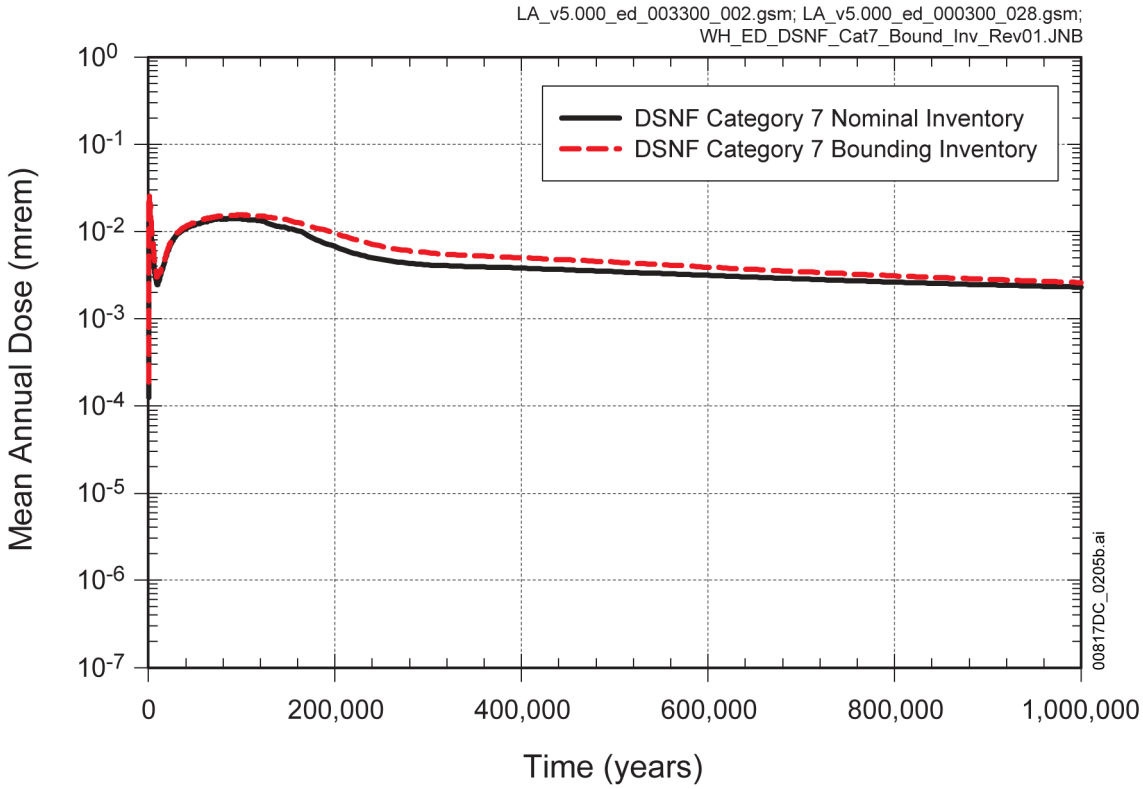

Source: Output DTN: MO0707TSPADSNF.000 [DIRS 182992].

Figure 7.5-26. Comparison of Mean Annual Dose from One Waste Package Failure of Uranium-Metal DSNF (Category 7) Using the Nominal Inventory with the Bounding Inventory (with no HLW)

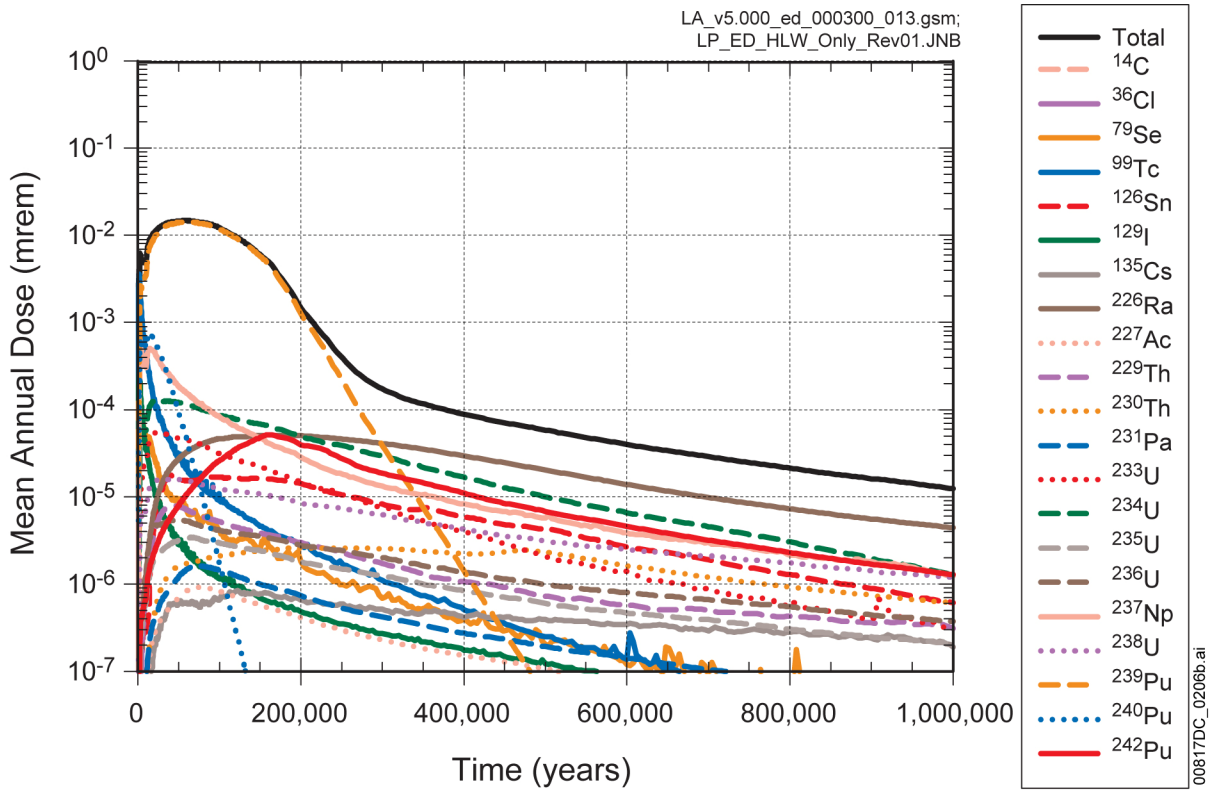

Source: Output DTN: MO0707TSPADSNF.000 [DIRS 182992].

NOTE: ^{226}Ra dose is the sum of ^{226}Ra and ^{210}Pb doses (secular equilibrium assumed).

Figure 7.5-27. Plot of Key Radionuclides that Contribute to Mean Annual Dose from Five Canisters of HLW (with no DSNF)

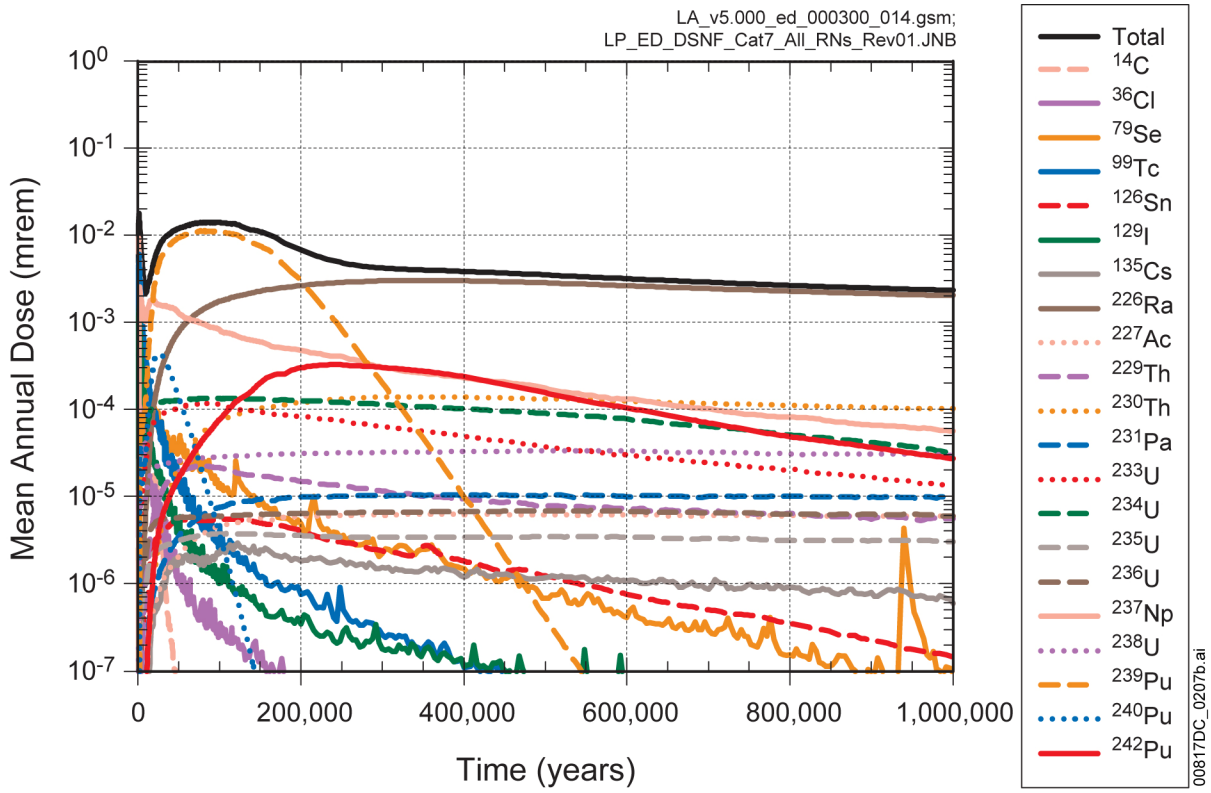

Source: Output DTN: MO0707TSPADSNF.000 [DIRS 182992].

NOTE: ^{226}Ra dose is the sum of ^{226}Ra and ^{210}Pb doses (secular equilibrium assumed).

Figure 7.5-28. Plot of Key Radionuclides that Contribute to Mean Annual Dose from One Waste Package Failure of Uranium-Metal Spent Fuel (Category 7) (with no HLW)

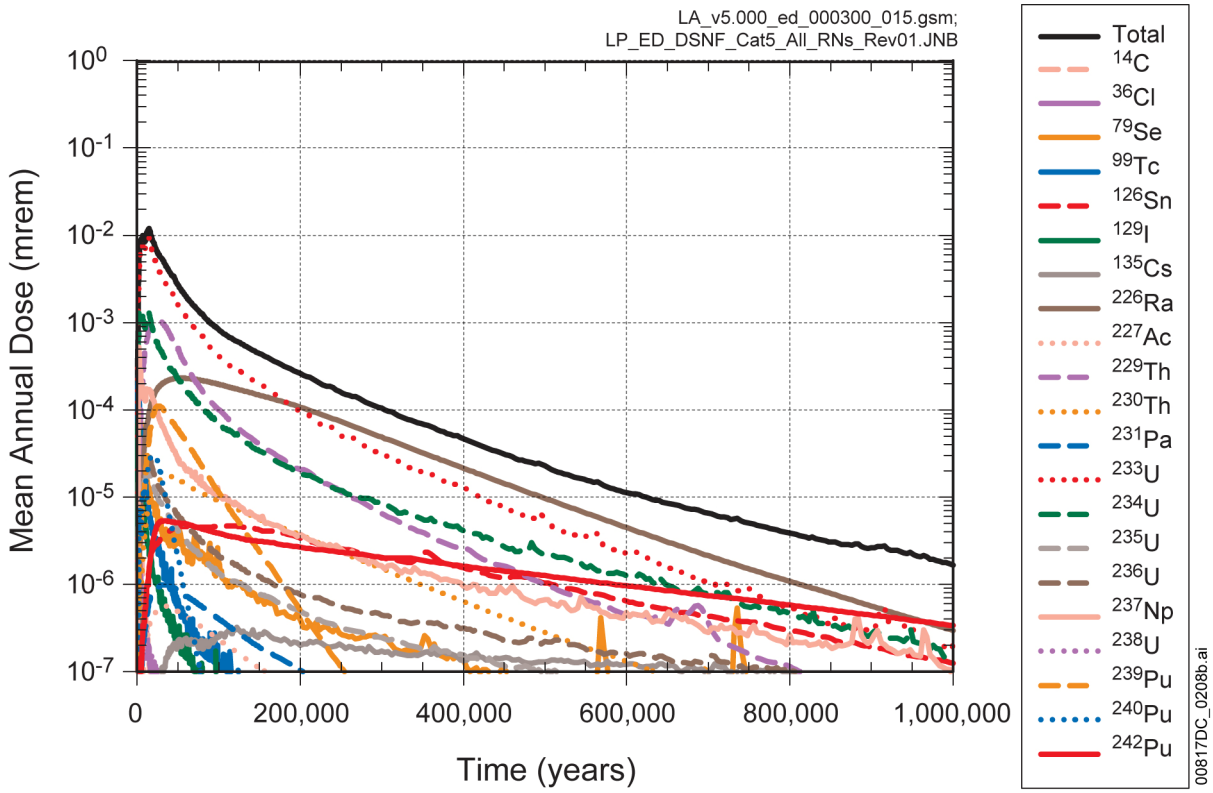

Source: Output DTN: MO0707TSPADSNF.000 [DIRS 182992].

NOTE: ^{226}Ra dose is the sum of ^{226}Ra and ^{210}Pb doses (secular equilibrium assumed).

Figure 7.5-29. Plot of Key Radionuclides that Contribute to Mean Annual Dose from One Waste Package Failure of Uranium/Thorium-Carbide Spent Fuel (Category 5) (with no HLW)

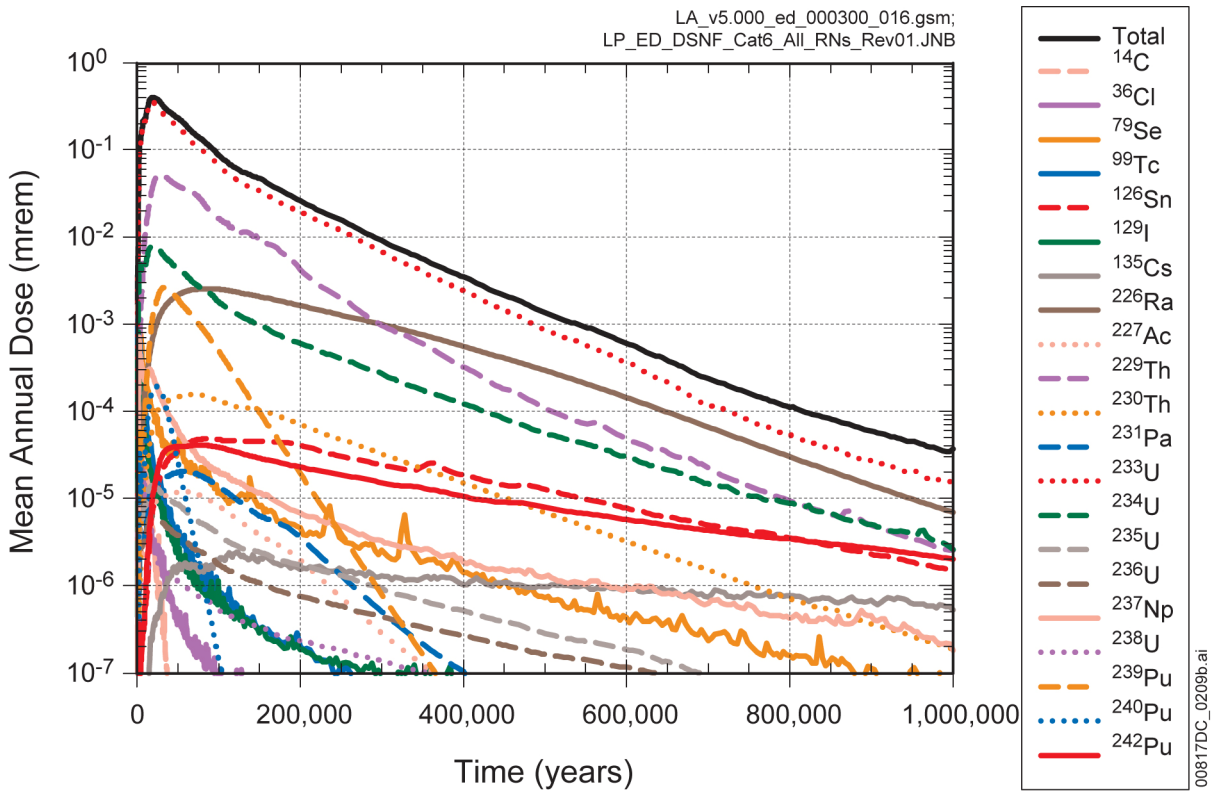

Source: Output DTN: MO0707TSPADSNF.000 [DIRS 182992].

NOTE: ^{226}Ra dose is the sum of ^{226}Ra and ^{210}Pb doses (secular equilibrium assumed).

Figure 7.5-30. Plot of Key Radionuclides that Contribute to Mean Annual Dose from One Waste Package Failure of Uranium/Thorium-Oxide Spent Fuel (Category 6) (with no HLW)

7.6 CORROBORATION OF ABSTRACTION MODEL RESULTS WITH VALIDATED PROCESS MODELS

Development of the TSPA-LA Model required abstraction of process models that serve as direct inputs and that provide parameter values as direct inputs to the TSPA-LA Model. SCI-PRO-006, *Models* lists corroboration of results of abstractions with their respective process models as one of nine post-development model validation criteria. For the TSPA-LA Model results to be valid, it is required that the abstractions are also accurately implemented in the TSPA-LA Model. Sections 7.2 (Computer Code and Input Verification) and 7.3 (Model Stability Testing) describe the implementation of the abstractions into the TSPA-LA Model. This section discusses the corroboration of the results of the abstractions with their respective process models and thus provides confidence that the TSPA-LA direct input parameters that were abstracted are technically sound for their intended purpose. The corroboration process provides the technical basis for the postclosure repository performance simulated by the TSPA-LA Model. Coupled with Table 7.6-1, this section summarizes the results of the corroboration, thus confirming that the TSPA-LA Model is based on technically defensible abstracted parameter values.

Section 7.6.1 provides a brief description of the processes used to develop the TSPA-LA Model. Section 7.6.2 describes the requirements and objectives for the verification of the model abstraction results. Section 7.6.3 explains the methods used in corroborating the abstraction model results, and the limitations associated with the results that are presented in Section 7.6.4.

7.6.1 Introduction

Figure 1-2 shows the key steps involved in the TSPA approach as four levels of a pyramid and the information flow and the feedback loops among the four levels. The foundation of the TSPA pyramid consists of a repository-system characterization involving the assimilation of the information collected in site characterization and engineering design activities. The repository system characterization entails data collection regarding waste properties and design of the repository facilities, as well as the regional geology, hydrology, and environmental characteristics of the Yucca Mountain site. The foundation of the pyramid represents more than a 20-year body of knowledge collected in the field, laboratory, and the design basis of the repository system.

The accumulated body of knowledge constitutes the technical database that was used to identify the set of possible FEPs that may affect the performance of the repository system after the repository closure and also provides the basis for the second stage of the TSPA pyramid; that is, development of conceptual models and process models (Figure 1-2). The TSPA-LA Model is built on the family of analyses of the identified FEPs, including analyses related to the exclusion of FEPs that are either very unlikely, are not required for regulatory reasons, or that have a low impact on performance. The second stage of the TSPA pyramid consists of the development and testing of models used to conceptually describe the retained probable FEPs and their outcomes regarding repository performance. The conceptual models consist of sets of hypotheses, assumptions, simplifications, and idealizations, which together describe the essential aspects of a system or subsystem of the repository relative to its performance. Model conceptualization identifies and selects FEPs that collectively comprise the scenarios (Section 1.5) considered in the conceptual models. The second stage of the TSPA pyramid (Figure 1-2) includes the

development of mathematical representations of the conceptual models of the FEPs or scenarios, or both, that contribute to overall repository performance.

The TSPA-LA Model includes a numerical representation of water flow through Yucca Mountain as an abstraction (Figure 7.1-1) consisting of a series of statistical or mathematical expressions, including look-up tables, equations representing response surfaces, probability distributions, linear transfer functions, or reductions of model dimensionality. Inputs developed by the abstraction process were either implemented directly into the TSPA-LA Model or through a series of simplifying steps, depending upon the relative complexity and/or importance of the FEPs being abstracted. This abstraction, or progressive simplification of the conceptual models to more compact and usable numerical models, is the essence of the third level of the TSPA pyramid. The models used to analyze the projected evolution through time of the various components of the repository system are abstracted models that capture the salient features of the process models, along with their associated uncertainties. The top level of the TSPA pyramid consists of the integrated total system model. The total system model is a numerical model used to simulate the behavior of the Yucca Mountain repository system. The TSPA-LA Model incorporates the abstracted process models and/or the results of analyses that describe the model components and their submodels from their development to their implementation.

7.6.2 Requirement and Objective

An abstraction is a quantitative simplification process required for the numerical implementation of the process models in the TSPA Model computation using a complex and integrated computer code such as GoldSim, which is used for computation of the TSPA-LA Model. It is essential, therefore, to ensure that the abstraction results corroborated by the underlying process model results. The abstractions quantitatively represent their respective process models before and after their implementation in the TSPA-LA Model. When the abstractions are applied together as the integral components of the TSPA-LA Model, they function coherently so that the TSPA-LA Model results are stable, and properly represent the contributing abstractions. This consistency is achieved by performing several steps: (1) ensuring that the individual abstractions are validated after abstraction for their intended use in the TSPA-LA Model, (2) performing input-verification activities during their implementation in the TSPA-LA Model, and (3) testing model stability during the model development process.

The abstractions and their underlying process models are validated during their individual development and post-development validation phases described in SCI-PRO-006. These validation activities and their results are documented in analysis and model reports. As a means of validating the abstractions, their results were corroborated with their underlying process models. Validated process models themselves feed the TSPA-LA Model when appropriate without further abstraction. The process models that served as the sources of the input parameters to the TSPA-LA Model are listed in Table 4-1. The input parameters are in the Parameter Entry Forms (PEFs) listed in Table 4-1. These inputs are referred to as direct input in Table 4-1 to reflect the fact that the process models that provide the inputs are supported by validated submodels. During implementation in the TSPA-LA Model development process, the integrity of the direct input models or analyses is ensured by performing: (1) independent checks to ensure that the direct inputs are accurately applied in the TSPA Model runs, and (2) independent verification, such as model re-runs, to confirm that the inputs produce the result

that is expected. These checking and verification activities are documented controlled processes. The verification activities are summarized in Section 7.1.2.1, and a detailed discussion of the verification analyses performed is provided in Section 7.2. The checking and verification activities ensure that the TSPA-LA Model is built with the inputs from the abstractions that have been accurately implemented. The development phase also involves determining whether or not the abstractions, when applied together as the integral components of the TSPA-LA Model, function coherently and provide stable TSPA-LA Model results. The TSPA-LA Model stability testing activities are summarized in Section 7.1.2.2 and discussed in Section 7.3.

Once the integrity of the implementation of the abstractions in the TSPA-LA Model is ensured through the verification process, and it is clear that the individual abstractions are functioning well when they are applied together as components of the TSPA-LA Model, certain post-development model validation and confidence building activities unrelated to the development of the TSPA-LA Model need to be performed in order to show that the TSPA-LA Model is valid for its intended use.

Ensuring the integrity of the direct-input models during abstraction and successful application of the abstractions to the TSPA-LA Model is the first step towards defining and executing these follow-up post-development validation and confidence building activities. The TSPA-LA Technical Work Plan (SNL 2008 [DIRS 184920], Section 2.3.5.2) identified corroboration of abstraction model results with validated process models as a TSPA-LA Model validation method in order to document in the TSPA-LA Model report that the results of the abstractions corroborate the results of the respective underlying process models. To accomplish this confirmation, corroboration of the abstraction results with those of the respective process models are evaluated in this section. The validation criterion, ensure that there is confidence in outputs from the models, and they are appropriate for their intended use in the TSPA-LA Model. The information on validation and the basis for confidence in the model outputs to the TSPA-LA Model are included in the discussion here and summarized in Table 7.6-1.

7.6.3 Methods Used

The model and analysis reports that were sources for the direct input parameters to the TSPA-LA Model are identified in Table 4-1. The functional relationships among these models and analyses as integral components of the TSPA-LA Model, and implementation of the parameters, are discussed in the individual subsections of Section 6 of the TSPA-LA Model report. The discussion here focuses on the corroboration of abstraction results with the underlying models and analyses that are referenced in Table 4-1 and Table 6-1. These references are cited in Table 7.6-1 as appropriate for transparency. As mentioned earlier, the direct input models are themselves usually based on a number of submodels and/or analyses. The submodels often need to be abstracted during their implementation in the models that serve as the direct input to the TSPA-LA Model. These submodels are not discussed here because their validation and confidence building activities and results are documented in the respective model or analysis reports. There are a few exceptions. For example, the UZ Site-Scale Process Model (SNL 2007 [DIRS 184614]), which is discussed here and shown in Table 7.6-1, is not a direct input. It is implemented in the TSPA-LA Model via the UZ Transport Model and MSTHM. However, the flow fields, rock properties, and percolation flux parameters from the UZ Site-Scale Process Model (SNL 2007 [DIRS 184614]) are parameters that form the basis for the predictions for

radionuclide transport in the UZ below the repository and the TH conditions in the repository. This relationship is shown on Figure 6.3.1-6. The validation and consistency of these models are presented in Section 7 of the respective model or analysis reports.

Table 7.6-1 shows the process models and analyses that served as direct input to the TSPA-LA Model computation are represented by the following groups: Natural System Environment, EBS Environment, Waste Form and Waste Package Degradation and Mobilization, Disruptive Events, and Biosphere.

The first column in Table 7.6-1 shows the general model area within individual groups. The second and the third columns identify the abstractions and the respective underlying process models or analyses. The column on the right in Table 7.6-1 provides the results. This column discusses the results of corroboration qualitatively, providing quantitative information when appropriate but mostly providing references to the figures and tables in the source model or analysis reports. A summary of the basis for the confidence in the output parameters used in the TSPA-LA Model preparation is also provided in the results column, again by largely deferring the detail to the cited respective source documents.

The results presented in the last column in Table 7.6-1 do not discuss the assumptions and uncertainties associated with the parameters from the abstractions and the underlying process models and analyses. The respective analysis reports describe the justifications of the assumptions and document the uncertainties of the output parameters. Assumptions used in the TSPA-LA Model are presented in Section 5. The treatment of uncertainty in the TSPA-LA Model is discussed in Section 6.1.3. The TSPA-LA parameter uncertainty characterization reviews and remedial actions on the findings are presented in Section 7.4. Appendix K discusses the uncertainty and sensitivity analyses conducted using the TSPA-LA Model. The auxiliary analyses presented in Section 7.7 provide confidence in the results of the TSPA-LA Model simulations based on the parameters from the direct input models and analyses discussed here.

7.6.4 Results of Corroboration

The following discussion focuses on the process models and the analyses that provide direct inputs to the TSPA-LA Model. The discussion follows the group sequence of Table 7.6-1: Natural System Environment, EBS Environment, Waste Form and Waste Package Degradation and Mobilization, Disruptive Events, and Biosphere.

7.6.4.1 Natural System Environment

This section presents results of corroboration of abstractions with the underlying validated process models of the natural system and provides information on the confidence built into the direct-input TSPA-LA Model parameters abstracted from these process models. The key models are on the UZ flow and SZ flow and transport processes.

7.6.4.1.1 UZ Flow Model

The model report that sources the input parameters on UZ flow to the TSPA-LA computation is *UZ Flow Models and Submodels* (SNL 2007 [DIRS 184614]).

Section 6.3.1 discusses implementation of the UZ flow model in the TSPA-LA Model. Figure 6.3.1-6 lists some activities on which the confidence in the output parameters from the UZ Site-Scale Flow Model is based. The details are provided in Section 7 of *UZ Flow Models and Submodels* (SNL 2007 [DIRS 184614]). The activities include corroborating the model-output parameters (hydrologic properties and percolation flux as inputs for the MSTHM and mountain-scale UZ flow fields as inputs for the UZ Transport Models). These parameters are shown in PEFs # 38, 39, 40, 42, and 43 in Table 4-1 with observations from numerous boreholes and the enhanced characterization of repository block (ECRB) and exploratory studies facility (ESF) tests and pretest predictions. For example, Figure 7.2-1 (SNL 2007 [DIRS 184614]) shows that the model prediction of water potential falls within the range observed in the ECRB, Figure 7.3-1 (SNL 2007 [DIRS 184614]) shows that the predicted water potential is consistent with the data observed in borehole WT-24, and Figures 7.5-1 and 7.5-2 (SNL 2007 [DIRS 184614]) demonstrate that the predicted groundwater ages in the UZ compare well with the measured 14C age in the samples from boreholes UZ-1 and SD-12. Similarly, Sections 7.6 to 7.8 (SNL 2007 [DIRS 184614]) demonstrate corroboration of predicted flow parameters with the fracture-flow infiltration and tracer test data from the Alcove 8/Niche 3 tests, Section 7.6 (SNL 2007 [DIRS 184614]) validates the flow model with the measured chloride data, and Section 7.7 (SNL 2007 [DIRS 184614]) corroborates fracture-flow percolation flux with the site-specific calcite deposition model. These numerous site-specific corroborative measurements and modeling activities serve to demonstrate that the UZ flow model parameters are technically sound.

In addition, the key flow and transport processes pertaining to the UZ at Yucca Mountain have been investigated through natural analogues (BSC 2004 [DIRS 169218]). These analogue studies contained both literature review and data analyses. One of the important case studies was the flow experiment and tracer infiltration test in fractured media at Box Canyon, Idaho. One of the desired confidence building activities is publication in a peer-reviewed journal. There have been numerous such publications on the UZ flow model by the YMP. These include the publications dealing with the following topics on the UZ flow model:

- A three-dimensional UZ numerical model was developed to simulate flow and distribution of moisture, gas, and heat at Yucca Mountain (Wu et al. 1999 [DIRS 117161]).

- Flow and transport processes within the UZ were characterized under current and future climates (Wu et al. 2002 [DIRS 160195]).

- Work on capillary barriers in the unsaturated rock of Yucca Mountain have been published (Wu et al. 2002 [DIRS 161058]).

- The perched-water phenomena in the UZ at Yucca Mountain have been investigated (Wu et al. 1999 [DIRS 117167]).

- Subsurface pressure variations have been used to determine the pneumatic diffusivity of important geological features (Ahlers et al. 1999 [DIRS 109715]).

- Subsurface borehole temperature data were used to estimate percolation flux (Bodvarsson et al. 2003 [DIRS 162477]).

- Chloride measurements were used to calculate infiltration rates along the ESF (Fabryka-Martin et al. 1998 [DIRS 146355]).

- Chloride data, in conjunction with hydrostructural and hydrogeological features, were used to constrain infiltration rates (Liu et al. 2003 [DIRS 162478]).

- Chloride and strontium geochemistry were investigated using three-dimensional modeling for insights into the hydrology of the UZ (Sonnenthal and Bodvarsson 1999 [DIRS 117127]).

The UZ Flow Model area in Table 7.6-1 shows two submodels: future climate analysis (BSC 2004 [DIRS 170002]) and infiltration (SNL 2007 [DIRS 182145]). These two submodels support the UZ Site-Scale Flow Model that provides the UZ flow fields, percolation flux, and rock properties parameters for the succeeding direct input models for the TSPA-LA Model: UZ radionuclides transport and MSTHM as shown on Figure 6.3.1-6. Figure 6.3.1-2 provides the flow of information and the basis for confidence in *Future Climate Analysis* (BSC 2004 [DIRS 170002]) outputs (PEF # 33) for use in the TSPA-LA Model, as described in Section 6.3.1. *Future Climate Analysis* (BSC 2004 [DIRS 170002], Section 7.1) presents an assessment of the confidence in the analysis results and concludes that the analysis is reasonable and defensible in that it is based on a consistent interpretation of available data, which include the earth orbital parameter and paleoclimate data. The defensibility is based on a body of data and a possibility rather than that the climate forecast by this analysis is much more likely to occur relative to other possible methods.

Figure 6.3.1-4 provides information on infiltration analysis (SNL 2007 [DIRS 182145]) and its output to the TSPA-LA as described in Section 6.3.1. The confidence building activities in the analysis results are described in Section 7 of *Simulation of Net Infiltration for Present-Day and Potential Future Climates* (SNL 2007 [DIRS 182145]). The report (SNL 2007 [DIRS 182145], Sections 7.1, 7.2, and 7.3]) also describes the activities performed on validation and confidence building in the infiltration parameters. The activities included: (1) comparison of MASSIF predictions of infiltration for present-day, monsoon, and glacial-transition climates for 40 realizations for each climate, with infiltration estimates from published models and data for the Yucca Mountain area, the southwestern United States, and the western United States, (2) comparison of MASSIF predictions of infiltration with seepage estimates observed in the South Ramp of the ESF in the winter of 2005; and (3) alternative model approach corroboration activity in which MASSIF results are compared to HYDRUS 1-D results for four different soil depths and using the same model inputs. Table 7.3-1 (SNL 2007 [DIRS 182145]) tabulates the output DTNs of the validation and confidence building activities. The results of these activities demonstrate that the infiltration parameters used in defining the UZ flow fields and percolation fluxes are technically sound and defensible.

7.6.4.1.2 UZ Radionuclide Transport Model

The model report that sources the input parameters on UZ radionuclide transport to the TSPA-LA computation is *Radionuclide Transport Models Under Ambient Conditions* (SNL 2007 [DIRS 177396]). The radionuclide transport computation utilizes the flow fields defined in *UZ Flow Models and Submodels* (SNL 2007 [DIRS 184614]) discussed in Section 7.6.4.1.1.

Figure 6.3.9-2 shows the model components and inputs for the TSPA-LA UZ transport computation. The UZ transport in the TSPA-LA Model is calculated using particle-tracking methodology as described in Section 6.3.9.2, and using the FEHM code (FEHM V2.24-01 [DIRS 179419]). The results of the Particle Tracking Model were compared, for the needed range of complexity, with the breakthrough curves developed from *Radionuclide Transport Models Under Ambient Conditions* (SNL 2007 [DIRS 177396]), which is a validated process model. Results show good comparisons. For example, Figure 7-11 of *Particle Tracking Model and Abstraction of Transport Processes* (SNL 2008 [DIRS 184748]) compares the FEHM results for several alternative conceptual models (ACMs) with the breakthrough curves from the process model using the code T2R3D. The dual-k results show the best match. The detail of the FEHM abstraction is presented in *Particle Tracking Model and Abstraction of Transport Processes* (SNL 2008 [DIRS 184748], Section 7).

7.6.4.1.3 SZ Flow and Transport Flow Models

The source of the SZ direct-inputs to the TSPA-LA computation are the breakthrough curves for the radionuclides of concern at the location of the RMEI. The breakthrough curves are developed using a three-dimensional transport model for the radionuclides without considering radioactive decay products. The effects of the decay products on the transport are accomplished separately through a one-dimensional transport model. Figure 6.3.10-2 summarizes the principal inputs and outputs, model features, and the foundations for confidence in the SZ Flow and Transport Model components as described in Section 6.3.10 of the TSPA-LA Model. These abstractions are described and validated in *Saturated Zone Flow and Transport Model Abstraction* (SNL 2008 [DIRS 183750]). The underlying validated process model is the SZ Site-Scale Transport Model (SNL 2007[DIRS 177392]).

For the three-dimensional simulations, breakthrough curves for a non-sorbing dissolved species (SNL 2008 [DIRS 183750], Figure 7-1 [a]) and moderately sorbing species of neptunium (SNL 2008 [DIRS 183750], Figure 7-2 [a]) of the 3-D SZ Transport Abstraction agree with those of the process model, based on visual inspection, within a few percent of relative mass of the respective species. For the non-sorbing case, one-million-year simulations were performed with an input condition of 1 g/yr for the first 1,000 years. The sum of the output mass was at 100.4 percent, 99.8 percent, and 101.6 percent of the median case, slow case, and fast case, respectively (SNL 2008 [183750], Figure 7-3 [a]). This demonstrates that the three-dimensional abstraction model represents the underlying process model with respect to total mass flux.

For the one-dimensional abstraction model, visual comparison of breakthrough curves for a non-sorbing dissolved species (SNL 2008 [DIRS 183750], Figure 7-4 [a]) and moderately sorbing species of neptunium (SNL 2008 [DIRS 183750], Figure 7-5 [a]) of the 1-D SZ

Transport Abstraction Model without radioactive decay and the 3-D SZ Transport Process Model indicate acceptable agreement. There is generally close agreement in the overall shapes of the breakthrough curves and generally good agreement at the mid-points of the breakthrough curves. The results of one-million-year simulations, expressed as the mean breakthrough curves of 200 realizations for a non-sorbing species and moderately sorbing species, indicate similar behavior for the two models, with somewhat less apparent dispersion exhibited by the 1-D SZ Transport Model relative to the three-dimensional process model. The validation testing indicates acceptable agreement of the one-dimensional transport model abstraction with the underlying 3-D process model.

7.6.4.2 Engineered Barrier System Environment

This section presents results of corroboration abstractions with the underlying validated models and analyses of the EBS environment. It provides information on the confidence built into the direct input TSPA-LA Model parameters that were abstracted from these process models and analyses. As shown on the first column in Table 7.6-1, the key models and analyses areas are seepage into drift, in-drift convection and condensation, repository thermo hydrology due to waste heat, and the EBS physical and chemical environment. The outputs from these TSPA-LA components are used in defining the WP and waste form degradation and release and transport of radionuclides through the EBS to the invert-UZ contact underlying the repository.

7.6.4.2.1 Seepage into Drift

The TSPA-LA seepage parameters were abstracted from the validated process models. The principal two process models that serve as direct inputs to the drift-seepage abstraction are: (1) Seepage Model for Performance Assessment (SNL 2007 [DIRS 181244], Section 6.4.2), and (2) TH Seepage Model (SNL 2007 [DIRS 181244], Section 6.4.3). Section 7.2 of *Abstraction of Drift Seepage* (SNL 2007 [DIRS 181244]) discusses the results of comparison of the abstracted seepage parameters with the underlying respective process models that were already validated for their intended use. The information flow for the drift-seepage abstraction for the TSPA-LA Model is shown on Figure 6.3.3-1. The TSPA-LA Model input parameters from *Abstraction of Drift Seepage* (SNL 2007 [DIRS 181244]) are shown in Table 4-1 (PEFs # 37, 44, and 45). The submodels of the Abstraction of Drift Seepage submodels are shown on Figure 6.3.3-2.

Abstraction of Drift Seepage (SNL 2007 [DIRS 181244], Section 7.2) provides evidence that the abstracted results of the drift seepage model satisfy the validation requirement (of Level 1 validation set by the technical workplan (BSC 2006 [DIRS 177465])) with agreement within 20 percent between the process models and abstracted results. Additional confidence in the abstracted TSPA-LA parameters was built by qualitative comparisons (SNL 2007 [DIRS 181244], Section 7.3) with: (a) the south ramp seepage predictions with actual observations, (b) Alcove 8-Niche 3 seepage tests results, and (c) observations with seepage in the Peña Blanca natural analogue. *Abstraction of Drift Seepage* (SNL 2007 [DIRS 181244, Section 7.3]) documents that the abstracted seepage value corroborates reasonably with the data from the above-mentioned analogues. The abstraction of Drift Seepage Model (SNL 2007 [DIRS 181244]) produces an upper-bound (i.e., a conservative) seepage value.

7.6.4.2.2 In-Drift Convection and Condensation

The information flow for the In-Drift Convection and Condensation Model (SNL 2007 [DIRS 181648]) in the TSPA-LA Model implementation is shown on Figure 6.3.3-1. The condensation model is based on the convection model and the average percolation flux derived from the MSTHM. The confidence in the MSTHM model outputs is described below. The convection model was validated by: (1) comparison of simulation results to small-scale (centimeter dimension) literature data for natural convection in horizontal concentric cylinders, (2) 44 percent of full-scale dimension tests, and (3) an independent technical review. The details of validation test and results are presented in *In-Drift Natural Convection and Condensation* (SNL 2007 [DIRS 181648], Sections 7.3, 7.4, and 7.5). The condensation model was validated by a technical review (AP-SIII.10Q, Section 5.3.2, c 5), the scope of which required affirmative answers by the reviewer to all six questions in its Technical Work Plan (BSC 2004 [DIRS 170950], Sections 2.3.3 and 2.3.4). The technical review also included in its scope a review of the convection model. The results are presented in *In-Drift Natural Convection and Condensation* (SNL 2007 [DIRS 181648], Section 7.6 and Appendix G).

7.6.4.2.3 Repository Thermohydrology Due to Waste Heat

The integrated MSTHM defines TH conditions in the drift due to waste-generated heat as a function of time and location. Figure 6.3.2-1 shows the integration of the component models for input to the TSPA-LA Model computation. Table 4-1 lists the parameters from the MSTHM that serve as the inputs to the TSPA-LA Model (PEFs # 79, 12, 15, 86, 16, 17, 18, 19, 20, 21, 22, 23, 24, 25, 26, 27, 28, 29, and 114). Section 6.3.2 discusses the implementation of the TH conditions in the drifts. The outputs from MSTHM (SNL 2007 [DIRS 181383]) produce percolation flux at the base of PTn at 3,264 locations and predict the in-drift thermohydrologic environment at these locations. The predictions consist of the following TSPA-LA parameters, which are implemented without further simplification: (1) temperature for drift-wall, DS, WP, and invert; (2) relative humidity of WP and invert; and (3) invert liquid-phase saturation. The MSTHM bases the predictions on application of its own methodology integrating its components (SNL 2007 [DIRS 181383]): (a) discrete-heat-source, drift-scale, thermal conduction; (b) smeared-heat-source, drift-scale, thermal conduction; and (c) smeared-heat-source, mountain-scale, thermal conduction, which are conduction-only calculations. The confidence in the predicted parameters was built by direct corroboration of test data (e.g., Large Block Test and Drift-Scale Test at the repository) and the results predicted by another model. The details are presented in Sections 7.3 through 7.6 of the MSTHM (SNL 2007 [DIRS 181383]). The results of these corroborative activities indicate that the parameters from MSTHM are technically sound for their intended use in the TSPA-LA Model.

The validation of the MSTHM involves the validation of both the MSTHM integrated prediction methodology as well as its supporting component submodels used in the integrated MSTHM. The MSTHM component, smeared-heat-source, drift-scale, thermal conduction, and smeared-heat-source, mountain-scale, thermal conduction are executed with the NUFT v3.0s code (Section 3.1.1). Because the smeared-heat-source, drift-scale, thermal conduction, smeared-heat-source, mountain-scale, thermal conduction, and discrete-heat-source, drift-scale, thermal conduction components are conduction-only calculations, which utilize standard scientific methods (e.g., Fourier's Law) to perform the calculations, they do not require separate

validation. Moreover, the smeared-heat-source, drift-scale, thermal conduction, smeared-heat-source, mountain-scale, thermal conduction, and discrete-heat-source, drift-scale, thermal conduction components are not applied as stand-alone models for analysis. Validation testing of the NUFT v3.0s code included conduction-only test problems (bmrk002 and verif02), which are described in the Validation Test Plan for NUFT 3.0s (LLNL 2002 [DIRS 170259]; LLNL 2000 [DIRS 170258]). These conduction-only test problems are sufficient to validate the usage of the conduction-only submodels in the MSTHM. Additional confidence building activity involving corroboration with results obtained from an alternate conduction-only mathematical model is described in *Multiscale Thermohydrologic Model* (SNL 2007 [DIRS 181383], Sections 6.2.5, 6.2.7, and 6.2.9), pertaining to the smeared-heat-source, mountain-scale, thermal conduction, smeared-heat-source, drift-scale, thermal conduction, and discrete-heat-source, drift-scale, thermal conduction components, respectively. This model-corroboration example is found in *Drift Degradation Analysis* (BSC 2004 [DIRS 166107], Section 6.2 and Figure 6-26).

The *Multiscale Thermohydrologic Model* (SNL 2007 [DIRS 181383], Section 7.4) documents the comparison of NUFT-predicted temperatures against those measured in the Drift Scale Test results and supports the ability of the MSTHM to predict a reasonable range of temperatures in the host rock. The confidence building activity for the ability of the MSTHM to predict a reasonable range of temperatures in the host rock is presented in *Multiscale Thermohydrologic Model* (SNL 2007 [DIRS 181383], Section 7.3), which documents the comparison of NUFT-predicted temperatures against those measured in the Large Block Test. The *Multiscale Thermohydrologic Model* (SNL 2007 [DIRS 181383], Section 7.6) also documents a comparison of the MSTHM-predicted in-drift temperature differences against those predicted by the FLUENT model, which supports the ability of the MSTHM to predict temperature differences between the drift wall and the DS and WP surfaces.

Section 7.4 of *Multiscale Thermohydrologic Model* (SNL 2007 [DIRS 181383]), which documents the comparison of NUFT-predicted liquid-phase saturations against those measured in the Drift Scale Test, also supports the ability of the MSTHM to predict a reasonable range of liquid-phase saturation in the invert. This ability of the MSTHM is supported by virtue of the relationship between liquid-phase flux and liquid-phase saturation, which is documented in Section 6.3.3 of *Multiscale Thermohydrologic Model* (SNL 2007 [DIRS 181383]). Note that for The TSPA-LA, the MSTHM-predicted liquid-phase flux is only applied to WPs that experience no seepage and no condensation. The ability of the MSTHM to predict a reasonable range of relative humidity on the drift wall and DS and liquid-phase saturation values is supported in *Multiscale Thermohydrologic Model* (SNL 2007 [DIRS 181383], Section 7.5) by virtue of a direct comparison between values predicted by the MSTHM and those predicted by a corresponding three-dimensional monolithic thermal-hydrologic model for a three-drift validation test case.

7.6.4.2.4 EBS Physical and Chemical Environment

The abstractions from the models in *Engineered Barrier System: Physical and Chemical Environment* (SNL 2007 [DIRS 177412]) are implemented by the EBS Chemical Environment Submodel. The inputs, outputs, and basis for model confidence for the EBS Chemical Environment Submodel are depicted on Figure 6.3.4-2. Table 4-1 lists the parameters inputs to

the TSPA-LA Model (PEFs # 75, 76, 77, and 78) from the Physical and Chemical Environment, and Section 6.3.4 discusses the TSPA-LA implementation.

The submodel provides seepage chemistry parameters (chloride ion concentration; nitrate ion concentration; and chloride to nitrate ion molar ratio, ionic strength, and pH) through the Seepage Dilution/Evaporation Abstraction Model (SNL 2007 [DIRS 177412]). It also provides the invert chemistry parameters (pH and I) via Seepage Dilution/Evaporation Abstraction Model (SNL 2007 [DIRS 177412]) and Integrated Invert Chemistry Abstraction Model (SNL 2007 [DIRS 177412]). The process models Near-Field Chemistry and In-Drift Precipitates Salts (IDPS) support the two abstraction models. The validation documentation for the abstraction models is presented in Section 7.2 of *Engineered Barrier System: Physical and Chemical Environment* (SNL 2007 [DIRS 177412]). Comparison of an interpolation of the look-up tables of the chemistry parameters with the underlying validated IDPS (SNL 2007 [DIRS 177412]) shows (Figure 7.2-2) that the difference is substantially less than the model uncertainty for the IDPS model for the model outputs from the same representative set of environmental conditions. In addition to these seepage and invert chemistry parameters, the validated Near-Field Chemistry model (SNL 2007 [DIRS 177412]) provides water rock interaction parameters and a range of in-drift partial pressure of carbon dioxide (pCO_2) values for the TSPA-LA. These Integrated Invert Chemistry Abstraction parameters are validated by the same set of test cases as those used for the Seepage Dilution/Evaporation Abstraction parameters because both models utilize the same look-up tables in the same manner.

7.6.4.3 Drip Shield, Waste Package, and Waste Form Degradation and Mobilization

This section presents corroboration of abstraction results with the underlying validated models or analyses on the DS, WP, and waste form degradation and mobilization. It also provides information on the confidence built into the direct-input TSPA-LA Model parameters derived from these process models or analyses.

7.6.4.3.1 Drip Shield, Waste Package, and Waste Form Degradation

Waste Package and Drip Shield Degradation, Section 6.3.5, discusses implementation of the SCC information in the TSPA-LA Model as shown graphically on Figure 6.3.5-8, which provides a summary and illustration of the information flow between the DS and WP SCC Abstractions. SCC is not implemented in the TSPA-LA Model for DS as discussed in Section 6.3.5.1.1. The outputs from the Alloy 22 slip dissolution-film rupture and WP SCC models (BSC 2006 [DIRS 169996]) provide direct feeds (parameters in PEF # 4 in Table 4-1) to the TSPA-LA Model. The outputs from the Alloy 22 and DS seismic crack density model feed Seismic Consequence Abstraction (SNL 2007 [DIRS 176828]), which is described below. These three models and the two key input parameters (threshold stress intensity factor and threshold stress for SCC initiation) to the slip dissolution-film rupture model are validated for their intended use, and the details of the validation activities and results are described in Sections 7.1 through 7.5 of *Stress Corrosion Cracking of Waste Package Outer Barrier and Drip Shield Materials* (SNL 2007 [DIRS 181953]).

Comparison with the literature data shows that the SCC growth rate is within two to three orders of magnitude of the literature data (SNL 2007 [DIRS 181953], Figure 7-2), which is considered

reasonable and acceptable because of the large scatter in experimental and literature data. Additionally, as a defensible approach, the threshold stress intensity factor and the threshold stress for SCC initiation under environmental conditions were established (SNL 2007 [DIRS 181953]).

General Corrosion and Localized Corrosion of Waste Package Outer Barrier—Figure 6.3.5-3 shows information flow from SCC and other corrosion submodels to WP and DS degradation modeling as a part of the WAPDEG analysis of WP and DS Degradation and PEF # 5, 7, and 117 in Table 4-1.

General Corrosion and Localized Corrosion of Waste Package Outer Barrier (SNL 2007 [DIRS 178519], Sections 7.1 and 7.2) provides detailed discussions on the comparison of experimental and literature data on general corrosion and localized corrosion parameters with the model predictions and present the validation and confidence building for the general corrosion and localized corrosion models. Figure 7-1 and Table 7-1 in *General Corrosion and Localized Corrosion of Waste Package Outer Barrier* (SNL 2007 [DIRS 178519]) provide comparison of the Project experimental data with literature data on general corrosion rates as a function of time and Table 7-4 for comparison of model prediction of localized corrosion susceptibility with experimental data of Alloy 22 crevice samples. The conclusion is that the general and localized corrosion models for the WP outer barrier corroborates well with the experimental data and those reported in the scientific literature.

Drip Shield Corrosion—Section 6.3.5.1 and Figure 6.3.5-3 show information flow from DS Corrosion (Titanium Grade 29) (SNL 2007 [DIRS 180778]) and other corrosion submodels to WP and DS degradation modeling as a part of the WAPDEG analysis of WP and DS degradation models (Parameters in PEF # 3 and 105 in Table 4-1). As is the case for most of the supporting submodels for the TSPA-LA Model, the long time of application involved does not allow validating these models in the usual way (i.e., by comparison of model-predicted values with those observed experimentally for the whole range of time (ASTM 1998 [DIRS 105725], Sections 19.3 and 20.4). Consequently, these models were validated by a combination of validating the input parameter values used and comparing these parameters and model predictions to experimental data that were not used (SNL 2007 [DIRS 180778], Figures 24, 25, and 27) and the available peer-reviewed data (e.g., Ogden 1960 [DIRS 160556], Chapter 10, Figure 30.18; Mattsson and Olefjord 1990 [DIRS 111885]; Molecke et al. 1982 [DIRS 161678]; Schutz and Thomas 1987 [DIRS 112147], Table 23); and Hua et al. 2004 [DIRS 167022]). The peer-reviewed data represent varied experimental designs. The fact that the parameters generally agree with these data provides confidence that the model predictions are appropriate. Further, comparison with the experimental data shows that the model predictions conservatively provide the upper bounds. Detailed description of the validation activities and results are provided in Sections 7.3 (dry oxidation), 7.4 (general corrosion), and 7.5 (localized corrosion) of *General Corrosion and Localized Corrosion of the Drip Shield* (SNL 2007 [DIRS 180778]). As discussed in Section 6.3.5.1.1, localized corrosion for DS was excluded and therefore not implemented in the TSPA-LA Model.

Waste Form Degradation—Section 6.3.7.4 of the TSPA-LA Model describes the TSPA-LA implementation of the three types (CSNF, DSNF, and Defense HLW glass) of waste-degradation (Table 7.6-1 and the parameters in PEF # 31, 82, 32, and 83 listed in Table 4-1). Figure 6.3.7-2

shows the inputs, outputs and the basis for confidence in the waste-form degradation models. The output from the three analyses is the mass-release rates of radionuclides due to degradation of the respective waste forms.

The rates developed by the three analyses were validated as required for their intended purpose of the calculations. The details of the validation and confidence building activities are documented in Section 7 of the respective documents: *CSNF Waste Form Degradation: Summary Abstraction* (BSC 2004 [DIRS 169987]); *DSNF and Other Waste Form Degradation Abstraction* (BSC 2004 [DIRS 172453]); and *Defense HLW Glass Degradation Model* (BSC 2004 [DIRS 169988]). The calculated release rates for the CSNF were corroborated with: (1) experimental and literature data that show that CSNF model rates and the experimental and literature data are within the range of associated uncertainty (Section 7.1 tables); (2) results of two ACMs (surface-complexation model and electrochemical model), which indicate the model dissolution rates are reasonable; and (3) comparison of the oxidative alteration rate and phases of relevant natural analogues with those of laboratory experiments, which indicates that the model results are reasonable. The natural analogues included the uranium deposits at Peña Blanca, Mexico; Koongarra, Australia; Pecos de Caldas, Brazil; and Shinkolobwe mine in Congo and Krunkelbach mine in Germany.

For the DSNF, the model data from the analysis were validated by comparison with alternate mathematical models (BSC 2004 [DIRS 172453], Section 6.1, Table 6-9), which showed complete degradation in one year, thus supporting the instantaneous release model for DSNF.

The degradation rate derived for the Defense HLW Glass Degradation analysis was validated by comparison with laboratory test results and relevant observations in studies with simulated HLW and natural analog glasses that were not used to develop the model. The details are presented in *Defense HLW Glass Degradation Model* (BSC 2004 [DIRS 169988], Section 7 and Table 7-1).

Drip Shield and Waste Package Early Failure—Section 6.4 discusses early failure and Figure 6.4-3 shows the information flow of inputs (parameters in PEFs # 2 and 118 in Table 4-1), outputs, and basis for confidence for the Early Failure Scenario Class. No validation is required. The Early Failure Scenario Class parameters were developed by an analysis using standard scientific and engineering practice and require no post-development validation. Nonetheless, confidence in the Early Failure Scenario Class parameters is based on: (1) the fact that the calculations were performed using manufacturing-industry defect-related controlled failure data sets, (2) conservative probability estimate of occurrences of flaws per WP and DS that lead to early failure, and (3) conservative estimate of impact on barrier containment properties.

7.6.4.3.2 Mobilization

Radionuclide Inventory—Section 6.3.7.1 of the TSPA-LA Model discusses the implementation of the data from *Initial Radionuclide Inventories* (SNL 2007 [DIRS 180472]) and its addendum. Figure 6.3.7-1 shows the information (parameters in PEFs # 72, 74, and 113 in Table 4-1) flow as implemented in the TSPA-LA Model. Figure 6.3.7-3 shows the basis for defining the waste inventory. The inventory was developed based on the latest available qualified and controlled dataset as stated in the source document in *Initial Radionuclide Inventories* (SNL 2007

[DIRS 180472], Section 7 and Table 7.1-1). The inventory is an analysis that was performed applying standard scientific principles and practices, pursuing the requirements of SCI-PRO-005, and thus providing confidence in the inventory presented in Table 7.1-1.

In-Package Chemistry—Section 6.3.7 discusses and Figure 6.3.7-5 shows the TSPA-LA Model implementation of the output parameters (PEFs # 12 and 79 in Table 4-1) from *In-Package Chemistry Abstraction* (SNL 2007 [DIRS 180506]). The in-package chemistry model is made up of two main underlying process models: the batch reactor model and the surface complexation model. The batch reactor model is made up of two water-influx models, the liquid-influx and the vapor-influx models, and several other component submodels, including the fuel-degradation and the steel-degradation submodels. The primary output parameters of the in-package chemistry model abstraction to TSPA are ranges of pH and ionic strength. The abstraction pH and ionic strength values were compared with the process-model output on Figures 7-1 through 7-8 in *In-Package Chemistry Abstraction* (SNL 2007 [DIRS 180506]) for a fixed flux and a range of fluxes. The abstracted values are consistent with the model outputs, and their reasonableness is evaluated by corroborating the values with natural analogues as presented in *In-Package Chemistry Abstraction* (SNL 2007 [DIRS 180506], Section 7.4.5) with favorable results.

Dissolved Concentration Limits of Elements with Radioactive Isotopes—Section 6.3.7.5 of the TSPA-LA Model discusses how the outputs from *Dissolved Concentration Limits of Elements with Radioactive Isotopes* (Parameters in PEFs # 9, 10, and 11 in Table 4-1) are implemented in the TSPA-LA Model. Figure 6.3.7.10 shows how the dissolved concentration limits are integrated with the WP sources, EBS flow and chemical environment and the in-package chemistry model outputs, as well as the inputs to the downstream submodels of radionuclide transport through EBS and invert. The solubility models used in TSPA-LA are based on four key components: (1) a thermodynamic database and modeling tool, (2) the environmental conditions of concern, (3) the construction of the conceptual model, and (4) the calculation of solubility limits using a geochemical modeling tool based on the conceptual model. Because the thermodynamic database used in this report and the EQ3/6 code are controlled products and are used within their valid ranges, the first and fourth components need no validation. The second component is represented by inputs to the model and also needs no validation. Therefore, the model-validation need focuses on the third component, the conceptual model (e.g., the solubility-controlling mechanism). The during-development and post-development model validation activities for the conceptual model are described in detail in *Dissolved Concentration Limits of Elements with Radioactive Isotopes* (SNL 2007 [DIRS 177418], Section 7). The solubilities of the radionuclides of interest predicted by the solubility models were corroborated with experimental data, publications in peer-reviewed journals (SNL 2007 [DIRS 177418], Table 7-1), and an independent technical review. The results of these activities provide confidence that the model solubilities of the radionuclides used as input in the TSPA-LA Model computations are appropriate for the purpose. The validation and confidence building activities for the solubilities models are discussed in detail in *Dissolved Concentration Limits of Elements with Radioactive Isotopes* (SNL 2007 [DIRS 177418], Sections 7.2.1 through 7.2.9).

Waste Form and In-Drift Colloids-Associated Radionuclide Concentrations—Section 6.3.7.6 of the TSPA-LA Model discusses the colloidal radionuclide transport in the TSPA-LA Model. Figure 6.3.7-13 conceptually displays the information flow. The colloid

model abstraction (parameters in PEFs # 53, 54, 55, 56, 57, and 58 in Table 4-1) is used in TSPA-LA to estimate the stability and concentration of colloid suspensions, as well as concentrations of radionuclides associated with the colloids, based on in-package and in-drift fluid chemistry and in-package dissolved radionuclide concentrations. The component models of colloidal transport, namely the: (a) mathematical; (b) stability and colloids-concentration (of CNSF, U-oxide, DHLWG, or WP); and (c) sorption of radionuclides to the colloids, are validated by corroboration with laboratory, field, and literature data. The validation activities and the results are documented in *Waste Form and In-Drift Colloids-Associated Radionuclide Concentrations: Abstraction and Summary* (SNL 2007 [DIRS 177423], Section 7). Table 7-1 of the above-mentioned report (SNL 2007 [DIRS 177423]) lists the corroborative data used to validate the specific requirements for the colloids component models. The mathematical form of the colloid model consists of a stability criterion based on the DLVO theory (DLVO theory is designed to account for the interactions between charged colloidal particles) with inputs from ionic strength and pH. By comparison with the literature data (SNL 2007 [DIRS 177423], Table 7-1), it was shown that the ionic strength and pH dependence of colloids stability is valid and a reasonable colloids stability threshold could be defined (SNL 2007 [DIRS 177423], Figure 7-1). The stability of waste-form colloids (of CNSF, U-oxide, DHLWG, or WP) is documented further in *Waste Form and In-Drift Colloids-Associated Radionuclide Concentrations: Abstraction and Summary* (SNL 2007 [DIRS 177423], Sections 7.1.2 and 7.1.3), which also discusses the confidence in the concentrations of radionuclides associated with colloidal sorption-desorption processes.

Sections 7.1.4 and 7.1.5 (SNL 2007 [DIRS 177423]) document the basis for confidence in the distribution-coefficient of radionuclide and predicted colloidal concentrations of radionuclides (SNL 2007 [DIRS 177423], Figure 7-5).

EBS Radionuclide Transport—Section 6.3.8 of the TSPA-LA Model discusses the EBS transport abstraction and implementation in the TSPA-LA Model. Figure 6.3.8-2 displays the abstraction model components, and the input parameters (in PEF # 59 of Table 4-1) to the TSPA-LA Model. Figure 6.3.8-2 also lists the activities performed that form the basis for confidence in the TSPA-LA Model input parameters from the supporting model components. The outputs (*EBS Radionuclide Transport Abstraction* (SNL 2007 [DIRS 177407], Table 8.2-1) from the submodels—EBS Flow, EBS Transport, and EBS-UZ Interface—were integrated as the EBS Radionuclide Transport Abstraction model and implemented unchanged. The submodels were validated for their intended use as required by SCI-PRO-006 and the confidence building was accomplished by corroborating the model outputs with an independent critical review. The results of the critical review on the flow and transport and the EBS-UZ interface submodels are documented in *EBS Radionuclide Transport Abstraction* (SNL 2007 [DIRS 177407], Section 7.2.3 and 7.3.2).

In addition, Section 7.1.1 of *EBS Radionuclide Transport Abstraction* (SNL 2007 [DIRS 177407]) documents the results of further validation of the flux-splitting portion of the EBS flow submodel by corroboration with experimental data (SNL 2007 [DIRS 177407], Tables 7.1-7 and 7.1-12). The corroboration demonstrates that the DS and WP flux data used in the EBS flow are conservatively credible. The diffusion portion of the EBS transport model was further validated through corroboration with alternate models as documented in *EBS Radionuclide Transport Abstraction* (SNL 2007 [DIRS 177407], Section 7.2). The alternate

models are based on the data available in the literature (SNL 2007 [DIRS 177407], Figure 7.2-4) in the EPRI Phase 5 report (EPRI 2000 [DIRS 154149]) and as shown on Figure 7-8 (SNL 2007 [DIRS 177407]), and also that included in the model by Lee et al. (1996 [DIRS 100913]) for diffusive releases from WP containers with multiple perforations. The results of these corroboration activities demonstrate that the input to the TSPA-LA Model parameters are technically sound.

7.6.4.4 Disruptive Events

This section presents results of corroboration of the abstractions with the underlying validated process models and analyses for the seismic and igneous events and provides information on the basis for confidence in the direct input TSPA-LA Model parameters.

7.6.4.4.1 Seismic Event

Seismic Consequence—Figure 6.6-2 shows the inputs to and out from the seismic scenario class modeling and analyses cases, and shows the basis for confidence in the output parameters from these cases. Section 6.6.1 of the TSPA-LA Model report discusses the implementation of parameters from the vibratory Seismic GM Modeling Case, and Section 6.6.2 of the report discusses that for the Seismic FD Modeling Case. The abstractions for damage to the WP and DS in response to vibratory ground motion are treated as models because they rely on analyses of structural response over a range of ground motion that is wider than typically covered by seismic designs for buildings or nuclear power plants. The abstractions for kinematic response of the WP and for the response of a WP surrounded by rubble was validated by: (1) corroboration of abstraction model results with the results of the validated structural response model from which the abstraction model is derived, and (2) a technical review by an independent reviewer. For the DS damage abstractions, the fragility curves for the DS and/or its plates and the abstraction for rubble accumulation was validated by: (1) corroboration of the abstraction results with the results of the validated structural response model or rockfall model from which the abstractions are derived, and (2) a technical review by an independent reviewer. The damage abstraction for fault displacement is a scientific analysis because it is based on a standard engineering approach that bounds component response through an analysis of clearances around the different types of WPs. Consequently, this abstraction does not require further validation.

Table 7-1 (SNL 2007 [DIRS 176828]) lists the figures and tables that corroborate the abstraction results with the underlying data. In addition to these, as mentioned above, an independent technical review is included as Appendix C (SNL 2007 [DIRS 176828]). Table 7-1 (SNL 2007 [DIRS 176828]) summarizes the results of the corroboration, which show that the abstractions for kinematic damage to the WP, for the WP surrounded by rubble, for the DS fragility curves, and for the damage to the DS provide reliable input parameters to the TSPA-LA Model. The independent technical review findings agree with this observation.

7.6.4.4.2 Igneous Event

Annual Frequency of Intersection—Section 6.5.1.1 of the TSPA-LA Model report discusses the TSPA-LA implementation of the annual frequency (i.e., probability) information. Figure 6.5-4 shows how the parameter (PEF # 60 in Table 4-1) from the probability estimate

flows to the eventual dose calculation by the TSPA-LA Model computation. The inputs to this scientific analysis report are the repository design elements and the results of the expert elicitation, *Probabilistic Volcanic Hazard Analysis for Yucca Mountain, Nevada* (CRWMS M&O 1996 [DIRS 100116]), conducted in a manner consistent with the guidance in the NRC Technical Position on Expert Elicitation (Kotra et al. 1996 [DIRS 100909]). The output parameter developed for the revised repository footprint was verified by ACMs and estimates. The combined output parameter for TSPA-LA Model is the annual frequency of intersection of the repository footprint by a volcanic event. Confidence in this parameter was established as summarized in Section 7.1 and discussed in *Characterize Framework for Igneous Activity at Yucca Mountain, Nevada* (BSC 2004 [DIRS 169989], Sections 6.3, 6.4.1.5, and 6.5).

7.6.4.4.3 Dike/Drift Interactions

Section 6.5.1 of the TSPA-LA Model discusses the TSPA-LA implementation of the parameters (parameters in PEFs # 13 and 14 in Table 4-1) and Figure 6.5-5 shows the inputs, outputs, and the basis for the confidence in the modeling case. Table 7-2 (SNL 2007 [DIRS 177430]) documents the methods used to validate and build confidence in the two submodels: dike propagation during intrusion and basalt cooling and solidification. The discussions in the sections cited in Table 7-2 and the appendices attached (SNL 2007 [DIRS 177430]) provide confidence in the output parameters from these submodels that support the TSPA-LA Model.

Briefly, the extensive post-development confidence building activities summarized below demonstrate the technical soundness of the parameters. Post-model development confidence in the dike propagation during intrusion submodel was built by the following four activities: (1) application of analytical solutions for a vertical self-similar dike. The results are documented in *Dike/Drift Interactions* (SNL 2007 [DIRS 177430], Section 7.3.1.1.3); (2) corroboration with analogue studies was conducted for effect of underlying geologic structure component (SNL 2007 [DIRS 177430], Section 7.3.2.3); (3) corroboration by comparison with data from independent, peer-reviewed research conducted for the effect of topography component (SNL 2007 [DIRS 177430], Section 7.3.1.2); and (4) corroboration with analogue studies conducted for effect of underlying geologic structure component (SNL 2007 [DIRS 177430], Section 7.3.2.3).

The basalt cooling and solidification submodel was validated by comparison with: (1) alternative analytic solutions; (2) alternative numerical models described in Sections 7.3.2.2.1.1 and 7.3.2.2.1.2, respectively, in *Drift/Dike Interactions* (SNL 2007 [DIRS 177430]); (3) field observations and associated mathematical model (SNL 2007 [DIRS 177430], Section 7.3.2.2.2); and (4) uncertainty studies (SNL 2007 [DIRS 177430], Section 7.3.2.2.3).

Number of Waste Packages Hit by Igneous Intrusion—Section 6.5.1.1 of the TSPA-LA Model describes the TSPA-LA implementation of the *Number of Waste Packages Hit by Igneous Intrusion* (SNL 2007 [DIRS 177432] and parameter in PEFs # 30 and 61 in Table 4-1). Figure 6.5-5 provides a graphical presentation of the inputs, outputs, and the basis for model confidence for the Igneous Intrusion and Volcanic Eruption Modeling Cases included in this calculation. The outputs of the calculation are:

- Igneous Intrusion Modeling Case: Number of WPs damaged by intrusion is CDF representing step function with values of 0 (no intersection of the repository) or 11,629 (intersection of repository and all WPs assumed damaged).

- Volcanic Eruption Modeling Case: Number of WPs intersected by conduits. CDF with a range of 0 to 7 and eruptive center probability—fraction of intrusion cases in which eruption also occurs.

Confidence in the three parameters is built by performing the calculations by following the established scientific process, and a traceable documentation of the process. Information on confidence building activities and results on the CDFs that were derived from the calculations is reported in *Number of Waste Packages Hit by Igneous Events* (SNL 2007 [DIRS 177432], Section 6.3).

Atmospheric Dispersal and Deposition of Tephra from a Potential Volcanic Eruption—The radioactive-waste mass concentration in the resuspendable layer of soil is determined from the results of the ASHPLUME and FAR Models (the FAR Model is described below). The implementation of the ASHPLUME in the TSPA-LA Model is described in Section 6.5.2.1.2 of the TSPA-LA Model. These two models produce the results in terms of waste volumetric concentrations, and the Biosphere Model uses the results. Section 6.3.11 of the TSPA-LA Model discusses TSPA-LA Model implementation in the Biosphere Model (presented below).

Confidence was built in the ASHPLUME Model by a number of post-model development buildings, including corroboration of the model results with: (a) the data collected for three volcanoes representative of volcanic ash deposits in the Yucca Mountain region (Cerro Negro, Nicaragua; Lathrop Wells, Nevada; and Cinder Cone, California); (b) an independent technical review performed to assess the applicability of the ASHPLUME Model (SNL 2007 [DIRS 177431], Appendix F) and the ash redistribution conceptual model (SNL 2007 [DIRS 177431], Appendix G); (c) comparison of the ASHPLUME model with published results of the ASHFALL model (SNL 2007 [DIRS 177431]); and (d) sensitivity analyses of the key parameters (SNL 2007 [DIRS 177431], Figures C-1 through C-11; Tables C-10 and C-11).

Redistribution of Tephra and Waste by Geomorphic Processes Following a Potential Volcanic Eruption at Yucca Mountain, Nevada—As mentioned above, the radioactive waste mass concentration in the resuspendable layer of soil is determined from the results of the ASHPLUME and Fortymile Wash Ash Redistribution (FAR) models. The FAR Model implements the FAR conceptual model. The implementation of the FAR Model in the TSPA-LA Model is described in Section 6.5.2.1.3. The Biosphere Model receives ash redistribution input as dynamically linked to the FAR code and ASPLUME code. Section 6.3.11 of the TSPA-LA Model discusses the TSPA-LA Model implementation in the Biosphere Model as discussed below.

Confidence in the FAR Model was built by corroborating the results with: (a) testing against measurements of radionuclides in soil at sites in the Nevada Test Site, using geomorphological data from the Fortymile Wash drainage basin, and measurements on ash redistribution in the Fortymile Wash due to the 1995 flood event to enhance confidence in the FAR Model inputs and the FAR Model during its development (SNL 2007 [DIRS 179347], Sections 7.1 and 7.2);

(b) corroboration of model results with relevant information published in a peer-reviewed journal (SNL 2007 [DIRS 179347], Section 7.3.1); and (c) independent technical review (SNL 2007 [DIRS 179347], Section 7.3.2). Details are documented in *Redistribution of Tephra and Waste by Geomorphic Processes Following a Potential Volcanic Eruption at Yucca Mountain Nevada* (SNL 2007 [DIRS 179347]).

7.6.4.5 Biosphere

This section presents outcome of corroboration of the abstraction results for the Biosphere Model with the underlying validated process models and analyses and provides information on the confidence built into the output parameters from the Biosphere Model.

7.6.4.5.1 Biosphere Model for Effects on RMEI

Biosphere Model—Figure 6.3.11-2 describes the inputs, outputs, and basis for model confidence for the Biosphere Model component of the TSPA-LA Model. The Biosphere Model outputs to the TSPA-LA Model are documented in Table 4-1 (PEFs # 67, # 68, and # 69). The Biosphere Model provides TSPA with the following inputs for dose calculation: (a) BDCFs and methodology to use these data to generate dose applicable to all modeling cases involving release of radionuclides to the accessible environment by pumping groundwater from the SZ, BDCFs, and (b) methodology to use these data to generate dose for the Volcanic Eruption Modeling Case and dose coefficients to calculate inhalation dose during the volcanic ash fall. In addition, the model also provides the data sets required for the TSPA to evaluate compliance with the ground water protection standard (alpha activities and beta-gamma dose derived from radionuclide concentrations developed in TSPA).

The Biosphere Model code, ERMYN, is used to generate both sets of BDCFs. ERMYN is a stochastic GoldSim model of the biosphere and provides TSPA with 1,000 random BDCFs for each radionuclide deemed important and tracked by TSPA in the appropriate modeling case. ERMYN itself was validated by comparisons at the submodel level with national and international peer-reviewed Biosphere Models.

The ground water protection standard and inhalation data sets are deterministic and are generated from the base data contained in Federal Guidance Report 13 (and the included database). Data for individual radionuclides were concatenated to provide the inputs required for the radionuclides considered in the TSPA-LA. These and the BDCF data are qualified in the Biosphere Model Report per SCI-PRO-006.

INTENTIONALLY LEFT BLANK

Table 7.6-1. Model Abstractions and Confidence in the Direct-Input TSPA-LA Parameters

General Model Area	Model Abstraction (Name and DIRS Number)	Underlying Process Model (Name and DIRS Number)	Model Abstractions and Confidence in the Direct-Input TSPA-LA Parameters
Natural System Environment			
Unsaturated Zone Flow	*UZ Flow Models and Submodels* (SNL 2007 [DIRS 184614]) Reference 1 in Table 6-1.	*UZ Flow Models and Submodels* (SNL 2007 [DIRS 184614]) Reference 1 in Table 6-1.	The UZ Flow Model is the validated supporting model implemented in the TSPA-LA Model via the UZ Transport Submodel and MSTHM discussed below. Comparison of the flow parameters predicted by the UZ Flow Model with the on-site borehole, Exploratory Studies Facility, and enhanced characterization of repository block tests data show that the predicted parameter values are supported by the range of observed data. Confidence in the values of the model parameters is further enhanced by comparison with natural analogues, and especially with a number of publications in peer-reviewed journals (Section 7.6.4).
	Future Climate Analysis (BSC 2004 [DIRS 170002]) Reference 3 in Table 6-1.	*Future Climate Analysis* (BSC 2004 [DIRS 170002]) Reference 3 in Table 6-1.	*Future Climate Analysis* (BSC 2004 [DIRS 170002], Section 7.1) presents an assessment of the confidence in the analysis results and concludes that the analysis is reasonable and, based on a consistent interpretation of available data that includes the earth orbital parameter and paleoclimate data it is, defensible.
	Simulation of Net Infiltration for Present-day and Potential Future Climates (SNL 2007 [DIRS 182145]) Reference 2 in Table 6-1).	*Simulation of Net Infiltration for Present-day and Potential Future Climates* (SNL 2007 [DIRS 182145]) Reference 2 in Table 6-1.	Confidence in the model output parameters was provided by a number of activities as summarized in Section 7.6.4 and listed on Figure 6.3.1-4. The activities included: (1) comparison of MASSIF predictions of infiltration for present-day, monsoon, and glacial-transition climates for 40 realizations for each climate, with infiltration estimates from published models and data for the Yucca Mountain area, the southwestern United States, and the western United States, (2) comparison of MASSIF predictions of infiltration with seepage estimates observed in the South Ramp of the Exploratory Studies Facility in the winter of 2005, and (3) alternative model approach corroboration activity in which MASSIF results are compared to HYDRUS one-dimensional results for four different soil depths and using the same model inputs. The results of these validation activities show that the predicted infiltration parameters fall within the range supported by these activities.

Table 7.6-1. Model Abstractions and Confidence in Direct-Input TSPA-LA Parameters (Continued)

General Model Area	Model Abstraction (Name and DIRS Number)	Underlying Process Model (Name and DIRS Number)	Model Abstractions and Confidence in the Direct-Input TSPA-LA Parameters
Natural System Environment (Continued)			
Unsaturated Zone Radionuclide Transport	*Particle Tracking Model and Abstraction of Transport Processes* (SNL 2008 [DIRS 184748]) Reference 14 in Table 6-1.	UZ Transport Model is implemented by particle-tracking methodology using FEHM (FEHM V2.24-01 [DIRS 179419]) and documented in *Particle Tracking Model and Abstraction of Transport Processes* (SNL 2008 [DIRS 184748]) Reference 14 in Table 6-1.	The breakthrough curves from the validated UZ Transport Model were compared with those of the underlying process model and several ACMs using FEHM and the results demonstrated reasonably good comparison, especially for the dual-k approach. For example, *Particle Tracking Model and Abstraction of Transport Processes* (SNL 2008 [DIRS 184748], Figure 7-11) compares the FEHM results with the breakthrough curves from the process model using the code T2R3D.
Saturated Zone Flow and Transport	*Saturated Zone Flow and Transport Model Abstraction* (SNL 2008 [DIRS 183750]) Reference 16 in Table 6-1.	SZ Site-Scale Transport Model (SNL 2007 [DIRS 177392]) Reference 18 in Table 6-1.	As discussed in detail in Section 7.6.4, and demonstrated in *Saturated Zone Flow and Transport Model Abstraction* (SNL 2008 [DIRS 183750], Figures 7-1 through 7.5), results of the sorbing and non-sorbing radionuclides from both the 3-D and 1-D Abstraction Models compare reasonably well with those of the underlying process models.
Engineered Barrier System Environment			
Seepage into Drift	*Abstraction of Drift Seepage* (SNL 2007 [DIRS 181244]) Reference 4 in Table 6-1.	The key process models are: (1) Seepage Model for Performance Assessment Including Drift Collapse (SNL 2007 [DIRS 181244], Section 6.4.2), and (2) Thermal Seepage Model (SNL 2007 [DIRS 181244], Section 6.4.3) Reference 5 in Table 6-1.	The *Abstraction of Drift Seepage* provides evidence that the abstracted results of the Drift Seepage Model satisfies the validation requirement (Level 1 validation set by the technical work plan (BSC 2006 [DIRS 177465], Section 7.2) with agreement within 20 percent between the process models and abstracted results. Additional confidence (Section 7.3) in the TSPA-LA Parameters was built by qualitative comparison with (a) the South Ramp seepage predictions with actual observations, (b) Alcove 8-Niche 3 seepage tests results, and (c) observations with seepage in the Pena Blanca natural analogue. Section 7.3 of the Abstraction of Drift Seepage Model documents that the abstracted seepage value is corroborated by the data from these analogues. The upper-bound seepage (i.e., a conservative) value is produced by the *Abstraction of Drift Seepage* (SNL 2007 [DIRS181244)] for the TSPA-LA parameters.

Table 7.6-1. Model Abstractions and Confidence in Direct-Input TSPA-LA Parameters (Continued)

General Model Area	Model Abstraction (Name and DIRS Number)	Underlying Process Model (Name and DIRS Number)	Model Abstractions and Confidence in the Direct-Input TSPA-LA Parameters
Engineered Barrier System Environment (Continued)			
In-Drift Convection and Condensation	The TSPA-LA used directly the condensation predictions for boiling and sub-boiling drift temperatures developed using the *In-Drift Natural Convection and Condensation Model* (SNL 2007 [DIRS 181648]) Reference 7 in Table 6-1.	*In-Drift Natural Convection and Condensation Model* (SNL 2007 [DIRS 181648]) Reference 7 in Table 6-1.	The Condensation Model is based on the Convection Model and the average percolation flux derived from MSTHM. The Convection Model was validated by: (1) comparison of simulation results to small-scale (centimeter dimension) literature data for natural convection in horizontal concentric cylinders, (2) 44 percent of full-scale dimension tests, and (3) independent technical review. The details of validation test plans and results are presented in *In-Drift Natural Convection and Condensation* (SNL 2007 [DIRS 181648], Sections 7.3, 7.4, and 7.5). The Condensation Model was validated by an independent technical review that included the supporting Convection Model. The results are presented in *In-Drift Natural Convection and Condensation* (SNL 2007 [DIRS 181648], Section 7.6 and Appendix G).
Repository Thermohydrology Due to Waste Heat	*Multiscale Thermohydrologic Model* (SNL 2007 [DIRS 181383]. The MSTHM produces direct predictions on the following TSPA-LA Parameters: (1) Temperature for drift-wall, DS, WP, and invert; (2) relative humidity of WP and invert; and (3) invert liquid-phase saturation. The MSTHM bases the direct predictions on application of its own methodology integrating SDT, SMT, and DDT (SNL 2007 [DIRS 181383]).	*Multiscale Thermohydrologic Model* (SNL 2007 [DIRS 181383]) Reference 6 in Table 6-1.	See Section 7.6.4 for additional discussion on the results of corroboration of the MSTHM predictions with test data and alternate model predictions with reasonable agreement. The predictions consist of the following TSPA-LA parameters, which are implemented without further simplification: (1) temperature for drift-wall, DS, WP, and invert; (2) relative humidity of WP and invert; and (3) invert liquid-phase saturation. The MSTHM bases the predictions on application of its own methodology integrating SDT, SMT, and DDT (SNL 2007 [DIRS 181383]), which are conduction-only calculations. The confidence in the predicted parameters was built by direct comparison of test data (e.g., Large Block Test and Drift-Scale Test at the repository) and results predicted by another model. The details are presented in Sections 7.3 through 7.6 of the MSTHM (SNL 2007 [DIRS 181383]), which indicate that the abstracted parameters are appropriate for their intended use in the TSPA-LA Model.

Table 7.6-1. Model Abstractions and Confidence in Direct-Input TSPA-LA Parameters (Continued)

General Model Area	Model Abstraction (Name and DIRS Number)	Underlying Process Model (Name and DIRS Number)	Model Abstractions and Confidence in the Direct-Input TSPA-LA Parameters
Engineered Barrier System Environment (Continued)			
EBS Physical and Chemical Environment	*Engineered Barrier System: Physical and Chemical Environment* (SNL 2007 [DIRS 177412]) produced the following abstractions: (a) Seepage Dilution/Evaporation Abstraction Model (abstracted parameters: chloride ion concentration; nitrate ion concentration; and chloride to nitrate ion molar ratio, ionic strength, and pH); (b) Integrated Invert Chemistry Abstraction Model (for pH and I).	*Engineered Barrier System: Physical and Chemical Environment* (SNL 2007 [DIRS 177412]) Reference 8 in Table 6-1. The process models are: (a) Validated Near-Field Chemistry (NFC) Model (for seepage water compositions, water-rock interaction parameters, and a range of in-drift partial pressure of carbon dioxide (pCO_2) values, and (b) Validated In-Drift Precipitates/Salt (IDPS) Model (provides the estimated uncertainties on the chemical parameters (pH, I, [Cl], [N]) as a function of in-drift relative humidity).	Comparison of an interpolation of the lookup tables of the chemistry parameters with the underlying validated In-Drift Precipitates/Salt (IDPS) model outputs (with uncertainty) for the same representative set of environmental conditions, show (SNL 2007 [DIRS 177412], Figure 7.2-2) that the difference is less than the model uncertainty for the IDPS model. Section 7.6.4 provides more information. The detail of the corroboration results are presented in *Engineered Barrier System: Physical and Chemical Environment* (SNL 2007 [DIRS 177412], Section 7).

Table 7.6-1. Model Abstractions and Confidence in Direct-Input TSPA-LA Parameters (Continued)

General Model Area	Model Abstraction (Name and DIRS Number)	Underlying Process Model (Name and DIRS Number)	Model Abstractions and Confidence in the Direct-Input TSPA-LA Parameters
Waste Form and Waste-Package Degradation and Mobilization			
Drip Shield, Waste Package, and Waste Form Degradation	SCC growth rate of the DS and the WP Outer Barrier (SNL 2007 [DIRS 181953]) Reference 11 in Table 6-1.	Three component process models of SCC feed the TSPA-LA model. These component process models are: (1) Alloy 22 SDFR, (2) drip shield SCC model, and (3) Alloy 22 and drip shield seismic crack density model.	The models and the two key input parameters (threshold stress intensity factor and the threshold stress for SCC initiation) to the SDFR model are validated for their intended uses (SNL 2007 [DIRS 181953], Sections 7.1, 7.2, 7.3, 7.4, and 7.5). Comparison with literature data show the SCC growth rate is within two to three orders of magnitude of the literature data, which is considered reasonable and acceptable. Additionally, as a defensible approach the threshold stress intensity factor and the threshold stress for SCC initiation under the relevant environmental conditions were established (SNL 2007 [DIRS 181953], Section 7.3.4).
	General Corrosion and Localized Corrosion of Waste Package Outer Barrier (SNL 2007 [DIRS 178519]) Reference 10 in Table 6-1.	*General Corrosion and Localized Corrosion of Waste Package Outer Barrier* (SNL 2007 [DIRS 178519]) constitutes a part of the WAPDEG analysis of waste-package and drip shield degradation (Reference 10 in Table 6-1).	Comparison of the project experimental data with literature data on general corrosion rates as a function of time (SNL 2007 [DIRS 178519], Figure 7-1 and Table 7-1) and comparison of model prediction of localized corrosion susceptibility with experimental data of Alloy 22 crevice samples (SNL 2007 [DIRS 178519], Table 7-4) lead to the conclusion that the general and localized corrosion models for the WP outer barrier corroborate well with the experimental data and those reported in the scientific literature.
	General Corrosion and Localized Corrosion of the Drip Shield (Ti - 29) (SNL 2007 [DIRS 180778]). The three parameters developed by DS Corrosion (Ti - 29) are: DS inner and outer surface corrosion rates and general corrosion rate ratio of Titanium Grade 29/Titanium Grade 7.	Drip Shield Corrosion (Ti - 29) (SNL 2007 [DIRS 180778]) Process models that produced the three corrosion parameters for the TSPA-LA Model are: (a) dry oxidation, (b) the general corrosion, and (c) the localized corrosion models for drip shield.	Comparison shows that the parameters generally agree with the data in the peer reviewed literature representing a wide range of environments, providing confidence that the model predictions are appropriate. Comparison with the experimental data shows that the model predictions provide the upper bound values of the parameters used in the TSPA-LA. The predictions are thus conservative. Detailed results are provided in Sections 7.3 (dry oxidation), 7.4 (general corrosion), and 7.5 (localized corrosion) of *General Corrosion and Localized Corrosion of the Drip Shield* (SNL 2007 [DIRS 180778]).

Table 7.6-1. Model Abstractions and Confidence in Direct-Input TSPA-LA Parameters (Continued)

General Model Area	Model Abstraction (Name and DIRS Number)	Underlying Process Model (Name and DIRS Number)	Model Abstractions and Confidence in the Direct-Input TSPA-LA Parameters
Waste Form and Waste-Package Degradation and Mobilization (Continued)			
Drip Shield, Waste Package, and Waste Form Degradation (Continued)	*CSNF Waste Form Degradation: Summary Abstraction* (BSC 2004 [DIRS 169987]).	*CSNF Waste Form Degradation: Summary Abstraction* (BSC 2004 [DIRS 169987]).	The basis for confidence in the TSPA-LA parameters from the three waste form degradation models is discussed in Section 7.6.4. The calculated release rates for the CSNF were compared with experimental and literature data that show (BSC 2004 [DIRS 169987], Tables in Section 7.1) CSNF model rates and the experimental and literature data are within the range of associated uncertainty. Additional confidence was built by comparing the: (1) results of ACMs (Surface-Complexation Model and Electrochemical Model), which indicate the model dissolution rates are reasonable; (2) oxidative alteration rate and phases with those of laboratory experiments, which indicates that the model results are reasonable, and (3) natural analogues that included the uranium deposits at Peña Blanca, Mexico; Koongarra, Australia; Pecos de Caldas, Brazil; Shinkolobwe mine in Congo; and Krunkelbach mine in Germany, which indicate consistency with the degradation modes.
	DSNF and Other Waste Form Degradation Abstraction (BSC 2004 [DIRS 172453]).	*DSNF and Other Waste Form Degradation Abstraction* (BSC 2004 [DIRS 172453]).	For the DSNF, the model output from the analysis were validated by comparison with alternate mathematical models (Section 6.1, Table 6-9), which showed complete degradation in one year, thus providing confidence in the instantaneous release model for DSNF.
	Defense HLW Glass Degradation Model (BSC 2004 [DIRS 169988]).	*Defense HLW Glass Degradation Model* (BSC 2004 [DIRS 169988]).	Validation of the defense HLW glass degradation rate model (rate expression) was accomplished by comparison with laboratory test results and relevant observations in studies with simulated HLW and natural analog glasses that were not used to develop the model. The details are presented in *Defense HLW Glass Degradation Model* (BSC 2004 [DIRS 169988], Section 7 and Table 7-1).
	Analysis of Mechanisms for Early Waste Package/Drip Shield Failure (SNL 2007 [DIRS 178765]).	*Analysis of Mechanisms for Early Waste Package/Drip Shield Failure* (SNL 2007 [DIRS 178765]).	Confidence in the Early Failure Scenario Class parameters is based on (1) the fact that the calculations were performed using controlled manufacturing industry defect-related failure data sets; (2) conservative estimate for probability of occurrences of flaws per WP and DS that lead to early; and (3) conservative estimate of impact on barrier containment properties.

Table 7.6-1. Model Abstractions and Confidence in Direct-Input TSPA-LA Parameters (Continued)

General Model Area	Model Abstraction (Name and DIRS Number)	Underlying Process Model (Name and DIRS Number)	Model Abstractions and Confidence in the Direct-Input TSPA-LA Parameters
Waste-Form and Waste-Package Degradation and Mobilization (Continued)			
Transport of Radionuclides Out of the EBS	*Initial Radionuclides Inventory* (SNL 2007 [DIRS 180472]; and SNL 2007 [DIRS 177422]) References 20 and 35 in Table 6-1.	*Initial Radionuclides Inventory* (SNL 2007 [DIRS 180472]; SNL 2007 [DIRS 177422]) References 24 and 39 in Table 6-1.	The inventory was developed based on the latest available qualified and controlled dataset as stated in the source document in *Initial Radionuclide Inventory* (SNL 2007 [DIRS 180472], Section 7 and Table 7.1[a]). The inventory is an analysis that was performed applying standard scientific principles and practices pursuing the requirements of SCI-PRO-005, and thus providing confidence in the inventory presented in Table 7.1[a].
	In-Package Chemistry Abstraction (SNL 2007 [DIRS 180506]) Reference 21 in Table 6-1.	In-Package Chemistry Model (SNL 2007 [DIRS 180506]). The In-Package Chemistry Model is made up of two main underlying process models: the batch reactor model and the surface complexation model. The batch reactor model is made up of two water-influx models, the liquid-influx and the vapor-influx models, and several other component submodels, including the fuel-degradation and the steel-degradation submodels. The In-Package Chemistry Model is presented in *In-Package Chemistry Abstraction* (SNL 2007 [DIRS 180506], Section 6) Reference 25 in Table 6-1.	See Section 7.6.4 for more information. The abstraction pH and ionic strength values were compared with the process-model output in *In-Package Chemistry Abstraction* (SNL 2007 [DIRS 180506], Figures 7-1 to 7-8) for a fixed flux and a range of fluxes. The abstracted values are consistent with the model outputs. The reasonableness of the abstracted values, was evaluated also by comparing the values with natural analogs as presented in *In-Package Chemistry Abstraction* (SNL 2007 [DIRS 180506], Section 7.4.5.8) with favorable results.

Table 7.6-1. Model Abstractions and Confidence in Direct-Input TSPA-LA Parameters (Continued)

General Model Area	Model Abstraction (Name and DIRS Number)	Underlying Process Model (Name and DIRS Number)	Model Abstractions and Confidence in the Direct-Input TSPA-LA Parameters
Waste-Form and Waste-Package Degradation and Mobilization (Continued)			
Transport of Radionuclides Out of the EBS (Continued)	*Dissolved Concentration Limits of Elements with Radioactive Isotopes* (SNL 2007 [DIRS 177418]).	*Dissolved Concentration Limits of Elements with Radioactive Isotopes* (SNL 2007 [DIRS 177418]).	The solubilities of the radionuclides of interest predicted by the solubility models were corroborated with the experimental data, publications in refereed journals (SNL 2007 [DIRS 177418], Table 7-1), and an independent technical review. The results of the comparison provide confidence that the model solubilities of the radionuclides used as inputs to the TSPA-LA Model computations are appropriate for the purpose. The validation and confidence building activities for the solubilities models are discussed in detail in *Dissolved Concentration Limits of Elements with Radioactive Isotopes* (SNL 2007 [DIRS 177418], Sections 7.2.1 through 7.2.9).
	Waste Form and In-Drift Colloids-Associated Radionuclide Concentrations: Abstraction and Summary (SNL 2007 [DIRS 177423]) Reference 27 in Table 6-1.	The component models of colloidal transport are: (a) mathematical, (b) stability and concentration of colloids (of CNSF, U-oxide, DHLWG, or WP), and (c) sorption of radionuclides to the colloids. These models were developed, validated, and applied to TSPA directly and documented in *Waste Form and In-Drift Colloids-Associated Radionuclide Concentrations: Abstraction and Summary* (SNL 2007 [DIRS 177423]) Reference 31 in Table 6-1.	*Waste Form and In-Drift Colloids-Associated Radionuclide Concentrations: Abstraction and Summary* (SNL 2007 [DIRS 177423], Sections 7.1.1 through 7.1.5, and Table 7-1) provides the basis for confidence in the parameters used in the TSPA-LA Model, which were derived from the colloids stability model, colloids concentration, and colloids-associated concentrations of radionuclides. The mathematical form of the colloid model consists of a stability criterion based on the DLVO theory with inputs from ionic strength and pH. By comparison with the literature data (SNL 2007 [DIRS 177423], Table 7-1), it was shown that the ionic strength and pH dependence of colloids stability is valid and a reasonable colloids stability threshold could be defined (SNL 2007 [DIRS 177423], Figure 7-1). The stability of waste form colloids (of CSNF, U-oxide, DHLWG, WP) is documented further in *Waste Form and In-Drift Colloids-Associated Radionuclide Concentrations: Abstraction and Summary* (SNL 2007 [DIRS 177423], Sections 7.1.2 and 7.1.3), which also discuss the confidence in the concentrations of radionuclides associated with colloidal sorption-description processes. Finally, *Waste Form and In-Drift Colloids-Associated Radionuclide Concentrations: Abstraction and Summary* documents the basis for confidence in the distribution-coefficient of radionuclides and predicted colloidal concentrations of radionuclides (SNL 2007 [DIRS 177423], Sections 7.1.4 and 7.1.5, and Figure 7-5).

Table 7.6-1. Model Abstractions and Confidence in Direct-Input TSPA-LA Parameters (Continued)

General Model Area	Model Abstraction (Name and DIRS Number)	Underlying Process Model (Name and DIRS Number)	Model Abstractions and Confidence in the Direct-Input TSPA-LA Parameters
Waste-Form and Waste-Package Degradation and Mobilization (Continued)			
Transport of Radionuclides Out of the EBS (Continued)	*EBS Radionuclide Transport Abstraction* (SNL 2007 [DIRS 177407]). The integrated EBS Radionuclide Transport Abstraction and its submodels: EBS Flow, EBS Transport, and EBS-UZ Interface, were developed for direct implementation into TSPA-LA. No simplification was involved.	EBS Radionuclide Transport Abstraction (SNL 2007 [DIRS 177407]) includes the following submodels for the EBS Radionuclide Transport Abstraction: (a) EBS Flow Model (b) EBS Transport Model – Invert diffusion submodel – WP corrosion products diffusion submodel – Waste form degradation rind diffusion submodel – Temperature dependence of diffusion coefficient – Colloid transport – Radionuclide sorption onto stationary corrosion products and mobile colloids – Two-cell (waste form and corrosion products) EBS implementation in TSPA (c) EBS–UZ Interface Model – Advection/diffusion across interface – Boundary condition based on transport through portion of UZ	Section 7.6.4 provides more discussion on the basis for confidence in the EBS parameters used in the TSPA-LA Model computation. The confidence was based on corroborating the model outputs with: (1) an independent review of the EBS Flow, EBS Transport, and EBS-UZ Interface Submodels; and (2) alternate models based on literature data, including the EPRI model (EPRI 2000 [DIRS 154149]) and a model developed by Lee et al., (1996 [DIRS 100913]). The results of these corroboration activities demonstrate that the input the TSPA-LA Model parameters are technically sound.

Table 7.6-1. Model Abstractions and Confidence in Direct-Input TSPA-LA Parameters (Continued)

General Model Area	Model Abstraction (Name and DIRS Number)	Underlying Process Model (Name and DIRS Number)	Model Abstractions and Confidence in the Direct-Input TSPA-LA Parameters
Disruptive Events			
Seismic Event	*Seismic Consequence Abstraction* (SNL 2007 [DIRS 176828]).	The parameters abstracted are based on kinematic and structural response calculations that were developed using finite element models. Details are presented in *Mechanical Assessment of Degraded Waste Packages and Drip Shields Subject to Vibratory Ground Motion* (SNL 2007 [DIRS 178851]) and the *Seismic Consequence Abstraction* (SNL 2007 [DIIRS 176828]).	The *Seismic Consequence Abstraction* lists the figures and tables that corroborate the abstraction results with the underlying data and summarizes the results of the corroboration, which show that the abstractions for kinematic damage to the WP, for the WP surrounded by rubble, for the DS fragility curves, and for the damage to the DS, provide technically reasonable input parameters to the TSPA-LA Model (SNL 2007 [DIRS 176828], Table 7-1). In addition to these, the results were corroborated with the results of an independent technical review (SNL 2007 [DIRS 176828], Appendix C) where the findings agreed with the above observation.
Igneous Event	Annual Frequency of Interaction (*Characterize Framework for Igneous Activity at Yucca Mountain, Nevada* (BSC 2004 [DIRS 169989]) Reference 29 in Table 6-1.	Annual frequency of intersection is a scientific analysis.	Confidence in the output parameter from the analysis (i.e., annual frequency of repository intersection by an igneous intrusion) was established in *Characterize Framework for Igneous Activity at Yucca Mountain, Nevada* (BSC 2004 [DIRS 169989], Sections 6.3, 6.4.1.5, 6.5, and 7.1). The inputs to this scientific analysis (i.e., annual frequency of intersection) are repository design elements (which were verified by alternate conceptual models and estimates) and the results of the expert elicitation, *Probabilistic Volcanic Hazard Analysis for Yucca Mountain, Nevada* (CRWMS M&O 1996 [DIRS 100116]).

Table 7.6-1. Model Abstractions and Confidence in Direct-Input TSPA-LA Parameters (Continued)

General Model Area	Model Abstraction (Name and DIRS Number)	Underlying Process Model (Name and DIRS Number)	Model Abstractions and Confidence in the Direct-Input TSPA-LA Parameters
Disruptive Events (Continued)			
Igneous Event (continued)	The outputs of the component models of the *Dike/Drift Interactions* (SNL 2007 [DIRS 177430]) Reference 9 in Table 6-1.	(a) Dike propagation (b) Magma cooling and solidification (SNL 2007 [DIRS 177430]). In addition, inputs for water chemistry are provided by *In-Package Chemistry Abstraction* (SNL 2007 [DIRS 180506]). The input to TSPA is drift centerline and rib temps for various times following intrusion.	Confidence in the dike propagation during intrusion submodel was built by corroboration of the results with: (1) analytical solutions for a vertical self-similar dike (SNL 2007 [DIRS 177430], Section 7.3.1.1.3); (2) corroboration with analogue studies conducted for effect of underlying geologic structure component (SNL 2007 [DIRS 177430], Section 7.3.2.3); (3) corroboration by comparison with independent peer-reviewed research conducted for the effect of topography component (SNL 2007 [DIRS 177430], Section 7.3.1.2); and (4) corroboration with analogue studies conducted for effect of underlying geologic structure component (SNL 2007 [DIRS 177430], Section 7.3.2.3). The basaltic magma cooling and solidification submodel was validated by comparison with (1) Alternative Analytic Solutions and (2) Alternative Numerical Models (SNL 2007 [DIRS 177430], Sections 7.3.2.2.1.1 and 7.3.2.2.1.2); (3) Field observations and associated mathematical model (SNL 2007 [DIRS 177430], Section 7.3.2.2.2); and (4) uncertainty studies (SNL 2007 [DIRS 177430], Section 7.3.2.2.3).
	Number of Waste Packages Hit by Igneous Intrusion (SNL 2007 [DIRS 177432]). The outputs of the calculation are: (1) CDF representing step function with values of 0 (no intersection of the repository) or 11,629 (intersection of repository and all WPs assumed damaged); (2) Number of WPs intersected by conduits; CDF with range of 0-7; and, (3) Eruptive center probability—fraction of intrusion cases in which eruption also occurs.	*Number of Waste Packages Hit by Igneous Intrusion* (SNL 2007 [DIRS 177432]).	Confidence in the three parameters is built by performing the calculations following established scientific process and developing traceable documentation of the process. Information on confidence building activities and results on the CDFs that were derived from the calculations is reported in *Number of Waste Packages Hit by Igneous Events* (SNL 2007 [DIRS 177432], Sections 6 and 7).

Table 7.6-1. Model Abstractions and Confidence in Direct-Input TSPA-LA Parameters (Continued)

General Model Area	Model Abstraction (Name and DIRS Number)	Underlying Process Model (Name and DIRS Number)	Model Abstractions and Confidence in the Direct-Input TSPA-LA Parameters
Disruptive Events (Continued)			
Igneous Event (Continued)	*Atmospheric Dispersal and Deposition of Tephra from a Potential Volcanic Eruption at Yucca Mountain, Nevada* (SNL 2007 [DIRS 177431]).	The ASHPLUME_DLL_LA V.2.1 [DIRS 181035] implements the mathematical model of atmospheric dispersal and deposition of tephra of Suzuki (1983 [DIRS 100489]) for estimation of the aerial density of tephra deposits on the surface of the earth following a volcanic eruption and provides direct input to the TSPA-LA computation.	Confidence was built in the ASHPLUME Model by corroboration of results with: (a) data collected for three volcanoes representative of volcanic ash deposits in the Yucca Mountain region: Cerro Negro, Nicaragua; Lathrop Wells, Nevada; and Cinder Cone, California (SNL 2007 [DIRS 177431], Section 7.3); (b) independent technical review performed to assess the applicability of the ASHPLUME Model (SNL 2007 [DIRS 177431], Section 7.4 and Appendix E) and the Ash Redistribution Conceptual Model (SNL 2007 [DIRS 177431], Appendix G); (c) published results of the ASHFALL Model (SNL 2007 [DIRS 177431], Section 7.5); and, (d) sensitivity analyses of the key parameters (SNL 2007 [DIRS 177431], Section 7.6 and Figures C-1 through C-11).
	Redistribution of Tephra and Waste by Geomorphic Processes Following a Potential Volcanic Eruption at Yucca Mountain, Nevada (SNL 2007 [DIRS 179347]).	The Fortymile Wash Ash Redistribution (FAR) model was implemented by the computer code FAR, which is coupled with the ASHPLUME code providing direct inputs to the TSPA-LA Model computation. That is, the ASHPLUME DLL and FAR DLL are coupled within GoldSim.	The methods and results of confidence building in the FAR model are discussed in detail in *Redistribution of Tephra and Waste by Geomorphic Processes Following a Potential Volcanic Eruption at Yucca Mountain, Nevada* (SNL 2007 [DIRS 179347], Section 7). These include corroborating the results with: (a) testing against measurements of radionuclides in soil at sites in the NTS, using geomorphological data from the Fortymile Wash drainage basin, and measurements on ash redistribution in the Fortymile Wash due to the 1995 flood event to enhance confidence in the FAR model inputs and as well as for the FAR model conceptual development process (SNL 2007 DIRS [179347], Sections 7.1 and 7.2); (b) corroboration of model results with relevant information published in a refereed journal (SNL 2007 [DIRS 179347], Section 7.3.1), and (c) independent technical review (SNL 2007 [DIRS 179347], Section 7.3.2).

Table 7.6-1. Model Abstractions and Confidence in Direct-Input TSPA-LA Parameters (Continued)

General Model Area	Model Abstraction (Name and DIRS Number)	Underlying Process Model (Name and DIRS Number)	Model Abstractions and Confidence in the Direct-Input TSPA-LA Parameters
Biosphere			
Biosphere Model for Effects on RMEI	*Biosphere Model Report* (SNL 2007 [DIRS 177399]).	*Biosphere Model Report* (SNL 2007 [DIRS 177399]).	Section 7.6.4 of the TSPA-LA Model report provides additional information. ERMYN is a stochastic GoldSim model used in the biosphere modeling. ERMYN was validated by comparisons of results at the sub-model level with national and international peer-reviewed biosphere models. The groundwater protection standard and inhalation data sets are deterministic and are generated from the base data contained in Federal Guidance Report 13 (and the included database). Data for individual radionuclides were concatenated to provide the input required for the radionuclides considered in TSPA. These and the BDCF data are qualified in the biosphere model report per SCI-PRO-006.

INTENTIONALLY LEFT BLANK